Seismic Performance of Precast Concrete Cladding Systems

A thesis submitted in partial fulfilment of the

requirements for the Degree of

Doctor of Philosophy

by

Andrew C. Baird

Supervised by

Dr. Alessandro Palermo

Professor Stefano Pampanin

Civil and Natural Resources Engineering

University of Canterbury

Christchurch, New Zealand

September 2014

This thesis is dedicated to my sister

Belinda Duncan

Abstract

Structural engineering is facing an extraordinarily challenging era. These challenges are driven by the increasing expectations of modern society to provide low-cost, architecturally appealing structures which can withstand large earthquakes. However, being able to avoid collapse in a large earthquake is no longer enough. A building must now be able to withstand a major seismic event with negligible damage so that it is immediately occupiable following such an event. As recent earthquakes have shown, the economic consequences of not achieving this level of performance are not acceptable.

Technological solutions for low-damage structural systems are emerging. However, the goal of developing a low-damage building requires improving the performance of both the structural skeleton and the non-structural components. These non-structural components include items such as the claddings, partitions, ceilings and contents. Previous research has shown that damage to such items contributes a disproportionate amount to the overall economic losses in an earthquake. One such non-structural element that has a history of poor performance is the external cladding system, and this forms the focus of this research.

Cladding systems are invariably complicated and provide a number of architectural functions. Therefore, it is important than when seeking to improve their seismic performance that these functions are not neglected. The seismic vulnerability of cladding systems are determined in this research through a desktop background study, literature review, and post-earthquake reconnaissance survey of their performance in the 2010 – 2011 Canterbury earthquake sequence.

This study identified that precast concrete claddings present a significant life-safety risk to pedestrians, and that the effect they have upon the primary structure is not well understood. The main objective of this research is consequently to better understand the performance of precast concrete cladding systems in earthquakes. This is achieved through an experimental campaign and numerical modelling of a range of precast concrete cladding systems.

The experimental campaign consists of uni-directional, quasi-static cyclic earthquake simulation on a test frame which represents a single-storey, single-bay portion of a reinforced concrete building. The test frame is clad with various precast concrete cladding panel configurations. A major focus is placed upon the influence the connection between the cladding panel and structural frame has upon seismic performance.

A combination of experimental component testing, finite element modelling and analytical derivation is used to develop cladding models of the cladding systems investigated. The cyclic responses of the models are compared with the experimental data to evaluate their accuracy and validity. The comparison shows that the cladding models developed provide an excellent representation of real-world cladding behaviour.

The cladding models are subsequently applied to a ten-storey case-study building. The expected seismic performance is examined with and without the cladding taken into consideration. The numerical analyses of the case-study building include modal analyses, non-linear adaptive pushover analyses, and non-linear dynamic seismic response (time-history) analyses to different levels of seismic hazard. The clad frame models are compared to the bare frame model to investigate the effect the cladding has upon the structural behaviour. Both the structural performance and cladding performance are also assessed using qualitative damage states. The results show a poor performance of precast concrete cladding systems is expected when traditional connection typologies are used. This result confirms the misalignment of structural and cladding damage observed in recent earthquake events.

Consequently, this research explores the potential of an innovative cladding connection. The outcomes from this research shows that the innovative cladding connection proposed here is able to achieve low-damage performance whilst also being cost comparable to a traditional cladding connection. It is also theoretically possible that the connection can provide a positive value to the seismic performance of the structure by adding addition strength, stiffness and damping.

Finally, the losses associated with both the traditional and innovative cladding systems are compared in terms of tangible outcomes, namely: repair costs, repair time and casualties. The results confirm that the use of innovative cladding technology can substantially reduce the overall losses that result from cladding damage.

Acknowledgments

This thesis would not have been possible without the support and encouragement from many people. The greatest thanks go to my primary supervisor Dr Alessandro Palermo for his unwavering support over the last four years. He has been a constant source of knowledge, inspiration and motivation, and I am sincerely grateful for his supervision of this thesis. I would also like to thank my co-supervisor Professor Stefano Pampanin for his exceptional technical support and for first inspiring me to pursue this research.

This project would not have been possible without the financial support provided by the Department of Civil and Natural Resources Engineering through a Doctoral Scholarship and the New Zealand Foundation for Research, Science and Technology (FRST) through the Natural Hazard Research Platform (NHRP). These contributions are gratefully acknowledged.

I would like to thank the technicians and staff of the Department of Civil and Natural Resources Engineering who helped me on this project. In particular, Gavin Keats, Mosese Fifita, Peter Coursey, Alan Poynter and John Maley for their assistance with the experimental programme, and Elizabeth Ackermann for her support with all administrative issues, big or small.

I would also like to acknowledge my post-graduate friends who made the PhD journey such an unforgettable experience, in particular: Tobias Smith, Sam McHattie, James O'Neill, Dennis Pau, Francesco Sarti, Craig Muir, Varun Joshi, Harry Johnston, Maxim Millen, Zeinab Chegini, Chris Watson and Daniel Moroder. Thanks for all the laughs and coffee chats that made the time spent writing this thesis so much more enjoyable.

Finally, I would like to acknowledge the support of my family. To my parents Tricia and Stuart, my sister Belinda, and my partner Lauren, thank you for your love, support, understanding and encouragement during these past years.

Table of Contents

1 Introduction

In recent years significant progress has been made in the development of low damage structures as well as in modelling and predicting the performance of structures during earthquakes. However, despite the enormous contribution of non-structural components to total economic losses, the seismic performance of non-structural components has received much less attention.

The objective of this research is to better understand the performance of cladding systems in earthquakes, the losses associated with this performance and propose solutions to reduce post-earthquake damage and disruption.

1.1 Motivation

Since the 1848 Marlborough earthquake, there have been 476 recorded deaths in New Zealand attributed to earthquakes (McSaveney, 2012). Of these, 176 are attributed to those who died due to building collapse in the 2011 Christchurch earthquake (New Zealand Police, 2012). Prior to this, over 80 years had passed since an earthquake fatality as a result of building collapse, even though this period includes a number of large earthquakes, including the 1942 Wairarapa earthquake, the 1968 Īnangahua earthquake and the 1987 Edgecumbe earthquake (McSaveney, 2012).

This improvement in building performance over the past century and a half can largely be attributed to lessons learnt in New Zealand and around the world about how buildings behave in earthquakes and the ensuing legislation prescribing how a building must perform in an earthquake. The New Zealand Building Code outlines the performance requirements of buildings built in New Zealand. One of the main goals of the building code is to ensure that even in a major earthquake, a building will not collapse and the occupants can escape from it, even if the building itself is badly damaged (MBIE, 2004). This performance requirement is

often referred to as the 'life-safety' performance requirement. When considering the 2010-11 Canterbury earthquakes, this life-safety objective was achieved by the large majority of modern building stock. The photo in Figure 1-1 taken following the February 22nd 2011 earthquake illustrates this by showing three typical large buildings in Christchurch that were all heavily damaged in the earthquakes but did not collapse (The Grand Chancellor Hotel, the central building in Figure 1-1 suffered a partial collapse, however, all occupants were able to escape the building so the structure achieved its life safety objective).

Figure 1-1: Christchurch CBD skyline following the 22nd February 2011 earthquake

Although the life-safety objective was often met, it is clear that the vast amount of damage to buildings in Christchurch was not an acceptable outcome for society (CERC, 2012a). The total rebuild costs facing Christchurch have been estimated at between $30 billion to $40 billion - the equivalent of almost 20 per cent of New Zealand's annual GDP (English, 2013).

A similar trend has been observed in the United States, where since 1970 only two people per year on average have died due to building collapse. However, on average the economic loss in the United State during this same period has been about US$2 billion per year (ATC-69, 2008). A FEMA study based on theoretical simulations suggests that future economic losses due to earthquakes could average US$4.5 billion per year (Kircher, 2003).

Clearly, such significant economic losses are not an acceptable outcome for society, even following a rare event such as an earthquake. Since September 2010, approximately 85 percent of the Christchurch CBD building footprint has been destroyed or demolished, as depicted in Figure 1-2 (Gates, 2012). The 2013 M_w 6.6 Lake Grassmere and 2014 M_w 6.2 Castlepoint earthquakes further heightened awareness of the risk earthquakes pose to the New Zealand community, particularly from a cost viewpoint – in both monetary and societal terms. It is clear that society expects better performing structures in the future, with calls from the public that new buildings built in Christchurch include 'earthquake resilient technology' to avoid a repeat of the large scale demolition that has occurred in the Christchurch CBD (Mussen, 2011).

Figure 1-2: Extensive demolition in Christchurch CBD

Over the past two decades, improving the seismic performance of the structural system has been a prime research topic in structural engineering (Wang, 1987). Elements of a structural system that are termed 'non-structural' have received less consideration from the structural engineering community. The implications of this inequity are now gaining attention, with extensive failures of non-structural elements contributing disproportionately to the overall economic losses (Filiatrault et al., 2002).

1.1.1 Non-Structural Damage

The term, 'non-structural', was coined by structural engineers to describe building elements which are not designed to contribute to the structural capacity of the building frame

(Wang, 1987). Unfortunately this term is misleading, since it implies that non-structural elements have no structural significance. 'Architectural elements' is another term which is sometimes used to describe "non-structural elements", but is confusing since the term also connotes a lack of structural significance; furthermore, it already has a very different and established usage in the architectural profession. Finally, 'secondary structural elements' is a term used by some researchers to distinguish non-structural building components with particularly great impact on the behaviour of the primary structure under seismic or wind forces, such as cladding from those which have relatively meagre effects on the structure, such as equipment. This term is less misleading; however, it is somewhat ambiguous and has not come into very common use (Wang & Bassler, 1992). The term 'non-structural', will be used in this thesis, and includes items such as cladding, partitions, ceiling systems, lights, mechanical equipment, piping and specialist equipment.

There are two key contributing factors to the high damage cost associated with non-structural elements. Firstly, non-structural elements typically make up the largest proportion of the overall structural cost. Research by Taghavi and Miranda (2003) showed that for a typical office building, the non-structural investment cost is 62% and for a typical hotel, the cost is 70%, as shown in Figure 1-3. The structural system of an engineered building typically only represents between 10% and 20% of the overall structural cost (ATC-69, 2008). The amount that the facade contributes to the overall construction cost varies depending on the system chosen, but typically represents between 10% and 20%. Taller buildings are more likely to be at the higher end of this range (Lam & Gad, 2002).

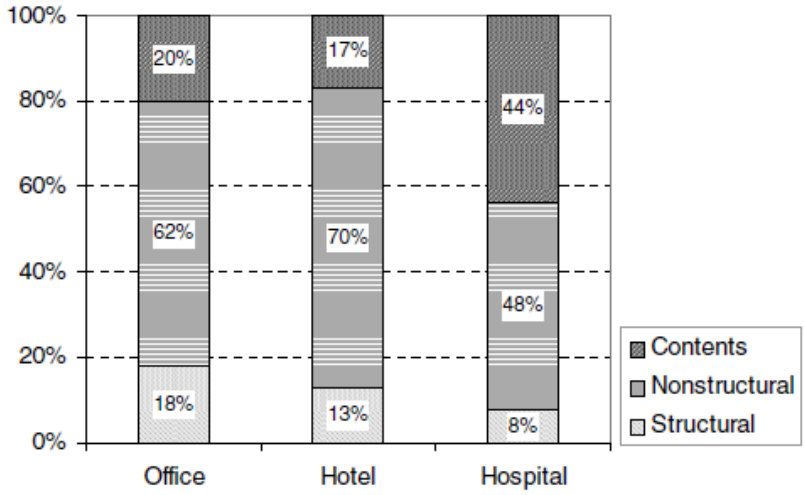

Figure 1-3: Building cost breakdown (Taghavi & Miranda, 2003)

As well as making up the largest proportion of the building's investment cost, non-structural elements are typically more vulnerable to seismic damage than structural elements. A study of the 66,000 buildings damaged by the 1994 Northridge earthquake showed that approximately three quarters of the buildings suffered damage to non-structural components alone (Charleson, 2008). Damage to most types of non-structural components in buildings is usually triggered at levels of deformation much smaller than those required to initiate structural damage (FEMA E-74, 2011). For example, damage to brittle partitions often begins at drift levels smaller than those required to induce damage to the structure. Similarly, high accelerations associated with small drifts can damage ceilings, piping, and other non-structural components with little or no damage to the structural members. The 2013 Lake Grassmere and 2014 Castlepoint earthquakes in New Zealand both served as an example of moderate earthquakes that resulted in limited structural damage, but extensive amounts of non-structural damage, such as that shown in Figure 1-4.

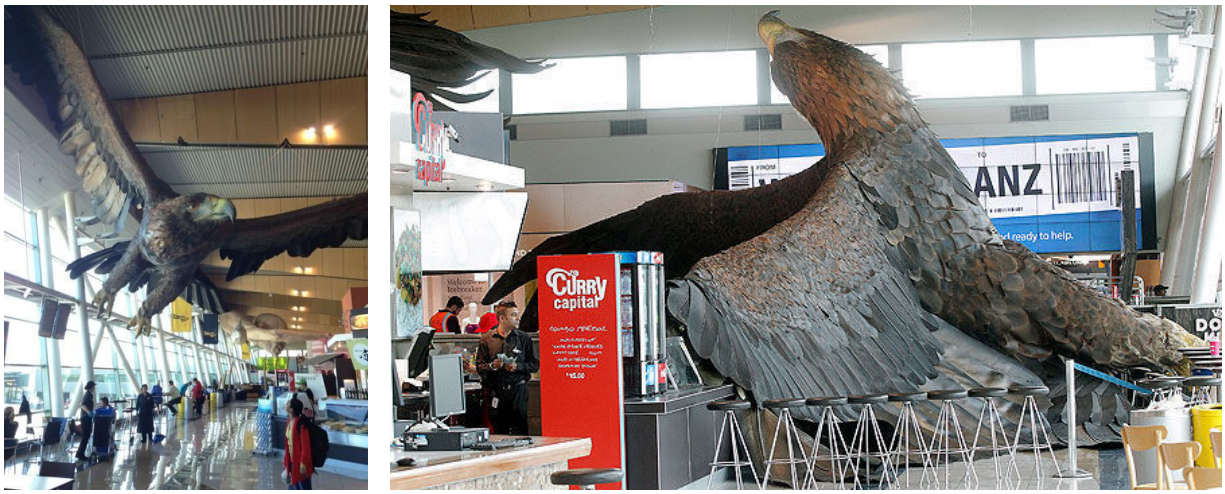

Figure 1-4: Bracing failure of eagle in Wellington Airport from the 2014 Castlepoint earthquake

Consequently, the direct and indirect costs associated with the damage of non-structural components in an earthquake can be significantly more than the costs associated with the damage to the structure itself. An analysis of the losses due to the 1994 Northridge earthquake indicated that of the approximate $6.3 billion of direct economic losses to non-residential buildings only about $1.1 billion was due to structural damage (Kircher, 2003). A post-disaster survey for the 1971 San Femando earthquake in California involving 355 high-rise buildings showed that 79% of the damage costs in dollar terms were non-structural (Arnold et al., 1987). A similar study completed in 2004 suggested that non-structural element damage contributed to on average 50% of the total cost of an earthquake in a developed country (Bachman, 2004).

Another implication of non-structural damage is that around the loss of functionality. If non-structural damage is substantial, significant economic losses can be produced from a temporary loss of function in a building. 1,300 staff were forced out of their office for six months following a ceiling collapse during the 2013 Lake Grassmere earthquake, as shown in Figure 1-5 (Vaughan, 2013). Negligible structural damage to this building was observed, however, the ceiling failure ruptured a sprinkler which caused extensive damage throughout the building. The indirect costs associated with the failure likely far outweighed the direct costs of the ceiling failure itself.

Figure 1-5: Ceiling failure in Wellington office building following the 2013 Grassmere earthquake

1.1.2 Cladding Performance

One such non-structural element that has a history of poor performance is that of the external cladding system, also referred to as the building facade. The external cladding is the shell, or covering of a structure. It often incorporate stiff, brittle materials such as glass, concrete and stone (Page, 2008). This makes them particularly susceptible to damage during an earthquake, as shown in Figure 1-6. Damage to cladding is such a common occurrence during an earthquake that the damage is often discussed only briefly in the engineering reconnaissance reports published after the earthquake (McMullin et al., 2004). Unlike other non-structural elements, cladding damage also presents a life safety hazard. Several cases exist of heavy exterior claddings that have dislodged during an earthquake resulting in the death of pedestrians (Adham & Brent, 1985; CERC, 2012b; Taly, 1988).

Significant cladding damage was reported from the 1964 Anchorage, 1971 San Fernando, 1978 Miyagiken-Oki, 1987 Whittier Narrows and the 1995 Hyogoken-Nambu

earthquakes. After the 1970s the significance of the economic loss of cladding damage began to emerge as a larger field of interest for earthquake engineers. Seike and Sakamoto (1997) reported on the damage to precast concrete cladding, curtain walls, windows and doors following the 1995 Hyogoken-Nambu earthquake.

Figure 1-6: Cladding damage following the 22nd February 2011 Christchurch earthquake

As well as being particularly susceptible to damage, cladding systems may also interact with the structure during an earthquake, affecting both the performance of the cladding and the structure (Cohen, 1995). Cladding systems, along with other non-structural elements, are typically regarded as separate from the primary structure and hence in most international design codes they are neglected in the structural design process. This approach simplifies the design process of both the structure and cladding, however, the potential for interaction between the cladding and the primary structure may be beneficial or detrimental to the seismic performance of the building (Goodno, 1983). Attempts are usually made to try and isolate the exterior cladding from the structure by using connections with flexible elements, slotted holes or gaps. However, in seismic events, the connections may be overstrained, the gaps too small, or the slotted holes too short, and interaction between the different elements often occurs, sometimes in the form of cracked partitions, falling cladding panels, or collapsed ceilings (Pinelli et al., 1995).

1.1.3 Reducing Seismic Risk

The field of earthquake engineering is rapidly changing due to the need to protect society not only from the direct harm caused by earthquakes, but also from the socio-economic risks that follow them. Performance-based earthquake engineering has become a

cornerstone on the path to reducing these risks to a more acceptable level. Implementation of performance-based earthquake engineering requires significantly expanding our knowledge about the design, construction, maintenance, and performance of both structural and non-structural components. As introduced in the previous sections, it is vital that we improve non-structural performance as we continue to also improve structural performance, particularly where loss control is of primary concern. The myriad of increasingly complex and costly non-structural systems and contents in modern buildings will continue to present new challenges to the overall seismic performance of buildings long after the seismic performance of structural systems has been improved (Filiatrault et al., 2002). Post-earthquake functionality and operability will not be delivered until effective strategies are devised to minimize non-structural damage.

1.2 Objectives

Considering the research motivations presented in the previous section, the main objective of this research is to better understand the performance of cladding systems in earthquakes, the losses associated with this performance and propose solutions to reduce such damage. In order to achieve this main research objective, the following eight objectives have been identified:

1. Collate the current state-of-art relating to the seismic performance of cladding systems;
2. Identify the most hazardous cladding systems that require research attention;
3. Experimentally gain a better understanding of the seismic behaviour of cladding components and their interaction with the structure;
4. Develop simple modelling tools for the assessment of cladding performance, including the implementation in numerical building models;
5. Examine the dynamic behaviour of cladding systems and their influence upon the structure using robust numerical modelling methods;
6. Quantify the expected seismic performance of cladding systems using qualitative damage limits;
7. Propose and evaluate innovative low-damage cladding system solutions;
8. Collect seismic loss data to perform probabilistic seismic loss assessment of cladding systems

This main research objective is broad, especially considering the large number of cladding systems both currently available and in use in existing buildings. Consequently, research boundaries have been established in order to provide a manageable scope, as well as the ability to achieve worthwhile research outcomes. These boundaries predominately relate to the type of cladding systems investigated. By limiting the research to a single cladding typology, namely, precast concrete cladding panel systems, it is possible to investigate the system following the entire performance based seismic assessment process. Various other cladding systems can subsequently be investigated following the same methodology. Precast concrete cladding systems were chosen for this research due to concerns over the life-safety risks they present, as will be elaborated on in Chapter 2 when their performance in the Canterbury earthquakes in discussed.

While the innovative cladding solutions will be mainly targeted at new buildings, the possibility of using the same concepts to enhance the performance of existing building systems will also be explored as a retrofit solution.

1.3 Organisation

This thesis contains twelve chapters which are organised into four parts, these are briefly summarised as follows:

Chapters 1 – 3 establish the seismic vulnerability of cladding systems through a desktop background study, literature review, and post-earthquake reconnaissance survey.

Chapters 4 – 7 experimentally and numerically investigate the performance of traditional heavy cladding systems used in both New Zealand and around the world.

Chapters 8 – 10 experimentally and numerically investigate the performance of innovative, low-damage heavy cladding systems.

Chapters 11 – 12 compare the performance of the traditional and innovative heavy cladding systems using a seismic loss assessment framework and present the conclusions of the thesis.

The individual chapters are summarised as follows:

Chapter 2 contains a background of general cladding systems including basic function, terminology and design information. Cladding damage observations made following the Canterbury earthquake sequence are presented to identify cladding systems that require the most urgent attention.

Chapter 3 forms a more traditional literature review of cladding systems in regards to their influence in the area of structural/earthquake engineering. This includes previous laboratory experiments and numerical investigations into understanding the behaviour of cladding systems and their interaction with the structure they are supported off.

Chapter 4 presents the results of experimental testing of a full-scale cladding-structure subassembly. The testing is performed on traditional heavy cladding systems using cyclic quasi-static loading to replicate earthquake loading in order to characterise the cladding's seismic performance.

Chapter 5 contains the development of numerical models for the traditional cladding systems included in Chapter 4. The models are developed using analytical methods and finite element analyses and are validated against the experimental results obtained in Chapter 4.

Chapter 6 implements the models of traditional cladding systems developed in Chapter 5 to a theoretical ten-storey case-study building. This case-study building is subjected to various analyses including dynamic non-linear response (time-history) analyses to determine the seismic response of the structure and cladding.

Chapter 7 quantifies the expected damage to both the structure and traditional cladding systems using the seismic response of the structure and cladding from the analyses performed in Chapter 6 and the experimental observations from Chapter 4.

Chapter 8 and **Chapter 9** are comparable to Chapters 4 and 5 but instead present the experimental tests and model development of an innovative low-damage cladding system.

Chapter 10 is comparable to Chapters 6 and 7 but instead presents the seismic response and expected damage of an innovative low-damage cladding system.

Chapter 11 compares the performance of the traditional and innovative cladding systems identified in Chapter 7 and 10, respectively. The systems are compared using a probabilistic seismic loss assessment that is based upon estimated repair costs and repair time data gathered following the Canterbury earthquake sequence. A novel method for assessing possible casualties from cladding failure is also presented.

Chapter 12 summarises the conclusions and the research and also presents recommendations for future work.

1.4 References

Adham, S. A., & Brent, B. (1985). The Borah Peak, Idaho Earthquake of October 28, 1983 – Buildings and Schools. *Earthquake Spectra, 2*(1).

Arnold, C., Hopkins, D., & Elsesser, E. (1987). *Design and Detailing of Architectural Elements for Seismic Damage Control*: Building Systems Development, KRTA Limited and Forell/Elesser Engineering Inc.

ATC-69. (2008). Reducing the Risks of Nonstructural Earthquake Damage: State-of-the-Art and Practice Report. Redwood City, CA., USA: Applied Technology Council.

CERC. (2012a). Canterbury Earthquakes Royal Commission - Final Report Retrieved 12 April 2012

CERC. (2012b). Canterbury Earthquakes Royal Commission – 43 Lichfield Street Retrieved 12 April 2012, from http://canterbury-hearings.royalcommission.govt.nz/tag/buildings/43-lichfield-street

Charleson, A. (2008). *Seismic Design for Architects: Outwitting the Quake*: Architectural Press.

Cohen, J. M. (1995). Seismic Performance of Cladding: Responsibility Revisited. *Journal of Performance of Constructed Facilities, 9*(4), 254-270.

English, B. (2013). Budget Speech Retrieved 16th May 2013, from http://www.treasury.govt.nz/budget/2013/speech/06.htm

FEMA E-74. (2011). Reducing the Risks of Nonstructural Earthquake Damage - A Practical Guide. Washington, DC., USA: Federal Emergency Management Agency.

Filiatrault, A., Christopoulos, C., & Stearns, C. (2002). *Guidelines, specifications, and seismic performance characterization of nonstructural building components and equipment*: Berkeley: Pacific Earthquake Engineering Research Center, University of California.

Gates, C. (2012). Our disappearing city centre, *The Press*. Retrieved from http://www.stuff.co.nz/the-press/news/christchurch-earthquake-2011/7744317/Our-disappearing-city-centre

Goodno, B. J. (1983). *Cladding-structure interaction in highrise buildings*: Schools of Civil and Aerospace Engineering, Georgia Inst. of Technology, Atlanta.

Kircher, C. A. (2003). *It Makes Dollars and Sense to Improve Nonstructural System Performance*. Paper presented at the ATC-29-2: Seminar on Seismic Design, Performance, and Retrofit of Nonstructural Components in Critical Facilities, Newport Beach, CA., USA.

Lam, N., & Gad, E. (2002). *An innovative approach to the seismic assessment of non-structural components in buildings*. Paper presented at the 2002 Australian Earthquake Engineering Society Conference, Adelaide, Australia.

MBIE. (2004). New Zealand Building Code *B1-Structure*. Wellington, New Zealand: Ministry of Business, Innovation and Employment.

McMullin, K., Wong, Y., Choi, C., & Chan, K. (2004). *Seismic Performance States of Precast Concrete Cladding Connections*. Paper presented at the 13th World Conference on Earthquake Engineering Conference, Vancourver, B.C., Canada.

McSaveney, E. (2012). Historic earthquakes. Te Ara - the Encyclopedia of New Zealand Retrieved 9th November 2012, from http://www.TeAra.govt.nz/en/historic-earthquakes

Mussen, D. (2011). Call for quake-resistant rebuild, *The Press*. Retrieved from http://www.stuff.co.nz/the-press/news/christchurch-earthquake-2011/5165252/Call-for-quake-resistant-rebuild

New Zealand Police. (2012). List of Deceased - Christchurch Earthquake Retrieved 9th November 2012, from http://www.police.govt.nz/list-deceased

Page, I. (2008). Cladding Types in New Zealand. *BUILD,* 55-56.

Pinelli, J. P., Craig, J. I., & Goodno, B. J. (1995). Energy-Based Seismic Design of Ductile Cladding Systems. *Journal of Structural Engineering, 121*(3), 567-578.

Seike, T., & Sakamoto, I. (1997). *A Report on the Damages of Precast Concrete Curtain Walls by the 1995 Hyogo-ken Nanbu Earthquake*. Paper presented at the International Conference on Building Envelope Systems and Technology, Bath, UK.

Taghavi, S., & Miranda, E. (2003). *Response Assessment of Nonstructural Building Elements*: Berkeley: Pacific Earthquake Engineering Research Center, University of California.

Taly, N. (1988). The Whittier Narrows, California Earthquake of October 1, 1987 - Performance of Building at California State University, Los Angeles. *Earthquake Spectra, 4*(2).

Vaughan, G. (2013). About 1,300 BNZ staff to start returning to Wellington's Harbour Quays building in December after ceiling strengthening, *interest.co.nz*. Retrieved from http://www.interest.co.nz/news/67103/about-1300-bnz-staff-start-returning-wellingtons-harbour-quays-building-december-after-ce

Wang, M. L. (1987). Cladding performance on a full-scale test frame. *Earthquake Spectra, 3*(1), 119-173.

Wang, M. L., & Bassler, B. L. (1992). *Cladding / Council on Tall Buildings and Urban Habitat*. New York, NY., USA: McGraw-Hill.

2 Background to Cladding Systems

2.1 Introduction

This chapter provides a background to cladding systems including descriptions of the basic function of cladding, terminology and design information. Whilst this thesis is primarily focussed on improving the seismic performance of cladding systems, it is vital that the primary functions of cladding are not neglected in the process. Cladding systems are not an area typically associated within the field of structural/earthquake engineering and therefore various architectural requirements are introduced here.

The vulnerability of cladding systems to earthquakes is presented, based on a cladding damage survey of 217 buildings within the Christchurch CBD following the Canterbury Earthquake sequence. Current design and construction practices are also presented for both New Zealand and overseas.

2.2 Cladding Function

Cladding systems are often considered as being the element which encloses a structure; however, they also influence the space inside and around the building. The cladding system is what is observed when looking at a building from the exterior and it also has impact on the interior and thus on the occupants. Aspects such as the lighting and ventilation are directly affected by the cladding and have a large influence on user comfort (Knaack et al., 2007).

The functions of the cladding system can be categorised as primary or secondary functions. The primary functions are functions that the cladding system is principally responsible for, these include the following:

1. Define the aesthetic image of the building;
2. Keep water out of the building;
3. Prevent air leakage;

4. Control the passage of light and heat (radiation and conduction);
5. Control sound from the outside;
6. Avoid thermal bridges;

The primary functions are often categorised as the cladding's architectural systems. The secondary functions are not the main responsibility of the cladding system and include the following:

1. Adjust to movement in the building due to wind, earthquakes, creep, etc.
2. Adjust to thermal expansions and contractions
3. Control the passage of water vapour
4. Resist fire
5. Resist weather conditions gracefully (without streaking, oxidation, corrosion, freeze-thaw spalling).

These secondary functions are somewhat also the main responsibility of the architect but do not always fall within an architect's expertise. For example, the ability to fire will be a functional requirement determined by a fire engineer. In a structural engineering context, the structural engineer will likely have input to all of these secondary functions. In particular, items 1 and 5 will be critical in determining the seismic performance of the cladding system.

Current research into cladding technology is primarily related to improving the primary functions of the cladding system (Brenden, 2006; Ruggiero, 1995). Such technology advances are often focussed on improving the energy efficiency and user comfort. Over the past decade, several international rating systems have been developed with the aim of developing sustainable 'green' buildings. Such examples include the 'Green Star' rating used by the New Zealand Green Building Council (NZGBC) and Leadership in Energy and Environmental Design (LEED) developed by the U.S. Green Building Council (USGBC). The Christchurch City Council Te Hononga Building shown in Figure 2-1 is the first renovated building and only second building in New Zealand to achieve a 6 green star rating. A double skin cladding system over the entire northern facing side of the building was integral in obtaining this rating (Sachdeva, 2010).

This shift towards 'sustainable buildings' has also placed increased reliance upon the cladding system in determining the overall performance of the internal building space. Where historically a heating, ventilation, and air conditioning (HVAC) system could be relied upon to moderate a building's temperature, it is becoming more common to rely upon the cladding

to do so. This can be either through passive methods, such as sunshades, or through active feedback devices that adjust the cladding depending on the internal environment (Phan & Taylor, 1996). This increased functional dependence upon the cladding system further heightens not only the investment cost of the cladding system but also the importance of preserving its functional integrity following an earthquake.

Figure 2-1: The six green star rated Christchurch City Council Te Hononga building.

2.3 Cladding Performance

Cladding design and performance assessment is a complex and broad structural research topic. One particular performance aspect cannot be examined without taking into account the numerous other functions of a building's cladding at the same time. While the primary objective of this research is to improve the seismic performance of cladding systems, it is important that the other aspects of cladding performance are not neglected whilst doing so. A brief background to the performance of architectural systems is therefore included in the following section. This subject is vast, and the information presented here is far from exhaustive, however, as mentioned above, it is important that a basic understanding of these functions is understood when considering cladding performance.

2.3.1 Architectural Performance

A brief background of the architectural performance of cladding systems, in particular, thermal, acoustic and weathertight performance is presented in this section.

2.3.1.1 Thermal Performance

The thermal performance of cladding defines the ability of the cladding to resist or transmit heat. Different metrics exist to determine thermal performance; however, it is common to quantify the thermal performance according to its thermal resistance (R value).

Thermal resistance is determined by the thickness of the material divided by the conductivity of that material. The conductivity of a material is the rate at which heat is transmitted, measured in watts per square metre of surface area for a temperature gradient of one Kelvin per metre thickness. Thermal resistance varies with temperature but it is common practice in construction to treat it as a constant value. The higher the R-value, the more efficient the cladding acts as an insulator. The cladding of the building shown in Figure 2-2 is evidently as a superior insulator to that of the door and window. The R-value accounts for convective and radiative heat transfer through the material. However it does not account for the radiative or convective properties of the materials surface, which may be an important factor for some cladding systems (Knaack et al., 2007).

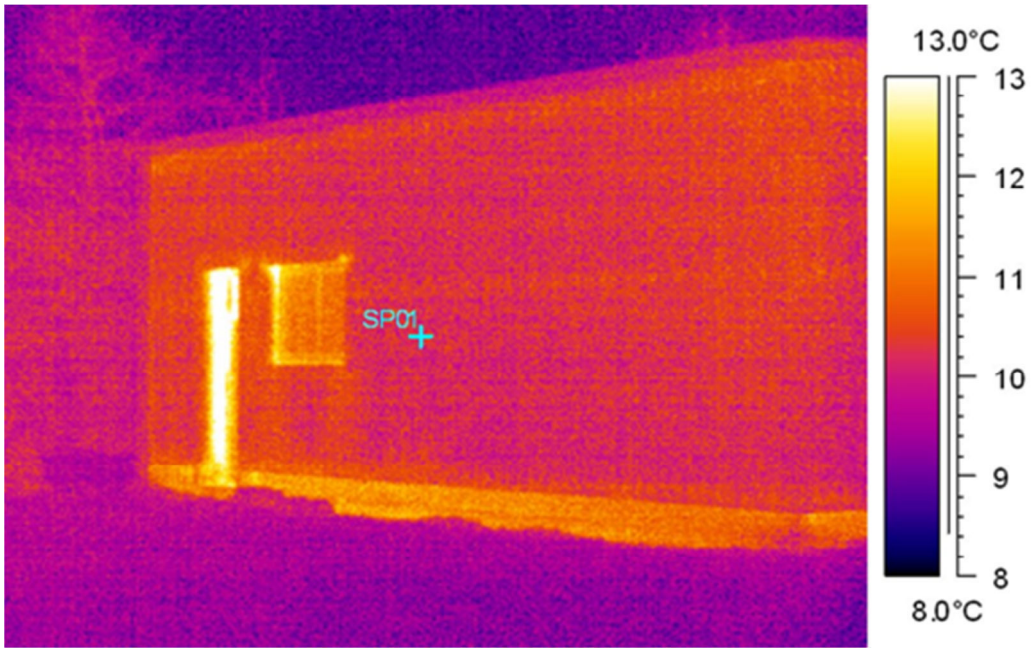

Figure 2-2: Thermal image of a small industrial building

Since thermal resistance does not capture radiative or convective properties, the thermal performance is also commonly assessed by its thermal transmittance (U value). Thermal transmittance is a measure of the rate of heat loss. It is expressed as watts per square metre, per degree Kelvin. The U-Value is calculated from the reciprocal of the combined thermal resistance of the materials in the element, air spaces and surfaces, also taking into account the effect of thermal bridges, air gaps and fixings.

The ability to quantify the effect of thermal bridges makes the U value a useful metric for quantifying a cladding's thermal performance. A thermal bridge is created when materials that are poor insulators come in contact, allowing heat to flow through the path created, as shown in Figure 2-3. Insulation around a bridge is of little help in preventing heat loss or gain due to thermal bridging: the bridging has to be eliminated, rebuilt with a reduced cross-section or with materials that have better insulating properties, or with an additional insulating component (BS EN ISO 6946, 2010).

Current building regulations require minimum thermal standards for cladding. The type of cladding adopted is a primary factor in the method through which thermal comfort will be achieved. Metal based cladding systems, for example, require separate layers of weathering and thermal protection. The ordering of these layers may in fact give rise to additional problems of thermal bridging and condensation. Generally most systems will require the inclusion of specific insulating layers.

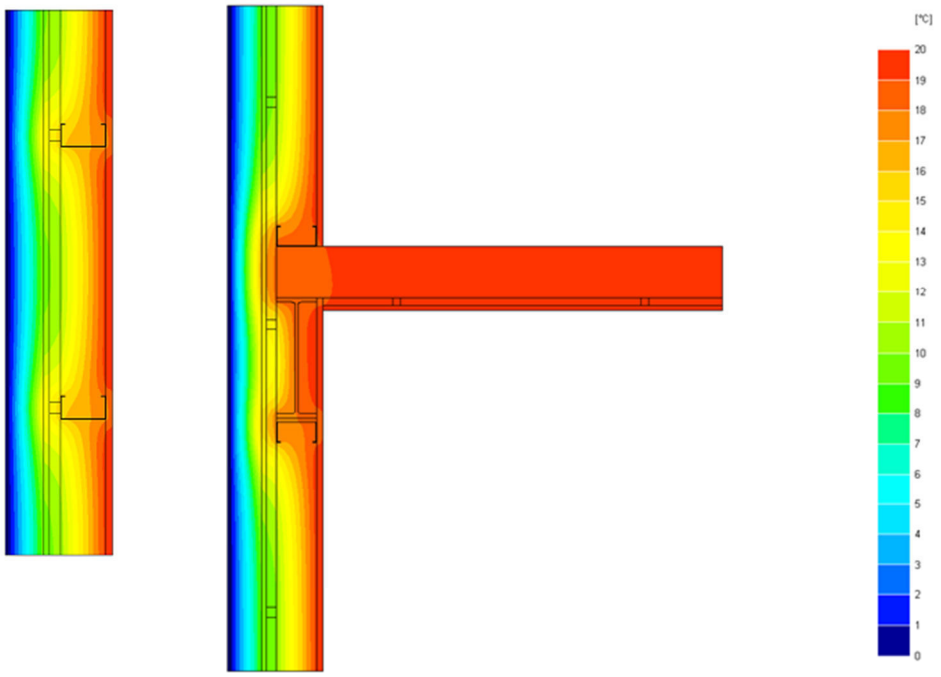

Figure 2-3: Thermal modelling to assess effect of thermal bridging

2.3.1.2 Acoustic Performance

The acoustic performance of cladding is similar to that of thermal performance, and is defined as the ability of the cladding to resist or transmit sound. Again, several metric can be used to assess the acoustic performance; however, it is common to quantify the acoustic performance by a Sound Transmission Class (STC). The STC is an integer rating that reflects

the decibel reduction in noise that a cladding can provide (BS EN ISO 10140-2, 2010). Examples of STC ratings are provided in Table 2-1.

Another commonly used metric for assessing acoustic performance is the Weighted Difference level D_w. This index is defined by measuring in decibels the difference in noise level produced on either side of the cladding.

The assessment of noise transmission through cladding systems is not normally critical in assessing the acoustic performance of a structure. This is due to noise flanking around the cladding through materials that have poorer acoustic properties than the cladding itself. The most critical noise paths are through roofs, eaves, windows, doors and penetrations.

Table 2-1: Sound Transmission Class examples (BS EN ISO 10140-2, 2010)

STC	Description
25	Normal speech can be understood quite easily and distinctly through cladding
30	Loud speech can be understood fairly well, normal speech heard but not understood
35	Loud speech audible but not intelligible
40	Onset of "privacy"
42	Loud speech audible as a murmur
45	Loud speech not audible; 90% of statistical population not annoyed
50	Very loud sounds such as musical instruments or a stereo can be faintly heard; 99% of population not annoyed.
60+	Superior soundproofing; most sounds inaudible

2.3.1.3 Weathertight Performance

Weathertight performance can be defined as the combined performance measure of a cladding system to be both airtight and watertight. Although similar in nature, the airtight and watertight performance levels are important for different reasons. The airtight performance is an important metric for determining the energy efficiency of a cladding system, whereas the watertight performance is important for determining the cladding's durability.

How airtight a cladding is directly influences the energy efficiency of the ability to heat or cool an internal building space. The airtight performance is therefore directly linked to the thermal performance, in particular the thermal transmittance (U value) as this is a measure of the rate of heat loss. Airtightness is typically measured experimentally using an air infiltration test or blower door test. This test is one of the most difficult tests to perform with a great degree of accuracy and it can be difficult to ensure that results of the cladding sample can be

extrapolated to describe the performance for the entire building envelope (AS/NZS 4284, 2008). An air infiltration test consists of a calibrated fan for measuring an airflow rate, and a pressure sensing device to measure the air pressure created by the fan flow.

A variety of airtightness metrics can be produced using the combination of building-to-outside pressure and fan airflow measurements. These metrics are useful for assessing the construction quality of a cladding system, how much ventilation is supplied by air leakage, energy losses resulting from air leakage and to assess compliance with building performance standards.

The airtight performance will also typically reflect the watertight performance of a cladding system, as a cladding that has large air infiltration result will often also be a 'leaky cladding' (AS/NZS 4284, 2008). Watertight performance is assessed in a similar way to that of the airtight performance, however, the testing regime is normally more rigorous. The watertight performance is assessed using water penetration testing that typically consists of both static and cyclic tests. These tests involve spraying the cladding with water whilst applying either static or varying air pressure, as shown in Figure 2-4 (left).

Figure 2-4: Testing air and water infiltration performance (left) and rotten structure resulting from a leaky cladding (right).

It is generally accepted that most claddings built in New Zealand are currently designed in accordance with the drained-joint and pressure equalisation principles. This means that water is allowed to penetrate the cladding at some points, however an allowance must be made for this to ensure that any water that does penetrate is able to drain back outside the cladding (AS/NZS 4284, 2008). When water is able to penetrate but is not able to drain it leads to serious durability issues. New Zealand currently faces an ongoing problem with

'leaky buildings' and one of the major causes of this problem was a lack of water drainage allowance. If water becomes trapped and cannot easily escape or evaporate it can leads to rotting of the structural frame, as shown in Figure 2-4 (right) (MBIE, 2011).

2.3.2 Seismic Performance

The seismic performance of cladding systems is primarily determined by earthquake induced deformation of the primary structure (FEMA P-58-1, 2012). For heavy cladding systems, inertial forces due to floor accelerations cause large out-of-plane demands in the connections. Consequently, floor accelerations are also an important consideration in determining the seismic performance of heavy cladding systems; however, designing for these inertial loads is well addressed in most international loading standards.

The principal structural deformation (and hence the most significant demand in terms of seismic performance) that occurs during earthquake shaking is storey sway (Wright, 1989). This is the lateral displacement of one level with respect to those adjacent, with the floors remaining essentially parallel to each other, resulting from predominantly flexural deformation of the building frame, as shown in Figure 2-5.

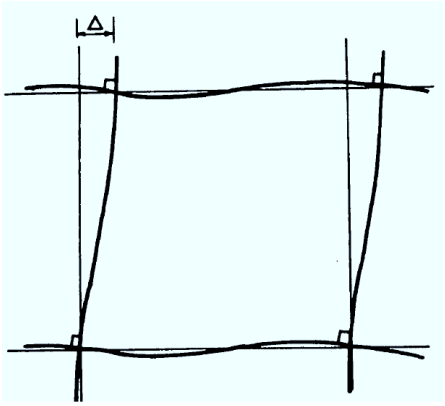

Figure 2-5: Frame sway mechanism (Wright, 1989)

Vertical deformations are typically negligible in frame structures. In shear wall dominant structures, vertical deformations only translate to cladding demands if the shear walls are located on the perimeter of the structure. Even so, vertical seismic deformations are not typically considered in the design or assessment of cladding systems. It should be noted that it is necessary to consider the vertical deflections due to perimeter beam sag when designing cladding systems.

Seismic deformation of the primary structure also includes several secondary deformations that place demand upon the cladding system. Secondary deformations are those

occurring in individual members of the building frame when it is subjected to the primary deformation shown in Figure 2-5. These will consist of the elastic curvature of both beams and columns and the localised rotation at plastic hinges due to storey sway (PCI, 2007). These secondary deformations are also typically neglected in the design or assessment of cladding systems.

Cladding systems respond to lateral structural deformation in a combination of translation and rotation modes. This movement can either be in-plane or out-of-plane depending on the orientation of the cladding to the storey sway, as shown in Figure 2-6.

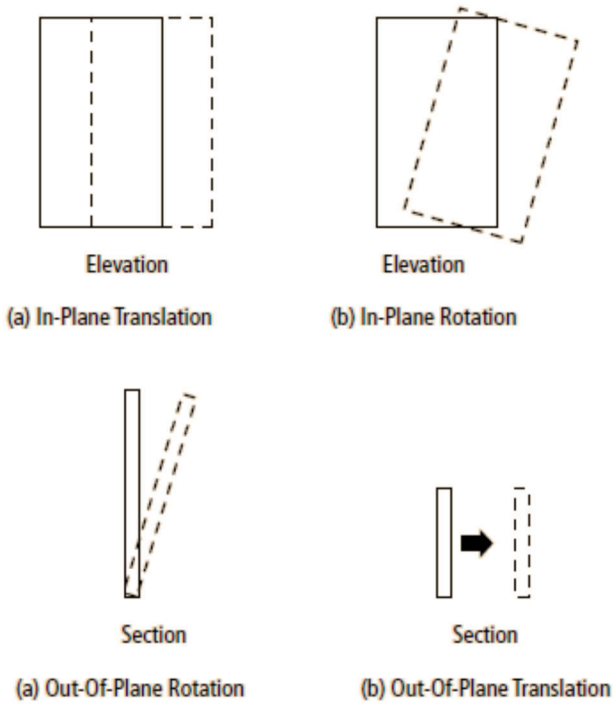

Figure 2-6: Modes of cladding response to lateral displacement (PCI 2007)

In-plane translation occurs when the cladding is fixed at one level and is subjected to in-plane movement, e.g. a spandrel panel fixed to a beam. The cladding translates laterally with that level, remaining vertical in elevation. In-plane rotation occurs when the cladding is supported at two levels and is subjected to in-plane movement, e.g. a column cover panel. This type of movement requires connections with slotted holes or gaps. Out-of-plane rotation occurs when the cladding is attached to two different levels and is subjected to out-of-plane movement (i.e. inter-story drift perpendicular to the plane of the cladding). This type of movement creates tension and compression forces in the connections of the cladding. Out-of-plane translation is the movement that occurs when the cladding is attached to one level of framing, such as a short spandrel panel, and is subjected to out-of-plane movement. The

movements that cause the most significant potential for structural interaction are the in-plane translation and in-plane rotation (Hunt & Stojadinovic, 2010).

When cladding panels are subject to in-plane inter-story displacement, the cladding connections may cause the panels to rock up on one corner or to translate without rocking. The difference in behaviour is dependent upon the connection type used as well as the arrangement of both the cladding and connections. For example, it can be seen that the cladding panel shown in Figure 2-7 (left) translates with the movement of the floor beam and thus the top connections have to be able to accommodate any lateral movement. The top connections are therefore critical in determining the behaviour and performance of the cladding system. In the case of panels like those shown in Figure 2-7 (right), a rocking mechanism is more likely (PCI, 2007). Thus, as the structure deforms, the column cover is forced to rock up on one side, and each of the bearing connections must be designed to withstand the force from the entire weight of the column cover panel. It is for this reason that the classification of these features is important, as will be expanded upon later in this chapter.

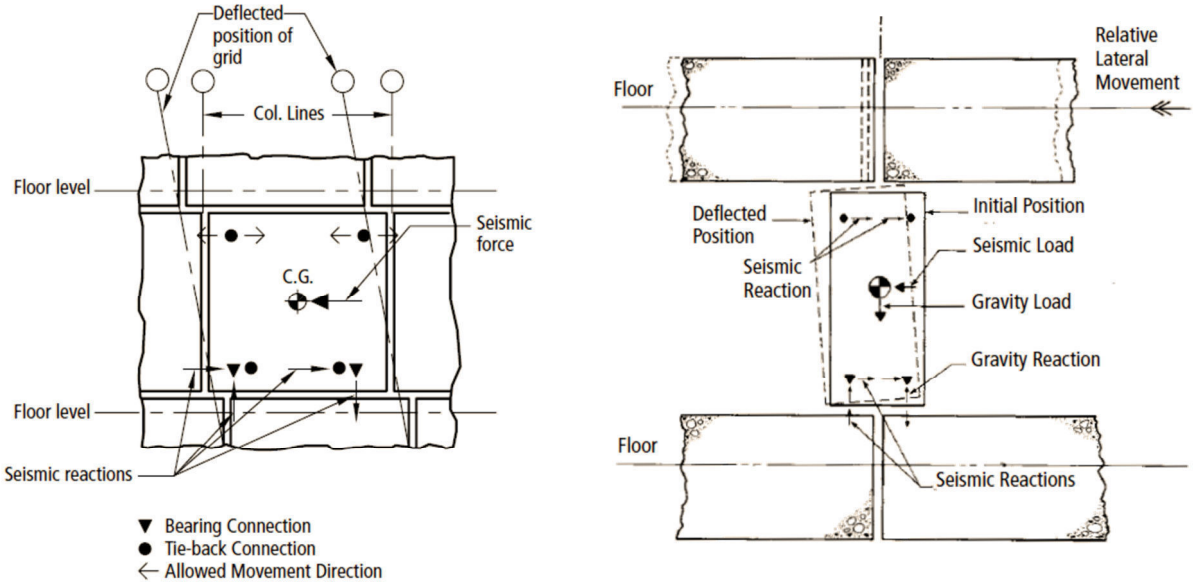

Figure 2-7: Translating (left) and rotating (right) cladding response (PCI 2007)

Once the mode of cladding response is understood, the seismic performance of the cladding is directly dependent upon how the connections are able to accommodate the movement demands. Connections may employ bending of steel and/or sliding of a bolt through a slotted hole. Bending connections must have sufficient ductility to withstand the inter-story drifts, and slotted connections must have slots long enough to account for movement without binding or shearing of the bolt. The weather and corrosion protection of

the slotted connections is also essential to ensure their long-term performance (Hunt & Stojadinovic, 2010).

2.3.2.1 Seismic Performance Levels

Building and component damage generally occurs as a continuum, with the scope and extent of damage increasing as the demand increases. Instead of a continuous range of possible performance levels, or damage states, modern performance-based engineering defines a series of discrete performance levels to characterize the different levels of damage that can occur. Each performance level is associated with a unique set of consequences relating to the probability of repair action, repair cost and repair time (FEMA P-58-1, 2012).

Various international codes provide guidance on how the 'damage continuum' should be discretised to a set of performance levels. In the case of New Zealand, the commentary to NZS 1170.5 (2004) provides SLS deformation limits which are defined by the onset of damage. It may seem obvious, but it can be concluded that these limits define the transition from an undamaged cladding system to a damaged cladding system. However, this statement raises several questions, including, what exactly constitutes a damaged cladding system and how badly damaged is the cladding system?

Modern performance-based engineering aims to address these questions by providing a qualitative description of the likely level of damage for each performance level. The qualitative descriptions used are intended to be meaningful to the general public and therefore employ basic terminology (i.e. Operational, Immediate Occupancy, Life Safety and Collapse Prevention). Descriptions of each of these terms are shown graphically in Figure 2-8.

Figure 2-8: Photos and graphical representations of cladding performance levels

The terms Operational, Immediate Occupancy, Life Safety and Hazards Reduced have been adopted from FEMA P-58-1 (2012) to describe the various performance levels for cladding systems. The term 'performance level' has been used to describe the qualitative damage. This term is interchangeable with the commonly used term 'damage state'. The final performance level of Hazards Reduced is applicable for non-structural elements. When considering structural performance levels, the term Collapse Prevention is used. Descriptions of each of the performance levels in relation to cladding damage are as follows.

Operational Performance Level

The cladding is able to support its pre-earthquake functions, although minor clean-up and repair may be required.

Immediate Occupancy Performance Level

Damage to the cladding is present but building access and life safety systems remain available and operable. Minor window breakage could occur. Presuming that the building is structurally safe, occupants could safely remain in the building, although normal use may be impaired and some clean-up required. The risk of life-threatening injury due to cladding damage is very low.

Life Safety Performance Level

Damage to the cladding is present but the damage is non-life threatening. Potentially significant and costly damage has occurred to the cladding but the majority of the system has not become dislodged or fallen. Egress routes within the building are not extensively blocked, but may be impaired by lightweight debris. While injuries may occur during the earthquake from the failure of cladding components, overall, the risk of life-threatening injury is very low. Restoration of the cladding may take extensive effort.

Hazards Reduced Performance Level

Damage to the cladding is present creating multiple falling hazards. Extensive damage has occurred to the cladding with the potential to seriously threaten life safety outside the building. Widespread window breakage is likely and disconnection of components of the cladding system from the structure is possible. Restoration of the cladding is likely only possible with a complete replacement of the system.

2.4 Cladding Classification

As introduced in the previous section, the prevailing trend in cladding technology is that of increasing complexity. The range of cladding systems is expanding constantly as technical solutions offer more ability to increase the user's comfort level (Knaack et al., 2007). The constantly evolving nature of cladding technology leads to difficulties in determining and thus comparing the seismic performance of new and existing cladding systems. One such reason for this is the difficulty in recognising the critical features that determine each cladding systems seismic performance. For example, the fixing of the cladding to the structure has a significant influence upon the performance of precast concrete cladding systems, whereas in a curtain wall cladding system it has minimal influence upon the performance (Taylor & Phan, 1997).

For this reason it is necessary to develop a cladding classification system that allows for simplifying the huge range of systems available. For the purpose of assessing seismic performance, it is also important that this classification is based upon grouping systems which have matching features that determine their seismic performance.

The classification system that has been proposed involves categorising each of the following four cladding system features:

- Cladding typology
- Cladding panel modularity
- Connection typology
- Connection modularity

Each of the above cladding features will be defined and expanded upon in the following sections.

2.4.1 Cladding Typology

As mentioned previously, the spectrum of cladding types available is virtually boundless. When we include residential as well as commercial cladding systems, this range increases even further. Numerous classification systems exist for cladding systems which are usually developed depending on the area of interest. For example, from a contractor's perspective, a cladding system can be categorised according to one of the following three typologies according to how they are assembled and installed (Das, 1986):

- Unit assemblies: generally arrive on site fully fabricated and are installed as floor-to-floor units
- Grid assemblies: consist of continuous vertical and horizontal mullions and transoms. Typically built up on site.
- Built-up Assemblies: generally built up on site. Examples include brick or stone veneer.

It can be seen how the above classification system is useful for a contractor for planning necessary labour and equipment needs, however, it is clear that this system is not suitable in order to categorise for seismic performance.

It is also necessary to mention here that there are types of building envelope systems that are not considered as being cladding systems. These systems are constructed within the frame of the structure and are often called infills. Examples of infill systems include masonry or timber infill, as shown in Figure 2-9.

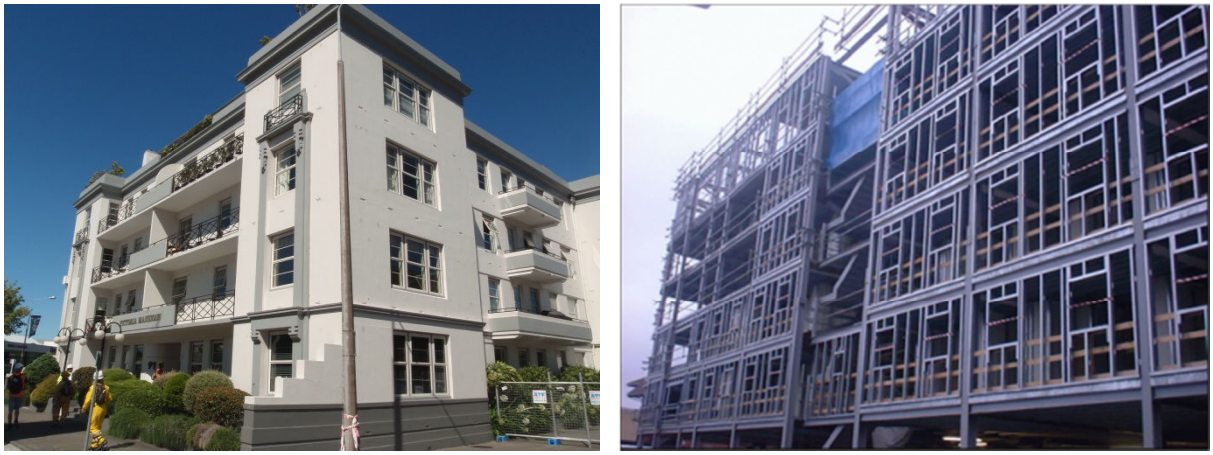

Figure 2-9: Infill systems – brick infill (left) and timber infill under construction (right)

Infill systems have similar performance requirements to that of cladding systems; however, their seismic behaviour is considered more similar to that of internal partitions (Dolsek & Fajfar, 2008). Infill systems are not considered in this research, however, a research campaign parallel to this has been undertaken at The University of Canterbury and reference should be made to Tasligedik (2014) for further information.

Since infill systems are constructed within the frame of the structure, the structure itself is part of the external envelope of the structure. This difference is a key difference that will be used here to define the difference between infills and cladding systems. Cladding systems are defined here as being external to the structure and form the complete building envelope. The

following typologies are therefore proposed for encompassing all possible external building envelope systems:

- Curtain wall
- Stick curtain
- Double skin
- Frameless glazing
- Monolithic cladding
- Masonry veneer
- Lightweight panels
- Heavy panels

It should be noted that a building can be clad in more than one of the above systems. In fact, it is rare for a building to have only a single cladding system. It is also common for an infill system, such as a timber stud frame, to be used in conjunction with one of the above cladding systems. This is necessary for concealing cladding connections, thermal insulation and services that are located around the perimeter of the building. A brief description of each cladding system is provided in the following sections.

2.4.1.1 Curtain Wall

Curtain walls systems include most generic types of lightweight cladding systems. They are typically designed with extruded aluminium members, although the first curtain walls were made of steel (Das, 1986). The aluminium frame typically contains glass or various panels which may include stone veneer, metal sheets, louvers, operable windows or vents, as shown in Figure 2-10. Lightweight cladding systems can either be installed as continuous or as discrete systems. Curtain walls are defined here as discrete lightweight cladding systems and continuous curtain walls are categorised as Stick Systems (covered in the following section).

The weight of the curtain wall can either be supported off the ground for low-rise systems, or supported off the structure. Curtain walls differ from store-front systems in that they are designed to span multiple floors. Unitised curtain walls entail factory fabrication and assembly of panels which may include factory glazing. These completed units are hung on the building structure to form the building envelope. Unitised curtain walls have the advantages of speed of construction, lower installation costs and quality control, however

they can be more expensive than other systems (Page, 2008). Economic benefits are typically only made on large projects or in areas of expensive labour.

Figure 2-10: Curtain wall cladding systems

2.4.1.2 Stick Curtain

The stick curtain, or stick system, is a metal 'stick' frame consisting of continuous perpendicular transoms and mullions surrounding pieces of glass or thin opaque panels. Stick curtains are a popular option in multi-storey buildings and are often used when a client wishes for a predominantly glass building envelope, like those shown in Figure 2-11. Framing members may be fabricated in a shop environment, but installation and glazing is typically performed on site.

Stick curtains are similar to curtain walls in that they are both lightweight systems that are made of mostly aluminium framing and glass, however, in terms of seismic performance, the differentiation between the two is necessary due to the different methods used to connect each system to the structure and how each system accommodates seismic movement. Due to the continuity of the stick curtain members, the transoms and mullions are detailed such that all movement must be accommodated between the glass and the frame. Silicone sealant is usually used to allow this movement while keeping the building weather tight. In contrast,

curtain walls typically use a combination of this technique, as well as seismic joints within the transoms and seismic head joints with the structure (Kaneki et al., 2008).

Figure 2-11: Stick curtain cladding systems

2.4.1.3 Double Skin

The double skin cladding system consists of two layers of material which create a sealed cavity to improve the thermal performance of a building. They are typically constructed as prefabricated units which are then hung on the building structure, as shown in Figure 2-12. Double skin cladding systems are not common in New Zealand buildings as they are usually the most expensive cladding option and hence are often beyond the scope of most New Zealand projects. However, they are being employed increasingly in high profile buildings, being touted as an exemplary 'green' building strategy (Sachdeva, 2010).

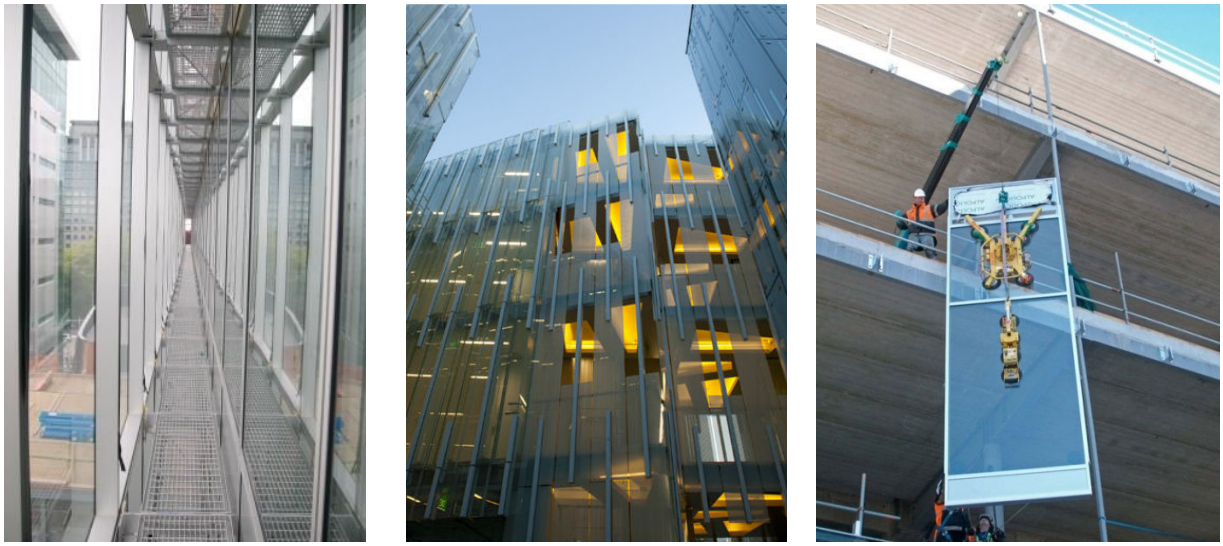

Figure 2-12: Double skin cladding systems

2.4.1.4 Frameless Glazing

Frameless glazing comprises of glass panes joined together by stainless steel bolted connectors in the corners of the glass, as shown in Figure 2-13. Also known as spider glazing, or suspended assemblies, frameless glazing is not a commonly used external cladding in New Zealand. It is more commonly utilised inside buildings, in locations such as hotel foyers and shopping malls. Due to these areas often being areas of high density people movement, it is imperative that they are engineered accordingly and that the glass specified is appropriate for overhead situations. As such, frameless systems typically always require typically require a specific engineering design solution.

Figure 2-13: Spider glazing cladding systems

Frameless glazing is typically hung from metal frames or tension wires. As the system does not have the benefit of movement joints or seismic receivers like a conventional

aluminium framed curtain wall, special consideration must be given to building movement, live load deflections and environment loads such as wind and seismic (Martins et al., 2012).

2.4.1.5 Monolithic Cladding

Monolithic cladding systems are claddings that have a seamless appearance, as shown in Figure 2-14, and are used mainly in residential construction. They typically consist of a sand-cement plaster applied over metal lath reinforcing on rigid or non-rigid backing material. The total system is either two or three coats, and it is finished with a layer of acrylic coating to make the cladding watertight. Uncoated plaster edges are very absorbent, and will also wick water from adjacent surfaces. The watertight performance is totally reliant upon the exterior coating system creating a face seal that is impervious to moisture.

Figure 2-14: Monolithic cladding systems

Monolithic cladding is brittle and cannot accommodate movement well making it vulnerable to cracking. Movement control joints are incorporated into the cladding to address this. Any faults in the cladding such as cracks in the plaster require immediate repair to ensure the system remains watertight. New Zealand currently faces an ongoing problem with 'leaky buildings', largely to do with incorrectly constructed monolithic cladding (MBIE, 2011). The traditional monolithic system is stucco which has been used in New Zealand since the 1920s. Modern monolithic systems include Exterior Insulation and Finish Systems (EIFS), which are multi-layered using polystyrene insulation and reinforced plaster.

2.4.1.6 Masonry Veneer

Masonry veneers consist of a single layer of masonry work, typically brick, separated from the main structure by an air cavity. The air cavity functions as a drainage plane, allowing any water that has penetrated the veneer to drain to the bottom of the cavity, where it encounters flashing (weatherproofing) and is directed to the outside through weep holes,

rather than entering the building. The cavity can also include insulation to increase the thermal performance of the cladding.

Masonry veneers, as shown in Figure 2-15, are commonly used in residential construction. They are only suitable for low-rise construction since it supports its own weight at ground level. Masonry veneers have low out-of-plane strength so require horizontal ties to the structure to provide out-of-plane restraint against wind and earthquake loads.

Figure 2-15: Masonry veneer cladding systems

2.4.1.7 Lightweight Panels

Lightweight panel cladding systems are one of the most economic cladding solutions and hence are a popular cladding choice for low-rise commercial, residential and industrial structures. This category includes a wide range of possible materials; including wood, metal and concrete. Examples of lightweight panels include simple metal sheets, plywood, insulated panels (or sandwich panels), autoclaved aerated concrete (AAC), and compressed fibre-cement panels, as shown in Figure 2-16.

Figure 2-16: Lightweight panel cladding systems

2.4.1.8 Heavy Panels

Heavy panel cladding systems includes concrete and stone cladding panels. Precast concrete panels have been the most popular cladding material in new non-residential buildings in New Zealand over the past decade (Page, 2008). Precast cladding can be made in a wide variety of shapes and sizes, as shown in Figure 2-17. Usually, cladding panels do not extend beyond the height of one story, and they are normally limited (by transportation and installation constraints) in width to less than or equal to the bay width of the structure (Hunt & Stojadinovic, 2010).

The cladding system for a building may use several different shapes and sizes of panels to create different architectural details. A variety of colours and textures are available by manipulating the aggregate selection, matrix colour, finishing process, and depth of exposure of the aggregate (PCI, 1989).

Heavy cladding panels are designed to resist wind forces, seismic forces generated from the panel self-weight, and the vertical forces required to transfer the self-weight to the supporting structure. In most cases, the forces generated in the panel during the manufacturing and erection stages of construction govern the reinforcement design of the panel (PCI, 2007). In cases when the expected design loads are relatively small, distributed reinforcement is needed to control cracking that may occur from fabrication, handling, erection, and stresses due to temperature changes of the panel.

Figure 2-17: Heavy panel cladding systems

Movement of the structure is accommodated in heavy panel cladding systems through the connections of the panel to the structure and joints between panels (PCI, 2007). In addition, the weight of the panel, volume changes in concrete frames, and rotation of supporting beams must be evaluated to ensure that the deformation compatibility between the panel and supporting structure is maintained (Hunt & Stojadinovic, 2010).

2.4.2 Cladding Modularity

Modularity describes the degree to which a system's components may be separated and recombined. In the context of cladding systems, the modularity refers to how a system is built up by combining smaller subsystems. The modularity of a cladding system thus provides a useful means of classifying the arrangement of the cladding components. The modularity of both the cladding panels and the cladding connections are required for classification, with the latter presented in the following section. The cladding modularity here refers to the degree to which the cladding panel components are built up to form the entire cladding system.

Classification of the modularity is important for determining the seismic performance of a cladding system since it has a direct influence upon how the system accommodates seismic movements. It is proposed that the cladding modularity is described based upon the number of cladding panel components that occupy a single storey and single bay of a structural frame. This modularity classification system is based upon previous work by Riccio (2010). A single panel may occupy more than one bay or one storey; however this can still be described adequately using this classification. One of the simplest examples of cladding modularity is that of a single panel that occupies a single bay and single storey of a structure, as shown in Figure 2-18. This cladding modularity is herein referred to as being a mono panel system. A mono panel cannot be separated or recombined within a single storey, single bay so can be deemed to have the simplest classification of cladding modularity.

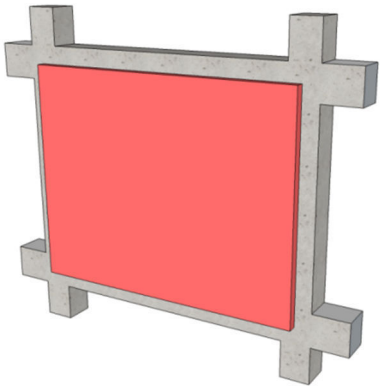

Figure 2-18: Mono panel cladding modularity

If the mono panel represents the simplest cladding modularity, the next level of complexity is represented by a cladding system with two panels that occupy a single storey and single bay of a structural frame. However, now there are multiple ways in which two panels can occupy this space. The space could be occupied by either two horizontally repeating panels or two vertically repeating panels, as shown in Figure 2-19. Two panels repeated horizontally is a commonly used system for precast concrete panels and this modularity will herein be referred to as being a dual panel system.

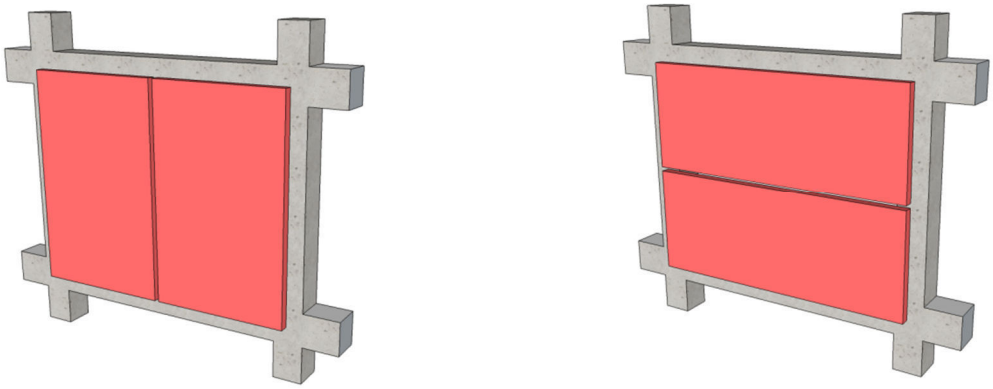

Figure 2-19: Horizontally (left) and vertically (right) repeating cladding modularity

The level of complexity of the panel modularity can further increase in both the vertical and horizontal direction. Such systems can therefore be described by the number of repetitions in the vertical direction (rows) and horizontal direction (columns). For example the system shown in Figure 2-20 (left) can be described as having a panel modularity of 4x3 and the system on the right as 1x3. This higher degree of modularity is common in glazed cladding systems since it is more economical to have a higher number of smaller glass panes than a single large pane (Behr & Worrell, 1998).

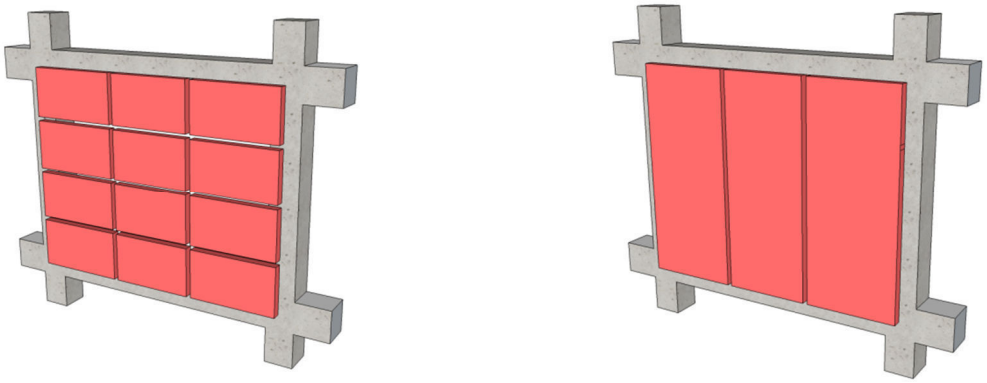

Figure 2-20: 4x3 (left) and 1x3 (right) cladding modularity examples

As well as increasing the repetition of panels both vertically and horizontally, the modularity can also vary in regards to panel arrangement. For example, it is common for precast concrete panels to be located only along the beam and/or column lines like that shown previously in Figure 2-17 (bottom right). Such panels are often called spandrel or cover panels, as shown in Figure 2-21.

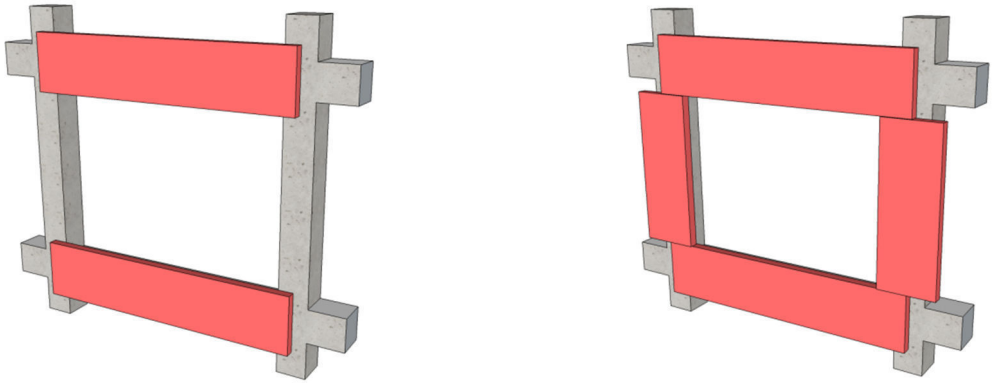

Figure 2-21: Spandrel (left) and spandrel with column cover (right) cladding modularity examples

Spandrel panels cover the beam and floor slab of the building structure. The vertical dimension of these panels may be small and only cover the beam or they may span the full height of the story. The horizontal dimension often extends the full bay width of the structure. Column cover panels are panels that cover the columns of the building structure. These panels are often used in conjunction with spandrel panels, like that shown in Figure 2-21 (right). The area between the panels is then filled with a simple glazing solution. The column cover panels may be attached to the building structure or to the spandrel panels above and below the column cover panel (Hunt & Stojadinovic, 2010).

A final consideration of cladding modularity is that of punched holes in panels. Such holes may be in the form of single central openings, or multiple randomly spaced openings. Large single punched openings are shown in Figure 2-22.

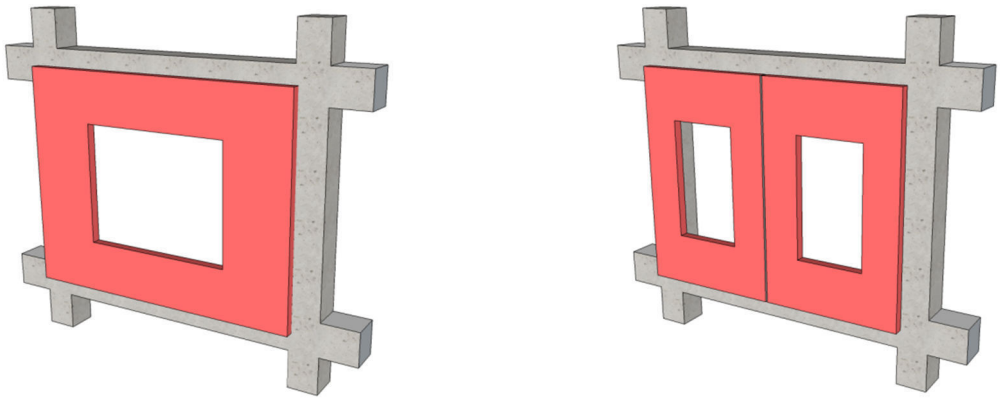

Figure 2-22: Single central punched hole in mono panel system (left) and dual panel system (right)

2.4.3 Connection Typology

The connection between the cladding system and the structure may consist of several components, including bolts, metal angles, cast-in fixings, nails, welds, etc. In order to define the different cladding connection typologies it is necessary to first understand the influence that each of these components has upon the seismic performance.

Although there are many different kinds of connection systems, all cladding systems are generally composed of five main components: the structural framing member, the attachment between structure and connection, the connector body, the attachment between connector body and the cladding panel (Pinelli et al., 1993). These five components are illustrated in Figure 2-23. The attachments (or fixings) of the connector body provide anchorage into the structure and cladding panel and are typically strong stiff elements that are designed to remain elastic, e.g. cast-in steel plates, welded fixings, or expansion anchors. The connector body forms the structural link between the cladding panel and the main structure. It is typically comprised of steel components, e.g. steel angles and bolts. There is considerable variation in the design of each of the attachments and connector body depending upon the function of the connection, the type of connection (welded or bolted), the architectural requirements, and other considerations (PCI, 2007).

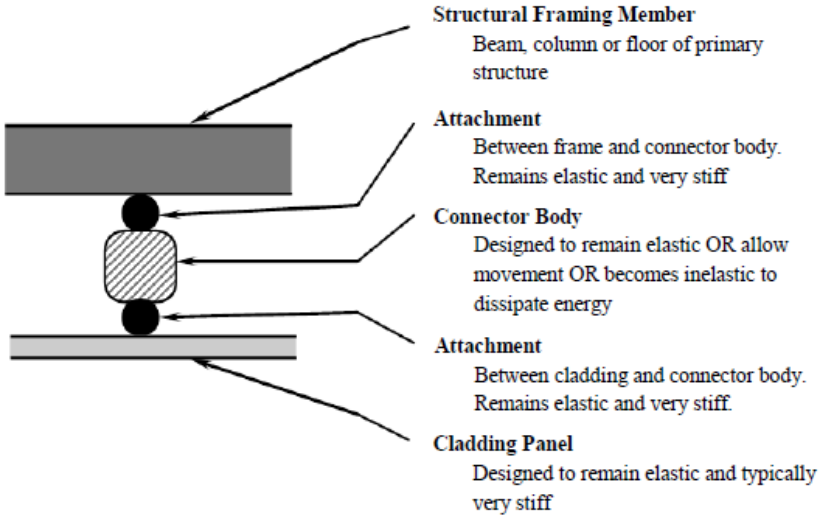

Figure 2-23: Cladding connection system composition (Pinelli et al., 1993)

The attachments of cladding connections may be subjected, in addition to possible shear and tension loads, to torsional and bending moments due to the eccentricity of the connection (Pinelli et al., 1995). Since it is usually assumed that these attachments are stronger than both the cladding and the connector body itself, they are not here considered

within the cladding classification. The attachments have not been included since they should play a very minor role in determining cladding performance due to strength hierarchy principles. However, as observed during the Christchurch earthquakes, mistakes where the attachment ends up being the weakest link are possible. When this is the case, the risk of complete detachment of the cladding is very high. Further information on experimental testing into the performance of attachments/anchors/fixings is presented in Chapter 3 for this reason.

If we assume that the connection attachments have been properly designed then, when we consider the components identified in Figure 2-23, the system can be simplified to that of the weakest link in the system. For most cladding panel systems the weakest (and least stiff) element in the system is the connector body. The connector body is usually required to accommodate relative movement between the cladding panel and the frame as well as provide out of plane restraint. The connector body is therefore expected to play a critical role in determining the seismic performance and as such, the connection classification is based upon the different possible connector body typologies. Several types of connector bodies are used in cladding systems. The following typologies are proposed for encompassing all possible connection types:

- Bearing connection
- Tie-back connection
- Slotted connection
- Fixed connection
- Dissipative connection

It should be noted that a cladding system will very commonly have more than one of the above connection types. A brief description of each connection type is provided in the following sections.

2.4.3.1 Bearing Connection

Bearing (or eccentric) connections are intended to transfer the vertical loads from the self-weight of the cladding panel to the building structure. Bearing connections are usually provided at no more than two points per panel as recommended by PCI (2007) so that an indeterminate force distribution of the gravity loads does not develop. The connections are also usually at just one level of the panel. Bearing can be either directly in the plane of the

panel along the bottom edge, or eccentric using concrete corbels, haunches, cast-in steel shapes, or attached panel brackets, as shown in Figure 2-24.

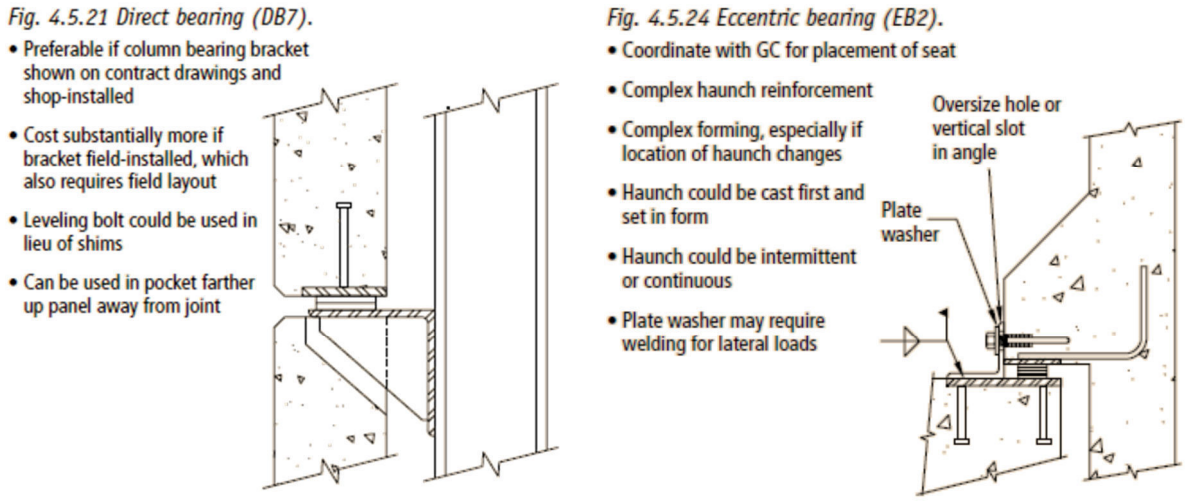

Figure 2-24: Bearing connection examples (PCI, 2007)

Eccentric bearing connections are usually used for cladding panels when movements of the support system are possible (Hunt & Stojadinovic, 2010). The most common types of eccentric bearing connections involve welding an angle or tube steel section to an embedment in the panel and using a levelling bolt to adjust the panel to the correct position.

2.4.3.2 Tie-Back Connection

Tie-back (or push-pull) connections are primarily intended to keep the panel in a vertical position and to resist wind and seismic loads perpendicular to the panel. Tiebacks may be designed to withstand forces in the plane of the panel, or isolate them to allow frame distortions independent of the panel and allow movement vertically and/or horizontally. Tie-back connections are often used in seismic areas to isolate the panels and keep them from participating in the lateral response of the building. The most common tie-back connections are made of threaded coil rods bolted or welded to angle or tube steel sections attached to the beam or column of the building structure, as shown in Figure 2-25.

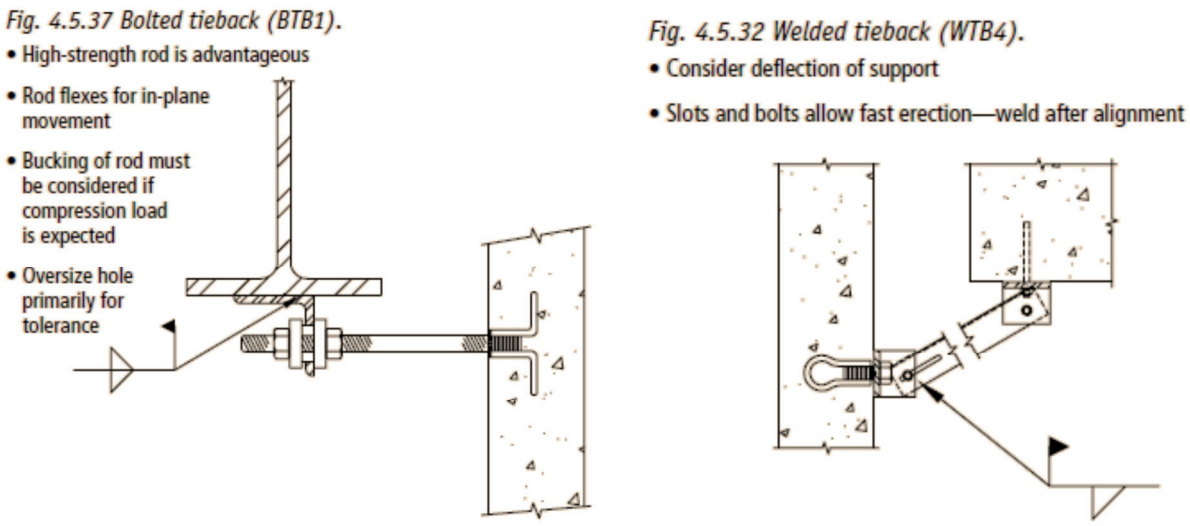

Figure 2-25: Tie-back connection examples (PCI, 2007)

2.4.3.3 Slotted Connection

Slotted (or slip) connections are similar to tie-back connections in that they keep the panel in a vertical position while allowing both vertical and horizontal in-plane movements. This is achieved by using an oversize hole or slot large enough to accommodate the design drift in each direction, as shown in Figure 2-26. Care must be taken to ensure that the bolt is not over-tightened so that the bolt is able to slide while at the same time, ensure that rattling of the connection does not occur.

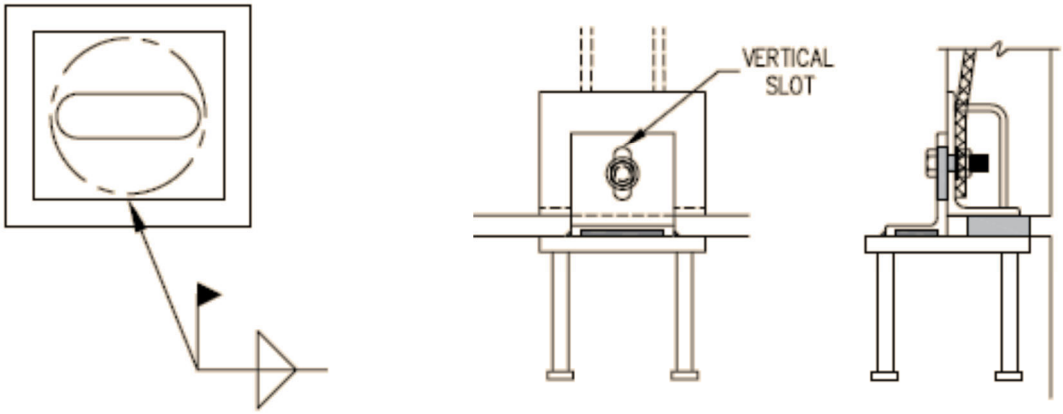

Figure 2-26: Slotted connection examples (PCI, 2007)

2.4.3.4 Fixed Connection

The fixed connection is similar to the bearing connection, however the differentiation has been made between the two since the bearing connection is designed to predominantly carry the self-weight of the panel only, the fixed connection is designed to loads imposed in

all directions (PCI, 2007). The fixed connection has a strong and rigid connector body and hence relative interstorey movement has to be accommodated within the cladding itself. Such a connection is commonly used in glazing systems with the interstorey movement accommodated by use of gaps around the glass and within the claddings itself (seismic frames).

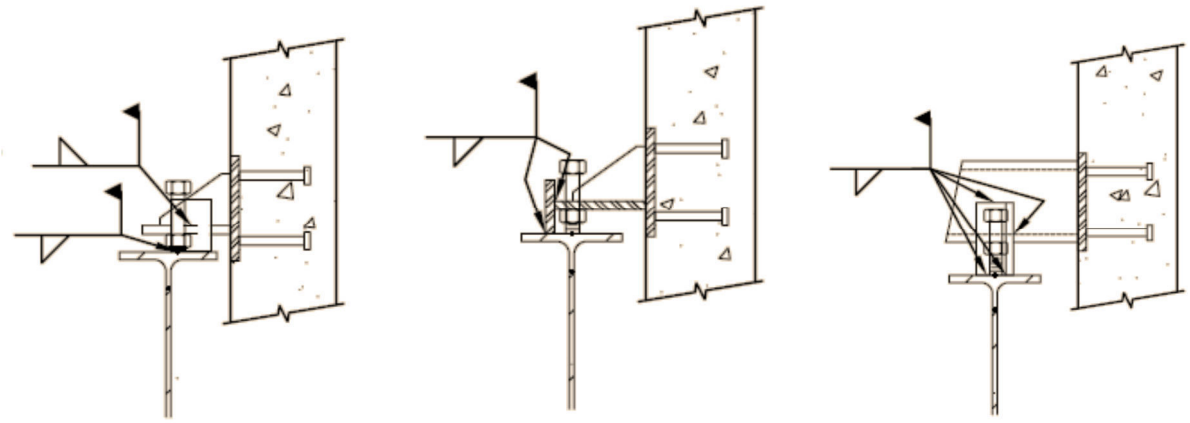

Figure 2-27: Fixed connection examples (PCI, 2007)

2.4.3.5 Dissipative Connection

Conventional connection designs aim to isolate the cladding from the structure. Slotted or flexible tie-back connections are recommended by PCI (2007) to allow movement in the plane of the panel, in this way lessening the panel interaction with the supporting frame. However, even when designed as isolated elements according to state-of-the-art connection design practice, it has been shown that cladding can add significantly to the lateral stiffness of the building (Goodno & Palsson, 1986; Henry & Roll, 1986; Smith & Gaiotti, 1989). Experimental studies and extensive analytical modelling point to the critical role that the cladding connections play in this process (Rihal, 1988; Sack et al., 1989).

Therefore, instead of minimising, or canceling the structural-cladding interaction, the dissipative connection takes advantage of this interaction to dissipate energy, thereby reducing the response of the main structure. These dissipative connections must exhibit superior properties of ductility and damping to result in high energy dissipation without failure during moderate or strong earthquakes. These connections must also limit the forces transmitted into the panel. By using dissipative cladding connections, studies have shown that significant advantages can be achieved over more conventional design (Goodno, 1998; Pinelli et al., 1995).

Dissipative connections typically form the same role of either a tie-back or slotted connection, in that they provide out-of-plane restraint while at the same time, allow horizontal and vertical movement. It is by this movement that the dissipative capacity is achieved. An example of a dissipative connection is shown in Figure 2-28.

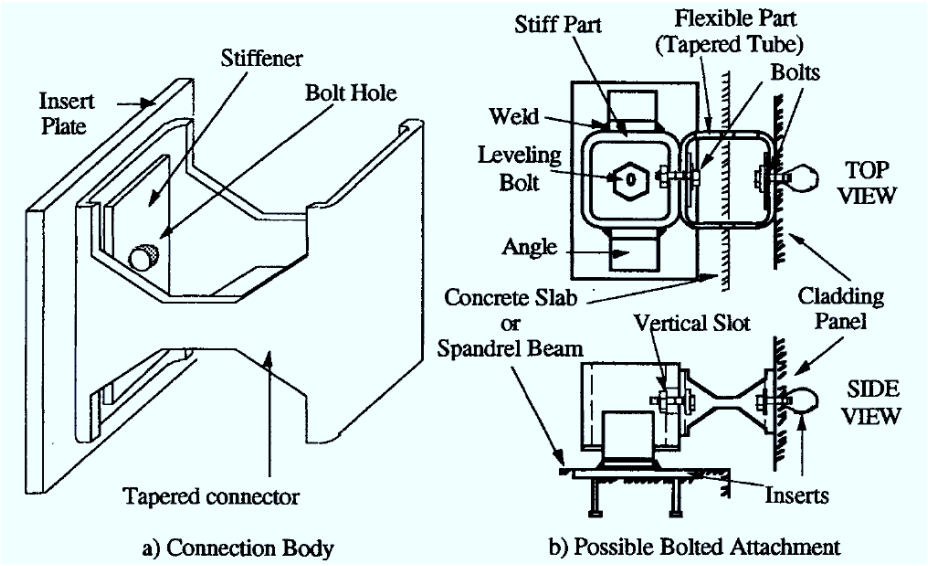

Figure 2-28: Dissipative connection example (Pinelli et al., 1995)

2.4.4 Connection Modularity

The definition of the connection modularity varies slightly from that defined for the cladding modularity since the connections are not built up by combining smaller subsystems. In the context of cladding connections, the modularity here describes the arrangement of the cladding connections.

The first characteristic of the cladding modularity that requires definition is whether the connection is continuous or discrete. Continuous connections are more common in infill panel systems or residential cladding solutions and utilise continuous timber or metal elements connected to the main structure with either adhesive or regularly spaced fixings. Discrete connections are more common in commercial cladding panel systems and allow for a huge range of possible connection arrangements.

Cladding connections can be located on the columns, beams, floor or any combination of these. Different panel shapes and types warrant different placements of the connections. For example, it is common for the bearing connections of rectangular panels to be located at the bottom of the panel and the tieback connections to be located in the top corners, as shown in Figure 2-29. For slender column cover panels, the bearing connections could be placed at

the bottom or centre of the panel. In spandrel panels, the self-weight is typically supported at the floor level and restrained at a column or vertical member rather than at the underside of the floor member. This connection arrangement prevents potential creep rotation of the edge member from affecting the alignment of the panel (PCI 2007). Lightweight cladding systems by definition do not have large gravity loads so bearing connections are not often essential and instead fixed connections are typically used at a regular spacing as required (Behr, 2006).

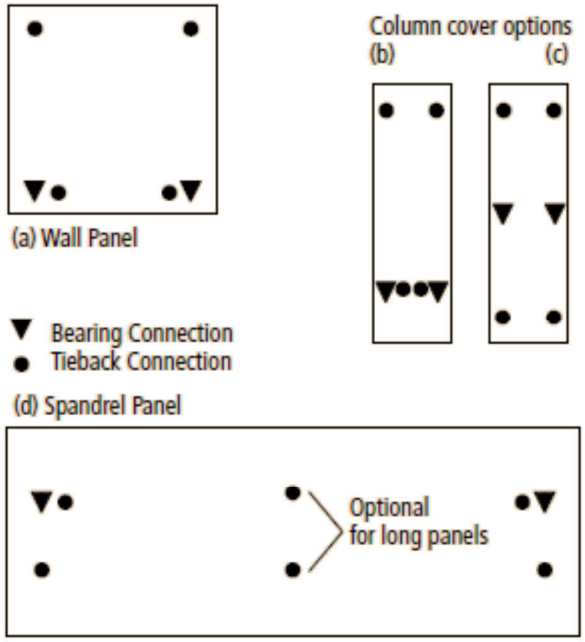

Figure 2-29: Typical cladding panel connection locations (PCI 2007)

2.5 Cladding Damage Survey

A cladding damage survey of 217 buildings in the Christchurch CBD was conducted following the 22nd February 2011 earthquake. The building survey was conducted within the four avenues (Bealey, Deans, Moorhouse and Fitzgerald) that encompass the Christchurch CBD. The buildings included in the survey were only those greater than three stories in height in order to exclude the majority of unreinforced masonry facades as well as to restrict the survey population. For buildings with multiple cladding systems, multiple assessments were conducted of the same building. In total, 266 cladding systems were included in the survey.

The survey based on what was visible from outside the building, making it equivalent to a Level 1, or rapid safety assessment of the exteriors only (ATC-20, 1989; NZSEE, 2006). A survey that focusses solely on cladding performance has not previously been conducted

and consequently, a new standard survey procedure was developed. A template of the survey form used is provided in Appendix A. This assessment is expected to underestimate the actual amount of damage since only visible damage is reported and undoubtedly less obvious forms of damage exist, e.g. warped frame, damaged connections. Only with a more detailed survey could the true extent of damage be determined. The full set of data collected from the survey is provided in Appendix B.

2.5.1 Earthquake Background Information

The magnitude 6.3 earthquake that struck New Zealand's second largest city on the afternoon of the 22nd February 2011 took the lives of 181 people; the second largest toll from a natural disaster in New Zealand (New Zealand Police, 2012). The epicentre was located approximately 10 km from the city at a shallow depth of 5 km. The close proximity of the earthquake resulted in severe ground shaking throughout Christchurch. The maximum felt intensity was MM IX and the maximum recorded peak ground acceleration (PGA) was 2.2 g. The recorded PGA within the Christchurch Central Business District (CBD) ranged from 0.6 and 0.8g (McVerry et al., 2012). The horizontal acceleration response spectra for four sites within Christchurch CBD are shown in Figure 2-1 for the 22nd February 2011.

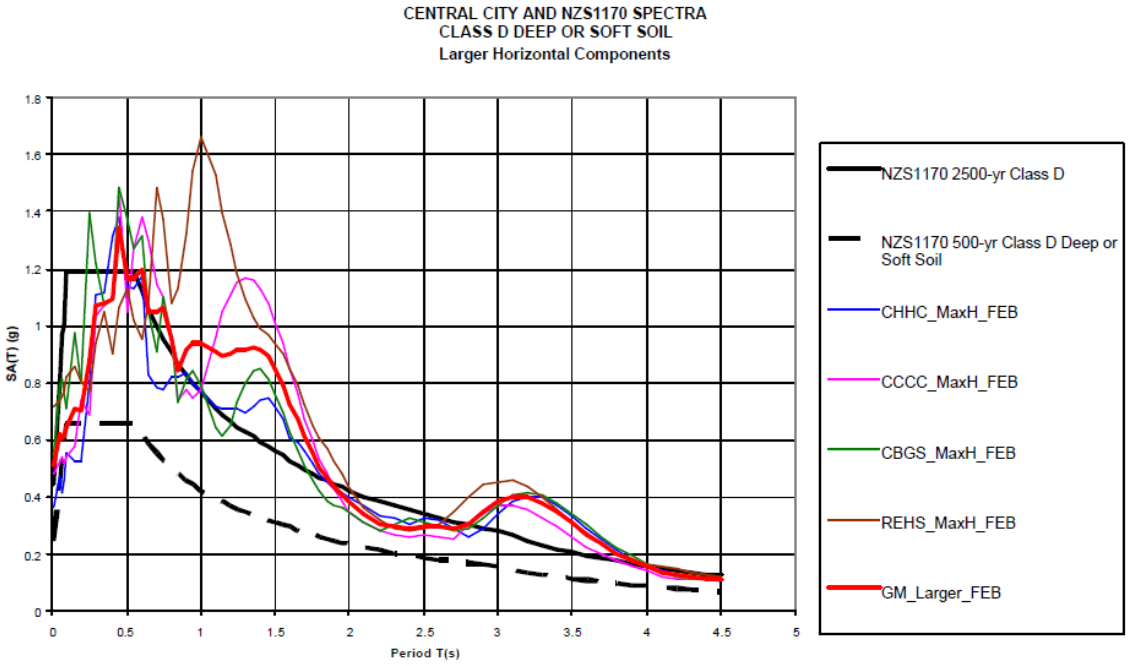

Figure 2-30: Comparison of 5% damped acceleration response spectra for four sites within Christchurch CBD and corresponding design spectra from NZS 1170.5 (2004) (McVerry et al., 2012)

The earthquake caused widespread failure to older unreinforced masonry (URM) structures, as well as the collapse of two reinforced concrete (RC) buildings. The majority of

buildings within the Christchurch CBD achieved the life-safety objective of the Building Code, however significant damage to both structural and non-structural elements was widespread (Kam et al., 2011). The cost to repair the extensive structural and non-structural damage resulted in many building being uneconomic to repair (Stylianou, 2014). Consequently, since September 2010, approximately 85 percent of the CBD building footprint has been destroyed or demolished (Gates, 2012).

Current seismic design provisions require that non-structural components be secured so as to not present a falling hazard or obstruct an egress route in a design level earthquake (NZS 1170.5, 2004); however, these components can still be severely damaged such that they cannot function following an earthquake. Cases of complete failure of cladding systems were observed, as shown in Figure 2-31, which shows that this design objective was not always achieved. Also of significance was the widespread amount of damage beyond serviceability limit state. This level of damage requires costly and time-consuming repairs which has considerable economic implications.

Figure 2-31: Examples of cladding failures during the Canterbury earthquake sequence: detached curtain wall (left) and detached coffered precast concrete panel (right)

2.5.2 Damage Survey Scope

After the February 22nd earthquake, all buildings were inspected by a structural engineer and given either a green, yellow or red placard to represent the safety of the building. A green placard indicated that a building had been assessed and no apparent structural or other safety hazards were found. A yellow placard indicated that a building had restricted access and a red placard indicated a building must not be entered because it was

deemed unsafe (ATC-20, 1989). As illustrated in Figure 2-32, 74% of the buildings in the survey received either a yellow or red placard.

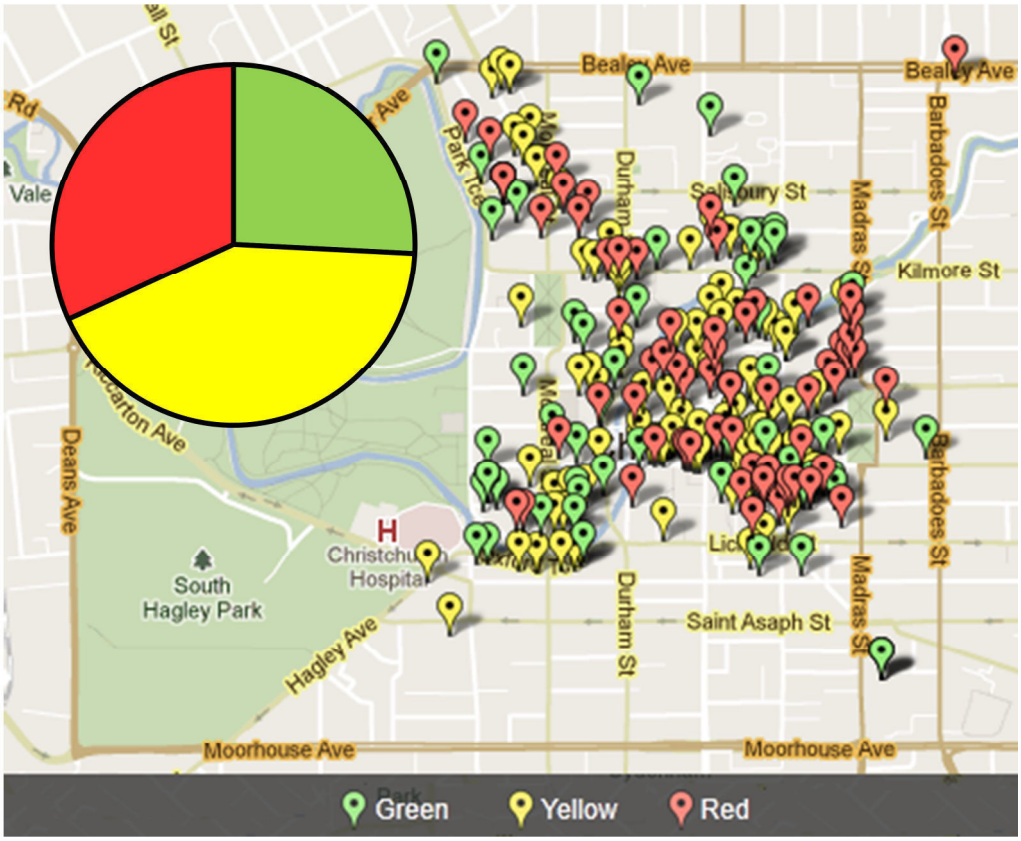

Figure 2-32: Locations of buildings surveyed and their placard composition

The building construction information of the 217 buildings included in the survey is illustrated in Figure 2-33. The majority of buildings surveyed were low to mid-rise in height and were of some variety of reinforced concrete construction. 65% of the buildings primary occupancy use was office use, followed by 18% apartments and 9% hotels. The building age was estimated at the time of survey or found from city records following further investigations. The majority of buildings were found to be less than 50 years old following a large boom in construction after the 1960s.

A total of 266 cladding systems were surveyed on the 217 buildings. Most buildings had more than one cladding system, however typically a single system would enclose the majority of the structure, and it was this 'primary' cladding system that was assessed in the damage survey. Where multiple systems existed and the primary cladding system was not obvious, multiple cladding systems were surveyed; hence the number of cladding systems included in the survey was slightly greater than the number of buildings surveyed.

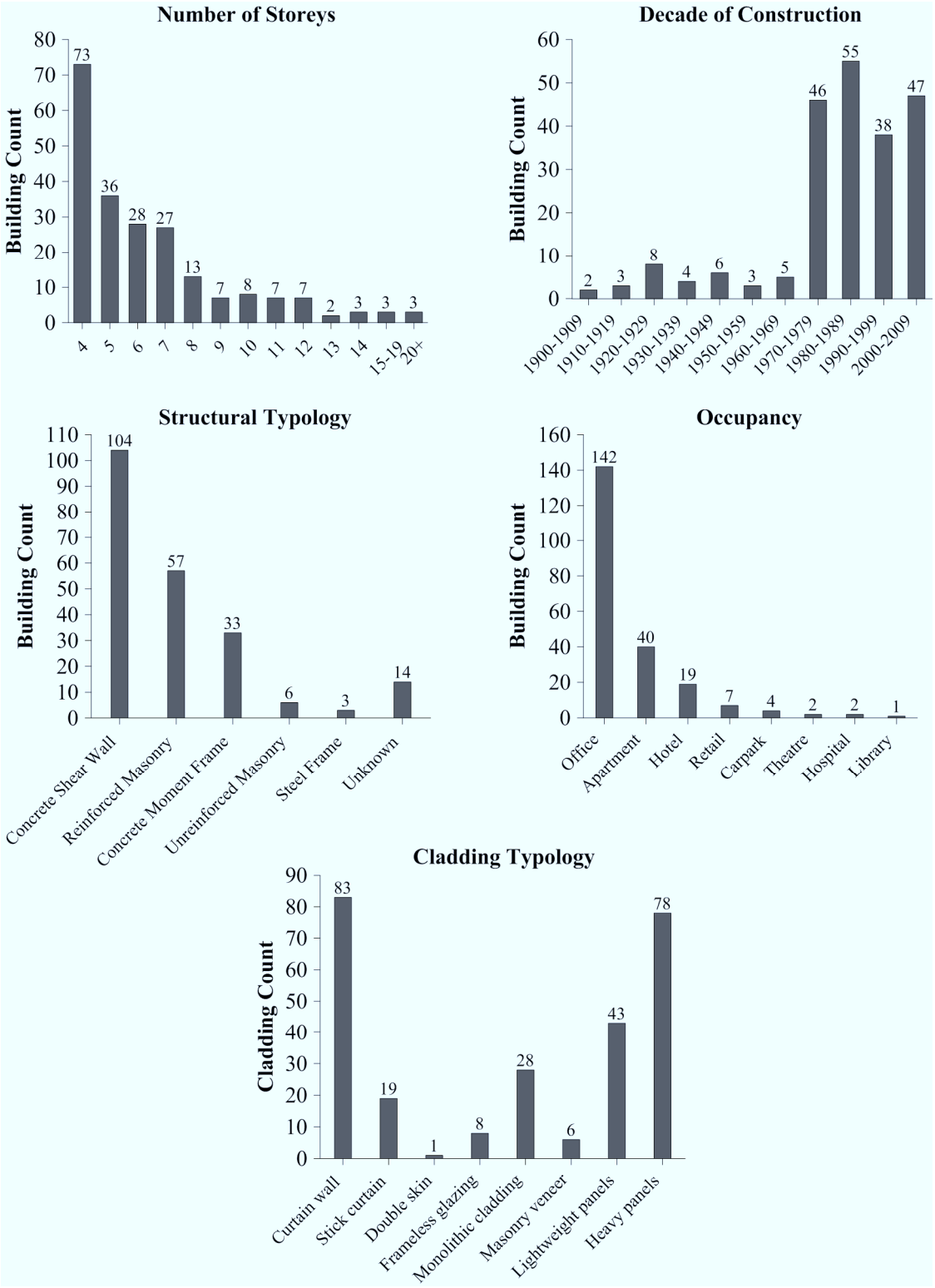

Figure 2-33: Construction information of buildings surveyed (clockwise from top left): building height, construction age, occupancy, cladding typology and structural typology

The survey classified each cladding systems according to the eight cladding typologies presented in Section 2.4.1. Figure 2-33 shows that curtain walls and heavy cladding panels were the most common cladding typology of buildings in the Christchurch CBD. With the

exception of the heavy panels, double skin and masonry veneer, all of the other cladding systems can be considered as being 'lightweight' cladding systems. These 'lightweight' systems make up approximately 70% of the cladding systems. The age of the cladding in relation to the building was also recorded. 97% of cladding systems appeared to be the same age of the building, with only eight systems appearing to be modern retrofits.

2.5.3 Cladding Damage

This section presents a summary of the typical cladding damage to each of the eight cladding typologies. Each summary is accompanied with examples of damage. These examples feature cases of the most heavily damaged cladding systems observed.

2.5.3.1 Curtain Wall

Curtain wall cladding systems often incorporate a large amount of glazing. Hence typical damage to curtain wall systems consisted of broken glass, as shown in Figure 2-34.

Figure 2-34: Damage to curtain wall cladding systems

Curtain walls of all ages showed various levels of damage. Older systems normally provide less movement allowance for the glass and consequently were more likely to exhibit glazing damage. Several buildings with older, non-seismic glazing frames were re-glazed between September 2010 and February 2011, only to be damaged again in the February

earthquake. Newer systems exhibited proportionately less moderate to severe damage. However, issues do still exist with current design and construction techniques since several curtain wall systems less than 20 years old were heavily damaged.

Damage to the frame of curtain walls was difficult to distinguish from street level, so it is likely this type of damage was overlooked. However there were observed cases of frames being bent and warped, as well as one case where the glass punctured through the frame itself. Failure of the frame was rare, with only one curtain wall system having a large-scale failure. This involved multiple sections of a curtain wall system completely detaching from the building, as shown in Figure 2-35. Almost the entire aluminium frame and glazing system that ran around three side of the building's second floor fell to the ground. Closer inspection showed that the frame was screwed into a wooden sub-frame and these screws had sheared off, possibly due to displacement incompatibility between the cladding and sub-frame.

Figure 2-35: Disconnection failure of curtain wall cladding systems

2.5.3.2 Stick Curtain

Similarly to curtain walls, stick curtain systems contain significant amounts of glazing. As would therefore be expected, cracked or broken glass was the most obvious form of

damage, as shown in Figure 2-36. The damage to stick curtains was not as heavy as it was to curtain walls, with no large-scale failures observed like that observed in curtain wall systems.

Figure 2-36: Damage to stick curtain cladding systems

Once the glass in the stick curtains (and also curtain walls) is broken, this presents a falling hazard to pedestrians. Managing the risk of falling glass is a difficult issue to deal with. Although most damage cases observed involved standard glass, it was evident that one approach to try and reduce the risk of falling glass was the use of laminated and toughened glass. Using these types of glass had both positive and negative consequences.

The use of laminated glass aims to prevent the glass being able to break up and fall as sharp pieces. This was successful in most damaged laminated glass observed; however, some cases were also observed where the entire laminated pane fell from frame, presenting a significant falling hazard.

Toughened (tempered) glass is stronger than normal glass and when it is damaged it breaks into thousands of small glass fragments that present a much smaller falling hazard. Damage to toughened glass was typically observed as an empty frame and a pile of glass fragments on the footpath. Although the use of toughened glass involves accepting that the

glass is going to fall if it is broken, it was clear the hazard of the falling fragments was lower than that of glass shards or entire panes.

2.5.3.3 Double Skin

Only one double skin system was observed in the cladding survey. This system was a modern system attached to the entire north side of a seven storey 1960's concrete moment frame building. Damage in the form of entire panes of shattered glass was observed to this double skin system following the 22nd February 2011 earthquake, as shown in Figure 2-37.

Toughened glass was used in the double skin and hence any glazing damage was in the form of entirely shattered panes. The remnants of the glass pane were typically small fragments left in the frame seals, as shown in Figure 2-37.

Figure 2-37: Damage to double skin cladding system

2.5.3.4 Frameless Glazing

Numerous cases of heavy damage were observed in frameless glazing, as can be seen in Figure 2-38. Frameless glazing is a reasonably modern system so it would be expected that it should have performed better than other systems, however this was not the case. It appeared that damage originated around the connector element that holds each corner of the glass

panes. This is likely a result of the connection creating stress concentrations in the glass due to the restraint of the connection to the structure.

Figure 2-38: Damage to frameless glazing cladding systems

One building that was due for construction completion soon after the 22nd February 2011 earthquake was clad with a large frameless glazing system. The frameless glazing system was so recently installed that the glass was still covered in protective wrapping. This system suffered widespread glazing failure, as can be seen in Figure 2-39 (top left).

The amount of movement a frameless glazing system can accommodate is not large (50 mm inter-storey displacement is approximately the maximum limit) and this was apparent by the amount of damage observed. Frameless glazing is not a commonly used as external cladding and it is more commonly utilised inside buildings, in locations such as hotel foyers and shopping malls, as shown in Figure 2-39. Due to these areas often being areas of high density people movement, the significant amount of glazing damage to these systems would have represented a significant fall hazard.

Figure 2-39: Damage to frameless glazing cladding systems

2.5.3.5 Monolithic Cladding

Monolithic cladding was mainly observed as a secondary cladding system. Since this type of cladding is brittle and does not have allowance for relative movement between itself and the structure, damage always consisted of cracking to the monolithic finish, as shown in Figure 2-40.

The degree of cracking damage varied from small hairline cracks to large cracking resulting in delamination of sections of cladding. Hairline cracks were often difficult to observe from ground level and it was also difficult to be certain that these were earthquake related damage. Cracks most commonly formed around window corners and also where joints between backing material were located. Any cracking to the panels may compromise the watertight performance of the cladding and lead to long-term serviceability issues.

Figure 2-40: Damage to monolithic cladding systems

2.5.3.6 Masonry Veneer

Only six masonry veneer cladding systems were included in the damage survey due to the survey only including buildings over three storeys in height. Masonry veneer systems are most typically used in residential construction and are therefore most common in single or double storey construction. There is also a limit to the height that masonry veneer can be used due to the requirement that it support its own weight.

Although widespread damage to unreinforced masonry was reported (Dizhur et al., 2011) as well as large amounts of damage to masonry veneer claddings in residential construction (Buchanan & Newcombe, 2010), masonry veneer cladding performed reasonably well in the few instances observed within the Christchurch CBD. One notable exception was the failure of a single panel of masonry veneer from a six storey medical facility, as shown in Figure 2-41 (right). This out-of-plane failure was likely the result of insufficient lateral restraint, since a minimal number of ties were visible from ground level.

Figure 2-41: Damage to masonry veneer cladding systems

2.5.3.7 Lightweight Panels

Lightweight panels can be made of a wide range of possible materials; including wood, metal and concrete. This cladding typology does not typically have allowance for relative movement between itself and the structure. Consequently, many lightweight panels were observed to be damaged, as shown in Figure 2-42. This damage either consisted of cracking of the panel, tearing of the panel, or disconnection of the panel. This damage typically occurred at the interface between adjacent panels, as can be seen in Figure 2-42.

Figure 2-42: Damage to lightweight panel cladding systems

Most lightweight panel cladding systems had a high degree of modularity (comprising numerous small sized panels). As such, it was concluded that the disconnection of lightweight panels may cause injury to pedestrians but the risk of failure result in death was low.

2.5.3.8 Heavy Panels

The majority of heavy claddings surveyed exhibited little to no damage. Visible damage to heavy panel cladding normally consisted of cracking or crushing of the concrete. Corner crushing was most likely due to pounding with adjacent panels, as shown in Figure 2-43 (left). Frame elongation caused significant damage to the connections and panels in a 17 story, mid-1980s reinforced concrete perimeter frame building within the Christchurch CBD. Cyclic plastic hinging in reinforced concrete beams has been shown to increase the length of beam members (Fenwick & Megget, 1993). In this particular reinforced concrete building, the plastic hinge regions of the frame were located between the precast concrete cladding panel connections. The movement apart of these connections due to frame elongation resulted in significant damage to the connection and panel, as shown in Figure 2-43 (centre). Minor damage was also observed in the form of panels having residual displacements and/or rotations. The ejection or rupture of sealing joints due to movement between panels was also common, as shown in Figure 2-43 (right).

Figure 2-43: Corner crushing of spandrel panels (left), precast panel and connection damage due to beam elongation (centre), torn polysulphide seal (right)

Within the Christchurch CBD only one case of panel disconnection was observed. The disconnection consisted of six precast concrete spandrel panels falling from the southern frontage of the building at levels 5, 6 and 7, as shown in Figure 2-44 (top left). The panel connection detail consisted of four 150x100x10 mm mild steel angle cleats that were welded onto a weld-plate cast in the side of the column, as shown in Figure 2-44 (bottom left). The angle had a 60x20 mm slotted hole; it would be presumed this was to provide relative movement between the frame and panel, however, on inspection, the bolt washers for the slot were found to be welded in place, effectively making the connections fixed, as shown in Figure 2-44 (top right).

The metal cleat suffered severe distortion as a result of the inter-story deformations induced by the earthquake. Since the bolts were unable to slide in the slotted holes, the bolts failed in shear at the cleat interface. The 60 mm slotted hole would have provided a maximum movement allowance of ± 20 mm (without allowance for installation tolerance) which would have unlikely been sufficient to accommodate the maximum inter-story displacement, however, would undoubtedly decreased the likelihood of failure. It was also found that the capacity of the fixings did not meet the code requirements of NZS 4203 (1992), the current code at time of construction. The fixings of the two panel sizes were found to be 15% and 33% of the capacity required by NZS 4203 (1992) (CERC, 2012). Unfortunately the falling panels, each weighing approximately 6 tons, fell onto a car, killing its occupant.

Figure 2-44: Disconnected precast spandrel panels (top left), metal cleat connection (top right), detail of precast spandrel panel connections (bottom left), car crushed by fallen panels (bottom right)

Complete disconnection of large coffered concrete panels was also observed after the magnitude 6.3 earthquake on 13th June 2011. Each panel was rigidly attached at its base to

the structure as well as to each adjacent panel. This effectively made the panels behave together as a cantilever shear wall. The top connection consisted of 12 mm bolts through the flange of the coffered panel, as shown in Figure 2-45. These top connections would not have been able to provide any significant degree of movement allowance and hence tore out through the panel resulting in the entire disconnection of the panels, as shown in Figure 2-45.

Figure 2-45: Coffered precast panels that failed in 13 June 2011 aftershock

2.5.4 Cladding Performance Data

This section identifies trends in the performance of cladding systems, particularly in relation to the structural information gathered for each building. It should be mentioned again that that the survey is based on what is visible from outside the building and consequently will always underestimate the true level of damage since less obvious forms of damage certainly exist, e.g. warped frame, damaged connections.

Firstly, the composition of performance levels for each cladding system is presented in Figure 2-46. The data has been normalised to 100% with the number of actual systems reported on each bar. The performance level of each cladding system was determined according to the criteria discussed in the previous section. Overall, 64% of cladding systems surveyed were deemed Operational, 14% deemed Immediate Occupancy, 12% deemed Life Safety and 10% deemed Hazards Reduced. This means that the performance of 22 cladding systems was outside an acceptable level for even a very rare earthquake event as it posed a significant risk to life safety.

Damage to heavy cladding was not frequently observed, however, it has to be recognised that the performance of heavy claddings is difficult to determine without being able to observe the extent of damage to the cladding connections. The cladding can appear to be completely undamaged from outside as well as inside the building. However, once the

internal linings are removed, it has been observed in several heavy claddings that the connections were damaged or even broken. The damage is not always consistent either, making inspection of virtually every connection necessary.

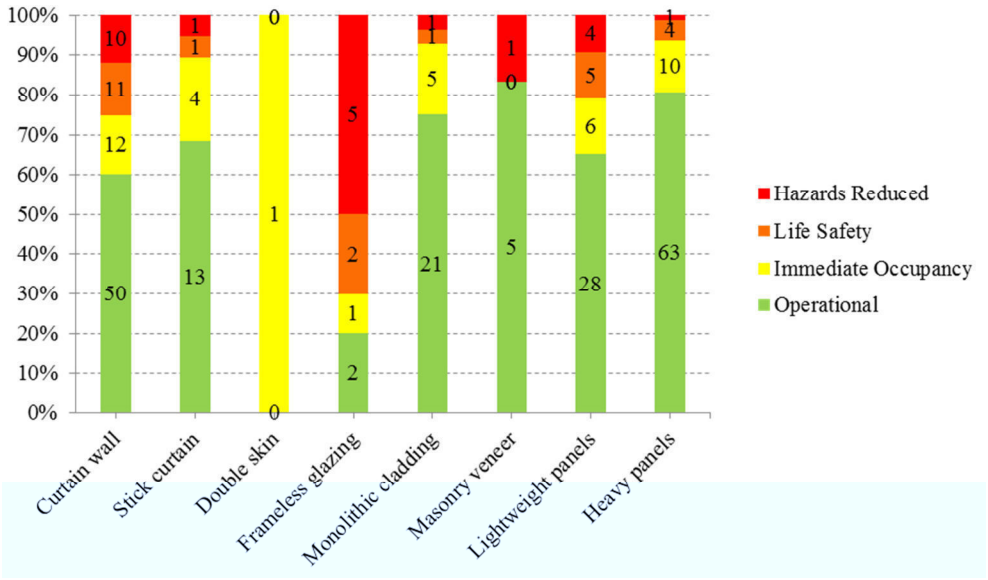

Figure 2-46: Cladding performance by cladding typologies

Overall, 78% of lightweight claddings were deemed either Operational or Immediate Occupancy. This typically meant that either no damage was observed or very minor damage such as ejected window seals, cracked glass, or cracked panels was observed. The poorest performing cladding system was clearly frameless glazing; with 50% being deemed Hazards Reduced. This was usually due to a significant portion of the glazing falling from the system as well as the potential for this falling glazing to seriously threaten life safety.

Shown in Figure 2-47 is the cladding performance grouped by building's structural typology. The typologies are listed from left to right in terms of the frequency that they were identified. As expected, cladding systems attached to unreinforced masonry performed by far the worst, likely a consequence of the poor structural performance. The remaining structural typologies showed fairly consistent cladding performance. One possible influence that structural typology may have upon cladding performance is related to the flexibility of the different structural systems. It can be seen that more damage was observed in concrete moment frame buildings compared to concrete shear wall buildings and it is possible that this is due to moment frame structures being more flexible than shear wall structures.

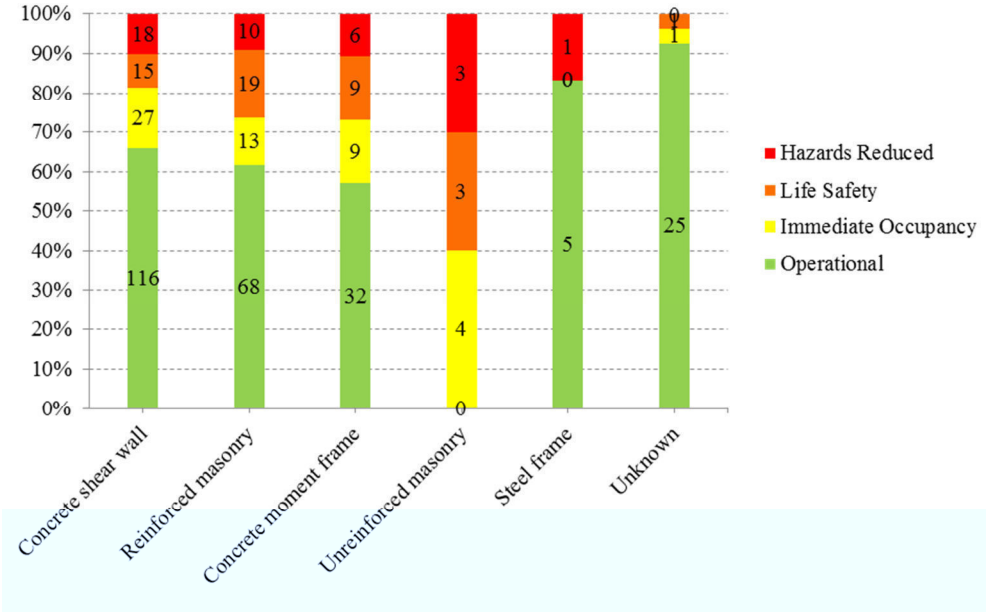

Figure 2-47: Cladding performance by structural typology

The cladding performance grouped by building construction age is presented in Figure 2-48. There is a clear trend that newer buildings had better cladding performance. Buildings built in the 1950s exhibited the highest number of Hazards Reduced cases. It is encouraging to see that facade systems built from 2000 onwards were clearly the best performing.

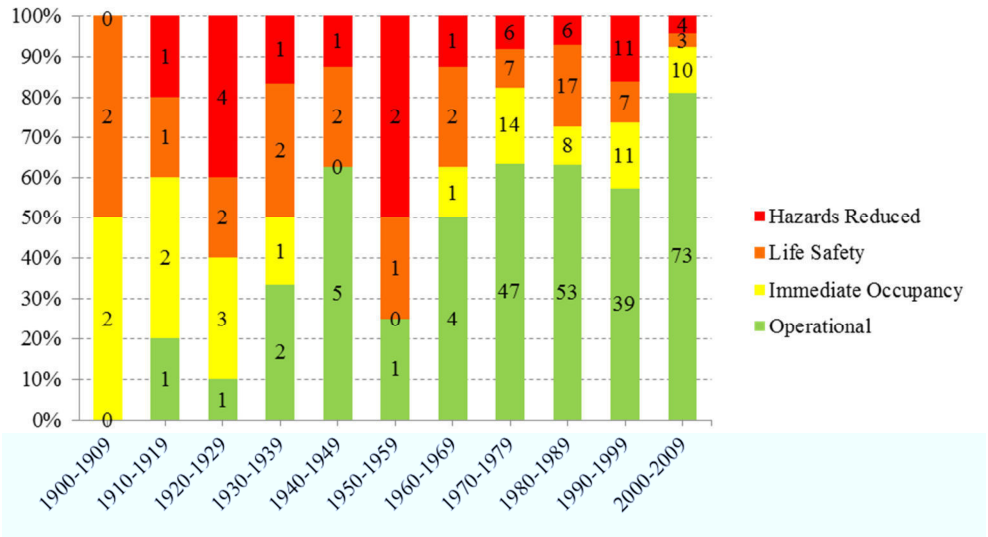

Figure 2-48: Cladding performance by building construction decade

Finally, the cladding performance grouped by the buildings height (number of storeys) is shown in Figure 2-49. A building's natural period is correlated to its height, so a possible hypothesis was that trends relating cladding damage to the earthquake spectra would have been observed. However it does not appear there is any such trend. The low amount of data

present for taller buildings is likely the reason for the apparent higher level of damage in buildings 14 storeys and taller.

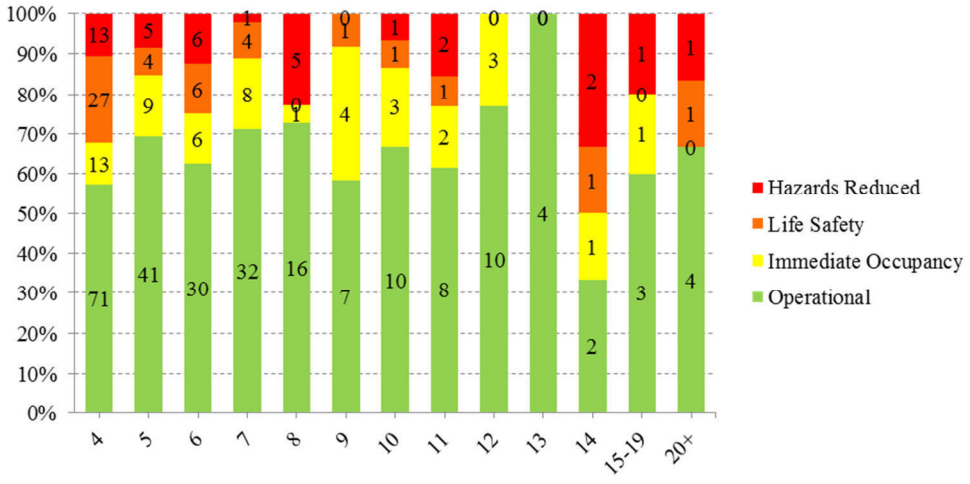

Figure 2-49: Cladding performance by building height

2.6 New Zealand Building Code Provisions

The New Zealand Building Code is a mandatory performance based building code which includes requirements for the performance of cladding systems. Compliance documents provide means of meeting the clauses of the Building Code. Another way to achieve compliance with the Building Code may involve a detailed product development and testing program through a registered laboratory. Buildings designed to the methods (Acceptable Solutions or Verification Methods) described in a compliance document are automatically deemed to comply with the Building Code. Acceptable Solutions provide simple step-by-step instructions that show one way to comply with the Building Code. Verification Methods are calculation methods or tests that prescribe one way to comply with the Building Code.

The seismic design loads for claddings and cladding connections are specifically defined in Section 8 "Requirements for Parts and Components" of NZS 1170.5 (2004). The risk and loadings for ULS and SLS are determined in conjunction with AS/NZS 1170.0 (2002). To be considered for ULS design, the cladding must weigh more than 10 kg and be able to fall more than 3.0 m onto a publicly accessible area.

The magnitude of the earthquake design loads for claddings is calculated by applying various coefficients to the peak ground acceleration from the site hazard spectra and multiplying these to the weight of the cladding, as given by Equation (2-1) and (2-2). These

coefficients take into account the period of the cladding, its risk classification, its height and the ductility of the cladding and its fixings. It should be noted that a ductility of 1.0 is adopted when assessing the SLS performance. For ULS, unless a greater ductility can be proven, the connections are typically designed for a nominal ductility of 1.25.

$$F_p = C_p(T_p) C_p R_p W_p \leq 3.6 W_p \quad \textbf{(2-1)}$$

where

F_p = design earthquake action
$C_p(T_p)$ = design coefficient of the part
C_p = part response factor
R_p = part risk factor
W_p = weight of the part

As shown in Equation (2-1), the horizontal design load is not allowed to be greater than 3.6 times the weight of the cladding. For the case of vertical loads, this limit is 2.5 times the weight of the cladding (NZS 1170.5, 2004).

$$C_p(T_p) = C(0) C_{Hi} C_i(T_p) \quad \textbf{(2-2)}$$

where

$C_p(T_p)$ = design response coefficient
$C(0)$ = site hazard coefficient for T=0
C_{Hi} = floor height coefficient for level i
T_p = period of the part
$C_i(T_p)$ = part spectral shape factor at level i

NZS 1170.5 (2004) also specifies that non-structural elements must be detailed so that they do not contribute in an unplanned way to the buildings seismic response and that damage of non-structural elements is kept to an acceptable level. The result of this prescription is that stiff elements such as cladding panels typically need to be fully separated from the structure. At present, except for heavy claddings, these requirements are seldom enforced by territorial authorities so it has been left to each industry sector to be self-regulating (MacRae et al., 2012).

2.6.1 Deformation Limits

The definition of appropriate engineering parameters to characterise each performance level represents the most critical and controversial phase of performance-based design. (Pampanin, 2005). Deformation limits, or damage limits, are values of an engineering demand parameter deemed most critical in defining the transition point between performance levels. For cladding systems this engineering demand parameter is typically the inter-storey displacement (or drift) (FEMA E-74, 2011).

The following sections include suggested deformation limits for various performance levels from various international codes. Evidently, these deformation limits are difficult to define precisely, so they should always be taken with a level of caution.

2.6.1.1 New Zealand

The commentary provided in Appendix C to NZS 1170.5 - Supp1 (2004) provides general guidance on the suggested inter-story displacements that different cladding systems can accommodate before the onset of damage. These therefore can be considered as SLS deformation limits.

Also included are suggested component ductility where testing of such systems is not possible. This information has been reproduced in Table 2-2 for convenience. Suggested ductility values are provided for the calculation of design forces.

Table 2-2: Suggested ductility and deformation limits (NZS 1170.5 - Supp1, 2004)

Cladding Type	**Ductility**	**Indicative deformation limits for onset of damage**
External wall or prefabricated cladding panel (lightweight – including metal faced, fibre-cement, tile)	3	H/200 (face loading), H/300 (in-plane)
External wall or cladding panel (precast concrete)	3	H/300 (face loading), H/400 (in-plane)
External wall or cladding (masonry – including glass blocks)	2	H/300 (face loading), H/600 (in-plane)
Masonry veneer attached to external wall	2	H/200 (face loading)
Curtain wall system (with framing elements)	2	H/150 (face loading), Clearance in frame (in-plane)
Structural glazing system	1	H/150 (face loading), Clearance (in-plane)

Note: H is in the height between supports. If H is the inter-storey height, which is a typical configuration, then the inter-storey drift can be found by letting H=1, e.g. H/200 = 0.5%

2.6.1.2 U.S.A.

The suggested acceptance criteria for cladding performance levels are given in FEMA P-750 (2009). The drift limits provided for the 'Life Safety' and 'Immediate Occupancy' performance levels of cladding systems are repeated in Table 2-3.

Table 2-3: Suggested deformation limits (FEMA P-750, 2009).

Element	Immediate Occupancy Drift	Life Safety Drift
Prefabricated panels	1.0%	2.0%
Glazed exterior	Clearance	Clearance

Since the type and extent of damage that a component will experience is uncertain, component fragility functions are increasingly being used to indicate the probability of incurring damage at a given value of demand (FEMA P-58-1, 2012). A unique fragility function is required for each damage state of each component. To allow for practical implementation of fragility and consequence data, the electronic Performance Assessment Calculation Tool (PACT) has been developed by the Applied Technology Council (ATC). PACT provides the ability to perform probabilistic loss computations for most common structural systems and building occupancies using fragility data collected from multiple sources (FEMA P-58-1, 2012).

2.6.1.3 Europe

The Eurocode (EC8, 2004) gives damage limitation requirements for non-structural elements in terms of the material of the element, as shown in Table 2-4. The definition for each classification is vague. It is unclear whether a heavy cladding which is a brittle material connected with ductile connections should be treated as a ductile or brittle element.

Table 2-4: Suggested deformation limits (EC8, 2004)

Element	Damage Limitation Drift
Brittle materials	0.5%
Ductile materials	0.75%
Fixed in a way as not to interfere with structural deformations	1.0%

2.6.2 Experimental Seismic Performance Assessment

The need to isolate cladding systems from the primary structure has been acknowledged in New Zealand since the 1931 Hawke's Bay earthquake. However, up until the late 1980s there was no standard procedure for assessing the seismic performance of

cladding systems in New Zealand or elsewhere around the world (Wright, 1989). Any effort made to isolate the cladding system was therefore mostly theoretical.

The Building Research Association of New Zealand (BRANZ) saw a need to better quantify cladding performance and consequently developed a standardised procedure and rig for testing the racking resistance of cladding systems. The testing procedure simulates a building under earthquake loading by imposing inter-storey deflection. The rig subjects the cladding to in-plane displacements (racking), as shown in Figure 2-50. The test imposes a lateral displacement along one axis to create an imposed inter-storey deflection. Consequently, vertical deflections, and other secondary deformations introduced previously such as beam curvatures and column rotations are ignored in this testing arrangement.

A racking test, similar to that developed by BRANZ has been adopted as a required test in the Australian/New Zealand Standard (AS/NZS 4284, 2008) which sets out a method for determining the performance of cladding systems. The tests performed are based upon proving compliance with the performance requirements of the New Zealand Building Code (MBIE, 2004) or higher project specific performance requirements. This includes substantiation of performance after Serviceability Limit State (SLS) inter-storey seismic movement tests and accommodation of Ultimate Limit State (ULS) inter-storey movements without endangering human life. The tests are applicable to all types of cladding systems, including low-rise, high-rise, commercial, industrial and residential systems. The following tests are performed (in the order given):

- Structural test at serviceability limit state
- Air infiltration test
- Water penetration test by static pressure
- Water penetration test by cyclic pressure
- Building Maintenance Unit (BMU) restraint test
- Strength test at ultimate limit state
- Seismic test
- Seal degradation test

The seismic test involves the in-plane, lateral displacement of the cladding sample for a number of cycles at a given period. The parameters used for displacement, number of cycles and period are specified by the structural designer in accordance with the specified serviceability and ultimate limit states appropriate to the geographic region.

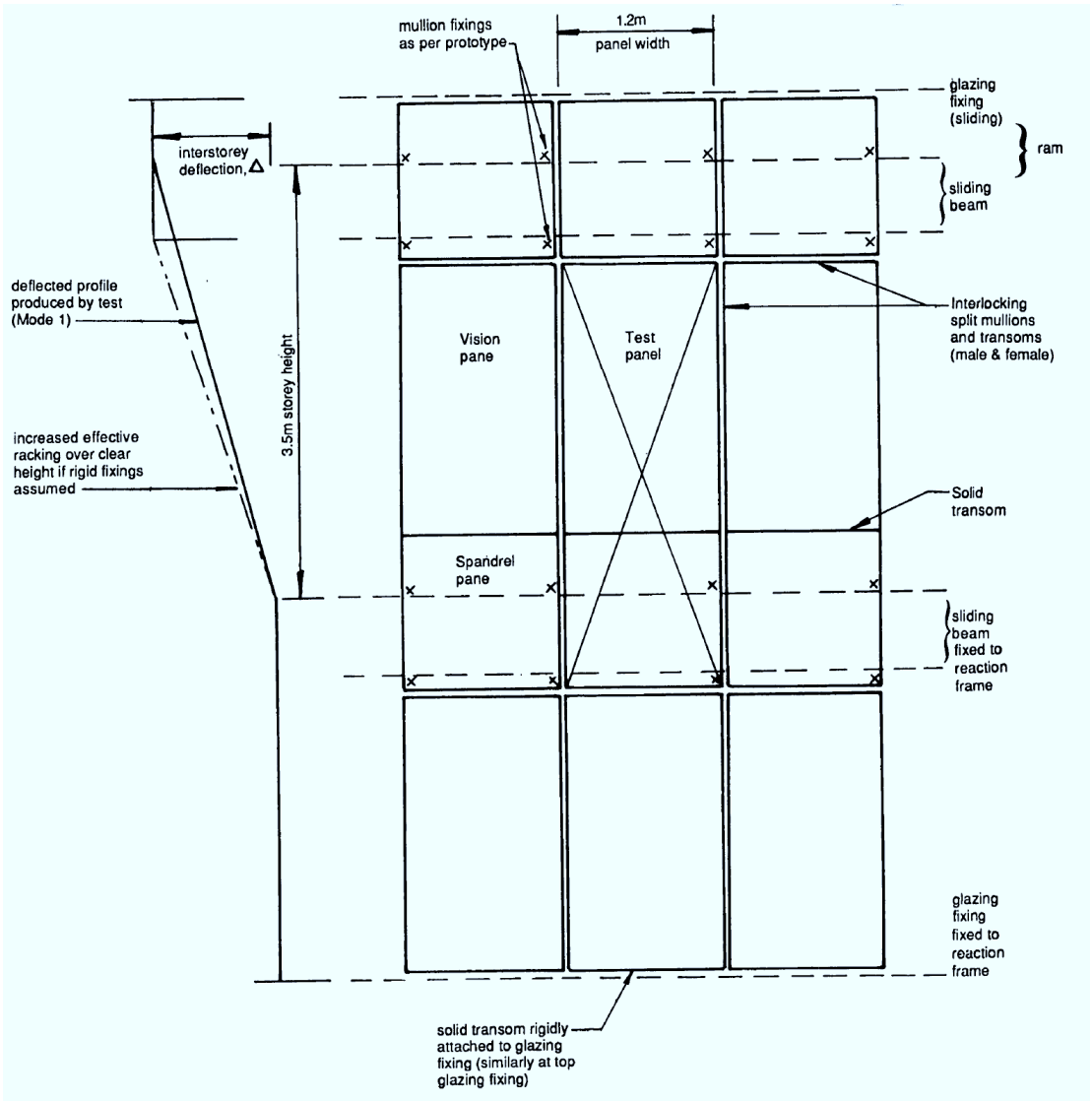

Figure 2-50: Schematic diagram of racking test (Wright, 1989)

The performance requirements for the testing are explicit and for a cladding to meet the requirements of AS/NZS 4284 (2008) it must meet all the test performance requirements. After being subjected to a racking test to SLS the cladding must not show any leaks from a cyclic water penetration test. At ULS there is to be no collapse of the test sample. Collapse of the cladding can include: disengagement of any framing member or cladding panel, failure of any fixings, repeated breakage of glass (glass may only be replaced once before the cladding is deemed to have collapsed).

2.7 Conclusions

This chapter presented a background to cladding systems in order to provide the necessary information for subsequent investigative chapters of this thesis. Since cladding

systems are not an area typically associated within the field of structural/earthquake engineering this chapter briefly summarised various architectural functions including how the performance of these functions are typically assessed.

Since performance-based assessment forms a major pillar to this research, this was introduced here in the context of cladding performance. This included a background to the assessment of both seismic and architectural performance. The seismic performance of cladding systems was shown to be primarily a function of the lateral inter-storey displacement of a structure.

A cladding classification framework was proposed for assessing the seismic performance of cladding systems. This classification framework is a necessary step in order to simplify the task of assessing the multitude of cladding systems and arrangements that exist. Although a significant portion of this thesis will focus on the performance of heavy cladding systems, it is possible that any of the cladding typologies presented here could have been the focus of this research. The classification system is therefore an important tool in order to provide the framework for all subsequent investigations into the seismic performance of cladding systems.

A survey of 217 buildings and their 266 respective cladding systems showcased all types of damage to all the different typologies of cladding systems. Earthquake damage to some cladding systems undoubtedly poses a large threat to life, with 22 cladding systems deemed outside an acceptable level of risk to life safety. The poorest performing cladding system was frameless glazing; with 50% of systems being categorised as having a Hazards Reduced performance level. This was usually due to a significant portion of the glazing falling from the system as well as the potential for this falling glazing to seriously threaten life safety.

The majority of heavy cladding systems were observed to be undamaged or have only suffered minimal damage such as cracking or torn seals. However, it is difficult to be able to observe damage to the cladding connections which were shown to be critical in determining the true cladding performance. Cladding can appear to be completely undamaged from outside as well as inside the building. However, once the internal linings are removed, it was observed that several heavy cladding systems had connections that were badly damaged or even broken. The damage is not always consistent either, making inspection of virtually every connection necessary. Examples of heavy cladding failure have a significant risk to life

safety. Unfortunately the failure of panels on one building within the Christchurch CBD, fell on to a car parked below, killing its occupant.

Due to the high risk to life-safety that precast concrete cladding presents, this research intends to focus on better understanding the behaviour of this heavy cladding systems and whether the methods used to isolate them from the structure are satisfactory. It was evident that many heavy cladding connections did not have adequate movement allowance. Several slotted connections of precast panels were also welded in place, eliminating the ability of the cladding to accommodate earthquake movement. It is vital that these common errors are communicated to ensure future failures are avoided.

2.8 References

AS/NZS 1170.0. (2002). Structural Design Actions, Part 0: General Principles. Wellington: Standards New Zealand.

AS/NZS 4284. (2008). Testing of Building Facades. Wellington: Standards New Zealand.

ATC-20. (1989). Procedures for Postearthquake Safety Evaluation of Buildings & Addendum. Redwood City, CA., USA: Applied Technology Council.

Behr, R. A. (2006). Design of Architectural Glazing to Resist Earthquakes. *Journal of Architectural Engineering, 12*(3), 122-128.

Behr, R. A., & Worrell, C. L. (1998). *Limit States for Architectural Glass Under Simulated Seismic Loadings*. Paper presented at the ATC-29-1: Seminar on Seismic Design, Retrofit, and Performance of Nonstructural Components, San Francisco, CA., USA.

Brenden, K. (2006). Dynamic Issues Drive Curtain Wall Design. *STRUCTURE Magazine*.

BS EN ISO 6946. (2010). Building components and building elements – Thermal resistance and thermal transmittance – Calculation method: International Organization for Standardization.

BS EN ISO 10140-2. (2010). Acoustics. Laboratory measurement of sound insulation of building elements. Measurement of airborne sound insulation: International Organization for Standardization.

Buchanan, A. H., & Newcombe, M. P. (2010). Performance of Residential Houses in the Darfield (Canterbury) Earthquake. *Bulletin of the New Zealand Society for Earthquake Engineering, 43*(4), 387-392.

CERC. (2012). Independent Assessment on Earthquake Performance of 43 Lichfield Street *Canterbury Earthquakes Royal Commission*.

Das, S. K. (1986). *A Study of Exterior Facades – Problems and Solutions*. Paper presented at the Application and Performance of Structural Materials and Exterior Facades, Boston, MA., USA.

Dizhur, D., Ingham, J., Moon, L., Griffith, M., Schultz, A., Senaldi, I., Magenes, G., Dickie, J., Lissel, S., Centeno, J., Ventura, C., Leite, J., & Lourenco, P. (2011). Performance of Masonry Buildings and Churches in the 22 February 2011 Christchurch Earthquake. *Bulletin of the New Zealand Society for Earthquake Engineering, 44*(4), 279-296.

Dolsek, M., & Fajfar, P. (2008). The Effect of Masonry Infills on the Seismic Response of A Four-Storey Reinforced Concrete Frame — A Deterministic Assessment. . *Engineering Structures, 30*(7).

EC8. (2004). Eurocode 8: Design of structures for earthquake resistance - Part 1: General rules, seismic actions and rules for buildings. Brussels, Belgium: CEN/TC 250.

FEMA E-74. (2011). Reducing the Risks of Nonstructural Earthquake Damage - A Practical Guide. Washington, DC., USA: Federal Emergency Management Agency.

FEMA P-58-1. (2012). Seismic Performance Assessment of Buildings *Volume 1 - Methodology*. Washington, DC., USA: Federal Emergency Management Agency.

FEMA P-750. (2009). NEHRP Recommended Seismic Provisions. Washington, DC., USA: Federal Emergency Management Agency.

Fenwick, R. C., & Megget, L. M. (1993). Elongation and load deflection characteristics of reinforced concrete members containing plastic hinge. *Bulletin of the New Zealand Society for Earthquake Engineering, 26*(1), 28 - 41.

Gates, C. (2012). Our disappearing city centre, *The Press*. Retrieved from http://www.stuff.co.nz/the-press/news/christchurch-earthquake-2011/7744317/Our-disappearing-city-centre

Goodno, B. J. (1998). *Ductile cladding connection systems for seismic design*: National Institute of Standards and Technology, Building and Fire Research Laboratory, Gaithersburg, MD.

Goodno, B. J., & Palsson, H. (1986). Analytical Studies of Building Cladding. *Journal of Structural Engineering, 112*(4), 665-676.

Henry, R. M., & Roll, F. (1986). Cladding-Frame Interaction. *Journal of Structural Engineering, 112*(4), 815-834.

Hunt, J. P., & Stojadinovic, B. (2010). *Seismic Performance Assessment and Probabilistic Repair Cost Analysis of Precast Concrete Cladding Systems for Multistory Buildings*: Berkeley: Pacific Earthquake Engineering Research Center, University of California.

Kam, W. Y., Pampanin, S., & Elwood, K. (2011). Seismic Performance of Reinforced Concrete Buildings in the 22 February Christchurch (Lyttelton) Earthquake. *Bulletin of the New Zealand Society for Earthquake Engineering, 44*(4), 239-278.

Kaneki, Y., Takeuchi, T., Miyazaki, K., & Iwata, M. (2008). Studies on Integrated Facade Engineering - Structural performance of integrated facades. *AIJ Journal of Technology and Design, 14*(27), 137-142.

Knaack, U., Klein, T., Bilow, M., & Auer, T. (2007). *Facades - Principles of Construction*. Berlin, Germany: Birkhauser Verlag AG.

MacRae, G. A., Pampanin, S., Dhakal, R. P., Palermo, A., Baird, A., & Tasligedik, A. S. (2012). Review of Design and Installation Practices for Non-Structural Components University of Canterbury.

Martins, L., Delgado, R., & Camposinhos, R. (2012). *Spider Glass Behaviour Under Seismic Action*. Paper presented at the 15th World Conference on Earthquake Engineering, Lisbon, Portugal.

MBIE. (2004). New Zealand Building Code *B1-Structure*. Wellington, New Zealand: Ministry of Business, Innovation and Employment.

MBIE. (2011). Consumer Build - Leaky Buildings Retrieved 12 Feb 2012, from http://www.consumerbuild.org.nz/publish/leaky.php

McVerry, G., Gerstenberger, M., Rhoades, D., & Stirling, M. (2012). *Spectra and PGAs for the Assessment and Reconstruction of Christchurch*. Paper presented at the 2012 New Zealand Society for Earthquake Engineering Conference, Christchurch.

New Zealand Police. (2012). List of Deceased - Christchurch Earthquake Retrieved 9th November 2012, from http://www.police.govt.nz/list-deceased

NZS 1170.5 - Supp1. (2004). Structural Design Actions, Part 5: Earthquake Actions - New Zealand - Commentary. Wellington: Standards New Zealand.

NZS 1170.5. (2004). Structural Design Actions, Part 5: Earthquake Actions - New Zealand. Wellington: Standards New Zealand.

NZS 4203. (1992). General structural design and design loadings for buildings. Wellington: Standards New Zealand.

NZSEE. (2006). Initial Seismic Assessment *Assessment and Improvement of the Structural Performance of Buildings in Earthquakes* New Zealand Society for Earthquake Engineering.

Page, I. (2008). Cladding Types in New Zealand. *BUILD,* 55-56.

Pampanin, S. (2005). Emerging Solutions for High Seismic Performance of Precast/Prestressed Concrete Buildings. *Journal of Advanced Concrete Technology, 3*(2), 207-223.

PCI. (1989). *Architectural Precast Concrete*. Chicago, IL., USA: PCI Architectural Precast Concrete Manual Committee.

PCI. (2007). *Architectural Precast Concrete*. Chicago, IL., USA: PCI Architectural Precast Concrete Manual Committee.

Phan, L. T., & Taylor, A. W. (1996). State of the Art Report on Seismic Design Requirements for Nonstructural Building Components. Gaithersburg, MD., USA: US National Institute of Standards and Technology.

Pinelli, J. P., Craig, J. I., & Goodno, B. J. (1995). Energy-Based Seismic Design of Ductile Cladding Systems. *Journal of Structural Engineering, 121*(3), 567-578.

Pinelli, J. P., Craig, J. I., Goodno, B. J., & Hsu, C. C. (1993). Passive control of building response using energy dissipating cladding connections. *Earthquake Spectra, 9*(3), 529-546.

Riccio, P. (2010). *Multi performance based design of facade systems in timber buildings.* Masters Thesis, Politecnico di Milano.

Rihal, S. S. (1988). *Earthquake resistance and behavior of architectural precast cladding and connections*. Paper presented at the Symposium on Architectural Precast Concrete Cladding, Chicago, IL., USA.

Ruggiero, S. (1995). Cladding's Ticking Time-Bombs. *Progressive Architecture, 76*.

Sachdeva, S. (2010). New building earns six-star green rating, *The Press*. Retrieved from http://www.stuff.co.nz/the-press/news/3351772/New-building-earns-six-star-green-rating

Sack, R. L., Beers, R. J., & Thomas, D. L. (1989). *Seismic Behavior of Architectural Precast Concrete Cladding*. Paper presented at the Architectural Precast Concrete Cladding - Its Contribution to Lateral Resistance of Buildings, Chicago, IL., USA.

Smith, B. S., & Gaiotti, R. (1989). *Interaction of Precast Concrete Cladding with a Story-Height Frame Module*. Paper presented at the Architectural Precast Concrete Cladding - Its Contribution to Lateral Resistance of Buildings, Chicago, IL., USA.

Stylianou, G. (2014). Insurance disputes put sites in limbo, *The Press*. Retrieved from http://www.stuff.co.nz/business/money/9881674/Insurance-disputes-put-sites-in-limbo

Tasligedik, A. S. (2014). *Damage Mitigation Strategies for Non-Structural Infill Walls.* Ph.D. Thesis, University of Canterbury, Christchurch, New Zealand.

Taylor, A. W., & Phan, L. T. (1997). *Seismic Design of Non-Structural Building Components in the United States*. Paper presented at the 29th Joint Meeting of U.S./Japan Government Cooperative Program on Natural Resources, Tsukuba, Japan.

Wright, P. D. (1989). The Development of a Procedure and Rig for Testing the Racking Resistance of Curtain Wall Glazing *SR17*: Building Research Association of New Zealand.

3 Recent Investigations into the Seismic Response and Performance of Cladding Systems

3.1 Introduction

Earthquake damage to non-structural elements has been recognised as an area of ongoing concern for several decades. One of the early recommendations that came out of a U.S. workshop into disaster mitigation, held over four decades ago, was:

> *"A multi-disciplinary programme of analytical, experimental and design studies should be conducted to acquire knowledge and develop standards for improving practices of design for non-structural building elements." (Wright et al., 1973)*

Over two decades later, a report prepared for U.S. Congress on the future needs for reducing earthquake losses to the built environment stated that:

> *"It is time for new building seismic engineering research to consider the next problem: reducing non-structural and contents damage"(U.S. Congress, 1995)*

Even so, in the past several decades, most of the research efforts in seismic engineering have focussed on improvements of the structural design of buildings to prevent collapse. This is consistent with the life-safety philosophy inherent in most international building codes. This is understandable since the consequence of collapse has more serious life safety implications than that of non-structural failure. As a result, most newly constructed buildings stand a good chance that they will not collapse during an earthquake (Phan & Taylor, 1996).

It is only recently that more attention has been paid to the performance of non-structural elements. This chapter presents a literature review of recent research into the seismic performance and behaviour of cladding systems. This includes a brief historical overview followed by a summary of previous analytical and experimental research. Since thesis will focus on the performance of heavy cladding systems, a greater emphasis will be placed upon previous research into these systems.

3.2 Background

Cladding is almost always designed as having no structural role. This approach simplifies the design process as it is assumed that any possible interaction with the primary structure is negligible. However, cladding systems are almost always connected between different parts of the structure, often spanning between two stories (Pinelli et al., 1995). Therefore, the potential for interaction between the cladding and the primary structure is apparent. This interaction may be beneficial or detrimental to the seismic performance of the building (Goodno, 1983) and this will be expanded upon later. However, firstly, understanding this interaction is of most interest.

As introduced in Chapter 2, it is common to attempt to isolate exterior cladding from the structure by using connections with flexible elements or slotted holes and placing gaps between the cladding and the structural elements (PCI, 2007). However, in seismic events, these connections may be overstrained, the gaps too small, or the slotted holes too short, and interaction between the different elements often still occurs, often resulting in cladding damage, cladding failure, or structural damage (Pinelli et al., 1995).

Interest in the effect of cladding on the structural strength and stiffness of multi-storey buildings has grown in the last 20 years. One of the first researchers to investigate the effect of cladding on the lateral response of buildings was Weidlinger (1973) who studied the behaviour of shear panels and suggested that cladding can be incorporated into the main lateral resistance system to brace against wind. Gjelvik (1973) studied the interaction between cladding panels and a supporting frame, and reported that the panels had an important effect on the lateral resistance of the supporting frame. The dynamic properties of a steel frame with cladding panels was first studied by Oppenheim (1973). The main result was that in designs where the panels have approximately the same stiffness as the supporting frame, the upper-storey panels undergo large deformations due to cladding system being in resonance with the structural frame.

3.3 Influence of Cladding on Structural Behaviour

This section contains research that examines the influence cladding has on the behaviour of the structure it is attached to. This includes the free vibration characteristics of the structure, the displacement of the structure under static loading and the displacement of the structure under dynamic loading. Some of the research summaries are adapted from abstract summaries by Cohen (1995) and Hunt and Stojadinovic (2010).

3.3.1 Participation in Seismic Resistance

The design and detailing of cladding panels, connections and the structural frame dictate how much the cladding panels and connections participate in the seismic resistance of the building. Arnold (1990) notably identified that the following four levels of cladding participation are possible:

1. Theoretical Detachment: The cladding, usually lying outside the structure, does not contribute to its lateral stiffness at all. In practice, this would very rarely be the case as in a building with hundreds of cladding panels it is likely that the detachment is not complete, and there is some transmission of forces from the structure to the panels and vice versa.
2. Accidental Participation: This occurs with connections such as slotted connections and sliding joints in which, because of being or errors in installation, the separation between the cladding and structure in not effective. The result is uncontrolled participation.
3. Controlled Stiffening or Damping: This involves the use of devices to connect the cladding to the structure in such a way that the damping of the structure is modified (usually increased) or the structure is stiffened.
4. Full Structural Participation: The cladding and the structure become a new integrated composite structure in which each element performs an assigned role. The cladding may participate in vertical support, and definitely contributes to lateral resistance.

In theory the fourth level of participation makes the most economic and dynamic sense because the cladding is removed from its role of dead weight to one of integral support. In

practice this level has proved difficult to achieve, and it has proved more economic (if not more performance effective) to use level one. Study of other structures in the dynamic environment, such as airplanes and automobiles, has shown a steady evolution from level one to level four. Today's building cladding compares to the doped fabric of a 1920s wood-structured airframe (Arnold, 1990).

The configuration or typology of the cladding can determine how much the cladding system participates in the load-resisting capacity of the structure. Arnold (1990) explains how each of these configurations might influence the behaviour of the structure:

1. Individual vertical and horizontal panels which cover the beams and columns do not effectively help in lateral resistance, but the panel system might form a composite structure to resist vertical loads.
2. Horizontal or spandrel beams cannot help in resisting lateral forces because they do not brace between the floors. Stronger panels and connections might lead to "short columns" or a strong beam / weak column situation.
3. The full-bay rectangular panels that span between floors provide the greatest chance for contribution to lateral strength.

Several research groups have investigated the interaction between cladding panels and the primary structure. Even when engineers try to isolate the panels from the structure using slotted or flexible connections, analytical and experimental studies have shown that the cladding may have a significant influence on the seismic response of the building (Henry & Roll, 1986; Palsson & Goodno, 1989; Smith & Gaiotti, 1989; Wang, 1987).

3.3.2 Free Vibration

The research team at the Georgia Institute of Technology led the way with research into the influence cladding has upon structural behaviour during the 1980s (Goodno, 1983, 1998; Goodno & Palsson, 1982, 1986; Goodno et al., 1984; Goodno et al., 1980; Palsson & Goodno, 1982). This early research studied the seismic response of steel frames with cladding panels attached. Comprehensive structural analyses were unable to predict the experimental results unless additional interstorey shear stiffness was added to the model. Goodno et al. (1980) suggested that the presence of the heavy precast cladding on the building was the cause of the variation between the numerical model and field results. Closer

examination of the cladding system, which was not designed for seismic loads, strongly suggested that the particular bolted connections using wedge insets in the cladding panels were easily capable of developing the needed additional interstorey stiffness to provide agreement between the structural model and measured modal frequencies.

Goodno (1983) compared the modal periods and dynamic response of analytical models with cladding panels to analytical models without cladding. The research created analytical models of a 25-storey steel-framed office structure to study the effect of cladding on its free vibration properties. The study building used for their models contains a central core with a moment-resisting frame in one direction and a braced frame in the other direction, as shown in Figure 3-1 (left). The core frames were designed for gravity and wind forces only. The cladding consisted of a dual panel precast concrete cladding system, with two panels per framing bay and 12 bays on each building face, as shown in Figure 3-1.

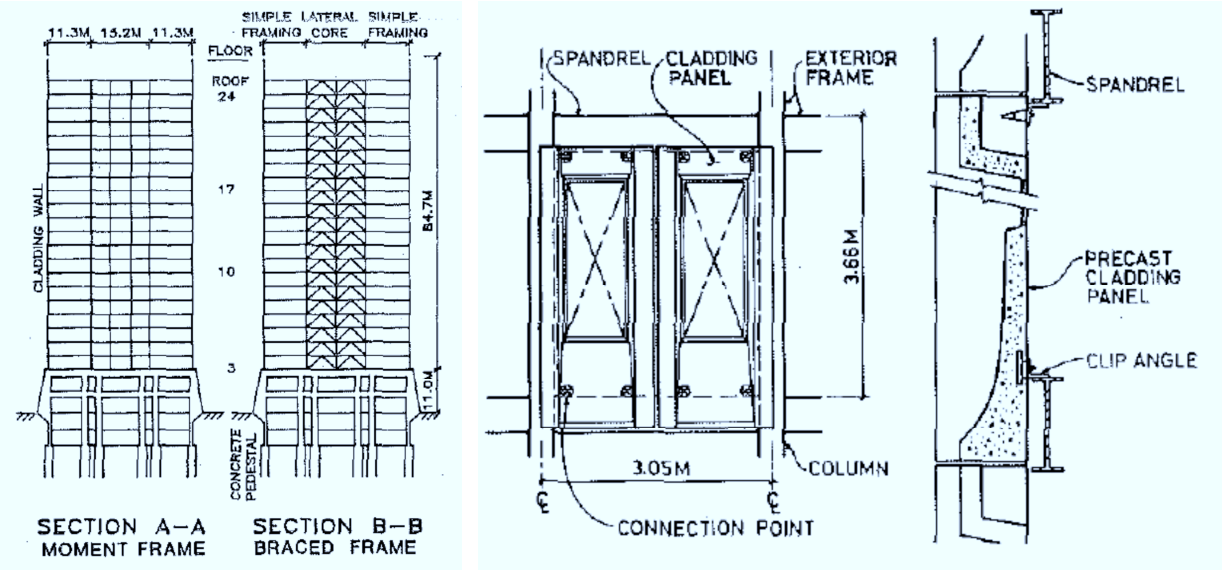

Figure 3-1: Structural system (left) and cladding system (right) investigated by Goodno (1983)

Three sets of ambient tests and one forced vibration test were performed on the building to determine the first three translational and torsional natural periods. A three-dimensional model of the bare frame structure of the building was also constructed to determine the natural periods analytically. The model was constructed as accurately as possible and considered the lateral stiffness of the interior and exterior frames and composite floor beams. When the analytical and measured periods did not agree, the researchers assumed that the difference in the periods was due to the effects of the cladding. The analytical periods of the bare frame structure were up to 34% and 48% greater than the measured translational and torsional periods, respectively (Goodno, 1983). The researchers

altered the stiffness matrix to correspond to a constant increase in interstorey shear stiffness value that represents the additional stiffness from the cladding. The value of the stiffness increase was varied until the periods of the analytical model were matched with the measured periods of the actual building. It was found a 110 kN/mm increase in stiffness to each floor best accounted for the difference in periods between analytical and actual building. Thus, the researchers concluded that the cladding decreased the translational periods by up to 34% and the torsional periods by up to 48%. The disadvantage of this approach is that the analytical model of the bare frame structure may not have accurately represented the bare frame of the real building. In addition, it is erroneous to assume that the cladding makes up for all of the difference between the analytical and measured periods. Other architectural elements would also likely contribute to the building's lateral stiffness, such as interior partitions, ceiling systems, and stairwells (Hunt & Stojadinovic, 2010).

The effect of a simple cladding system on the modal properties of a multi-storey concrete framed building was investigated with analytical models by Henry and Roll (1986). The study building was a two-dimensional, nine-storey, three-bay concrete moment-framed structure. The cladding system consisted of spandrel panels attached to the structural frame at the panel corners, as shown in Figure 3-2.

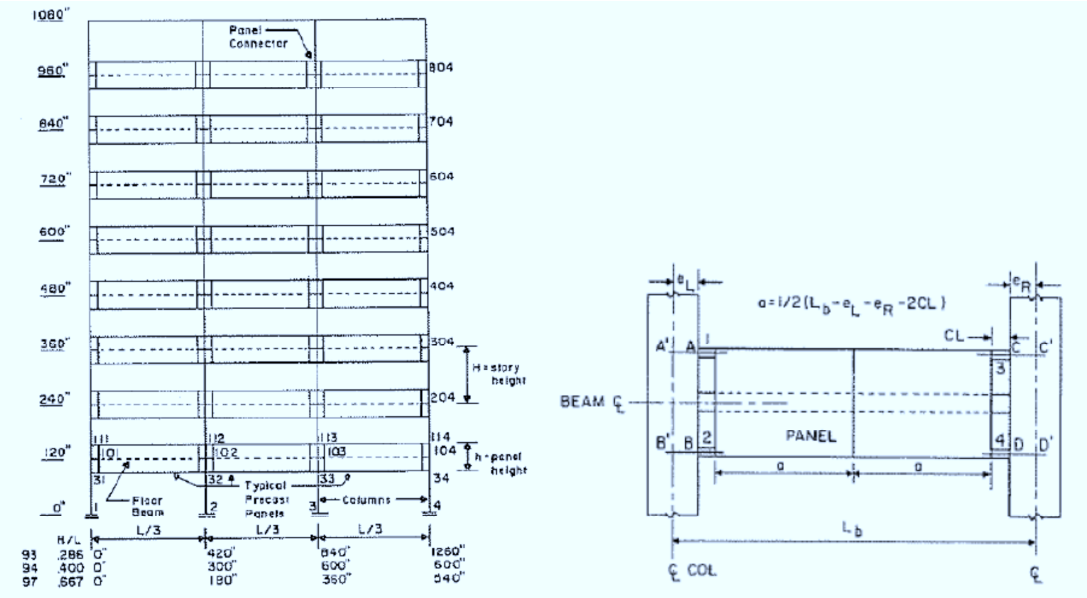

Figure 3-2: Structural system (left) and cladding system (right) investigated by Henry and Roll (1986)

The cladding panels were modelled using four-node shear elements, and the stiffness matrices for the cladding connections were modelled as rigid elastic elements with their end conditions fixed. Using this approach, all of the deformations in the cladding system occur in the panels themselves. Several models of the building were constructed to vary different

parameters: three variations of bay widths (10.7 m, 7.6 m and 4.6 m), five variations of panel heights (0.9 m, 1.5 m, 2.1 m, and 2.9 m), and two variations of concrete weight for the panels (25 kN/m^3 and 16 kN/m^3). The storey height was taken as 3.0 m. Modal analyses were performed on the bare frame structure and the structure with cladding. The inclusion of cladding was found to reduce the fundamental period of the building by between 18 and 55%.

The disadvantage of the Henry and Roll modelling approach is that the authors assume that all of the deformations in the cladding system occur in the panels themselves. Modelling the cladding system in this manner overestimates the contribution of the cladding to the lateral stiffness of the building. In reality, the shear stiffness of the cladding connectors is much lower than the panels.

The vibration properties of a high-rise building were measured while construction was in progress in order to trace the changes in the values of the parameters with construction (Meyyappa et al., 1981). The measuring process began after erection of the steel structure, prior to the installation of the cladding. The study building was a 24-storey steel office tower with a lightweight precast concrete cladding and glazing system. Ambient tests were performed to determine the free vibration periods of the first three translational modes and torsional modes.

The test results found that the first translational period of the bare frame in the N-S direction was 2.09 sec and this increased to 2.25 sec when the building was completely clad. The first translational period of the bare frame in the E-W direction was 3.11 sec and this increased to 3.13 sec when the building was completely clad. The first torsional period of the bare frame was 1.37 sec and this increased to 1.45 sec when the building was completely clad. The elongation of the periods went against previous research which suggested that the additional stiffness provided from cladding reduces the building's periods. Meyyappa et al. (1981) concluded that the period elongation could be largely attributed to the additional mass of the cladding as well as other elements that were moved into the building during construction. In this case, the stiffness of the cladding was not large enough to overcome the effects of the additional mass it provided to the building.

3.3.3 Inter-storey Displacements

The influence of cladding upon the structural behaviour of buildings was also studied by comparing the drifts of frames with and without cladding. Lateral static forces were applied by Henry and Roll (1986) to their nine-storey three-bay model shown in Figure 3-2.

Equivalent lateral static forces were applied to the structure, with and without cladding included and the lateral displacement of the frame were measured. The lateral roof displacement decreased by 75% for the case of panels that occupied 60% of the frame. As discussed previously, the drawback to these analyses is that the connectors are modelled as rigid elements and all the deformations in the cladding systems occur in the finite elements of the panels.

The effect of precast concrete cladding on the lateral response of multi-storey buildings was investigated by Charney and Harris (1989). They performed analytical studies to determine the effect that a cladding system has on the lateral displacements of a steel moment-resisting frame building. The building was four stories tall and two bays wide. The cladding system and connection details are shown in Figure 3-3,

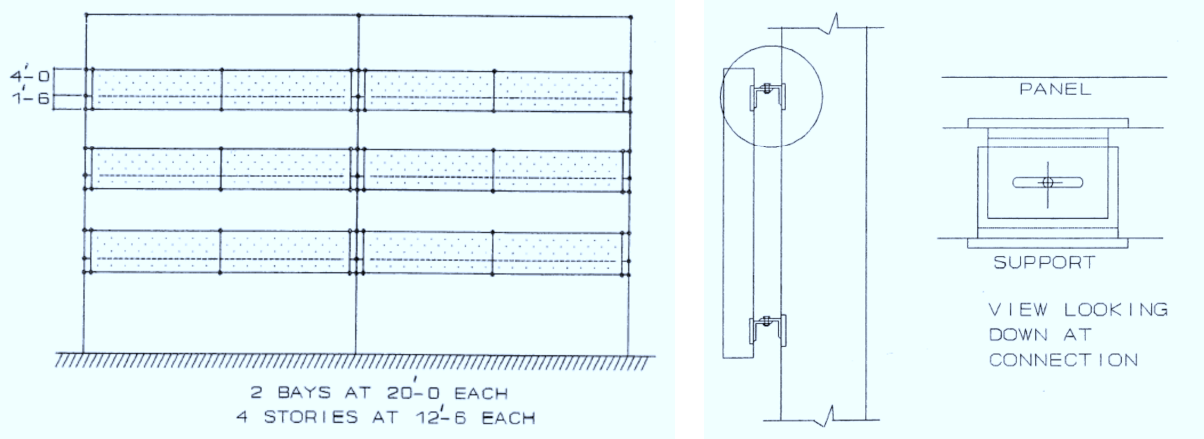

Figure 3-3: Structural system (left) and cladding system (right) investigated by (Charney & Harris, 1989)

The cladding panels were modelled with two shear elements per bay, and the cladding connections were modelled as short beams (with fixed-end conditions) 100 mm in length with a cross section of 13 x 150 mm. It was assumed the connections were bending about their minor axis. The analytical model was subjected to lateral loads of 90 kN at the first three stories and 45 kN at the roof, and the lateral displacement of the third storey was recorded. The primary variable in the analysis was the panel thickness. The effect of the third floor displacement was computed in terms of beam deformation, column deformation, connection deformation, and panel deformation, with the results reproduced in Table 3-1.

The inclusion of a thin 50 mm (2 inch) thick panel decreases the total lateral drift by approximately 28%. For this panel, the connectors and panels contributed 14.4% and 8.4%, respectively, to the total drift. However, when the panel thickness is increased to 150 mm, the percentages change to 20.3% and 4.3% for the connectors and panels. For the 1.5 m thick panel (which represents the infinitely rigid case), the total drift reduced to 7 mm, with the

connector being responsible for 24.4% of the total. The total panel-connector contribution was approximately 24% in each of the analyses that included the effect of cladding. This would seem to suggest that in some applications, negligible loss of accuracy would result from modelling panels as infinitely rigid.

Table 3-1: Panel thickness effect upon deformation contributions (Charney & Harris, 1989)

Panel Thickness (inches)	Deformation Source (inches)				
	Beams	Columns	Connections	Panels	Total
0.0	0.1940	0.2580	-	-	0.4520
2.0	0.0713	0.1796	0.0468	0.0272	0.3249
4.0	0.0614	0.1738	0.0575	0.0174	0.3101
6.0	0.0577	0.1716	0.0619	0.0130	0.3042
60.0	0.0503	0.1700	0.0714	0.0004	0.2921

As mentioned in Henry and Roll (1986), the panels may redistribute the shear forces and bending moments in the beams and columns. The authors concluded that the cladding can cause the effective height of the column to decrease, and consequently, the shear force in the column increases drastically. This situation may result in a short-column shear failure mode, as shown in Figure 3-4.

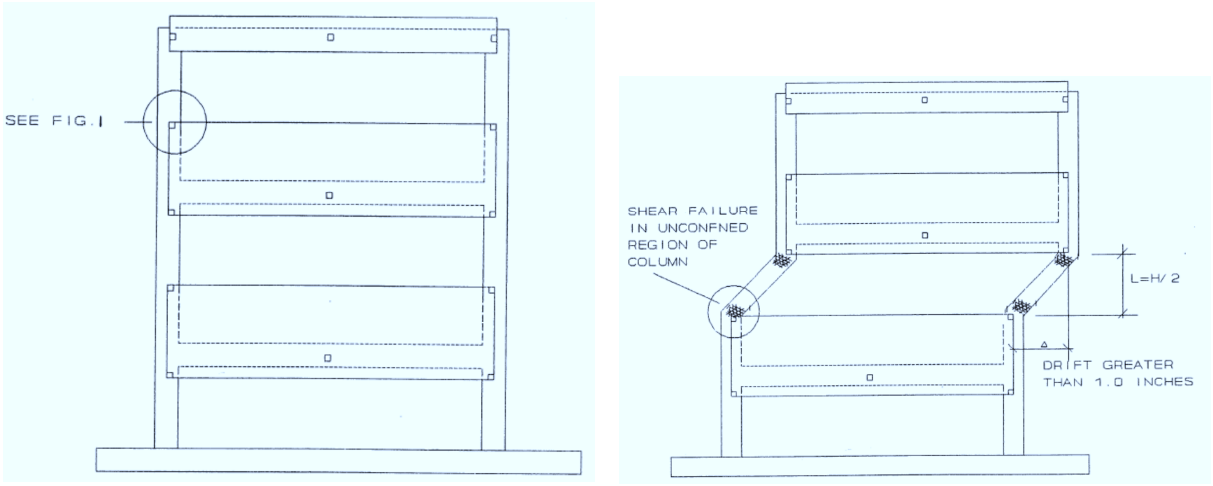

Figure 3-4: Frame with cladding panels (left) and short column effect (right) (Charney & Harris, 1989)

The researchers at the Georgia Institute of Technology performed a limited number of time-history analyses using the analytical model of the 25-storey study building shown previously in Figure 3-1. Four different analytical models of the cladding system were considered. The first involved adding a constant interstorey shear stiffness value (calculated by matching the modal periods of the analytical bare frame model and measured period of the actual building) to the stiffness matrix of the bare frame model. As discussed previously, the

drawback in estimating the interstorey stiffness of the cladding with this approach is that it assumes that the analytical model of the bare frame is perfectly predicts the modal periods of the building's bare frame. Also, this approach neglects the other important non-structural contributions to the interstorey shear stiffness. As was previously identified, the cladding was represented by a constant interstorey shear stiffness of 110 kN/m.

Time-history analyses were performed by Goodno and Palsson (1986) when they subjected the 25-storey building to the 1940 El Centro and 1966 Parkfield earthquake ground motion records. The maximum seismic drifts for the two earthquakes are shown in Figure 3-5. The drifts are slightly higher in the clad frame than the bare frame structure for the El Centro motion, while for the Parkfield motion, the drifts in the frame with cladding are less than the drifts in the bare frame structure in the upper stories. The results were found to be highly sensitive to the ground motion used.

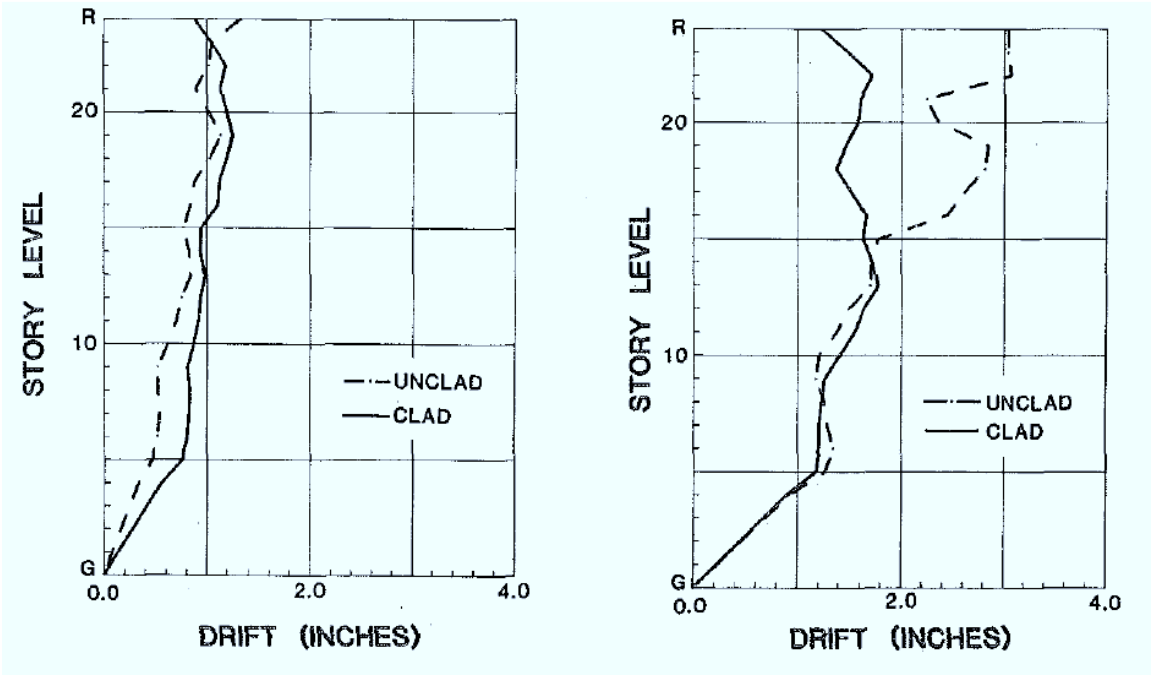

Figure 3-5: Peak inter-storey drift for clad and unclad building during the 1940 El Centro earthquake (left) and 1966 Parkfield earthquake (right) (Goodno & Palsson, 1986)

Goodno and Palsson (1986) also investigated different methods to represent the stiffness of the cladding. These methods included an incremental failure model, hysteresis model and slotted connection model. The incremental failure model represented a progressive failure of the cladding. Failure was defined as graduated loss of cladding stiffness as allowable drift limits were exceeded at different levels. The hysteresis model contained an elasto-plastic hysteretic rule but load degradation was not considered. The slotted connection model was implemented in the form of a piecewise-linear force-drift relationship that sharply

increases in stiffness once the slot length was exceeded (the slot length was 18 mm). Drift envelopes for the hysteretic, slotted and inter-storey shear stiffness models were very similar.

A similar study was conducted which subjected the same analytical model to time-history analyses of six other ground motions, and the maximum roof displacements were recorded for each motion (Goodno et al., 1980). The maximum roof displacements of the frame with cladding were less than the maximum roof displacements of the bare frame for three of the ground motions (14%, 22%, and 38% decrease). For the other three ground motions, the maximum roof displacements in the frame with cladding were larger than those in the bare frame (54%, 67%, and 82% increase). These results emphasised the high sensitivity the ground motions selected have in determining the effect cladding has upon structural behaviour.

Wolz et al. (1992) used an analytical model and time-history analyses to study the response of a building with cladding. The study building was a six-storey, ¼ scale model of a moment-resisting frame that had two cladding panels per bay. The cladding panels were represented by truss members and were assumed to be rigid in-plane with attachment points located at the beam-column joints and at the mid-span of the beams on two successive floor levels. The lower two cladding connectors were rigid, while the upper two cladding connectors were flexible. The horizontal force-deformation relationship of the flexible connections was assumed to be bi-linear with an arbitrarily assigned initial stiffness of 17.5 kN/m. The model was subjected to one input of ground acceleration, a two-sided pulse with maximum amplitude of 0.3 g. The time-history of the roof displacement of the bare frame model and the model with cladding were recorded and are shown in Figure 3-6. The maximum roof displacement of the model with cladding was approximately 33% less than the roof displacement of the bare frame model.

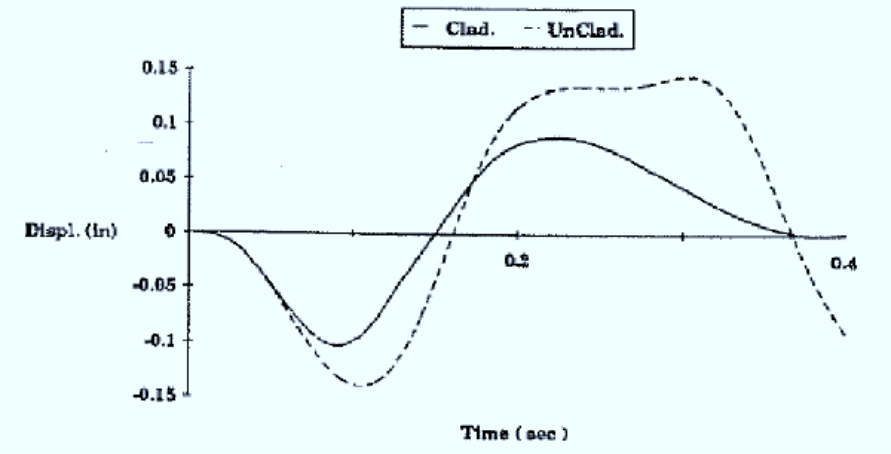

Figure 3-6: Time-history of roof drift (Wolz et al., 1992)

Thiel et al. (1986) studied the effect that the cladding had on the damping properties of a ductile steel moment-frame. The researchers performed non-linear time-history analyses of a hypothetical 15-storey building of uniform mass and stiffness. The cladding was represented by dampers lumped at each floor and idealised as having elastic-perfectly plastic behaviour. The building was subjected to a base motion accelerogram and the roof displacement and equivalent base shear were recorded during the time-history analyses. Considering 2% viscous damping in the frame, the cladding dampers reduced the maximum roof displacement response by approximately 40% and the base shear by 45%. The authors argued that the effective damping of a building can be increased through activation of part of the lateral force resistance capacity of the cladding panels and controlled hysteretic behaviour of their connections to the structure. However, the cladding connections require unrealistically high stiffness to be as effective as the research suggests.

3.4 Experimental Investigations

Up until recently, there has been relatively little attention given to experimentally testing the structural performance of either cladding panels themselves, their connection elements, or of cladding-structure systems. When testing of cladding is performed, the objective is almost always to determine the architectural performance of the cladding, e.g. sealant performance, resistance to wind, thermal rating, etc. (refer to Chapter 2 for further information on architectural performance). Information on structural performance is usually only of interest when problems are encountered during the tests. Such information is almost always not shared due to it being highly commercially sensitive.

There is a general feeling that cladding connections that aim to isolate the cladding from the structure, such as the tie-back or slotted connection presented in Chapter 2, will work properly (Goodno & Craig, 1989). As a result, there is only a limited amount of test data available today, and much of it is for structural components that are also employed in other applications, e.g. concrete anchor systems. There have been almost no experimental studies of cladding panels themselves, a situation that may be due to the complexity of such tests and their relatively high cost compared to component level tests.

The earliest experimental studies of cladding were concerned with validating numerical studies which demonstrated the significant lateral stiffening that cladding may introduce. These studies involved full-scale testing of high-rise buildings. Both ambient level vibration measurement and force vibration testing were used to determine overall building natural

frequencies, modal damping, and mode shapes for multi-axis bending and torsion modes. The inter-storey shear stiffness of the cladding was estimated using this approach, and while the identified stiffness were well within the capacities of the particular precast panels employed on the study building, the governing factor was the connection between the panels and structure, rather than the panels themselves (Goodno & Craig, 1989).

Rihal (1989) carried out similar in-plane dynamic tests of a large precast concrete cladding panel, shown in Figure 3-7, measuring the displacement of the connection elements.

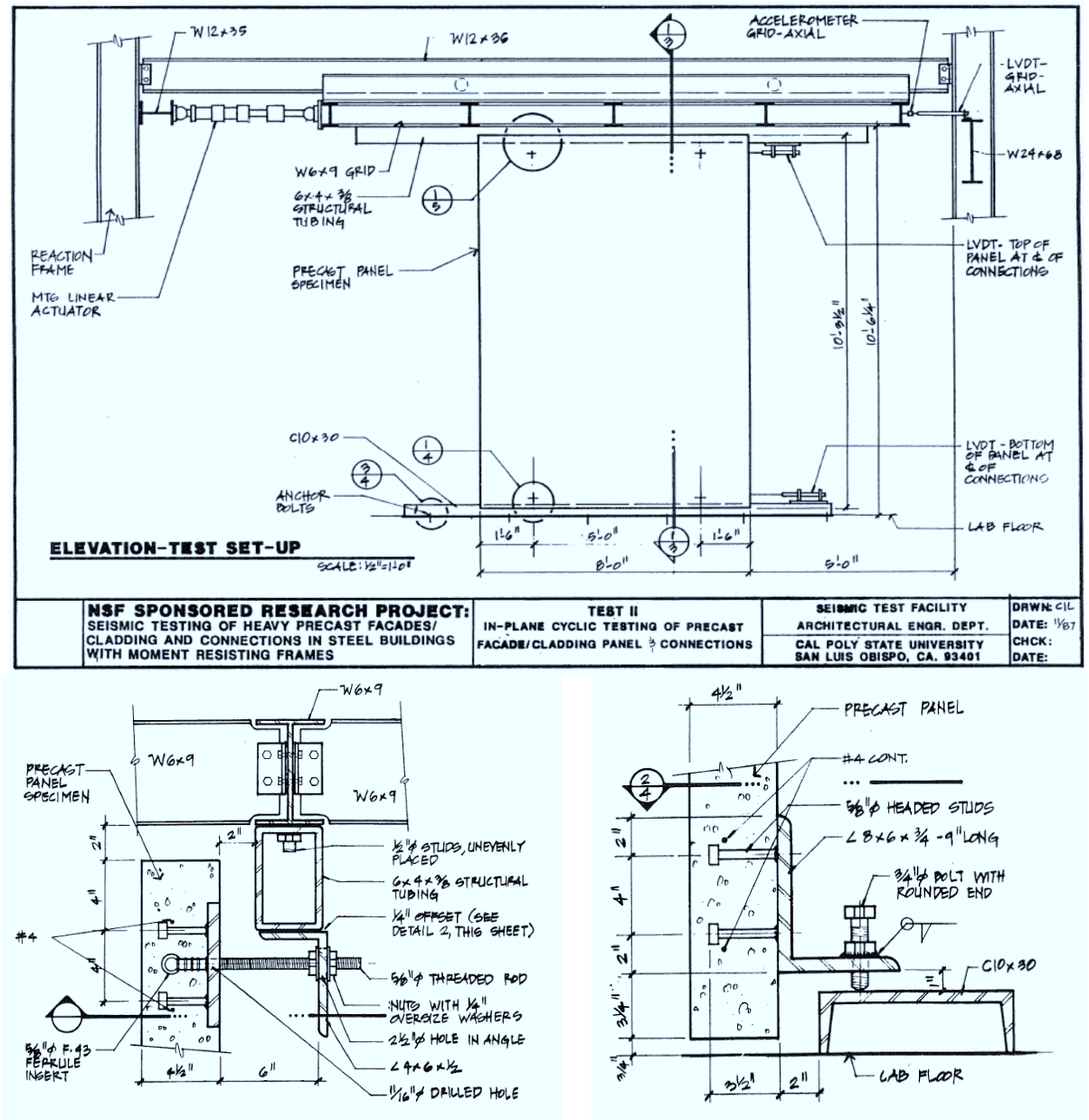

Figure 3-7: Cladding panel test setup (top), cladding speciment connection details – top tie-back connection (bottom left), bottom bearing connection (bottom right) (Rihal, 1989)

The test structure was a two-storey steel moment-resisting frame structure with one bay in each direction. The precast cladding panels were 115 mm thick, and the width and height

of the panels were established so that the mass of the cladding panels expressed as a percentage of the mass of the steel test structure is the same as in a full-scale building.

The cladding configuration and connection details were developed in consultation with a precast manufacturer who fabricated the cladding system in accordance with current U.S. practices. The modal response of the test structure was measured experimentally using random and sinusoidal excitations. The first two translational modal periods of the bare frame structure in the N-S direction were 0.14 sec and 0.05 sec. With cladding attached, the first two translational modal periods were 0.17 sec and 0.06 sec. One possible explanation offered by Rihal for the increase in period after adding the cladding is that the effects of the added mass of the precast panels seems to have overcome the additional stiffening offered by the cladding panels and connection assemblies to the test structure.

3.4.1 Full Scale Static Testing

In 1979, a U.S.–Japan testing program was performed on a full-scale steel structure to determine the seismic performance of non-structural elements (Wang, 1986, 1987; Wang & Bassler, 1992). The test building was six stories tall with storey heights of 3.4 m, as shown in Figure 3-8. There were two bays of framing 7.5 m wide in each direction of the building.

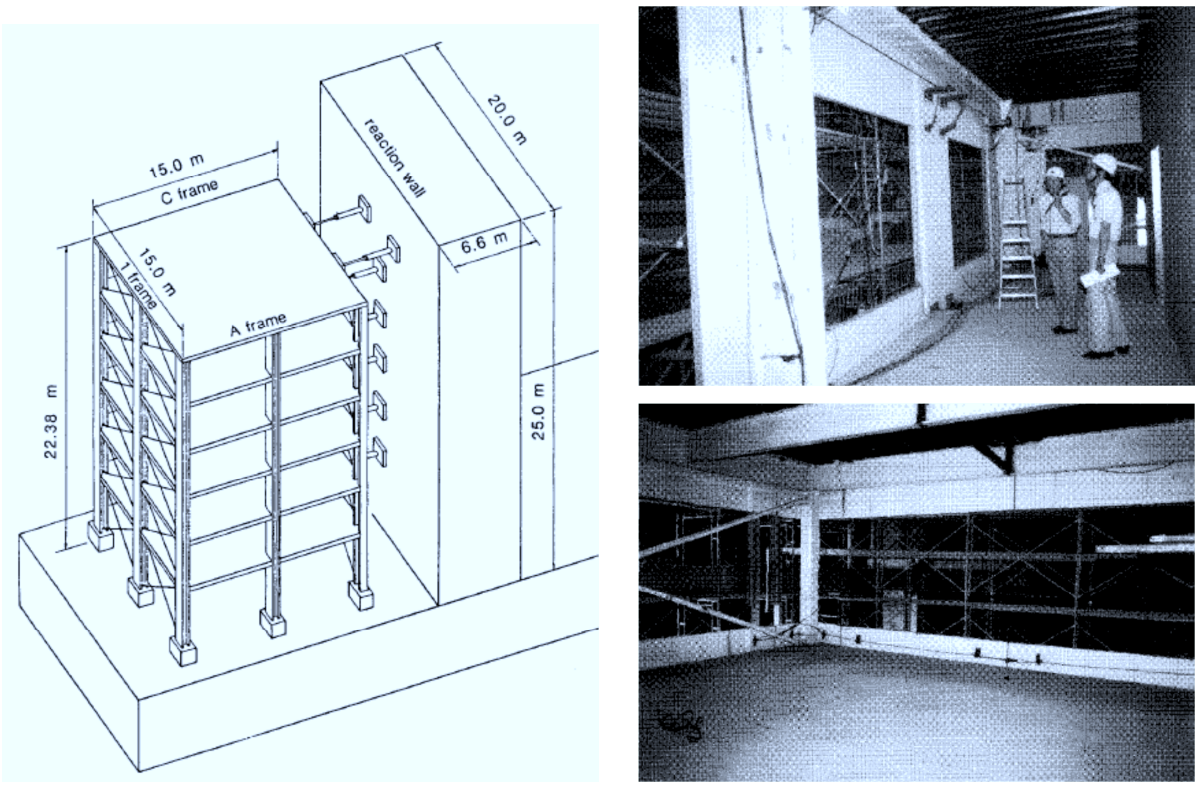

Figure 3-8: Six storey test frame (left) and precast concrete cladding connected to frame (right) (Wang, 1987)

The three-dimensional test specimen demonstrated the behaviour and interaction of cladding that isolated assemblages would not. The test building was constructed with interior partitions, ceilings, doors, and exterior cladding. Both Japanese and U.S. precast cladding systems were attached to the building, as shown in Figure 3-9.

A statically applied loading sequence was applied to the building to determine the seismic performance of the non-structural elements. However, prior to the static testing of the frame, the Japanese side conducted free vibration and forced vibration tests before and after the installation of the non-structural elements to ascertain the stiffness and period of the structure. The addition of the non-structural elements reduced the natural period of the building by 30%, which suggests that the overall structural stiffness was increased by more than 100% (Foutch et al., 1986). However, after 8 cycles of testing at a storey drift of 0.3%, most of this additional stiffness had been lost. The stiffness was deemed to have decreased due to damage of the non-structural elements. Despite these insights from the free vibration tests, it is not possible to separate the contribution of the cladding because the free vibration tests included either all or none of the non-structural components.

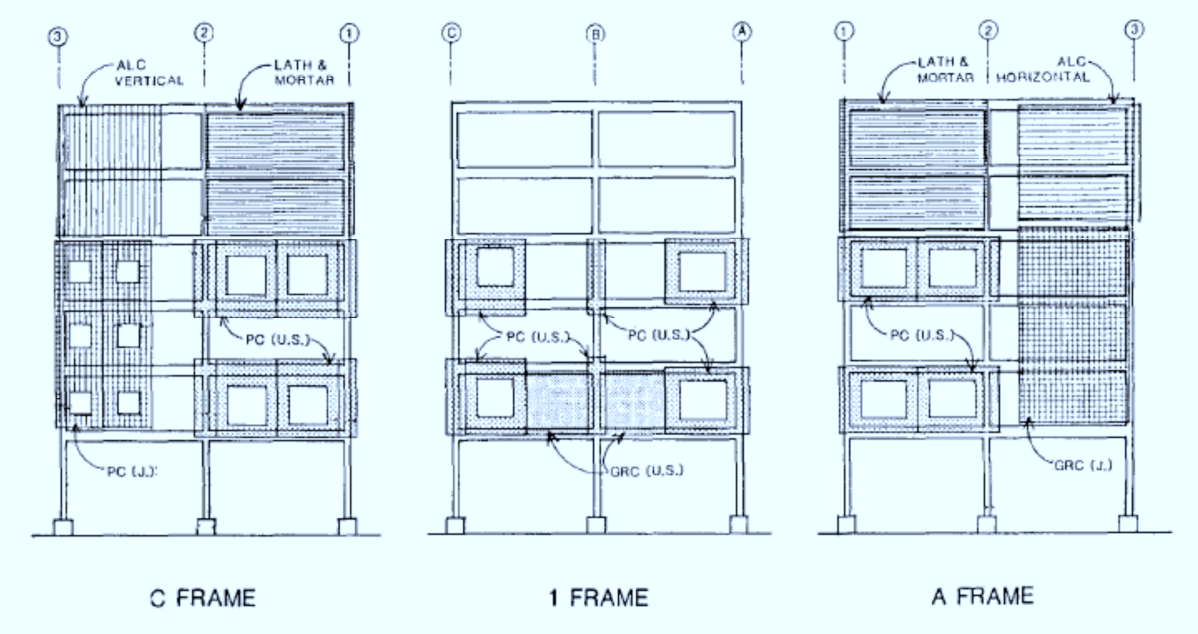

Figure 3-9: Elevation of frame with US and Japan cladding elements (Wang, 1987)

The six-storey structure was tested statically with actuators that provided horizontal forces at each storey. The structure was displaced so that each storey had approximately the same interstorey drift (linear shape) with a loading sequence that consisted of alternate positive and negative displacements. The loading sequence started with drifts of 0.1%, increasing to 0.8% for several cycles and then finally up to 2.5%. Several different cladding

systems were attached to the structure, including rocking systems and sway systems with deformable connections. The panels on floor 2 were connected with angle bearing connections and long-rod lateral connections, and the panels on floor 4 were connected with tube bearing connections and slotted angle lateral connections. Details of the connections are illustrated in Figure 3-10.

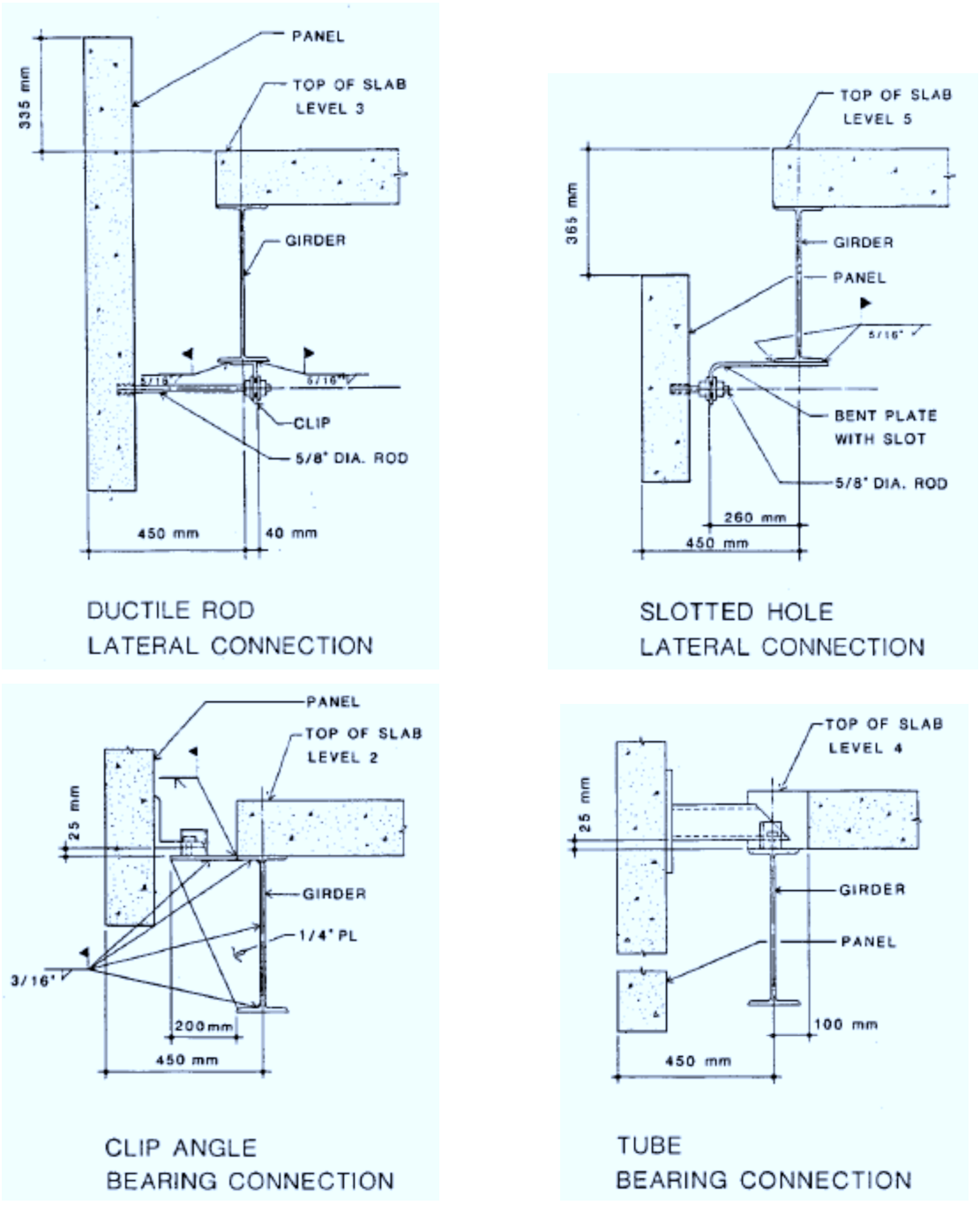

Figure 3-10: U.S. lateral (top) and bearing (bottom) connection details for cladding panels (Wang, 1987)

Many of the sliding connections were the first to exhibit visible deterioration, which quickly accelerated into total failure at many points. Visible failure of a short-rod slotted

connection began at a drift of 0.8%. This early progression of damage was attributed to the fact that some of the slotted connections were incorrectly installed by over tightening the bolts. The test was stopped and the connections were loosened, after which they started sliding as intended. However, it was found that the slot width was inadequate to accommodate the structural drift. The long-rod connections were found to perform much better and possessed significant ductility. Some cracking of the concrete in the cladding panels occurred at the bearing connections because these connections were so stiff.

3.4.2 Shake Table Component Testing

Full-scale precast concrete cladding panels were tested in 2011 on a full-scale five-story steel frame building at the E-Defence shake table facility in Japan by McMullin et al. (2012). The testing was aimed at evaluating the acceleration of the cladding panels and the effectiveness of the current slotted-bolt sliding connection to allow for inter-story earthquake motion. The panels were designed according to common U.S. practice. The panels were cast in Japan and the steel connections were designed and fabricated in the US to accurately simulate the behaviour of American cladding construction. A 50 mm vertical seismic joint was installed between the two panels. Two full-height column cover panels were tested, a return cover 3D shape, and a flat panel, as shown in Figure 3-11.

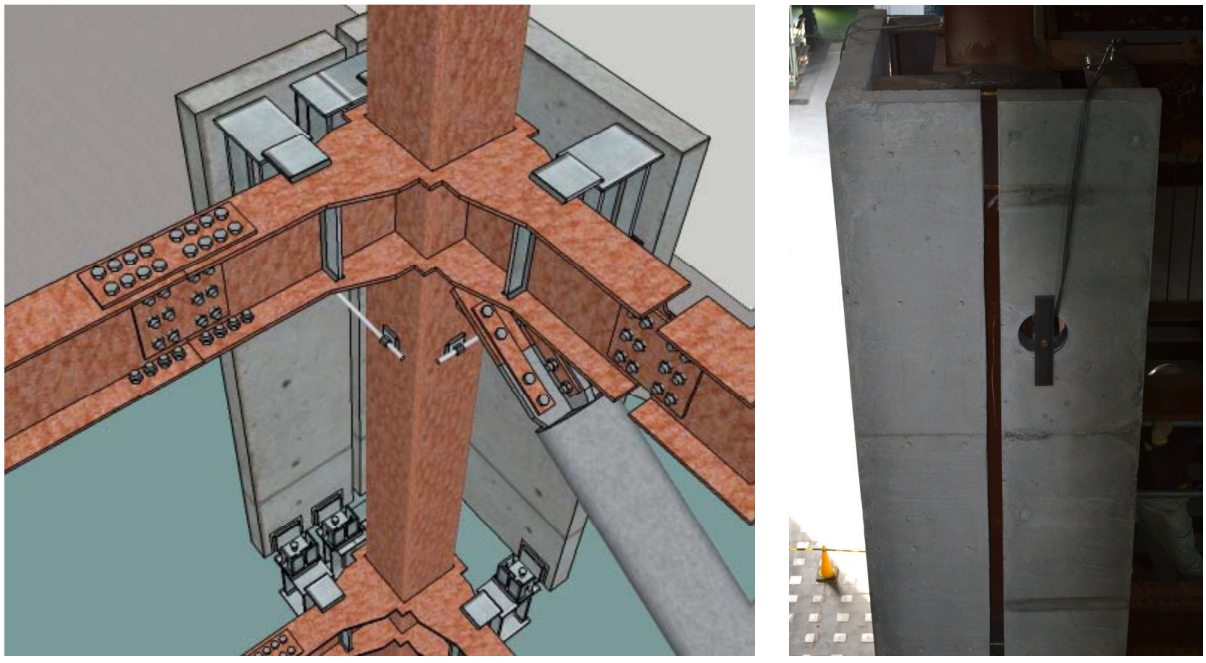

Figure 3-11: Cladding panels tested on E-Defence Shake Table in Japan (McMullin et al., 2012)

Instrumentation measured the acceleration of the panels and the movement of the slotted connections. Findings include the ability of slotted connections to slide while being

accelerated in a full scale 3D seismic motion and development of fragility curves relating damage to panel and/or floor acceleration. The connections were slotted vertically to accommodate inter-story drift though racking of individual panels, as shown in Figure 3-12.

The study found that the cladding performed very well under dynamic seismic loading. Peak floor accelerations of 0.8 g were applied simultaneously to the test specimen with no observed damage. Peak panel accelerations of 1.3 g were recorded. The rocking action of the bottom connections allowed inter-story drifts of 0.2%.

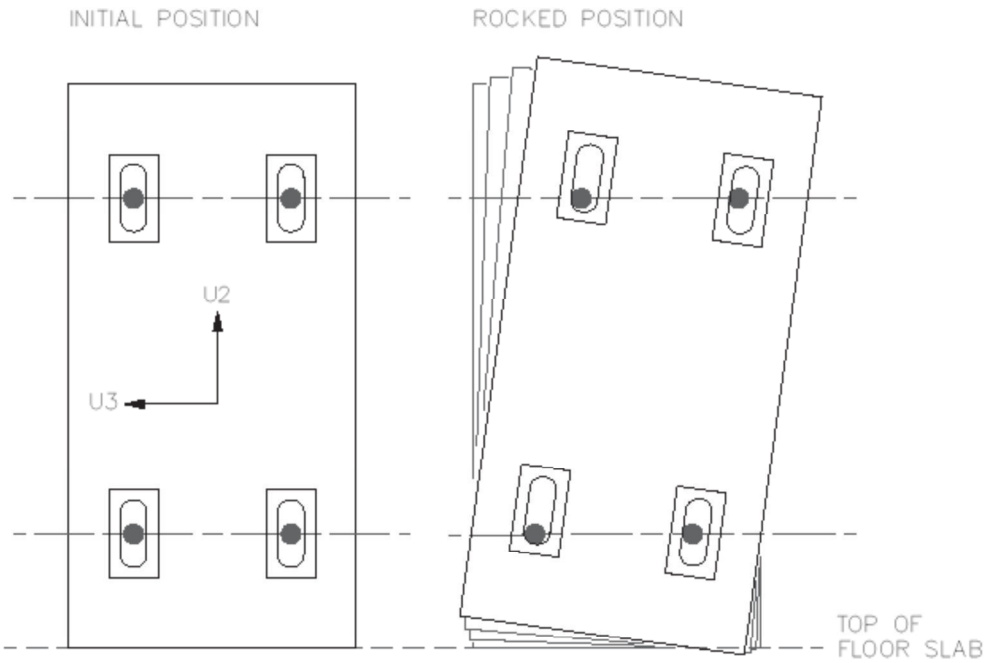

Figure 3-12: Racking of individual panels by use of vertically slotted connections (McMullin et al., 2012)

3.4.3 Full Scale Shake-Table Testing

A landmark experimental testing project was undertaken at the University of California, San Diego in 2012. The Building Non-structural Components and Systems (BNCS) Project involved the seismic testing of a five-story building, as shown in Figure 3-13, which was completely furnished with non-structural elements, including a functioning passenger elevator, partition walls, cladding and glazing systems, piping, HVAC, ceiling, sprinklers, building contents, as well as passive and active fire systems (Chen et al., 2012; Hutchinson et al., 2013; Pantoli et al., 2013).

The full-scale five-story building was tested on the Network for Earthquake Engineering Simulation (NEES) Large Outdoor High-Performance Shake Table at the University of California, San Diego.

Figure 3-13: Five storey shake-table test for the Building Non-structural Components and Systems (BNCS) Project University of California, San Diego (Hutchinson et al., 2013)

Two different types of façades were installed on the building, namely a lightweight metal stud system overlaid with stucco (bottom half of building) and a punched window-style precast concrete cladding system (top half of building). Tie-back, sliding, flexing, and a new yielding connection were investigated within the cladding system. A variation to the panel corner detail was also tested.

The tie-back connections tested investigated the ratio of rod length to rod diameter. The testing found that these connections benefit from longer rod lengths. The longer rod length helps reduce inelastic strains in the rod for a given displacement. However, it should be noted that from a practical point of view, long rods may require too much space, infringing on interior finishes rather than being concealed in the perimeter framing spaces.

The sliding (or slotted) connections consisted of a rod and oversized hole in the support clip angle, with long plate washers either side to maintain contact. Sliding connections can also be constructed with an embedded channel that allows the bolt to slide inside the channel

on the panel side of the connection. This configuration was not tested. It was found that, a sliding connection works best when the surface with the slot is close to the surface that is sliding, i.e. when the rod is short. If the sliding rod is too long, bending and rotation of the rod will cause the connection to bind, limiting the connections ability to slide and overstressing the connection. This in turn may lead to yielding of the rod, damage to its connecting elements, or damage to the panel itself. Several rod lengths were tested for each of the sliding and flexing rod connections.

Pictures of the long tie-back rod connection and sliding connection are shown in Figure 3-14 along with diagrams to explain how each connection accommodates inter-storey drift. The panels on the west side of the building were installed with sliding rod connections, while those on the eastern side were installed with long tie-back rod connections.

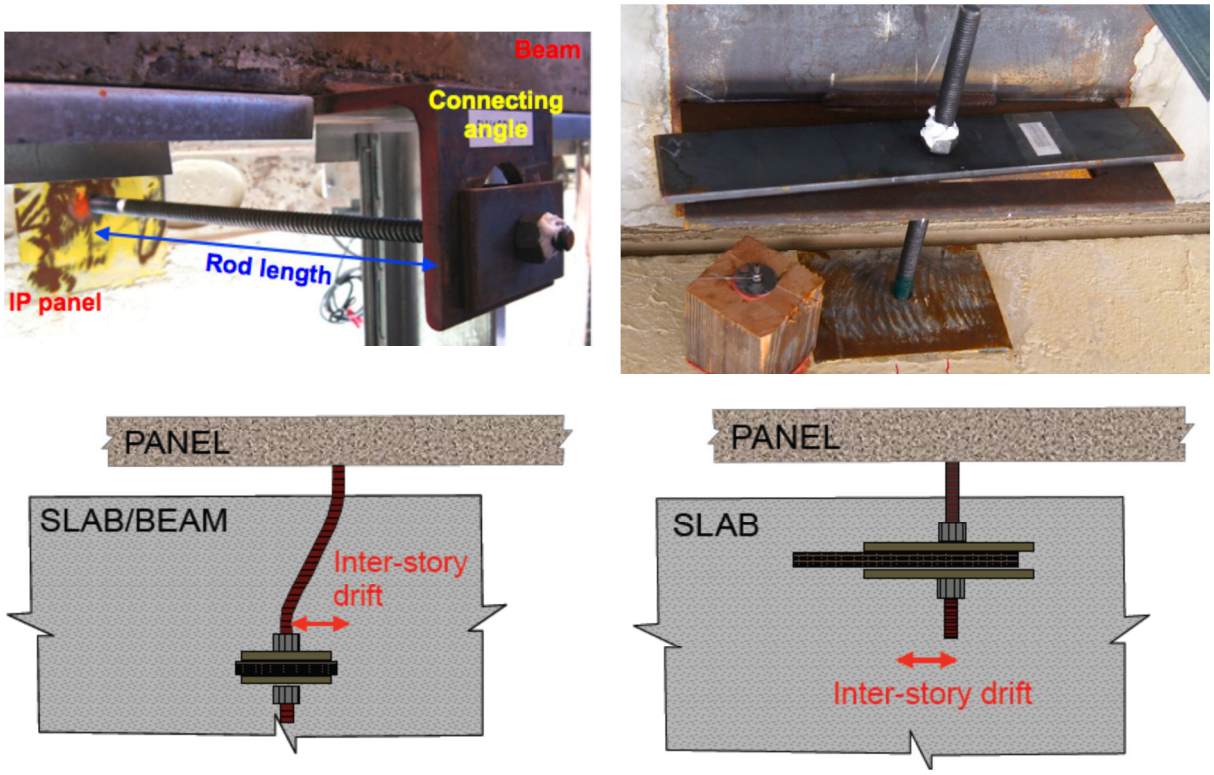

Figure 3-14: Long tie-back rod connections (left) and slotted connections (right) tested for the Building Non-structural Components and Systems (BNCS) Project (Pantoli et al., 2013)

The building was initially tested while isolated from the shake table with four high damping rubber bearings installed between at each of the four corners of the structure. Following the base isolation test phase, the foundation was fixed to the table and the building was then tested with a fixed base configuration. The building was subjected to a suite of earthquake motions of increasing intensity. In addition, white noise and pulse-based excitation were input before and after each earthquake motion input. Initial motions were

selected and scaled to an intensity associated with a serviceability event. Motions from the Maule, Chile (2010) and the Pisco, Peru (2007) earthquakes were chosen due to their inherently long duration of strong shaking. The latter record was also input into the model multiple times at increasing amplitudes. Two final motions were scaled records obtained during the Denali earthquake in Alaska (2002). The goal of these motions was to reach and exceed the design level earthquake.

Inspection of residual damage after each test motion revealed that the connections did not have any substantial damage during the base-isolated motions. During the fixed-base tests however, plastic yielding of both the flexing rod and sliding rod connections was observed, with the exception of the sliding short rod connections, which showed no signs of damage under any test. Sliding rods of a medium length showed minor plastic yielding in most of the tests. Flexing rod connections behaved better, with plastic yielding observed during the design and maximum credible scaled earthquake motions.

Displacement absorbed by the connection was compared with the interstorey drift for all of the panels. In contrast to static testing, the peak deflection of the panel and connection was found to often exceed the peak inter-storey displacement. This was believed to be due to frictional effects in the slotted connections, as well as from the dynamic interaction between the structure and cladding panels.

3.5 Cladding Panel Connections

The behaviour of the panel-to-structure connections has a significant influence on the amount of interaction between the cladding panel system and supporting framing (Hunt & Stojadinovic, 2010). If very stiff and high-strength connections are used along with inadequate joint widths, the cladding system may act as an external shear wall and cause significant damage to the cladding. If attached in this way, research presented previously identified that the cladding system may shorten the fundamental period of the building resulting in an unintended increased in seismic forces. If the cladding is rigidly attached, the panels may induce force redistribution in the lateral-force-resisting system, causing increased shear or moment forces in the columns or beams.

The stiffness and strength of panel connections vary widely among different buildings (Smith & Gaiotti, 1989). The large variety of cladding and connection configurations limits the ability to collect and document data on how cladding systems affect the response of buildings. This lack of data has made it difficult to develop realistic models for cladding

systems (Goodno & Craig, 1989). This section summarises previous research on the behaviour of panel connections.

3.5.1 Connection Strength, Stiffness and Ductility

The two most important qualities of cladding connections are sufficient strength and adequate ductility (Iverson, 1989). Cladding connections must have adequate strength to transfer wind loads and inertial loads from the cladding to the structure. They must also have adequate ductility to be able to deform under lateral displacement to accommodate any differential movements between the stiff cladding and flexible frame under seismic events without transferring large forces into the cladding (Korista, 1989). It is typically the responsibility of the engineer to ensure that the connection possesses these two qualities. Adequate anchorage of the connection to the panel is also required to avoid failure and ensure stability. Engineers may use "confining hoops, deformed bar anchors, or long reinforcing bars welded to plates" to create sufficient anchorage of the connection to the concrete panel (Cohen, 1995).

Rihal (1989) undertook a testing program to investigate the earthquake resistance and behaviour of precast cladding and connections in medium-rise steel-framed buildings. As presented previously in Figure 3-7, a cladding panel with bearing connections at the bottom and threaded rod push-pull connections at the top were tested with a cyclic loading pattern. The precast cladding panel was 2.4 m wide x 3 m high x 114 mm thick. Two 16 mm diameter threaded rods were attached to the top of the panel, and two bearing connections were attached to the bottom. The in-plane resistance was controlled by the lateral deformation capacity of the top threaded rod connections. The 200 mm long threaded rod failed at an applied load of 5 kN and an interstorey drift of 1.2%.

Behaviour of threaded-rod connections showed evidence of strain-hardening. Rihal (1989) recommended that this strain-hardening should be taken into account in the seismic design of precast concrete cladding. While the tests provided good data on the elast-plastic beahviour of the connection components, they also revelaed that the rods are highly susceptible to low-cycle fatigue failure after as few as 20 cycles of loading at displacements within currently allowable interstorey drift limits. This work demonstrated that low-cyle fatigue of this popular isolating connection element may be a problem.

The work by Sack et al. (1989) included tests of certain types of connection elements under in-plane dynamic loading. The connection tests included rod elements connected to the

structure with steel angles and threaded inserts in the concrete. In contrast to typical anchor tests, which generally report pull-out capacity, these tests were designed to explore the behaviour of the connections and anchors under lateral loads representative of cladding applications. The results of the test demonstrate that the panel connections perform as ideally elastic perfectly plastic materials. It was noted that the steel face plates did not enhance the behaviour of connections using single inserts and threaded bars, and the energy dissipation characteristics of the connections could be based on the product of the interstorey drift and the plastic load limit. During the cyclic tests, the concrete of the panels maintained its integrity.

The behaviour of steel inserts in cladding panels was investigated by Craig (1986) to determine their lateral stiffness, energy dissipation, and ductility. The test specimens were angle inserts placed in a 900 x 900 x 160 mm concrete panel, and the inserts were subjected to shear, moment, and pull-out tests, as shown in Figure 3-15. The method of failure was the undesirable mode of concrete fracture, with the research suggesting that a better design would be to integrate the insert with the panel reinforcing steel (Craig et al., 1989).

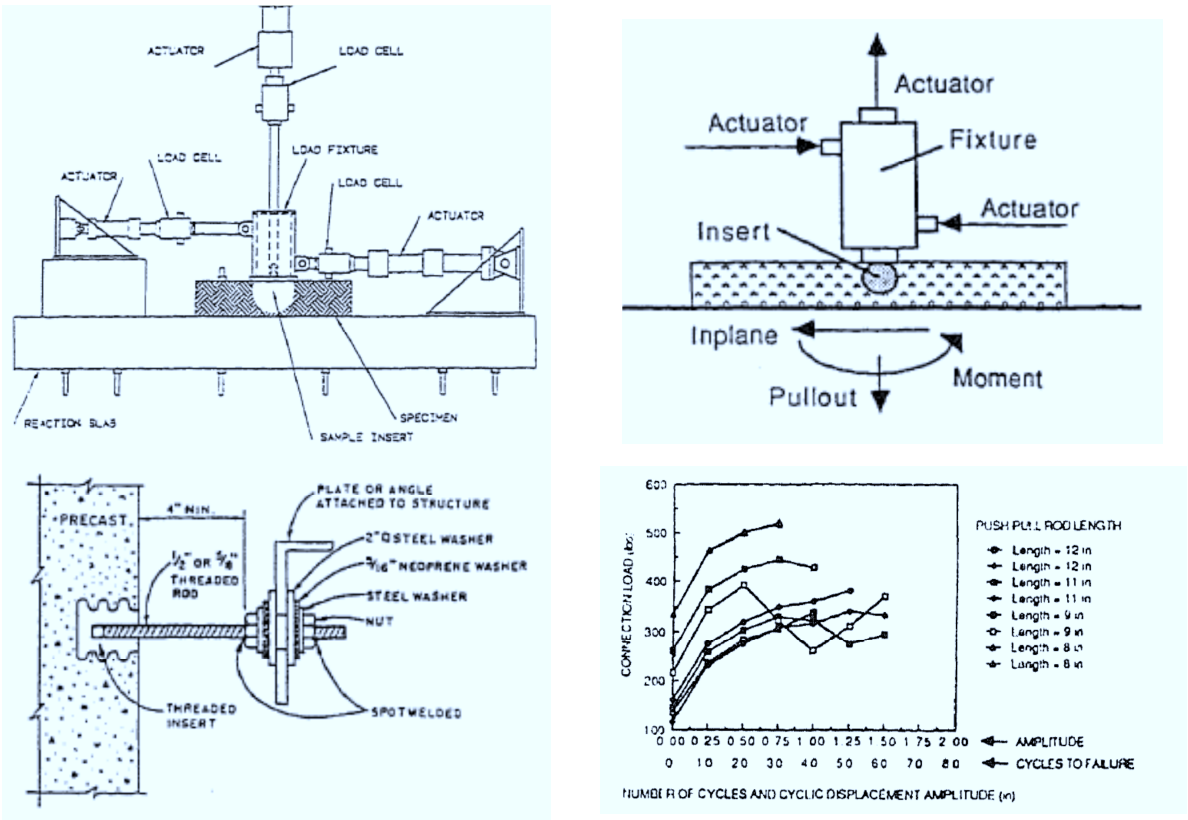

Figure 3-15: Connection test setup (top left), loading schematic (top right), tie-back connections tested (bottom left), connection force-displacement behaviour (bottom right) (Craig et al., 1989)

Seven different steel plate inserts for cladding connections were tested by Pinelli and Craig (1989). The embedded inserts were supported with either welded 90-degree rebar or welded rebar parallel to the surface of the concrete, as shown in Figure 3-16. The stiffness of the connections was found to be 58 kN/mm. The maximum resisted loads were approximately 27 kN, and the inserts showed limited energy dissipation.

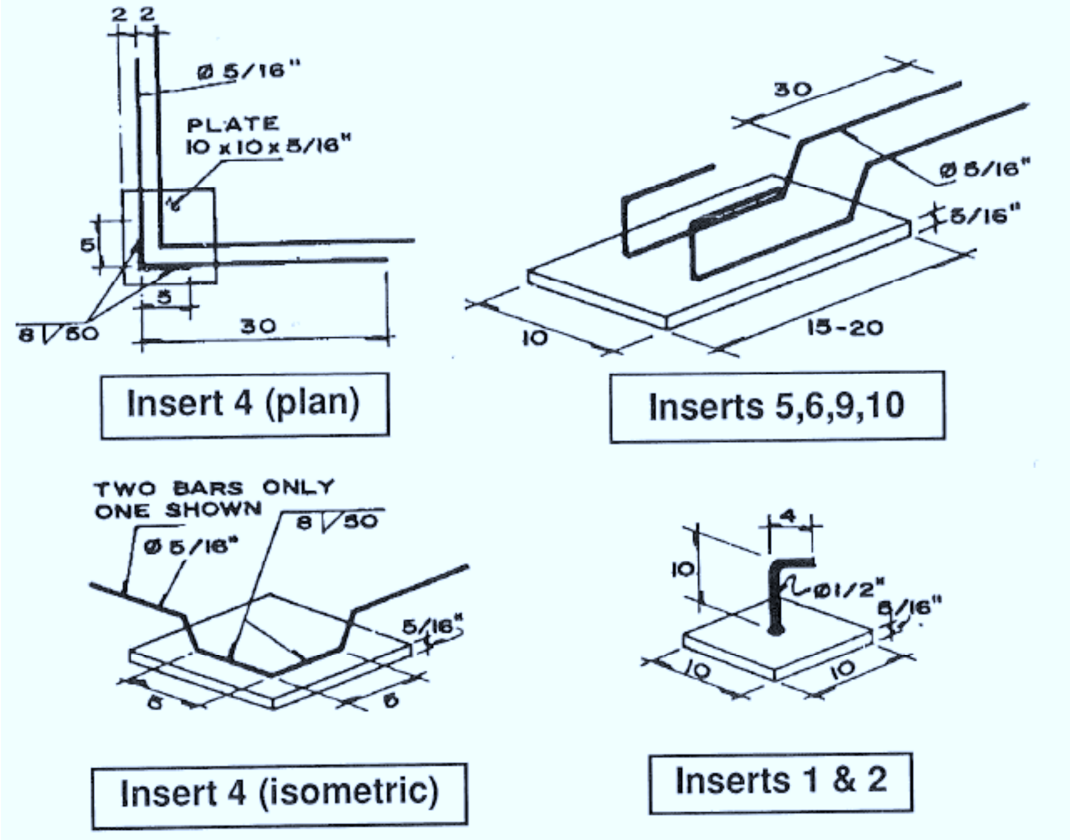

Figure 3-16: Insert geometry tested by Pinelli and Craig (1989)

The cyclic load tests revealed pinching in the hysteretic loops, as shown in Figure 3-17 (left). This behaviour can be explained by the interaction between the steel insert and the surrounding concrete. At low load, the stiffness is provided primary by the concrete surrounding the insert. As the magnitude of the load increases, the insert is blocked against the concrete and further stiffness is provided by the steel properties of the insert. As the magnitude of the load increases further, the concrete began to deteriorate. In many cases the concrete failed suddenly in a brittle manner, especially where the concrete suffered from a lack of confinement. Once the concrete failed, the connections began acting like a hinge, with the steel insert experiencing large displacements. Ultimately, the connection failed by a total collapse of the concrete of a failure of the weld between the steel plate and the reinforcement.

As expected, inserts located along the edge of the specimens behaved better than the inserts located at the corners. The values of ductility were found to vary substantially with the type of insert, its location in the concrete specimen, the load type, and the magnitude of the load cycles, as shown in Figure 3-17 (right). In all cases, a tendency towards an increase in ductility with increase in magnitude of the load was observed. More specifically and as expected, the ductility increased dramatically once the concrete started to crack.

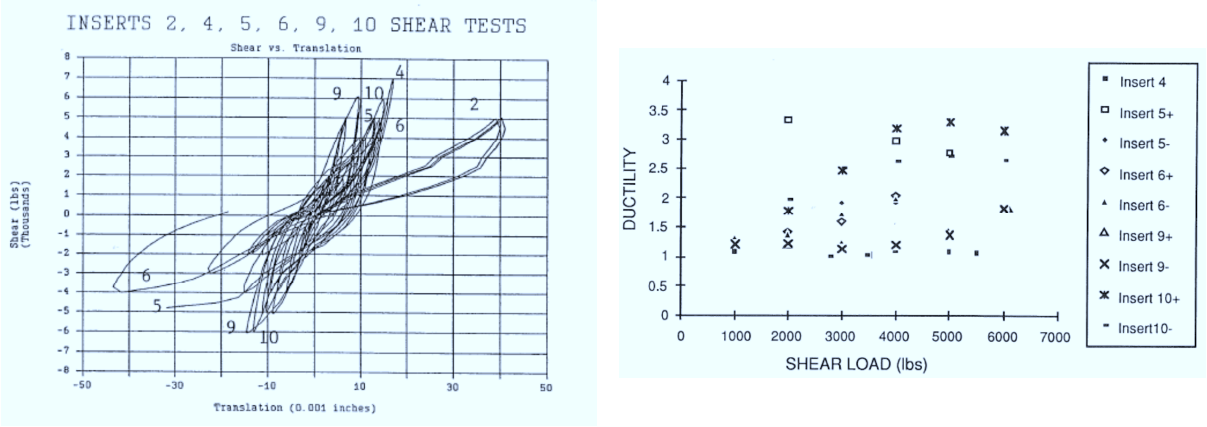

Figure 3-17: Shear deformation (left) and ductility (right) for all inserts tested by Pinelli and Craig (1989)

Seven full-scale threaded rod tie-back and welded plate cladding connections were tested by McMullin et al. (2004) to determine their force-deformation behaviour. The 25 mm diameter rods were subjected to monotonic tension, compression and flexural loading. The connections exhibited very ductile behaviour, achieving deformations of 150 mm without a loss of strength, as shown in Figure 3-18.

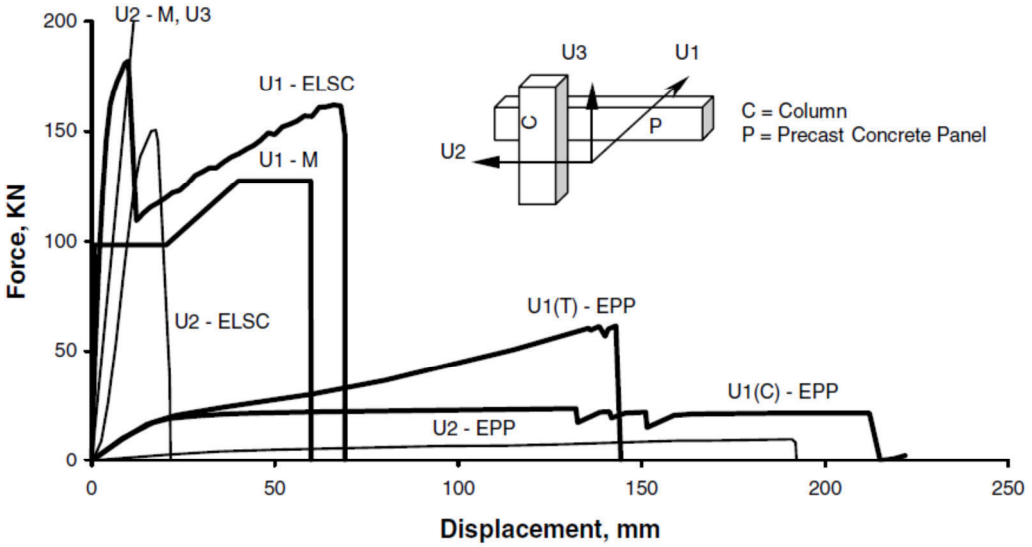

Figure 3-18: Tension, compression and bending of threaded rod connections (McMullin et al., 2004)

Some of this deformation resulted from bending of the supporting plate connecting the threaded rod to the column. The connections failed in a very ductile manner and the bending

of the supporting plate further accentuated this ductile failure. However, monotonic loading is not a very good representation of earthquake loading due to it not capturing any cyclic actions or possible strength and stiffness degradation. The results of the testing by McMullin et al. (2004) therefore likely overestimate the ductility of the connections.

3.5.2 Isolating Connections

Because a structure is often designed neglecting the cladding system, the current practice in seismically active countries such as Japan, USA and New Zealand is to isolate the cladding from the frame (Charleson, 2008). Two philosophies exist to achieve this isolation: using seismic gaps in the cladding system or using isolating connections. Seismic gaps accommodate interstorey movement by use of gaps around the glass and within the claddings itself in seismic frames. Isolating connections consist of flexible or sliding connections which allow the cladding to move and rotate relative to the frame when undergoing seismic excitation. An investigation into autoclaved lightweight aerated concrete (ALC) panel connections showed that these panels could be successfully isolated from the structure, even under a large inter-storey drift of 4% (Okazaki et al., 2007). The test structure was a three-storey, two-bay by one-bay steel moment frame with a plan dimension of 13m in the longitudinal loading direction and 8.25m in the transverse direction, as shown in Figure 3-19 (left). The ALC panels were attached to floor beams located at the edge of the floor slab. Figure 3-19 (right) shows the northeast side of the test structure, with the ALC panels attached to the far side of the structure.

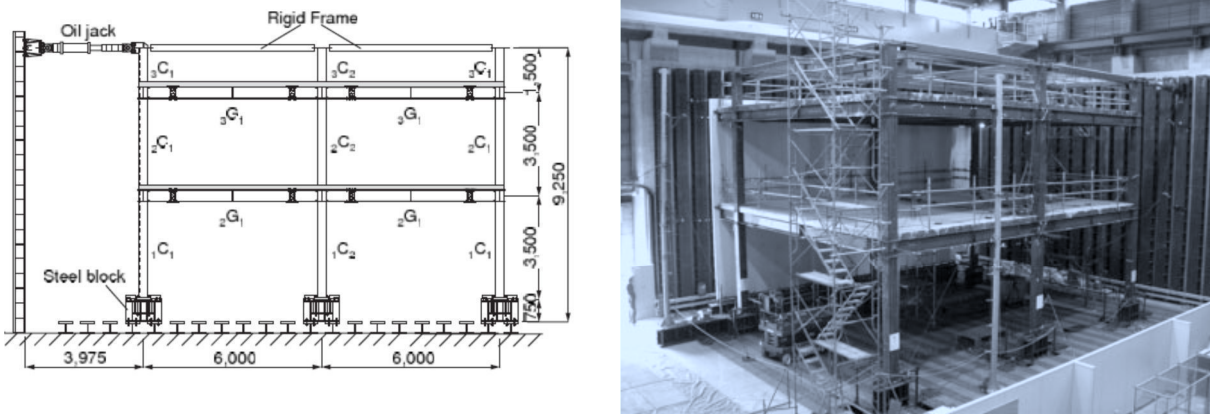

Figure 3-19: South elevation of test structure (left) and overview of test structure with ALC panels on far side (right) (Okazaki et al., 2007)

The test structure was subjected to quasi-static cyclic loading with increasing overall drift angles, with two or three cycles repeated for each increase. The overall drift angle was

defined as the horizontal displacement at the loading point divided by the distance between the loading point and grade level, measured as 8.5 m. The overall drift was increased from 0.5% to 1.0%, 1.3%, 2.0%, 4.0%, and then, to 5.0% drift, shown in Figure 3-20 (left). After loading at ±5.0% drift was completed, 600 mm thick shims were added to extend the stroke of the jacks, and loading was continued monotonically to an overall drift angle of 12.5%.

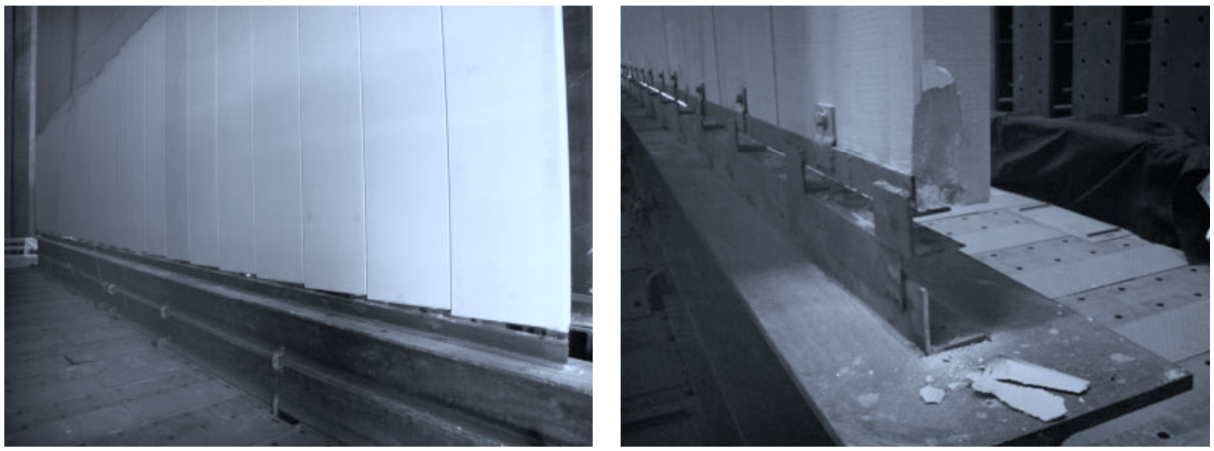

Figure 3-20: Deformed aerated lightweight concrete (left), and spalling at base of panels (right) (Okazaki et al., 2007)

The structure exhibited stable cyclic behaviour up to the loading cycles at ±5.0%. Although small cracks were observed at the beam end flange welds during and after the loading at 4.0% drift rad, these cracks had little influence on the overall behaviour of the structure until after the loading at 5.0% was completed.

The hysteresis curve at the first storey showed a pinching behaviour, which was not seen in the second storey. The pinching behaviour was caused primarily by plastic elongation of the anchor bolts at the column bases. The small difference between the bare frame hysteresis and the clad frame hysteresis indicates that the ALC panels had little effect on the stiffness or strength of the structure. During the loading at 1.3% drift cycle, the bottom of the first storey ALC panels contacted the supporting steel angle. This contact caused minor cracking at the bottom edges of the ALC panels, as shown in Figure 3-20 (right). Otherwise, no cracking or damage was noted in the body of the ALC panels.

Relying upon sliding connections to isolate cladding panels is seen as undesirable in some countries due to the possibility of the bolt not being able to slide as intended. This may be due to incorrect bolt alignment, jamming or binding due to unwanted materials left after installation, jamming due to geometrical change of the structural frame under horizontal forces, or from the bolts being over-tightened. These concerns arise since the sliding mechanism may be called upon to work instantaneously decades after their installation.

The full-scale test performed by Wang (1986) that were presented earlier tested sliding connections using a short rod and angle with a slotted hole details (refer to Figure 3-10). These connections can be seen as desirable since they can fit where long tie-back rods cannot. However, the sliding connections tested did not have a good performance, even during initial forced vibration tests. At that point, it was discovered that the Japanese construction crew who had never worked with such details, had over-tightened the connections making them unable to slide as intended.

Although the U.S. Principal Investigator requested that these connections be loosened, the Japanese side preferred to maintain a uniform policy of leaving installation "as is" in all cases, so that the specimen would be consistently unaltered. Although initially there was concern by the American side that the decision to not loosen the connections would compromise the tests, in retrospect, the decision was sound for it resulting in more dramatic, revealing and credible results. Though some of the over-tightened connections worked better than expected, the extent of failure were numerous and severe. Visible failure of a short rod began at 0.4% drift. Aside from the problems associated with over-tightening, another inherent problem with the sliding detail was discovered. The battered edge of the angle slot shown in Figure 3-21 illustrates that the slot length was insufficient to accommodate the motion of the short rod in the slot.

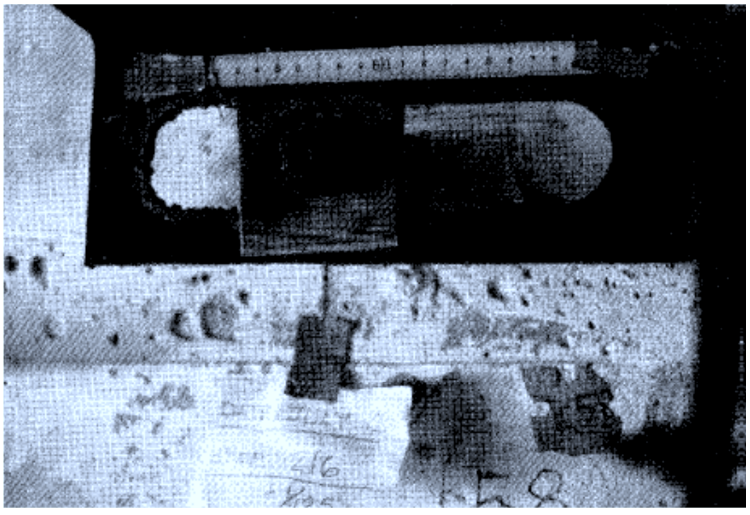

Figure 3-21: Insufficient slot length of sliding connection (Wang, 1987)

The serious problem with connections being unable to slide resulting from over-tightening is also applicable to connections that are unable to slide for various other reasons, and therefore this testing presented a 'worst-case-scenario'.

It was clear from the Japanese results that given "exceptional detailing, meticulous workmanship and other ideal conditions, sliding parts of rocking connections can work very

well" (Wang, 1987). Despite ideal conditions, there was the early failure of a sliding component of the rocking connection due to an incorrect installation. The rest of the Japanese connections performed excellently. There was concern that the Japanese connections were too exceptionally detailed and installed by workmen from the product association who were experts in their field, and consequently, the exceptional results is slightly unrealistic for a typical construction. This research shows that the use of sliding connections to isolate cladding requires care, skill and a thorough understanding to be implemented correctly.

3.5.3 Passive Control with Advanced Cladding Connections

A building fully clad in precast concrete cladding presents an increase of approximately 20-30% in the inertial mass of multi-storey building (Pall, 1989). This increased mass means increased seismic forces during earthquake excitation. However, unlike other cladding types, precast concrete cladding has inherent strength and stiffness that is typically ignored. Current design philosophies attempt to isolate cladding from interacting with the frame during deformations due to wind and earthquake loading (Arnold, 1990). As shown in the prior section, bolted connections with slotted or oversized holes are commonly used to isolate panels as well as accommodate erection tolerances. However, as identified earlier, research has shown how even when attempts to isolate the cladding are made, precast concrete cladding can still substantially increase the overall stiffness of a structure.

Instead of attempting to isolate the structure-panel interaction, others have proposed to instead take advantage of it to form an integrated building-cladding system that offers improved stiffness, energy dissipation, and ductility. This type of system is often referred to as a passive control of the seismic behaviour of a structure (Pinelli et al., 1993). Such a system makes use of the relative displacement between the cladding and structure. Controlling the cladding participation requires the an advanced connection that has high ductility and damping qualities that results in high energy dissipation without failure during moderate or strong earthquakes (Pinelli et al., 1993). These connections utilise the interaction between the panels and the building structure to dissipate energy. At the same time, like other passive control devices, they provide additional lateral stiffness to the structure and alter its dynamic characteristics. By using such a system, deformations of the main structure can be reduced, preventing damage in both structural and non-structural components. It also makes more economic and dynamic sense because the cladding is no longer simply a dead weight to the frame.

Several research studies have focused on developing such advanced panel connections. These connections must also be simple to design, highly robust and limit the forces transmitted into the panel. Both analytical and experimental testing has been performed to quantify the benefits to the response of the building as a whole. One of the first to propose an advanced cladding connection was Kemeny and Lorant (1989). They performed experimental testing on elastomeric panel-to-structure connections to determine their effect on interstorey displacements and seismic forces. The connections used interlocking keyed steel-rubber isolators, as shown in Figure 3-22 (top), that provide very low stiffness at low excitation and increased stiffness and strength for larger drifts and forces.

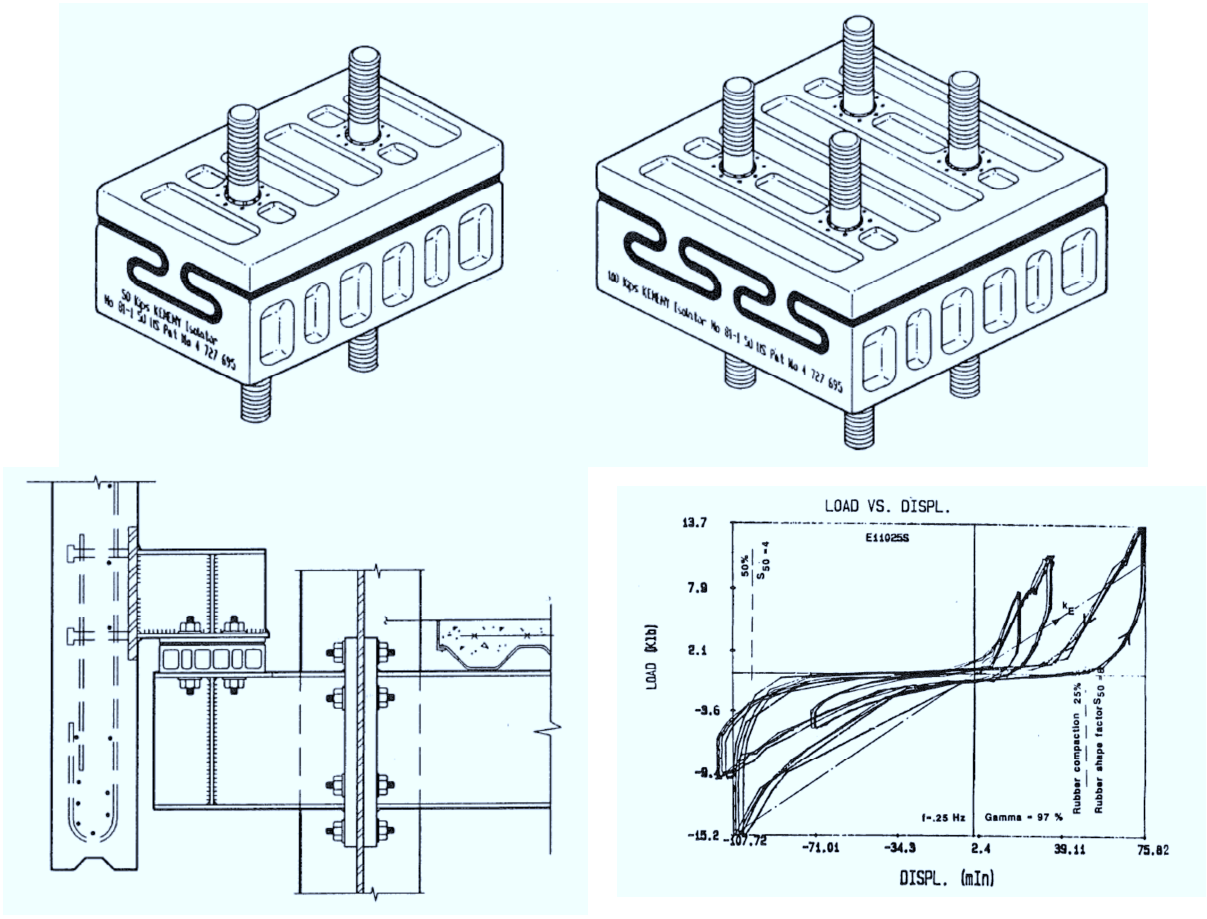

Figure 3-22: Interlocking keyed steel-rubbed isolator connections (top), bearing connection detail (bottom left) and experimental force-displacement behaviour (bottom right) (Kemeny & Lorant, 1989)

The interlocking keyed steel-rubber isolator connections were placed between the bearing connections of the panel and structure, as shown in Figure 3-22 (bottom left). The experimental behaviour of the connections that displays this delayed activation of the connections is shown in Figure 3-22 (bottom right). The authors concluded that the isolators might reduce 3 – 8% from the seismic structure since the isolator connection system could reduce seismic forces on the structure by 25–67%.

Another type of advanced cladding connection is a friction-damped connection developed by Pall (1989), as shown in Figure 3-23 (left). He performed analytical studies to compare the response of a frame using the advanced connections to the response of a bare frame. Time-history analyses revealed that the advanced connections reduced the deflections and column moments to 60–70% of those in the bare frame as shown in Figure 3-23 (right). Results also showed that torsional resistance of the building with the advanced connections was improved by four times compared to the bare frame.

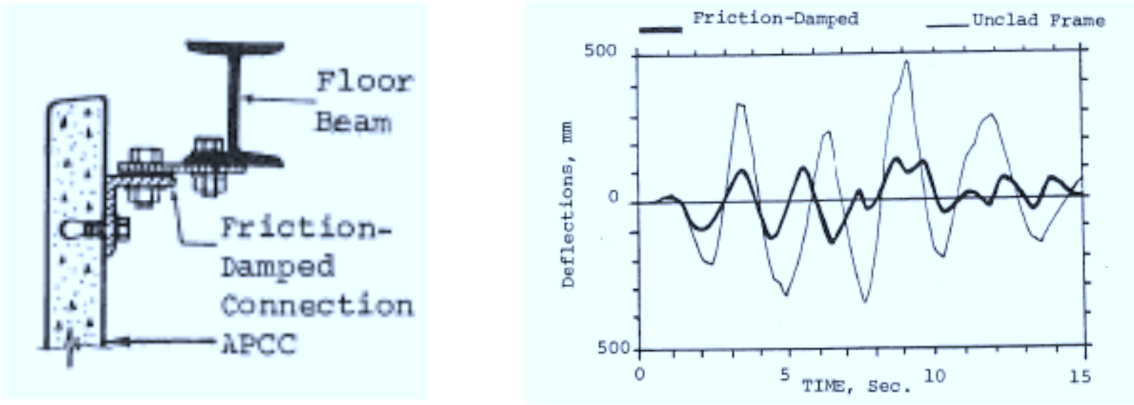

Figure 3-23: Friction-damped connection (left), displacement during time-history (right) (Pall, 1989)

Most of the research on advanced cladding connections and passive control has been carried out by B. J. Goodno, J. I. Craig, and their research team at the Georgia Institute of Technology from 1989–2000 (Craig et al., 2000; El-Gazairly et al., 1990; Goodno, 1998; Goodno et al., 1991; Pinelli et al., 1995; Pinelli et al., 1993; Pinelli et al., 1996; Wolz et al., 1992). Their work focussed on the use of an advanced tapered connection, shown in Figure 3-24 (left). The connection provides stiffness and damping through yielding of a tapered section. The hysteretic behaviour of the connection is shown in Figure 3-24 (right).

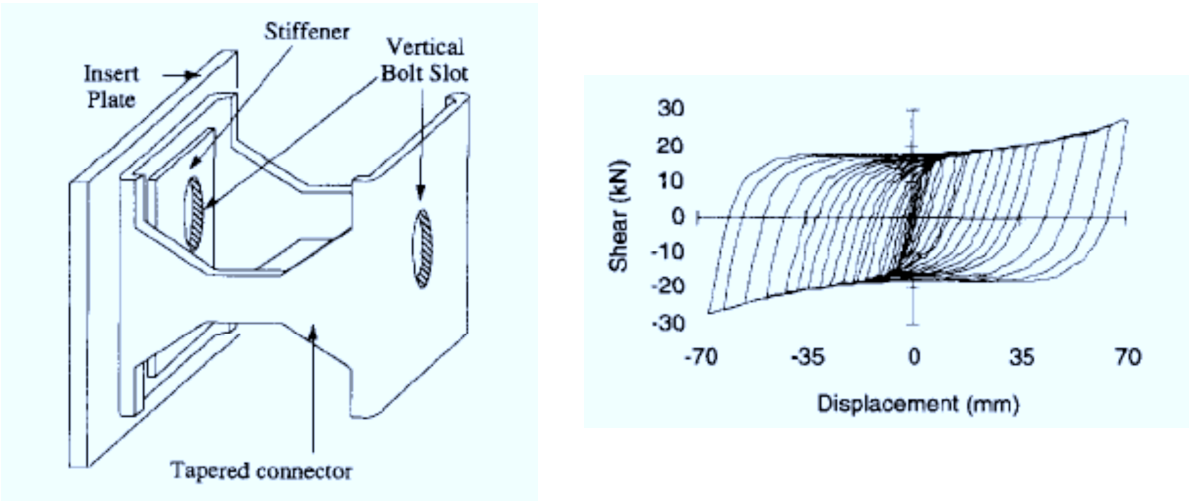

Figure 3-24: Advanced tapered connection (left) and its hysteretic behaviour (right) (Pinelli et al., 1995)

The analytical test structure used to assess the potential of the advanced tapered connections was a six-story, three-bay moment-resisting frame, with two cladding panels per bay. Each panel was attached to the structure with four connections: two bearing connections at the bottom and two advanced tapered connections at the top. The authors also describe an energy-based design methodology to determine the material properties and size of the connections. Several dynamic time-history analyses were performed. The analyses that included the advanced connections reduced the interstorey drifts by 53–58% compared to the bare frame for some earthquakes. In most cases, up to 70% of the input energy was dissipated by the connectors, as shown in Figure 3-25 (Pinelli et al., 1996).

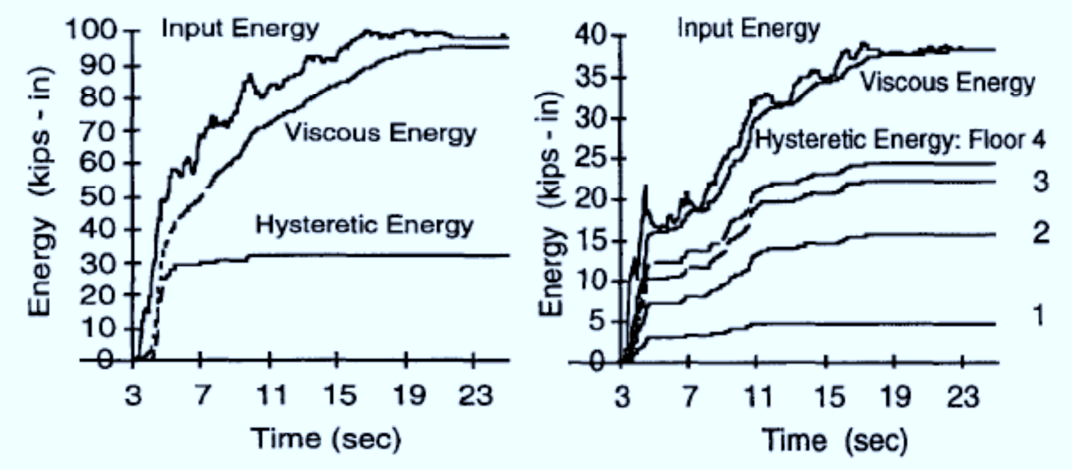

Figure 3-25: Energy time-history of conventional cladding (left) and cladding utilising advanced tapered connections (right) (Pinelli et al., 1996))

The use of ductile cladding panels to act as passive energy dissipators was also explored by analytical studies by Weston et al. (2002). Non-linear time history analyses were performed utilising the advanced tapered connection developed by Pinelli et al. (1996). The results showed that it is not necessary to cover the entire facade of the building with ductile connections to achieve the desired improvement in performance. With a small number of strategically placed connections on the building's exterior, the primary structure can effectively be protected from seismically induced damage (Weston, 2000).

Studies into the use of advanced cladding connections have shown they can be a very effective and efficient method to reduce building demands. However, most studies are purely numerical investigations, and limited experimental data exists to verify some of the claims of such research. The implementation of these connections in practice this has also proved difficult to achieve. Currently, it has proved more economic (if not more performance effective) to use isolation rather than passive control (Arnold, 1991).

3.6 Cladding Panels

As mentioned previously, testing of cladding is almost always to determine the architectural performance of the cladding being investigated. Consequently, there is only a very limited amount of test data available on cladding panels. This situation also likely arises due to the complexity of such tests and their relatively high cost compared to component level tests.

Experimental research has more commonly been performed on reinforced concrete panels when they are intended to behave as wall elements. Tassios and Tsoukantas (1978) examined the monotonic and reversing cyclic loading of reinforced concrete panels. This early research gave an indication of the likely shear strength and stiffness of precast concrete panels and is also applicable to panels used as cladding. Experimental testing was also undertaken by Sudarno (2003) to examine thin precast concrete panels. The testing involved shake table testing of rocking panels, but again, was more focussed on panels which act primarily as wall elements for warehouse buildings.

Matthewson and Davey (1979) analysed a six-storey building that incorporated energy dissipating steel members into precast concrete panels. The panels were reinforced by diagonal cross bracing, as shown in Figure 3-26 (left), consisting of hollow mild steel sections, which yielded axially when subjected to inter-storey differential displacement. The panels were attached to the columns of the building through welded steel attachment plates, and therefore increased the stiffness of the building structure. Non-linear time history analyses were conducted using several different earthquake ground motions. These studies revealed that the energy dissipated by the yielding of the diagonal cross bracing in the panels kept the deformations of the frame within the elastic range.

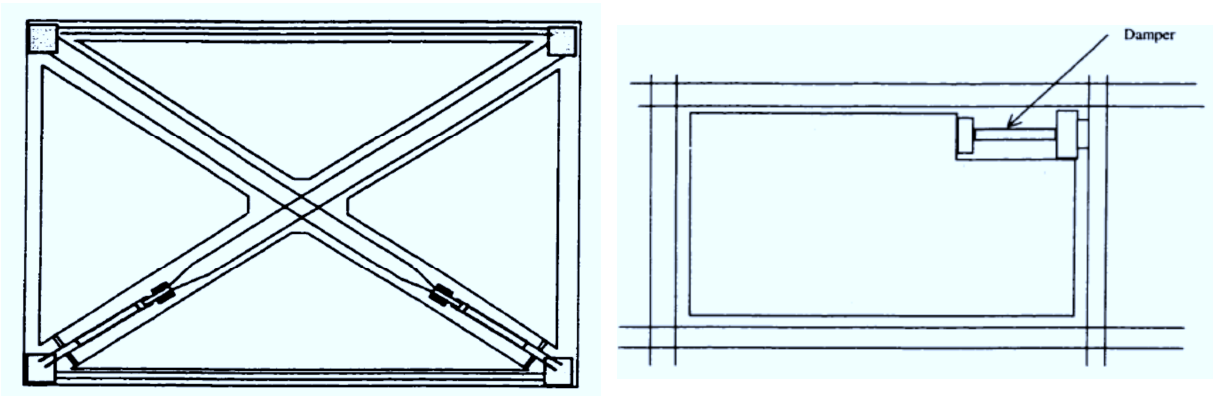

Figure 3-26: Energy-dissipating cladding panel (left) Matthewson and Davey (1979) and sketch of cladding panel including damping device (right) (Bruneau et al., 1998)

Another configuration, as pictured in Figure 3-26 (right), used the precast panel to implement different damping devices such as friction dampers, lead extrusion dampers, and fluid viscoelastic dampers (Bruneau et al., 1998). The devices were again activated by the differential movement between the panel and the structure.

Finite element modelling of a reinforced concrete cladding panels was undertaken by Maneetes and Memari (2009). The cladding system investigated consisted of a single spandrel panel connected to a steel frame with two bearing connections, a single slotted connection and a friction damper connection, as shown in Figure 3-27 (top left).

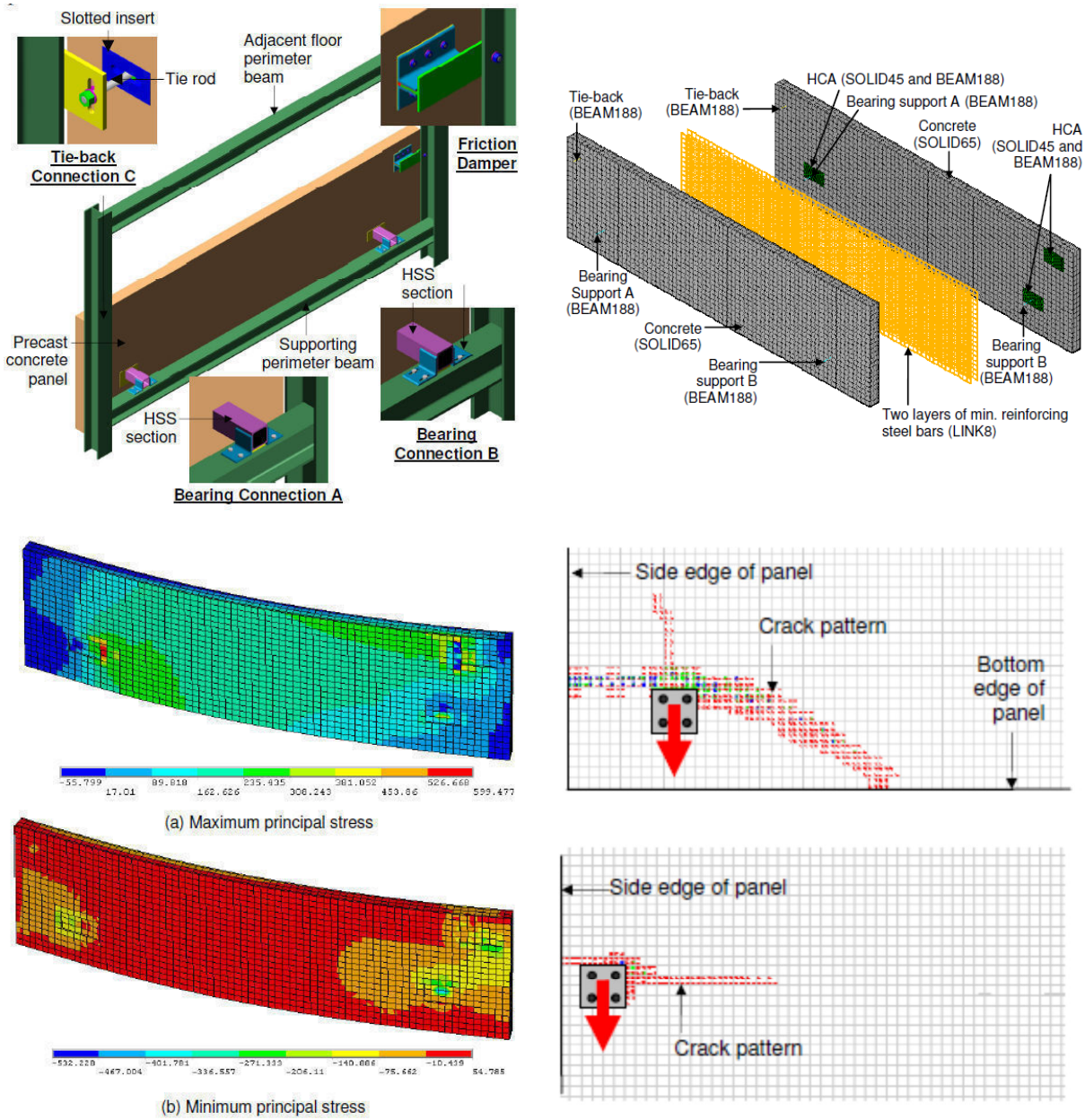

Figure 3-27: Cladding system investigated by Maneetes and Memari (2009) (top left), finite element models (top right), stress distributions (bottom left) and crack patterns (bottom right)

Under moderate or high intensity seismic motions, the in-plane forces developed in the cladding panel would exceed the design slip load of the friction damper, causing it to slip horizontally and dissipate part of the building input energy. The proposed design relies on the ability of the precast concrete panel to carry the high in-plane loads and this was investigated using finite element modelling techniques. Finite element analyses (FEA) allow important parameters like stress-strain relationships and cracking models to be investigated. Several 3D finite element models of the cladding panel were developed using elements verified by experimental testing of reinforced concrete beams. The elements used to model the cladding panels are shown in Figure 3-27 (top right). The cladding panel models were subjected to differential displacement between connections in order to find the stress-strain distribution throughout the panel. The maximum and minimum principal stresses are shown in Figure 3-27 (bottom left). Determining crack initiation and the crack propagation pattern was also possible using the results of FEA. The effect of the location of the connections in relation to the edge of the panel was explored, and the differences in crack patterns found are shown in Figure 3-27 (bottom right).

3.7 Loss Modelling

Research into the seismic performance of cladding systems has historically been guided by the objective to reduce potential casualties and injuries resulted directly from the failure of cladding components. More recently, this objective has changed to focus on mitigation of the ensuing economic costs associated with cladding damage, due to loss of function, repair costs and repair time.

Direct replacement costs of cladding can be only a small part of the total costs which include the loss of function and repair costs. Such indirect costs can be two to three times the cost of replacing the damaged structure (Phan & Taylor, 1996). Cladding systems in low-moderate seismic regions deserves attention even in situations where the risk of structural damage seems very low. For example, buildings responding elastically can produce high periodic floor motions which can be very damaging to even at very low intensity (Lam & Gad, 2002).

The main outputs of the research presented in this chapter are useful for engineers and researchers; however, end-users and decision-makers are not able to translate these results into a quantity useful for making decisions on post-earthquake repair cost scenarios. The Pacific Earthquake Engineering Research Centre developed a performance-based

methodology for calculating post-earthquake repair costs and repair times based on the seismic hazard at the building site. These decision variables (repair cost and repair time) are more readily understandable by the building owner.

Hunt and Stojadinovic (2010) undertook a performance-based repair cost analysis of precast concrete cladding systems like that shown in Figure 3-28 (left). The seismic response of the cladding systems was evaluated using the maximum inter-story drift and the maximum deformations in the cladding connectors found from time-history analyses of nine storey building shown in Figure 3-28 (right).

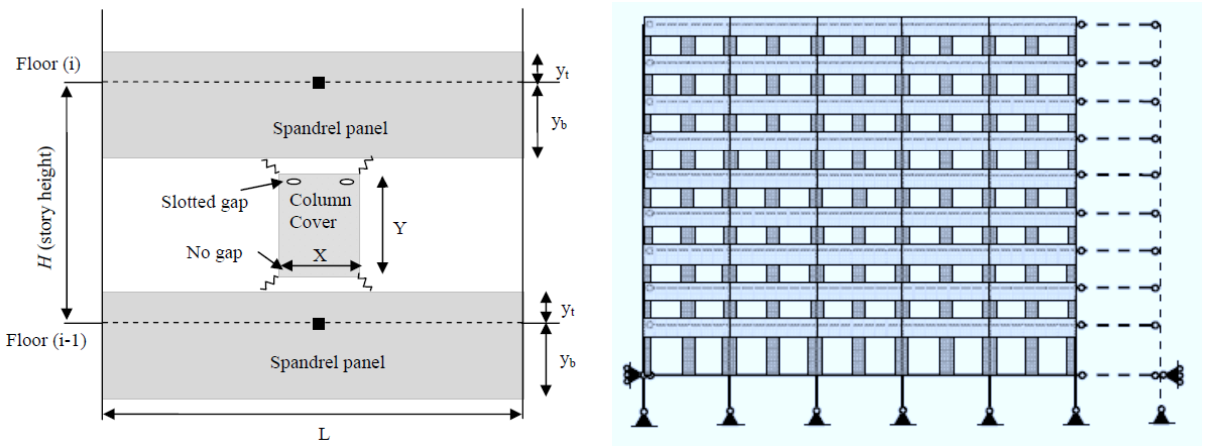

Figure 3-28: Elevation of precast cladding system assessed for performance-based repair cost analysis by Hunt and Stojadinovic (2010)

The total repair cost of the cladding was expressed in terms of different repair cost ratio. The first repair cost ratio was calculated as the total repair cost of the cladding system divided by the replacement cost of the cladding system. At spectral accelerations of 0.11g and 0.65g the repair cost ratios were 4.0% and 65.8%, respectively. The second repair cost ratio was calculated as the total repair cost of the cladding system divided by the replacement cost of the complete building. At spectral accelerations of 0.11g and 0.65g the repair cost ratios were 0.8% and 13.7%, respectively. The third repair cost ratio was calculated as the total repair cost of the cladding system divided by the total repair cost of the complete building. Again, at spectral accelerations of 0.11g and 0.65g, the ratios were 11.1% and 50.4%, respectively.

The mean annual repair cost was calculated as the product of the mean repair cost of the cladding system conditioned on intensity measure and slope of the hazard curve at each intensity measure, integrated over the range of intensity measure. The mean annual total repair cost of the cladding system was US$40,000.

3.8 Conclusions

This chapter presented a literature review of recent research into the seismic performance and behaviour of cladding systems. This included a brief historical overview and a summary of previous analytical and experimental research into heavy cladding systems. This chapter also aids in the motivation and scope of the research undertaken in the remaining chapters of this thesis. Commentary is provided here that identifies issues in the current state-of-art that this research will aim to explore.

Analytical research showed that cladding can decrease the translational periods by up to 34% and the torsional periods by up to 48%. Various other studies also showed the potential lateral stiffening effect cladding has to a bare frame structure. However, several flaws were identified in the methods used to illustrate the stiffening effect of cladding. These were typically attributed to simplifications made in the modelling approach, e.g. assuming the cladding is the sole element for the difference in stiffness between the bare frame and complete structure, or due to erroneous assumptions made in the modelling of the cladding, e.g. assuming the connections or cladding were extremely rigid. This research will aim to more rigorously examine the stiffening effect cladding has upon a structure.

Limited experimental research exists into the performance of cladding systems, with the majority of research undertaken on individual cladding components. The exception to this is the recent shake-table testing performed at the University of California, San Diego in 2012. This research will therefore experimentally examine a full-scale precast concrete cladding system that represents a typical cladding solution used in New Zealand and other high seismic countries. This will include the identification of damage limits in order to assess the seismic performance.

The seismic performance of cladding is believed to be most dependent on the panel-to-structure connections. If very stiff and high-strength connections are used along with inadequate joint widths, the cladding system may act as an external shear wall and cause significant damage to the cladding. If attached in this way, it has been found that the cladding system may shorten the fundamental period of the building resulting in an unintended increased in seismic forces. Consequently, the current practice in seismically active countries such as Japan, USA and New Zealand is to isolate the cladding from the frame using sliding connections. Research into the use of these connections has shown that they can successfully eliminate the interaction between the cladding and structure. However, the use of sliding connections to isolate cladding requires care, skill and a thorough understanding to be

implemented correctly. This research will subsequently seek to determine how these typical connections influence the behaviour of a structure and aim to provide advice on the detailing that should be used.

Instead of attempting to isolate the structure-panel interaction, others have proposed to instead take advantage of the cladding to form an integrated building-cladding system that offers improved stiffness, energy dissipation, and ductility. Studies into the use of these advanced cladding connections show they offer a very effective and efficient method to reduce building demands. However, most studies are purely numerical investigations, and limited experimental data exists to verify some of the claims of such research. The implementation of these connections in practice this has also proved difficult to achieve. Currently, it has proved more economic (if not more performance effective) to use isolation rather than passive control. This research will aim to both experimentally and numerically examine the potential of an innovative cladding connection as a means to provide additional stiffness and damping to the building-cladding system.

Finally, research has shown that direct replacement costs of cladding only forms a small part of the total damage cost. This total damage cost includes the loss of function, repair costs and repair time. Such indirect costs can be two to three times the cost of replacing the damaged structure. Consequently, cladding systems in low-moderate seismic regions still require attention even in situations where the risk of structural damage appears very low. This research will aim to better quantify these costs for both a typical precast concrete cladding system, as well as an innovative low-damage system.

3.9 References

Arnold, C. (1990). Architectural Precast Cladding *Cladding Design: Recent Architectural Trends and Their Impact on Seismic Design* (pp. 29-30). Chicago, IL., USA.

Arnold, C. (1991). *The seismic response of nonstructural elements in buildings*. Paper presented at the Pacific Conference on Earthquake Engineering, Auckland, New Zealand.

Behr, R. A. (1998). Seismic Performance of Architectural Glass in Mid-Rise Curtain Wall. *Journal of Architectural Engineering, 4*(3), 94-98.

Behr, R. A., & Belarbi, A. (1996). Seismic Test Methods for Architectural Glazing Systems. *Earthquake Spectra, 12*(1), 129-143.

Behr, R. A., Belarbi, A., & Brown, A. T. (1995). Seismic performance of architectural glass in a storefront wall system. *Earthquake Spectra, 11*(3), 367-391.

Behr, R. A., Belarbi, A., & Culp, J. H. (1995). Dynamic racking tests of curtain wall glass elements with in-plane and out-of-plane motions. *Earthquake Engineering & Structural Dynamics, 24*(1), 1-14.

Behr, R. A., & Worrell, C. L. (1998). *Limit States for Architectural Glass Under Simulated Seismic Loadings*. Paper presented at the ATC-29-1: Seminar on Seismic Design, Retrofit, and Performance of Nonstructural Components, San Francisco, CA., USA.

Bouwkamp, J. G., & Meehan, J. F. (1960). *Drift Limitations Imposed by Glass*. Paper presented at the Second World Conference on Earthquake Engineering, Tokyo.

Brueggeman, J., Behr, R., Wulfert, H., Memari, A., & Kremer, P. (2000). Dynamic Racking Performance of an Earthquake-Isolated Curtain Wall System. *Earthquake Spectra, 16*(4).

Bruneau, M., Uang, C. M., & Whittaker, A. S. (1998). *Ductile Design of Steel Structures*: McGraw-Hill, Inc.

CERC. (2012). Canterbury Earthquakes Royal Commission - Final Report Retrieved 12 April 2012

Charleson, A. (2008). *Seismic Design for Architects: Outwitting the Quake*: Architectural Press.

Charney, F. A., & Harris, J. R. (1989). *The Effect of Architectural Precast Concrete Cladding on the Lateral Response of Multistorey Buildings*. Paper presented at the Architectural Precast Concrete Cladding - Its Contribution to Lateral Resistance of Buildings, Chicago, IL., USA.

Chen, M., Pantoli, E., Wang, X., Espino, E., Mintz, S., Conte, J., Hutchinson, T., Marin, C., Meacham, B., Restrepo, J., Walsh, K., Englekirk, R., Faghihi, M., & Hoehler, M. (2012). Design and Construction of a Full-Scale 5-Story Base Isolated Building Outfitted with Nonstructural Components for Earthquake Testing at the UCSD-NEES Facility *Structures Congress 2012* (pp. 1349-1360): ASCE.

Cohen, J. M. (1995). Seismic Performance of Cladding: Responsibility Revisited. *Journal of Performance of Constructed Facilities, 9*(4), 254-270.

Craig, J. I. (1986). *Hysteretic behavior of precast cladding connections*. Paper presented at the Dynamic Response of Structures, Los Angeles, CA., USA.

Craig, J. I., Goodno, B., Towashiraporn, P., & Dogan, T. (2000). *Ductile Cladding Systems for Seismic Design*. Paper presented at the 12th World Conference on Earthquake Engineering, Auckland, New Zealand.

Craig, J. I., Leistikow, R., & Fennell, C. J. (1989). *Experimental studies of the performance of precast cladding connections*. Paper presented at the Ninth World Conference on Earthquake Engineering, Tokyo, Japan.

El-Gazairly, L. F., Goodno, B. J., & Craig, J. I. (1990). *Analytical investigation of advanced connections for precast cladding on buildings*. Paper presented at the Fourth U.S. National Conference on Earthquake Engineering, Palm Springs, CA., USA.

FEMA 450. (2003). NEHRP Recommended Provisions and Commentary for Seismic Regulations for New Buildings and Other Structures. Washington, DC., USA: Federal Emergency Management Agency.

Foutch, D. A., Goel, S. C., & Roeder, C. W. (1986). Preliminary Report on Seismic Testing of a Full-Scale Six-Story Steel Building, Ch. 6 on Phase III and Phase IV – Moment Frame Test and Nonstructural Component Test *Structural Research Series No. 527*: University of Illinois.

Gjelvik, A. (1973). Interaction between Frames and Precast Wall Panels. *Journal of the Structural Division, ASCE, 100*(2).

Goodno, B. J. (1983). *Cladding-structure interaction in highrise buildings*: Schools of Civil and Aerospace Engineering, Georgia Inst. of Technology, Atlanta.

Goodno, B. J. (1998). *Ductile cladding connection systems for seismic design*: National Institute of Standards and Technology, Building and Fire Research Laboratory, Gaithersburg, MD.

Goodno, B. J., & Craig, J. I. (1989). *Historical Overview of Studies on the Contribution of Cladding to Lateral Resistance of Buildings*. Paper presented at the Architectural Precast Concrete Cladding - Its Contribution to Lateral Resistance of Buildings, Chicago, IL., USA.

Goodno, B. J., Craig, J. I., & Hsu, C. C. (1991). *Experimental studies and analytical evaluation of ductile cladding connections*. Paper presented at the Pacific Conference on Earthquake Engineering, Auckland, New Zealand.

Goodno, B. J., & Palsson, H. (1982). *Earthquake performance of building cladding systems*. Paper presented at the Sino-American Symposium on Bridge and Structural Engineering, Beijing, China.

Goodno, B. J., & Palsson, H. (1986). Analytical Studies of Building Cladding. *Journal of Structural Engineering, 112*(4), 665-676.

Goodno, B. J., Palsson, H., & Pless, D. G. (1984). *Localized cladding response and implications for seismic design*. Paper presented at the Eighth World Conference on Earthquake Engineering, San Francisco, CA., USA.

Goodno, B. J., Will, K. M., & Palsson, H. (1980). *Effect of cladding on building response to moderate ground motion*. Paper presented at the Seventh World Conference on Earthquake Engineering, Istanbul, Turkey.

Henry, R. M., & Roll, F. (1986). Cladding-Frame Interaction. *Journal of Structural Engineering, 112*(4), 815-834.

Hunt, J. P., & Stojadinovic, B. (2010). *Seismic Performance Assessment and Probabilistic Repair Cost Analysis of Precast Concrete Cladding Systems for Multistory Buildings*: Berkeley: Pacific Earthquake Engineering Research Center, University of California.

Hutchinson, T., Restrepo, J., Conte, J., & Meacham, B. (2013). Overview of the Building Nonstructural Components and Systems (BNCS) Project *Structures Congress 2013* (pp. 1485-1498): ASCE.

ICC. (2000). International Building Code. Falls Church, Va., USA: International Code Council.

Iverson, J. K. (1989). *Concrete Cladding Connections in Earthquake Country*. Paper presented at the Architectural Precast Concrete Cladding - Its Contribution to Lateral Resistance of Buildings, Chicago, IL., USA.

Kemeny, Z. A., & Lorant, J. (1989). *Energy Dissipating Elastomeric Connections*. Paper presented at the Architectural Precast Concrete Cladding - Its Contribution to Lateral Resistance of Buildings, Chicago, IL., USA.

Korista, D. S. (1989). Exterior Façade System – Building Structure System: Load-Deformation Behavioral Inter-Relationships *Exterior Claddings on High Rise Buildings.* Chicago, IL., USA.

Lam, N., & Gad, E. (2002). *An innovative approach to the seismic assessment of non-structural components in buildings*. Paper presented at the 2002 Australian Earthquake Engineering Society Conference, Adelaide, Australia.

Lim, K. Y. S., & King, A. B. (1991). The Behaviour of External Glazing Systems Under Seismic In-Plane Racking *SR39*: Building Research Association of New Zealand.

Maneetes, H., & Memari, A. M. (2009). Finite Element Modeling of Reinforced Concrete Cladding Panels. *Journal of Structural Engineering, 9*.

Matthewson, C. D., & Davey, R. A. (1979). Design of an Earthquake Resisting Building Using Precast Concrete Cross-Braced Panels and Incorporating Energy Absorbing Devices. *Bulletin of the New Zealand Society for Earthquake Engineering, 12*(4), 340-349.

McMullin, K., Ortiz, M., Patel, L., Yarra, S., Kishimoto, T., Stewart, C., & Steed, B. (2012). *Response of Exterior Precast Concrete Cladding Panels in NEES-TIPS/NEESGC/ E-Defense Tests on a Full Scale 5-Story Building*. Paper presented at the Structures Congress 2012, Chicago, IL., USA.

McMullin, K., Wong, Y., Choi, C., & Chan, K. (2004). *Seismic Performance States of Precast Concrete Cladding Connections*. Paper presented at the 13th World Conference on Earthquake Engineering Conference, Vancourver, B.C., Canada.

Memari, A. M., Behr, R. A., & Kremer, P. A. (2003). Seismic Behavior of Curtain Walls Containing Insulating Glass Units. *Journal of Architectural Engineering, 9*(2), 70-85.

Memari, A. M., Behr, R. A., & Kremer, P. A. (2004). Dynamic Racking Crescendo Tests on Architectural Glass Fitted with Anchored Pet Film. *Journal of Architectural Engineering, 10*(1), 5-14.

Memari, A. M., Kremer, P. A., & Behr, R. A. (2006). Architectural Glass Panels with Rounded Corners to Mitigate Earthquake Damage. *Earthquake Spectra, 22*(1), 129-150.

Meyyappa, M., Palsson, H., & Craig, J. I. (1981). *Modal Parameter Estimation for a Highrise Building Using Ambient Response Data Taken During Construction.* Paper presented at the 2nd Specialty Conference Dynamic Response of Structures: Experimentation, Observation, Prediction, and Control, New York, NY., USA.

O'Brien, W. C., Memari, A. M., Kremer, P. A., & Behr, R. A. (2012). Fragility Curves for Architectural Glass in Stick-Built Glazing Systems. *Earthquake Spectra, 28*(2), 639-665.

Okazaki, T., Nakashima, M., Suita, K., & Matusmiya, T. (2007). Interaction between cladding and structural frame observed in a full-scale steel building test. *Earthquake Engineering & Structural Dynamics, 36*(1), 35-53.

Oppenheim, I. J. (1973). *Dynamic Behavior of Tall Buildings with Cladding*. Paper presented at the Fiftth World Conference on Earthquake Engineering, Rome, Italy.

Pall, A. S. (1989). *Friction Damped Connections for Precast Concrete Cladding*. Paper presented at the Architectural Precast Concrete Cladding - Its Contribution to Lateral Resistance of Buildings, Chicago, IL., USA.

Palsson, H., & Goodno, B. J. (1982). *A degrading stiffness model for precast concrete cladding*. Paper presented at the Seventh European Conference on Earthquake Engineering, Athens, Greece.

Palsson, H., & Goodno, B. J. (1989). *Influence of interstory drift on cladding panels and connections*. Paper presented at the Ninth World Conference on Earthquake Engineering, Tokyo, Japan.

Pantoli, E., Wang, X., Chen, M., Hutchinson, T., Meacham, B., & Park, H. (2013). Shake Table Testing of a Full-Scale Five-Story Building: Performance of the Major Nonstructural Components - Egress and Facades *Structures Congress 2013* (pp. 1447-1459): ASCE.

PCI. (2007). *Architectural Precast Concrete*. Chicago, IL., USA: PCI Architectural Precast Concrete Manual Committee.

Phan, L. T., & Taylor, A. W. (1996). State of the Art Report on Seismic Design Requirements for Nonstructural Building Components. Gaithersburg, MD., USA: US National Institute of Standards and Technology.

Pinelli, J. P., & Craig, J. I. (1989). *Experimental Studies of the Performance of Mexican Precast Cladding Connections*. Paper presented at the Architectural Precast Concrete Cladding - Its Contribution to Lateral Resistance of Buildings, Chicago, IL., USA.

Pinelli, J. P., Craig, J. I., & Goodno, B. J. (1995). Energy-Based Seismic Design of Ductile Cladding Systems. *Journal of Structural Engineering, 121*(3), 567-578.

Pinelli, J. P., Craig, J. I., Goodno, B. J., & Hsu, C. C. (1993). Passive control of building response using energy dissipating cladding connections. *Earthquake Spectra, 9*(3), 529-546.

Pinelli, J. P., Moor, C., Craig, J. I., & Goodno, B. J. (1996). Testing of Energy Dissipating Cladding Connections. *Earthquake Engineering & Structural Dynamics, 25*(2), 129-147.

Rihal, S. S. (1989). *Earthquake Resistance and Behavior of APCC and Connections*. Paper presented at the Architectural Precast Concrete Cladding - Its Contribution to Lateral Resistance of Buildings, Chicago, IL., USA.

Sack, R. L., Beers, R. J., & Thomas, D. L. (1989). *Seismic Behavior of Architectural Precast Concrete Cladding*. Paper presented at the Architectural Precast Concrete Cladding - Its Contribution to Lateral Resistance of Buildings, Chicago, IL., USA.

Schoeneck, F. (1971). Evaluation of the Effects of Earthquake Racking Tests on a StanLock Preformed Glazing Gasket: Standard Products Company, Port Clinton, Ohion.

Smith, B. S., & Gaiotti, R. (1989). *Interaction of Precast Concrete Cladding with a Story-Height Frame Module*. Paper presented at the Architectural Precast Concrete Cladding - Its Contribution to Lateral Resistance of Buildings, Chicago, IL., USA.

Sudarno, I. (2003). *Performance of Thin Precast Concrete Wall Panels Under Dynamic Loading.* Masters Thesis, University of Canterbury.

Tassios, T. P., & Tsoukantas, S. G. (1978). *Serviceability and Ultimate Limit States of Large Panel Connections Under Static and Dynamic Loading*. Paper presented at the Symposium on Mechanican and Insulating Properties of Joints in Precast Reinforced Concrete Elements, Athens, Greece.

Thiel, C. C., Elsesser, E., Lindsay, J., Kelly, T., Bertero, V. V., Filippou, F., & McCann, R. A. (1986). *Seismic Energy Absorbing Cladding System: A Feasibility Study*. Paper presented at the ATC-17 Seminar and Workshop on Base Isolation and Passive Energy Dissipation, San Francisco, CA., USA.

Thurston, S. J., & King, A. B. (1992). Two-Directional Cyclic Racking of Corner Curtain Wall Glazing *SR44*: Building Research Association of New Zealand.

U.S. Congress. (1995). Reducing Earthquake Losses. U.S. Government Printing Office, Washington D.C.: Office of Technology Assessment.

Wang, M. L. (1986). *Nonstructural element test phase: U.S.-Japan Cooperative Research Project on a Full Scale Steel Test Frame*: Center for Environmental Design Research, Univ. of California, Berkeley.

Wang, M. L. (1987). Cladding performance on a full-scale test frame. *Earthquake Spectra, 3*(1), 119-173.

Wang, M. L., & Bassler, B. L. (1992). *Cladding / Council on Tall Buildings and Urban Habitat*. New York, NY., USA: McGraw-Hill.

Weidlinger, P. (1973). Shear Field Panel Bracing. *Journal of the Structural Division, ASCE, 99*(7).

Weston, N. R. (2000). *Development of Energy Dissipating Ductile Cladding for Passive Control of Building Seismic Response.* Ph.D. Thesis, Georgia Institute of Technology.

Weston, N. R., Craig, J. I., & Goodno, B. J. (2002). *Passive control of seismic response using ductile cladding panels*. Paper presented at the Seventh U.S. National Conference on Earthquake Engineering Boston, MA., USA.

Wolz, M. W., Hsu, C. C., & Goodno, B. (1992). *Nonlinear Interaction between Building Structural Systems and Nonstructural Cladding Components*. Paper presented at the ATC-29 Seminar and Workshop on Seismic Design and Performance of Equipment and Nonstructural Elements in Buildings and Industrial Structures.

Wright, R. N., Kramer, S., & Culver, C. (1973). *Building Practices for Disaster Mitigation.* Paper presented at the National Workshop on Building Practices for Disaster Mitigation, Building Science Series 46.

Zarghamee, M. S., Schwartz, T. A., & Gladstone, M. (1996). Seismic behavior of structural silicone glazing *Science and technology of building seals, sealants, glazing and waterproofing*: American Society for Testing and Materials.

4 Quasi-Static Testing of Traditional Heavy Cladding Systems

4.1 Introduction

The opening chapters of this thesis identified that precast concrete cladding presents a significant life-safety risk to pedestrians, and that the effect it has upon the primary structure is not well understood. This chapter therefore aims to experimentally examine the behaviour of heavy cladding systems that utilise traditional connection typologies. The traditional connection typologies tested are variations of tie-back rod and slotted plate connections. These have been introduced in Chapter 2 – Background to Cladding Systems. A test frame which represents a single-storey, single-bay portion of a reinforced concrete (RC) building is used to test the cladding systems. The cladding-frame system is tested under uni-directional quasi-static cyclic loading.

The cyclic response of the cladding-structure system is compared to a benchmark test of the frame without any cladding present. This allows the effect of the cladding presence upon the lateral resistance of the frame to be investigated. Values found for the lateral stiffness of the cladding connections and cladding panel can be inferred by measuring the difference in force-displacement behaviour of the system with and without cladding. The testing also investigates the performance limits of the cladding system when traditional connections are used.

4.2 Design and Construction of the Experimental Sub-assembly

A racking test is the typical experimental testing procedure used to test the seismic performance of cladding (AS/NZS 4284, 2008). A racking test aims to replicate the relative

inter-storey displacements observed during an earthquake. This is achieved by having a fixed beam on one level and the other beam being able to slide back and forth to simulate lateral seismic motion. Racking tests are traditionally undertaken using a cyclic, quasi-static loading protocol. The cladding is attached to each of the beam and subjected to increasing levels of positive and negative displacement. This cyclic, quasi-static loading enables deformation limits to be established using damage observations (Wang, 1987).

The experimental setup used was a variation of a simple racking test, however it was able to capture some effects that a simple racking test cannot, which will be discussed later. The setup consists of a full scale, single-bay, single-storey reinforced concrete frame which represents a portion of a moment-resisting frame, as shown in Figure 4-1.

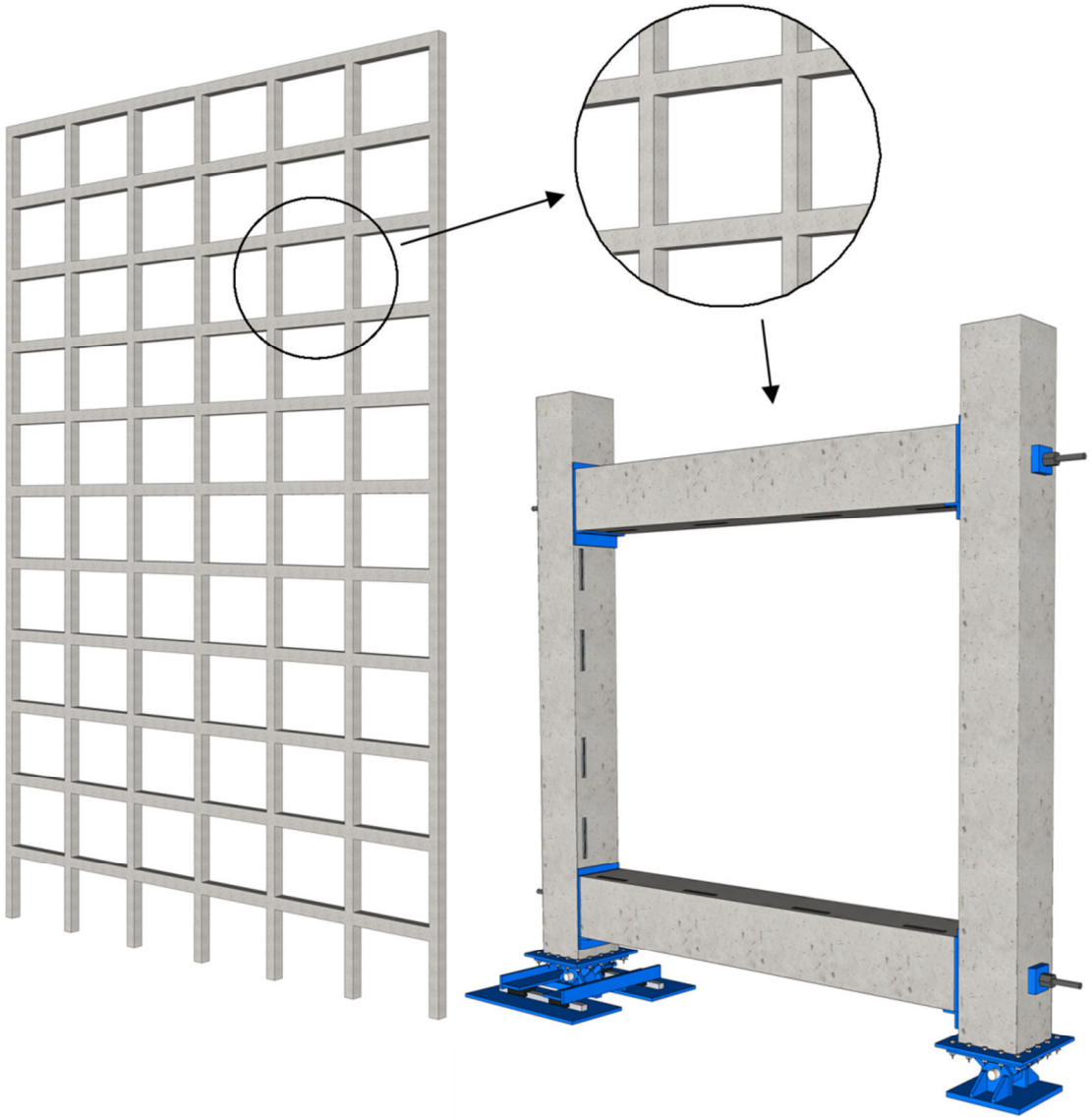

Figure 4-1: Experimental test frame which represents a single-bay single storey portion of a concrete moment-resisting frame building

4.2.1 Test Frame

The design of the test frame was dictated by the requirement that it behave elastically each time it was loaded. This was necessary so that the frame could be loaded repeatedly to high drift levels with negligible damage. It was also required in order to accurately separate the cladding's contribution to the system's strength and stiffness from that of the frame itself.

The frame was pinned at the base and loaded from the top of one column to create a relative inter-storey deflection, similar to that of a racking test. The beams and columns were both made of reinforced concrete, the material properties of which can be seen later in this chapter in Section 4.4. The beam and column members were cast separately and were tied together using post-tensioning bars to provide moment resistance. Steel plates were cast into the ends of the beam and the sides of the columns to provide armouring of the concrete at the beam-column interface. The beam-column connections of the frame utilised Precast Seismic Structural System (PRESSS) technology. As opposed to a monolithic system, the PRESSS connections allowed the frame to be tested repeatedly to high drift levels without sustaining significant structural damage (Priestley et al., 1999). The type of PRESSS connections used for the test frame are referred to as post-pension (PT) only connections as they do not include any form of supplemental dissipation in the beam-column joint region. This PT only connection is only used in structures if it is intended that dissipation will be provided from another mechanism outside of the beam-column joint, e.g. dissipative braces. Since the intention of the testing is to isolate the influence of the cladding from the structure, this PT only connection is the ideal connection type.

The use of PRESSS connections results in some differences in behaviour to that of a monolithic frame. One such difference is that the curvature of the frame elements is not the same. Rather than the beams having a large amount of curvature through the member, this rotation is all concentrated at the beam-column interface. The effect of this is that the cladding connections do not have to undergo any rotation or vertical deformation when connected to the PRESSS frame as they would when connected to a monolithic frame. Since the magnitudes of these deformations are second-order compared to the horizontal deformations of the frame, the effect of these deformations is believed to be negligible for the top (movement) connections. However, for the bearing connections this effect may be more important. Likewise, the effect of plastic-hinging and cracking in the beams may result in the loss of carrying capability of these bearing connections in a monolithic frame; however this is not captured by the test frame. The scope of this research is predominantly focussed on the

top connections and the cladding panels, with the assumption that the bottom bearing connection is completely fixed. Further research into the performance of performance of bearing connections is recommended.

The frame was constructed at full-scale so that real-size connections and cladding components could be used. The inter-storey height was 3.0 m and bay spacing was 3.8 m. The columns were 400 mm wide by 400 mm deep and the beams were 400 mm wide by 450 mm deep. The aspect ratio of the frame was 1.27:1. The frame was connected to a 300 kN hydraulic jack at the top of the western column. The hydraulic jack was attached to a steel reaction frame which was braced against the strong floor of the laboratory. An elevation of the test frame setup can be seen in Figure 4-2.

The frame was connected to a strong floor by pinned connections at the base of each column. One pinned connection was fixed and the other was mounted on two rails with bearing sliders. The bearing sliders allowed the transfer of large vertical forces from the frame to the strong floor but provided no in-plane resistance to allow for frame-elongation during testing.

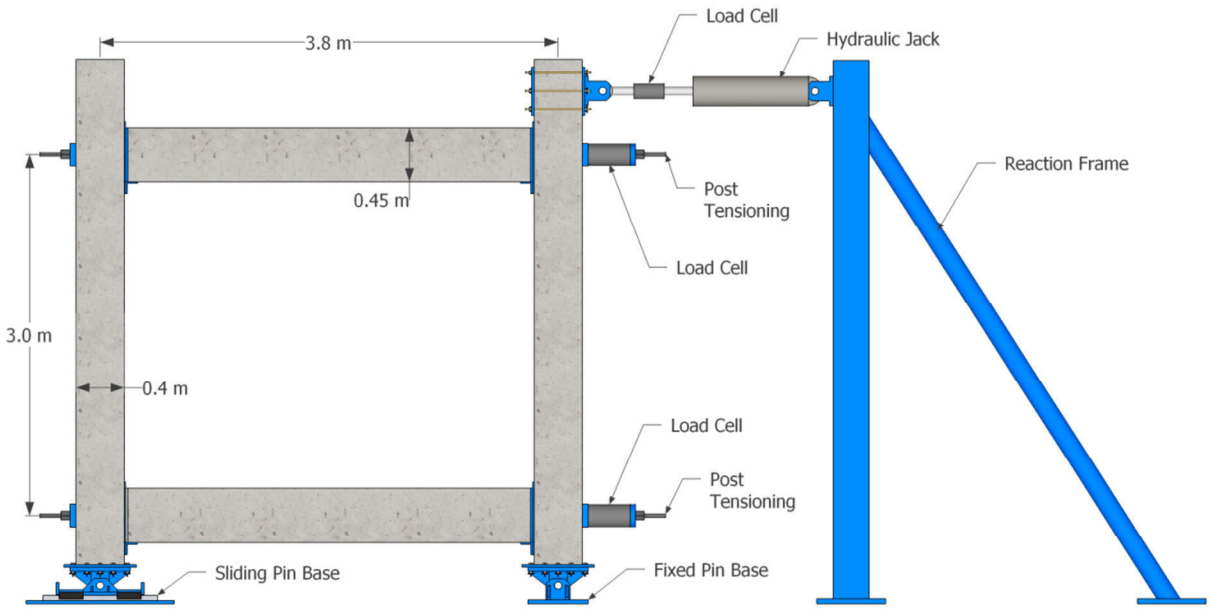

Figure 4-2: Experimental test set-up including loading apparatus

A design level drift of 4.0% was chosen for the test frame. This is double the maximum design drift of 2.0% permitted by the International Building Code (IBC) (ICC, 2000). Even though a typical structure would not be expected to endure repeated 4.0% drift cycles it was decided to design for such a high level of drift to ensure that the frame could test all cladding systems to their ultimate capacity. Further design information for the frame is provided in Appendix C.

In order to design the frame to be able to obtain an inter-storey drift of 4.0%, it was necessary for the frame to be more flexible than a typical structural frame. This could be accomplished by one of two means, either through flexible members or flexible beam-column joint (BCJ) connections. As stated earlier, it was critical that the frame was elastic, therefore this ruled out using flexible members, as designing the beams and/or columns to be flexible would result in plastic (unrecoverable) damage. Thus, it was decided to make the BCJs flexible. This suited the use of PRESSS connections, as the joint stiffness could easily be varied by adjusting the post-tensioning force.

4.2.1.1 PRESSS Connections

The use of post-tensioned connections was essential in order to allow the frame to be tested repeatedly to high drift levels without sustaining significant structural damage. The PRESSS construction system was introduced in the late 1990s at the University of California, San Diego (Priestley, 1991, 1996). It is based on dry, jointed, ductile connections that are held together by unbounded post-tensioning tendons or bars. The inelastic demand is accommodated within the connection itself through opening and closing of an existing gap, as shown in Figure 4-3.

Then PRESSS connections used in the test frame were similar to that shown in Figure 4-3, except that the test frame did not have any non-prestressed (mild) steel passing through the joint. Mild steel provides additional moment capacity as well as dissipation as it yields through axial elongation and compression. Because of the aforementioned design objective of the frame being elastic, mild steel was not included in the PRESSS connections. This also simplified the design as the moment capacity of the joint was directly dependent on the level of post-tensioning.

The theoretical moment-rotation behaviour of the PRESSS connection in both positive and negative directions is shown in Figure 4-3 for an initial post-tensioning force of 60 kN. It can be seen that the decompression point occurs at such a low moment that the moment-rotation behaviour of the connection essentially follows a linear elastic relationship. This behaviour is also akin to a pure hinge connection. Because the behaviour of the connections defines the behaviour of the frame, the moment-rotation behaviour of the frame was also essentially linear elastic. The ability of the frame to re-centre when unloaded is also demonstrated in Figure 4-3. It can be seen that when the connections are unloaded the rotation returns to zero. Consequently, the frame returns back to vertical when unloaded.

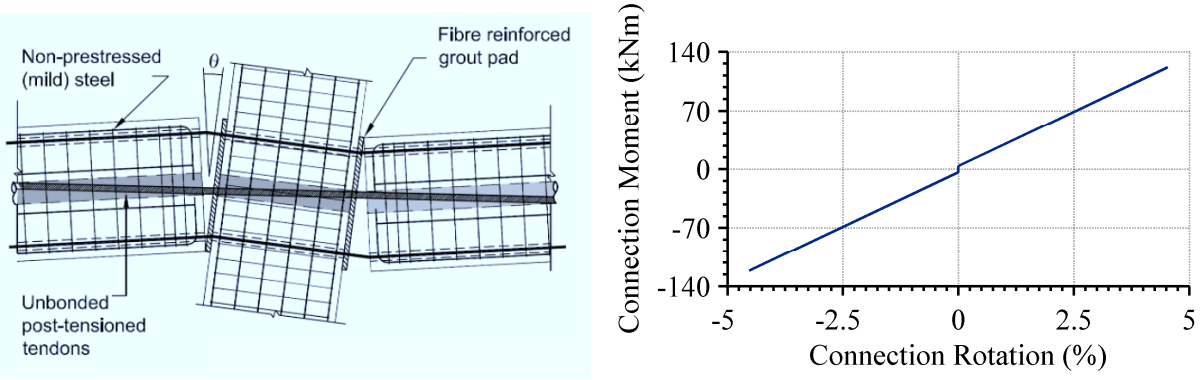

Figure 4-3: PRESSS connection with post-tensioning and internal mild-steel dissipation (left) (Pampanin, 2005) and moment – rotation behaviour of test frame connections (right)

4.2.1.2 Concrete Frame Members

The design of the concrete frame members used a capacity design approach. This approached ensured that the frame members remained elastic by designing for the yield capacity of the beams and columns to be being greater than the moment expected in the PRESSS connections at 4% drift.

The reinforced concrete beams were designed for a yield moment capacity of 290 kNm which was over two times that of maximum moment capacity of the PRESSS connections. This would ensure elastic behaviour of the frame members and the response of the frame would be governed by the characteristics of the PRESSS connections.

The moment-curvature of the beams and columns was calculated using the MATLAB programme CUMBIA (Montejo & Kowalsky, 2007) and is shown in Figure 4-4 along with section diagrams showing reinforcement layouts. The nominal capacity of the beams and columns was found to be 395 kNm and 469 kNm respectively.

A 28 day concrete compressive strength of 50 MPa was specified for both the beams and columns. Grade 500 steel was used for both longitudinal and transverse reinforcement (full material properties of the concrete and reinforcing steel can be found in Section 4.4).

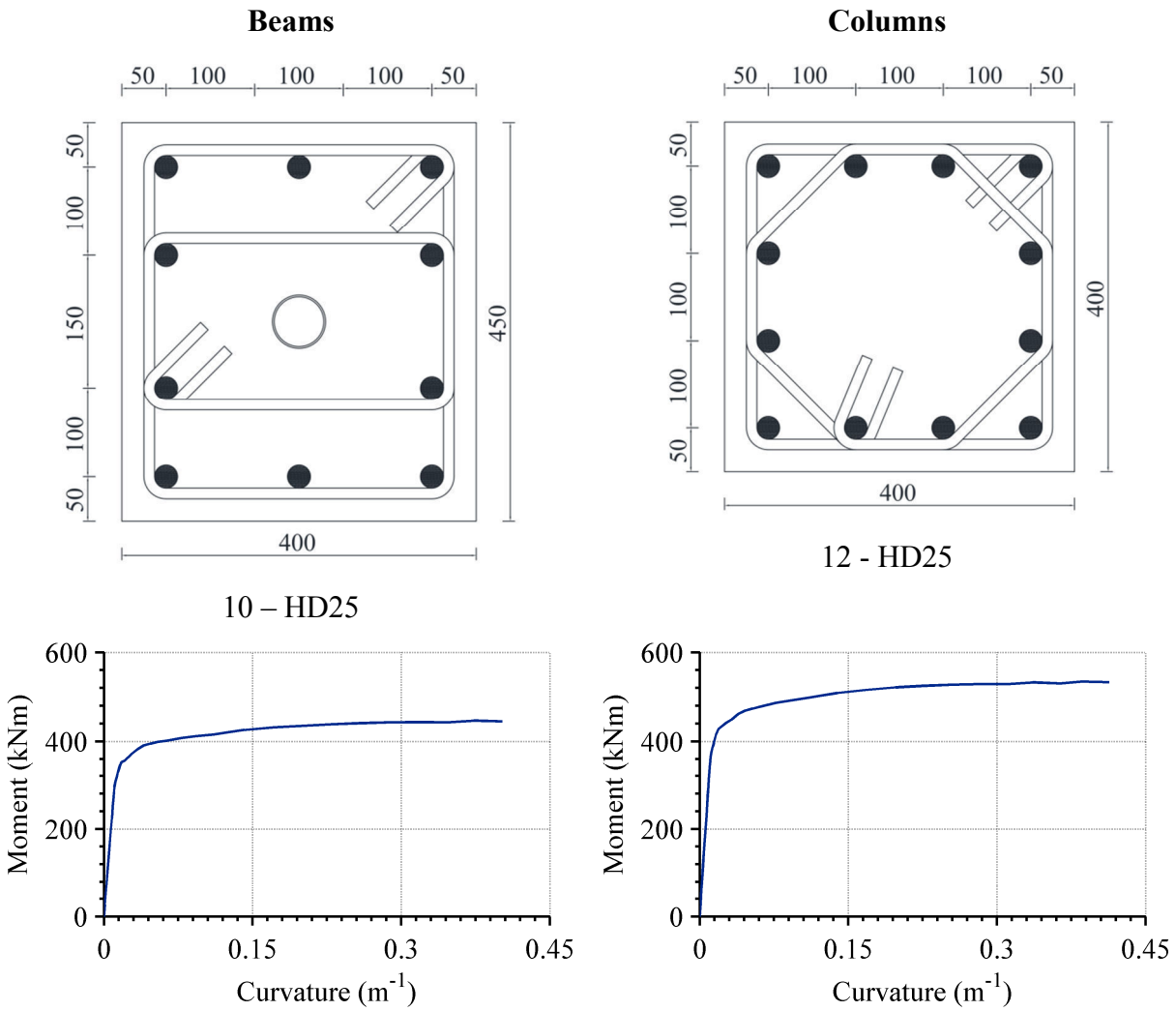

Figure 4-4: Reinforcement section layout (top) and moment-curvature behaviour (bottom) for beam and column members

The frame members reinforcing cage was tied and then the longitudinal steel was welded to the end plate, as shown in Figure 4-5. The members were cast at the Stahlton precast yard in Hornby, Christchurch where they were cured on heated casting beds, also shown in Figure 4-5. A hollow duct was cast the length of the beams, as shown in Figure 4-5, to allow the post-tensioning to pass through. A duct was also cast horizontally through the columns at the beam level for the same purpose. Steel plates were cast into the side of the columns, as shown in Figure 4-5, to provide a smooth rocking interface for the beams and to armour the column concrete.

Figure 4-5: Reinforcement cages of beam and column members including welded end plates

4.2.2 Precast Concrete Panels

Two sizes of precast concrete panels were tested. One size panel was a full-bay, single-storey panel and the other a half-bay, single storey. Both panel sizes had a central, single opening where a window would normally be located. The panels were 120 mm thick and contained a single layer of reinforcement in each direction. The dimensions of the panels, including a typical cross section and the reinforcement layout are shown in Figure 4-6. The panels are reinforced with D12's at 200 mm centres and D16 bars around the opening and external perimeter. 1.0 m length D16s also run diagonally at each corner opening.

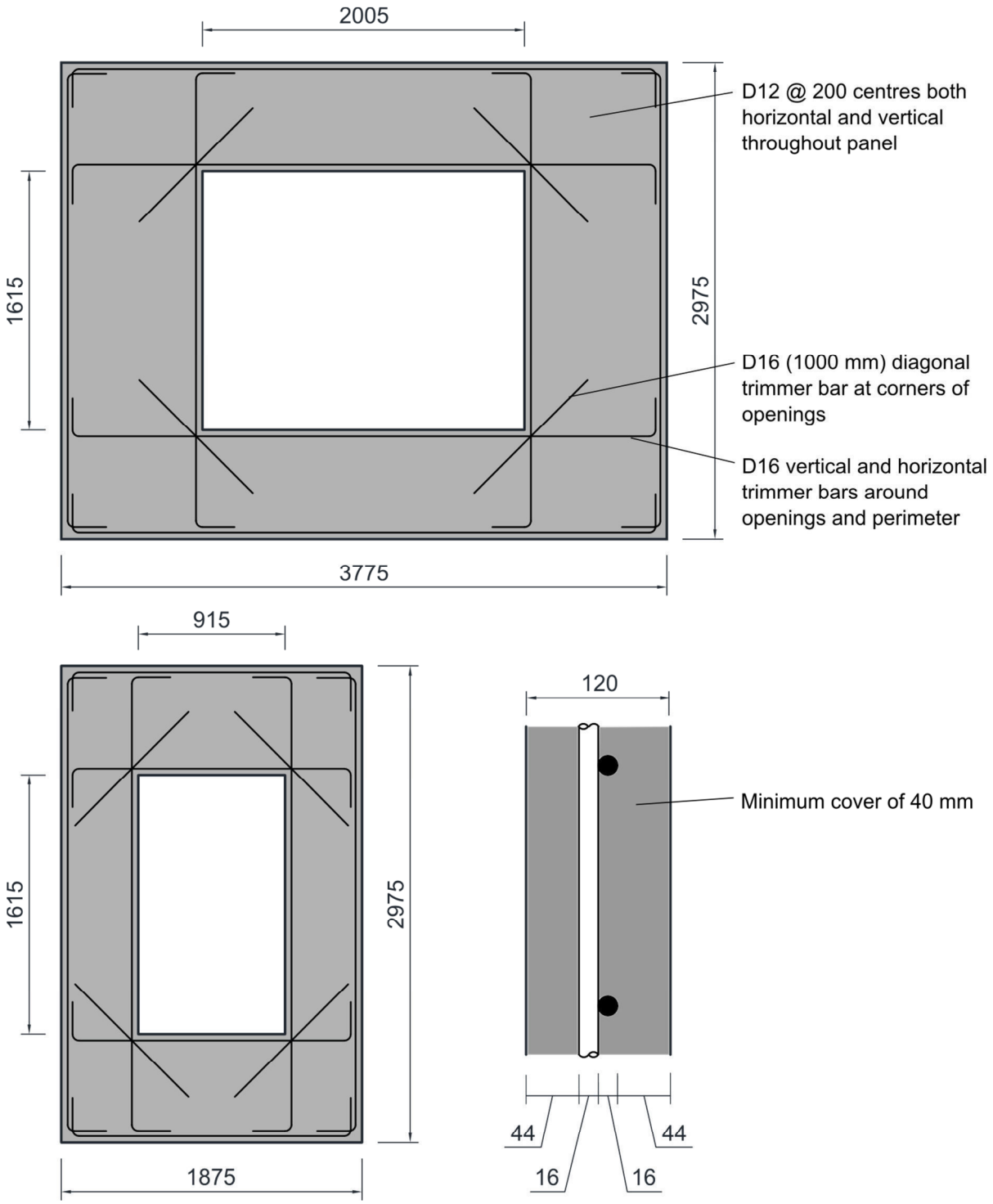

Figure 4-6: Mono panel (top) and dual panel (bottom) panel sizes including cross section

The large panel will herein be referred to as the mono panel system, as tests of this panel included one panel only. Similarly, the two smaller panels will herein be referred to as the dual panel system as both smaller panels were tested simultaneously.

A 28 day concrete compressive strength of 40 MPa was specified for the panels. Grade 300 steel was used for reinforcement (full material properties of the concrete and reinforcing steel can be found in Section 4.4).

A minimum concrete cover of 40 mm was specified for the panels based on an intended life of 50 years and an exposure classification of B2. An exposure classification of B2 is used for surfaces of members in above-ground exterior environments in areas that are located in coastal frontage (NZS 3101, 2006). This corresponds to the maximum environmental exposure for such a panel in all major New Zealand cities.

The panels were designed for serviceability by aiming to limit deflection and cracking of the panel. NZS 3101 (2006) recommends maximum surface width cracks of 0.3 mm at serviceability limit state for reinforced concrete of exposure classification B2. The reinforcement bar size was kept small with a higher spacing in order to improve stress distributions in an attempt to control crack width. The other design consideration was the strength requirement of the panels when performing an edge lift.

The panels were cast at the Stahlton precast yard in Hornby, Christchurch where they were cured on heated casting beds, also shown in Figure 4-7. Also shown in Figure 4-7 is the cast-in lifting insert with hanger bar.

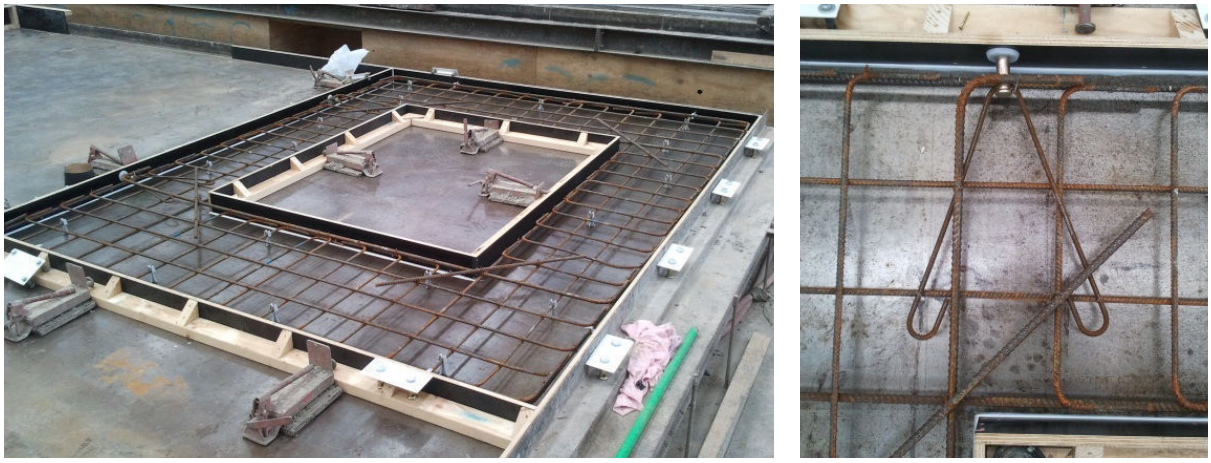

Figure 4-7: Reinforcement cage of mono panel prior to casting (left) lifting insert with hanger bar (right)

4.2.3 Panel Connections

The precast concrete panels were attached to the frame using two different connection types: bearing connections and movement connections, as shown in Figure 4-8. Such an arrangement is the typical method precast panels are attached to a multi-storey structure (Phan & Taylor, 1996). The bearing connections were designed to carry the gravity load of

the panel back to the frame and were located at the base of the panels. Metal angles were used as the bearing connections and were bolted into place using two M20 ferrule anchors cast into the panel and frame. The bearing connection was not able to accommodate movement and acted as a fixed connection between the panel and the frame.

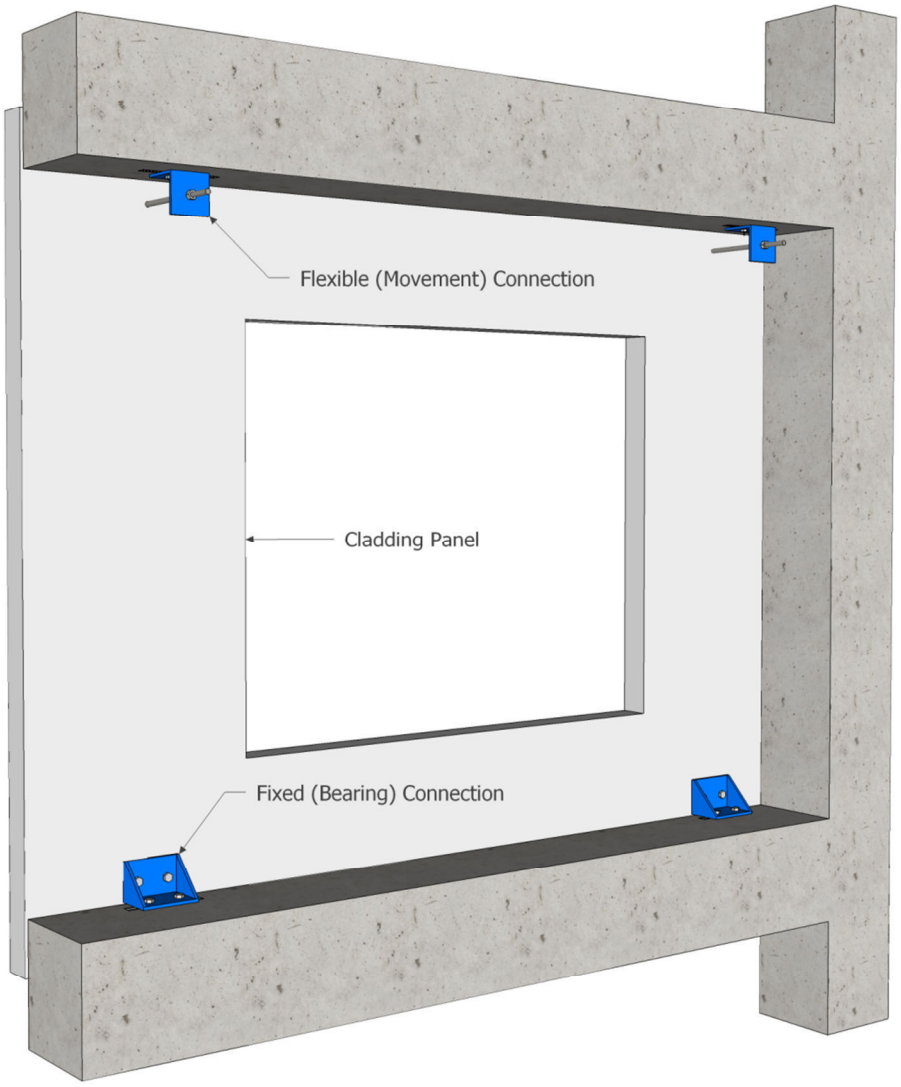

Figure 4-8: Cladding panel connection types and locations

The other connection type was a flexible, or movement connection, and was located at the top of the panels. The movement connections were designed to resist out-of-plane forces due to wind and earthquake loading. Since the panel is very stiff in the in-plane direction and is fixed securely at its base, the top connections also have to be able to accommodate in-plane relative movement between the frame and the cladding panel during earthquake induced movement. The movement connections were varied during testing, which will be explained further in Section 4.3.

4.2.3.1 Design Actions

The panel connections were designed according to the requirements for parts and components of NZS 1170.5 (2004). These define the horizontal and vertical actions using the elastic site hazard spectra for the structure of interest. The actions are found using the peak ground acceleration and the weight of the part when it is multiplied by factors which take into account floor height, period of the part, ductility of the part and the risk factor of the part (please refer to Section 2.5 for more details regarding the code requirements of cladding design). The horizontal and vertical design actions are repeated in Equations (4-1) and (4-2) respectively for convenience.

$$F_{ph} = C_p(T_p)C_{ph}R_pW_p \leq 3.6W_p \quad \textbf{(4-1)}$$

where

F_{ph} = Horizontal design earthquake action on part
$C_p(T_p)$ = Horizontal design coefficient of the part
C_{ph} = Part horizontal response factor
R_p = Part risk factor
W_p = Weight of the part

$$F_{pv} = C_{pv}C_{vh}R_pW_p \leq 2.5W_p \quad \textbf{(4-2)}$$

where

F_{pv} = Vertical design earthquake action on part
C_{pv} = Parts vertical response factor
C_{vd} = Vertical design action coefficient
R_p = Part risk factor
W_p = Weight of the part

Since the precast concrete panels were considered a hazard to life outside the structure (they weighed more than 10 kg and would be able to fall more than 3 m) they were given a part risk factor, R_p of 1.0 and designed for Ultimate Limit State. The cladding connections were designed for a ductility of 1.0.

The horizontal and vertical design actions are determined from the weight of the panels. The weight of the mono panel and dual panels are given by (4-3) and (4-4) respectively.

$$W_{p(MP)} = \rho_c V_{p(MP)} = 23.0\ kN \quad \textbf{(4-3)}$$

$$W_{p(DP)} = \rho_c V_{p(DP)} = 11.8\ kN \quad \textbf{(4-4)}$$

where

W_p = Weight of panel (kN)

ρ_c = Density of concrete (kN/m^3)

V_p = Volume of panel (m^3)

The horizontal and vertical actions for the two panel sizes are presented in Equations (4-5) and (4-6). These actions found to be equal to the upper limits prescribed by Equations (4-1) and (4-2) of 360% and 250% of the weight of the panel for horizontal and vertical actions respectively. The bearing connections were designed to resist the vertical and horizontal action and the movement connections were designed to resist the horizontal action alone.

$$F_{ph} = 3.6W_p \quad \textbf{(4-5)}$$

$$F_{ph} = 2.5W_p \quad \textbf{(4-6)}$$

where

F_{ph} = Horizontal design earthquake action on part

F_{pv} = Vertical design earthquake action on part

The corresponding horizontal and vertical actions for each panel size are given in Table 4-1.

Table 4-1: Design actions for each panel size in accordance with NZS 1170.5 (2004)

	Horizontal Action (kN)	Vertical Action (kN)
Mono Panel	84.6	58.8
Dual Panel	43.4	30.2

4.2.3.2 Connection Design

The threaded rod diameter required to resist the horizontal actions in Table 4-1 is determined according to the strength design for tension members prescribed in Chapter 7 of NZS 3404 (1997). This aims to prevent failure of either excessive elongation (yield over the gross area) and sudden strength decrease (fracture over the effective net area) according to

Equation (4-1) and (4-8) respectively. The net area of a threaded rod is found from the shank diameter of the rod, as given by ISO 68-1 (1998).

$$N^* \leq \emptyset_t A_g f_y \quad \textbf{(4-7)}$$

$$N^* \leq 0.85\emptyset_t A_n f_u \quad \textbf{(4-8)}$$

where

N^* = Tension force

$\emptyset_t$ = Strength reduction factor for tension = 0.9

A_g = Gross area

A_n = Net area

f_y = Yield stress

f_u = Ultimate tensile stress

The panel actions will be resisted by two threaded rods. It was found that in order to satisfy both Equation (4-1) and (4-8) two rods of 20 mm diameter or four rods of 12 mm diameter were required to resist the horizontal actions.

The design of the connection fixings was also made using parts and components of NZS 1170.5 (2004). Ferrule anchors were used in the panel and slotted t-channels were used in the frame. The anchors were cast into the panel in various locations allowed various connection arrangements. Slots in the angle connections and the t-channels in the frame provided construction tolerance in all three directions.

Construction and fabrication of all connections was carried out in the Civil Engineering workshop at the University of Canterbury. The connections used commonly available materials.

4.3 Details of Specimens

The movement connection is the most influential component of the interaction between the frame and cladding. Consequently, the testing programme consisted of testing several variations of movement connections. Three typical movement allowance connections types were tested: long threaded rod tie-backs (commonly referred to as push-pull connections in the USA), short threaded rod tie-backs, and slotted angle connections. The number, size, length and location of the three connection types were varied in order to assess

the influence these parameters had on the connection behaviour. The possible location of all connections is shown in Figure 4-9.

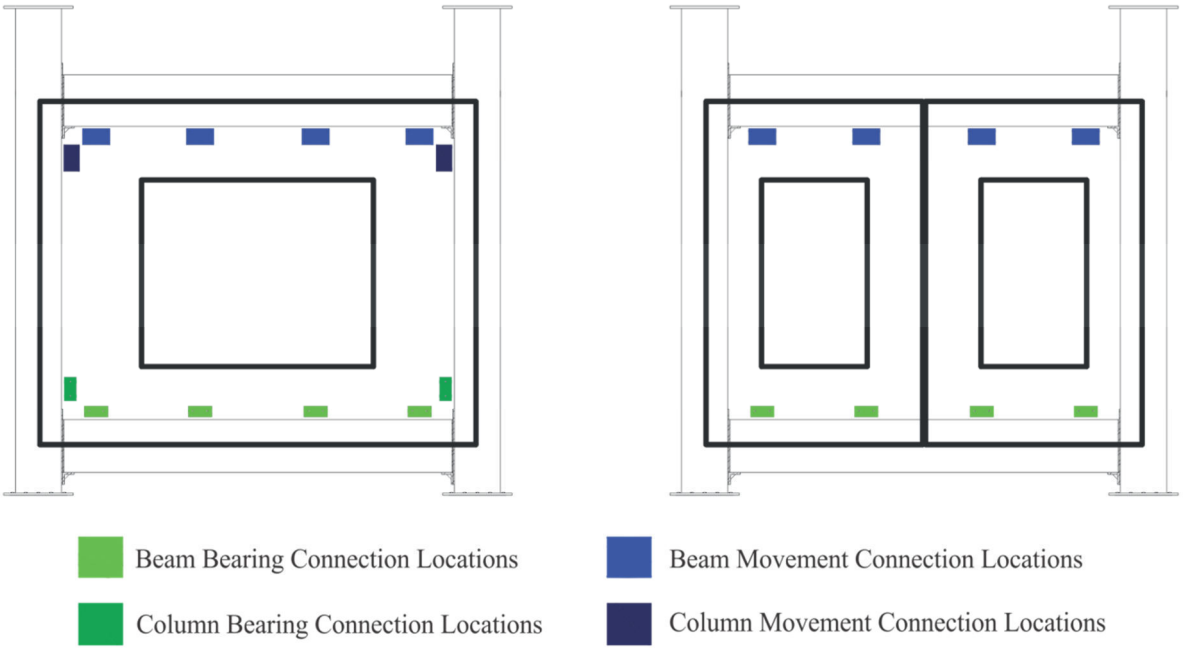

Figure 4-9: Possible connection locations for mono panel (left) and dual panel (right)

Each of the connection types were tested when attached to both of the sizes of precast concrete panels. A total of 14 cladding systems were tested, with the same bearing connections being used for each test. The testing sequence was such that the connections which risked damage to the panels were tested last so the panels remained undamaged for most of the testing.

The interface with the cladding panel at the top movement is a 10 mm thick steel plate that is bolted to four anchors cast into the concrete. A small recess was made behind the steel plate during casting so that the connections would be bolted to the plate, as shown in Figure 4-10. Such a connection fixing is not typically used but allowed a variety of connections to be simply attached to the cladding panels. A typical connection fixing that is used in New Zealand is a weld-plate or drilled chem-set anchor. Such fixings do not provide the 'plug-and-play' capability that was required for the testing programme. The fixings of the connections were not included in the scope of the testing programme, hence it has been assumed that the connection fixing has been sufficiently designed to provide a capacity of greater than the force required to fail the movement connection. If the connection fixing is strong and rigid then the bolted plate is an acceptable substitute for a typical fixing.

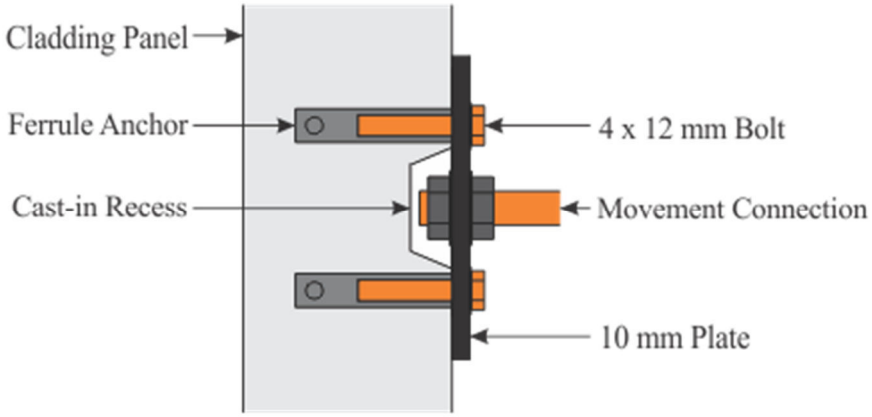

Figure 4-10: Movement connection fixing to cladding panel

Testing of the long threaded rod connections was undertaken first since these connections were not expected to cause any damage to the panels. The long threaded rod connection tested consisted of two mild steel rods of 20 mm diameter connecting the panels to the underside of the beam. The exposed length of the rods was 250 mm; this excluded the region of the rod inside the nut at each end. The steel type, end fixity, location, number and rod diameter were varied to assess how these influenced the connection behaviour. Table 4-2 summaries the long threaded rod systems tested. Each system was tested three times with the rods replaced after each test.

Table 4-2: Long threaded rod tie-back tests

Test ID	Panel Size	Rod Size	Number/ Location	Details	Steel Grade
MP-LTR1	Mono Panel	20 mm	2 Beam	Fixed-fixed ends	4.6
MP-LTR2	Mono Panel	20 mm	2 Beam	Fixed-fixed ends	8.8
MP-LTR3	Mono Panel	20 mm	2 Beam	Fixed-pinned ends	4.6
MP-LTR4	Mono Panel	20 mm	2 Column	Fixed-fixed ends	4.6
MP-LTR5	Mono Panel	12 mm	4 Beam	Fixed-fixed ends	4.6
DP-LTR1	Dual Panel	20 mm	4 Beam	Fixed-fixed ends	4.6

Testing of the slotted connections was undertaken following the testing of long threaded rods. These were tested before the short threaded rods were tested since the latter were expected to result in damage to the panel. The slotted connections tested consisted of two mild steel rods of 20 mm diameter connecting the panels to the underside of the beam through a horizontally slotted steel angle. The length of the rods was 120 mm and was able to slide horizontally through the slot in the angle. A large washer was used on either side to ensure the rod could not pull through the slot. A variation of the connection was proposed by placing a tubular spacer between the washers and tightening the two washers against the tube.

A 3D exploded view of this connection detail is shown in Figure 4-11. This ensured that the washers on either side were firmly held in place and could not rattle.

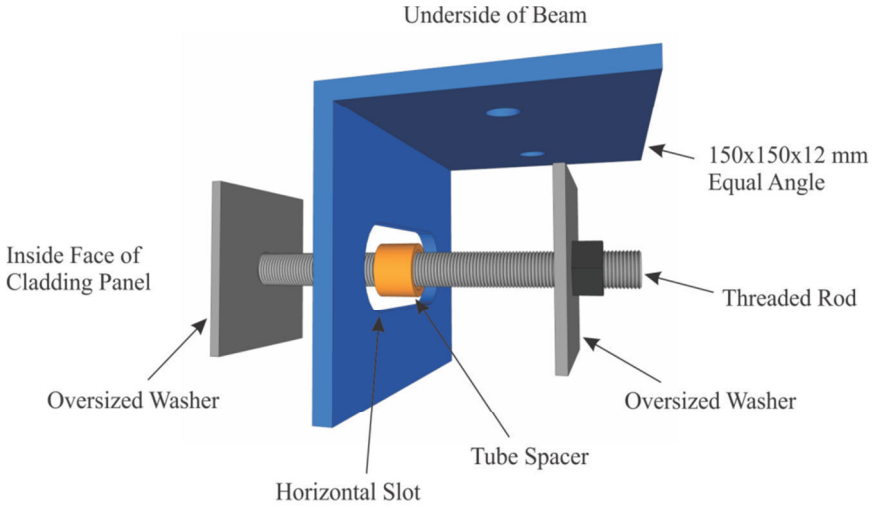

Figure 4-11: Exploded 3D view of slotted connection with tube spacer

A section and elevation of the slotted connection are shown in Figure 4-12. The slotted region of the angle was offset from the panel face due to the location of the cast-in fixing to the underside of the concrete beam. The offset from slotted face to the back of the panel was 110 mm; however, the length of exposed rod was 50 mm. This exposed rod length was the same as that of the short threaded rod connections.

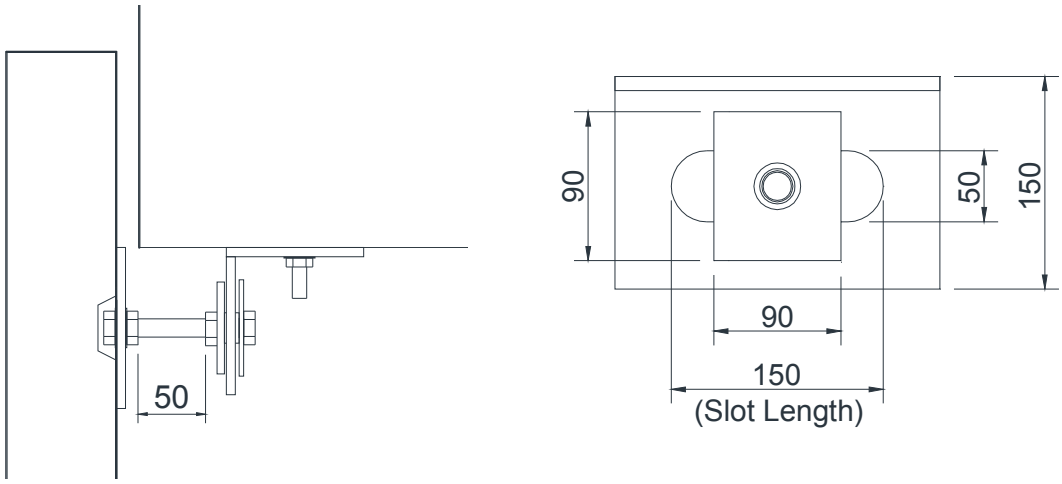

Figure 4-12: Section (left) and elevation of slotted connection (right)

The slot length was varied so that the effects of displacement beyond the slot length could be examined. Table 4-3 summaries the slotted connections tested. Each system was tested three times with the rods and washers replaced after each test.

Table 4-3: Slotted connection tests

Test ID	Connection Type	Slot Length	Number/ Location	Details
MP-SL1	Mono Panel	300 mm	2 Beam	No spacer
MP-SL2	Mono Panel	300 mm	2 Beam	Spacer inside slot
MP-SL3	Mono Panel	150 mm	2 Beam	No spacer
MP-SL4	Mono Panel	150 mm	2 Beam	Spacer inside slot
DP-SL1	Dual Panel	300 mm	4 Beam	Spacer inside slot

Testing of the short threaded rod connections was undertaken last first since these connections were expected to result in damage to the cladding panels. Similarly to the long threaded rod system, the system consisted of two mild steel rods of 20 mm diameter connecting the cladding panel to the underside of the beam. The exposed length of the rods was 50 mm. The key area of interest from testing the short threaded rod connections was to observe the performance of the cladding panel, therefore, the connection configurations tested consisted of two and four rods to look at the largest likely load transferred into the panels. Table 4-4 summaries the short threaded rod systems tested. Each system was tested three times with the rods replaced after each test.

Table 4-4: Short threaded rod tie-back tests

Test ID	Connection Type	Rod Size	Number/ Location	Details
MP-STR1	Mono Panel	20 mm	2 Beam	Mild steel; Fixed-fixed ends
MP-STR2	Mono Panel	20 mm	4 Beam	Mild steel; Fixed-fixed ends
DP-STR1	Dual Panel	20 mm	4 Beam	Mild steel; Fixed-fixed ends

4.4 Material Properties

4.4.1 Concrete

Casting of concrete frame members and cladding panels was undertaken at Stahlton precast yard. The 28 day concrete strength targeted was 40 MPa for the precast concrete panels and 50 MPa for the precast frame members. The concrete strength was tested at 28 days and 90 days. The 90 day strength was obtained during testing and should give a good indication of the concrete strength during testing. The average material properties of the concrete are presented in Table 4-5.

Table 4-5: Concrete material properties

	40 MPa		50 MPa	
	28 Day	**90 Day**	**28 Day**	**90 Day**
Compressive Strength (MPa)	44.9	58.3	55.8	70.8
Tensile Strength (MPa)	6.9	7.3	7.5	7.8
Elastic Modulus (GPa)	35.6	41.6	36.2	41.2

4.4.2 Steel Reinforcement

The steel reinforcement was supplied by Fenwick Reinforcing Ltd according to specification AS/NZS 4671 (2001). Grade 500E deformed bars were used in the precast frame members and Grade 300 deformed bars were used for the precast panels. From tensile tests the average yield stress of the Grade 500E and Grade 300 steel was found to be 568 MPa and 388 MPa respectively.

4.4.3 Post-tensioned Reinforcement

Macalloy 1030 post-tensioning bars were used to provide the post-tensioning force to the frame. Macalloy bar is a high strength carbon chrome steel bar with high strength properties achieved by either cold working or heat treatment. 32 mm Macalloy bars were used which had an ultimate tensile strength of 1030 MPa and yield strength of 835 MPa.

4.5 Experimental Laboratory Test Setup

A photograph of the experimental setup of the test frame is shown in Figure 4-13. A displacement controlled loading protocol was used to undertake the quasi-static, cyclic loading. The displacement was controlled via a rotary pot mounted on an auxiliary frame to the east of the frame. The rotary pot measured the displacement of the eastern column at the ram level. A 300 kN load cell was attached to the ram at the top of the western column to measure the force applied to the frame. 1000 kN load cells measured the post-tensioning force at each level. Instrumentation of the frame was mostly placed on the rearward facing side as to avoid being obstructed by the cladding.

Steel columns and channels were used for the reaction frame as well as to provide out-of plane support. Two adjustable plastic rollers were attached to the steel channels on either side of the frame. These were mounted at the top beam level and adjusted to be flush against the beams, as shown in Figure 4-14 (left). These ensured the beams moved uni-directionally during loading and also provided out-of-plane support against aftershocks.

Figure 4-13: Photographs of experimental test set-up

The eastern pinned support was seated on two rails with bearing sliders, as shown in Figure 4-14. The sliders allowed the transfer of large vertical forces from the frame to the strong floor but provided no in-plane resistance to allow for frame-elongation during testing.

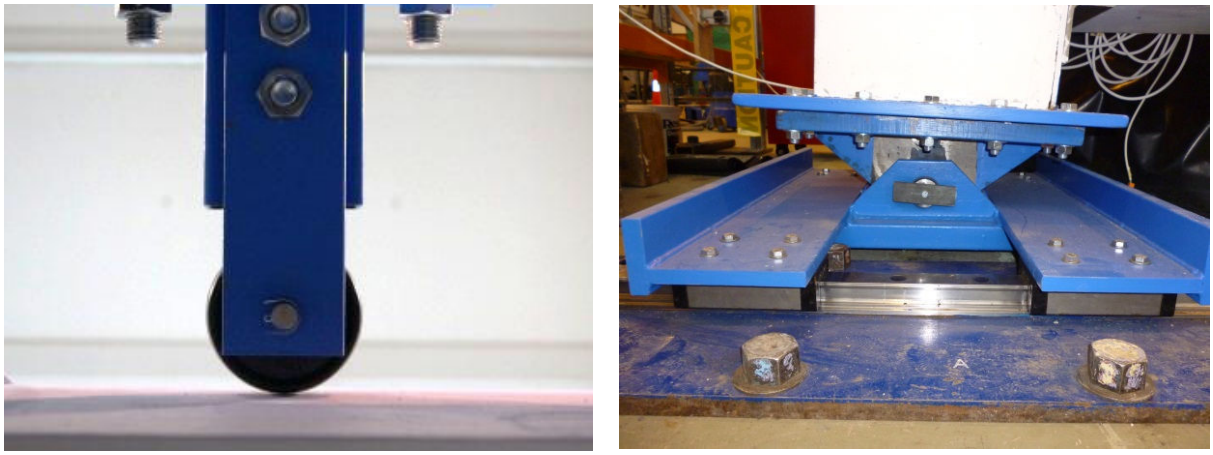

Figure 4-14: Adjustable plastic rollers to ensure frame stayed straight (left), pinned base connection on bearing sliders (right)

4.5.1 Loading Protocol

The quasi-static loading regime consisted of three cycles at each specified drift ratio, as shown in Figure 4-15. The procedure defining the loading protocol was adopted from the ACI recommendations "Acceptance criteria for moment frames based on structural testing" (ACI - 374.1R, 2005). This standard defines the typical MCE displacement demand for moment resisting frames as being a drift ratio of not less than 3.5%. Therefore 3.5% was chosen as the maximum inter-storey drift ratio.

The loading protocol shown in Figure 4-15 was selected since is allows for identification of increasing levels of damage as well as comparison with other structural experiments since it is a commonly used regime. Further research considering different loading protocols is required, particularly since threaded rods are particularly susceptible to low-cycle fatigue and as such their performance may vary depending on the protocol used.

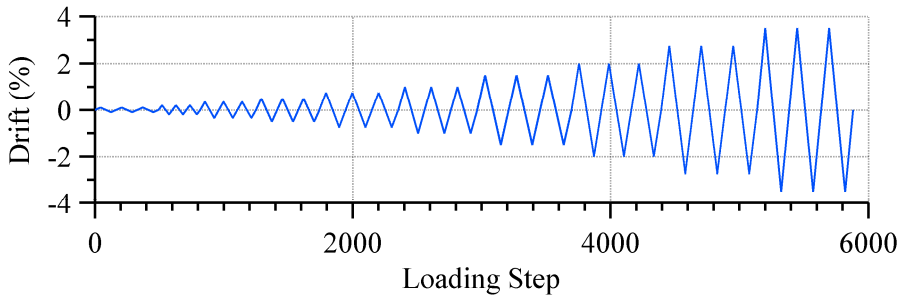

Figure 4-15: Quasi-staitc loading protocol

The loading protocol was controlled by the top displacement of the eastern column. The frame's behaviour was slightly asymmetric due to frame elongation. In the positive direction, frame elongation caused slightly higher drifts than intended and in the negative direction, slightly lower drifts than intended. Frame elongation occurs in traditional concrete frames as a result of the formation of plastic hinges, leading to slab damage and a reduced seating for precast floor elements. Post-tensioned rocking frames also suffer this detriment through the gapping that occurs at the beam-end-to-column-face joint (Amaris et al., 2008).

4.5.2 Erection of Panels

The panels were lifted using a gantry crane and spreader bar which attached to inserts in the top of the panel, as shown in Figure 4-16. A laser level was used to bring the panel up to the correct height and then the bearing connections were bolted into place. The movement connections were then attached and adjusted to bring the panel to vertical. This was again measured using the laser level.

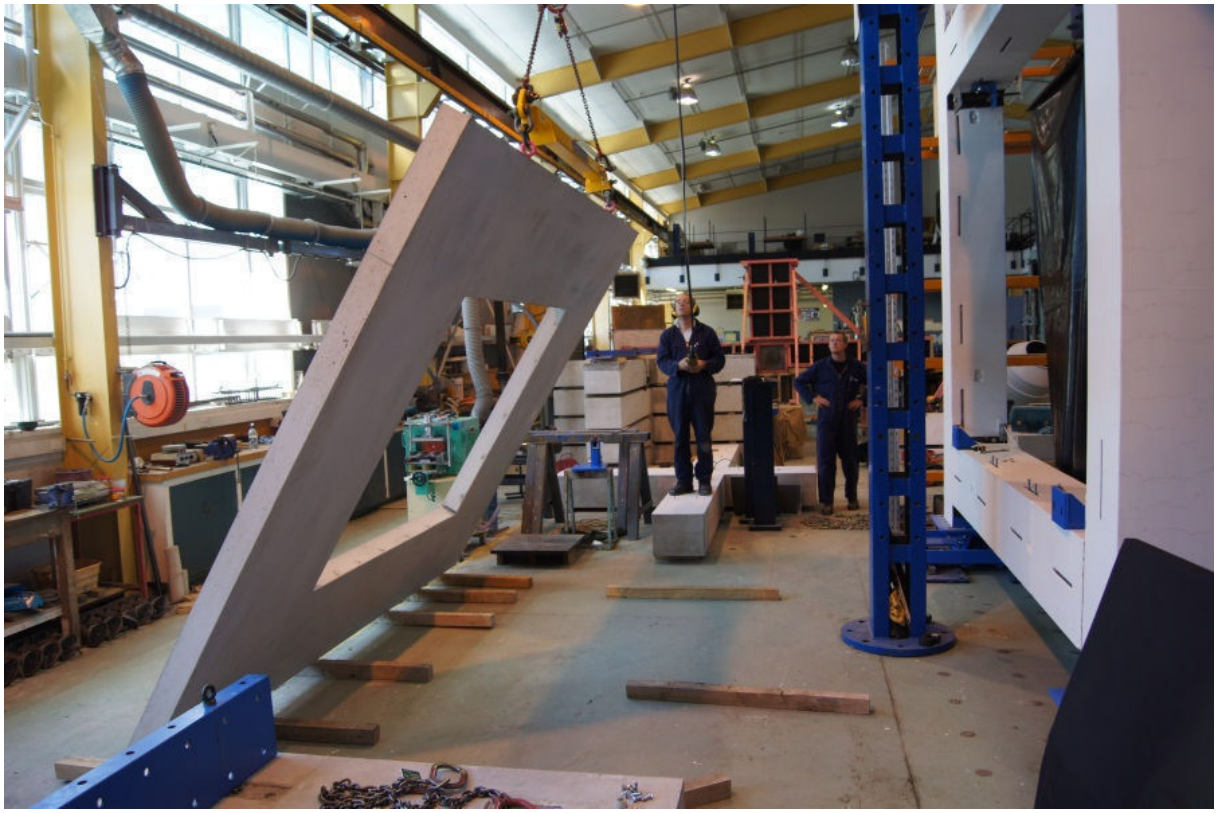

Figure 4-16: Edge lifting of mono panel

A clearance of 25 mm was left between the panel and the frame, as shown in Figure 4-17. This clearance is employed to ensure that the movement of the panel relative to the frame is unobstructed and also to prevent thermal bridging. A stub was placed mounted on

one of the reaction frame columns, as shown in Figure 4-17. It was near to touching the outside face of the cladding panel to prevent the panel from falling outwards when the top panel connections failed.

Figure 4-17: Erection of mono panel (top left), out-of-plane stub restraint (bottom left) and 25 mm clearance between panel and test frame (right)

4.5.3 Instrumentation

The PRESSS connections were thoroughly instrumented during bare-frame testing in order to form a good understanding of the frame's behaviour. 30 mm and 50 mm linear potentiometers (pots) were used on the beam column joint region, as shown in Figure 4-18. These were arranged so that they were able to measure joint rotation, beam curvature, joint deformation and neutral axis position. Spring pots were also attached to the columns to measure the uplift of the beams during rocking. A spring pot was also used to measure the movement of the sliding base.

Rotary pots fixed to an auxiliary frame measured the drift of the frame from the eastern and western column. This gave the ability to capture both the drift of the frame at the two levels as well as the frame elongation. The loading protocol was also controlled by the top displacement of the eastern column.

1000 kN load cells were used to measure the level of post-tensioning force at each level, as shown in Figure 4-18 and a 300 kN load cell was used to measure the force applied to the frame by the hydraulic jack.

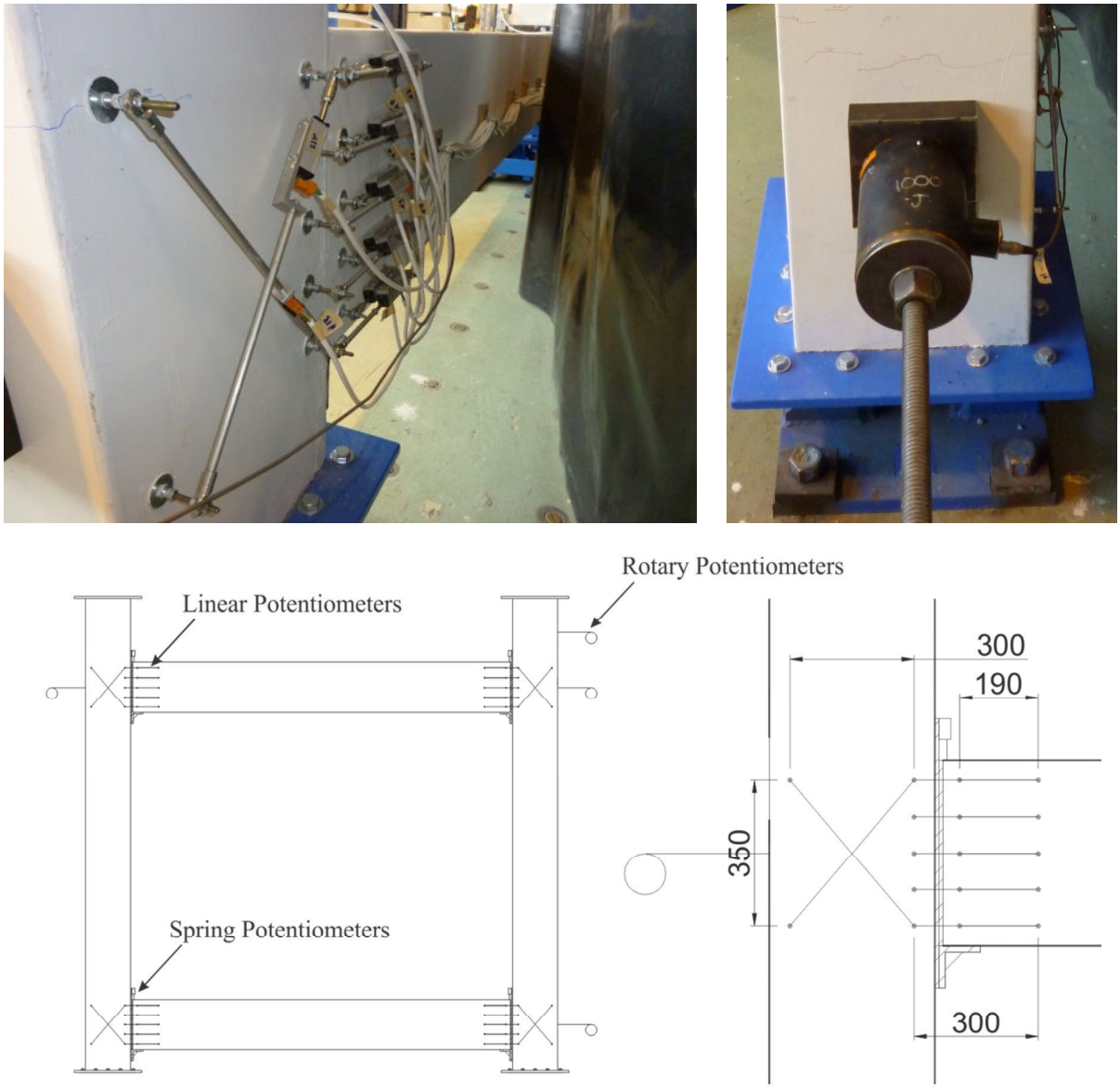

Figure 4-18: Test frame instrumentation

A range of instrumentation was used to capture the deformations in the cladding panels and relative movement between the panels and the frame. Rotary pots were attached between diagonally opposite top and bottom connections to measure the diagonal strut deformation of the panel. Linear pots were attached to the panel around the corner openings as these regions were expected to have the highest local deformations due to the stress concentrations arising from in plane loading. These linear pots were arranged to be at the same angle as the rotary pots measuring diagonal strut deformation.

Spring pots were attached to the top corners of the panel to measure the out-of-plane movement and vertical in-plane movement of the panels relative to the frame. Linear tempsonics were also used to measure the relative in-plane movement between the panels and the frame. These were fixed to the underside of the beams and measured the relative in-plane displacement at the movement location. 30 mm linear pots were used to measure movement between the smaller two panels. The instrumentation of the panels is shown in Figure 4-19.

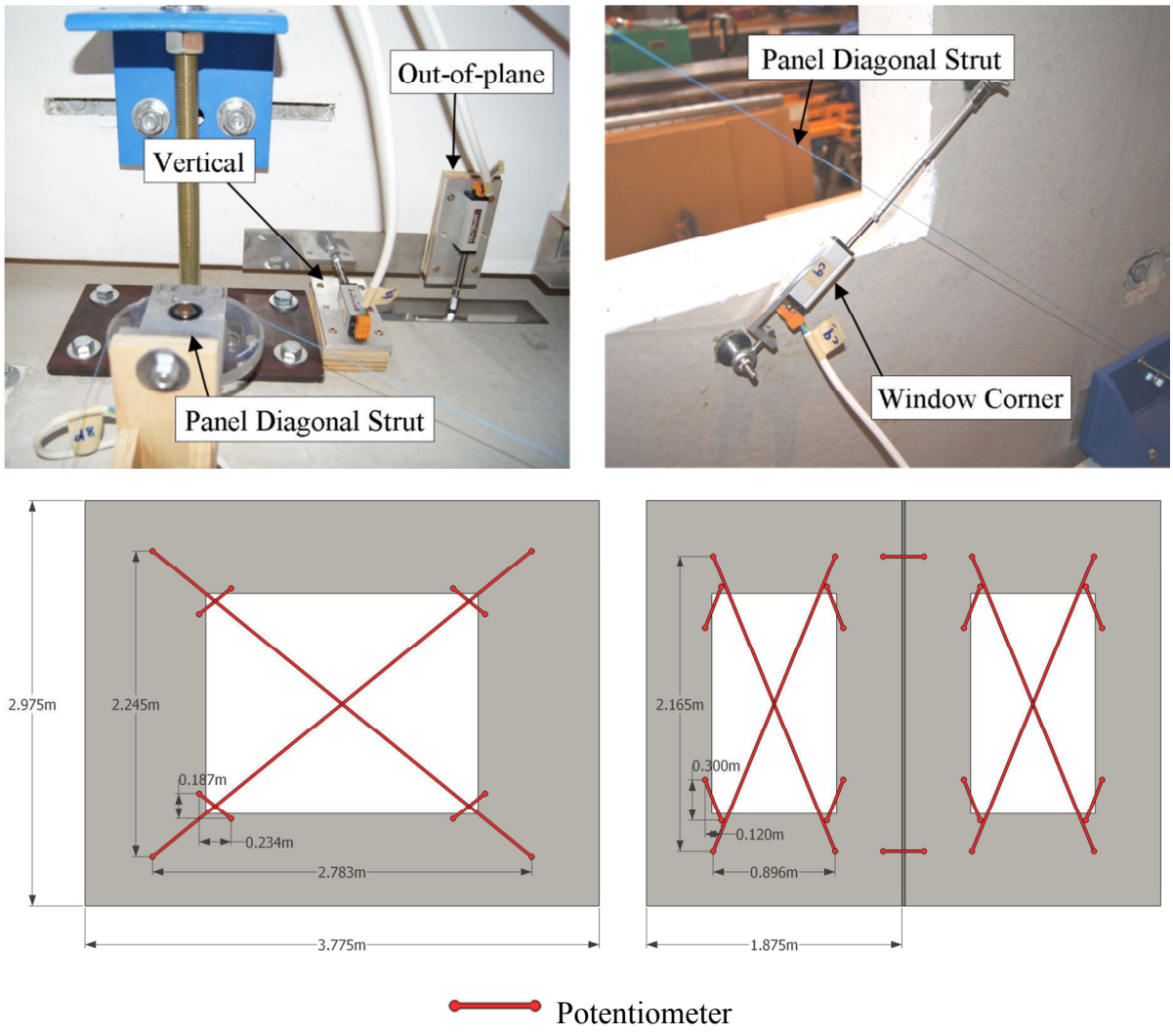

Figure 4-19: Cladding panel instrumentation

4.6 Test Results

The test results will be summarised according to the general connection type. The connections will be grouped according to the following types: long-threaded rod, slotted and short threaded rod. Connection types within these groups showed similar behaviour so the results are presented in this way and any interesting differences within each type will be

discussed. Refer to Table 4-2 and Table 4-3 for a list of all connection types tested and to Appendix D for full test results.

4.6.1 Bare Frame Response

The bare frame response was established by undertaking three consecutive tests of the same specimen without any cladding attached. Three tests were undertaken to ensure a repeatable behaviour in the test frame was established. In this way, the interaction of the cladding with the bare frame could be accurately determined. A small difference between the first and second test force-displacement behaviour was observed, however, the difference between the second and third tests was negligible.

The force-drift response of the bare frame is shown in Figure 4-20 (left). The behaviour is approximately linear elastic, as was theoretically predicted. There were two differences observed between the predicted linear elastic behaviour and the experimental behaviour. These included a small amount of hysteretic behaviour and lower frame stiffness for drifts less than ±1.0%. The small amount of hysteretic behaviour is likely attributed to friction in the beam-column joint and the pin base connections. Minor localised damage around the beam-column joint provided evidence for this theory. The lower stiffness of the frame for drifts less than ±1.0%. was not expected but was concluded to be due to the fact the frame had multiple PRESSS connections. Each PRESSS connection would have a neutral rotation angle at which it would re-centre to when unloaded; however, it is very unlikely the neutral position of all four connections would coincide at 0% drift of the frame (corresponding to when the columns are exactly vertical). This is due to the surfaces not all being perfectly square during construction. Consequently, the stiffness of the frame is reduced at low drifts as each PRESSS connection moves through its neutral position.

The force in each of the two post-tensioning bars for the bare frame test is shown in Figure 4-20 (right). This demonstrates how the neutral position at each level in the frame does not coincide. It can be seen that the level of post-tensioning decreases in the bottom beam under small positive drifts and similarly decreases in the top beam under small negative drifts. This explains the lower stiffness of the frame for small drift levels. The bottom level beam has the lowest level of post-tensioning at approximately +0.7% drift. The top level beam has the lowest level of post-tensioning at approximately -0.4% drift.

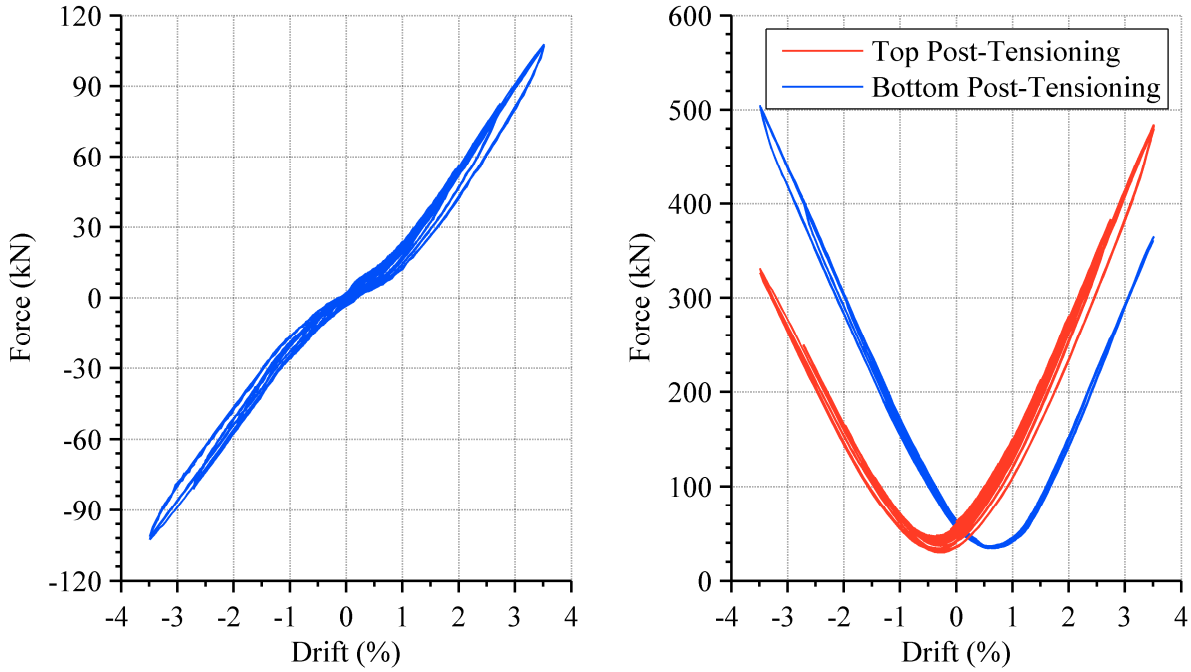

Figure 4-20: Force-drift behaviour (left) and post-tensioning force (right) of bare frame

Three bare frame tests were undertaken before cladding was attached in order for the frame to develop a repetitive cyclic behaviour. The difference in the resisting force of the frame was compared between tests in order to determine whether the frame had developed a repetitive behaviour. The maximum difference in resisting force between the first and second bare frame tests was approximately 15 kN. This is most likely due to the PRESSS joints and post-tensioning moving from initial stressing to find their natural equilibrium as well as minor damage from the first bare frame. The absolute difference between the second and third test decreased to less than 2 kN. By the third test the behaviour of the frame appeared to be repetitious and it could therefore be concluded that when comparing any results the force being resisted by the frame has a level of uncertainty of ±2 kN.

The frame and connections at 3.5% drift are shown in Figure 4-21 (top left and top right). Minor cover cracking was observed in the first bare frame test between 2.0 and 3.5% drift. The cracking was flexural cracking located in the columns, as shown in Figure 4-21 (bottom left), and had a maximum crack width of 0.2 mm. A very small amount of localised crushing was also observed behind the armouring plates of the columns, as shown Figure 4-21 (bottom right).

Figure 4-21: Test frame at +3.5% drift (top left and top right), column cracking (bottom left) and localised crushing (bottom right)

4.6.2 Long Threaded Rod Connections

The long threaded rod connections all had an exposed length of 250 mm and were connected to the frame with steel angles. The exposed length takes into account the fact the rod is essentially fixed in the regions where the nut and washer is. The experimental testing examined the effect the following variables had on the cladding-frame interaction: steel grade, bar diameter, end fixity and location.

The setup of connection MP-LTR1 is shown in Figure 4-22 after being installed (left) and at its maximum drift deformation of 2.0% (right). This connection consists of two 20 mm diameter mild steel threaded rods attached to the underside of the top beam. The steel angle is fixed so that no end rotation of the threaded rod is possible. These connections are designed so that the relative movement between the cladding and frame is accommodated by the flexibility of the threaded rod. It can be observed in Figure 4-22 when the cladding has moved 60 mm relative to the frame that most of this movement is accommodated by inelastic rotation of the threaded rods in the end regions of the rods.

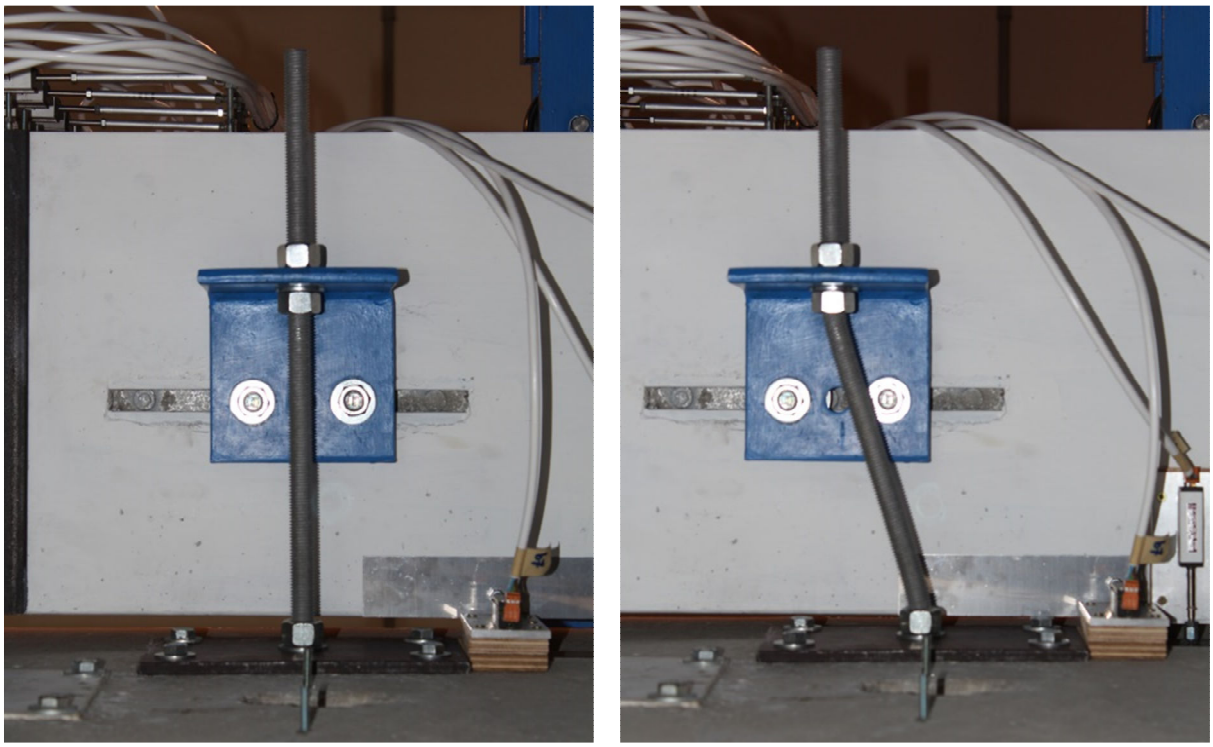

Figure 4-22: Long threaded rod connections at neutral position (left) and 2.0% drift (right)

The force-drift behaviour of the frame when a single precast concrete panel is attached to the frame with connection MP-LTR1 is shown in Figure 4-23 (left). The bare frame behaviour has been limited to the relevant ±1.5% for comparison purposes. It can be seen that

there is a small increase in the strength of the frame as well as the amount of hysteretic damping.

The force difference between test MP-LTR1 and the bare frame test can be computed and is shown below in Figure 4-23 (right). It can be observed that the cladding adds a maximum of approximately 7 kN to the bare frame system. The level of force added by the cladding evidently varies depending on the drift level of the frame. The yield point of the connections also appears to occur at approximately 0.2% drift.

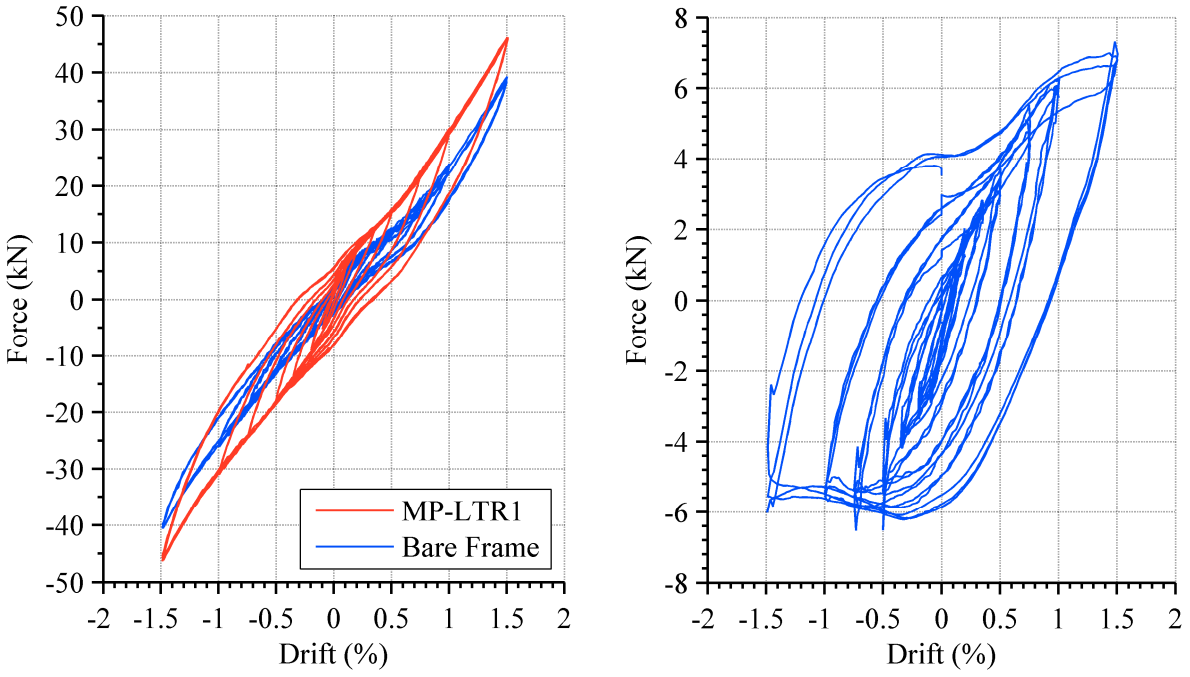

Figure 4-23: Force-drift behaviour (left) and difference between clad and unclad frame (right) for long threaded rod connection test specimen MP-LTR1

There was no evident degradation in the strength of the connection between yield and failure, however different damage states were observed in the form of localised damage. At 0.5% drift, visible cracks parallel to the threads of the threaded rods were observed in between the threads, similar to those shown in Figure 4-24 (top left). At 1.0% drift, cracking perpendicular to the threads was observed, as shown in Figure 4-24 (top right). The cracking occurred in the end regions of the threaded rods. The eastern threaded rod failed on the first negative 2.0% drift cycle. The rod failed at the interface with the nut connecting it to panel, as shown in Figure 4-24 (bottom left). The failure was due to the crack in the threaded rod being worked open as the rod was cycled, ultimately failing in tension due to the reduced capacity. A close-up of the end of the failed rod is shown in Figure 4-24 (bottom right).

Figure 4-24: Parallel cracks (top left), perpendicualr cracks (top right) and rupture (bottom left and bottom right) of long threaded rods

One of the secondary effects observed from the use of the threaded rod tie-back connection type was the out-of-plane movement of the cladding panel. Due to the geometry of the threaded rod, as the cladding panel moves relative to the frame, the panel was drawn in towards the frame. This magnitude of this movement was measured by the out-of-plane spring potentiometers located at the top of the panel. The out-of-plane displacement of the panel relative to the frame's drift is shown in Figure 4-25 (left) with positive displacements representing the panel moving away from the frame. The panel was drawn in a maximum of 10.0 mm towards the frame at 2.0% drift. The original gap between frame and panel was 25 mm. The behaviour was unsymmetrical due to frame elongation and failure of the connection after a single positive 2.0% drift cycle.

The threaded rods also lengthened as cracks developed and opened up. This is shown by the residual positive displacement that develops around 0% drift in Figure 4-25 (left). At the end of the three 1.5% drift cycles the panel had moved 1.0 mm away from the frame. Following the first positive 2.0% drift cycle, the panel moves 1.6 mm away from the panel before failing at the interface with the panel, as shown in Figure 4-25 (right).

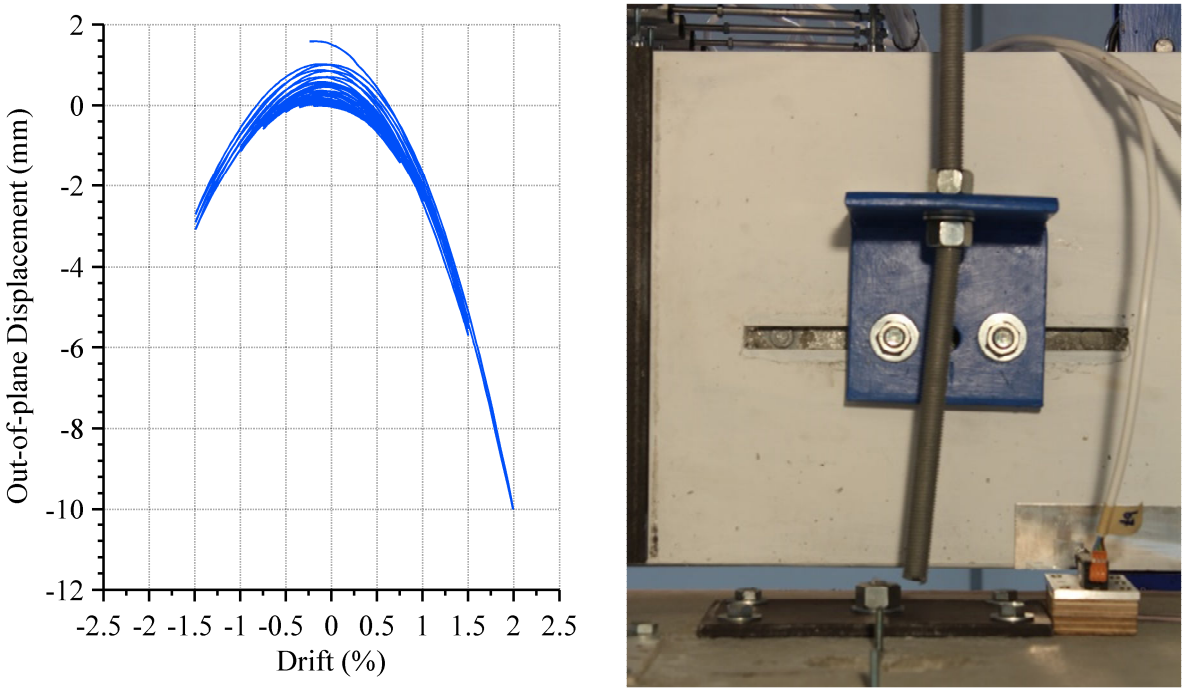

Figure 4-25: Out-of-plane movement of the cladding panel during test MP-LTR1 (left) and long threaded rod connection failure (right)

A total of six long threaded rod connection types were tested in order to gain an understanding of how different connection detailing affects the overall system behaviour. The maximum force results for the six connection types are presented in Table 4-6. The maximum force values are averaged over the three tests undertaken for each connection type. Both the maximum pushover force of the cladding-frame system and the difference between the cladding-frame system and the bare frame (refer to Figure 4-23) at 1.5% drift are presented. The failure drift and cycle number are also presented for each connection and correspond to when one or more threaded rods has completely ruptured.

Table 4-6: Summary of long threaded rod connection test results

Test ID	**MP-LTR1**	**MP-LTR2**	**MP-LTR3**	**MP-LTR4**	**MP-LTR5**	**DP-LTR1**
Rod Size	20 mm	20 mm	20 mm	20 mm	12 mm	20 mm
Location	2 Beam	2 Beam	2 Beam	2 Column	4 Beam	4 Beam
Steel Grade	4.6	8.8	4.6	4.6	4.6	4.6
End Fixity	Fix-fix	Fix-fix	Fix-pin	Fix-fix	Fix-fix	Fix-fix
Max Pushover Force (1.5% Drift)	46.5 kN	52.6 kN	48.7 kN	54.7 kN	44.9 kN	55.2 kN
Max Force Increase (1.5% Drift)	7.2 kN	13.1 kN	8.1 kN	15.0 kN	5.6 kN	15.4 kN
Failure Drift (Cycle Number)	2.0% (1) 1.5% (3) 2.0% (1)	2.0% (1) 2.0% (2) 2.0% (1)	2.0% (2) 2.0% (1) 2.0% (2)	1.5% (3) 1.5% (2) 1.5% (3)	2.75% (1) 2.75% (2) 2.75% (2)	1.5% (3) 1.5% (3) 2.0% (1)

Test MP-LTR1 was effectively the base case for the long-threaded rod connection, with the other connection tests examining the sensitivity of various connection parameters. The use of high-tensile (grade 8.8 steel) was expected to result in an earlier failure compared to the use of mild steel due to it being less ductile, however, this was not the case, with this high tensile threaded rods undergoing more cycles on average. High-tensile steel had a larger maximum lateral force than mild steel, as expected.

The end fixity of the threaded rods was typically fix-fix; however one variation which had a single bolt to the underside of the beam allowed the rod to rotate at this end, effectively making it a pinned end connection. It was expected that this connection typology would not fail as early as the fix-fix connection, and this was the case, however the connection was typically only able to undergo an additional 2.0% drift cycle before it also failed.

Having the connections located on the columns causes the relative displacement between top and bottom connections to be reduced since the connections are closer together than when located on the beams. It would be expected that this would improve the performance of the connections; however, this was found to not be the case. This is possibly attributed to the greater deformation that the connections undergo as a result of the geometric frame elongation of the frame. The connections located on the inside of the columns were found to fail the earliest of all long-threaded connection types tested.

The use of smaller diameter rods reduced the maximum lateral resistance of the cladding system even though more rods were used to connect the panel to the frame. The 12 mm diameter threaded rod connections were also the only connections tested that did not fail prior to reaching the 2.75% drift cycle.

The dual panel system essentially represented a doubling of the base test case (MP-LTR1). The maximum lateral resisting force of the dual panel system was exactly double that of the base case.

4.6.3 Slotted Connections

The slotted connections were formed from 150x150x10 equal angle steel sections with a horizontal slot cut out of one side. The experimental testing examined the effect the slot length and detailing of slotted cladding connections had upon the cladding-frame interaction. The setup of connection MP-SL1 is shown in Figure 4-26 after being installed (left) and at the maximum drift deformation of 3.5% (right). The out-of-plane force of the panel is carried by a 20 mm diameter mild steel threaded rod that is fixed to the inside face of the panel and

passes through the slot of the steel angle. Oversized washers are used to ensure the bolt cannot pass through the slot (refer to Figure 4-11 and Figure 4-12 for details of the connections). The maximum slot length tested is 300 mm. This length was determined based on the maximum expected relative movement between the panel and frame for the maximum drift cycle of 3.5%. It can be observed in Figure 4-26 when the frame is at 3.5% drift that the steel bolt is at the furthest extent of the slot and is not deformed.

Figure 4-26: Slotted connection (300mm slot) at neutral position (left) and 3.5% drift (right)

The force-drift behaviour of the frame when a single precast concrete panel is attached to the frame with connection MP-SL3 is shown in Figure 4-27 (left). The slot length for test MP-SL3 was 150 mm which corresponded to a drift allowance of 1.5%.

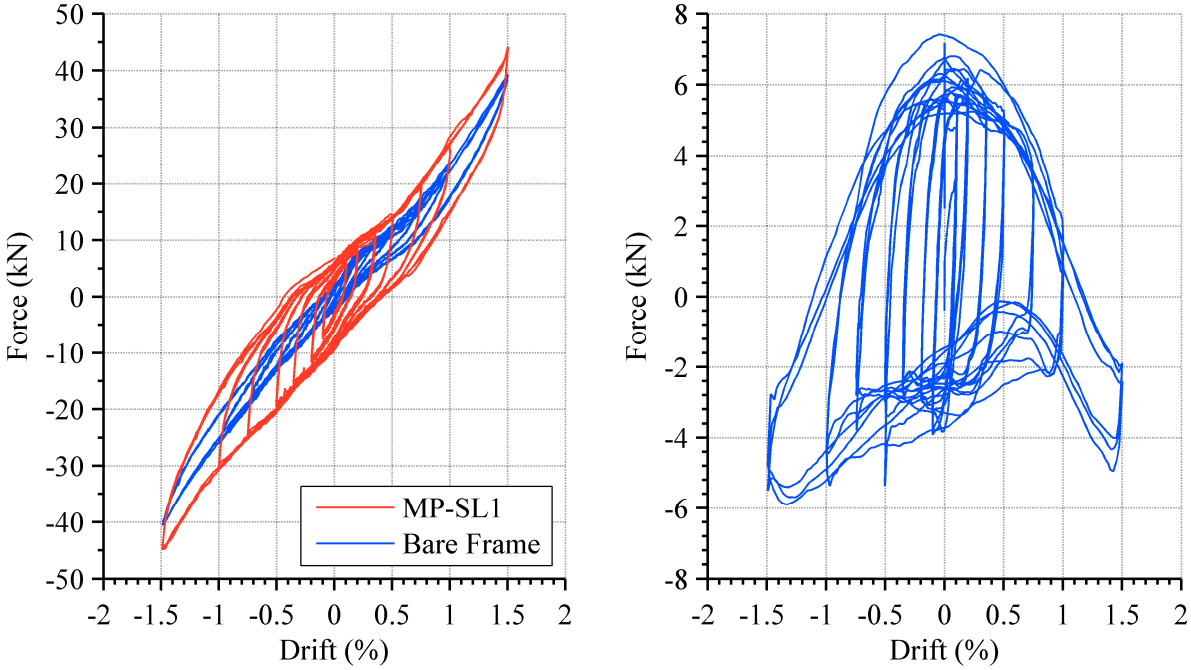

Figure 4-27: Force-drift behaviour (left) and difference between clad and unclad frame (right) for slotted connection test specimen MP-SL3

The results of the test for ±1.5% drift have been presented in order to show the behaviour when movement is within the slots capacity. The bare frame behaviour has been limited to the relevant ±1.5% for comparison purposes. It can be seen that there is a small increase in the strength of the frame when clad with this connection as well as the amount of damping from friction within connection. The force difference between test MP-SL3 and the bare frame test can be computed and is shown below in in Figure 4-27 (right). The cladding adds a varying amount of force to the system. The force difference is presume to be due to the varying amount of friction in the connection between the washers and slotted steel angle.

No damage was observed to either the panel or connections when the slotted connections were tested within the drift allowance of their slot with the exception of one test. During the second MP-SL1 test, one of the bolts became stuck and resulted in cracking in the panel and damage to the connection. The outside washer of the bolt became bent and was drawn into the slot, also bending the slotted angle and bolt as shown in Figure 4-28.

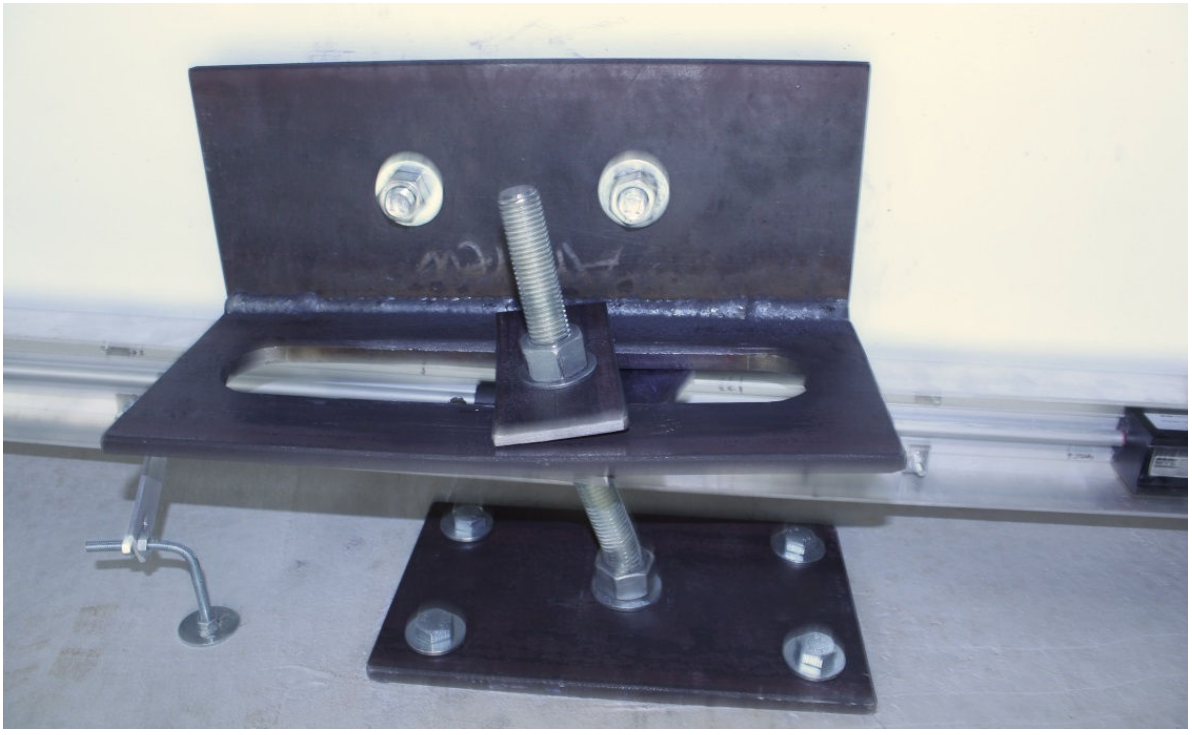

Figure 4-28: Bolt washer that became stuck during testing of slotted connection

It appeared the thinness of the washer was a major factor in the washer becoming stuck. As the washer slid back and forth along the slotted angle, the out-of-plane force likely created a slight bend in the washer causing stress concentrations to form along the edge of the slot and the inside of the washer. After many cycles the steel of the washer began galling, as shown in Figure 4-29 (top left) and consequently the friction between the two surfaces

increases. As a consequence of this the washer became stuck and bent further into the slot. Figure 4-29 (bottom left) shows the final state of the bent washer. 6mm washers were used for the tests, however if thicker washers were used it is believed the chance of the washer getting stuck would be greatly reduced. The bolt becoming stuck resulted in a maximum force of approximately 40 kN being transferred into the panel. Consequently, a crack formed on the inside of the panel adjacent to the connection as shown in Figure 4-29 (right).

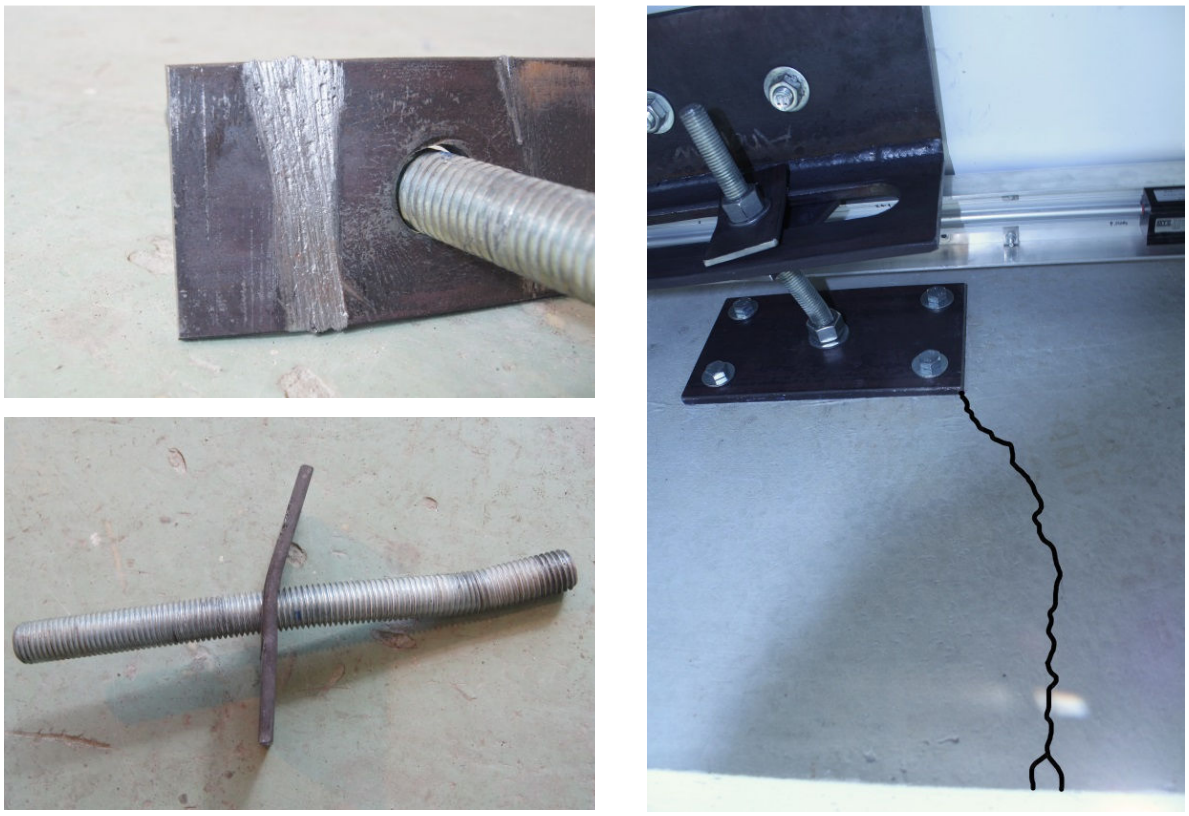

Figure 4-29: Galling of stuck washer (top left), bent washer (bottom left) and crack in cladding panel due to stuck slotted connection (right)

Of particular interest in the detailing of slotted connections was the behaviour of the connection beyond the slot's capacity. Tests MP-SL3 and MP-SL4 tested slotted connections with a slot length of 150 mm, equivalent to a drift allowance of ±1.5%. Beyond 1.5% drift, significantly more force was transferred into the panel. Figure 4-30 (left) shows the force difference between test MP-SL3 and the bare frame test for the full test drift range of ±3.5%.

Also evident is a drop in strength between subsequent cycles, indicating permanent damage is occurring to the precast concrete panel. This was confirmed by the first cracks developing in the panel window corners, shown in Figure 4-30 (right), which will be elaborated on in Section 4.6.5. The out-of-plane displacement of the panel was negligible for all slotted connections tested, as expected.

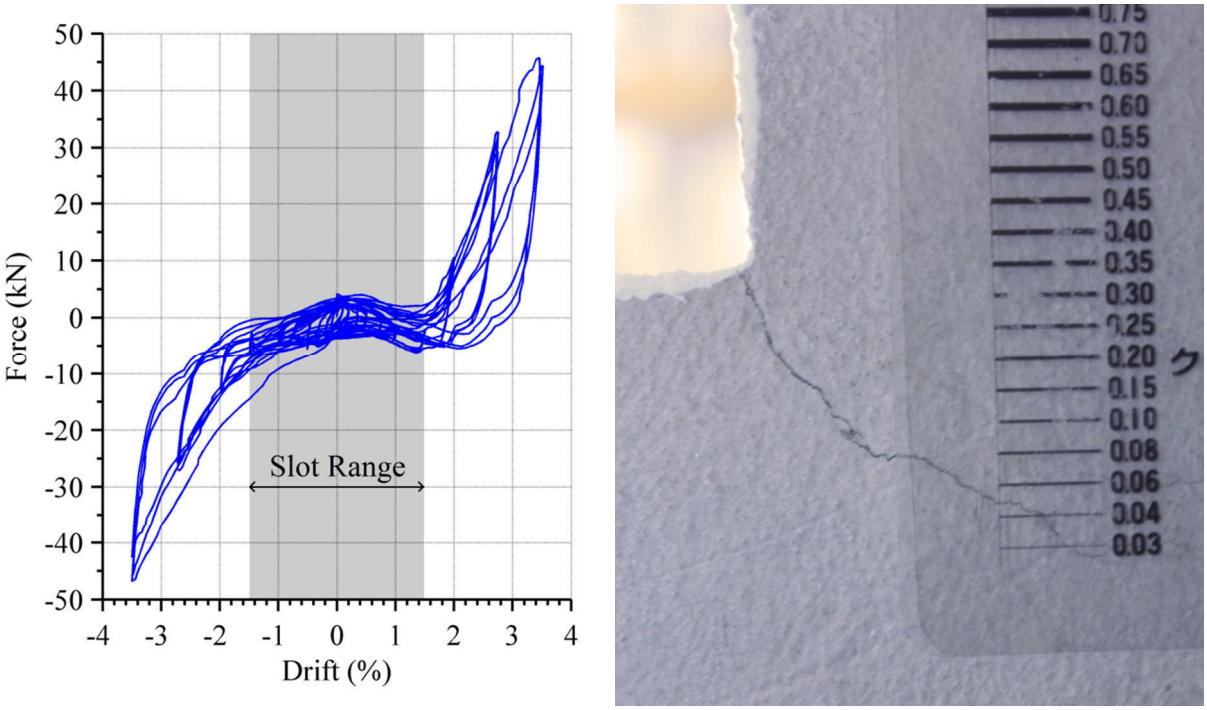

Figure 4-30: Difference between clad and unclad frame for slotted connection test MP-SL3 (left) and cracking damage to cladding window corner (right)

A total of four slotted connection types were tested in order to gain an understanding of how different connection detailing affects the overall system behaviour. The maximum force results for the four connection types are presented in Table 4-7. The maximum values are averaged over the three tests undertaken for each connection type. Both the maximum force of the cladding-frame system and the difference between the cladding-frame system and the bare frame (refer to Figure 4-27 and Figure 4-30) at 1.5% and 3.5% drift are presented.

Table 4-7: Summary of slotted connection test results

Test ID	**MP-SL1**	**MP-SL2**	**MP-SL3**	**MP-SL4**	**DP-SL1**
Slot Length	300 mm	300 mm	150 mm	150 mm	300 mm
Tube Spacer	None	Present	None	Present	Present
Location	2 Beam	2 Beam	2 Beam	2 Beam	4 Beam
Max Pushover Force (1.5% Drift)	45.8 kN	45.4 kN	46.1 kN	44.8 kN	50.6 kN
Max Force Increase (1.5% Drift)	7.8 kN	7.2 kN	8.3 kN	7.4 kN	13.0 kN
Max Pushover Force (3.5% Drift)	109.8 kN	109.2 kN	152.1 kN	156.8	115.6 kN
Max Force Increase (3.5% Drift)	7.7 kN	7.4 kN	46.8 kN	51.1 kN	13.6 kN

After one of the tests of MP-SL1 became stuck, a tube spacer was used to provide a way of ensuring the washers are not able to rattle. The tube spacer used was approximately

14 mm long (4 mm longer than the 10 mm plate of the slotted angle) and was placed between the washers, as shown in Figure 4-11. By having the tube longer than the plate thickness the connection was able to be tightened to restrain the oversized washers making them unable to rotate and avoid becoming stuck. It also meant the connection could be tightened without clamping the connection fixed. This detail made the connection more stable without altering the behaviour of the connection.

The use of two slotted connections per panel for the dual panel system approximately doubled the lateral resistance of the cladding system which shows that the friction force provided from the connection is relatively constant.

4.6.4 Short Threaded Rod Connections

The short threaded rod connections all had an exposed length of 50 mm and were connected to the frame with steel angles. The experimental testing examined the effect the number of short threaded rods had on the frame-cladding interaction. All short threaded rod connections used 20 mm diameter mild steel threaded rods connected to the frame beams.

The setup of connection MP-STR1 is shown in Figure 4-31 after being installed (left) and at the maximum drift deformation of 1.5% (right). This connection consists of two 20 mm diameter mild steel threaded rods attached to the underside of the top beam.

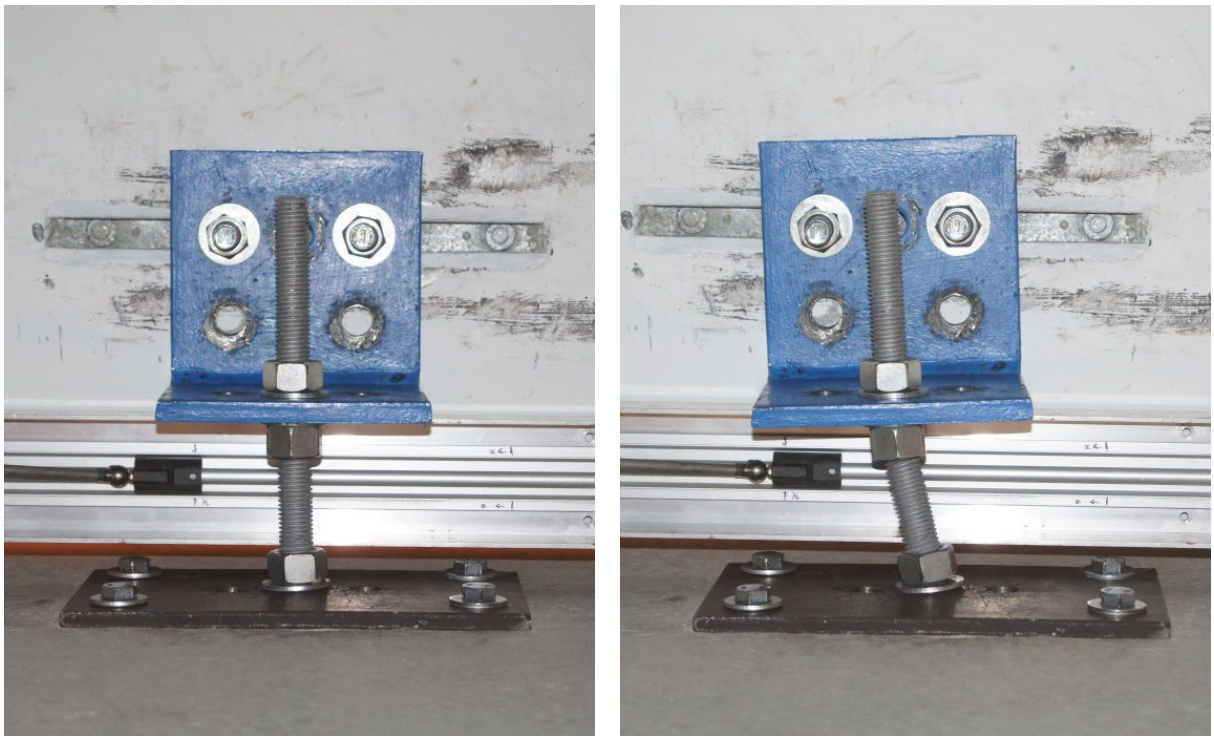

Figure 4-31: Short threaded rod connection at neutral position (left) and 1.5% drift (right)

The steel angle is fixed so that rotation of the threaded rod is minimal. Because of the short length of the threaded rod, only a small amount of movement can be accommodated by the flexibility of the rod. It can be observed in Figure 4-31 when the top beam has moved 45 mm relative that deformation is occurring in the rod as well as the connection fixings. It would also appear that the top of the panel has not moved the full 45 mm relative to the frame which suggests that a significant amount of deformation is occurring in the panel. This is confirmed in the analysis of the panel observations in Section 4.6.5.

The force-drift behaviour of the frame when a single precast concrete panel is attached to the frame with connection MP-STR2 is shown in Figure 4-32 (left). The bare frame behaviour has been limited to the relevant ±2.0% for comparison purposes. It can be seen that there is a significant increase in the strength of the frame and in the amount of hysteretic damping.

The force difference between test MP-STR1 and the bare frame test can be computed and is shown below in Figure 4-32 (right). It can be observed that the cladding adds a maximum of 62 kN to the bare frame system.

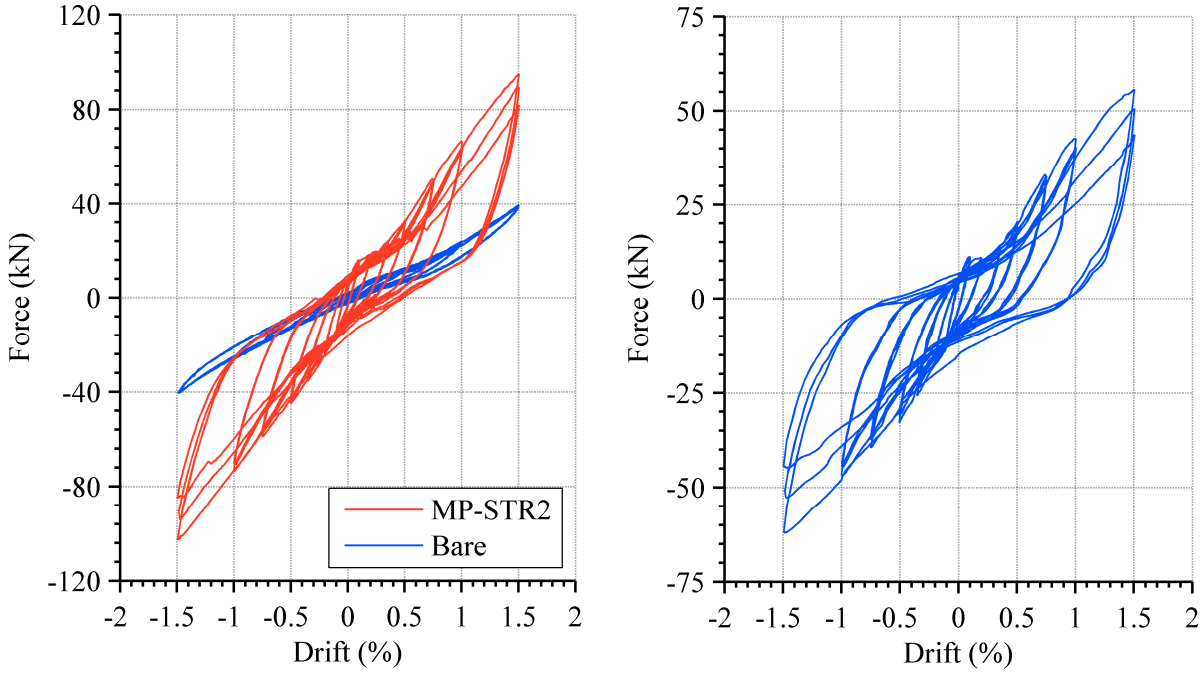

Figure 4-32: Force-drift behaviour (left) and difference between clad and unclad frame (right) for short threaded rod connection test specimen MP-STR2

Also evident is a drop in strength between subsequent cycles of displacement, indicating permanent damage is occurring to the precast concrete panel, as well as to the connection. The damage to the panel was clearly visible as cracking over the entire panel, as

shown in Figure 4-33 (left). The damage to the precast panel is discussed in further detail in Section 4.6.5

Damage to the connection was similar to that observed in long threaded rod connections (refer to Section 4.6.2) although it was evident that because more force was being transferred through the connections, deformation was also observed in the connection fixings. The 8 mm steel plate that fixed the threaded rod to the panel was warped out-of-plane and the bolts connecting the steel angle to the top beam were also damaged.

Localised cracking in the threaded rods was observed at 0.5% drift. This cracking was the precursor to the failure mechanism of the connection with the cracks being cycled open and eventually failing in tension at the interface with the nut, as shown in Figure 4-33 (right).

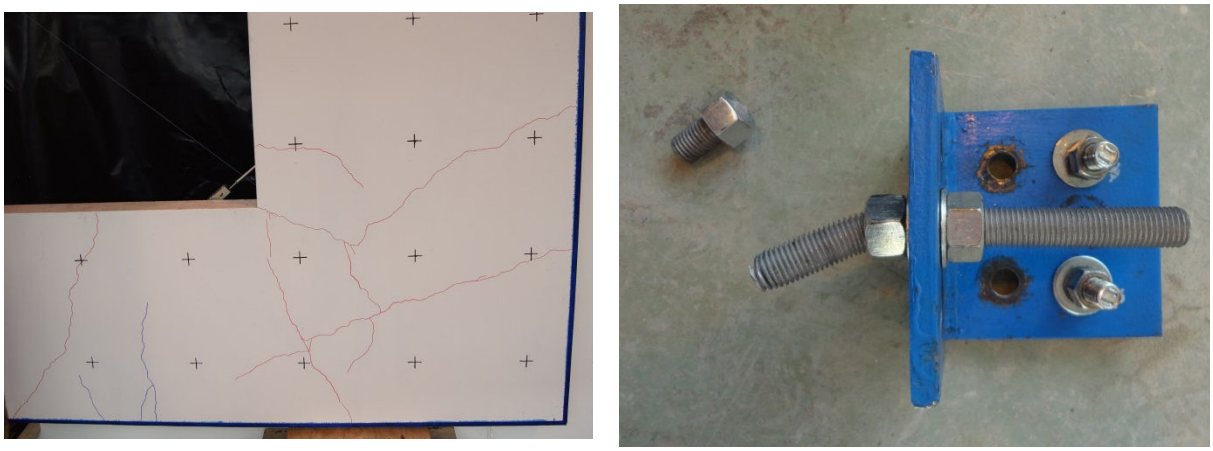

Figure 4-33: Cracking to the cladding panel during testing of short threaded rod connections (left) and failure of short threaded rod showing large permanent deformation (right)

A total of three different short threaded rod connection variations were tested in order to gain an understanding of how threaded rods with limited movement capability affect the interaction between the frame and cladding. The maximum force results for the two connection types are presented in Table 4-8.

Table 4-8: Summary of short threaded rod connection test results

Test ID	MP-STR1	MP-STR2	DP-STR1
Number of Rods	2 x 20 mm	4 x 20 mm	4 x 20 mm
Max Pushover Force (1.5% Drift)	71.5 kN	102.6 kN	101.2 kN
Max Force Increase (1.5% Drift)	30.9 kN	62.0 kN	60.4 kN
Failure Drift (Cycle Number)	2.0% (1) 1.5% (3) 1.5% (3)	1.5% (3) 1.5% (3) 2.0% (1)	1.5% (3) 1.5% (3) 1.5% (3)

The maximum values are averaged over the three tests undertaken for each connection type. Both the maximum force of the cladding-frame system and the difference between the cladding-frame system and the bare frame (refer to Figure 4-32) at 1.5% are presented. The effect of doubling the number of connections (for both the mono panel and dual panel system) results in a doubling of the lateral resistance of the cladding system as would be expected.

4.6.5 Panel Observations

The panel deformations were measured in both a global and local scale. Global scale deformations were measured by the diagonal strut displacement and the shear deformation of the panels. The diagonal strut displacement measured the displacement between diagonally opposite corners of the panel using rotary potentiometers. The shear deformation between the top and bottom of the panels could be computed by finding the difference between the inter-storey displacement and the relative movement between the top of the panel and the frame. Local scale deformations were measured by linear potentiometers placed diagonally around all window corners. These gave an indication of when cracking had occurred at the window corners. The window corners were where stress concentrations were assumed to be highest and hence where the largest local deformations should be expected (refer to Section 4.5.3 for further details on instrumentation).

The testing order was planned so that the precast concrete panels would remain undamaged for most of the testing and only be damaged in the final several tests. This aim was achieved with the panels remaining undamaged until the testing of slotted connections beyond their slot capacity.

4.6.5.1 Mono Panel

The first cracks were observed in the mono panel during test MP-SL3 during drift cycles greater than 1.5% drift when significant forces were transferred into the panel. Figure 4-34 presents how the cracks developed in the panel for the three drift largest cycles. The connection locations are shown by grey rectangles. During the 2.0% drift cycle a hairline crack appeared in the bottom right hand corner of the window opening. In the 2.75% drift cycle, cracks develop in all four window corners which have a maximum width of 0.4 mm. In the 3.5% drift cycle, the cracks initiated in the 2.75% cycle extend to the edge of the panel and new perpendicular cracks develop in the bottom corners of the panel.

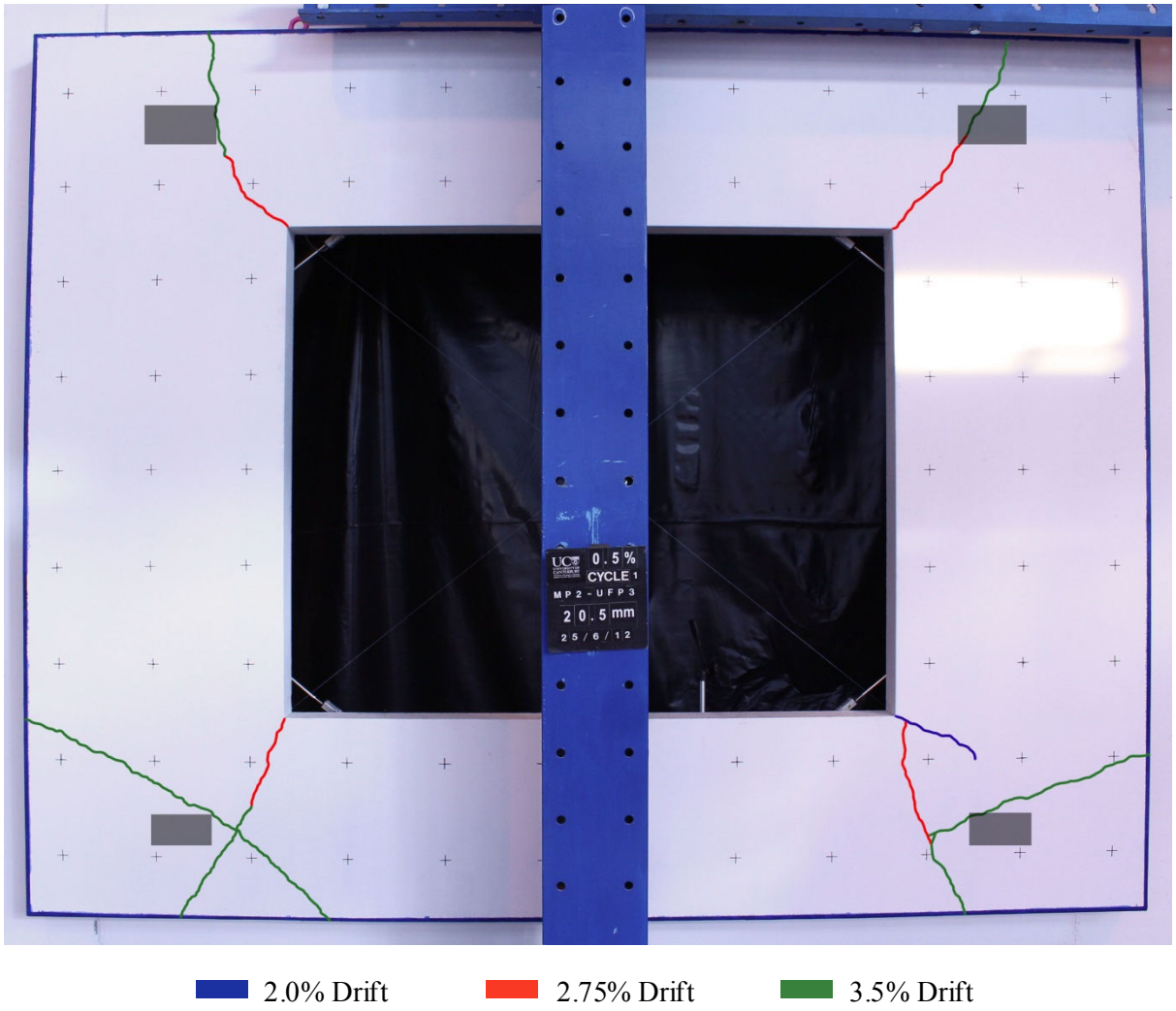

Figure 4-34: Crack pattern development in mono panel during test MP-SL3

The diagonal strut displacement for test MP-SL3 is shown in Figure 4-35 (left). A positive strut displacement corresponds to an extension of the strut, when the panel is in tension. For drift cycles up to and including 1.5% drift, the maximum strut displacement was 0.2 mm. The maximum strut displacement for the long threaded rod connections was also 0.2 mm. Because no damage was observed in the panel for these drift cycles, this displacement is within the elastic deformation limit of the panel.

In the 2.0% drift cycle, when significant forces are being transferred into the panel, the strut displacement becomes less trivial, reaching a maximum of 2.9 mm. This returns to approximately zero so it would suggest very little damage has occurred which agrees with crack observations. In the 2.75% and 3.5% drift cycles, the strut displacement increases to a maximum of 10.0 mm and it can also be seen in Figure 4-35 (left) that significant residual displacements occur in the panel.

The diagonal opening and closing of the four window corners was measured using linear potentiometers. The opening of the window corners is measured as a positive displacement and is shown in Figure 4-35 (right). Similarly to the diagonal strut displacement, the measurements are negligible for drift cycles up to and including 1.5%. At 2.0% drift, the maximum displacement was 0.2 mm. This increased to 0.5 mm at 2.75% drift and subsequently to 0.6 mm at 3.5% drift. It can also be seen that a residual corner displacement developed during the larger drift cycles.

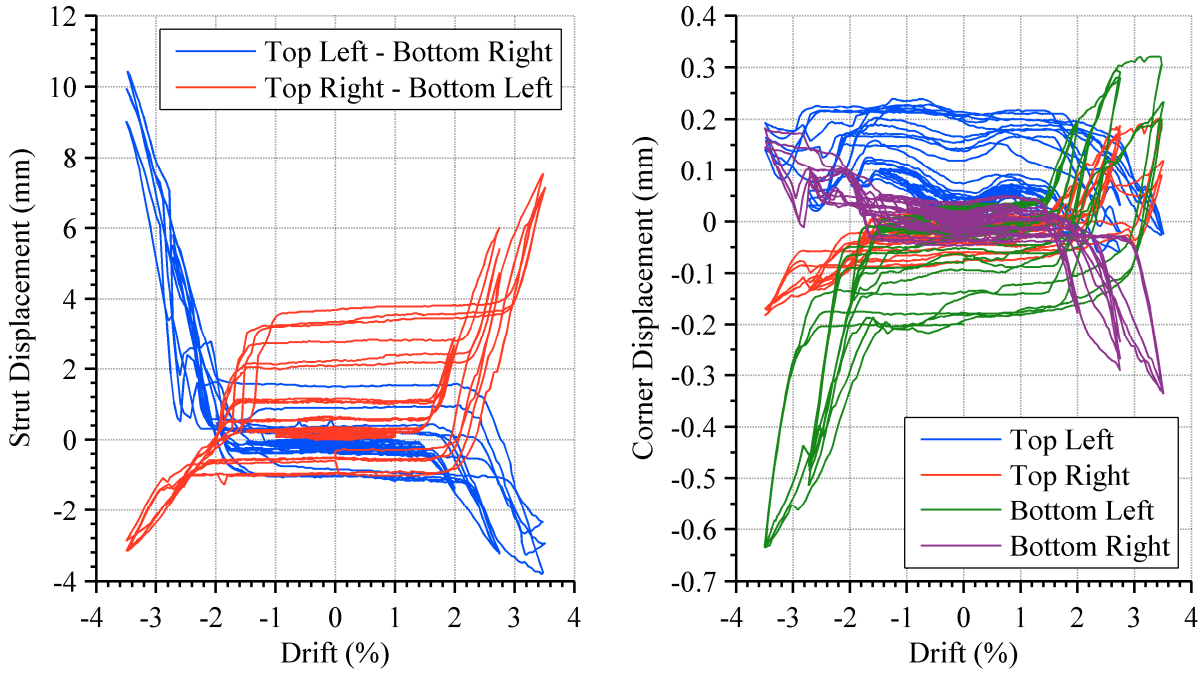

Figure 4-35: Diagonal strut displacement (left) and window corner displacement (right) for mono panel during test MP-SL3

The tests of short threaded rod connection systems were undertaken following the testing of slotted connection systems. The short threaded rod tests generated the largest amount of force being transferred into the panel and as such the heaviest damage to the panel.

A maximum crack width of 0.3 mm is observed during the 1.0% drift cycle and this increases to a maximum of 0.8 mm during the 1.5% drift cycle. The crack pattern for test MP-STR2 is presented in Figure 4-36 for the drift limits that the damage occurred.

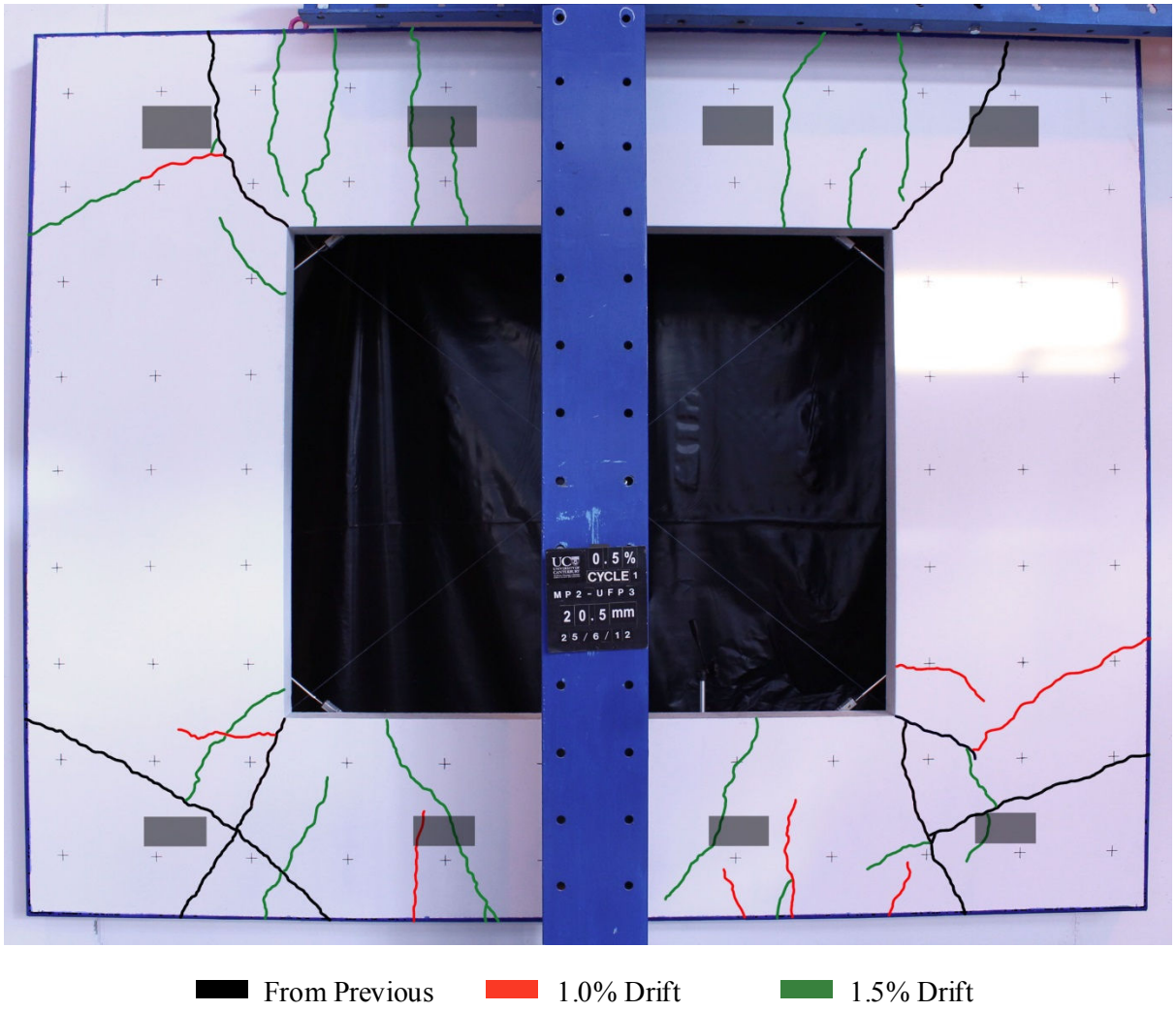

Figure 4-36: Crack pattern development in mono panel during test MP-STR2

When examining the global deformation of the panel, if the panel is assumed to act as either a diagonal strut or as a member in shear then the characteristics of these elements can be determined since the force being transferred into the panel and the panel deformations are known. The horizontal force transferred into the panel during test MP-STR2 is compared with the diagonal strut displacement in Figure 4-37 (left). It can be observed that the stiffness of the panel degrades as the strut goes through large deformations and damage occurs to the panel.

A slightly larger maximum strut displacement of 12.7 mm is observed during test MP-STR2 compared to the slotted connection test MP-SL3. This result agrees with the additional cracks formed during these tests. Crack initiation in test MP-SL4 occurred at a strut displacement of approximately 3 mm. It can be inferred that crack initiation for short threaded rod connections would likely occur during the 0.5% drift cycle.

The force transferred into the panel during test MP-STR2 is compared against the shear deformation of the panel in Figure 4-37 (right). The shear deformation was computed by finding the difference between the inter-storey displacement and the relative movement between the top of the panel and the frame. A maximum of 15.4 mm shear deformation occurred during the test of MP-STR2. This corresponds to 51% of the required inter-storey deformation between the top and bottom beams being accommodated by the panel, with the remaining being taken by the connections. The maximum shear deformation in the tests of long threaded rod connections was 6.8 mm and of slotted connections was 5.6 mm (when within slot range).

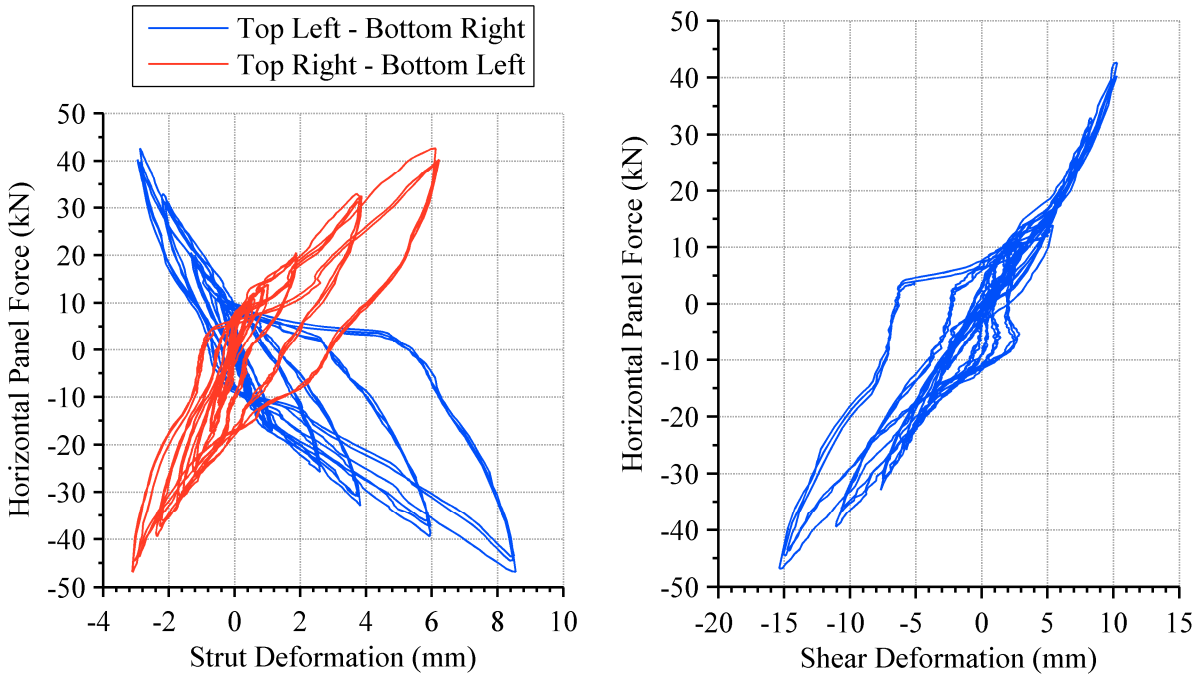

Figure 4-37: Lateral force compared with strut deformation (left) and shear deformation (right) during test MP-STR2

4.6.5.2 Dual Panel

The first damage was observed in the dual panels during testing of the short threaded rod connections. Figure 4-38 presents how the crack patterns developed during test DP-STR1. The first corner cracks were observed during the 0.5% drift cycle. During the 0.5% drift cycle hairline cracks appeared in the bottom corners of both window openings. Further cracks develop in the top and bottom of both panels during the subsequent drift cycles, as shown in Figure 4-38. A maximum crack width of 0.3 mm is observed during the 0.75% drift cycle and this increases to a maximum of 1.5 mm during the 1.5% drift cycle.

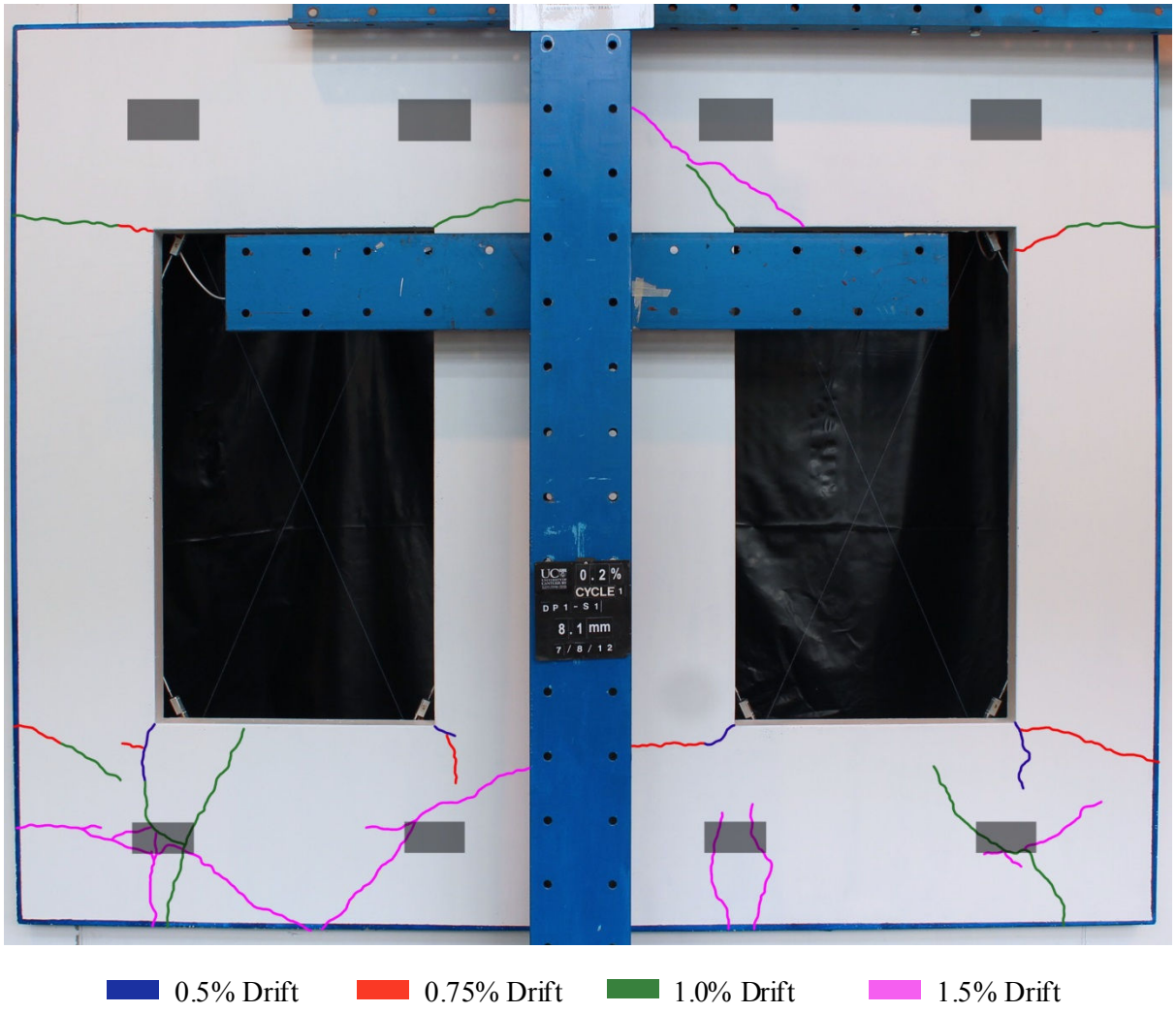

Figure 4-38: Crack pattern development in dual panels during test DP-STR1

The force transferred into the panel during test DP-STR1 is compared against the shear deformation of the panels in Figure 4-39 (left). A maximum of 20.6 mm shear deformation occurred during the test of MP-STR2. This corresponds to 46% of the required inter-storey deformation between the top and bottom beams being accommodated by the panels, with the remaining being taken by the connections.

The diagonal opening and closing of the eight window corners was also measured using linear potentiometers. Deformation in the window openings were observable from low drift levels during test DP-STR1 as illustrated in Figure 4-39 (right) which shows corner displacements for the western panel. Both positive and negative maximum displacements occur in the top right hand corner. The maximum opening of the corner was measured to be 0.5 mm.

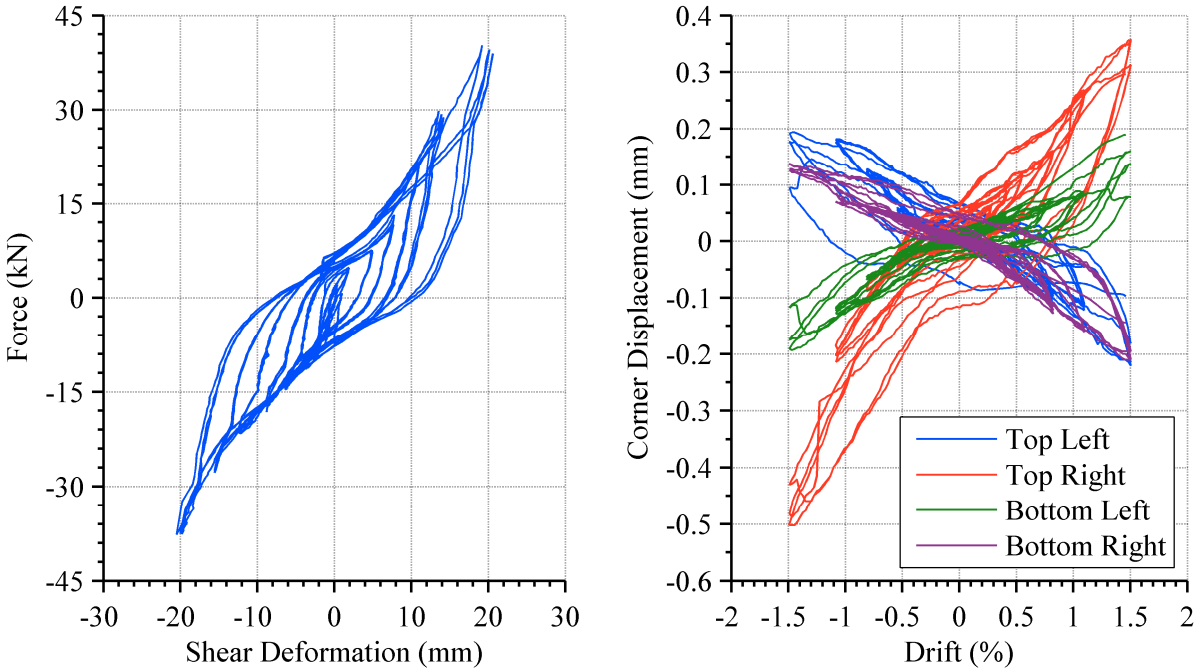

Figure 4-39: Lateral force compared with lateral (shear) deformation (left) and window corner displacement (right) for dual panel during test DP-STR1

4.7 Experimental Modelling Outputs

The key outputs from the experimental testing programme are presented in this section. These include parameters which are essential for modelling purposes and inter-storey drift limits which quantitatively describe the cladding damage states. The latter will be used in the seismic performance assessment of cladding systems presented in Chapter 7 and the probabilistic seismic loss assessment presented in Chapter 11.

4.7.1 Cladding Damage Parameters

For modelling purposes as well as for defining damage states it is necessary to know several key output parameters of the cladding connections and precast panels tested. Where possible the following parameters are presented: initial stiffness, yield force, yield displacement, failure force and failure displacement. Failure is defined here as the rupture of the connection.

The key parameters of the connections are grouped by the connection types presented previously: long-threaded rod, short threaded rod and slotted. The average values for a single connection are shown below in Table 4-9.

Table 4-9: Single cladding connection modelling parameters

	Connection Type		
	Long Threaded Rod	Short Threaded Rod	Slotted
Initial Stiffness	600 kN/m	2,000 kN/m	-
Yield Force	2 kN	6 kN	3 kN(1)
Yield Displacement	3 mm	3 mm	-
Failure Force	4 kN	16 kN	-
Failure Displacement	50 mm	30 mm	-

(1) The yield point refers to the friction force that needs to be overcome to initiate sliding of the connection.

The key damage parameters of the precast panels are related to crack initiation since this determines whether repair work is required. The panels were not tested to failure since it is highly unlikely that the forces generated through typical cladding connections would ever be large enough to cause a failure. The key damage parameters of the precast panels are presented below in Table 4-10.

Table 4-10: Single cladding panel modelling parameters

	Large Panel	Small Panel
In-Plane Shear Stiffness	4800 kN/m	800 kN/m
Shear Force at First Crack	33 kN	10 kN
Shear Deformation at First Crack	6.9 mm	12.5 mm
Shear Force at 3 mm Crack	39 kN	18 kN
Shear Deformation at 3 mm Crack	12.2 mm	22.5 mm

4.8 Conclusions

Traditional heavy cladding panel connection typologies (tie-back rod and slotted) were tested in order to investigate the effect of heavy cladding systems upon the lateral resistance of a reinforced concrete frame. A test frame which represents a single-storey, single-bay portion of a reinforced concrete building was used to test the cladding systems. The cladding-frame system was tested under uni-directional quasi-static cyclic loading.

The magnitude of the lateral resistance provided by the cladding was found to vary significantly depending on the type of top connection used. The minimum lateral force provided by the cladding was found to be 5.6 kN. This was observed when four 250 mm long 12 mm threaded rod connections were used. The maximum lateral force provided was found to be 62.0 kN. This was observed when four 50 mm long 20 mm threaded rod connections were used. When slotted connections were used, the cladding added between 7.0 – 52.0 kN to the lateral resistance of the frame. This large range was dependent upon whether the drift of

the frame caused the relatively displacement between the cladding and the frame to exceed the slot length of the connections. When the relative displacement was less than the slot length, the maximum force added was between 7.0 – 13.0 kN. This was of similar magnitude to that of the long threaded rod connections. However, when the slot length was exceeded, significantly more lateral resistance was provided by the cladding. Since the length of the exposed rod between the slot and the panel was the same as the short threaded rod connection (50 mm), the connection essentially became a short threaded rod connection once the slot length was exceeded. The lateral resistance of the slotted connection mimicked the short threaded rod connection once the slot length was exceeded so this comparison appears to be accurate.

The testing also investigated the performance limits of the cladding system. For the cladding connections the performance limits relate to the onset of damage and failure. Long threaded rods were repeatedly found to fail during the 1.5 – 2.0% inter-storey drift cycles of the test frame. The increased length / diameter ratio of the 12 mm rods meant that these rods did not fail until the 2.75% drift cycle. No connection failure was observed in the slotted connections, even when the slot length was exceeded over multiple cycles. Short threaded rods were also found to repeatedly fail during the 1.5% drift cycle. The short threaded rod connections on average failed earlier than long threaded rods, however, the difference between the two connection types was not as prominent as expected. This may be due to the low-cycle fatigue characteristics of the threaded rods requiring a given number of cycles in order to cause rupture of the rods. However, it was also observed that the cladding panel underwent significant lateral deformation during the testing of the short-threaded rod connections. Consequently, the 1.5% drift of the frame was accommodated both by deformation of the connections and the cladding panel. This mechanism was likely critical in order for the short threaded rods to not fail until a drift of 1.5%. The composition of this deformation will be explored in subsequent chapters.

For the cladding panel the performance limits relate to onset of damage and when the maximum crack width reached 3 mm. Cracking was initiated in the panel during the slotted connection tests when the slot length was exceeded. Cracks initially formed in the window corners of the panel and subsequently spread around the connection locations as more force was transferred through the panel. The lateral stiffness of the panel was found to degrade over time as the cracking propagated.

4.9 References

ACI - 374.1R. (2005). Acceptance Criteria for Moment Frames Based on Structural Testing and Commentary: American Concrete Institute.

Amaris, A., Pampanin, S., Bull, D. K., & Carr, A. J. (2008). *Experimental Investigation on a Hybrid Jointed Precast Frame with Non-tearing Floor Connections*. Paper presented at the 2008 New Zealand Society for Earthquake Engineering Conference, Wairakei, New Zealand.

AS/NZS 4284. (2008). Testing of Building Facades. Wellington: Standards New Zealand.

AS/NZS 4671. (2001). Steel reinforcing materials. Wellington: Standards New Zealand.

ICC. (2000). International Building Code. Falls Church, Va., USA: International Code Council.

ISO 68-1. (1998). ISO General Purpose Screw Threads - Basic Profile - Part 1: Metric Screw Threads: International Organization for Standardization.

Montejo, L. A., & Kowalsky, M. J. (2007). CUMBIA - Section and Member Response of Reinforced Concrete Members. Department of Civil, Construction and Enviromental Engineering, North Carolina State University.

NZS 1170.5. (2004). Structural Design Actions, Part 5: Earthquake Actions - New Zealand. Wellington: Standards New Zealand.

NZS 3101. (2006). Concrete Structure Standard - Part 1. Wellington: Standards New Zealand.

NZS 3404. (1997). Steel Structures Standard. Wellington: Standards New Zealand.

Pampanin, S. (2005). Emerging Solutions for High Seismic Performance of Precast/Prestressed Concrete Buildings. *Journal of Advanced Concrete Technology, 3*(2), 207-223.

Phan, L. T., & Taylor, A. W. (1996). State of the Art Report on Seismic Design Requirements for Nonstructural Building Components. Gaithersburg, MD., USA: US National Institute of Standards and Technology.

Priestley, M. J. N. (1991). Overview of the PRESSS Research Program. *PCI Journal, 36*(4), 50-57.

Priestley, M. J. N. (1996). The PRESSS Program Current Status and Proposed Plans for Phase III. *PCI Journal, 41*(2), 22-40.

Priestley, M. J. N., Sritharan, S., Conley, J., & Pampanin, S. (1999). Preliminary Results and Conclusions from the PRESSS Five-Story Precast Concrete Test Building. *PCI Journal, 44*(6).

Wang, M. L. (1987). Cladding performance on a full-scale test frame. *Earthquake Spectra, 3*(1), 119-173

5 Development of Numerical Models for Heavy Cladding

5.1 Introduction

This chapter presents the development of modelling techniques for heavy cladding systems that utilise traditional connection typologies. The traditional connection typologies tested are variations of tie-back rod and slotted plate connections. These have been introduced in Chapter 2. Analytical derivations based on fundamental engineering principles are first used as a framework to determine key modelling parameters. These analytical derivations are compared against experimental results and used to develop finite element models. The finite element models are verified using experimental results of the traditional heavy cladding systems investigated in Chapter 4. Once verified, a series of parametric analyses are undertaken to expand the experimental data set in order to best characterise the behaviour of cladding components when certain geometric parameters are varied. Key modelling parameters of cladding components are then presented using the combination of experimental, analytical and numerical results,

These modelling parameters are used to develop local lumped plasticity cladding models that can be easily incorporated into frame analyses. Finally, these simplified cladding models are compared to the experimental results obtained in Chapter 4 to examine their suitability.

5.2 Cladding Component Characterisation

The cladding connections and cladding panels will each be characterised separately. This will allow the development of a simplified two component cladding model. A separate connection and panel model also allows for the non-linear behaviour of the connections to be

isolated from the panel, which may be treated as elastic for the majority of modelling situations.

The cladding components can be characterised through three means: experimentally, analytically and numerically. The combination of all three methods provides a robust process for deriving reliable modelling parameters for the cladding components tested experimentally when certain geometric parameters are varied. Complementing experimental testing with numerical modelling is essential as it provides the ability to greatly increase the quantity of test data. This is due to the fact that numerical modelling is much faster and uses fewer resources than experimental testing.

The experimental testing of the cladding components will be presented first and then compared with analytical derivations of cladding component properties based on basic engineering principles. Finite element modelling of cladding components are then developed and verified against the experimental results. The geometric parameters of the finite element models are varied to increase the quantity of cladding component data. This large data set is subsequently used in the development of cladding models.

5.2.1 Experimental Testing

5.2.1.1 Threaded Rod Connections

In order to characterise the behaviour of the threaded rod cladding connections, a series of six different threaded rod connections were prepared and tested using an Instron Materials Testing Machine. The threaded rod cladding connections can be represented by fixed-end beams with an imposed lateral displacement, Δ, at one end, as shown in Figure 5-1 (left). This fixed-end beam is analogous to a three-point bending test of the same length with pinned ends, as shown in Figure 5-1 (right). However, it can be seen that the equivalent displacement of the three-point bending test is exactly half that of the fixed-end beam.

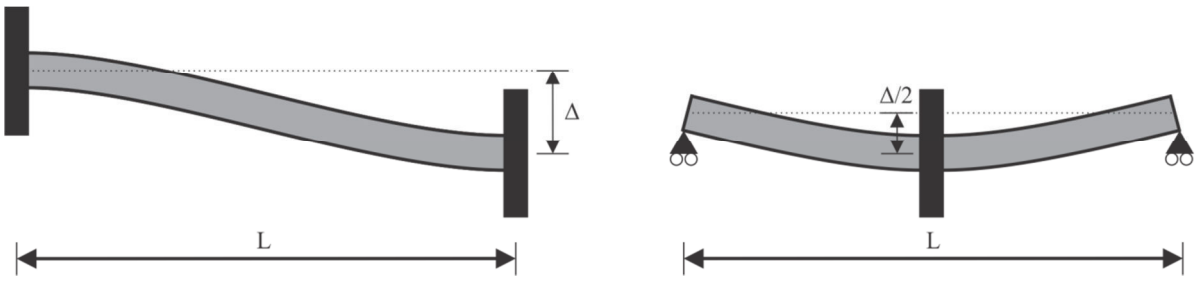

Figure 5-1: Threaded rod connection represented by a fixed-end beam (left) and three-point bending beam (right)

Because the test was cyclic it was necessary to construct a test rig that restrained the threaded rods so they could be loaded in both vertical directions but also allowed for the geometric shortening of the rods without adding large axial loads. A steel test rig was constructed that achieved this using supports that were pinned at both ends, as shown in Figure 5-2. This allowed the external loading points of the rod to both rate as well as move in the plane of the rod to allow for the geometric change in length of the rod between supports due to large displacements.

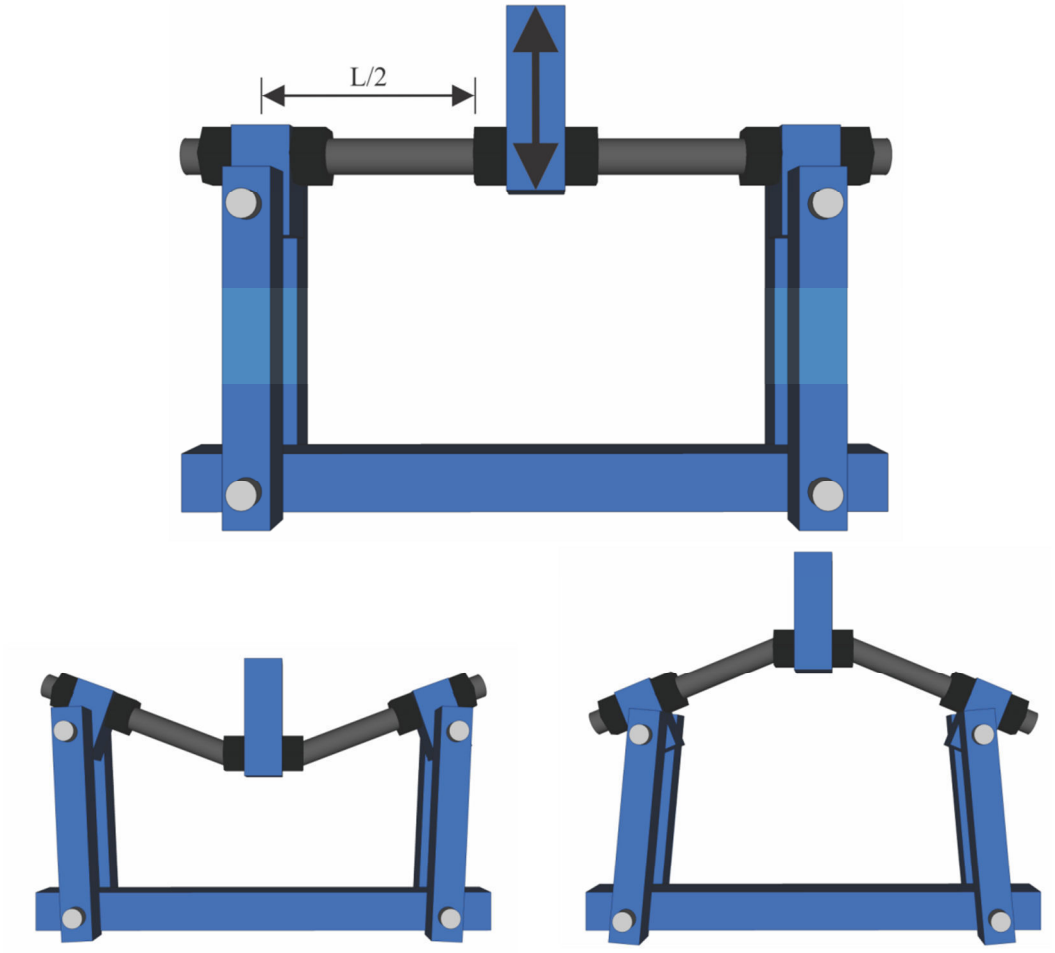

Figure 5-2: Graphical representation of three-point bending test of threaded rod

The rods were loaded at a rate of 0.2 mm/sec using a loading regime that matched that used for the systems testing in Chapter 4. The loading regime consisted of three cycles at each specified displacement with the displacement and load applied being recorded. The procedure defining the loading protocol was adopted from the ACI recommendations (ACI - 374.1R, 2005). A photograph of a 150 mm long threaded rod test prior to commencement of the test is shown in Figure 5-3.

Figure 5-3: Threaded rod of 150 mm length loaded in Instron Materials Testing Machine

The six different rod tests varied the rod length, l_r, as well as the rod diameter, d_r. Several tests were also duplicated. These rod lengths and rod diameters include those that were tested experimentally in Chapter 4. The rod diameters represent the low end of possible threaded rod connections; however the rod lengths are very typical of those observed during investigations into current cladding systems. A rod length of 50 mm represents a threaded rod connection with minimal ability to accommodate movement between the cladding and frame (referred to here as a 'short threaded rod'). A rod length of 250 mm represents a connection assumed to have an acceptable ability to accommodate movement between the cladding and frame (referred to here as a 'long threaded rod). Table 5-1 shows the dimensions and diameters of the rods tested.

Table 5-1: Geometry of threaded rods tested experimentally

	Rod Length (mm)		
20 mm Rod Diameter	50	150	250
12 mm Rod Diameter	50	150	250

The results from the six tests performed are shown in Figure 5-4. The top row of Figure 5-4 displays the force-displacement behaviour of the 20 mm diameter rods for increasing rod length from left to right. The bottom row shows the same increasing rod length for the 12 mm

diameter rods. Note that the scale of the force axis for the 12 mm rods is smaller than that of the 20 mm rods.

The tests were performed until failure and it can be seen that the 50 mm rods failed during the 22.5 mm cycle, the 150 mm rods during the 45 mm cycle and the 250 mm rods during the 60 mm cycle. Also evident is the drop in both the strength and stiffness as the rod length increases as well as when the rod size decreases. The 50 mm long rods show strength degradation during the higher displacement cycles, whereas the longer rods exhibit more stable hysteretic behaviour. This trend is consistent for both size rod sizes. The strength degradation for the shorter rods could possibly be attributed to flexure-shear interaction since during large displacements it is unlikely that pure bending would be occurring in the 50 mm long rods.

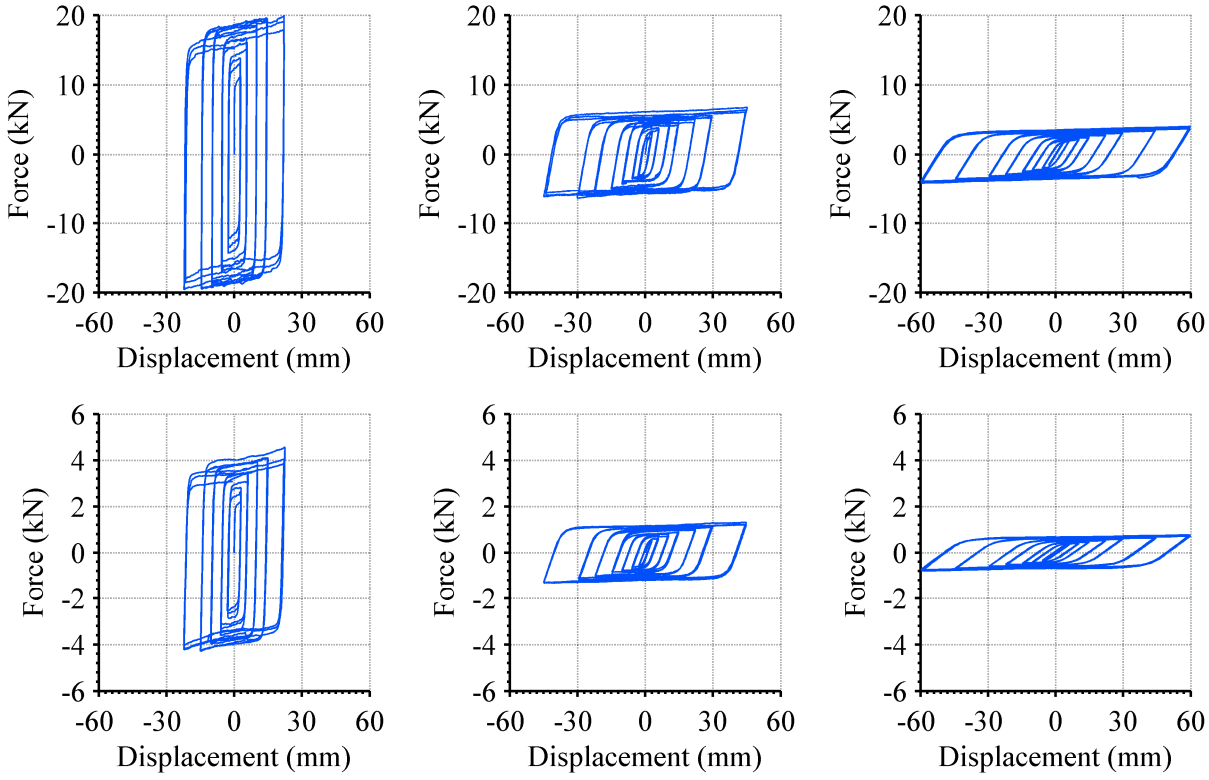

Figure 5-4: Force-displacement results of experimental testing of threaded rod connections: 20 mm diameter rods (top row), 12 mm diameter rods (bottom row); 50 mm length (left), 150 mm length (cetnre), 250 mm length (right)

The yield force, yield displacement, initial stiffness and maximum force were visually interpreted from each test. The values for each of these parameters are presented in Table 5-2 for each threaded rod test. As would be expected, the initial stiffness, yield force and maximum force are greatest for the threaded rods of shortest lengths and largest diameter.

Table 5-2: Experimental results of threaded rod tests

	Rod Length (mm)	Yield Force (kN)	Yield Disp. (mm)	Initial Stiffness (kN/m)	Maximum Force (kN)
20 mm Rod Diameter	50	10.0	0.5	20,000	17.6
	150	2.8	1.2	2,300	5.9
	250	1.6	3.4	470	3.3
12 mm Rod Diameter	50	2.2	0.6	3,700	4.2
	150	0.7	2.2	320	1.4
	250	0.4	4.6	90	0.7

5.2.1.2 Slotted Connections

The key parameter for modelling slotted cladding connections is the resisting force due to sliding friction. A separate component test was not undertaken for the slotted connections. The slotted connections tested experimentally were presented in Chapter 4 and the average values of resisting force are repeated in Table 5-3.

Table 5-3: Experimental sliding force of slotted connections

	Large Panel	Small Panel
Average Sliding Force (kN)	3.0	1.5

5.2.1.3 Panels

The key parameter for modelling cladding panels is determining their in-plane stiffness. This is necessary in order to determine how much of the inter-storey displacement demand can be accommodated by the in-plane deformation of the cladding panel, with the remaining deformation being taken up by the cladding connections. A separate component test was not undertaken for the cladding panels. The in-plane stiffness of the two cladding panels tested was determined experimentally in Chapter 4 and is repeated in Table 5-4.

Table 5-4: Experimental stiffness of cladding panel

	Large Panel	Small Panel
In-Plane Stiffness (kN/m)	4,800	800

5.3 Analytical Derivation

5.3.1.1 Threaded Rod Connections

The key parameters that can be derived analytically for threaded rod cladding connections are the yield force, yield displacement and maximum force. Also of interest is

the out-of plane shortening of the rod due to bending since this can result in closing of the gap between the cladding panel and the structure as well as additional axial load in the connection. The analytical model chosen is a fixed end beam with an imposed lateral displacement, as shown in Figure 5-5.

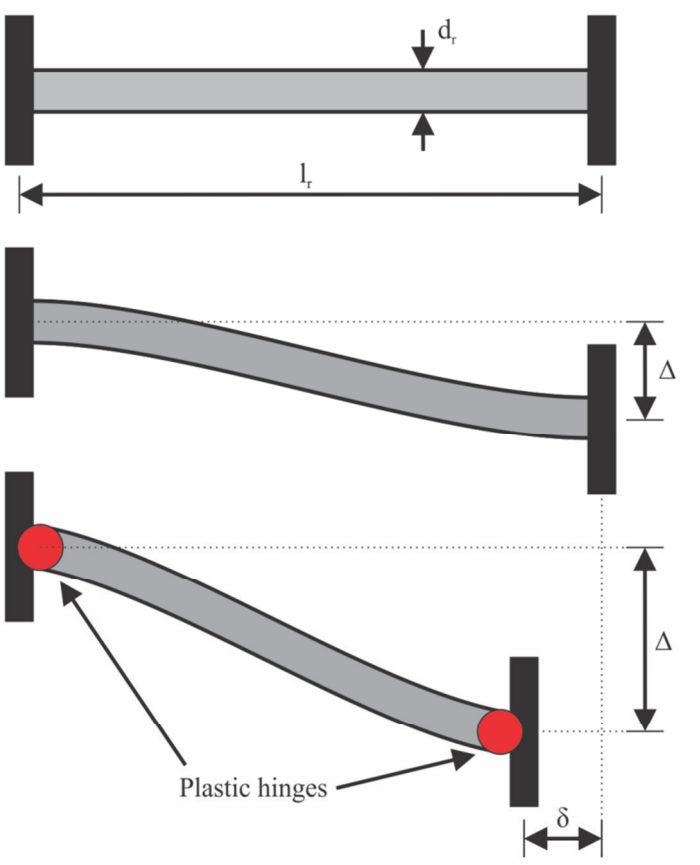

Figure 5-5: Fixed-end beam representation of threaded rod connections

For a fixed-fixed beam, as the imposed lateral displacement is increased, plastic hinges develop at each of the beam to form a plastic mechanism, as shown in Figure 5-5. The reaction force and moment for a fixed-fixed beam can be related by Equation (5-1).

$$F = \frac{2M}{l_r} \tag{5-1}$$

where

l_r = Length of threaded rod

The relationships for the yield moment and plastic moment are provided by Equations (5-2) and (5-3) respectively. Hence the yield force can be found using the yield moment and Equation (5-1). Likewise, the maximum theoretical force provided by the threaded rod corresponds to when a plastic mechanism has formed so can be found using the plastic

moment and Equation (5-1). It is assumed that the yielding is governed by bending stresses alone. This assumption is valid so long as the rod is of a reasonable length so that shear stresses are negligible compared to bending stresses. For a 50 mm long rod of 20 mm diameter (the lowest l_r/d_r considered) the maximum bending stress is 10 times greater than the maximum shear stress, so clearly bending governs and the assumption is valid.

$$M_y = Zf_y \quad \textbf{(5-2)}$$

$$M_p = Sf_y \quad \textbf{(5-3)}$$

where

Z = Elastic section modulus

S = Plastic section modulus

f_y = Yield stress of threaded rod

The displacement at yield and at the onset of the plastic mechanism forming can be found using Equation (5-4) and the corresponding force value.

$$\Delta = \frac{F{l_r}^3}{12EI_r} \quad \textbf{(5-4)}$$

where

E = Elastic modulus

I_r = Moment of inertia of threaded rod

The threaded rods can be approximated as solid circular sections and as such, have the following section moduli:

$$I_r = \frac{\pi {d_r}^4}{64} \quad \textbf{(5-5)}$$

$$Z = \frac{\pi {d_r}^3}{32} \quad \textbf{(5-6)}$$

$$S = \frac{{d_r}^3}{6} \quad \textbf{(5-7)}$$

where

d_r = Nominal diameter of threaded rod

The ratio between the plastic section modulus, *S*, and elastic section modulus, *Z*, provides the ratio between the maximum force and yield force. For a circular section, this

ratio is 1.7:1. The displacement when this maximum force is reached can be obtained by finding the yield displacement and multiplying this by an expected level of ductility. Obviously there are limitations in the level of accuracy in such values; however, they give a useful first estimate of the performance upon which numerical models can be verified.

By substituting Equations (5-2) and (5-6) into (5-1), the yield force of a threaded rod can be represented by Equation (5-8). By substituting Equations (5-5) into (5-4), the yield displacement for a threaded rod can be represented by Equation (5-9).

$$F_y = \frac{\pi f_y {d_r}^3}{16 l_r} \quad \textbf{(5-8)}$$

$$\Delta_y = \frac{f_y {l_r}^2}{3E d_r} \quad \textbf{(5-9)}$$

The diameter of the threaded rod is limited to standard metric sizes. Figure 5-6 shows the yield force and yield displacement curves for a range of standard threaded rod diameters using a yield stress of σ = 300 MPa.

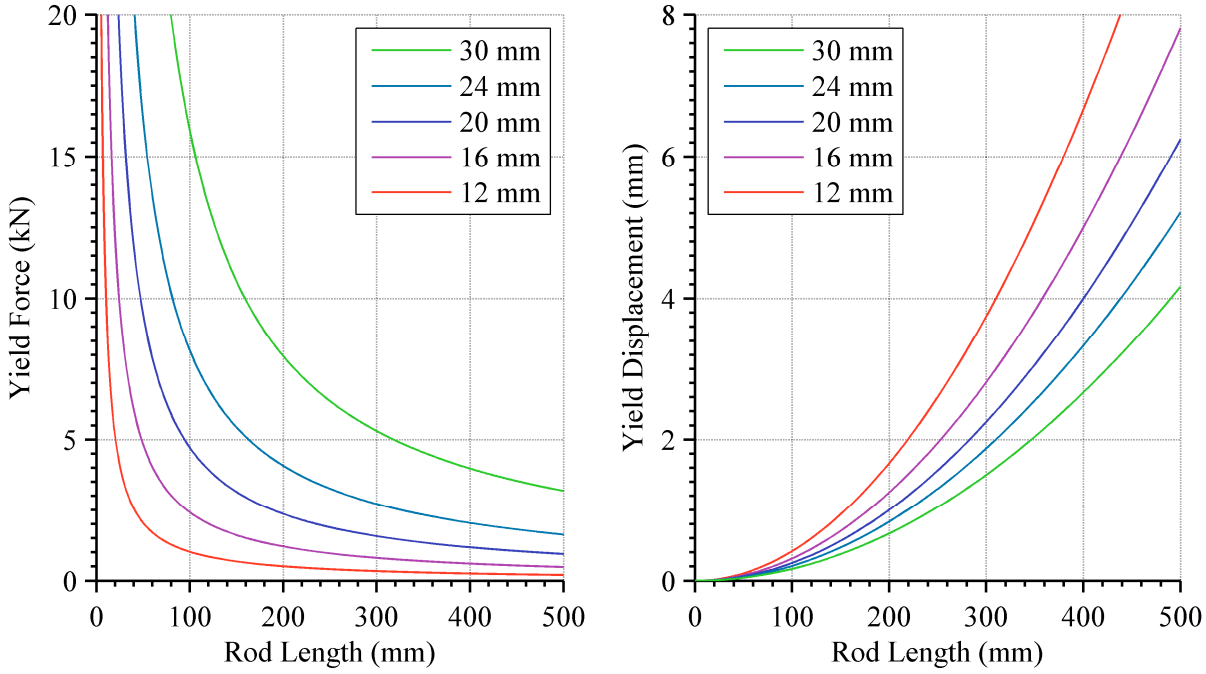

Figure 5-6: Analytical yield force and yield displacement of various threaded rod geometry

Two different threaded rod diameters were tested experimentally at three different lengths, as presented in Section 5.2.1.1. The analytically predicted force-displacement behaviour for these rods is compared with the results obtained experimentally in Figure 5-7. The threaded rods tested were mild steel so are assumed to have a yield strength of 300 MPa.

A ductility of 10 was used for all rods in finding the displacement when the maximum force was reached. It can be seen that this ductility is a reasonable estimate for some cases, e.g. the 250 mm long rod of 12 mm diameter; however in other cases it underestimates or overestimates the post-yield stiffness of the threaded rods.

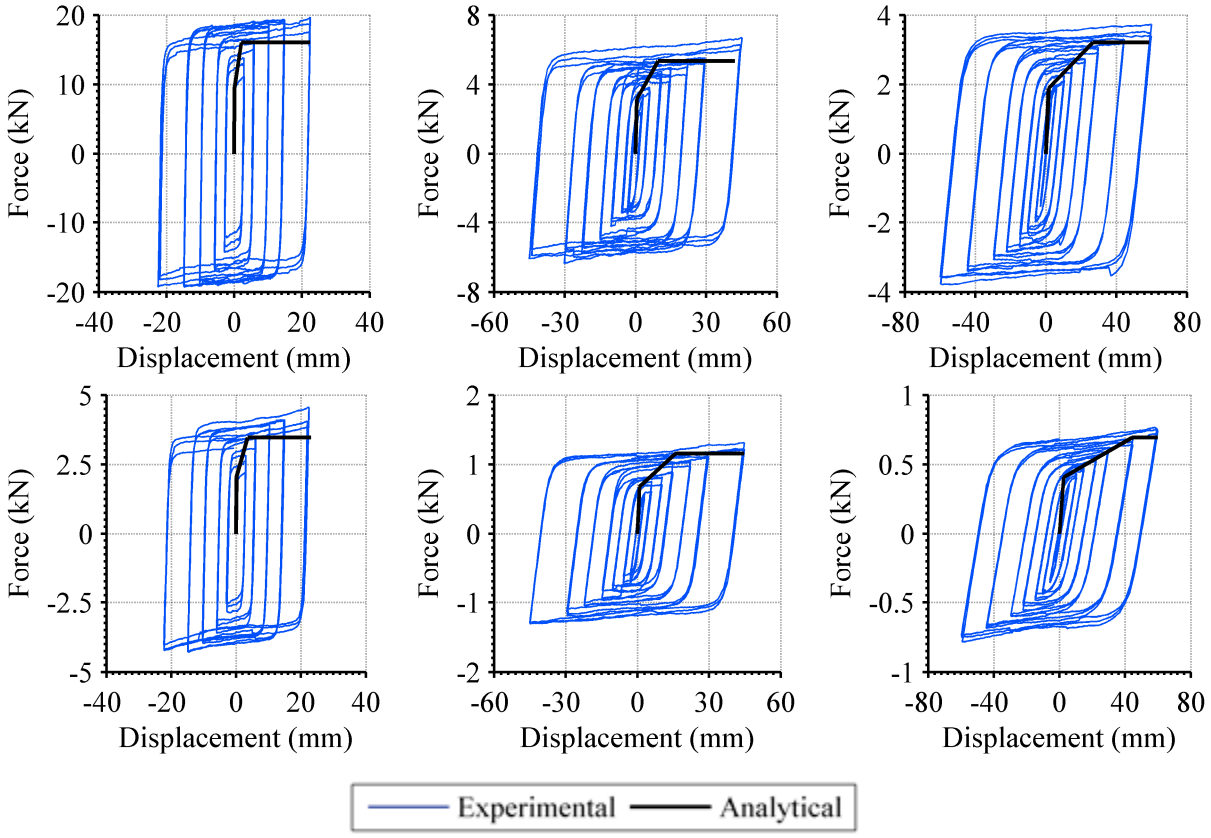

Figure 5-7: Force-displacement comparison of experimental and analytical threaded rod connections: 20 mm diameter rods (top row), 12 mm diameter rods (bottom row); 50 mm length (left), 150 mm length (cetnre), 250 mm length (right)

The experimental yield force and yield displacement are compared with the analytical values in Table 5-5. It can be seen that that the analytical solution for the yield force given by Equation (5-8) is reasonably accurate in predicting the yield force for all rods tested. However, the yield displacement is significantly under-predicted.

Table 5-5: Comparison of experimental and analytical threaded rod yield force and yield displacement

		Yield Force (kN)		Yield Displacement (mm)	
	Rod Length (mm)	Experimental	Analytical	Experimental	Analytical
20 mm Rod Diameter	50	10.0	9.4	0.5	0.1
	150	2.8	3.1	1.2	0.6
	250	1.6	1.9	3.4	1.6
12 mm Rod Diameter	50	2.2	2.0	0.6	0.1
	150	0.7	0.7	2.2	0.9
	250	0.4	0.4	4.6	2.6

The prediction of the maximum force being 1.7 times greater than the yield force slightly under-predicts the observed maximum force, as shown in Table 5-6. However this maximum force is still reasonably accurate for the rod sizes tested. The initial stiffness is found based on the yield force and yield displacement. Since the yield displacement was significantly under-predicted, Table 5-6 shows that the analytical prediction of the stiffness of the rods is significantly over-predicted.

Table 5-6: Comparison of experimental and analytical threaded rod stiffness and maximum force

		Initial Stiffness (kN/m)		Maximum Force (kN)	
	Rod Length (mm)	**Experimental**	**Analytical**	**Experimental**	**Analytical**
20 mm Rod Diameter	50	20,000	94,000	19.6	16.0
	150	2,300	5,200	6.4	5.3
	250	470	1,200	3.7	3.2
12 mm Rod Diameter	50	3,700	20,000	4.5	3.4
	150	320	780	1.3	1.2
	250	90	150	0.7	0.7

Also of interest is the geometric shortening of the threaded rod during large lateral displacement. The out-of-plane shortening can result in the gap between the panel and structure closing, as witnessed during experimental testing. It also results in additional axial demands upon the connection since the panel will resist being pulled in towards the structure due to its own out-of-plane stiffness and the potential presence of thermal or acoustic packing material. These additional forces may coincide with out-of-plane forces arising from earthquake accelerations, amplifying the demands on the connection. Referring to Figure 5-5, assuming the rod stays at a constant length and rotates about the two ends, the out-of-plane displacement can be related to the lateral displacement by Equation (5-10).

$$\delta = l_r - \sqrt{{l_r}^2 - \Delta^2} \qquad \textbf{(5-10)}$$

where

Δ = Lateral displacement

The analytical out-of-plane displacement, δ, is presented for a range of possible threaded rod lengths in Figure 5-8. The experimentally observed out-of-plane displacement for two different threaded rod lengths is also shown in Figure 5-8. It can be observed that the analytical solution does a reasonably accurate job of predicting the out-of-plane displacement

for the two experimental rod lengths. The experimental out-of-plane displacement changes through testing due to the plastic hinging resulting in cracking and lengthening of the rods.

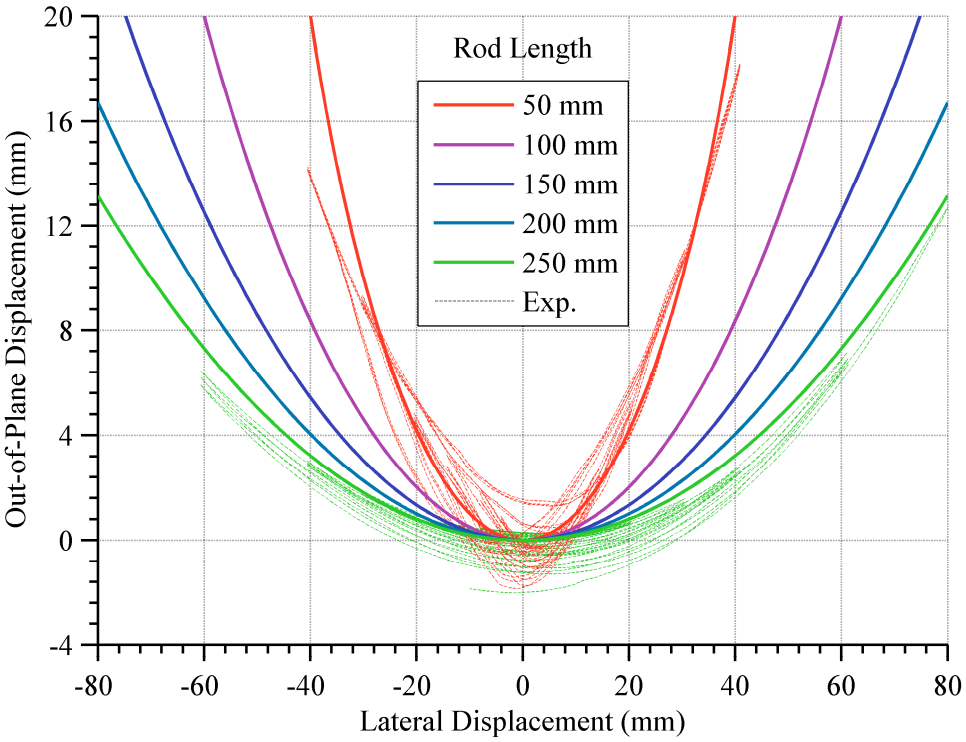

Figure 5-8: Experimental geometric shortening of threaded rods compared with analytical solution

5.3.1.2 Slotted Connections

Slotted connections dissipate energy due to sliding friction. This sliding friction is a constant force opposing the sliding motion which is independent of surface area, displacement or velocity (Serway & Jewett, 2009). This type of sliding friction is often called Coulomb damping and is defined as product of the coefficient of friction, μ, and the normal force, N, as given by Equation (5-11):

$$F_f = \mu N \qquad \textbf{(5-11)}$$

where

F_f = Friction force (static or kinetic)

μ = Coefficient of friction (static or kinetic)

N = Normal force

In order to estimate the sliding friction, it is necessary to know the coefficient of friction for steel on steel, as this is the typical sliding interface of a slotted connection, as well as the normal force on the slotted connection.

The coefficient of static friction, μ_s, for clean and dry steel on steel is 0.7 and the coefficient of kinetic friction, μ_k, is 0.6 (Sullivan, 1988). For these analytical derivations, it will be conservatively assumed that the coefficient of friction is constant and equal to 0.7.

The normal force acting against the sliding surface of the slotted connections is brought about by the eccentricity of the panels' weight from the bearing support as shown in Figure 5-9. This eccentricity creates an overturning moment that must be resisted by the top connection.

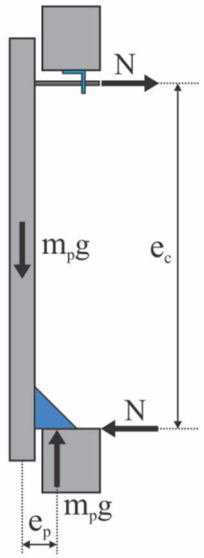

Figure 5-9: Normal force in connections due to panel eccentricity

The magnitude of this force can be found by summing the moments about the fixed (bearing) connection of the panel, as given by Equation (5-12).

$$N = \frac{m_p g e_p}{e_c} \qquad \textbf{(5-12)}$$

where

m_p = Mass of panel

g = Gravity

e_p = Horizontal eccentricity between panel and connection

e_c = Vertical eccentricity between connections

Thus, the friction force, F_f, can be defined by the following:

$$F_f = \frac{\mu m_p g e_p}{e_c} \quad \textbf{(5-13)}$$

For the experimental panel configurations, a horizontal eccentricity of 300 mm and vertical eccentricity of 2400 mm provides the analytical sliding forces in Table 5-7. It can be seen that the analytical sliding force underestimates the average experimental sliding force by 50%. The experimental sliding forces observed initially are around the analytical values calculated; however these values increase during testing due to galling of the steel. Galling is a form of wear caused by sliding between two metal surfaces. It results in the surface steel being pulled from one surface and being deposited or friction welded onto the adjacent surface (Davis, 2001). Galling results in an increase in the coefficient of friction and consequently, the sliding force of the connection to increase to approximately double the initial sliding force.

Table 5-7: Comparison of experimental and analytical sliding forces

	Large Panel	**Small Panel**
Average Experimental Sliding Force (kN)	3.0	1.5
Analytical Sliding Force μ = 0.7 (kN)	2.0	1.0
Adjusted Sliding Force μ = 1.0 (kN)	2.9	1.4

It is suggested in order to take into account the likelihood of galling between steel surfaces of slotted connections, a coefficient of friction equal to 1.0 is used. This brings the analytical sliding forces in line with the average observed experimental sliding forces. It is also recommended to use either a lubricant or a form of gasket using a material which will not gall, e.g. brass or rubber.

5.3.1.3 Panels

The lateral in-plane stiffness is the key modelling parameter required when modelling the in-plane behaviour of precast concrete cladding panels. A suitable structural model for determining the stiffness of a solid and prismatic cladding panel without openings and with constant cross section, like that shown in Figure 5-10, is that of a deep beam theory. In deep beams, cross-sections are assumed to remain plane after deformation but, unlike the Bernoulli beam model, don't remain perpendicular to the beam axis (Neuenhofer, 2006).

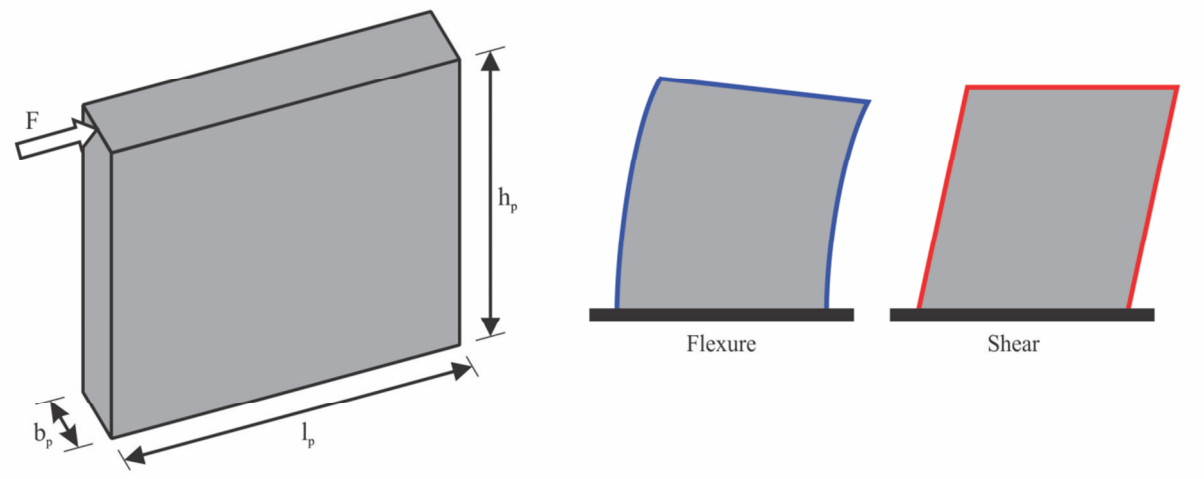

Figure 5-10: Cladding panel parameters when represented as a 'deep-beam' (left), flexure and shear components of deep-beam theory (right)

The in-plane stiffness of a deep beam is determined by both the shear and flexural stiffness. The panel is assumed to be in single curvature since it is assumed the top connections of the panel would allow small vertical deformations. It is typical for the top connections to be able to provide deformation capacity so this assumption is correct for most situations (PCI, 1989). If the top connections were rigid then the panel should be assumed to be in double curvature, and the flexural stiffness would be quadrupled.

The equations for stiffness of a rectangular cantilever in pure flexure and pure shear can be derived from engineering fundamentals and are given in Equations (5-14) and (5-15) respectively.

$$k_f = \frac{3EI_e}{{h_p}^3} \quad \textbf{(5-14)}$$

$$k_s = \frac{GA}{\chi h_p} \quad \textbf{(5-15)}$$

where

E = Elastic modulus

I_e = Effective moment of inertia of panel section

h_p = Panel height

G = Shear modulus

A = Area of section

χ = Shear shape factor

It follows that for a combination of flexure and shear that the relationship between the horizontal displacement, δ, and applied load, F, is as follows:

$$\delta = \left(\frac{{h_p}^3}{3EI_e} + \frac{\chi h_p}{GA}\right)F \quad \textbf{(5-16)}$$

For concrete, the effective moment of inertia of a section is not typically given by the gross section size. It is unknown what proportion of the gross section is applicable for the derivation of cladding panel stiffness. Table C6.6 in The New Zealand Concrete Structures Standard, NZS 3101 (2006) suggests the effective moment of inertia of walls with zero axial load is taken to be 32% of the gross moment of inertia so this will be used as a starting point. This reduction in the moment of inertia will be introduced to Equation (5-20) with the inclusion of a constant, α_e.

The shear modulus can also be equated to the elastic modulus by assuming a Poisson's ratio of 0.2 for concrete (NZS 3101, 2006) as follows:

$$E = 2G(1 + \upsilon) \quad \textbf{(5-17)}$$

where

υ = Poisson's ratio

hence

$$E = 2G(1 + 0.2) = 2.4G \quad \textbf{(5-18)}$$

For a rectangular section we can make the following geometric substitutions:

$$\chi = 1.2 \quad \textbf{(5-19)}$$

$$I_e = \alpha_e \frac{b_p {l_p}^3}{12} \quad \textbf{(5-20)}$$

$$A = b_p l_p \quad \textbf{(5-21)}$$

where

α_e = Effective percentage of moment of inertia

b_p = Panel thickness

l_p = Panel width

Using equations (5-16) - (5-21), the lateral stiffness of the panel, k_p, can be simplified to the following:

$$k_p = \frac{F}{\delta} = \frac{E b_p}{\frac{4}{\alpha_e}\left(\frac{h_p}{l_p}\right)^3 + \frac{2.88}{\alpha_e}\left(\frac{h_p}{l_p}\right)} \quad \textbf{(5-22)}$$

where

$\frac{h_p}{l_p}$ = Panel aspect ratio

This provides us with an equation to determine the stiffness of a rectangular concrete section that includes both flexural and shear deformations. It can be seen that the relationship between the stiffness and the thickness of the panel, b_p, is linear, whereas the relationship with the aspect ratio, h_p/l_p, determines whether the stiffness is predominantly shear or flexure based. For an arbitrary panel, Figure 5-11 shows how the contribution from flexural deformation and shear deformation changes for different aspect ratios. It can be seen that as the height of the panel increases relative to the width the total stiffness transitions from being governed by shear to flexure.

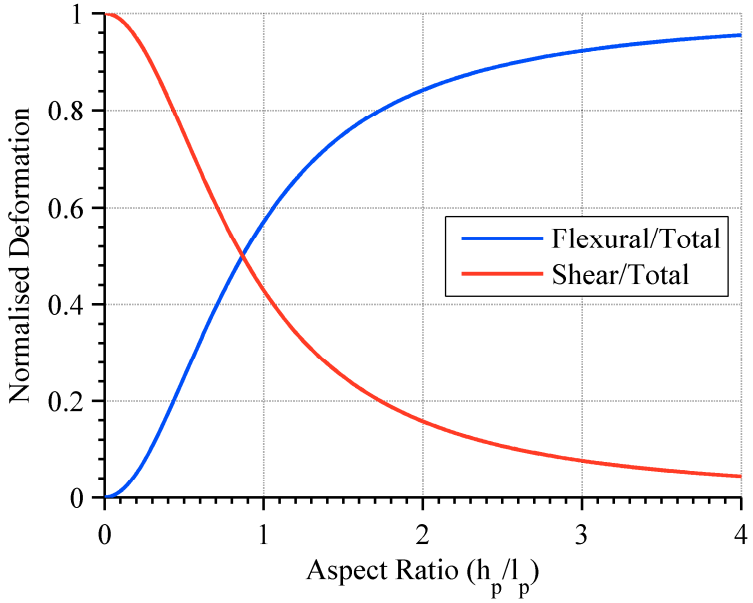

Figure 5-11: Contribution of flexure and shear to overall deformation for various panel aspect ratio

The theoretical stiffness of the two panel sizes that were tested experimentally are found using Equation (5-22) and are presented in Table 5-8. The elastic modulus used for the analytical calculations was that of the concrete panels tested in the lab, which was found to be 35 GPa. The effective moment of inertia was taken as 32%. It can be seen that Equation

(5-22) overestimates the stiffness by approximately 3-5 times. This overestimation is likely attributed to the opening in the panel being neglected since this can cause a significant reduction in the panel stiffness, as will be examined in the following section using finite element modelling.

Table 5-8: Comparison of experimental and analytical in-plane panel stiffness

	Large Panel	Small Panel
Experimental Stiffness (kN/mm)	4.8	0.8
Analytical Stiffness (kN/mm)	19.9	2.7

5.3.2 Finite Element Modelling

The ABAQUS finite element programme (ABAQUS Inc., 2011) was used to model the force-displacement behaviour of the threaded rod connections and concrete cladding panels. Finite Element Models (FEM) were created of each cladding component and validated against the experimental data by modifying the material properties. Using the experimentally validated model, a parametric investigation of cladding connections and panels has been performed.

5.3.2.1 Threaded Rod Connections

A 3D deformable solid made up of 2 mm tetrahedral mesh elements was used to model the threaded rod connections tested experimentally. Initially a FEM was developed which included the threads of the rod; however, the difference in behaviour when compared to a rod with no threads was found to be minor (around 2-3% reduction in force). The inclusion of threads on the rods also added a large computational expense because of the highly refined mesh that was required. Consequently, the threads of the rod have been neglected for this numerical investigation.

The steel material was modelled using a plastic isotropic yield model with (combined) cyclic hardening. The boundary conditions of the rods were set in order to mimic as closely as possible the realistic loading. This consisted of two regions 15 mm long on each end of the rods, one being fixed and one having a lateral displacement imposed on it. To reduce computational expense, the models made use of symmetry to reduce the model to a half of the threaded rod. The mesh arrangement and boundary conditions are shown in Figure 5-12.

The FEM was run using the same displacement cycles as testing however only a single cycle was applied at each displacement level. The FEM was verified against the six

experimental models by calibrating the plastic material properties. The elastic modulus of the FEM material was set at 200 GPa and a yield stress of 320 MPa was found to best match the yield point. Combined cyclic hardening with a Q-infinity of 200 MPa and Hardening Parameter of 15 was found to best match the experimental post-yielding behaviour.

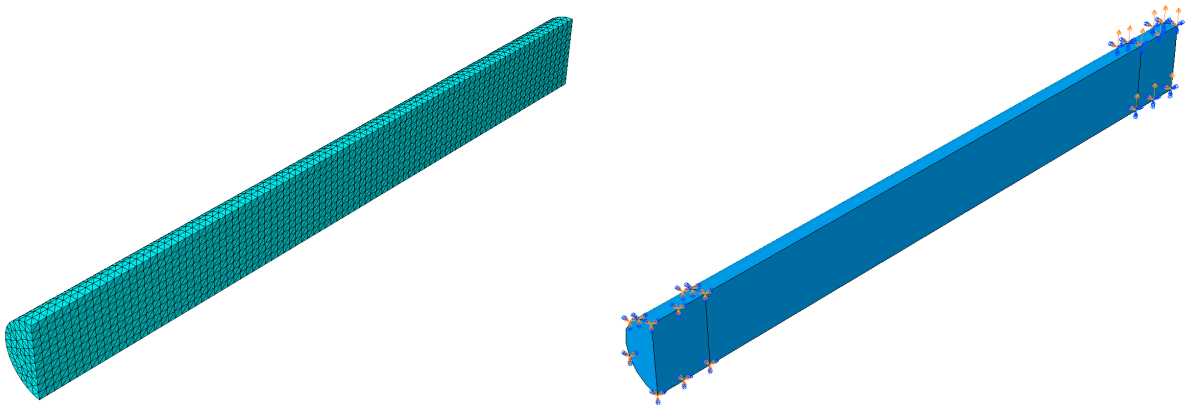

Figure 5-12: Finite element mesh (left) and boundary conditions (right) of threaded rod analyses

The 30 mm lateral deformation of a 20 mm diameter rod with a length of 150 mm is shown in Figure 5-13. A contour plot of the stress distribution in the rod is also projected on the deformed shape. The von Mises stress distribution is shown in the top of Figure 5-13 and the maximum principal stresses in the bottom of the figure. The contour plot shows how stress concentrations develop at the ends of the rods where the rotation is restricted. This region would correspond to where the nut of the threaded rod is located.

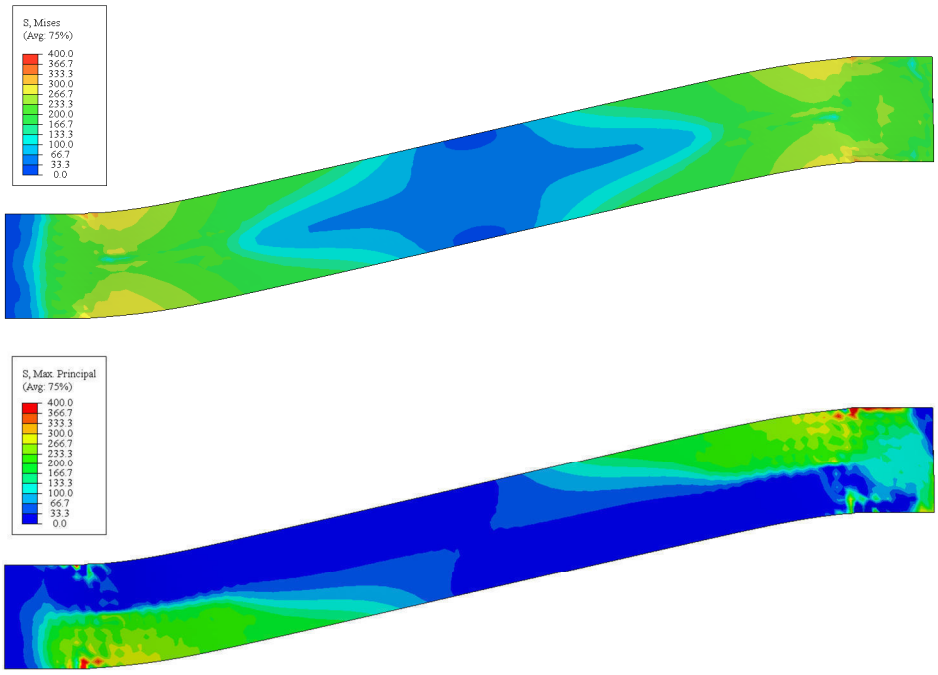

Figure 5-13: von Mises (top) and maximum principal (bottom) stress distributions of threaded rod

The numerical force-displacement behaviour of the six rod sizes tested experimentally is shown in Figure 5-14 along with the corresponding experimental and analytical behaviour. The numerical model evidently models the cyclic behaviour of threaded rods very well, capturing the yielding of the rods and the post-yield behaviour very accurately.

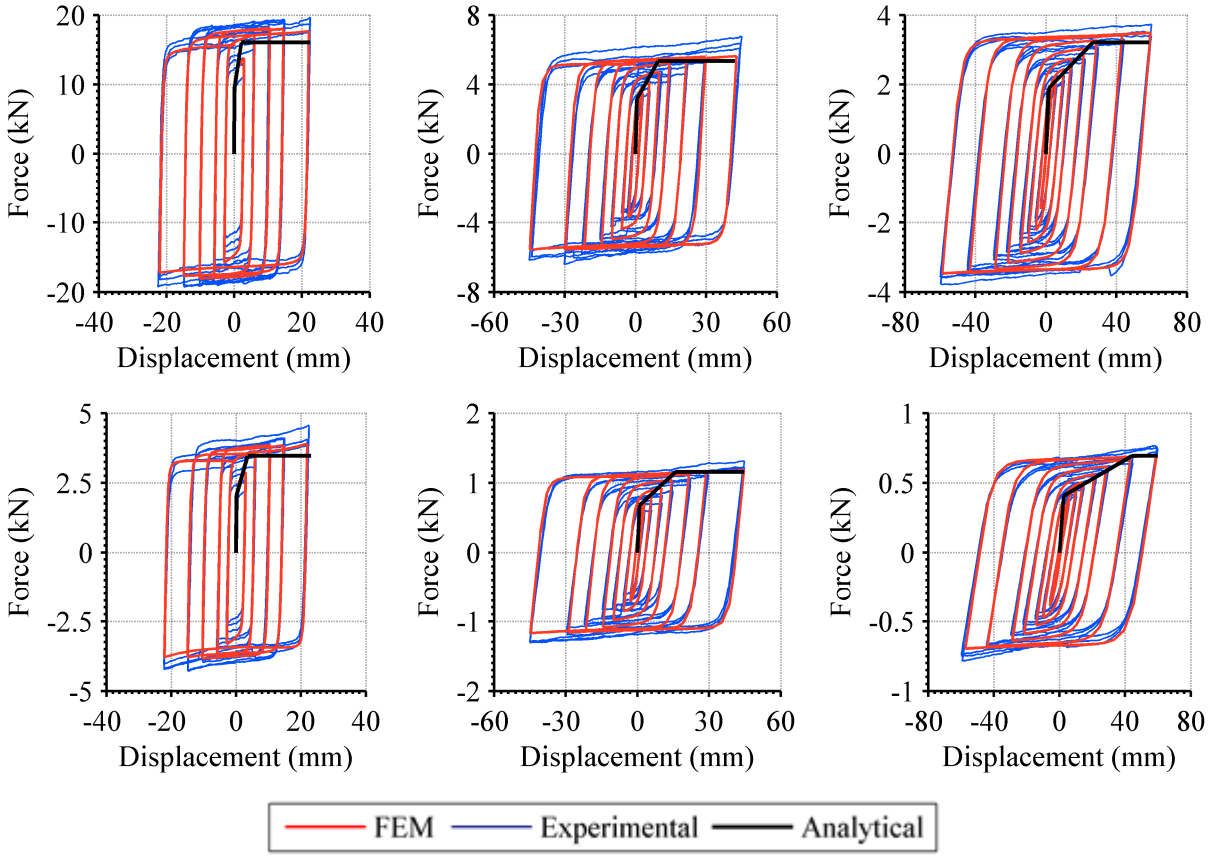

Figure 5-14: Force-displacement comparison of experimental, analytical and finite element modelling of threaded rod connections: 20 mm diameter rods (top row), 12 mm diameter rods (bottom row); 50 mm length (left), 150 mm length (cetnre), 250 mm length (right)

The numerically obtained yield force, yield displacement, initial stiffness and maximum force values are compared against experimental values in Table 5-9 and Table 5-10.

Table 5-9: Comparison of experimental and analytical threaded rod forces

		Yield Force (kN)		Yield Displacement (mm)	
	Rod Length (mm)	**Experimental**	**Numerical**	**Experimental**	**Numerical**
20 mm Rod Diameter	50	10.0	9.1	0.5	0.3
	150	2.8	3.2	1.2	1.5
	250	1.6	1.9	3.4	3.8
12 mm Rod Diameter	50	2.2	2.1	0.6	0.3
	150	0.7	0.7	2.2	2.3
	250	0.4	0.4	4.6	5.0

Similarly to the analytical solutions, the finite element models slightly under-predict both the yield force and maximum force of the threaded rods. However it can be seen that the yield displacement (and hence the initial stiffness) are predicted with much more accuracy by the numerical models than by the analytical solutions.

Table 5-10: Comparison of experimental and analytical threaded rod forces

		Initial Stiffness (kN/m)		Maximum Force (kN)	
	Rod Length (mm)	**Experimental**	**Numerical**	**Experimental**	**Numerical**
20 mm Rod Diameter	50	20,000	35,000	19.6	18.1
	150	2,300	2,100	6.4	5.6
	250	470	500	3.7	3.5
12 mm Rod Diameter	50	3,700	6,000	4.5	3.9
	150	320	300	1.3	1.2
	250	90	80	0.7	0.7

The threaded rod FEM developed are subjected to a monotonic loading protocol in order to approximate the non-linear behaviour with the non-linear Ramberg-Osgood hysteretic rule (Ramberg & Osgood, 1943). The Ramberg-Osgood hysteresis is suited for representing steel behaviour since it shows a smooth elastic-plastic transition, as shown in Figure 5-21. The Ramberg–Osgood hysteresis that relates force and displacement is given by Equation (5-23). It can be seen that the hysteretic rule requires the definition of just three parameters: the initial stiffness, yield force and R factor. It should be noted that the R factor used to define the Ramberg-Osgood hysteresis is not analogous to the R factor used to define a bi-linear relationship where it is a percentage of initial stiffness. For the Ramberg-Osgood function, the larger the R factor value, the closer the post-yielding behaviour is to being perfectly plastic (Kaldjian & Fan, 1967).

$$\delta = \frac{F}{k_0}\left[1 + \left(\frac{F}{F_y}\right)^{(r-1)}\right] \quad \textbf{(5-23)}$$

where

δ = Displacement

F = Force

k_0 = Initial stiffness

F_y = Yield force

r = R factor

A Ramberg-Osgood function is fitted to each numerical test using a MATLAB regression function that estimates the function coefficients using an iterative least squares estimation (MathWorks Inc., 2011). The initial stiffness can be extracted directly from the numerical data, leaving only the yield force and R factor to require fitting. Figure 5-15 shows a Ramberg-Osgood function that has been fitted to the numerical data of one test, along with the definition of the functions parameters. It can be seen that the Ramberg-Osgood function is an excellent representation of the behaviour. Also shown in Figure 5-15 is a bi-linear function with the same yield force determined by the Ramberg-Osgood regression function.

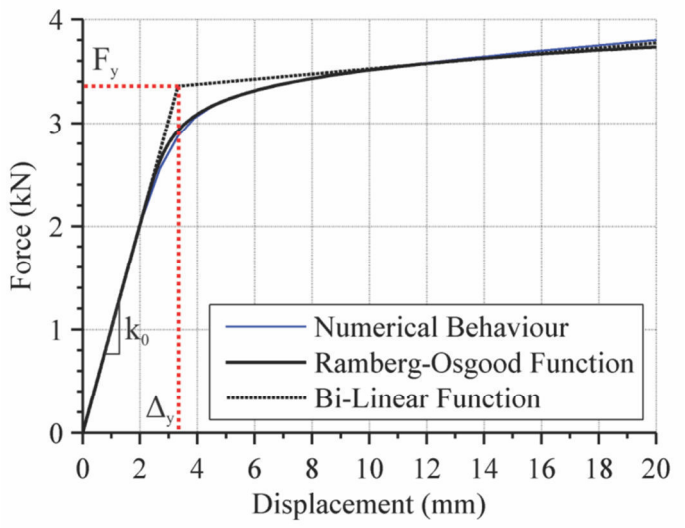

Yield Force, F_y (kN)	3.4
Yield Displacement, Δ_y (mm)	3.3
Initial Stiffness, k_i (kN/mm)	1.01
R factor	15

Figure 5-15: Curve fitting of Ramberg and Osgood (1943) function to numerical behaviour obtained by finite element analyses (left) with example parameters (right)

A parametric investigation of the threaded rods has been performed using the FEM developed from the experimental results. The parametric investigation of the threaded rod connections involves varying the threaded rod diameter and length and examining how these parameters affect the yield force, yield displacement, initial stiffness and R factor. Each numerical analysis consists of a monotonic loading to produce a force-displacement plot similar to that shown in Figure 5-15. A Ramberg-Osgood function is fitted to each numerical analysis in order to define the aforementioned parameters.

The diameters of threaded rods analyses were based on commercially available metric sizes. These included 12, 16, 20, 24 and 30 mm diameter rods. The threaded rod length was varied from 50 mm to 500 mm in 50 mm increments. In total, 50 numerical analyses were performed.

The yield force, yield displacement, initial stiffness and R factor are presented in Figure 5-16 for the 50 numerical analyses. The figures show that as rod length increases or rod

diameter decreases the yield force and stiffness decrease and the yield displacement increases. The stiffness of the rods is presented in logarithmic scale because of the large range of stiffness values. The R factor values are quite erratic, varying between 5 and 16.

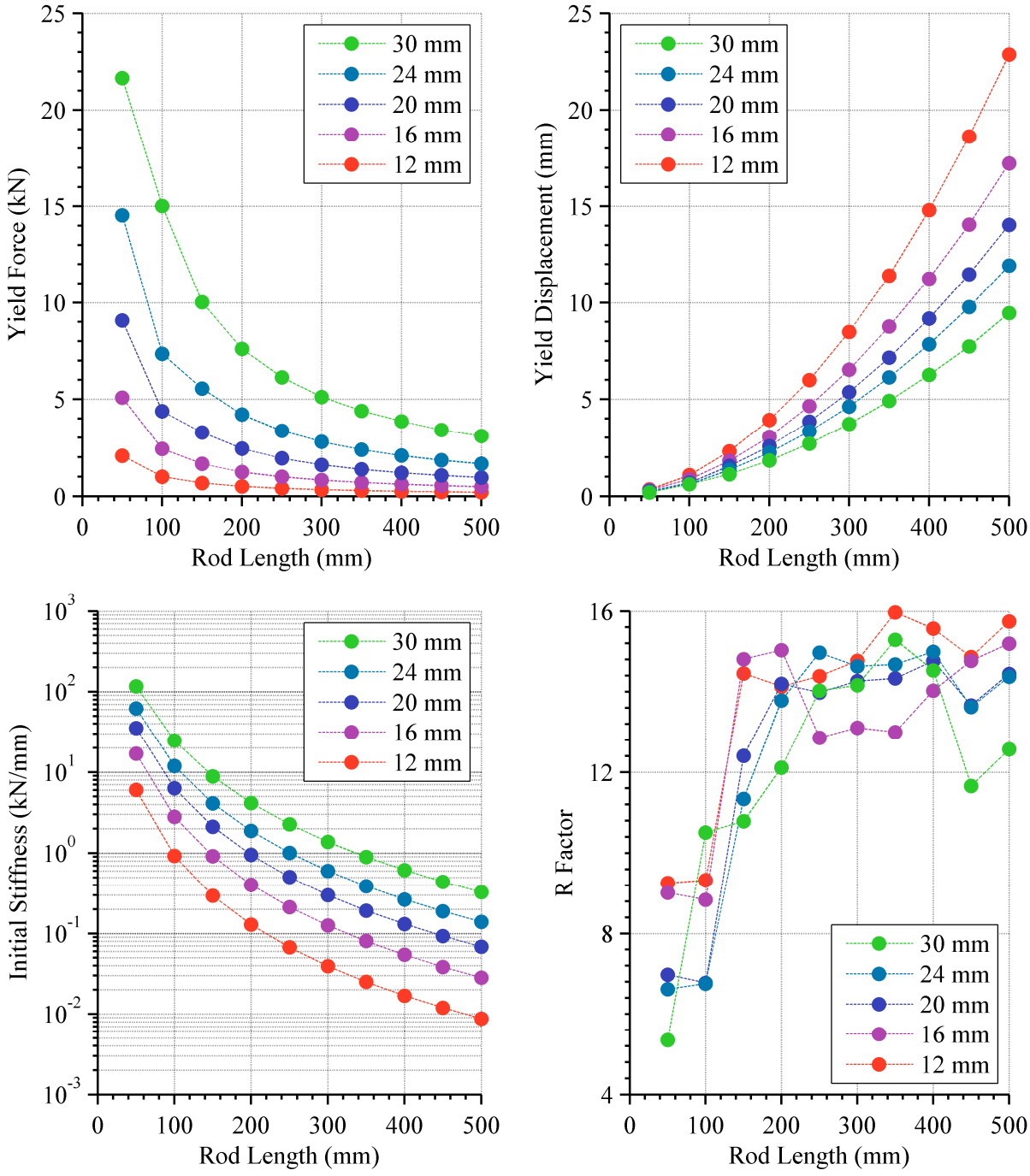

Figure 5-16: Results of finite element parametric analysis: yield force (top left), yield displacement (top right), initial stiffness (bottom left) and R factor (bottom right)

When the numerical and experimental results are compared against the analytical solutions for yield force and yield displacement obtained in Section 5.3.1.1, it can be seen in

Figure 5-17 that the analytical solution for yield force accurate predicts the yield force of the FEM for the rod diameters and rod lengths investigated.

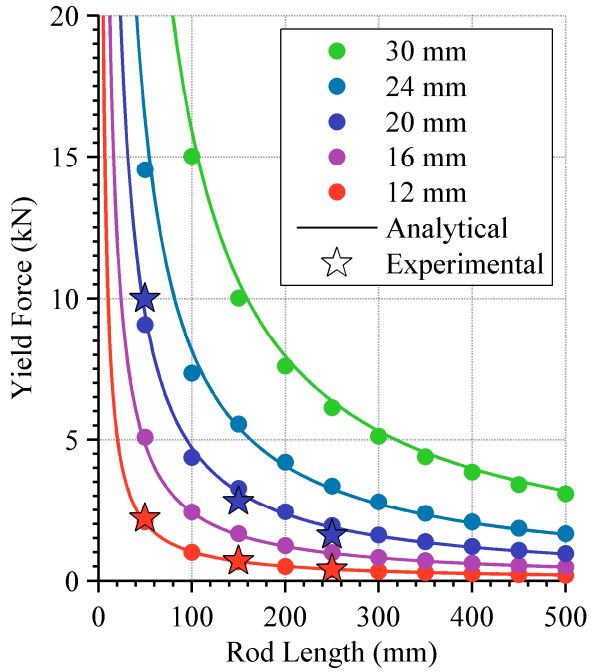

Figure 5-17: Comparison of yield force values obtained experimentally, analytically and numerically

The analytical solution for yield displacement under-predicts the observed numerical and experimental yield displacements, as shown in Figure 5-18 (left).

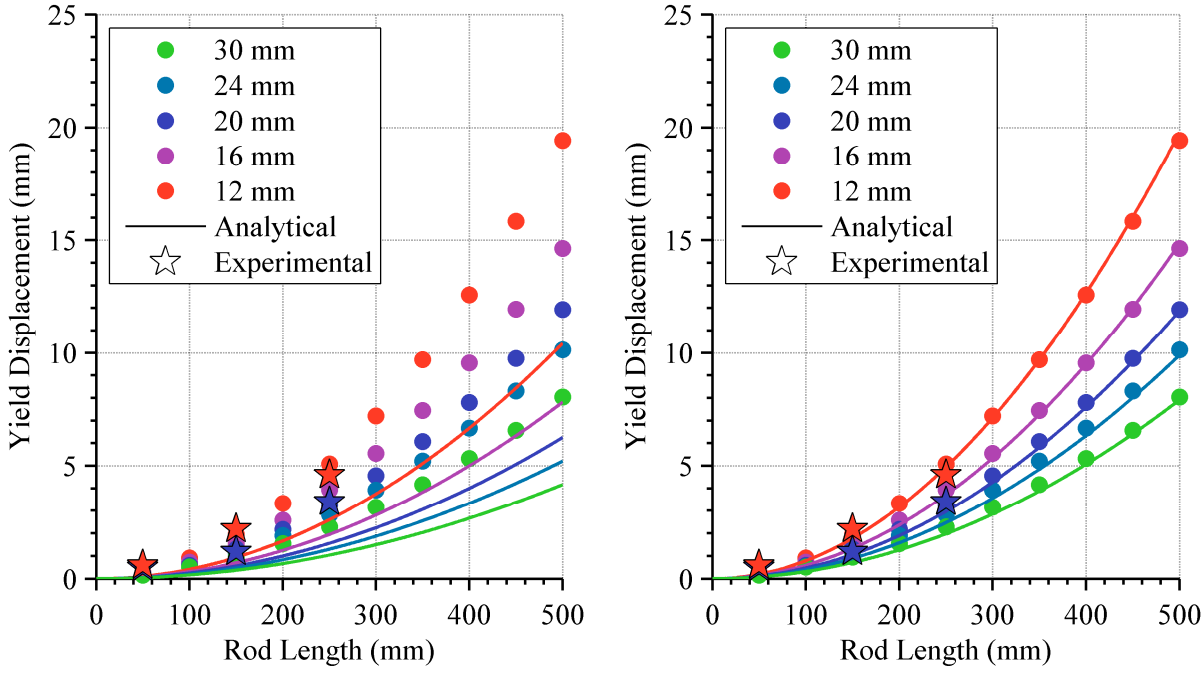

Figure 5-18: Comparison of yield displacement values obtained experimentally, analytically and numerically (left) when analytical yield displacement is doubled (right)

This may be attributed to the way in which the yield displacement is defined. Referring back to Figure 5-15 it can be seen that the numerical definition of the yield displacement is slightly greater than the displacement where the stiffness of the numerical test first changes. If the analytical solution for yield displacement is multiplied by two, as shown in Figure 5-18 (right), it can be seen that the analytical solution matches the numerical and experimental observations well.

The original analytical solution for initial stiffness over-predicts the observed numerical and experimental initial stiffness values; however, if the correction to the yield displacement is taken into account then the analytical solution accurately predicts the observed values, as shown in Figure 5-19. The analytical solution becomes less accurate when the rod is shorter and thicker, as shown by the numerical data points on the left of the plot not meeting the lines. This is likely attributed to the analytical solution being based purely on flexure of the rods and as the rods become shorter and thicker, the influence of shear becomes greater.

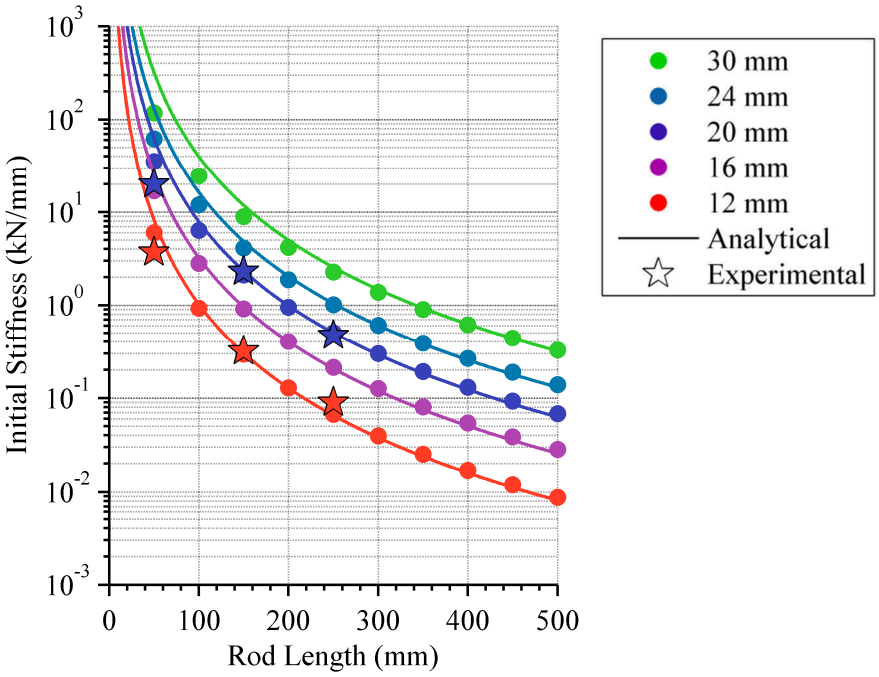

Figure 5-19: Comparison of initial stiffness values obtained experimentally, analytically and numerically

The R factor values show no discernible trend for rod diameter, however, the R factor does tend upwards for increasing rod length, as shown in Figure 5-20. This increase appears to flatten out for longer rod lengths, suggesting a logarithmic function would be a good fit to approximate the data.

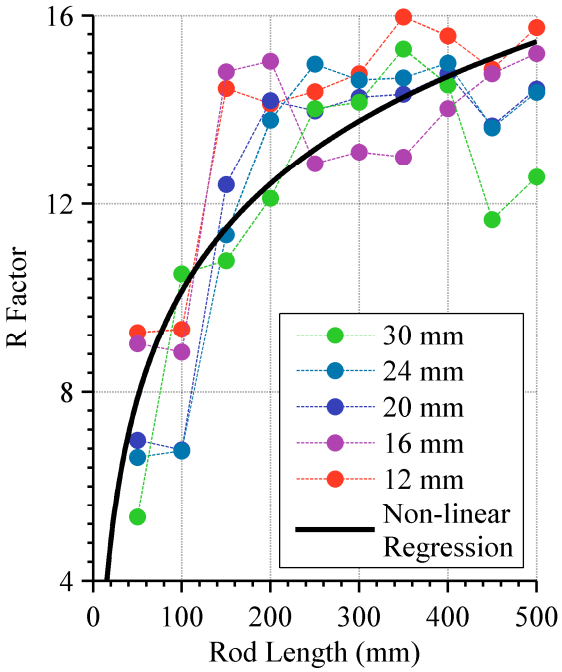

Figure 5-20: R factor values of Ramberg and Osgood (1943) function when fitted to numerical results

A logarithmic function is fitted to the data using an iterative approach to minimise the squares of the difference between the function and data points and is shown in Figure 5-20. The fitted logarithmic function is given by Equation (5-24). Obviously this is only applicable for the rod lengths considered here.

$$R = 3.3 \ln l_r - 5.0 \qquad \textbf{(5-24)}$$

where

R = R factor

5.3.2.2 Panels

The idealisation of a cladding panel as a cantilever wall for the analytical derivations undertaken previously assumes that the panel is fixed entirely along the base. In reality the panel is likely able to deform along both the top and bottom edges as the connections are typically discretely located near the corners of the panel. A fixed base assumption would be considered appropriate when the panel connection is in the form of a continuous in-situ connection cast along the length of beam/floor of the structure. Cladding panels also often have large openings and thus cannot be assumed to be a single quadrilateral element.

In order to more accurately predict the lateral deformation of cladding panels, a finite element model (FEM) of a cladding panel has been developed. The model consists of a 3D

deformable solid made up of 50 mm hexahedral mesh elements was used. The hexahedral element is a cube shaped, linear, reduced integration element (ABAQUS Inc., 2011). The material was modelled using an elastic isotropic material. The boundary conditions of the panel were set in order to mimic as closely as possible the loading of the panel. This consisted of two rectangular regions where the elements were fixed to represent the fixed bearing connections and two rectangular regions where the elements had a lateral movement imposed to represent the movement connections. The mesh arrangement and boundary conditions are shown in Figure 5-21.

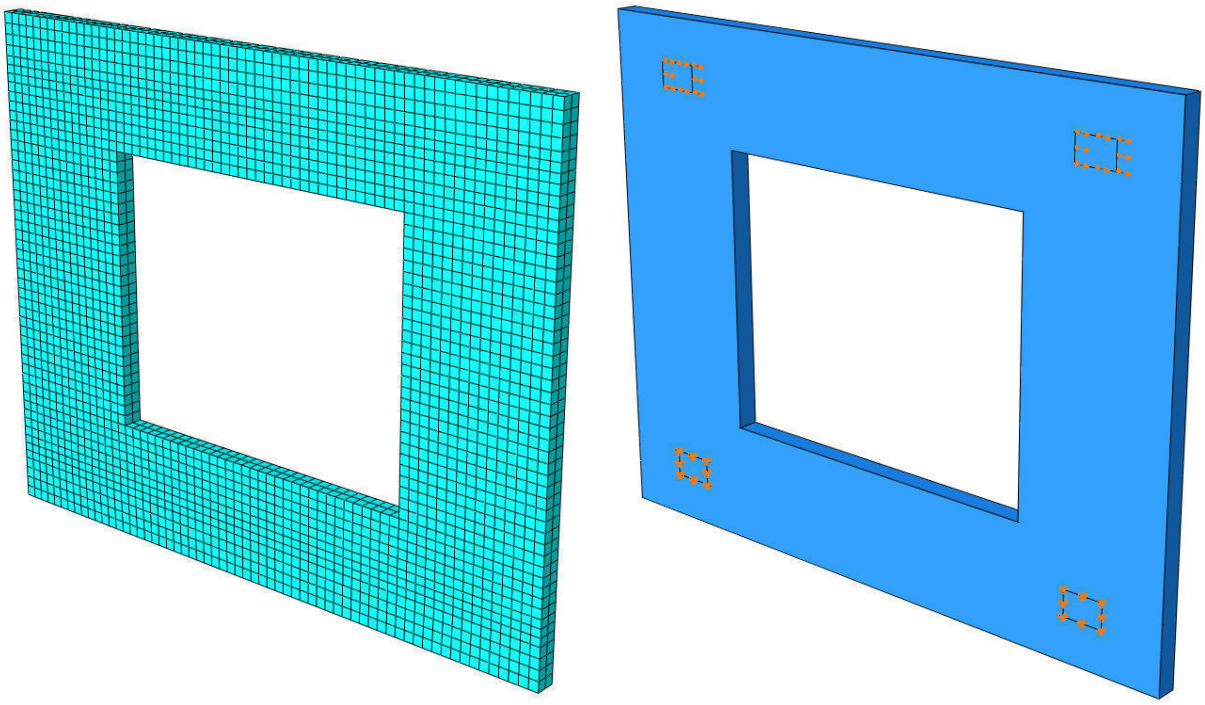

Figure 5-21: Finite element mesh (left) and boundary conditions (right) of cladding panel analyses

The size of the panel model was chosen to replicate the large panel tested experimentally. The elastic modulus of the FEM material was adjusted in order to obtain an in-plane stiffness equivalent to that obtained experimentally. An elastic modulus of 29 GPa was found to best fit the experimental data. This was less than the elastic modulus of the concrete tested experimentally, which was found to be 35 GPa.

The panel size was then altered to that of the smaller panel. The numerical stiffness matches the experimental results well which suggests the model provides a good estimation of the in-plane stiffness of precast concrete cladding panels. In order to fully validate the model, further experimental investigation of different panel aspect ratios and opening width ratios would be needed. A comparison between the experimental stiffness and FEM stiffness is presented in Table 5-11.

Table 5-11: Comparison of experimental and numerical in-plane panel stiffness

	Large Panel	Small Panel
Experimental Stiffness (kN/mm)	4.8	0.8
Numerical Stiffness (kN/mm)	4.8	0.9

The in-plane deformation of the large panel is shown in Figure 5-22. A contour plot of the principal stress distribution in the panel is also projected on the deformed shape. The largest principal stresses are shown in red. The contour plot shows how tensile stress concentrations develop at the connections and window corners. The location of the largest principal stresses indicate where cracking will first be observed since by definition they denote the maximum tensile stress (Park & Paulay, 1975). Thus the model accurately predicts that first cracking occurs in the window corners. The bottom connections in particular also have large stress concentrations since these regions are more rigid and do not allow any vertical or rotational movement. It is also apparent that both the top and bottom edges of the panel are deforming. Therefore, as alluded to earlier, the assumption made during the analytical derivation that the bottom edge of the panel is fixed is not entirely accurate.

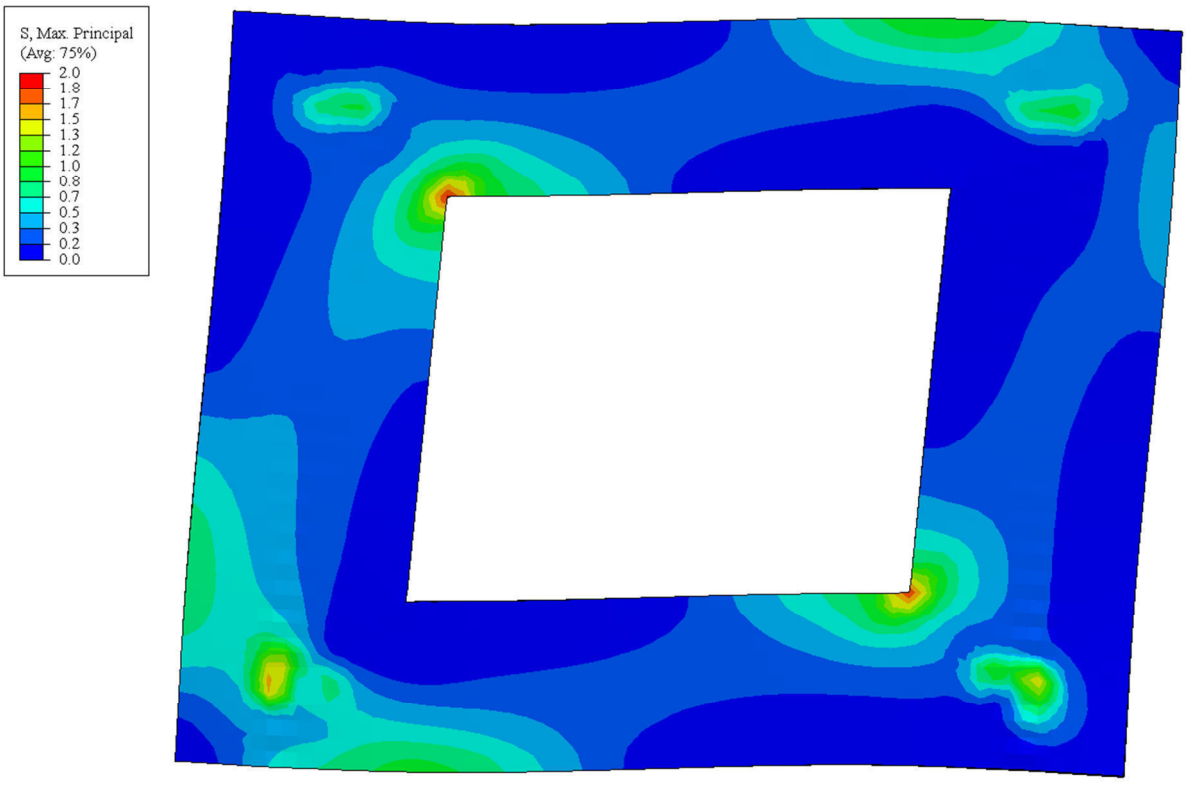

Figure 5-22: Maximum principal stress distribution in cladding panel when deformed laterally in-plane

Using the model validated from the experimental data, a parametric investigation of cladding panels has been performed. The parametric investigation of the cladding panel

model involves varying the panel aspect ratio and opening width ratio to examine how these parameters affect the stiffness.

Firstly, cladding panels with no opening have been modelled in order to compare with the analytical stiffness obtained in Section 5.3.1.3. The in-plane stiffness of the panels is presented in Figure 5-23 for varying panel aspect ratios. The analytical stiffness has been presented with an effective moment of inertia factor equal to the gross moment of inertia as well as with reduction factors of both 32% and 25%. It can be observed that using the gross moment of inertia significantly overestimates the stiffness. The 32% reduction factor suggested for a concrete cantilever wall with zero axial load by (NZS 3101, 2006) also overestimates the stiffness slightly. The best fit was found when a 25% reduction factor was used. This reduction is likely attributed to the additional flexibility brought on by the panel not having a fixed base since the analytical solution is based on a fixed base assumption.

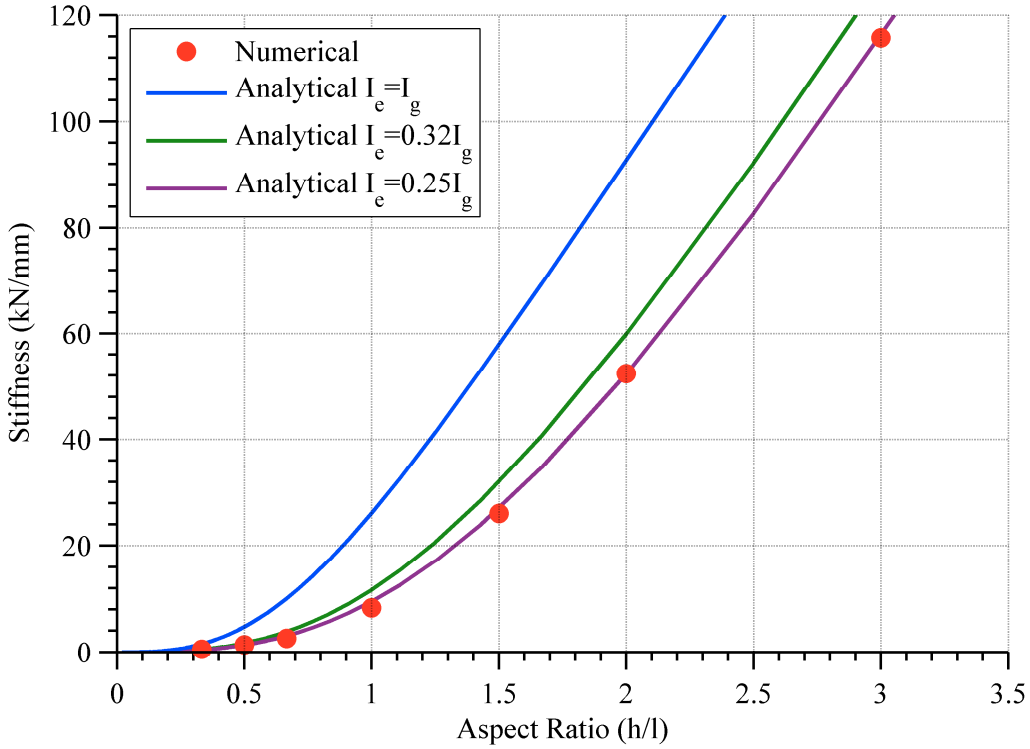

Figure 5-23: Comparison of numerical and analytical panel stiffness for varying panel aspect ratio and effective moment of inertia

A panel opening was introduced to the panel aspect ratios modelled to understand how this affected the panel stiffness. The opening has been defined by the opening width ratio, which is equal to the width of the opening divided by the width of the panel. Only symmetric panels have been investigated, thus the opening is located in the centre of the panel and the ratio of the opening height to panel height is that of the opening width ratio. Presented in

Figure 5-24 are the stiffness values of the nine aspect ratios investigated, including the two experimental panel aspect ratios, when the opening width ratio is increased from zero (no opening) to 80% of the panel width. It can be seen that the stiffness drops away considerably when the opening width ratio is between 20 – 60%.

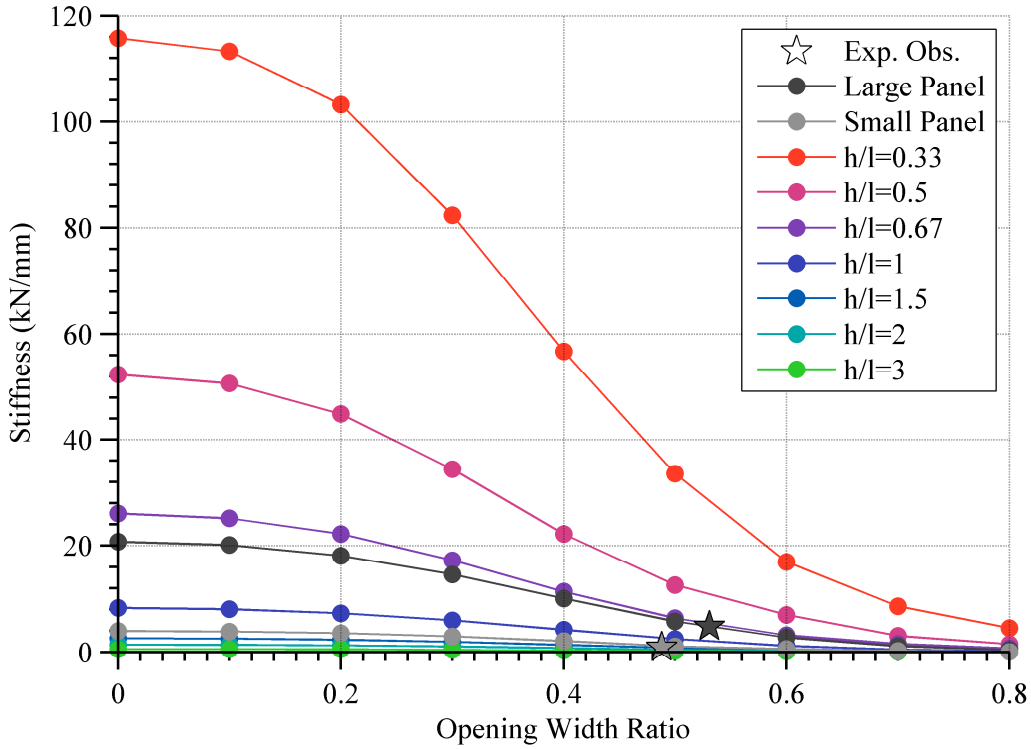

Figure 5-24: Numerical panel stiffness considering central opening compared with experimental results

The general shape for each panel aspect ratio in Figure 5-24 is also approximately the same. Therefore, the data points have been normalised by the maximum stiffness for that aspect ratio, which is the stiffness of the panel with no opening. The data points of all FEM models are presented in Figure 5-25. It can be observed that the data points lie approximately along the same curve, suggesting the stiffness at different opening width ratios is not greatly dependent upon the aspect ratio. The data has been fitted with a non-linear regression curve based on an exponential function that estimates the functions coefficients using an iterative least squares estimation. An exponential function appears to fits the data well.

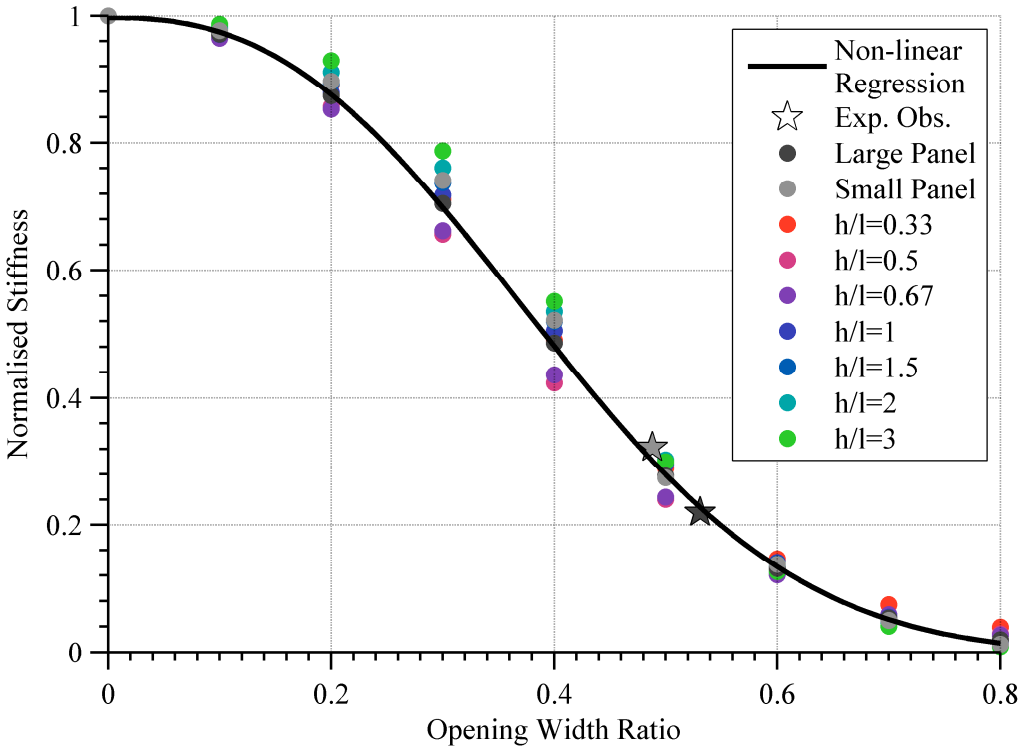

Figure 5-25: Experimental and numerical normalised panel stiffness considering central opening

The stiffness of a symmetric panel with a symmetric opening can thus be calculated using Equation (5-25) which is a combination of the analytical equation derived previously for a panel with no opening and the empirical function presented in Figure 5-25 which considers the central opening in the panel.

$$k_p = \frac{E b_p}{328{\eta_p}^3 + 12.5\eta_p} \cdot e^{-7.1{\chi_p}^{2.5}} \qquad \textbf{(5-25)}$$

where

$\eta_p = \frac{h_p}{l_p}$ = Panel aspect ratio

$\chi_p = \frac{l_o}{l_p}$ = Opening width ratio

l_o = Opening width

A comparison can now be made between the stiffness of the panels tested experimentally and the analytical stiffness given by Equation (5-25), with the values presented in Table 5-12. The experimental, numerical and analytical force-displacement behaviour for the two panel sizes tested is shown in Figure 5-26.

Table 5-12: Comparison of experimental, numerical and analytical in-plane panel stiffness

	Large Panel	Small Panel
Experimental Stiffness (kN/mm)	4.8	0.8
Analytical Stiffness (kN/mm)	4.9	0.8

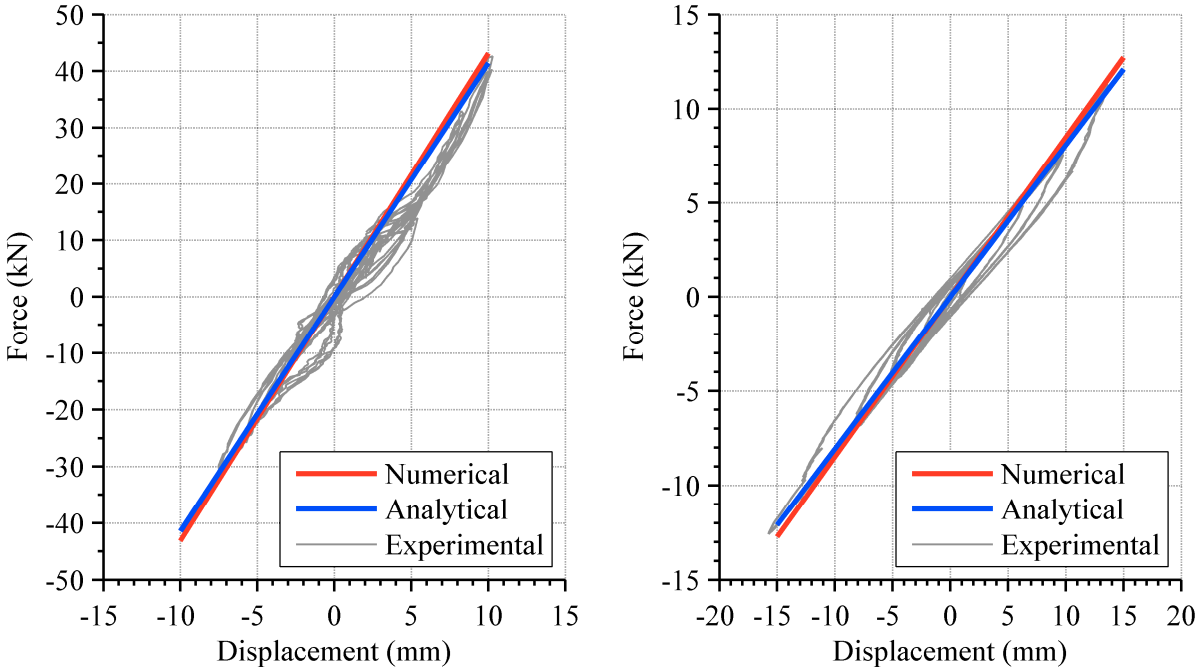

Figure 5-26: Comparison of panel stiffness values obtained experimentally, analytically and numerically for large panel (left) and small panel (right)

5.3.3 Summary of Recommended Modelling Parameters

Using the combination of experimental, analytical and numerical results, the key parameters to numerically model cladding components are given in this section.

5.3.3.1 Threaded Rod Connections

The yield force, initial stiffness and Ramberg-Osgood R factor for threaded rod connections are given in Equations (5-8), (5-25) and (5-24).

$$F_y = \frac{\pi f_y {d_r}^3}{16 l_r} \quad \textbf{(5-8)}$$

$$k_0 = \frac{3\pi E {d_r}^4}{32 {l_r}^3} \quad \textbf{(5-26)}$$

$$R = 3.3 \ln l_r - 5.0 \quad \textbf{(5-24)}$$

where

d_r = Diameter of threaded rod

l_r = Length of threaded rod

E = Elastic modulus of steel

f_y = Yield Stress

5.3.3.2 Slotted Connections

The friction force for slotted steel on steel connections is given by Equation (5-13).

$$F_f = \frac{\mu m_p g e_p}{e_c} \quad \textbf{(5-13)}$$

where

μ = Coefficient of friction (1.0 for steel on steel)

m_p = Mass of panel

g = Gravity

e_p = Horizontal eccentricity between panel and connection

e_c = Vertical eccentricity between connections

5.3.3.3 Panels

The initial in-plane stiffness of a reinforced concrete panel with a central, symmetric opening is given by Equation (5-25).

$$k_p = \frac{E b_p}{328{\eta_p}^3 + 12.5\eta_p} \cdot e^{-7.1{\chi_p}^{2.5}} \quad \textbf{(5-25)}$$

where

E = Elastic modulus of concrete

b_p = Panel thickness

$\eta_p = \frac{h_p}{l_p}$ = Panel aspect ratio

$\chi_p = \frac{l_o}{l_p}$ = Opening width ratio

h_p = Panel height

l_p = Panel width

l_o = Opening width

5.4 Cladding Model Development

Two different models have been developed to represent the cladding system in a frame building: the quadrilateral cladding model and the spring cladding model. Both models were developed using the seismic response analysis programme Ruaumoko2D (Carr, 2010). The quadrilateral model is a more physical representation of the cladding system, with the ability to define each component individually. However, the computational expense of the quadrilateral model is much greater than that of the spring model. Each cladding panel system that is modelled using the quadrilateral model requires 20 nodes and 12 elements to be defined. The spring model is a much simpler model, requiring the definition of just four nodes and three elements per cladding panel. This makes the spring model less expensive computationally, however, it requires a higher level of understanding and calibration to ensure the model best represents the cladding. The stiffness of the cladding panel is defined for the quadrilateral cladding model by only the elastic modulus and dimensions of the panel, whereas the spring model requires the stiffness to be explicitly provided. Quadrilateral elements in Ruaumoko 2D are elastic only elements and thus the quadrilateral model can only model the panel as being elastic, whereas the spring model is able to capture non-linear behaviour in the cladding panel.

5.4.1.1 Quadrilateral Cladding Model

Linear elastic quadrilateral elements are used to represent the cladding panel for modelling situations where the panel is assumed to remain elastic and undamaged. The stiffness of the quadrilateral elements is based on the material properties and dimensions of the precast concrete cladding panel.

The quadrilateral elements are connected to the frame using linear springs at the top and rigid links at the bottom to represent the cladding connections, as shown in Figure 5-27. The rigid links represent the bearing connections which carry the gravity load of the cladding to the frame and are unable to deform in both axial directions as well as rotationally. The springs used at the top of the panel represented the flexible connections. For slotted

connections, these linear springs are replaced with damper (dash-pot) elements since for slotted connections the force is dependent upon velocity instead of displacement. These elements undergo most of the lateral deformation and as such, dictate the magnitude of force transferred through the cladding system. The top connections do not have any rotational or vertical stiffness so only provide horizontal resistance. All non-linear behaviour in the cladding system occurs in the top springs alone when this system is used.

The mass of the cladding is assigned as being distributed evenly throughout the quadrilateral elements. This mass is lumped at each of the quadrilateral element corner nodes for computation.

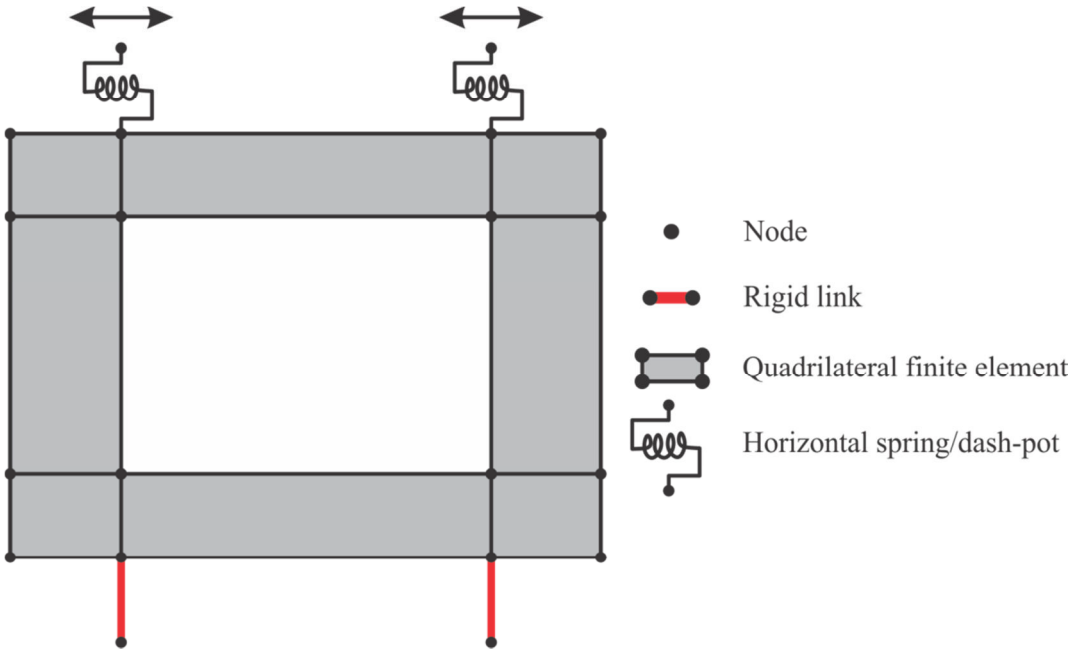

Figure 5-27: Quadrilateral cladding model

5.4.1.2 Equivalent Spring Cladding Model

The equivalent spring cladding model consists of a single linear spring to represent the cladding panel and a single top and bottom connection, represented by a horizontal spring/dash-pot and rigid link respectively, as shown in Figure 5-28.

This model provides a simple representation of the cladding system which can easily be added between floors of a structure. The rotations and axial displacements of the connection and panel elements were restrained so that they can only deform horizontally. The mass of the cladding panel is assigned as being distributed evenly along the panel spring element. This mass is then lumped at each end of the spring for computation.

It is possible to model each connection separately, as was done in the quadrilateral cladding model, however, since both connections will typically be subjected to the same displacement and velocity demands it is possible to simplify the model to a system where the connections are represented with a single horizontal element. It is then necessary to assign this single element the parameters equivalent to two identical elements in parallel. This model is the simplest representation of a cladding system where the cladding and connections are represented separately. Modelling the cladding panel with an equivalent spring element provides more freedom to how the cladding is modelled, including the ability to capture damage within the panel but this also allows for greater inaccuracy if not done correctly.

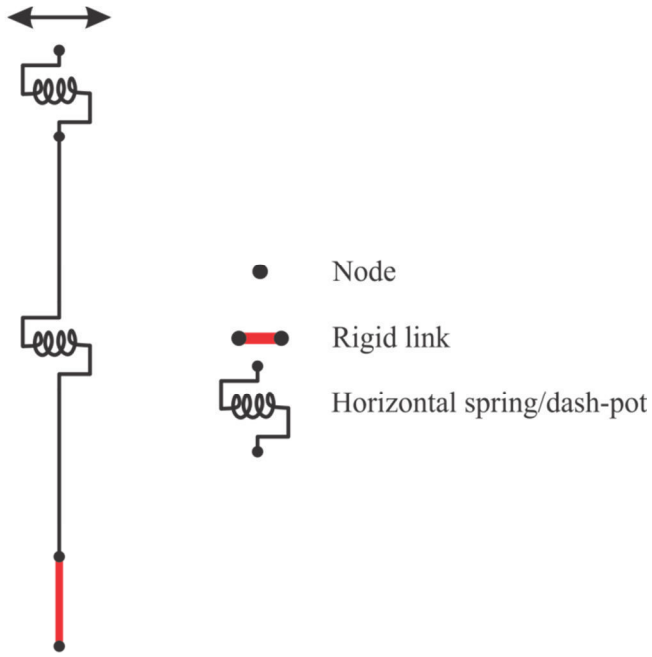

Figure 5-28: Equivalent spring cladding model

5.5 Cladding Model Implementation

In order to implement the cladding models, a 2D model of the experimental testing frame has been developed using the seismic response analysis programme Ruaumoko2D (Carr, 2010). A representation of the experimental frame model is shown in Figure 5-29. The frame elements remained elastic during experimental testing so was modelled using linear frame elements with the appropriate section properties. Multi-spring elements springs were used to model the PRESSS connection between beam column joints of the frame (Speith et al., 2004). The multi-spring consisted of two springs in parallel which acted in compression only, located at the centroid of compression force for each rocking direction. The use of the

multi-spring meant the elongation of the frame was able to be accurately captured. Linear springs between columns were used to model the post-tensioning bars. These springs were pre-loaded with the initial post-tensioning force and could only provide axial resistance. Rotational springs were also used adjacent to the multi-spring in order to capture model local column deformation. During casting of the columns, a small space was left behind the plates on the face of each column. This resulted in a reduction of the moment capacity in each beam column joint for small rotations as this space was consumed. The rotation springs reduced the moment capacity of the PRESSS connections for small rotations to capture this softening effect.

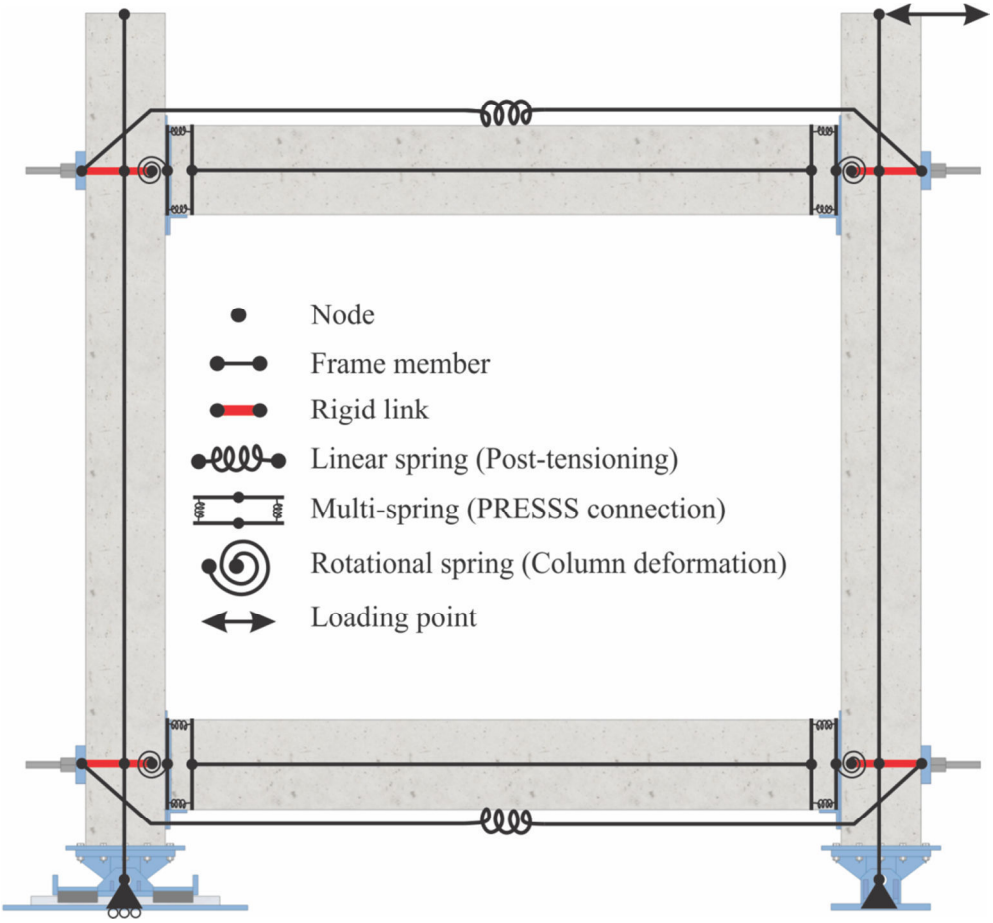

Figure 5-29: Experimental test frame model

Material properties were used for the frame members, multi-spring elements and linear springs. The stiffness of the rotation springs was calculated using local deformation measurements made using linear potentiometers placed over the PRESSS joint. For a full description of the modelling parameters used, refer to Appendix E. The model was subjected to the same displacement controlled loading protocol that was used during experimental testing in Chapter 4. A comparison of the experimental and numerical force-displacement

behaviour is shown in Figure 5-30 (left) and a comparison of the experimental and numerical post-tensioning force is shown in Figure 5-30 (right). The numerical model accurately models the force-displacement behaviour of the frame, although it does not capture the small amount of dissipative behaviour in the frame. This is likely occurring within the column deformation as it can be seen the numerical post-tensioning stiffness is greater than the experimental stiffness for small drift levels. This results in the post-tensioning force being slightly over-estimated by the numerical model.

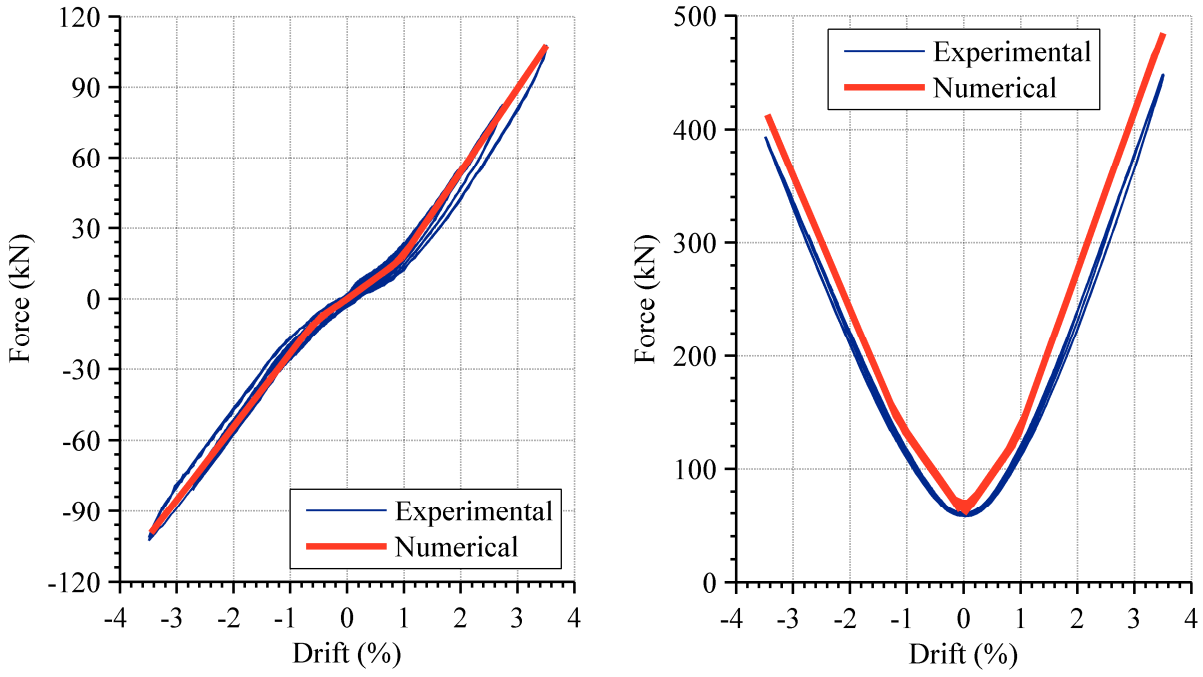

Figure 5-30: Comparison of experimental and numerical force-displacement behaviour (left) and top level post-tensioning force (right) of experimental test frame

5.5.1 Experimental Frame Cladding Models

The two cladding models (quadrilateral and equivalent spring) introduced in Section 5.4 are incorporated into the bare frame model of the experimental test rig. The cladding system modelled is that of the mono panel experimental setup with two top and bottom connections. The parameters used to represent the panel and the top connections are based on those developed in this Chapter and summarised in Section 5.3.3 for different connection types.

A representation of the experimental frame model including the cladding system modelled with quadrilateral elements is shown in Figure 5-31. The vertical length of the connections is exaggerated and the size of the panel reduced for clarity.

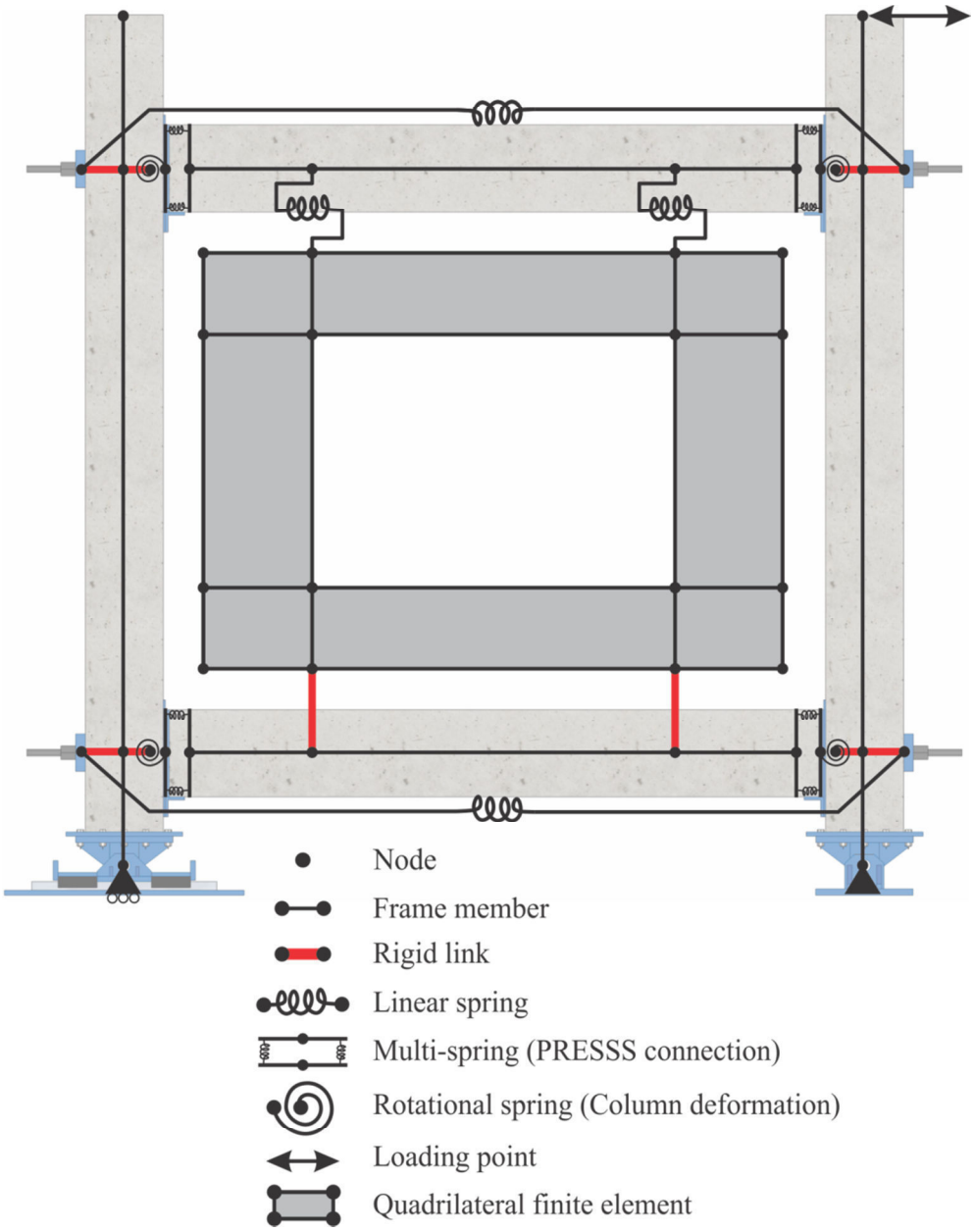

Figure 5-31: Quadrilateral cladding model incorporated in test frame

A representation of the experimental frame model including the cladding system modelled with the equivalent spring cladding model is shown in Figure 5-32. The horizontal spring connecting the panel spring to the beam represents both top movement connections and is thus equivalent to two individual connection springs in parallel.

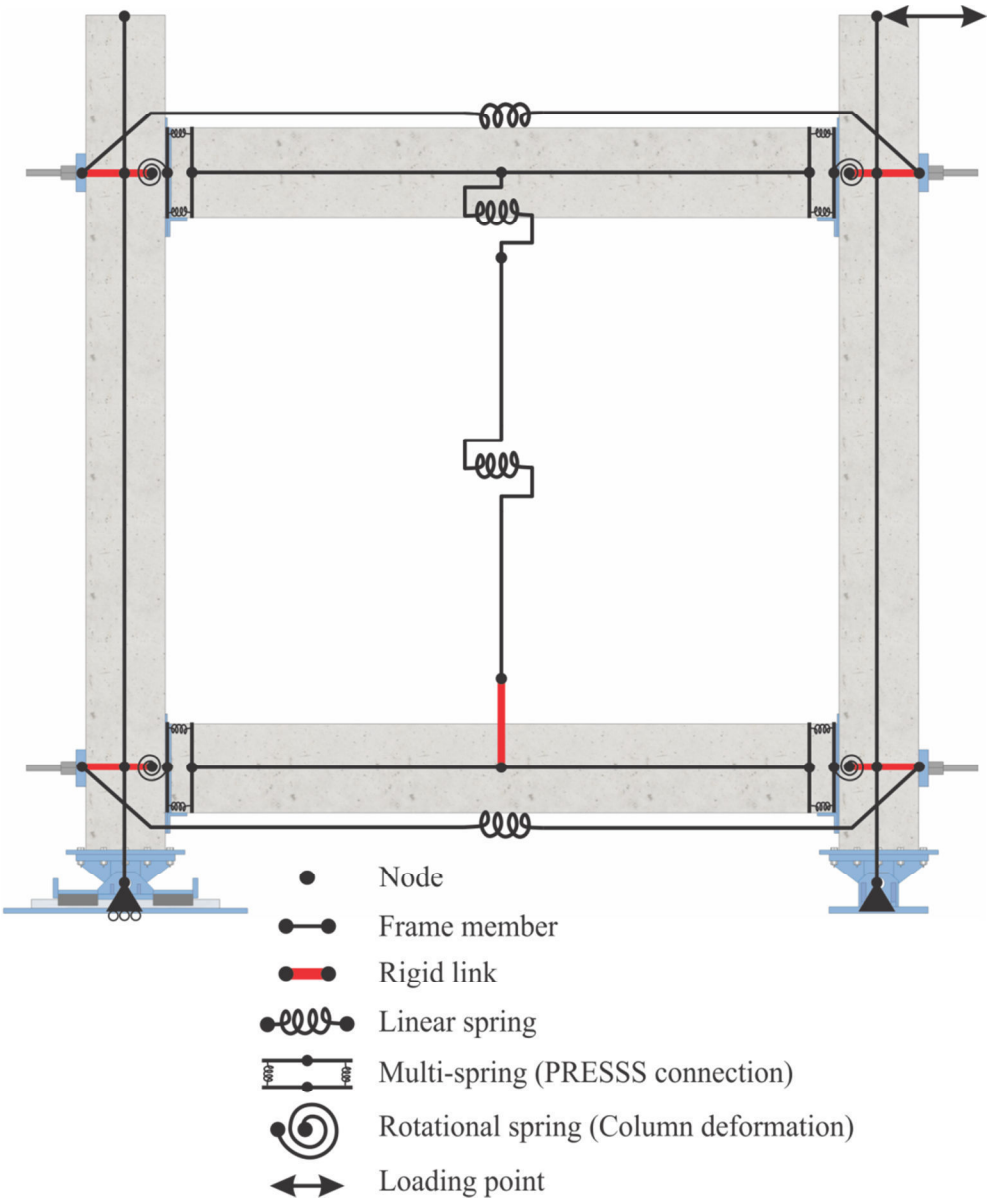

Figure 5-32: Equivalent spring cladding model incorporated in test frame

5.6 Cladding Model Verification

This section compares the force-displacement behaviour of the numerical cladding models developed against the observed experimental behaviour in order to verify their accuracy. The different connection types tested experimentally in Chapter 4 are implemented as numerical cladding model using both the quadrilateral and equivalent spring models. These connection types are long threaded rod connections, slotted connections and short threaded rod connections. Multiple models are presented for each connection type where appropriate. Each model was developed using the recommended modelling parameters presented in Section 5.3.3.

To compare the force-displacement behaviour of the numerical models with the experimental behaviour the models were subjected to the same displacement controlled loading protocol that was used during experimental testing. The force-displacement behaviour of the numerical bare frame (refer to Figure 5-30) is subtracted from the overall numerical frame behaviour to display the force-displacement contribution of the cladding system for each connection type modelled.

5.6.1 Long Threaded Rod Connections

A quadrilateral and an equivalent spring model have been developed to represent the cladding system with 250 mm long threaded rod connections. Both models represent the long threaded rod connections with linear springs. The amount of force transferred through the cladding system being dictated by the hysteretic behaviour of these springs. The non-linear behaviour of the connection springs for both models was represented using the Bounded Ramberg-Osgood hysteretic rule. The bounded version of the Ramberg-Osgood hysteretic rule produces a modified loop on small cycle reloading. This is necessary for cycle loading since the original version of the hysteretic rule tends to exhibit un-realistic forces if the loop reverses and has not moved very far from the back-bone curve (Carr, 2008).

The yield force, initial stiffness and R factor for the threaded rods modelled using Ramberg-Osgood are given in Equations (5-8), (5-25) and (5-24).

$$F_y = \frac{\pi f_y {d_r}^3}{16 l_r} = 1.9\ kN \qquad \textbf{(5-8)}$$

$$k_0 = \frac{3\pi E {d_r}^4}{32 {l_r}^3} = 600\ kN/m \qquad \textbf{(5-26)}$$

$$R = 3.3 \ln l_r - 5.0 = 13 \qquad \textbf{(5-24)}$$

Strength degradation was incorporated into the definition of hysteretic behaviour so that when the connection displacement exceeded 50 mm, the strength of the connections sharply dropped off to zero. This drop in strength represents the failure of the threaded rod connection that was observed experimentally and corresponds to a ductility of 17.

The cladding panel was represented in the quadrilateral model using the geometry of the panel and an elastic modulus of 35 GPa (the elastic modulus of the panel concrete tested experimentally). The equivalent spring model stiffness was defined using Equation (5-25).

$$k_p = \frac{E b_p}{16{\eta_p}^3 + 2.88\eta_p} \cdot e^{-7.1{\chi_p}^{2.5}} = 4800 \text{ kN/m} \qquad \textbf{(5-25)}$$

The force-displacement behaviour of the quadrilateral cladding model compared with the experimental behaviour of the corresponding long threaded rod cladding system is illustrated in Figure 5-33. It can be observed that the numerical model accurately represents the behaviour of the cladding system. The failure of the connections can be observed by the return to bare frame behaviour for drifts above 1.5%. Also shown in Figure 5-33 is the force-displacement contribution from the cladding system and the parameters of the hysteretic rule for an individual connection. It should be noted that the force-displacement contribution of the cladding includes the behaviour of the two connections and the panel. Therefore the yield force and failure force is double that of the parameters given in the table for the hysteretic parameters of an individual connection.

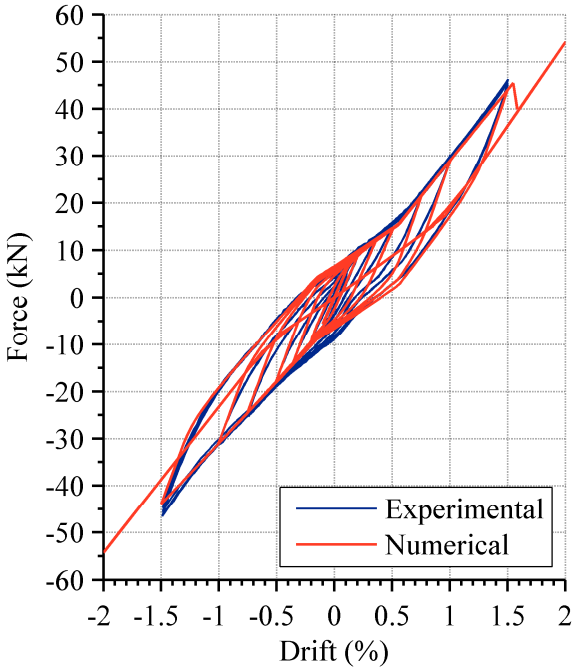

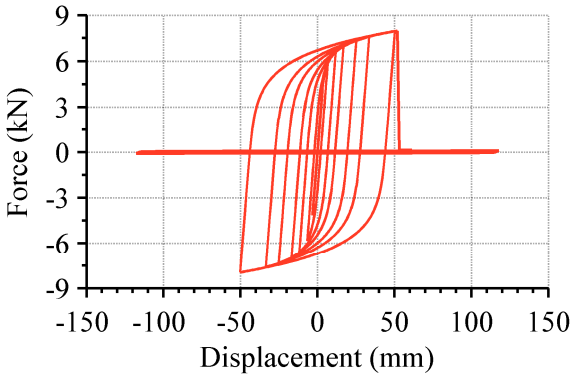

Model Type	Quadrilateral
Hysteretic Rule	Bounded Ramberg-Osgood
Initial Stiffness	600 kN/m
Yield Force	2 kN
R factor	13
Failure Force	4 kN
Failure Displacement	50 mm

Figure 5-33: Long threaded rod cladding model (quadrilateral model) compared with experimental results of test MP-LTR1

The force-displacement behaviour of the equivalent spring cladding model compared with the experimental behaviour of the corresponding long threaded rod cladding system is illustrated in Figure 5-34. The single connection spring of the model was assigned double the stiffness and yield force to make it equivalent to two connection springs being in parallel. It can be observed that the behaviour of the model is virtually identical to that of the previous

model presented in Figure 5-33. Also shown in Figure 5-34 is the force-displacement contribution from the cladding system and the parameters of the hysteretic rule for the equivalent spring connection.

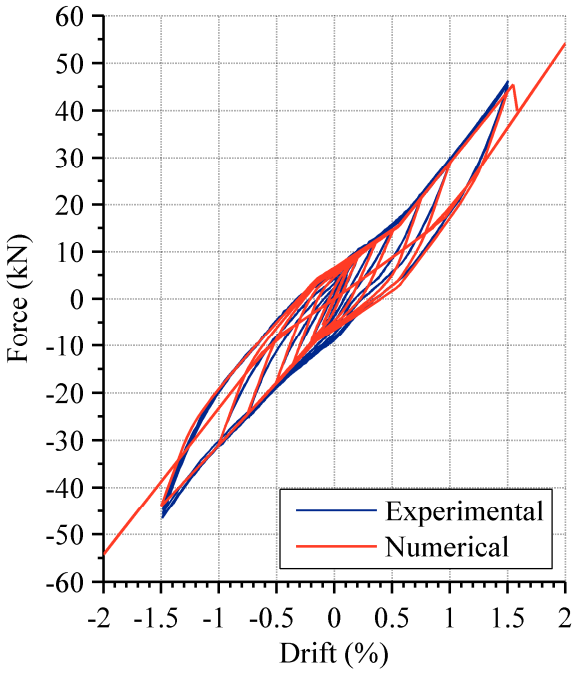

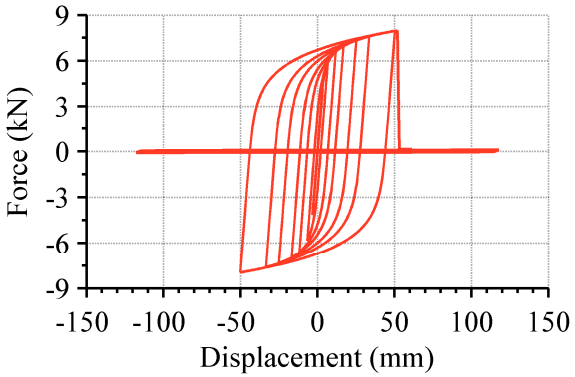

Model Type	Equivalent Spring
Hysteretic Rule	Bounded Ramberg-Osgood
Initial Stiffness	1200 kN/m
Yield Force	4 kN
R factor	13
Failure Force	8 kN
Failure Displacement	50 mm

Figure 5-34: Long threaded rod cladding model (equivalent spring model) compared with experimental results of test MP-LTR1

5.6.2 Slotted Connections

Two slotted connection models were developed for both the quadrilateral and equivalent spring cladding models. The different models are based upon whether the slot capacity of the connection is exceeded or not. The first two models (one quadrilateral and one equivalent spring model) correspond to slotted connections when the displacement demand is within the capacity of the slot and utilise a simple elasto-plastic hysteresis. The subsequent two models (one quadrilateral and one equivalent spring model) correspond to slotted connections when the displacement demand exceeds the slot capacity and thus significantly more force is transferred into the cladding system.

Damper (dash-pot) members are used to model the slotted connections when displacements are within the capacity of the slot. The friction force provided by the connections is assumed to be constant, i.e. not dependent upon displacement or velocity. This type of sliding friction is referred to as Coulomb damping (Serway & Jewett, 2009). The

dampers require definition of a damping coefficient (force/velocity) and the maximum friction force. The damping coefficient was set at 30,000 kNs/m so that the maximum friction force is reached virtually immediately but not so high that instability of the model occurs. The friction force that the dash-pot of the slotted connection is limited to is determined by Equation (5-13).

$$F_f = \frac{\mu m_p g e_p}{e_c} = 3.0\ kN \qquad \textbf{(5-13)}$$

When the dash-pot element is used, the force from the connection is constant, which is analogous to a slotted connection of infinite slot length. However, when the displacement demand exceeds the slot capacity, the force transferred into the cladding system is much greater than the friction force alone. The effect this has upon the system and its behaviour is of particular interest; hence new models are required to capture this effect. This has been achieved by adding a horizontal spring which utilised the Bi-linear with Slackness hysteresis in parallel with each dash-pot element. The use of this hysteretic rule allows for a delay in the initiation of the hysteresis (slackness) which means that the spring does not affect the behaviour whilst the displacement demand is within the slot capacity. A slackness (or gap) of ±50 mm was used, which corresponds to the slotted connection slot length which was tested in the experimental programme. Once engaged, the model provides additional strength and stiffness according to the bi-linear hysteresis specified. The definition of this stiffness has been achieved by assuming that the connection behaves like a threaded rod connection once engaged. This assumption is made since the experimental connections tested had a length of 150 mm between the slotted plate and the cladding panel, therefore, when the capacity of the slot was exceeded the connection effectively became a fixed end threaded rod connection of 120 mm length. The stiffness was defined by the relationships established for threaded rods and is given below for a 20 mm rod of 120 mm length. When unloaded, the hysteresis is disengaged and the behaviour returns to that of the slotted region alone.

$$k_0 = \frac{3\pi E {d_r}^4}{32 {l_r}^3} = 2{,}800\ kN/m \qquad \textbf{(5-26)}$$

The first and second connection models have a theoretically infinite slot length and as such are only applicable when it can be assured that the displacement demand within the slot length of the connection. The third and fourth models are useful for defining the behaviour once the slot length is exceeded; however, require definition of the stiffness once the slot is

exceeded. The cladding panel was modelled in the same way for the slotted connections as it was for the long threaded rod models presented previously. A summary of the four slotted connections models is shown in Table 5-13.

Table 5-13: Summary of slotted connection models

Slotted Connection Model Number	**1**	**2**	**3**	**4**
Model Type	Quadrilateral	Equivalent Spring	Quadrilateral	Equivalent Spring
Connection Elements	Coulomb Dash-pot	Coulomb Dash-pot	Coulomb dash-pot + Bi-linear with Slackness Spring	Coulomb dash-pot + Bi-linear with Slackness Spring
Slot Length	Infinite	Infinite	50 mm	50 mm

The second slotted connection model is for use when the displacement demands are within the slot allowance so no damage is expected in either the connection or cladding panel The force-displacement behaviour of the quadrilateral cladding model compared with the experimental behaviour of the corresponding slotted cladding system is illustrated in Figure 5-35. It can be observed that the numerical model accurately represents the behaviour of the cladding system. Also shown in Figure 5-35 is the force-displacement contribution from the cladding system and the parameters of the dah-pot elements for an individual connection.

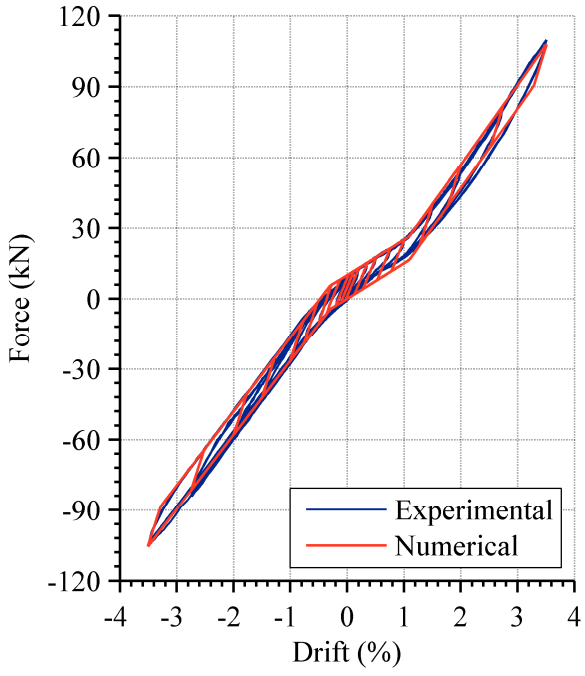

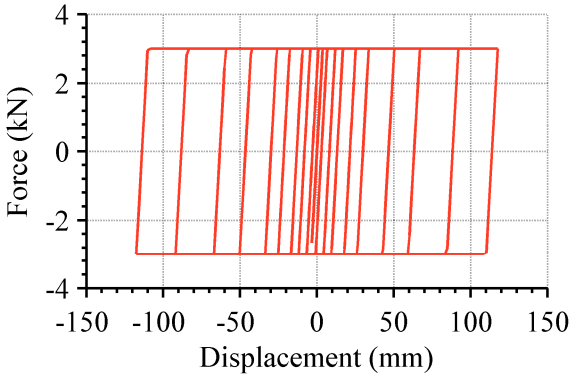

Model Type	Quadrilateral
Connection Element	Coulomb Dash-pot
Max Force	3 kN
Damping Coefficient	30,000 kNs/m

Figure 5-35: Slotted cladding model 1 (quadrilateral) compared with experimental results of test MP-SL1

The second slotted connection model makes use of the equivalent spring model and is again for use when the displacement demands are within the slot allowance so no damage is expected in either the connection or cladding panel. The force-displacement behaviour compared with the experimental behaviour is illustrated in Figure 5-36. It can be observed that the numerical model accurately represents the behaviour of the cladding system.

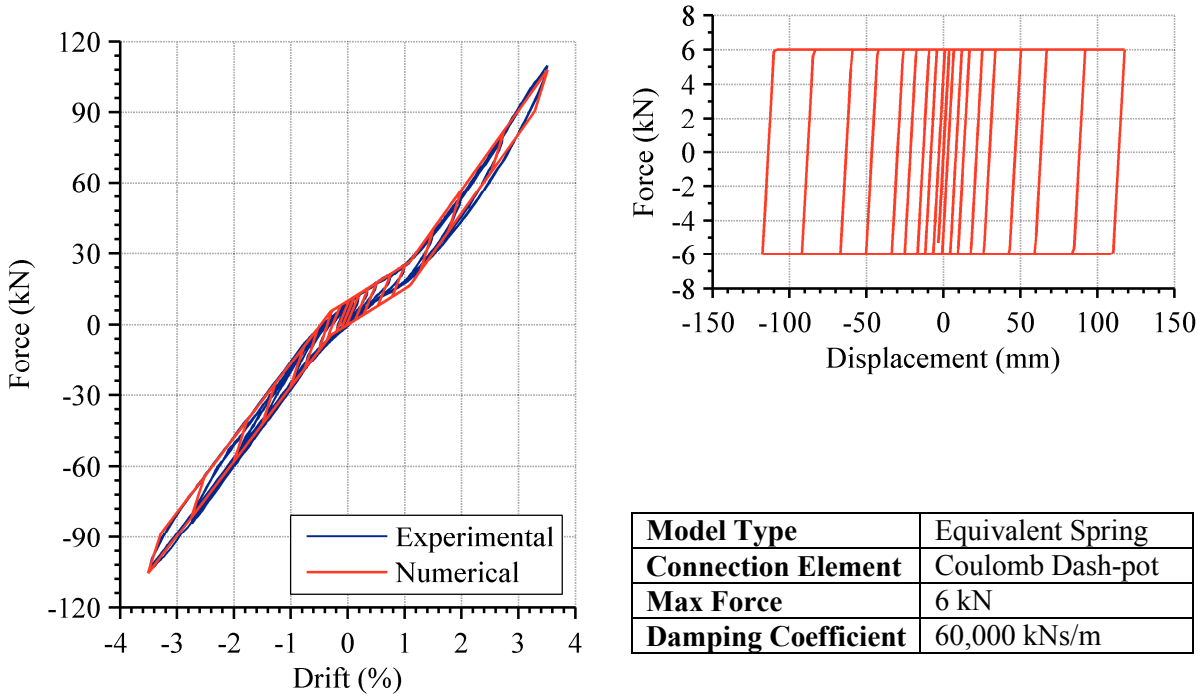

Model Type	Equivalent Spring
Connection Element	Coulomb Dash-pot
Max Force	6 kN
Damping Coefficient	60,000 kNs/m

Figure 5-36: Slotted cladding model 2 (equivalent spring) compared with experimental results of test MP-SL1

The third slotted cladding model made use of the quadrilateral cladding model and the combination of dash-pot and spring connections. The force-displacement behaviour of the system and connections is presented below in Figure 5-37. The strength degradation occurring in the panel of the experimental tests during the higher cycles is not captured since it is assumed that the panel's stiffness is constant; however, the overall force-displacement envelope is accurately captured so this model is accurate where strong panels are used, or when strength degradation is to be ignored.

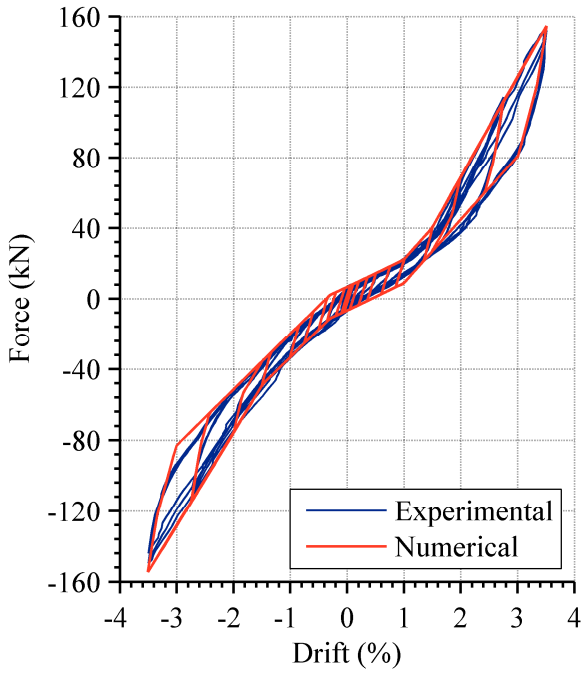

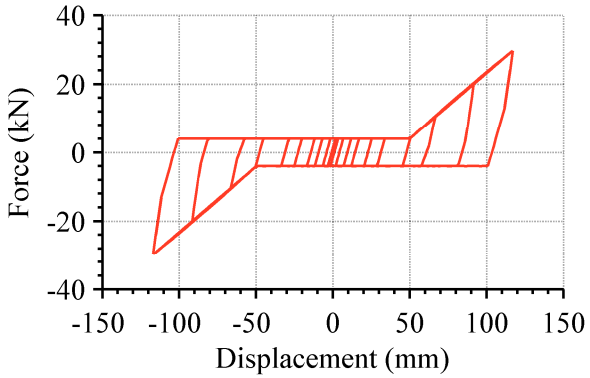

Model Type	Quadrilateral
Connection Elements	Coulomb dash-pot + Bi-linear with Slackness Spring
Initial Force	3 kN
Stiffness Gap	± 50 mm
Secondary Stiffness	2,800 kN/m

Figure 5-37: Slotted cladding model 3 (quadrilateral) compared with experimental results of test MP-SL3

The fourth model utilised the equivalent spring cladding model and the combination of dash-pot and spring connections. The strength and stiffness for the single spring and dash-pot was calculated from the equivalent two elements in parallel. The force-displacement behaviour of the cladding system and connections is illustrated in Figure 5-38. It can be observed that the behaviour of the model is virtually identical to that of the previous model presented in Figure 5-37 so the equivalent spring model can be used to accurately represent the behaviour of slotted connections when beyond the slotted region and strength or stiffness is assumed. The parameters of the hysteretic rule used for the equivalent spring model are presented in Figure 5-38.

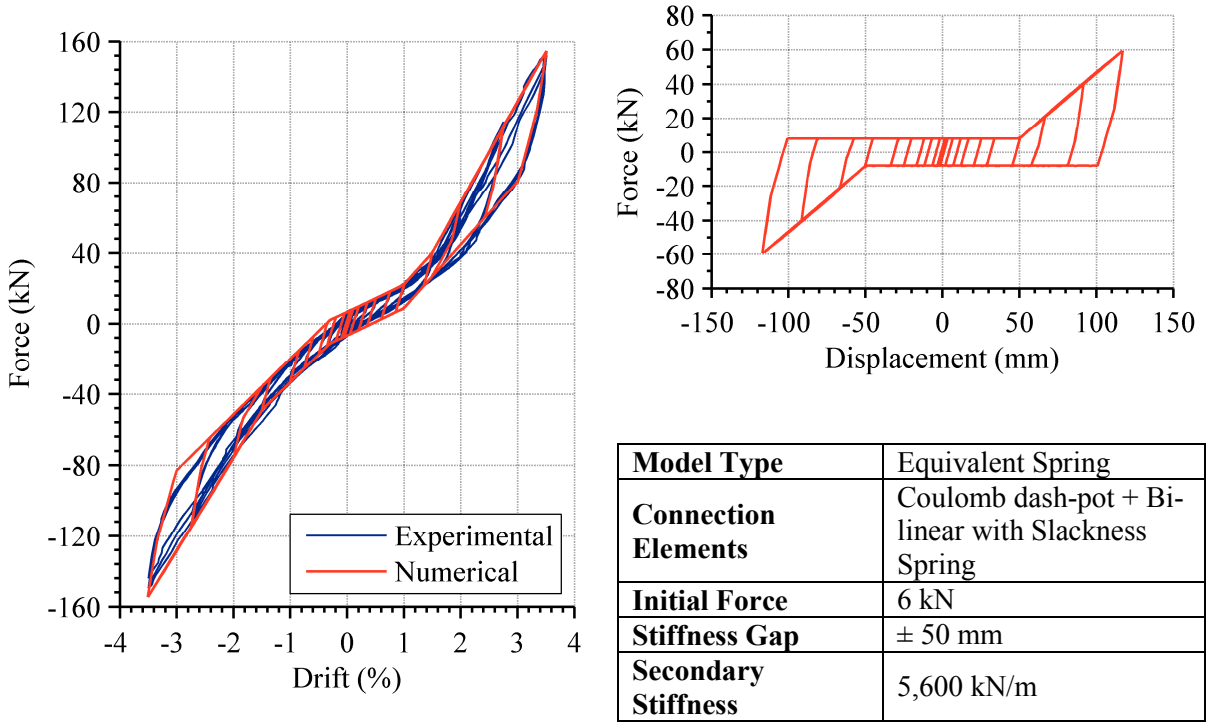

Model Type	Equivalent Spring
Connection Elements	Coulomb dash-pot + Bi-linear with Slackness Spring
Initial Force	6 kN
Stiffness Gap	± 50 mm
Secondary Stiffness	5,600 kN/m

Figure 5-38: Slotted cladding model 4 (equivalent spring) compared with experimental results of test MP-SL3

5.6.3 Short Threaded Rod Connections

Two cladding models were developed to represent the cyclic behaviour of short threaded rod connection type. Both models represent the short threaded rod connections with linear springs. The amount of force transferred through the cladding system being dictated by the hysteretic behaviour of these springs. The non-linear behaviour of the connection springs for both models was represented using the Bounded Ramberg-Osgood hysteretic rule.

One variation specific to the short threaded rod connection cladding models was that four top spring elements were used instead of the two used for previously presented models. These top springs represent four short threaded rod connections. The experimental test of this cladding system (refer to test MP-STR2 in Chapter 4) transferred the most force into the cladding panel so this configuration is of most interest.

The yield force, initial stiffness and R factor for the threaded rods modelled using Ramberg-Osgood are given in Equations (5-8), (5-25) and (5-24).

$$F_y = \frac{\pi f_y {d_r}^3}{16 l_r} = 9.4\ kN \qquad \textbf{(5-8)}$$

$$k_0 = \frac{3\pi E {d_r}^4}{32 {l_r}^3} = 75{,}000\ kN/m \quad \textbf{(5-26)}$$

$$R = 3.3 \ln l_r - 5.0 = 8 \quad \textbf{(5-24)}$$

A model utilising the quadrilateral cladding model is first presented. The force-displacement behaviour of the cladding system and connections is illustrated in Figure 5-39.

It can be observed that the unloading portion of the numerical hysteresis does not follow the experimental behaviour. This is likely attributed to the inability of the model to capture the damage to the cladding panel that was observed during testing of the short threaded rod connections. The damage to the panel results in degradation of the stiffness and what would appear a non-linear response in the panel. The use of a linear relationship (albeit one which takes into account damage through a reduced second moment of area) for modelling the cladding panel when both the connection and cladding panel are undergoing inelastic deformation does not accurately capture the force-displacement response of the cladding system. The model does provide an envelope of the maximum force the connection transfers into the cladding system.

Strength degradation was incorporated into the connection hysteretic behaviour so that when the connection displacement exceeded 30 mm, the strength of the connections sharply drops off to zero. This drop in strength represents the failure of the threaded rod connection. The failure of the connections can be observed by the return to the bare frame behaviour for drifts greater than 1.5%. When the force-displacement behaviour of the cladding system is examined, it can be observed that this failure occurs at a relative displacement between the cladding and frame of 50 mm. The additional 20 mm of deformation is due to in-plane deformation of the cladding panel. This observation agrees with the experimentally observed values. The parameters of the hysteretic rule are also presented in Figure 5-39.

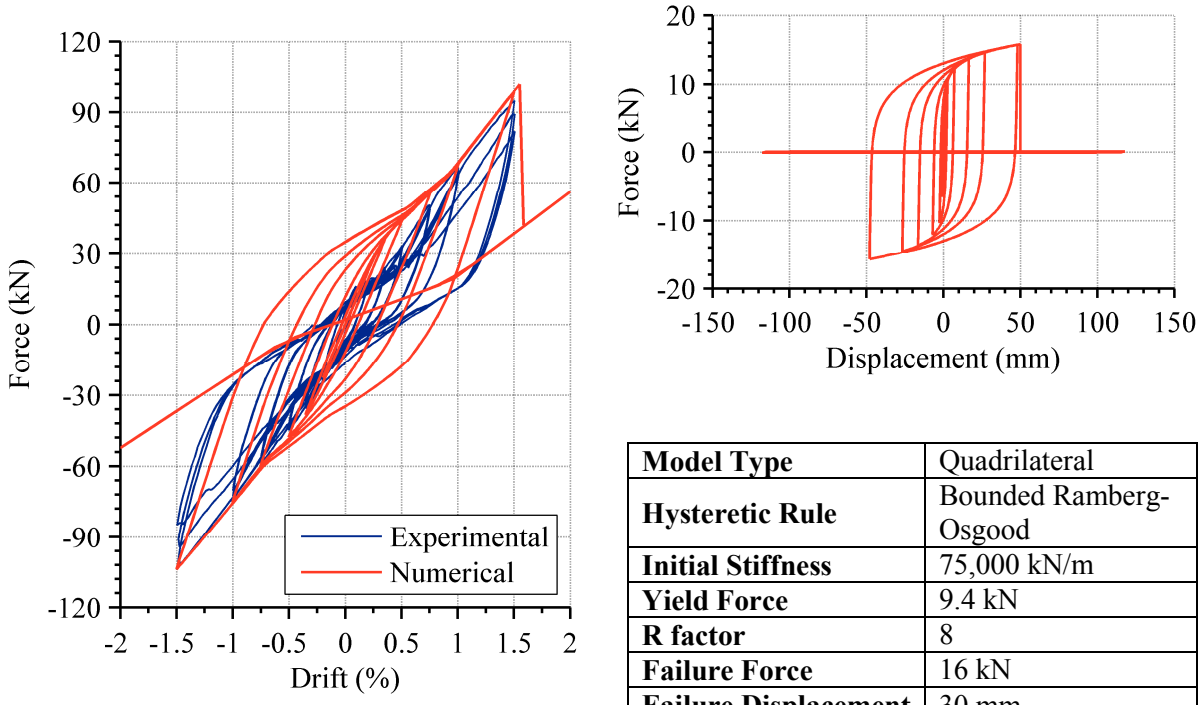

Model Type	Quadrilateral
Hysteretic Rule	Bounded Ramberg-Osgood
Initial Stiffness	75,000 kN/m
Yield Force	9.4 kN
R factor	8
Failure Force	16 kN
Failure Displacement	30 mm

Figure 5-39: Short threaded rod cladding model (quadrilateral model) compared with experimental results of test MP-STR1

The second model utilised the equivalent spring cladding model. The equivalent strength and stiffness for the single connection spring was calculated according to the four connection springs being in parallel. The same hysteresis rules developed to model the short threaded rod connections in the quadrilateral model were used. In this way the connection behaviour is identical to the previously calibrated model.

The force-displacement behaviour of the system and panel spring is presented in Figure 5-40. It can be seen that the model does not accurately capture the force-displacement response of the cladding system similarly to the quadrilateral model. The connection fails at a displacement of 30 mm, with a maximum deformation in the panel spring of 20 mm, which corresponds to a maximum inter-storey drift of 1.5%. This is the same as the quadrilateral model and agrees with experimental observations. After failure of the connections the behaviour returns to bare frame behaviour for drifts above 1.5%. The parameters of the hysteretic rule are also presented in Figure 5-40.

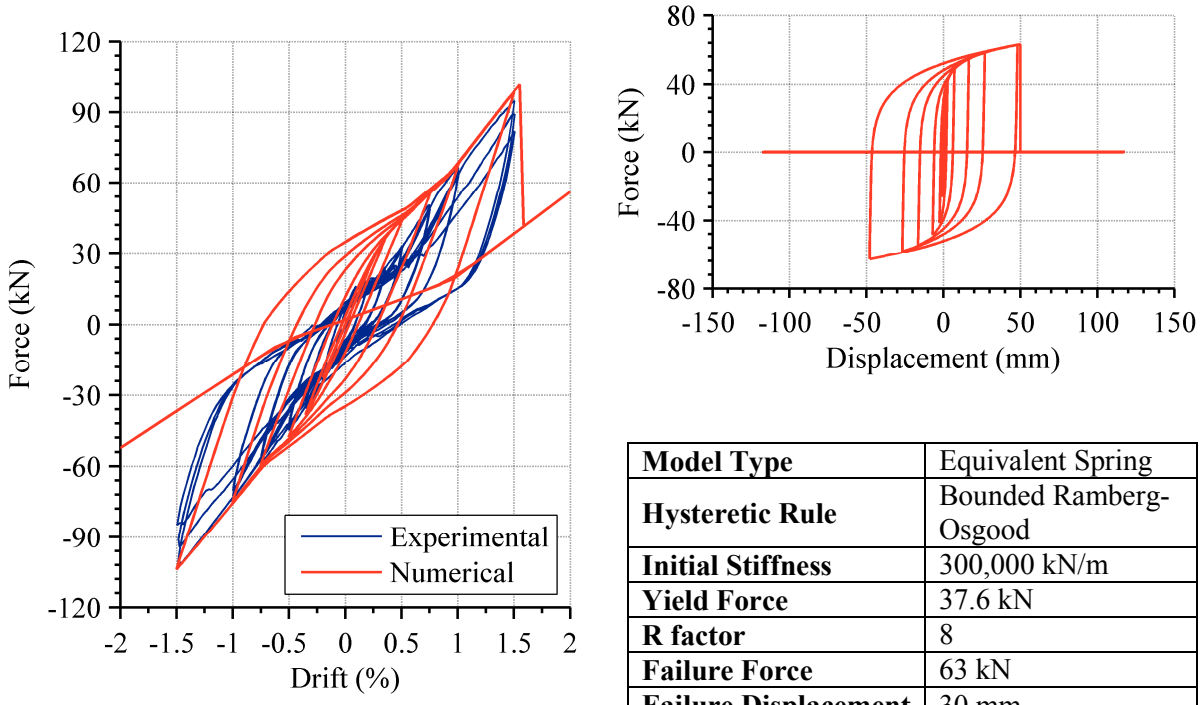

Model Type	Equivalent Spring
Hysteretic Rule	Bounded Ramberg-Osgood
Initial Stiffness	300,000 kN/m
Yield Force	37.6 kN
R factor	8
Failure Force	63 kN
Failure Displacement	30 mm

Figure 5-40: Short threaded rod cladding model (equivalent spring model) compared with experimental results of test MP-STR1

5.7 Conclusions

Cladding components can be characterised through three means: experimentally, analytically and numerically. The combination of all three methods provides a robust process for deriving reliable modelling parameters. This chapter presented the development of numerical models for heavy cladding systems that utilise traditional connection typologies. The traditional connection typologies tested are variations of tie-back rod and slotted plate connections

Analytical derivations based on fundamental engineering principles were used where possible to derive non-linear characteristics of cladding connections and linear characteristics of cladding panels. The analytical derivation of the yield and maximum force in a threaded rod cladding connection and slotted connection formed a good representation of experimentally obtained data. However, the analytical models were not able to accurately represent all of the experimental parameters necessary for the development of the cladding models. Therefore, the experimental dataset was expanded using finite element analyses. Finite element models were calibrated to the experimental results and a parametric study was undertaken that varied the cladding component geometry. Using the results of the

experimental testing and finite element modelling, the analytical solutions were refined and new relationships proposed that provided all of the necessary parameters required to model heavy cladding systems.

The suitability of these modelling parameters was then verified by developing numerical models in the seismic response analysis programme Ruaumoko2D to represent the cladding systems tested experimentally in Chapter 4. First, a lumped plasticity model of the test frame was developed and verified against the bare frame behaviour using a combination of the multi-spring and rotational spring to represent the PRESSS connections of the test frame. Two types of cladding models were then implemented into the test frame model: the quadrilateral model and the equivalent spring model. The quadrilateral model requires less derivation but is more computationally expensive, whereas the equivalent spring model requires more derivation but is computationally efficient. The numerical models were both developed using the modelling parameters developed previously.

The force-displacement results were compared against the experimental behaviour for the long threaded rod connection, slotted connection and short threaded rod connection. An excellent fit was observed for the long threaded rod connection, with the numerical model capturing the increase and strength and stiffness the connections provided nearly perfectly. The failure of the connections when the 1.5% drift cycle was exceeded was also captured.

The slotted connections were represented in two different ways, firstly when the slot length was assumed to be infinite, and secondly when the slot length was ±50 mm. The infinite slot represented the experimental case excellently when the slot length exceeded the displacement demand of the cladding. When the slot length was exceeded, this effect was incorporated by using the parameters for a short threaded rod connection, but with an initial slackness. This model captured the force increase of the slotted connection when the slot was exceeded; however, it was unable to capture some of the degradation in stiffness that occurred as a result of damage to the cladding panel.

A similar result was observed in the short threaded rod connections, the maximum force transferred through the cladding was able to be captured with reasonable accuracy. However, it was observed that the unloading portion of the numerical hysteresis did not follow the experimental behaviour. This was likely attributed to the inability of the model to capture the non-linear degradation of the cladding panel strength and stiffness.

5.8 References

ABAQUS Inc. (2011). Abaqus FEA: Providence, RI., USA.

ACI - 374.1R. (2005). Acceptance Criteria for Moment Frames Based on Structural Testing and Commentary: American Concrete Institute.

Carr, A. J. (2008). Ruaumoko Programme for Inelastic Dynamic Analysis - Appendices: Department of Civil Engineering, University of Canterbury, New Zealand.

Carr, A. J. (2010). Ruaumoko Programme for Inelastic Dynamic Analysis - User Manual: Department of Civil Engineering, University of Canterbury, New Zealand.

Davis, J. R. (2001). Surface Engineering for Corrosion and Wear Resistance: ASM International.

Kaldjian, M. J., & Fan, W. R. S. (1967). Earthquake Response of a Ramberg-Osgood Structure. Industry Program of the College of Engineering: The University of Michigan.

MathWorks Inc. (2011). MATLAB 7.11. Natick, MA., USA.

Neuenhofer, A. (2006). Lateral Stiffness of Shear Walls with Openings. Journal of Structural Engineering, 132(11), 1846-1851.

NZS 3101. (2006). Concrete Structure Standard - Part 1. Wellington: Standards New Zealand.

Park, R., & Paulay, T. (1975). Reinforced Concrete Structures. New York, NY., USA: Wiley.

PCI. (1989). Architectural Precast Concrete. Chicago, IL., USA: PCI Architectural Precast Concrete Manual Committee.

Ramberg, W., & Osgood, W. R. (1943). Description of stress-strain curves by three parameters (Version Technical Note No. 902). Washington, DC.,USA: National Advisory Committee for Aeronatics.

Serway, R. A., & Jewett, J. W. (2009). Physics for Scientists and Engineers (8 ed.): Cengage Learning.

Speith, H. A., Carr, A. J., Pampanin, S., Murahidy, A. G., & Mander, J. B. (2004). Modelling of Precast Prestressed Concrete Frame Structures with Rocking Beam-Column Connections: Department of Civil Engineering, University of Canterbury.

Sullivan, J. F. (1988). Technical Physics. USA: Wiley.

6 Seismic Response of Multi-Storey Buildings with Heavy Cladding

6.1 Introduction

This chapter presents the seismic response of multi-storey buildings with cladding interaction by use of numerical analyses. The numerical analyses include modal analyses, non-linear adaptive pushover analyses, and non-linear dynamic seismic response (time-history) analyses. The numerical cladding system models developed from experimental and numerical calibration in Chapter 5 are implemented into a 2D model of a case-study building frame. The seismic responses of the clad frame models are compared to the bare frame model to investigate the cladding-structure interaction. This chapter also presents the seismic hazard and ground motion selection procedure used for the numerical seismic response analyses in this chapter as well as subsequent chapters. The cladding systems investigated comprise the traditional heavy cladding systems tested experimentally in Chapter 4.

6.2 Global Cladding Model Development

A case-study structure has been chosen to showcase the influence cladding has upon the structural behaviour. A 2D model of the case-study structure was developed using the seismic response analysis program Ruaumoko2D (Carr, 2010). The model represents a typical concrete structure and has been modelled using conventional non-linear frame elements.

A total of 18 frame model configurations with cladding were analysed to understand the effect cladding has upon the response of a structure. The 18 frame models included the three cladding configurations (mono panel, dual panel and fully clad), two cladding models types (quadrilateral and equivalent spring) and three connection hysteretic rules (long threaded rod, short threaded rod, slotted).

6.2.1 Case Study Structure

To illustrate the global cladding-structure interaction a New Zealand case study reinforced concrete structure is used. The structure is based on the Red Book building (Bull & Brunsdon, 1998) which acts as a design example of the New Zealand Concrete Code (NZS 3101, 2006). The building is designed for Christchurch prior to the increase in seismic hazard factor from 0.22 to 0.3 (MBIE, 2011). Figure 6-1 illustrates plan and elevation views of the building layout. The primary lateral load carrying system consists of four one-way perimeter moment resisting frames which are each three bays long. Vertical loads are transferred primarily through interior columns with gravity beams supporting one-way floor units. The beam extensions that form the corner of the building have been neglected since in 2D analyses these should have minimal effect upon the frame behaviour. The bottom floor has a storey height of 4 m while the upper floors have a storey height of 3.6 m. Design loads, forces and seismic masses have been calculated according to New Zealand Design Standards (NZS1170:1, 2002 and NZS1170:5, 2004).

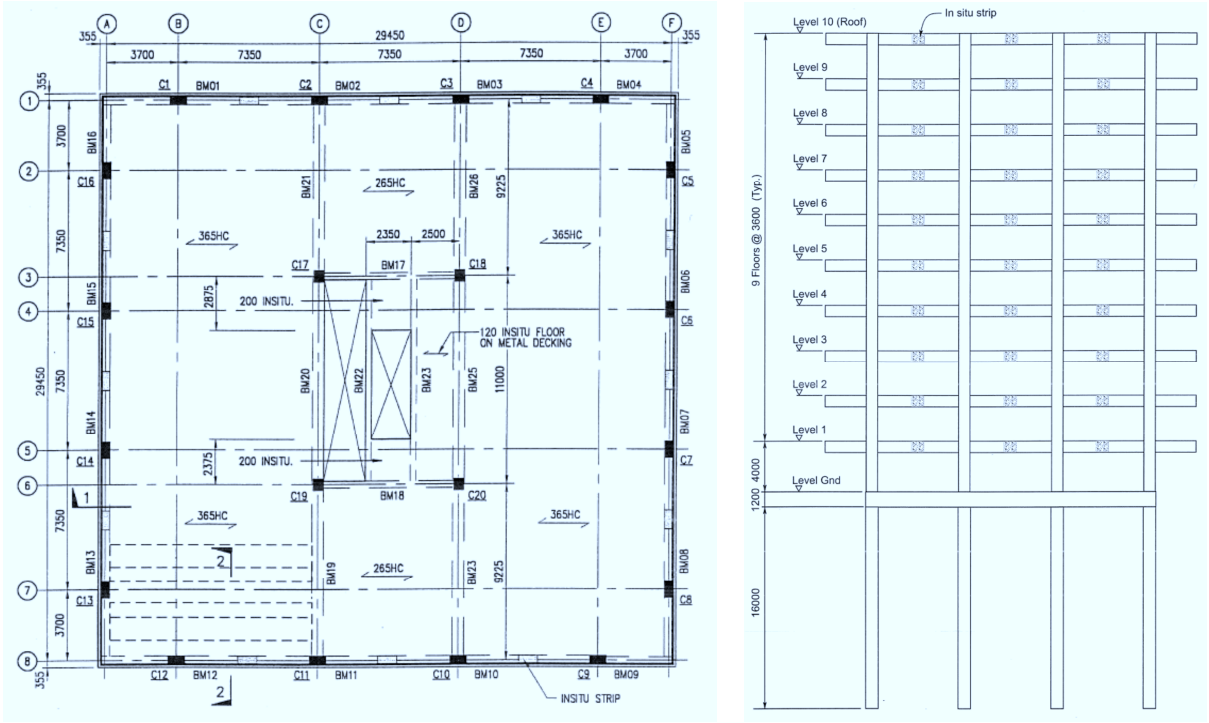

Figure 6-1: Plan and elevation of Red Book building (Bull & Brunsdon, 1998)

A 2D model of the perimeter frame was developed using the seismic response analysis program Ruaumoko2D (Carr, 2010). A fixed-base model was used in the analysis and as a result soil-structure interaction was neglected. The structure was modelled using a lumped mass model and non-linear frame elements that utilised the Giberson One Component Beam

model (Giberson, 1967), as shown in Figure 6-2 (left). The non-linear behaviour was based on the Modified Takeda hysteresis (Otani & Sake, 1974), with the appropriate section properties determined using section modelling programme CUMBIA (Montejo & Kowalsky, 2007), as shown in Figure 6-2 (right).

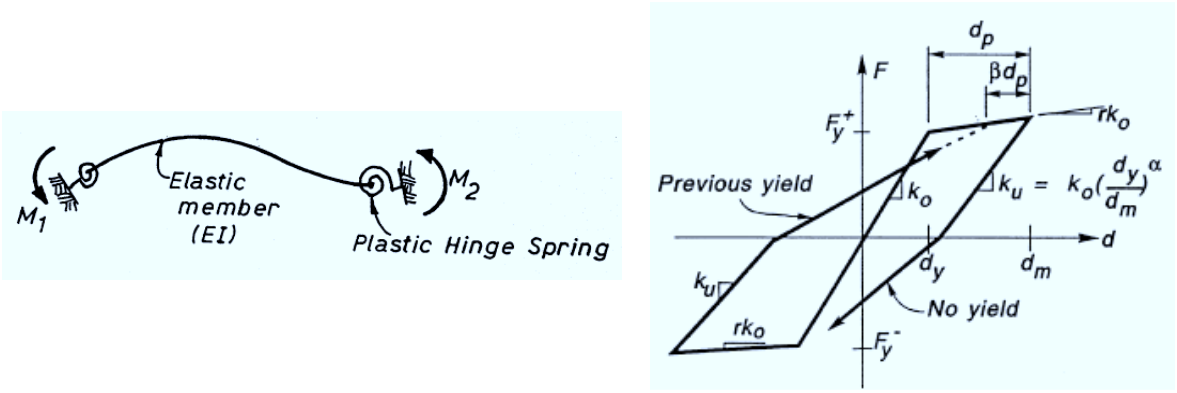

Figure 6-2: Giberson One Component Beam (Giberson, 1967) (left) and Modified Takeda Hysteretic Rule (Otani & Sake, 1974) (right)

The column members also were defined a moment-axial yield interaction surface to account for the effect axial load has on the moment capacity (Park & Paulay, 1975). The beam-column-joint regions of the frame were assumed to be rigid and were represented with rigid links as shown in Figure 6-4. For a full description of the modelling parameters used, refer to Appendix E.

6.2.2 Cladding-Structure Models

The 2D model of the frame, herein referred to as the bare frame model, was used as the base to form the cladding-structure models. Three models that include precast concrete panel cladding were developed. The modularity and size of the cladding panel is varied to include three typical cladding configurations. The first model includes a single storey height panel in each bay and in every floor except the ground floor. Having cladding on every floor except the ground floor is the most commonly observed system as this open floor is typically used for retail space in a commercial building or as a foyer in residential or apartment buildings (PCI, 1989). This model will herein be referred to as the mono panel (MP) configuration. The second model includes two storey height cladding panels in each bay and in every floor except the ground floor. This model will herein be referred to as the dual panel (DP) configuration. The third model includes a single storey height panel in every bay and in every floor, including the ground floor. This model will herein be referred to as the fully clad (FC)

configuration. Figure 6-3 shows diagrams of the bare frame, mono panel configuration, dual panel configuration and fully clad configuration prototype building models.

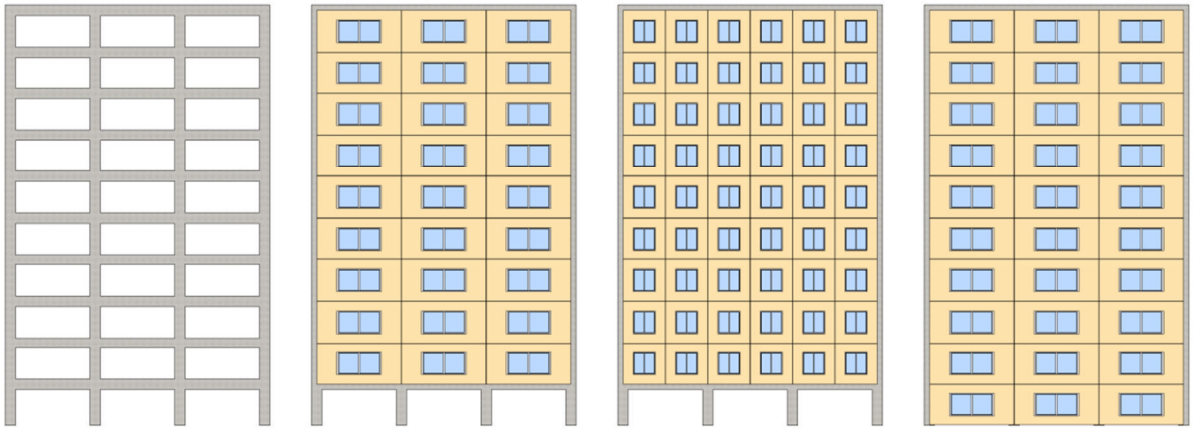

Figure 6-3: Bare frame and three cladding configurations investigated

The prototype clad building models presented in Figure 6-3 have been implemented in Ruaumoko2D (Carr, 2010) using both the quadrilateral and equivalent spring cladding models developed in Chapter 5. The mono panel and fully clad configurations implement the cladding models in the same way that they were developed, with a single panel in each bay. The quadrilateral model consists of quadrilateral elements to represent the cladding panel, connected to the beams of the frame via two rigid link connections at the bottom and two spring connections at the top. The equivalent spring model consists of a single spring for the cladding panel, a single rigid base connection and a single spring to represent the top movement connections. A visual representation of the quadrilateral and equivalent spring models implemented in the mono panel configuration is shown in Figure 6-4.

The dual panel configuration model utilises the same connection models, however, since it has two panels per bay, two cladding models are implemented adjacent to each other in each frame bay, giving it double the number of cladding members.

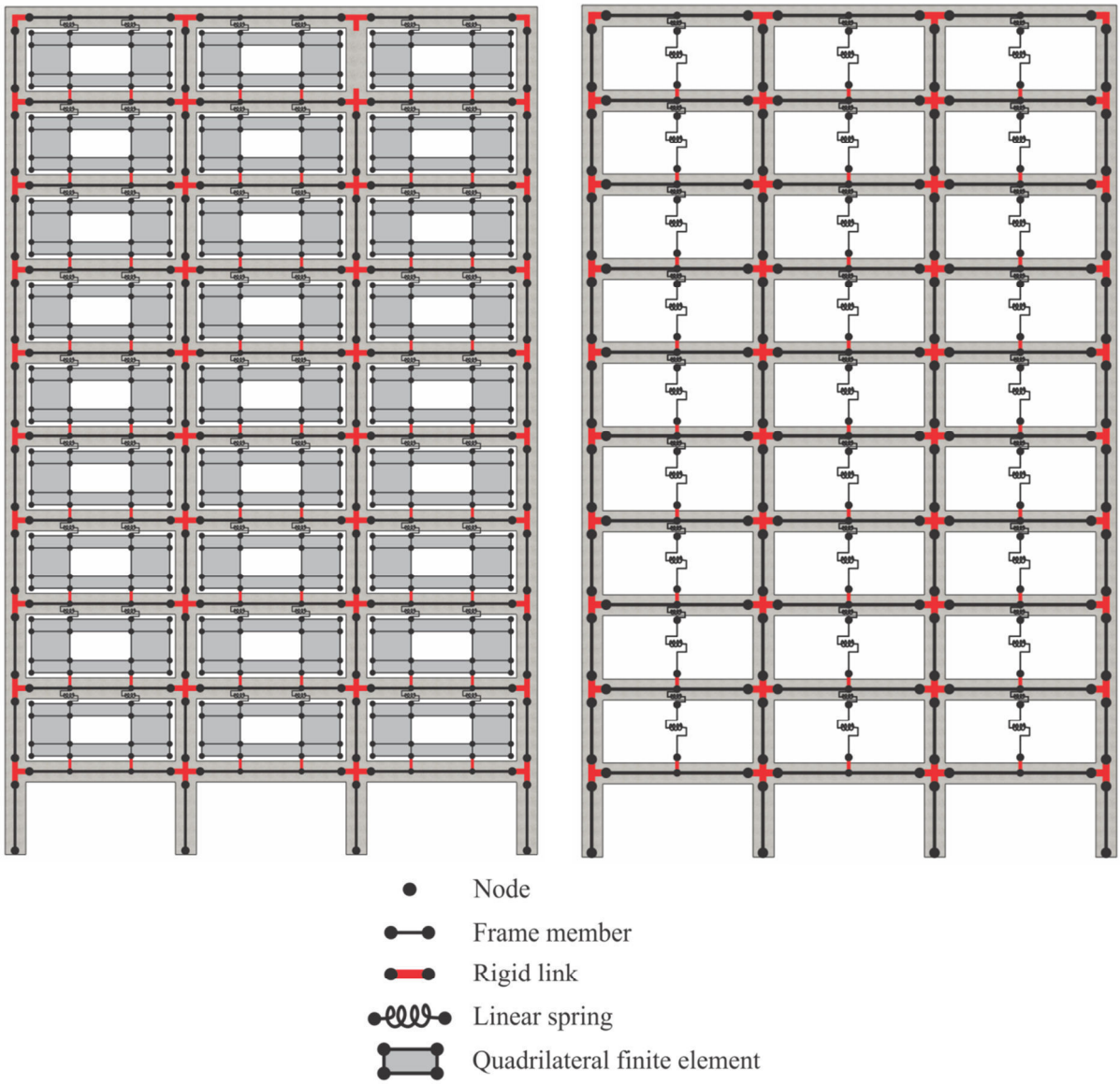

Figure 6-4: Quadrilateral (left) and equivalent spring (right) model implementation of mono panel configuration

6.2.3 Development of Cladding Models

The development of cladding models for the case study structure requires the definition of several modelling parameters. These include the panel weight, panel stiffness, connection stiffness, and connection yield properties. In order to determine these parameters, the cladding connections must be designed in accordance with NZS 1170.5 (2004) to carry the earthquake design actions of the cladding system.

6.2.3.1 Design Actions

The horizontal and vertical design actions are determined from the weight of the panels. The weight of the mono panel and dual panels are given by (6-1) and (6-2) respectively. The panel sizes were chosen as the inter-storey bay size of 7.35 x 3.6 m (or 4.0 m for the bottom floor).

$$W_{p(MP)} = \rho_c V_{p(MP)} = 56.5\ kN \quad \textbf{(6-1)}$$

$$W_{p(DP)} = \rho_c V_{p(DP)} = 28.1\ kN \quad \textbf{(6-2)}$$

where

W_p = Weight of panel (kN)

ρ_c = Density of concrete (kN/m^3)

V_p = Volume of panel (m^3)

The horizontal and vertical actions are conservatively assumed to be the limits prescribed to the requirements for parts and components of NZS 1170.5 (2004) given in Equations (6-5) and (6-4) respectively.

$$F_{ph} = 3.6W_p \quad \textbf{(6-3)}$$

$$F_{ph} = 2.5W_p \quad \textbf{(6-4)}$$

where

F_{ph} = Horizontal design earthquake action on part

F_{pv} = Vertical design earthquake action on part

The corresponding horizontal and vertical actions for each of the two panel sizes considered are given in Table 6-1.

Table 6-1: Horizontal and vertical panel actions

	Horizontal Action (kN)	Vertical Action (kN)
Mono Panel	203	141
Dual Panel	101	70

6.2.3.2 Threaded Rod Connections

The threaded rod diameter required to resist the horizontal actions in Table 6-1 is determined according to the strength design for tension members prescribed in Chapter 6 of NZS 3404 (1997). This aims to prevent failure of either excessive elongation (yield over the gross area) and sudden strength decrease (fracture over the effective net area) according to Equation (6-5) and (6-6) respectively. The net area of a threaded rod is found from the shank diameter of the rod, as given by ISO 68-1 (1998).

$$N^* \leq \emptyset_t A_g f_y \quad \textbf{(6-5)}$$

$$N^* \leq 0.85\emptyset_t A_n f_u \quad \textbf{(6-6)}$$

where

N^* = Tension force

$\emptyset_t$ = Strength reduction factor for tension = 0.9

A_g = Gross area

A_n = Net area

f_y = Yield stress

f_u = Ultimate tensile stress

The panel actions will be resisted by two threaded rods. It was found that in order to satisfy both Equation (6-5) and (6-6) two rods of 24 mm diameter were required to resist the actions of the mono panel and two rods of 20 mm diameter were required to resist the actions of the dual panel.

Two threaded rod lengths have been considered: 50 mm and 250 mm. The corresponding yield force, initial stiffness and Ramberg-Osgood R factor, as determined using the process developed in Chapter 5, are shown in Table 6-2 for the two threaded rod sizes.

Table 6-2: Threaded rod cladding connection modelling parameters

	Rod Length (mm)	Yield Force (kN)	Initial Stiffness (kN/mm)	R factor (kN)
20 mm Rod Diameter	50	9.4	75.4	8
	250	1.9	0.6	13
24 mm Rod Diameter	50	16.3	156.3	8
	250	3.3	1.25	13

6.2.3.3 Slotted Connections

The maximum friction force in the slotted connection is required to define the dash-pot behaviour of the cladding model. The friction force is dependent upon the weight of the panel and it's eccentricity from the frame, as given by Equation (6-7).

$$F_f = \frac{\mu W_p e_p}{e_c} \quad \textbf{(6-7)}$$

where

μ = Coefficient of friction (static or kinetic)

e_p = Horizontal eccentricity between panel and connection

e_c = Vertical eccentricity between connections

For the case study building panel configurations, a horizontal eccentricity of 300 mm and vertical eccentricity of 2700 mm have been assumed. The vertical eccentricity corresponds to the distance between the top and bottom faces of adjacent inter-storey beams. A coefficient of friction of 1.0 has been used as this was found to best match the experimental data (refer to Chapter 5). The analytical friction forces used to define the dash-pots are given in Table 6-3.

Table 6-3: Slotted cladding connection modelling parameters

	Mono Panel	Dual Panel
Friction Force (kN)	6.3	3.1

Both slotted connection models developed in Chapter 5 are included in the numerical response analyses. This includes the simplest slotted connection model of infinite slot length and the model of a restricted slot length. The infinite slot length requires the definition of the friction force only. The restricted slot length is given a slot length of ±25 mm. For a 20 mm bolt this would correspond to a 70 mm long slot. The behaviour beyond the slotted connection length is defined by the threaded rod connection model for a 24 mm diameter rod of 50 mm length.

6.2.3.4 Panels

Each cladding panel is modelled using either the quadrilateral or equivalent spring model introduced in Chapter 5. The quadrilateral model is more computationally expensive than the equivalent spring model because of the additional nodes and elements required, however, the quadrilateral element model represents the cladding using physical properties

and does not require calibration whereas the equivalent spring model does require some degree of calibration in order to accurately represent the stiffness of the cladding panel. Any interaction between adjacent panels, due to stiffness provided by silicone sealant or from contact of the panels is ignored. Since the panels are essentially fixed at beam level, the relative movement between panels was found to be very minimal both experimentally and numerically, so the assumption is acceptable for a 2D analysis.

A panel opening was included with each panel and has been defined by the opening width ratio, which is equal to the width of the opening divided by the width of the panel. An opening width ratio of 50% was chosen for both panel sizes. The opening is located in the centre of the panel and the ratio of the opening height to panel height is that of the opening width ratio.

The stiffness of a symmetric panel with a symmetric opening can be calculated using Equation (6-8) which is a combination of analytical and empirical derivation undertaken in Chapter 5. The elastic modulus is taken to be equal to 30 GPa.

$$k_p = \frac{E b_p}{328{\eta_p}^3 + 12.5\eta_p} \cdot e^{-7.1{\chi_p}^{2.5}} \quad \textbf{(6-8)}$$

where

$\eta_p = \frac{h_p}{l_p}$ = Panel aspect ratio

$\chi_p = \frac{l_o}{l_p}$ = Opening width ratio

l_o = Opening width

The in-plane stiffness of the two panel sizes is shown in Table 6-4.

Table 6-4: Cladding panel modelling parameters

	Mono Panel	Dual Panel
Analytical Stiffness (kN/mm)	23.3	3.2

6.3 Seismic Hazard and Ground Motions

The rigorous selection of ground motions is an important consideration in the seismic assessment of an engineered system as it provides the link between seismic hazard (seismology) and seismic response (earthquake engineering) (Bradley, 2010a).

The selection of ground motions firstly requires the definition of a seismic hazard. Probabilistic Seismic Hazard Analysis (PSHA) (Cornell, 1968) has been used to define the seismic hazard for this study since it has become the most unanimously adopted method by which seismic hazards are quantitatively assessed (Bradley, 2010a). The seismic hazard is based on a site in Christchurch, New Zealand prior to the knowledge of the fault systems that caused the 2010 Darfield and subsequent Canterbury earthquakes. This is consistent with the seismic hazard the case study building was designed for (Bull & Brunsdon, 1998).

Ground motion selection was subsequently performed to best represent the seismic hazard identified by PSHA. A generalised conditional intensity measure (GCIM) approach has been used for the selection of ground motions (Bradley, 2010a). This method was chosen as it allows an increased number of ground motion intensity measures to be considered in the ground motion selection.

6.3.1 Seismic Hazard

The seismic hazard due to earthquake induced ground motion is quantified by performing PSHA (Cornell, 1968). PSHA combines the magnitude recurrence relationships of various earthquake sources, and a ground motion prediction relationship. The ground motion prediction relationship describes the level of ground motion shaking at a site as a function of the magnitude of the earthquake and faulting type; source-to-site distance and path effects; local site effects; and soil amplification (Bradley, 2009). The result of a PSHA is a ground motion hazard curve which gives the annual frequency of exceeding specific values of ground motion intensity. This investigation uses the ground motion hazard for Christchurch based on that developed by Bradley (2010b) for New Zealand specific ground motion prediction.

The spectral acceleration at the fundamental period of the case-study structure was chosen as the ground motion intensity measure (IM) for the PSHA. The fundamental period of the structure is taken as 2.0 seconds, as this was the period used in the design. The fundamental period of the model was found to b 1.97 seconds so this assumption was suitable. The use of spectral acceleration as the ground motion IM is based on observations from past research that the spectral acceleration at the fundamental period of the structure is an ‘efficient’ IM at predicting the drift demands in the structure (Shome & Cornell, 1999). An efficient IM is desired as a reduction in the uncertainty in the structural response will also result in a reduction in the uncertainty for calculating expected damage and losses which will

be explored in subsequent Chapters (Bradley, 2009). The seismic hazard curve for the spectral acceleration obtained via PSHA is shown in Figure 6-5.

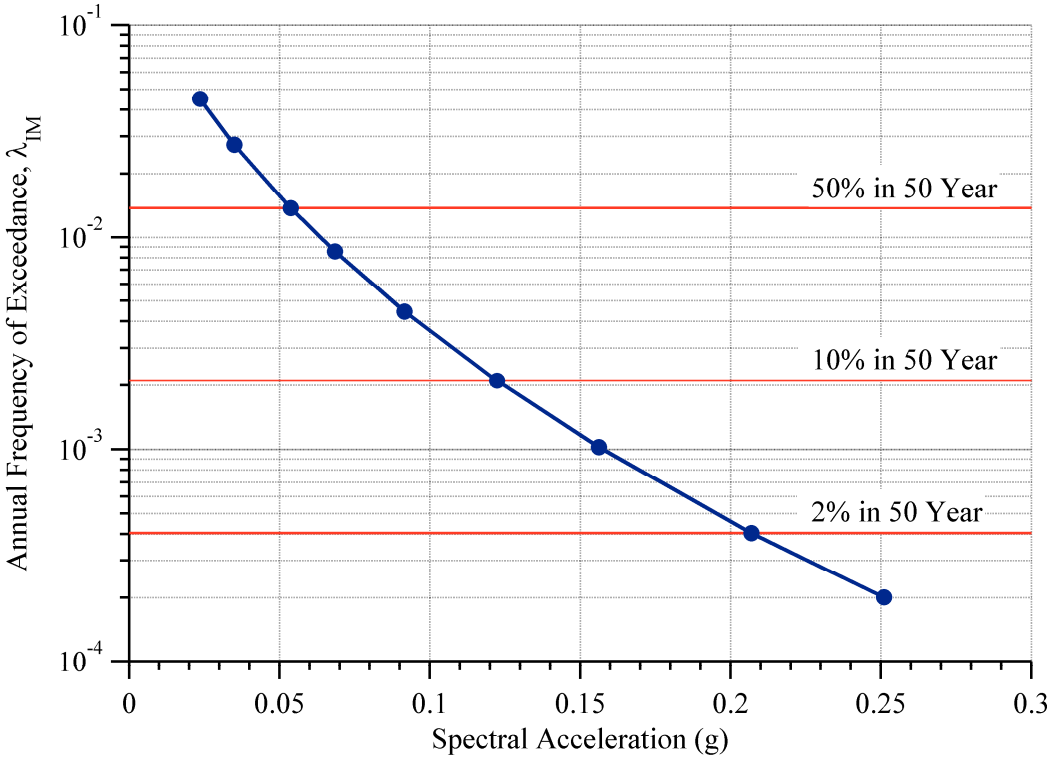

Figure 6-5: Spectral acceleration seismic hazard curve for Christchurch, New Zealand

Nine earthquake intensity levels have been considered to represent the seismic hazard, as presented in Figure 6-5 and Table 6-5. The majority of the seismic response analyses presented in this chapter will focus on three of the earthquake intensity levels; these three intensity levels are based on the following probabilities of exceedance: 50% in 50 years, 10% in 50 years and 2% in 50 years, as suggested for performance-based seismic assessment by FEMA 450 (2003). These three intensity levels are illustrated in by horizontal lines in Figure 6-5.

Table 6-5: Spectral acceleration seismic hazard data for Christchurch, New Zealand

IM Level	SA (g)	Probability of Exceedance in 50 Years	Annual Rate of Exceedance	Return Period (years)
1	0.024	90%	4.50×10^{-2}	22
2	0.035	75%	2.73×10^{-2}	37
3	0.054	50%	1.38×10^{-2}	73
4	0.059	35%	8.58×10^{-3}	117
5	0.092	20%	4.45×10^{-3}	225
6	0.122	10%	2.10×10^{-3}	475
7	0.156	5%	1.03×10^{-3}	975
8	0.207	2%	4.04×10^{-4}	2475
9	0.251	1%	2.01×10^{-4}	4975

Referring to the performance objectives matrix developed by SEAOC (1995), the Basic Safety Objective is attained when a structure achieves Immediate Occupancy performance for the 50%/50 intensity level, Life Safety performance for the 10%/50 intensity level and Collapse Prevention performance for the 2%/50 intensity level.

6.3.1.1 Seismological Signature of Christchurch

The determination of the seismic hazard for Christchurch using PSHA presented in Figure 6-5 requires the definition of local soil conditions. These are required in order to predict the local site effects on the level of ground shaking.

Geophysical surveys completed by Tonkin & Taylor Ltd. (2011) following the Christchurch earthquakes indicate that most sites within the central city are likely to be assigned a site subsoil Class D (deep or soft soil site), in accordance with the requirements of Section 3 of NZS 1170.5 (2004). The predominant 30 m averaged shear wave velocity (Vs_{30}) of the subsoil in the Christchurch CBD was found to be in the range of 200-400 m/s, therefore Vs_{30} was taken as equal to 250 m/s. For further information on the seismic hazard disaggregation, refer to Appendix F.

6.3.2 Ground Motion Selection

The ground motions selected for seismic response analyses have been selected from the Pacific Earthquake Engineering Research Centre (PEER) ground motion database (PEER, 2010). The PEER ground motion database contains ground motions records of earthquake events from 1935 to 1999 and includes a multitude of information regarding each ground motions seismological signature (i.e. magnitude, source-to-site distance and faulting mechanism).

A generalised conditional intensity measure (GCIM) approach (Bradley, 2010a) has been used for the selection of ground motions for the seismic response analysis performed. The GCIM approach is based on a two-step procedure that uses numerical simulation to generate a set of ground motion intensity measures (IM) for a given seismic hazard. The IM distributions generated through GCIM are subsequently used to select ground motions that have similar IM distributions. For further information on the ground motion selection process used as well as the records used, refer to Appendix F.

6.3.2.1 Comparison of Ground Motion Records

A comparison of the twenty ground motions selected at the three key intensity levels is shown in Figure 6-6. The mean of the ground motion spectrums are shown alongside the seismic hazard spectrum.

It can be observed that the spectral accelerations at low periods (high frequencies) are lower than that of the design spectrum. This is due to the ground motions being predominantly far-field, as shown in Figure 6-7. Far-field ground motions have lower energy in the high frequency range of the spectrum since high frequency earthquake waves attenuate faster than low frequency waves (Serway & Jewett, 2009).

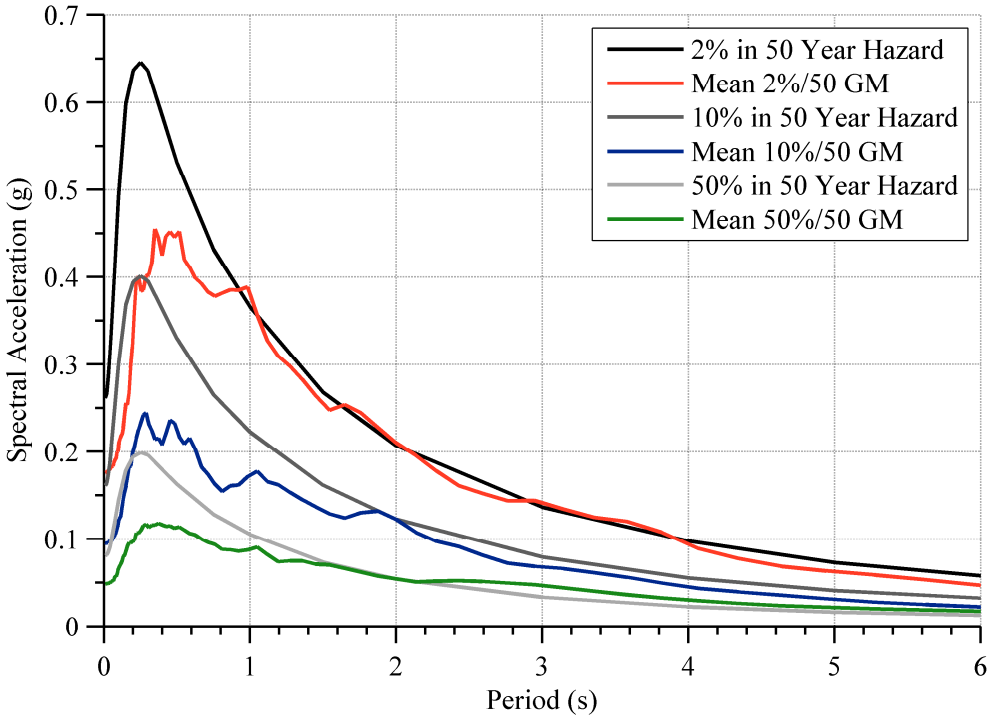

Figure 6-6: Mean spectral acceleration curves compared to Uniform Hazard Spectrum for 50%/50, 10%/50 and 2%/50 year seismic hazard

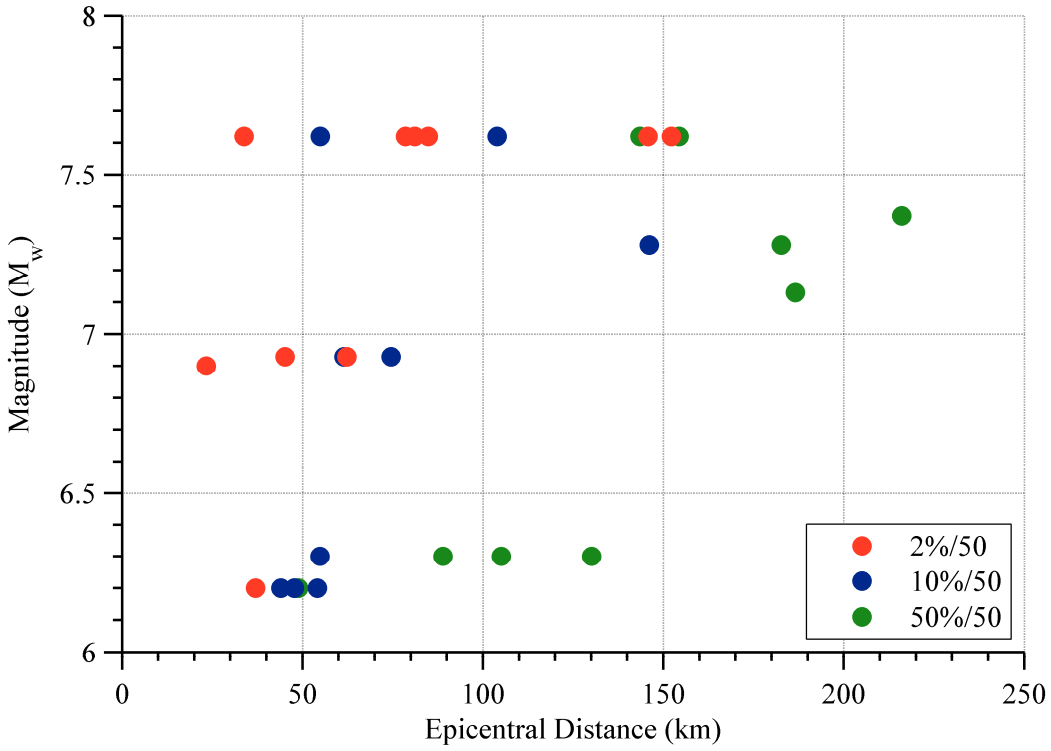

Figure 6-7: Magnitude and epicentral distance of ground motions for 50%/50, 10%/50 and 2%/50 year seismic hazard

6.4 Static Analyses

Adaptive non-linear push-over analyses were undertaken to show the difference in stiffness and strength between the bare frame and cladding frame models (Carr, 2010). An adaptive pushover is a succession of static analysis performed by subjecting the frame to a load pattern that is adapted as the structure deforms. The initial load pattern used was that prescribed for the equivalent static method in NZS 1170.5 (2004).

Pushover analyses were performed up to a maximum frame drift of 2.0% for the bare frame (BF), mono panel (MP), dual panel (DP) and fully clad (FC) models, with the force-drift behaviour is shown in Figure 6-8. The clad frame models utilise the quadrilateral cladding model of long threaded rod connections. The behaviour of the four frame systems up to 0.20% is shown in Figure 6-8 (left) in order to compare the initial stiffness and yield point of the systems. The initial stiffness of the bare frame is 19.2 kN/mm. The inclusion of cladding increases this stiffness by between 4 and 7% with the threaded rod cladding system. The fully clad and mono panel systems results in the greatest increase in initial stiffness, followed by the dual panel systems.

The full pushover behaviour of the four frame systems up to 2.0% frame drift is shown in Figure 6-8 (right). Also shown on the right axis is the percentage of beams in the bare frame model that have yielded and formed plastic hinges for increasing levels of drift. The frame remains elastic up to a drift of 0.16%, or a corresponding top displacement of 58 mm. Progressive yielding of the beams throughout the structure occurs due to the adaptive nature of the pushover analysis and it can be seen that at 2.0% drift, 75% of the beam ends have formed plastic hinges. The initial yield point and progressive yielding behaviour of the clad frame systems was very similar to the bare frame behaviour, so these have been omitted from the figure for clarity.

At 0.5% frame drift, the bare frame has a base shear force of 1470 kN. The inclusion of cladding with slotted connections increases the base shear force by between 3 and 6%. The dual panel system results in the greatest increase in base shear, followed by the fully clad and mono panel systems.

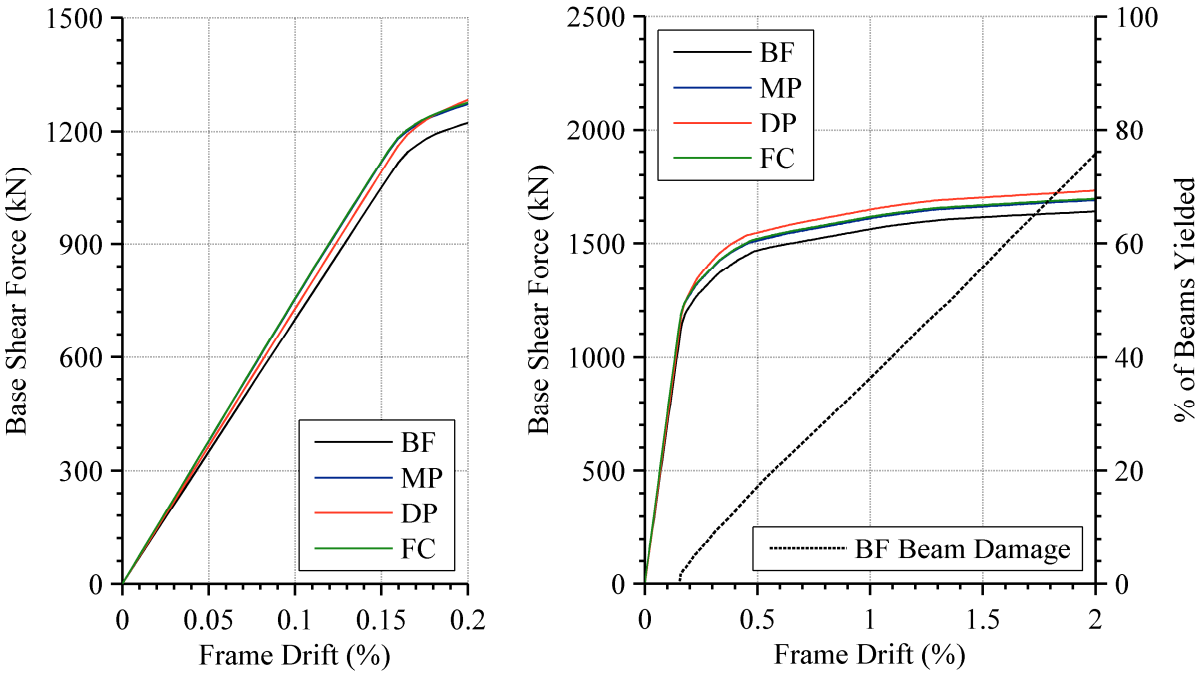

Figure 6-8: Initial (left) and complete (right) pushover behaviour for different frame configurations

Pushover analyses were also performed on the mono panel configuration model for each of the different connection types up to a maximum frame drift of 2.0%, with the force-drift behaviour is shown in Figure 6-9. The quadrilateral element cladding model was used to compare the connection types. The behaviour of the equivalent spring models was virtually identical to that of the quadrilateral model so has been omitted for clarity. The behaviour of the four cladding systems up to 0.20% is shown in Figure 6-9 (left) in order to compare the

initial stiffness and yield point of the systems. The long threaded rod (LTR) and slotted (SL) connections increase the frame stiffness by 7% and the short threaded rod (STR) connections increase the frame stiffness by 28%.

The full pushover behaviour of the four connection systems up to 2.0% frame drift is shown in Figure 6-8 (right) along with the percentage of beams in the bare frame model that have yielded and formed plastic hinges. The dashed line for slotted connections represents the slotted connections with a 50 mm length slot and the solid line represents the slotted connections with an infinite slot length.

At 0.5% frame drift, the inclusion of cladding with long threaded rod connections increases the base shear by 4%, the slotted connections increase the base shear by 3% and the short threaded rod connections increase the base shear by 14%. It can be observed that at a frame drift of 2.0% the increase in base shear is approximately the same for the long threaded rod and slotted connections with infinite slot length, however the short threaded rod connections have increased the base shear by 17% and the slotted connections with a slot length of 50 mm have increased the base shear at 2.0% by 13%. The slot length is exceeded initially around 0.8% drift, as shown by the divergence of the dashed line from the solid line. This is due to the connections providing increasing resistance as relative displacement increases once the slot length is exceeded.

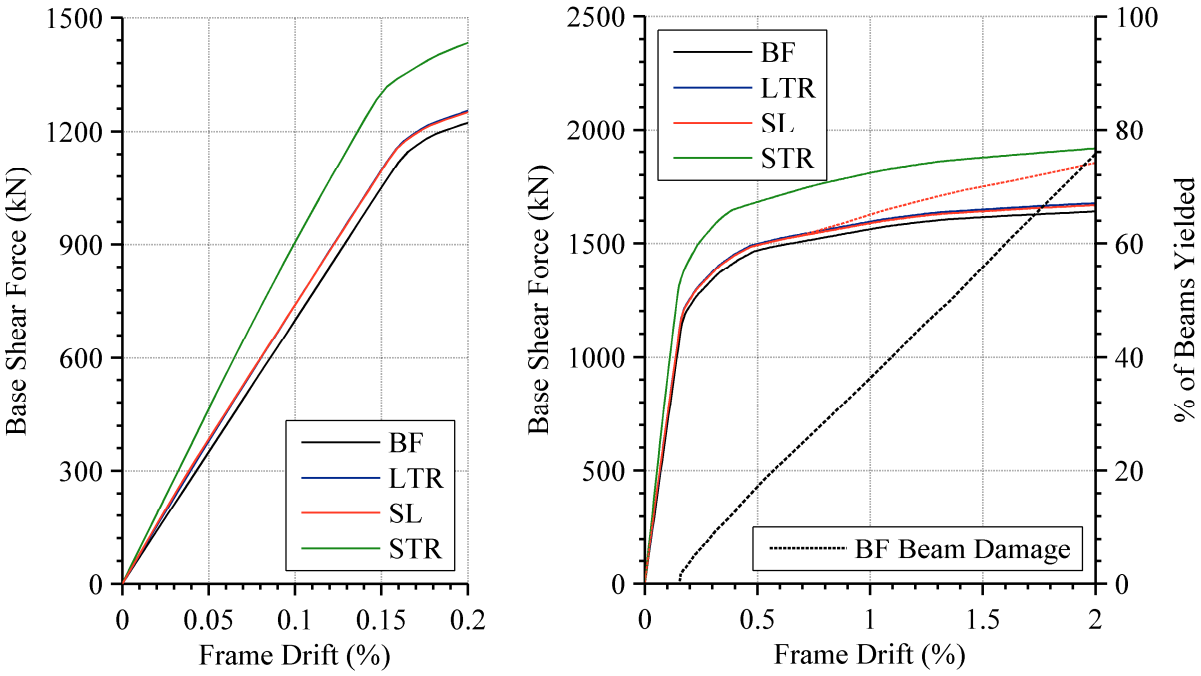

Figure 6-9: Initial (left) and complete (right) pushover behaviour for different cladding connection types

6.5 Dynamic Analyses

The dynamic behaviour of the case-study structure with and without cladding is explored in this section through numerical analyses. The numerical analyses include a modal response spectrum analysis as well as time-history analyses (seismic response analyses) using the earthquake ground motions identified in Section 6.3.2.

6.5.1 Modal Response

A modal response spectrum analysis was undertaken on each of the numerical building models to investigate how the inclusion of cladding affects the dynamic behaviour. Modal analysis separates a structure into several single degree of freedom systems. Each single degree of freedom corresponds to one of the structure's elastic periods of free vibration. The effective mass of each mode determines the amount to which each mode contributes to the overall building motion.

The first four periods of free vibration in the bare frame structure are shown in Figure 6-10. The fundamental period of the bare frame model was found to be 1.97 seconds. This matches well with the period obtained by the authors of 2.02 seconds (Bull & Brunsdon, 1998).

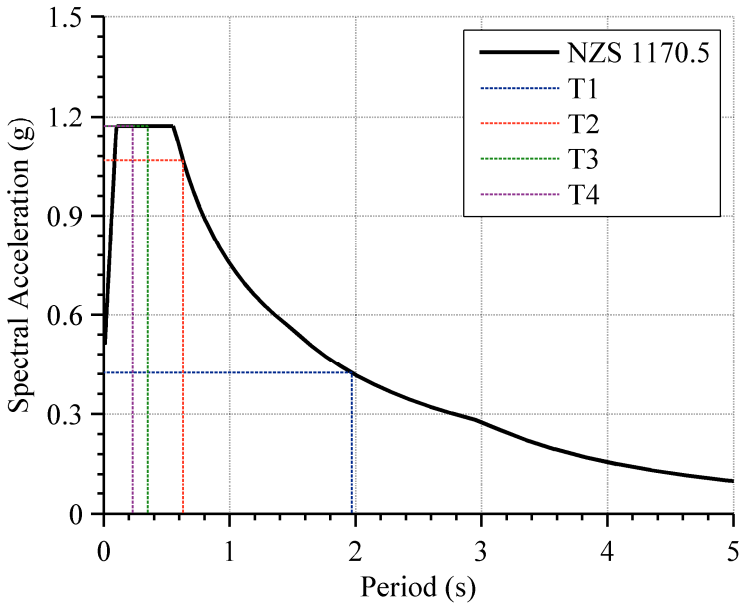

Mode	Period	Mass Participation
1	1.97 s	82 %
2	0.63 s	10 %
3	0.35 s	4 %
4	0.23 s	2 %

Figure 6-10: First four models of modal response analysis

The spectral acceleration demands for each of the first four modes of free vibration are shown in Figure 6-10 considering an elastic site spectra for horizontal loading obtained from the New Zealand Standard for earthquake actions (NZS 1170.5, 2004). A seismic hazard of

0.22, corresponding to the building being located in Christchurch prior to the increase in seismic hazard post September 2010 (MBIE, 2011), soil type D (Tonkin & Taylor Ltd., 2011) and annual probability of exceedance of 1/1000 (R_s = 1.3) are considered.

The mode shapes and the amount that each mode participates in the displacement and floor force is shown in Figure 6-11. It can be seen that the first mode dominates the lateral displacement of the building, as we would expect from the high mass participation found for this mode. However, the higher modes all provide significant contribution to the peak floor force throughout the building, particularly to the top two floors of the building. Site effects due to factors such as directivity and soil properties that could also further activate these higher modes so it is important that they are included. As shown in Figure 6-10, the first four modes contribute to approximately 98% of the total lateral response, indicating that these four modes capture essentially all of the lateral dynamic response of the building. The first mode contributes over 80% to the total response, which is typical of a moment-resisting frame building with an approximately uniform distribution of structural properties and mass (Hunt & Stojadinovic, 2010).

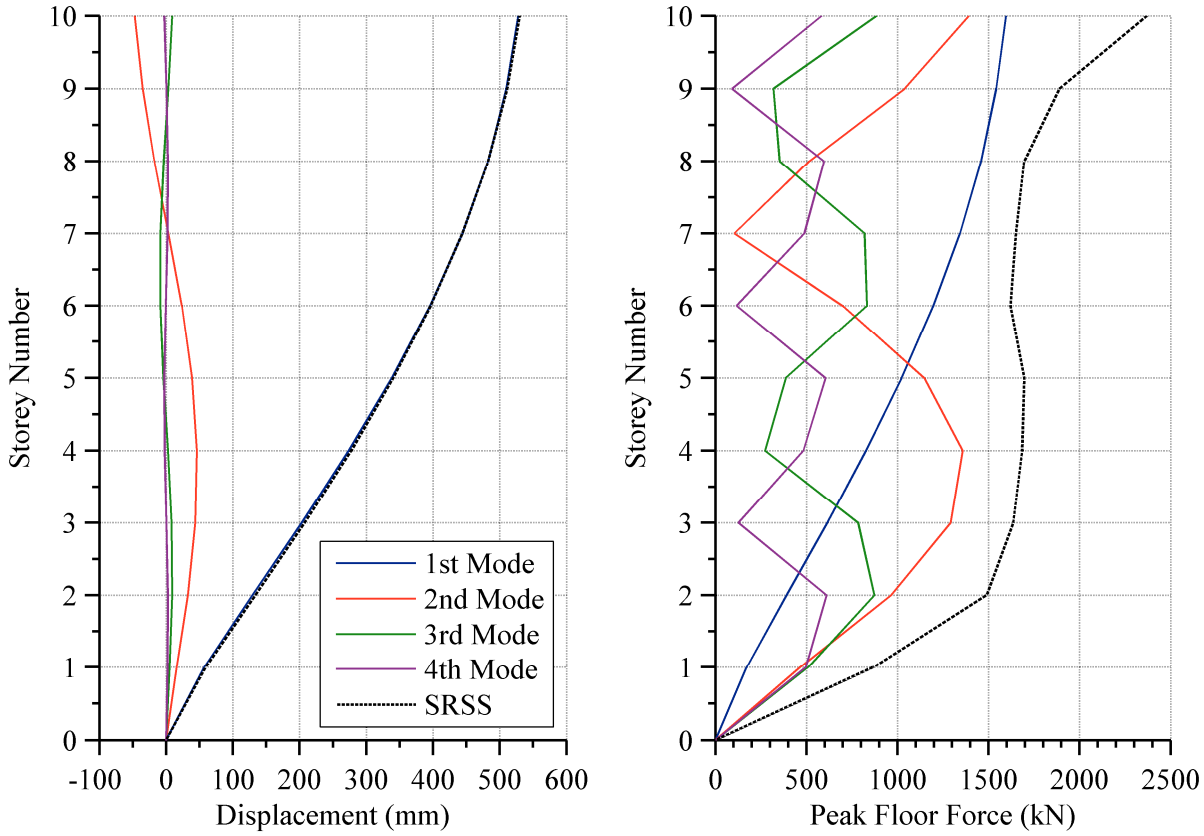

Figure 6-11: Displacement profile (left) and peak floor force profile (right) of first four modes and combined square root of the sum of the squares

The interstorey displacements and peak forces of each mode are combined by carrying out a square root of the sum of the squares (SRSS) at each level of the structure. It can be seen that the combined displacement profile is virtually identical to that of the fundamental period and that the peak floor force is between 1500 – 2000 kN throughout most of the building.

The modal analysis procedure is repeated for the three different cladding configurations as well as for each of the cladding models developed in Section 6.2.3. The inclusion of cladding accounted for an increase in mass of 7% for the mono panel and dual panel configurations and an 8% increase for the fully clad configuration. Where the mass of a building part is in excess of 20% of the combined mass of the part and the primary structure a special study must be carried out according to NZS 1170.5 (2004). Therefore, the cladding systems interaction with the structure would typically be ignored in a numerical analysis.

The difference in the mode shapes between the bare frame model and the clad frame models is negligible; however, the inclusion of cladding does increase the participation factors for the higher modes, as shown in Table 6-6. The effect this has upon the overall displacement demands for the case study structure is minimal since the fundamental mode is dominant. However, for structures where the higher modes have a larger influence upon the structure's overall dynamic behaviour, the effect the cladding has upon exciting these higher modes may be significant.

Table 6-6: Participation factors of first four modes for different frame configuration

Mode	Bare Frame	Mono Panel	Dual Panel	Fully Clad
1	1.29	1.29	1.29	1.29
2	0.45	0.45	0.45	0.45
3	0.26	0.32	0.28	0.30
4	0.18	0.28	0.25	0.38

When the SRSS envelopes for frame displacements and peak floor forces found above for the bare frame are compared to those found for clad frame cases, it can be observed in Figure 6-12 that there is a reduction in the maximum displacements and increase in peak floor force due to the presence of cladding. The connection model used to compare the different cladding configurations is the quadrilateral cladding model of slotted connections. The displacement at the top of the bare frame was found to be 530 mm for this seismic hazard, equivalent to 1.45% frame drift. This is reduced by 6-7% when the frame had the different cladding configurations included. The peak floor force in the bare frame was found to be 2370 kN. This maximum force increases by between 10-13% when cladding is

included, it can also be seen in Figure 6-12 that this increase is apparent throughout the structure and not just at the top, as is the case for the increase in displacement profile. There is not a significant difference between each cladding system (the mono panel envelopes in blue is almost completely concealed by the dual panel envelopes in red); however, the fully clad system has the most effect upon decreasing the displacements and increasing the peak floor forces.

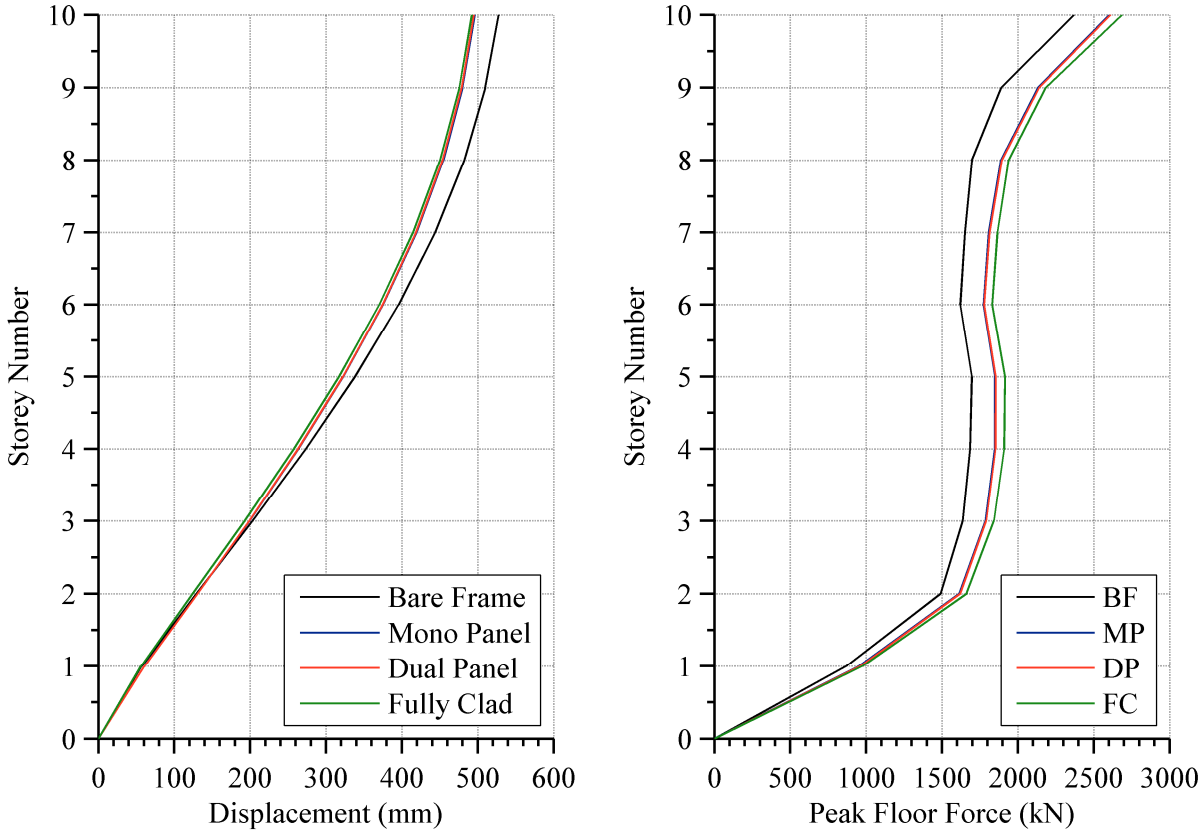

Figure 6-12: Displacement profile (left) and peak floor force profile (right) for different frame configurations

A summary of the periods for the first four modes for each of the four frame systems is presented in Table 6-7. The periods for the cladding cases are taken as an average of the six different cladding models used (three connection types, using both the quadrilateral element and equivalent spring models).

Table 6-7: Period of first four modes for different frame configurations

Mode	Bare Frame	Mono Panel	Dual Panel	Fully Clad
1	1.97 s	1.90 s	1.90 s	1.89 s
2	0.63 s	0.61 s	0.61 s	0.61 s
3	0.35 s	0.34 s	0.34 s	0.34 s
4	0.23 s	0.23 s	0.23 s	0.23 s

The SRSS envelopes for frame displacements and peak floor forces are now compared for each of the three connection types, as shown in Figure 6-13. The frame model used to compare the different connection types is the fully clad frame. It can be observed that the short threaded rod connections reduce the displacements and increase the floor forces the most out of the three connections investigated. It is worthwhile noting that the long-threaded rod connections decrease the peak displacements by only 1.2%, but increase the peak floor force by 7.5%.

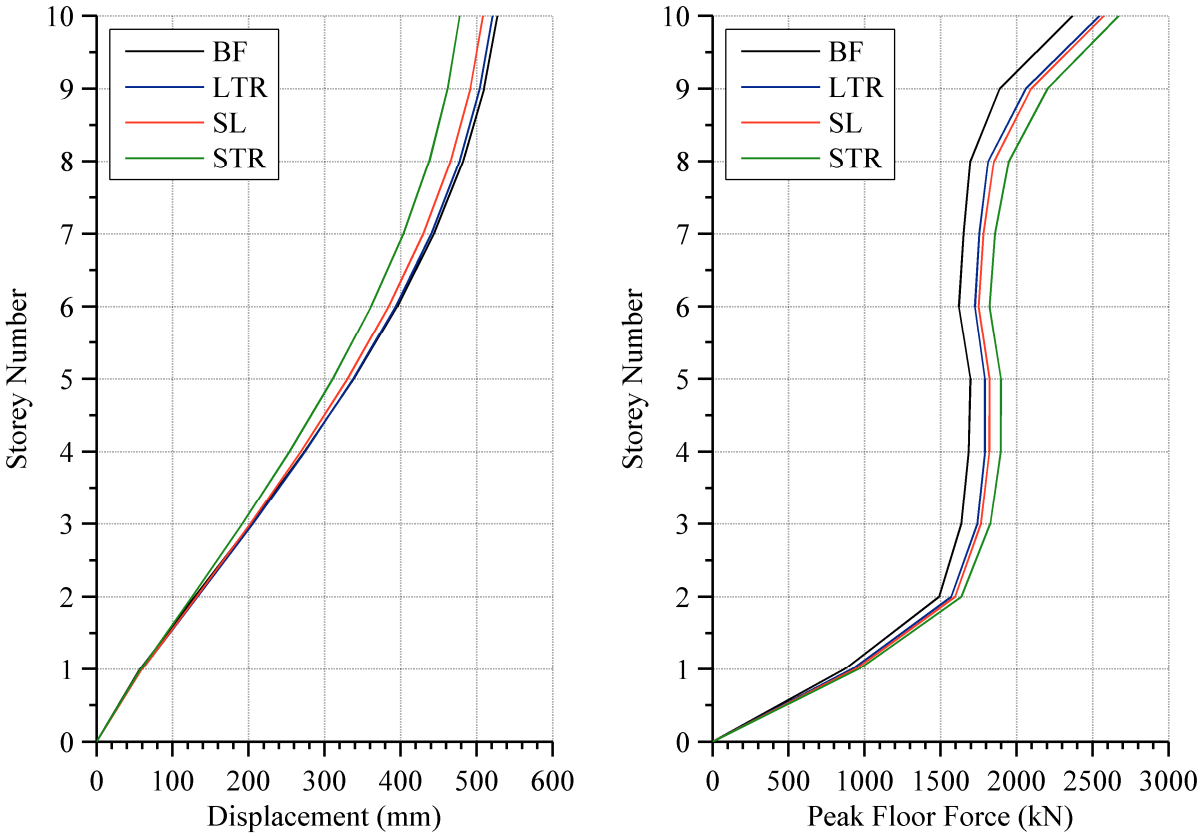

Figure 6-13: Displacement profile (left) and peak floor force profile (right) for different cladding connection types

A summary of the periods for the first four modes for each of the three connection types is presented in Table 6-8 along with that of the bare frame. The periods for the cladding cases are taken as an average of the six different cladding models used (three cladding configurations using both the quadrilateral element and equivalent spring models).

Table 6-8: Period of first four modes for different cladding connection types

Mode	Bare Frame	LTR	SL	STR
1	1.97 s	1.95 s	1.90 s	1.79 s
2	0.63 s	0.62 s	0.61 s	0.58 s
3	0.35 s	0.35 s	0.35 s	0.33 s
4	0.23 s	0.23 s	0.23 s	0.22 s

Many factors contribute to the uncertainty surrounding the periods of free vibration of a structure. The additional strength and stiffness provided by claddings contribute to this uncertainty; however, this research shows that the difference between free vibration periods of a building with and without cladding is significantly less than that suggested by some research. In previous analytical studies, summarised in Chapter 3, a decrease of 11-52% in the fundamental period of a bare frame structure was presented (Goodno et al., 1980; Henry & Roll, 1986; Su et al., 2005). This research has shown that the cladding causes at most a 9% reduction in fundamental period. These results are limited to this case-study building and it is possible that results will vary for different structural typologies, however, this result agrees better with the measured data that indicate a cladding system affects the fundamental period of a multi-storey building by only a small amount (Meyyappa et al., 1981).

6.5.2 Structural Response

The structural response to the seismic response analyses has been quantified according to the following engineering demand parameters (EDP): maximum base shear force, maximum inter-storey drift, residual inter-storey drift and peak floor acceleration. This section explores how the inclusion of cladding in the structural model affects these EDPs. Quantifying the structural performance (in terms of damage) to both the structure and the claddings is explored in Chapter 7.

Twenty unique data points exists for each EDP from each of the twenty ground motion records. The mean and standard deviation are found at each intensity level using a lognormal distribution. The lognormal distribution is used since the EDPs are the multiplicative product of many independent variables, e.g. stiffness, mass, acceleration. Since the EDPs represent absolute values the lognormal distribution is also useful since it does not allow negative data, unlike a normal distribution. The skew of the distributions is negligible for some results, e.g. base shear results, making the distributions approximately normally distributed. However, some EDPs, such as drift and acceleration, exhibit a positive skew. This is where the probability distribution ‘leans’ to the right side of the mean. This is due to the fact that once a structure goes non-linear, deformations increase at a higher rate. For example, a ground motion with a slightly stronger than average intensity can lead to significantly larger than average deformations. Whereas, a ground motion with slightly weaker than average intensity will only usually cause slightly smaller than average deformations.

6.5.2.1 Bare Frame Behaviour

The bare frame was subjected to each of the twenty ground motions at the nine intensity levels specified previously. The maximum base shear recorded for each of the 180 ground motions (20 records at nine intensity measures) is presented in Figure 6-14 for the corresponding spectral acceleration at a period of two seconds (refer to Table 6-5). The spectral acceleration at each intensity level is constant since the generalised conditional intensity measure (GCIM) approach (Bradley, 2010a) scales records according to this condition.

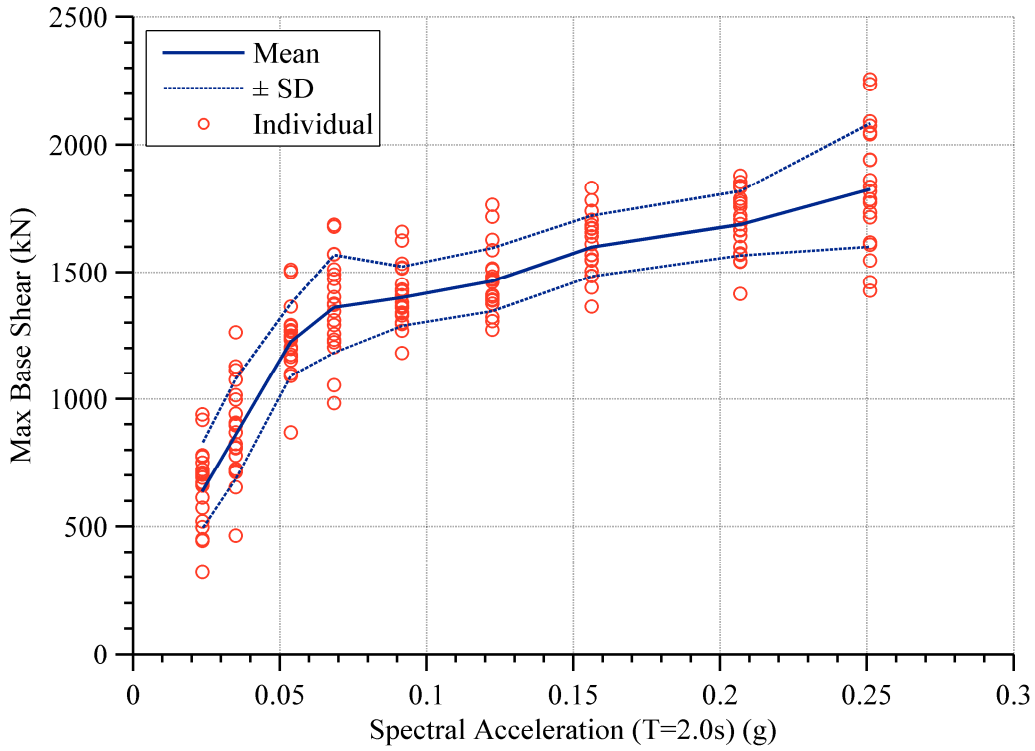

Figure 6-14: Maximum base shear of bare frame at corresponding spectral acceleration of each ground motion

The mean of the maximum base shear at each intensity levels is found using a lognormal distribution and is shown in Figure 6-14 along with the upper and lower standard deviation. The distribution is reasonably consistent for each intensity level and exhibits minimal skew. It can be seen that the shape of the mean base shear in Figure 6-14 is similar to a force-displacement push-over curve, being monotonic in nature with an initial steep increase in base shear for low acceleration demands, followed by a plateau for higher demands. As will be presented in the following chapter, the frame remains completely elastic for the majority of records at the lowest two intensity levels. The mean of the maximum base shear for the three key intensity levels is presented in Table 6-9.

Table 6-9: Mean of maximum base shear at three key intensity levels

	50%/50 Year	10%/50 Year	2%/50 Year
Base Shear (kN)	1225	1465	1688

The EDPs (maximum inter-storey drift, residual drift and maximum floor acceleration) are herein presented for the three key intensity levels of interest. This allows the presentation of the distribution of these EDPs throughout the structure and thus the ability to determine where maximum demands occur. Using the location of maximum demands, a probabilistic response analysis is presented using the nine intensity level at one location in the structure. This produces data similar to that shown previously for base shear (refer to Figure 6-14) relating the EDP to the intensity measure (spectral acceleration).

Maximum inter-storey drifts are commonly used to compare the maximum displacement deformation profile observed during an earthquake. The inter-storey drift was recorded at each floor in order to form the maximum inter-storey drift envelopes shown in Figure 6-15. It should be noted that the maximums at each floor do not necessary occur at the same time during the ground motion record.

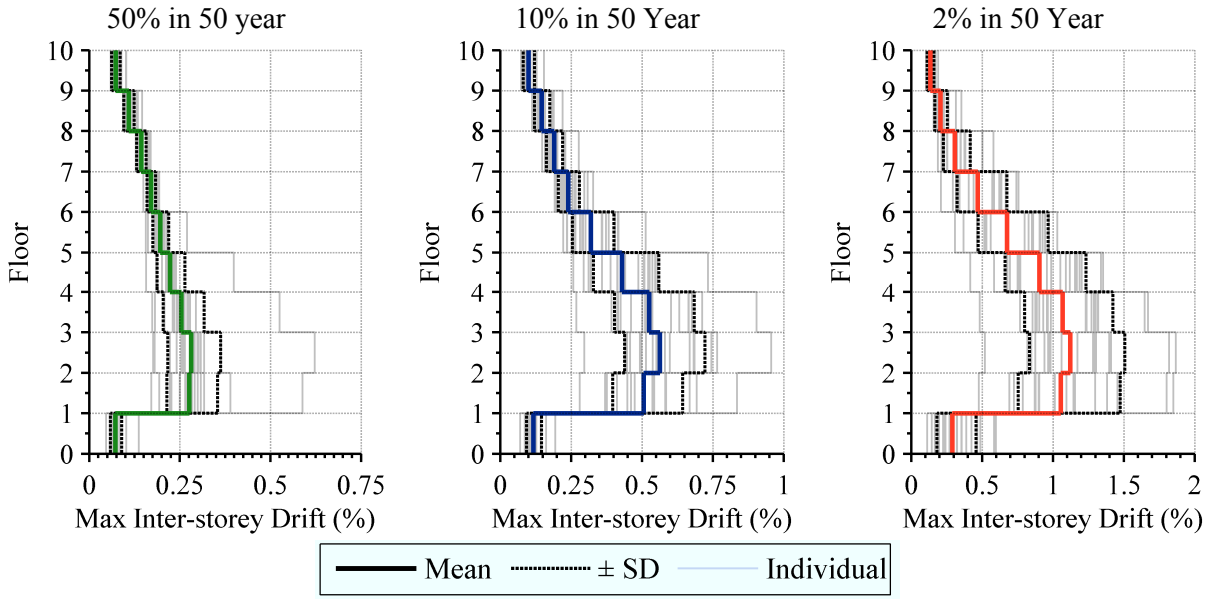

Figure 6-15: Maximum inter-storey drift envelopes of bare frame

Figure 6-15 displays the maxima envelope obtained for each individual ground motions as well as the mean and standard deviation based on a lognormal distribution. It can be observed that the largest inter-storey drifts typically occur around the third and fourth floor. It can be observed that significantly larger than average drifts were observed for some cases. On inspection, these records were ground motions which were classified as exhibiting directivity (Shahi, 2013). Furthermore, the period of the directivity pulse was found to be

near the fundamental period of the structure. It would therefore appear that the larger than average drifts that result from these records are linked to the presence of directivity (Champion & Liel, 2012).

As shown in Figure 6-21, the maximum inter-storey drifts in the structure occurred around the third floor of the structure. The maximum inter-storey drifts in the third and sixth floor of the structure are presented in Figure 6-16. This includes each of the nine intensity levels analysed. It can be seen that very large drifts are observed for several ground motions at the highest intensity level considered. These cases correspond to collapse of the structure which will be defined and quantified in the following section.

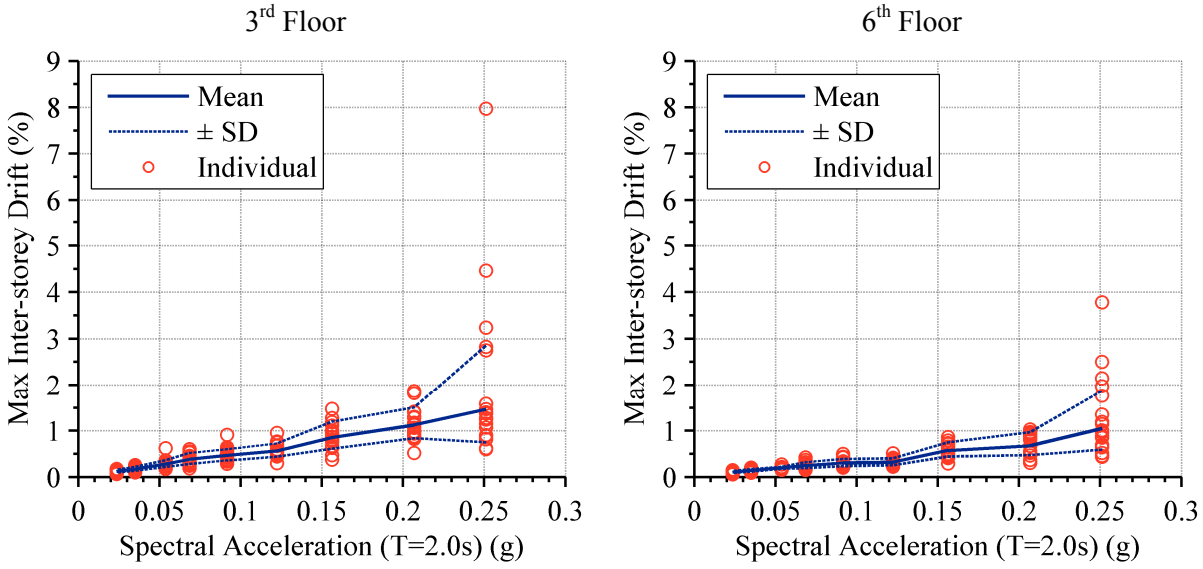

Figure 6-16: Maximum inter-storey drift of bare frame at corresponding spectral acceleration of each ground motion

Residual inter-storey drifts are commonly used to compare the amount of unrecoverable structural deformation that has occurred during an earthquake. The absolute drift values at the end of each analysis were recorded and the distributions of these values throughout the structure are presented in Figure 6-17. It can be observed that the largest residual drifts typically occur around the fourth floor for 50%/50 intensity level ground motions, however, for higher intensity ground motions, the largest residual drifts occur in the ground floor. This shows that the largest transient deformations, like those observed in Figure 6-15 do not necessarily coincide with the largest residual deformations. While no universally accepted criteria for residual drift limits exist, it has been suggested that residual drifts of less than 0.10% are negligible (Prasad et al., 2008) and would therefore be acceptable for the Immediate Occupancy requirement of (ASCE 31-03, 2003).

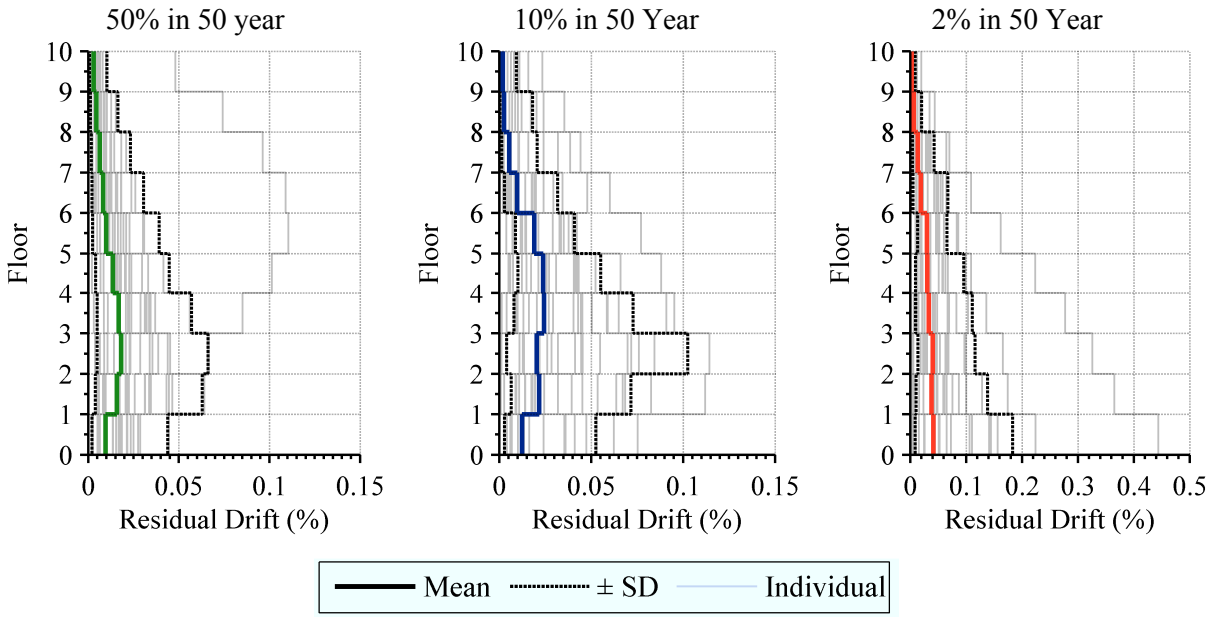

Figure 6-17: Residual inter-storey drift envelopes of bare frame

The maximum residual inter-storey drifts in the structure occurred in the first floor for stronger ground motions and around the third floor in weaker ground motions. The maximum absolute residual inter-storey drifts in the first and third floor of the structure are presented for the nine intensity levels in Figure 6-18. Collapse cases have been excluded in order to present only the cases of interest. The residual drifts in the first and third floors are reasonably equivalent for all of the nine intensity levels.

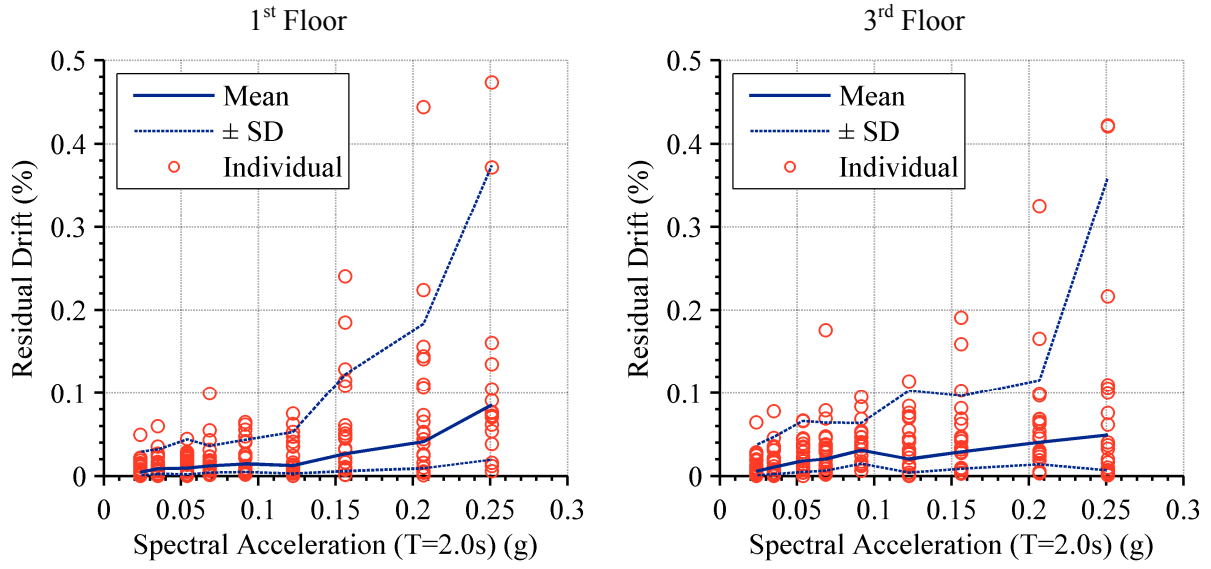

Figure 6-18: Residual inter-storey drift of bare frame at corresponding spectral acceleration of each ground motion

Maximum floor accelerations are commonly used to compare the maximum force profile in a structure observed during an earthquake. The acceleration at each floor was

recorded in order to form the maximum acceleration envelopes shown in Figure 6-19. It should be noted that the maximums at each floor do not necessary occur at the same time during the ground motion record. Figure 6-19 displays the maxima envelope obtained for each individual ground motions as well as the mean and standard deviation. It can be observed that the largest accelerations are reasonably constant throughout the structure. Slightly larger accelerations are visible in the tenth floor, particularly for the 2%/50 year intensity level. This is due to higher mode effects; it would appear the second mode in particular begins to have a more pronounced influence on the accelerations as the second mode shape becomes clearly visible (refer to Figure 6-11 for mode shapes of structure).

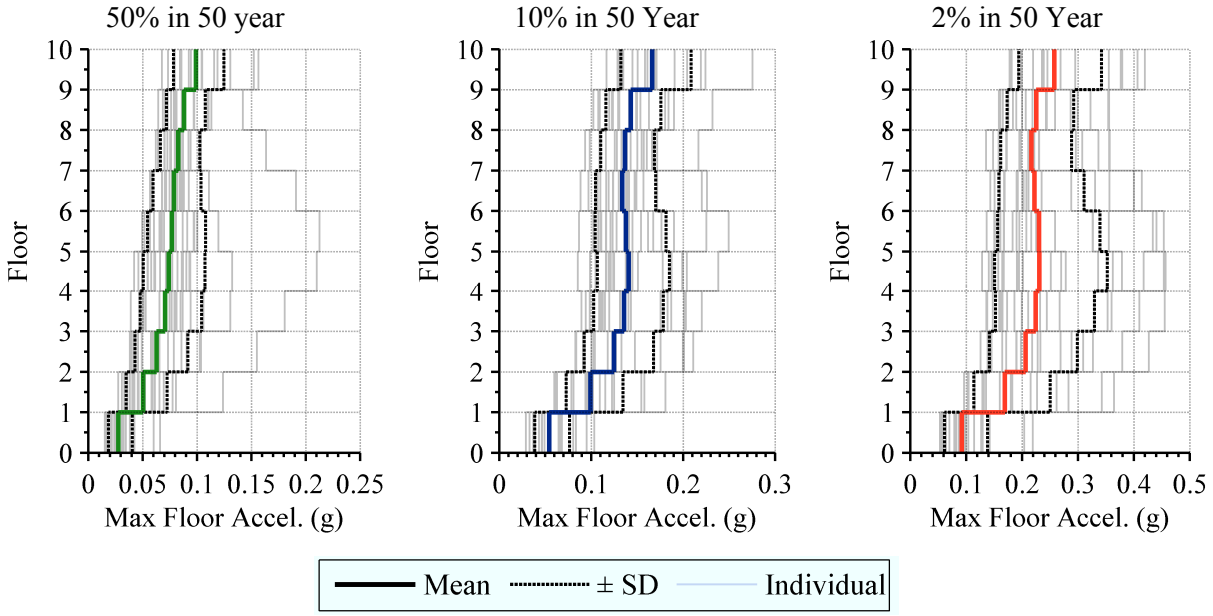

Figure 6-19: Maximum floor acceleration envelopes of bare frame

The maximum floor accelerations in the third and tenth floor of the structure are presented for the nine intensity levels in Figure 6-20. It can be seen that on average, the maximum floor acceleration is approximately equivalent to the spectral acceleration of the input ground motion. Slightly larger floor accelerations are observed in the top floor, as identified in Figure 6-19. It can also be seen that one earthquake record produces significantly larger than average floor accelerations at the 35%/50 intensity level (SA = 0.059 g). On inspection, this particular record is found to have significant energy in the high frequency range when scaled for the target spectral acceleration at two seconds. This high frequency energy has evidently excited higher modes of the structure, resulting in floor accelerations nearly ten times greater than those at a spectral acceleration of two seconds.

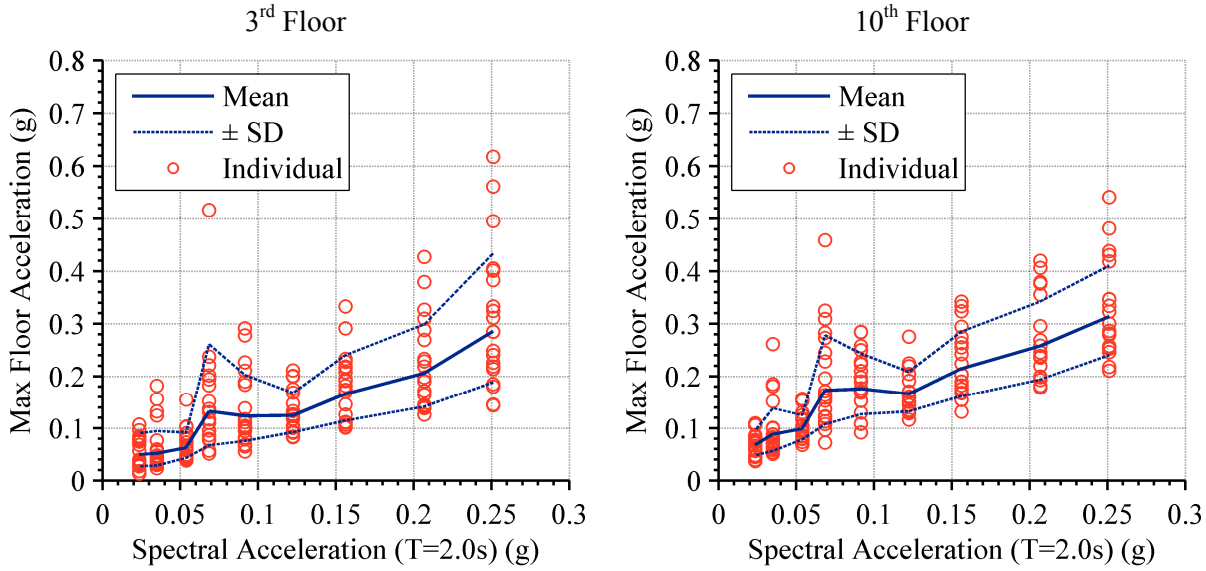

Figure 6-20: Maximum floor accelerations of bare frame at corresponding spectral acceleration of each ground motion

The mean envelopes for maximum drift, residual drift and maximum floor acceleration at the three intensity levels (shown in green, blue and red in the previous figures) is presented in Figure 6-21. It can be seen that the shape of the maximum drift and maximum floor acceleration envelopes is consistent for increasing seismic hazard, however as seismic hazard increases, residual drift increases proportionately more in the bottom levels of the structure. The ratio between the 50%/50, 10%/50 and 2%/50 demands is reasonably consistent for the three engineering demand parameters considered.

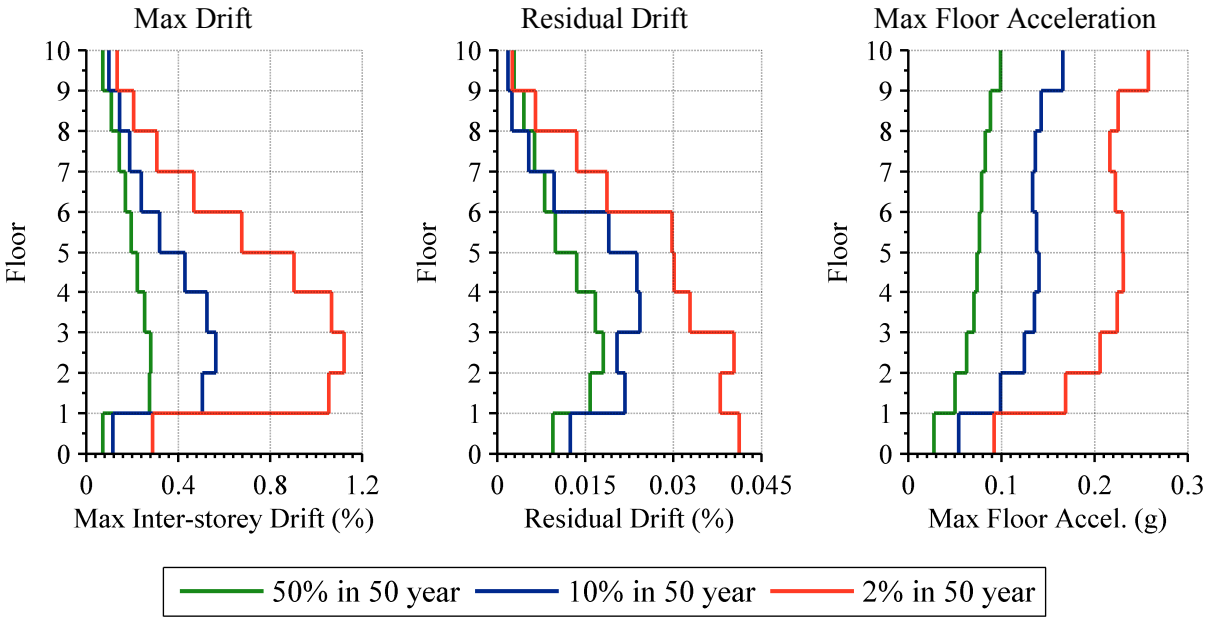

Figure 6-21: Comparison of maximum inter-storey drift, residual inter-storey drift and maximum floor acceleration envelopes at three key intensity levels

6.5.2.2 Structural Collapse

In assessing the structural response as well as for loss assessment purposes it is vital to identify global collapse of a numerical model (Shome & Cornell, 2000). Traditionally, the occurrence of structural collapse has been associated with some prescribed level of seismic demand, such as interstorey drift or component plastic deformation. This however does not account for the redundancy of structural systems which allows for redistribution of damage and global stability despite local failures (Zareian & Krawinkler, 2007). Collapse is here defined as the state in which lateral instability occurs in one or more storeys. Collapse due to loss of vertical carrying capacity (due to axial and critical shear failures) is not considered due to a lack of structural analysis tools which can reliably capture these phenomena. This lateral instability is therefore conditional on the hysteretic behaviour of the structural elements. As shown previously in Figure 6-2, the hysteretic behaviour of these elements considers strength and stiffness degradation but does not include cyclic degradation. Strength degradation is based on the maximum curvature ductility of the frame members, which is initiated at a curvature ductility of 16.6 and decreases linearly to near zero at a curvature ductility of 46.3. These curvature ductilities were found using CUMBIA (Montejo & Kowalsky, 2007) based on the case-study member sections and the model for confined concrete proposed by (Mander et al., 1988).

The probability of collapse is initially estimated from the proportion of ground motion records that cause structural collapse and are presented in Table 6-10 for the nine intensity levels investigated. It can be seen that collapse is only observed at the maximum intensity level investigated: 1% in 50 year probability of exceedance. Figure 6-14 showed that five of the records produced inter-storey drifts of over 2.0% in the third floor. On inspection, these five records resulted in global instability and hence correspond to structural collapse.

Table 6-10: Probability of collapse data for case study frame

IM Level	SA (g)	Probability of Exceedance in 50 Years	Probability of Collapse
1	0.024	90%	0%
2	0.035	75%	0%
3	0.054	50%	0%
4	0.059	35%	0%
5	0.092	20%	0%
6	0.122	10%	0%
7	0.156	5%	0%
8	0.207	2%	0%
9	0.251	1%	25%

The probability of collapse is generally assumed to have a lognormal distribution (Zareian & Krawinkler, 2007), hence the values found at the nine intensity levels were used to determine the parameters of this distribution using a generalized linear model with a probit link (Kutner et al., 2005). A generalised linear model is used as it allows for non-constant variance as opposed to conventional Gaussian regression (Bradley et al., 2010). Figure 6-22 illustrates the cumulative probability of structural collapse as a function of the spectral acceleration at two seconds. The data points in Figure 6-22 represent the probabilities of collapse presented in Table 6-10.

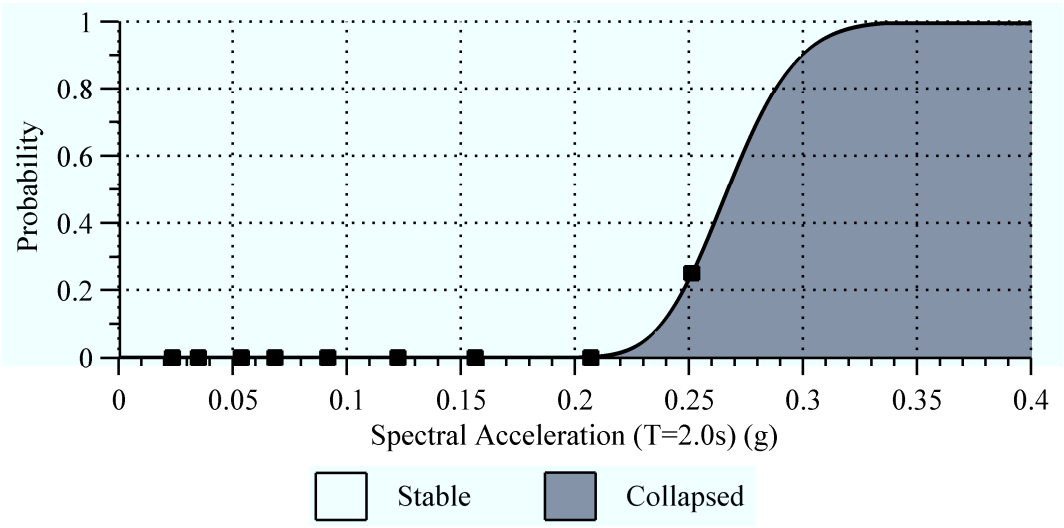

Figure 6-22: Cumulative probability distribution of collapse of case study frame

6.5.2.3 Clad Frame Behaviour

A total of 24 frame model configurations with cladding were analysed to understand the effect cladding has upon the dynamic response of the case-study structure. The 24 frame models included the three cladding configurations (mono panel, dual panel and fully clad), two cladding models types (quadrilateral and equivalent spring) and four connection models (long threaded rod, infinite slotted, 50 mm slotted and short threaded rod). A matrix of the clad frame models investigated is presented in Table 6-11.

Each of the 24 frame models was subjected to twenty ground motion records (ten earthquakes that include both orthogonal directions) at each of the nine intensity levels presented in Section 6.3.1. The maximum base shear for each ground motion was recorded and the mean for each of the intensity levels calculated. The mean base shear of the clad frames can then be compared to that of the bare frame when subjected to the same ground motion records. The effect the cladding presence has upon the maximum base shear is

presented in the following tables for each of the three key intensity levels analysed. Each table groups the results by the parameter of interest: connection type, cladding configuration and cladding model type.

Table 6-11 Cladding frame model matrix

		Cladding Configuration		
		Mono Panel	**Dual Panel**	**Fully Clad**
Connection Hysteresis	**Long Threaded Rod**	Quad / Spring	Quad / Spring	Quad / Spring
	Slotted with Infinite Slot	Quad / Spring	Quad / Spring	Quad / Spring
	Slotted with 50 mm Slot	Quad / Spring	Quad / Spring	Quad / Spring
	Short Threaded Rod	Quad / Spring	Quad / Spring	Quad / Spring

The influence different cladding connection types have upon the base shear is presented in Table 6-12 along with the bare frame values for comparison purposes. Each mean base shear presented takes the average of the 20 ground motion records for the three cladding configurations and both numerical cladding models for a total of 120 analyses.

It can be seen that the cladding presence results in a decrease in base shear for the 50%/50 year intensity level and increase in base shear for the 2%/50 year intensity level for all of the connection types considered. The long threaded rod and slotted connections result in a similar change to the frame's maximum base shear. The short threaded rod connections increase the base shear by 12% at the 2%/50 year intensity level. It can also be observed that the restriction in the slot length causes an increase in base shear when subjected to a greater seismic hazard.

Table 6-12: Mean of maximum base shear for connection types

	50%/50 Year	**10%/50 Year**	**2%/50 Year**
Bare Frame	1225 kN	1465 kN	1688 kN
Long Threaded Rod	1174 kN	1471 kN	1723 kN
Slotted with Infinite Slot	1145 kN	1465 kN	1727 kN
Slotted with 50 mm Slot	1145 kN	1465 kN	1815 kN
Short Threaded Rod	1208 kN	1599 kN	1889 kN

The mean base shear of the bare frame is compared against those obtained for the clad frames for each of the four connection types in Figure 6-23. It can be observed that the influence of the long threaded rod and slotted (infinite) connection cause a minimal change in the base shear, regardless of the earthquake intensity level. However, the short threaded rod and slotted (50 mm) connections have an increased influence upon the base shear for larger intensity levels. Obviously the influence of the slotted connection with the 50 mm slot only becomes significant once the displacement capacity of the slot is exceeded. This would appear to occur around a spectral acceleration of 0.13 g. Thereafter, the maximum base shear increases considerably as the seismic hazard level increases due to the cladding system becoming more rigid. The short threaded rod connections cause a consistent increase in the maximum base shear of approximately 10% but this only appears to occur for ground motions where the frame has become inelastic, as shown up the negligible influence they have up until 0.07 g.

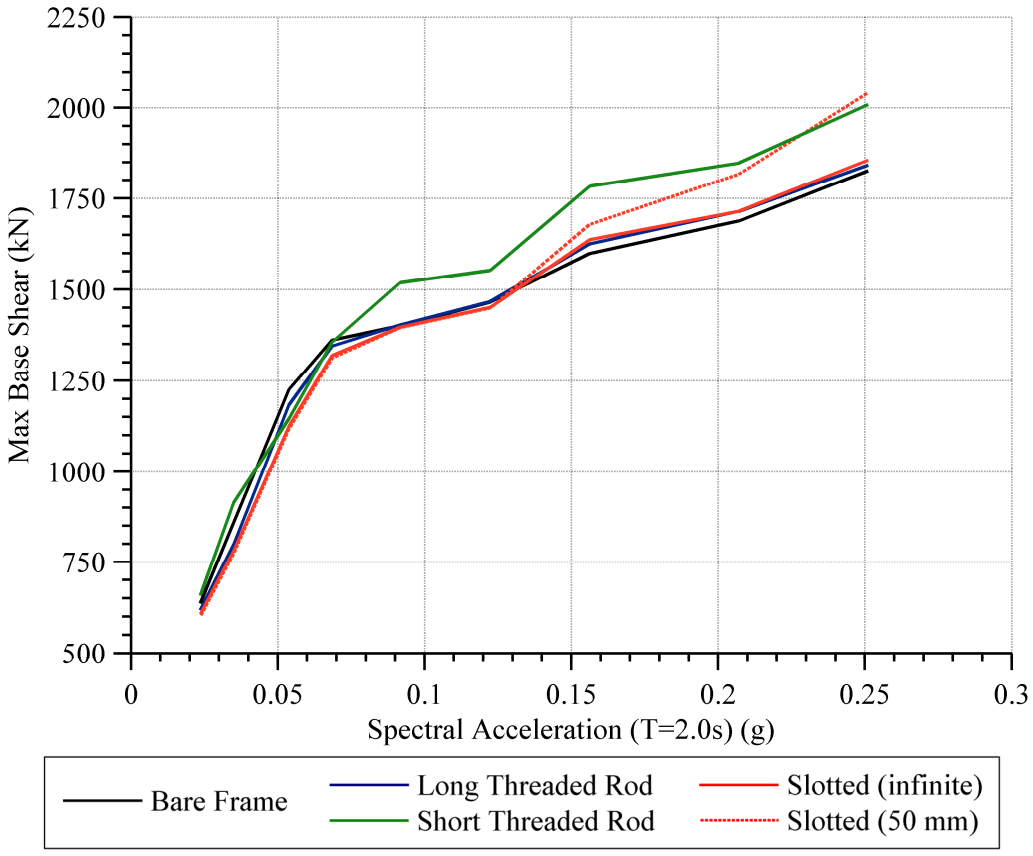

Figure 6-23: Effect of cladding upon maximum base shear at different earthquake intensity levels

The influence different cladding configurations have upon the base shear is presented in Table 6-13 along with the bare frame values for comparison purposes. Each mean base shear

presented takes the average of the 20 ground motion records for the four cladding connection types and both numerical cladding models; a total of 160 analyses.

It can be seen that the cladding presence results in both the mono panel and dual panel configurations has a similar effect upon the base shear of the frame. The dual panel system has more cladding connections but these provide less lateral resistance since they are smaller, consequently, the overall influence of the cladding is very similar. The fully clad configuration provides a significant increase in the base shear compared to the other configurations for higher intensity ground motions. For the 2%/50 year intensity level, the fully clad configuration increases the base shear on average 10% compared to the 3% average increase provided by the mono panel and dual panel configurations.

Table 6-13: Mean of maximum base shear for different frame configurations

	50%/50 Year	10%/50 Year	2%/50 Year
Bare Frame	1225 kN	1465 kN	1688 kN
Mono Panel	1163 kN	1486 kN	1769 kN
Dual Panel	1158 kN	1489 kN	1745 kN
Fully Clad	1183 kN	1522 kN	1849 kN

The influence the different cladding model types have upon the base shear is presented in Table 6-14 along with the bare frame values for comparison purposes. Each mean base shear presented takes the average of the 20 ground motion records for the four cladding connection types and for all cladding configurations; a total of 240 analyses.

It can be seen that there is a different of 1-2% in base shear response for the two cladding model types. The equivalent spring cladding model consistently provides slightly larger base shear values of the two model types. This level of error is well within the level of error used in defining the models. Since both models predict similar results, the computational savings provided by the equivalent spring model make it the preferred model.

Table 6-14: Mean of maximum base shear for cladding model type

	50%/50 Year	10%/50 Year	2%/50 Year
Bare Frame	1225 kN	1465 kN	1688 kN
Quadrilateral	1162 kN	1490 kN	1767 kN
Equivalent Spring	1174 kN	1508 kN	1807 kN

The inter-storey drift envelopes for the four connection types at the three key intensity levels are shown in Figure 6-24. The inter-storey drift envelopes are the mean of the maximum inter-storey drifts recorded for all analyses of that particular connection type at the corresponding earthquake intensity. These envelopes are compared to the bare frame envelope obtained previously.

It can be seen that all of the connection types reduce the maximum inter-storey drift throughout the entire height of the structure. The short threaded rod connections reduce the drifts the greatest amount, followed by the slotted connections and the long threaded rod connections reduce drifts the least. The drifts are reduced proportionately more during the 50%/50 year intensity level, however at such low drift levels this only corresponds to a reduction of 1-4 mm. It can also be seen that the influence of the 50 mm slotted connection has a significant influence on the drifts in the lower levels of the building for the 2%/50 year intensity level.

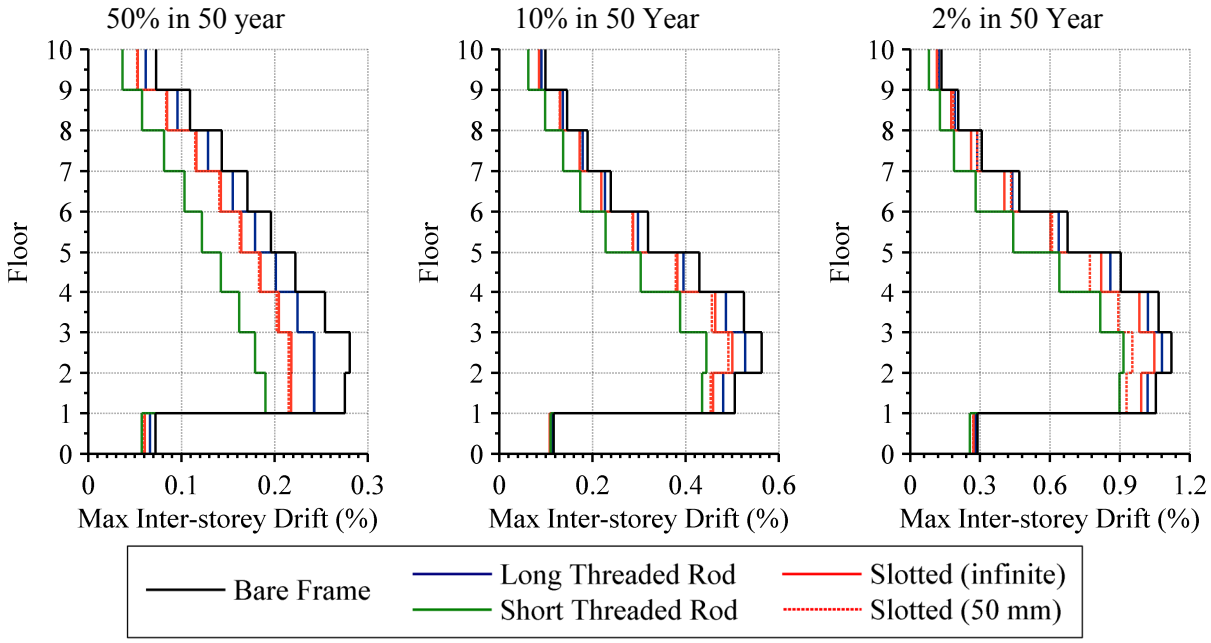

Figure 6-24: Effect of cladding upon maximum inter-storey drift envelopes

Similarly to what was presented previously for the bare frame, the mean maximum inter-storey drifts at the third and 6th floor at all nine intensity levels are presented for the clad frame cases in Figure 6-25. The intensity measure is defined by the spectral acceleration at two seconds that the ground motions were scaled to. The larger inter-storey drifts observed in the third floor result in a greater reduction in drift from the 50 mm slotted connection than those observed in the sixth floor. It is also apparent that the short threaded rod connections cause a substantial decrease in the inter-storey drifts observed in the sixth floor in comparison

with the other connection types. It would appear that the overall influence of the cladding when connected with short threaded rod accumulates throughout the structure. This can be examined by looking at the difference in reduction at the same hazard level at the different floor levels. For example, consider the hazard level that causes a mean maximum bare-frame inter-storey drift of 1.00%. In the third floor this occurs at a spectral acceleration of 0.18 g. At this hazard level, the maximum mean third floor inter-storey drifts of the frame clad with short threaded rod connections is 0.82%. However, at the sixth floor, a spectral hazard level of 0.24 g results in a mean maximum bare frame inter-storey drift of 1.00%. At this hazard level, the maximum mean inter-storey drift of the frame clad with short threaded rod connections is 0.61%.

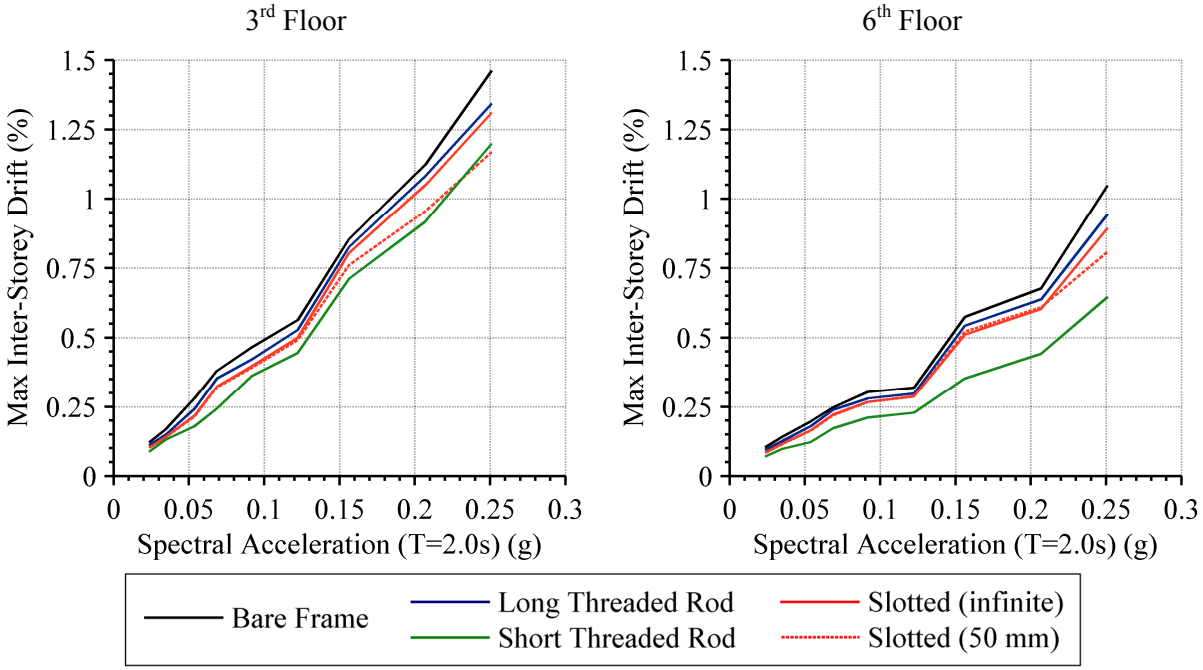

Figure 6-25: Effect of cladding upon maximum inter-storey drift at different earthquake intensity levels

The residual inter-storey drift envelopes for the four connection types at the three key intensity levels are shown in Figure 6-26. These envelopes are compared to the bare frame envelope obtained previously.

It can be seen that for the 50%/50 year intensity level all of the connection types reduce the residual drift throughout the entire height of the structure. Such reductions are negligible since the drifts are so small at this level. At greater earthquake intensities, no reduction in the residual drift is evident. In fact, the residual drift is larger in some clad cases; however no discernible trend is evident.

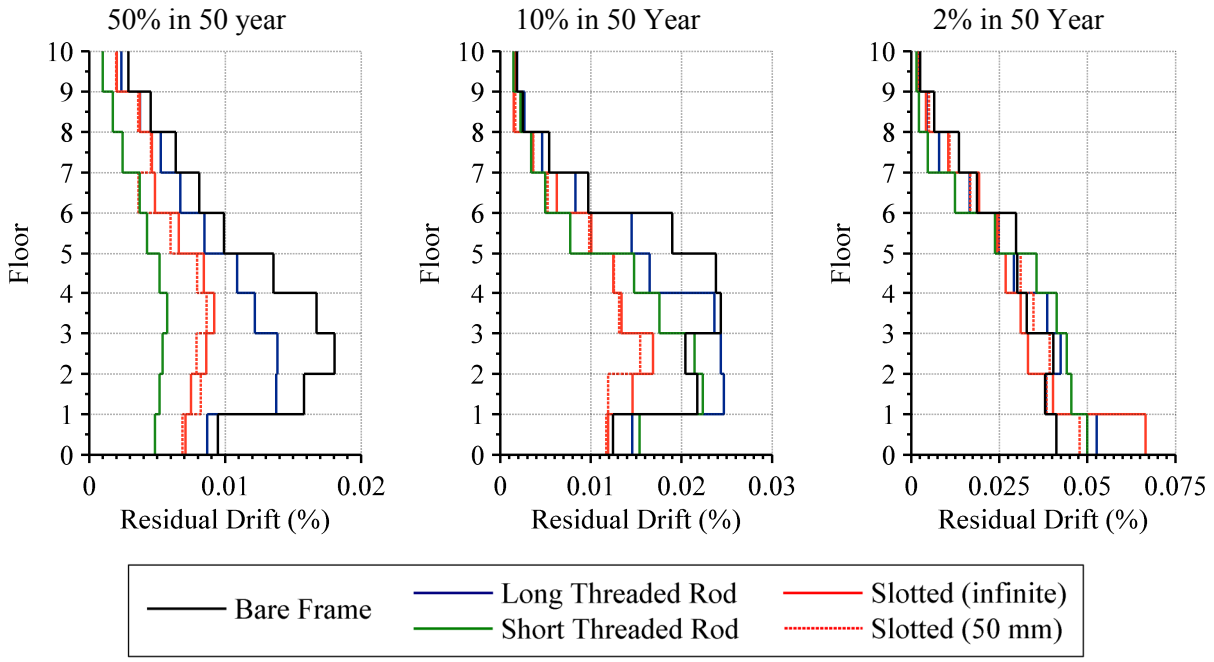

Figure 6-26: Effect of cladding upon residual inter-storey drift envelopes

The lack of a discernible trend in the influence cladding has upon the residual drift is further illustrated in Figure 6-27. The figure shows the residual drifts of the clad frames compared to the bare frame at the first and third floor for the nine intensity levels. At some intensity levels the cladding presence has a positive effect upon the residual drift and others a negative effect. In all cases the effect is minimal and corresponds to less than 5 mm difference from the bare frame behaviour.

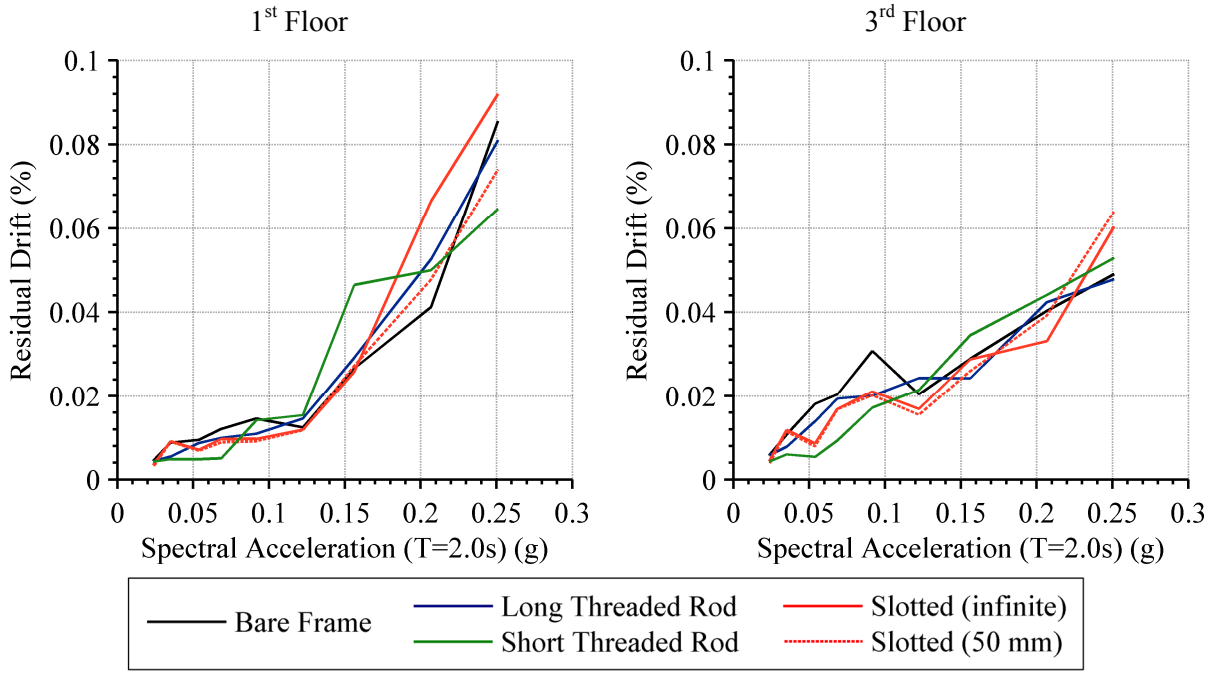

Figure 6-27: Effect of cladding upon residual inter-storey drift at different earthquake intensity levels

The maximum mean floor acceleration envelopes for the four connection types at the three key intensity levels are shown in Figure 6-28. These envelopes are compared to the bare frame envelope obtained previously.

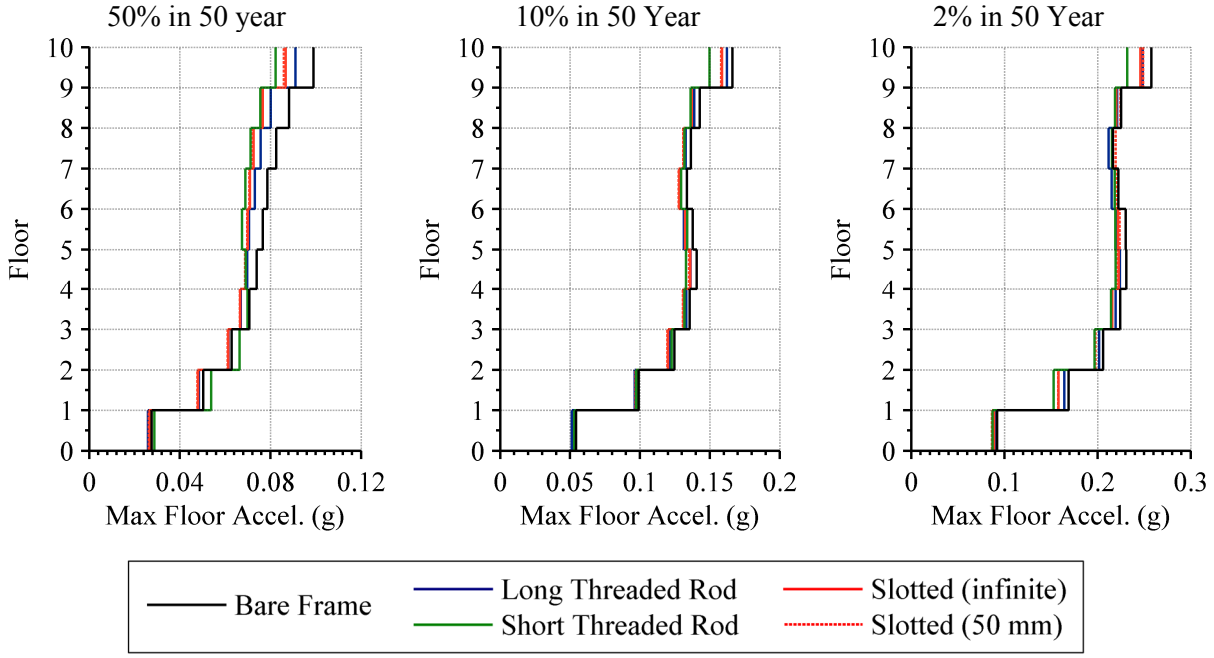

Figure 6-28: Effect of cladding upon maximum floor acceleration envelopes

Figure 6-29 portrays the mean maximum floor accelerations of the third and tenth floor of the clad frames compared to the bare frame at the nine intensity levels.

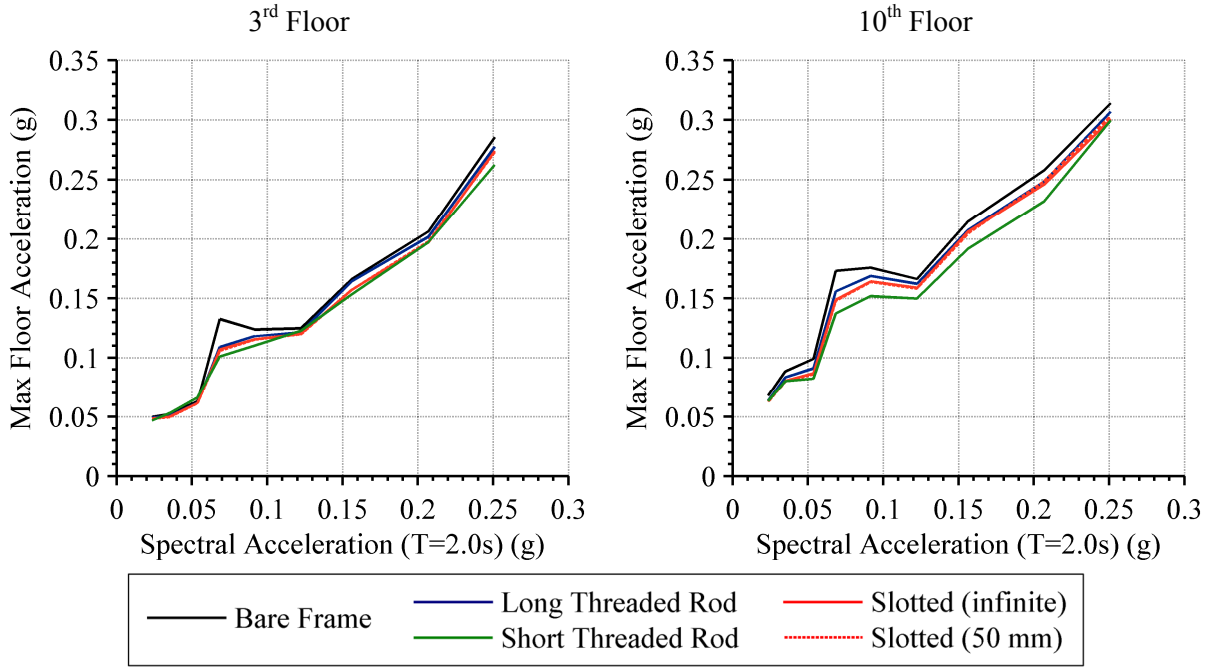

Figure 6-29: Effect of cladding upon maximum floor acceleration at different earthquake intensity levels

Evidently, the cladding presence has a very minimal influence upon the structure's maximum floor accelerations, regardless of the connection type or earthquake intensity. It can be seen that the cladding registers a minor reduction in maximum floor accelerations in both floors, with the short threaded rods having the greatest influence of the connection types.

The influence the different cladding configurations have upon the structural response is illustrated in Figure 6-30. The figure presents the mean envelope of the three structural response EDPs for the bare frame and a frame clad with long threaded rod connections. The intensity level used to compare the influence is that of the 2%/50 year probability of exceedance as it was found earlier that the cladding typically has a greater influence upon the structural response during stronger earthquake shaking. The different coloured envelopes in Figure 6-30 represent the three cladding configurations investigated. It can be seen that the cladding configuration does not appear to have any influence upon the three structural EDPs.

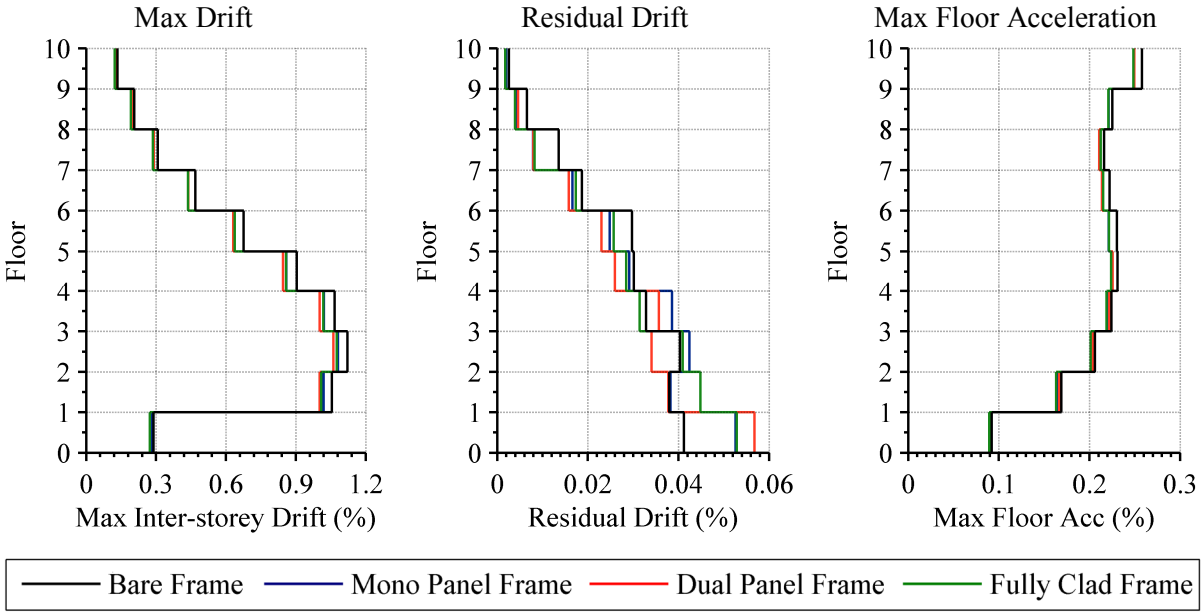

Figure 6-30: Comparison of maximum inter-storey drift, residual inter-storey drift and maximum floor acceleration for different frame configurations

6.5.3 Cladding Response

The engineering demand parameters (EDPs) used to quantify the cladding performance during the overall systems seismic response are the maximum lateral connection displacement, the maximum lateral panel displacement and the maximum connection acceleration. The maximum connection acceleration is analogous to the maximum acceleration at the top of the cladding panel.

Twenty unique data points exists for each EDP from each of the twenty ground motion records. The mean and standard deviation of each EDP is found from this data using a lognormal distribution. Unlike structural EDPs, multiple data points exist for each cladding EDP on each floor due to the presence of multiple cladding connections and panels. The data point used to represent each floor is herein taken as the absolute maximum from each floor (in the damage analysis presented in Chapter 7, the displacement of each individual component is assessed). In reality, the difference in the EDP values of the cladding components on each floor was found to be very minimal.

6.5.3.1 Cladding Displacements

The mean envelopes of maximum connection displacement and maximum inter-storey frame displacement are presented in Figure 6-31 for the three connection types subjected to the 2% in 50 year intensity level. The displacements are presented for the fully clad configuration. The displacement in the connection is defined by the relative displacement between the cladding panel and the structure. The frame displacement is defined by the displacement between floors. It should be noted that the maximums at each floor do not necessary occur at the same time during the ground motion record.

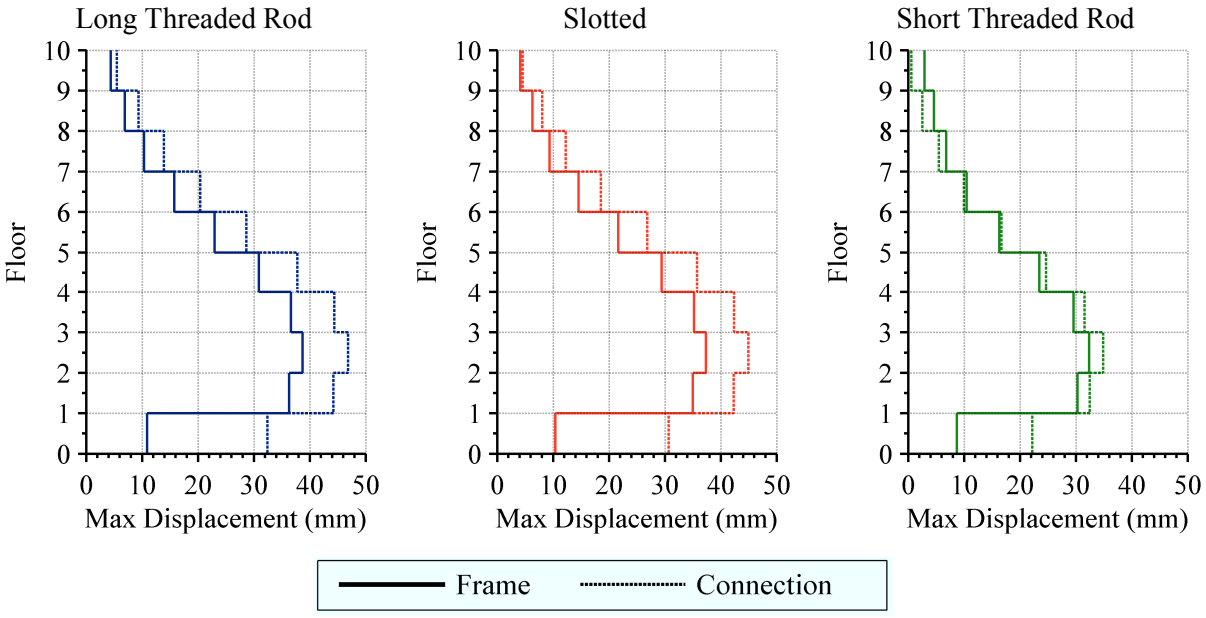

Figure 6-31: Maximum cladding connection displacement envelope compared with inter-storey frame displacement envelope for different connection typologies at 2%/50 year intensity level

It can be seen that in some cases the displacement in the connection is greater than the displacement between floors of the frame. This is true throughout the structure for both the long threaded rod and slotted connections. The difference in displacement between the frame

and connection is less for the short threaded rod connections and the displacement in the connection less than the frame at higher floors. The greatest connection displacements occur around the third floor of the structure.

The mean maximum displacement of each of the connection types at the third and sixth floor is presented in Figure 6-32 for the nine different earthquake intensity levels. The connection displacement demand increases approximately linearly with increasing spectral acceleration hazard. In accordance with the envelopes presented in Figure 6-31, the connection displacements are on average less in the sixth floor than the third floor. The displacements in the short threaded rod connections are clearly less than the other connections, with the exception of the 50 mm slotted connection. It can be seen that for an earthquake intensity greater than approximately 0.12 g (10% in 50 year hazard level), the maximum displacement of the slotted connections is affected by the slot length. Understandably, this occurs when the maximum connection displacement is around 25 mm (the length of the slot in one direction). The maximum displacement of the 50 mm slotted connection is considerably less than the infinitely slotted connection at the highest hazard level, also being less than that of the short threaded rod connection in the third floor.

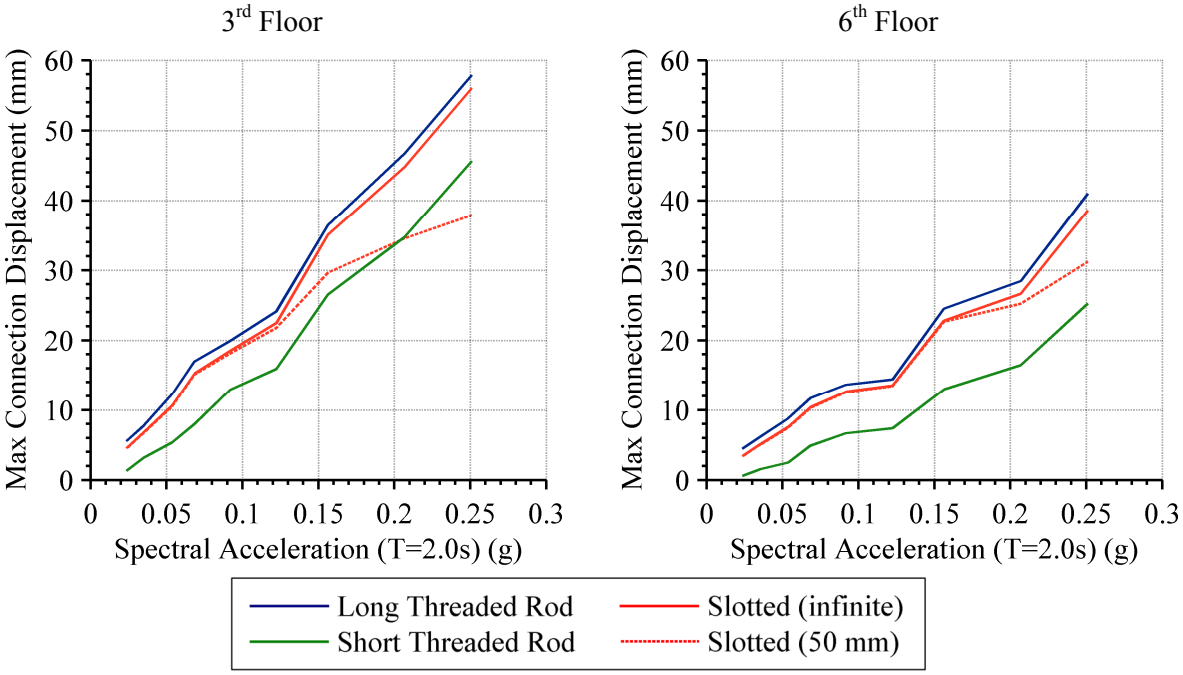

Figure 6-32: Maximum connection displacement at different earthquake intensity levels

As presented earlier, the cladding presence does not greatly reduce the magnitude of the inter-storey drift (refer to Figure 6-24 and Figure 6-25), hence the difference in maximum connection displacement observed between connection types does not equate to a difference

in frame displacement. Instead, this difference is expected to be accommodated by displacement of the cladding panel.

The mean envelopes of maximum panel displacement and maximum inter-storey frame displacement are presented in Figure 6-33 for the three connection types subjected to the 2% in 50 year intensity level. The displacement in the panel is defined by the relative displacement between the top and bottom of the panel's connections. The panel displacement is considerably less than the maximum frame displacement (and the connection displacement presented previously); however, it is apparent that the displacement in the panel is not negligible. As expected, the shape of the displacement envelope is the same as that of the frame, with the largest displacements being around the third floor.

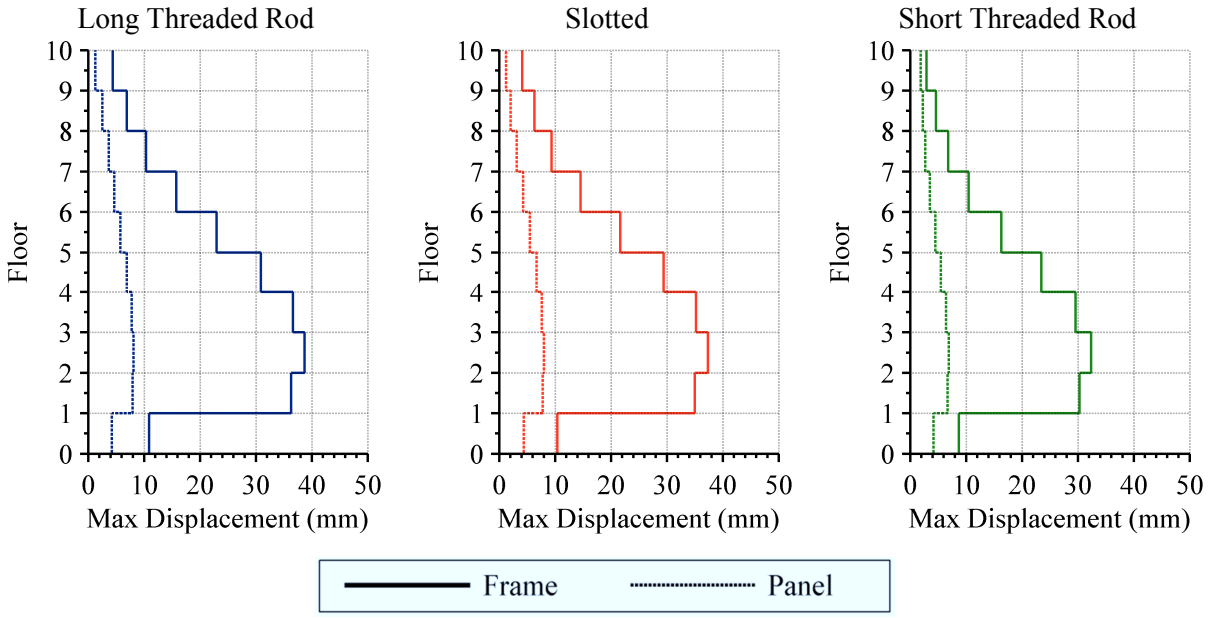

Figure 6-33: Maximum panel displacement envelope compared with inter-storey frame displacement envelope for different connection typologies at 2%/50 year intensity level

When considering the panel displacement in the third and sixth floor for increasing seismic hazard, a similar trend to that of the connection displacement is observed, as shown in Figure 6-34 for the nine different earthquake intensity levels.

This result is slightly counterintuitive to what may be expected. Considering that the connection displacements presented previously showed that the long threaded rod connections had the greatest displacement demands and the short threaded rods the least. It may therefore be expected that the magnitude of the displacements in the panels of the long threaded rods would be less than those for the short threaded rods. This is since we would expect that the more flexible connections would be able to accommodate the majority of the inter-storey displacement. However, the result in Figure 6-34 shows that the panel

displacements are greatest for the long threaded rod connections and least for the short-threaded rods.

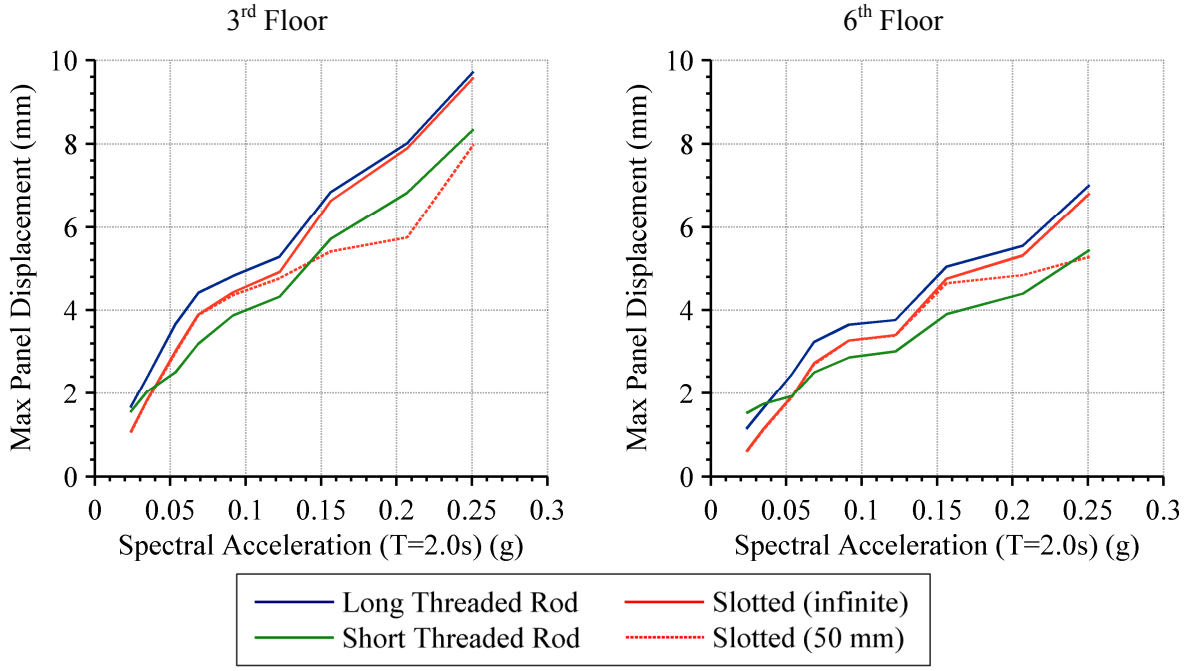

Figure 6-34: Maximum panel displacement at different earthquake intensity levels

This result reveals that the dynamic displacement demand upon the individual connection and panel components does not necessarily sum to the inter-storey displacement demand of the structure. This can be examined by finding the ratios of the connection and panel displacements relative to the frame displacement, as shown in Figure 6-35 for the three connection types when subjected to the 2% in 50 year intensity level.

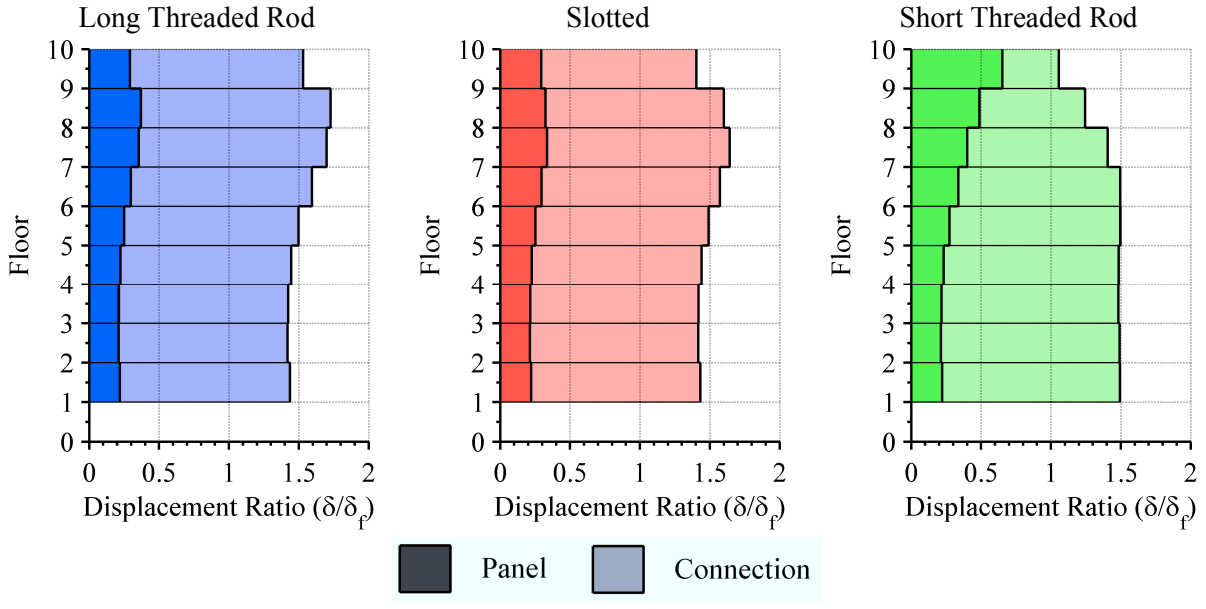

Figure 6-35: Connection and panel displacement ratios for different connection typologies of mono panel cladding system at 2%/50 year intensity level

The displacement ratio is found by non-dimensionalising the maximum panel and connection displacements by the respective maximum inter-storey frame displacement. The panel and connection displacement ratios in Figure 6-35 are found for each floor and are stacked alongside each other. It can be observed that the sum of the displacement ratio exceeds 1.0 (the frame displacement) throughout the structure for all three connections. The ratios consistently sum to approximately 150% of the frame displacement.

It is of interest whether this ratio varies depending on the earthquake intensity, hence presented in Figure 6-36 are the displacement ratios of the connection and panel for the nine intensity levels investigated. The displacement ratio at each intensity level is taken as the average of the ten floors. It can be seen that the sum of the displacement ratios is fairly consistent for all three connections at around 140 – 160% that of the frame displacement.

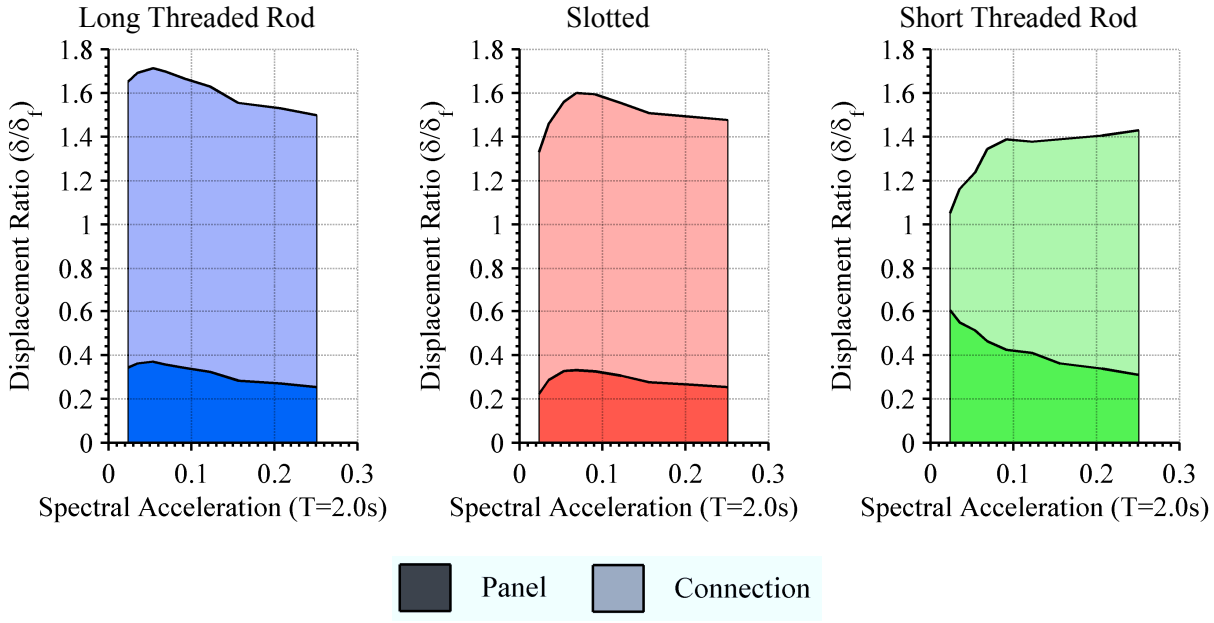

Figure 6-36: Connection and panel displacement ratios of mono panel cladding system at different earthquake intensity levels

In order to explain this amplification in displacement demand upon the cladding system, it is necessary to consider the cladding system in a dynamic sense. In terms of its system, the cladding is essentially a fixed base cantilever with a top restraint. The more flexible this top restraint is, the more the system can be considered purely as a cantilever. The input excitation for the cladding is through its fixed base, i.e. the bottom beam level. Due to the cladding panels having high in-plane stiffness, the fundamental periods of the panels are much shorter than that of the structure, as shown in Table 6-15. Consequently, the panels are subjected to the higher accelerations generally present at the high frequency end of the response spectrum. It would therefore appear that these larger high frequency accelerations

excite the cladding panels creating displacement demands greater than those due to frame induced displacements.

Table 6-15: Period of cladding panels

	Mono Panel	Dual Panel
Panel Mass (kg)	5760	2860
Panel Stiffness (kN/m)	23,300	3,200
Panel Period (s)	0.10	0.19

The larger cladding displacements are also likely attributed to the movements of the frame and cladding being out of phase. If the cladding panel and frame movement are out of phase the connections are subjected to larger displacement demands and consequently the sum of the displacement ratios is greater than one. An example of the difference in movement of the top of the cladding panel and the beam of the above floor are compared in Figure 6-37. The displacement is shown relative to the beam of the floor at which the cladding panel is connected. It can be seen that the relative displacements are in fact completely out of phase. This means that as the bottom floor moves in one direction, the displacement of the panel in the same direction is delayed due to the inertia of the panel. Consequently, the distance between the top of the panel and the floor above (the difference between the two lines in Figure 6-37) is greater than the inter-storey displacement (shown as blue in Figure 6-37). This type of amplified displacement response was observed during shake-table testing of precast concrete cladding panels by Pantoli et al. (2013).

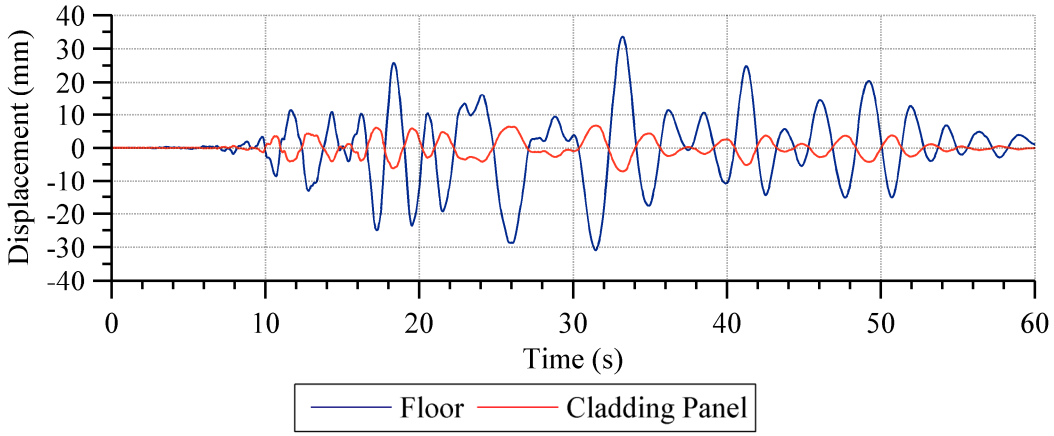

Figure 6-37: Example response history of floor displacement compared with cladding panel displacement

The stiffness of the top connection thus directly influences the feedback of the relative movement between the panel and frame, i.e. a stiffer connection reduces the degree to which the cladding movement is out of phase with the frame. This trend was evident in the connections examined, with the stiffer short threaded rod connections having smaller

cladding displacements compared to its longer, more flexible counterpart. Furthermore, the flexibility of the panel will directly affect the displacement of both the cladding connection and the panel itself. In a static sense, a more flexible panel results in less displacement demand upon the cladding connections since the panel is able to accommodate a larger portion of the frame's inter-storey displacement itself. However, due to the concepts described beforehand, when subjected to dynamic earthquake excitation a more flexible panel results in greater displacements in both the cladding and the connections. This was clearly evident when comparing the behaviour of the two panel sizes analysed. When excited by the same ground motion records, the more flexible dual panel produced significantly larger displacement demands in the cladding connections than the stiffer mono panel. Presented in Figure 6-38 are the average connection and panel displacement ratios of the dual panel system with the three connection types subjected to the 2% in 50 year intensity.

The most apparent difference of the dual panel displacement ratios compared to the corresponding mono panel system results (refer to Figure 6-35) are the large displacements in the upper floors of the structure. The connection displacements in particular are significantly greater, up to five times the inter-storey frame displacement. It should be noted that the frame displacement in the upper floors is significantly less than that in the lower floors (refer to Figure 6-30). Therefore, a connection displacement in the top floor that is five times that of the frame in reality has a displacement of similar magnitude to that of the connection displacements in lower floors.

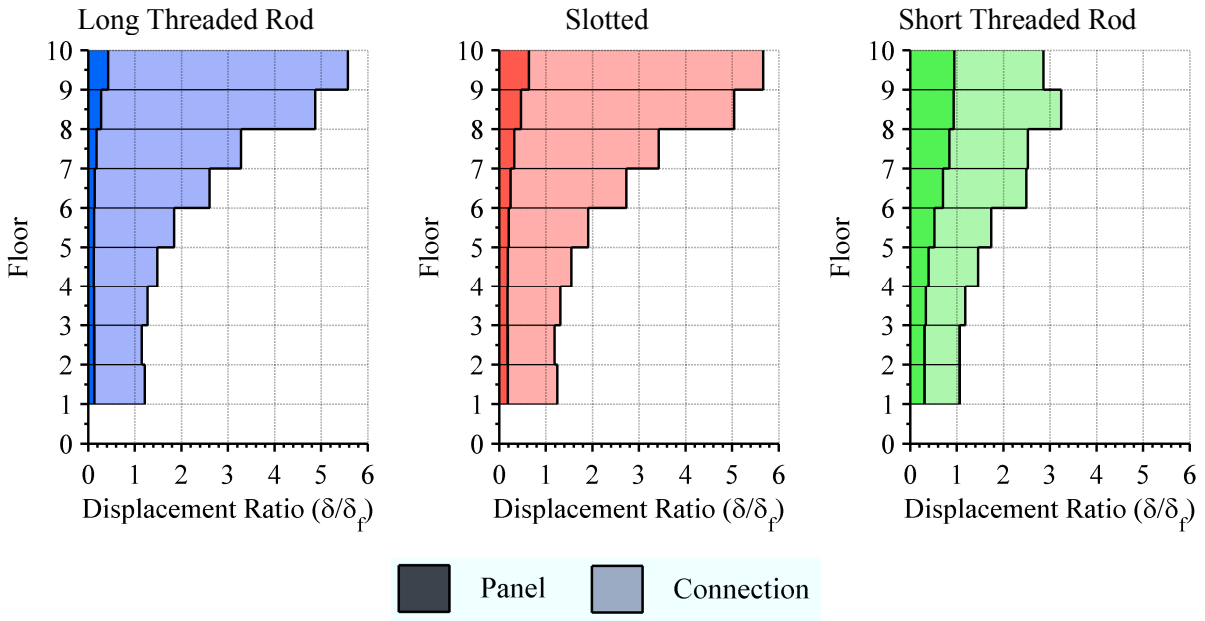

Figure 6-38: Connection and panel displacement ratios for different connection typologies of dual panel cladding system at 2%/50 year intensity level

The average panel and connection displacement ratios at each of the nine intensity levels are presented in Figure 6-39. Since the displacement ratios of the dual panel systems presented in Figure 6-39 take the average over the height of the structure, the large displacement ratios found in the upper floors skew the average displacement ratio so that it is significantly greater than that of the mono panel systems presented in Figure 6-36.

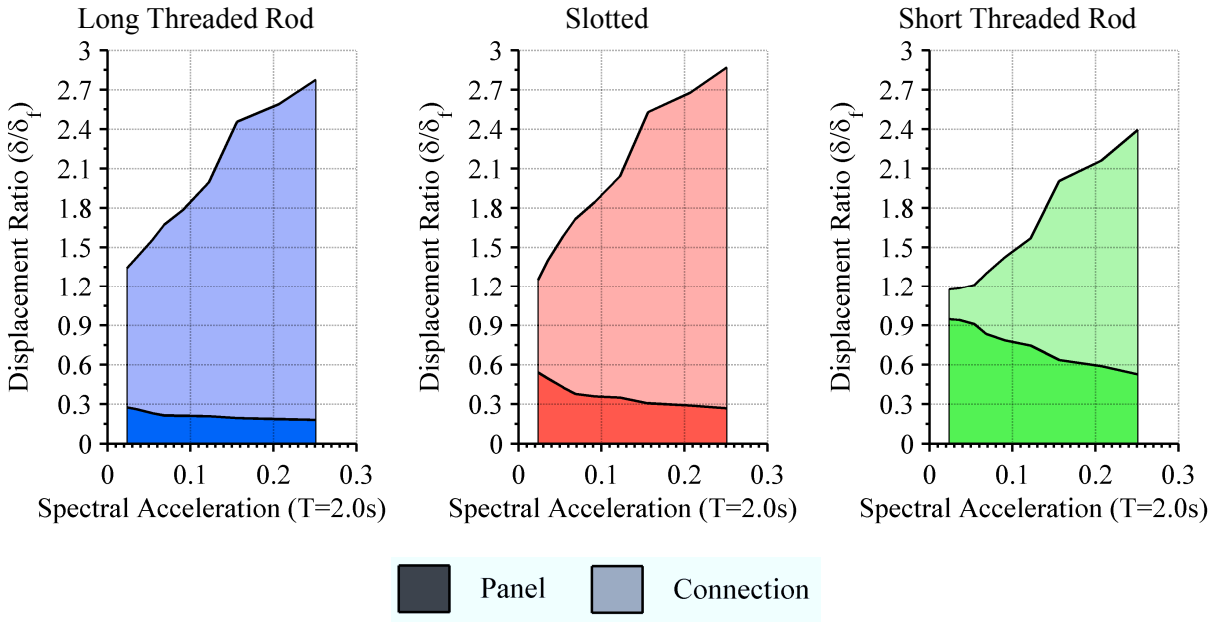

Figure 6-39: Connection and panel displacement ratios of dual panel cladding system at different earthquake intensity levels

Also evident in Figure 6-39 is the increasing displacement ratio of the connection for increasing intensity level. The average displacement ratio of the long threaded rod cladding connections increases to be 260% of that of the frame displacement at the 1%/50 year intensity level. Such an increase was not the case for the cladding systems with the larger, stiffer mono panel, which had a reasonably constant displacement ratio. It can be seen in Figure 6-39 that the displacement ratio of the panel itself is fairly constant for the dual panel system when subjected to different intensity levels. The magnitude of the panel displacement ratio is also similar to that of the mono panel.

6.5.3.2 Cladding Accelerations

The lateral acceleration of the cladding during each response history analysis has been recorded at the top and bottom of each cladding panel. The acceleration of the bottom of the cladding panel is identical to that of the floor acceleration since the bottom connection is rigid. The acceleration at the top of the panel is of most interest since it also corresponds to

the acceleration at the top cladding connection. This acceleration is of interest since it defines the lateral forces that the top connection is subjected to.

The mean envelopes of the maximum acceleration at the top connection (herein referred to as the connection acceleration) and the maximum floor acceleration are presented in Figure 6-40 for the three connection types subjected to the 2% in 50 year intensity level.

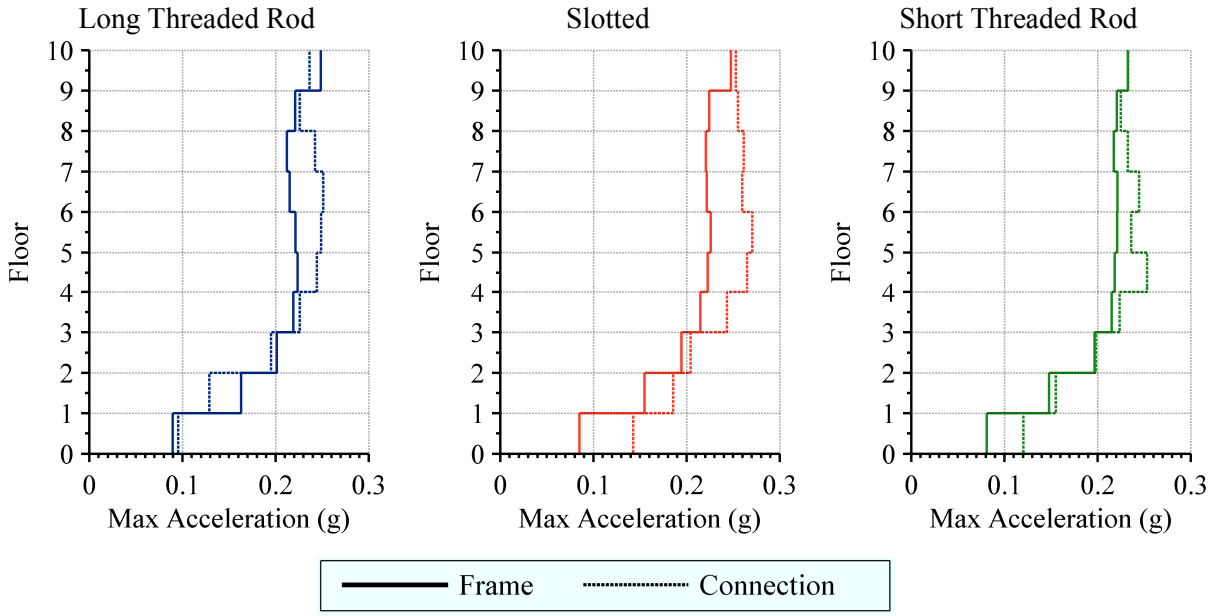

Figure 6-40: Maximum cladding connection acceleration envelope compared with maximum floor acceleration envelope for different connection typologies at 2%/50 year intensity level

The accelerations are presented for the fully clad configuration. It should be noted that the maxima at each floor do not necessary occur at the same time during the ground motion record. The connection acceleration envelopes are of a similar shape to the floor acceleration envelopes with the exception that the connection envelopes do not exhibit an increase in acceleration in the top floors associated with higher mode effects that are evident in the floor accelerations. Rather, the maximum accelerations are consistent throughout the top five floors for all connection types.

The maximum connection accelerations are on average slightly greater than the floor accelerations throughout the structure. This is most likely due to the cladding having a short fundamental period which results in the cladding being excited by the higher accelerations generally present at the high frequency end of the response spectrum.

The ratio between the connection and floor acceleration, herein referred to as the acceleration ratio, is of interest since it provides the ability to find the connection accelerations and subsequently the forces that the cladding connections must be designed for without requiring the presence of cladding in the numerical model. The acceleration ratio

throughout the structure of the three connection types when subjected to the three key intensity levels is presented in Figure 6-41. It can be seen that the connection acceleration varies from around 80% to 120% of the floor acceleration, and does not appear to be dependent upon connection type, intensity level or floor height.

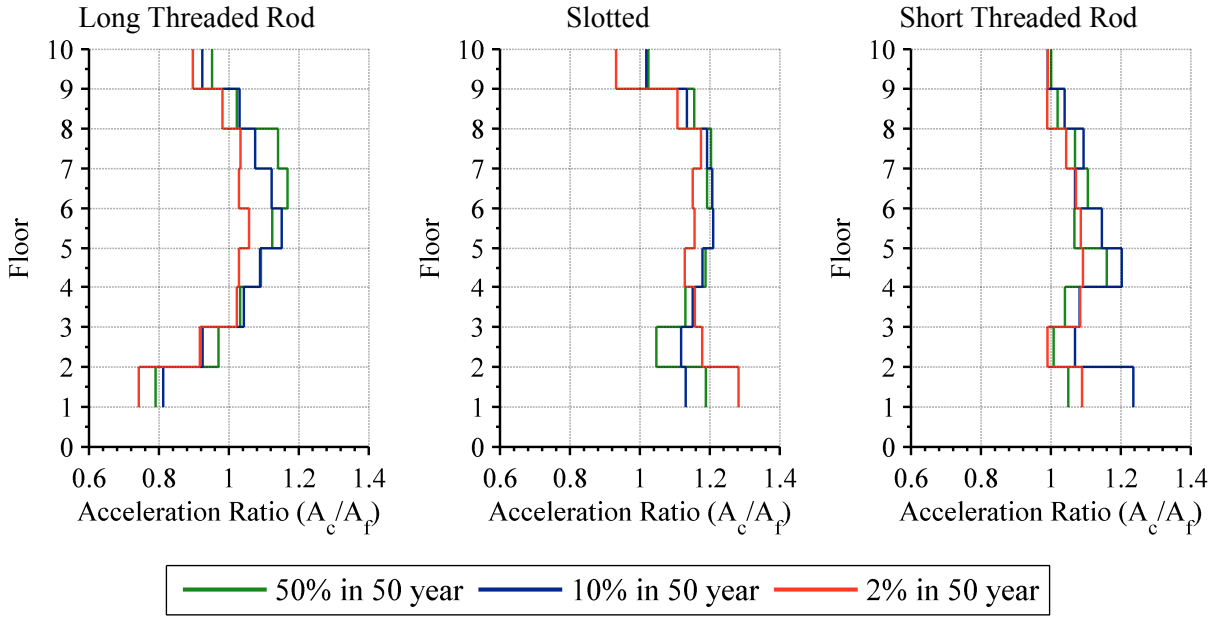

Figure 6-41: Acceleration ratios for different connection typologies

An example of the difference between the connection acceleration and corresponding floor acceleration during an earthquake is presented in Figure 6-42. The accelerations are shown for the third floor of the fully clad configuration when subjected to the Loma Prieta earthquake at 2%/50 year intensity level (refer to EQ#731 in Appendix F). It can be seen that the cladding connection accelerations are slightly greater than the floor accelerations and also exhibit more high frequency energy. This can be seen in Figure 6-42 by the cladding's higher frequency mode being superimposed upon the lower frequency modes of the structure.

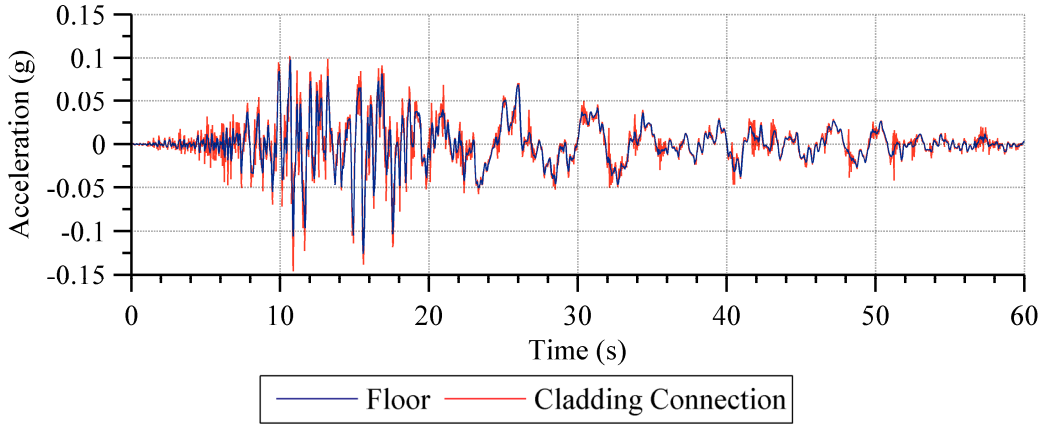

Figure 6-42: Example response history of floor acceleration compared with cladding connection acceleration

When not explicitly included in a structural model, design guides typically propose that the acceleration demand at the cladding connection is found by multiplying the PGA by a response coefficient. The New Zealand design code, NZS 1170.5 (2004), defines this response coefficient by the elevation of the support height of the cladding and the period of the cladding, as given in Equation (6-9).

$$C_p(T_p) = C(0)C_{Hi}C_i(T_p) \quad \textbf{(6-9)}$$

where

$C_p(T_p)$ = Horizontal acceleration coefficient

$C(0)$ = Site hazard coefficient for T = 0 (PGA)

C_{Hi} = Floor height coefficient

T_p = Period of the cladding

$C_i(T_p)$ = Spectral shape factor

The floor height coefficient is a bi-linear function with height and has a maximum value of 3.0. The spectral shape factor is a tri-linear function dependent upon the period of the cladding. For a period of less than 0.75 s the coefficient is equal to 2.0. Consequently, the largest the acceleration coefficient can be is six times the PGA. Presented in Figure 6-43 are the mean envelopes of the maximum connection accelerations for the three different connection types at the three key intensity levels.

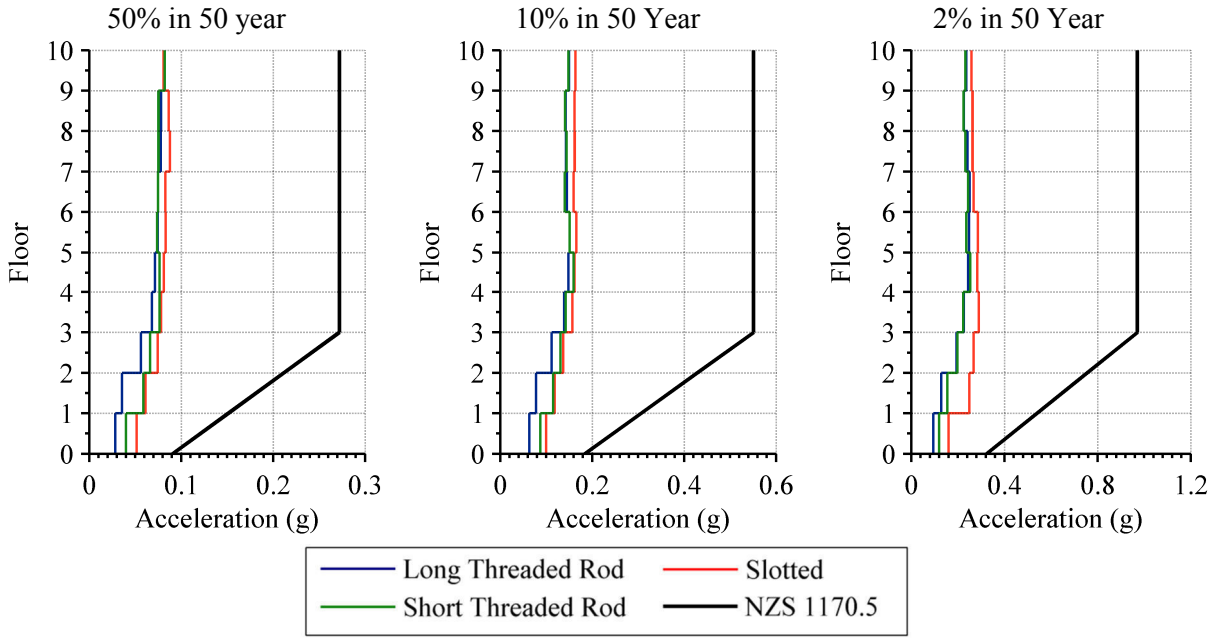

Figure 6-43: Maximum cladding connection acceleration envelopes compared with design acceleration envelope provided by NZS 1170.5 (2004)

Also shown is the mean envelope calculated using NZS 1170.5 (2004). This is found by taking the mean PGA for each ground motion and multiplying this value by the acceleration coefficient. Evidently, the use of Section 8 of NZS 1170.5 (2004) provides a conservative estimation of the cladding connection accelerations. Consequently, the use of a part response factor allows for the corresponding force to be reduced when the ductility of the cladding can be assured. For all of the three intensity levels and connection types, the accelerations NZS 1170.5 (2004) suggests are approximately three times greater than what was measured.

As shown in Figure 6-43, the maximum connection accelerations occurred in the top five floors of the structure. The mean of the maximum connection accelerations in the third and tenth floor of the structure are presented in Figure 6-44 for the nine different earthquake intensity levels. It can be seen that the connection acceleration is not highly dependent upon the connection type. The 50 mm slotted connection does cause greater accelerations than the other connections, but this difference is only apparent in the lower floors. As opposed to the significant difference in connection displacements found between the mono panel and dual panel systems, the connection accelerations of mono panel and dual panel systems were found to be of equivalent magnitudes.

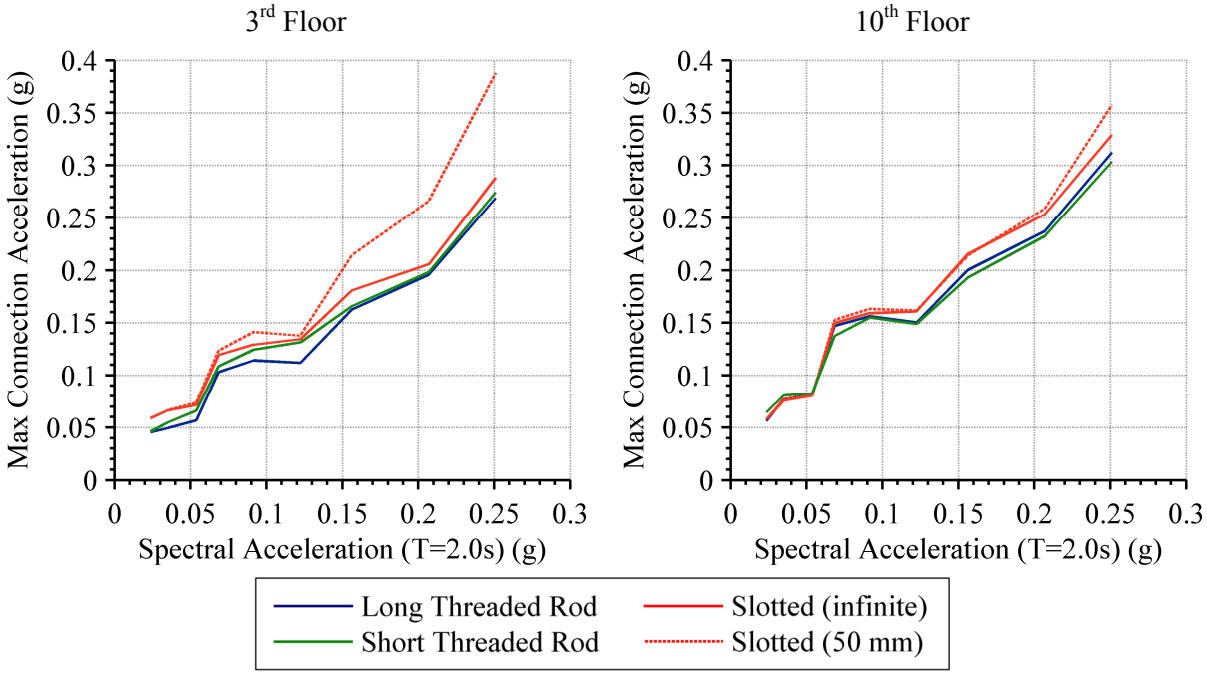

Figure 6-44: Maximum connection acceleration at different earthquake intensity levels

6.6 Conclusions

The numerical cladding system models developed in Chapter 5 were implemented into a model of a case-study reinforced concrete structure. The case-study structure acts as a

design example for the New Zealand Concrete Code for a building designed in Christchurch. A total of 18 frame model configurations with cladding were developed using the seismic response analysis program Ruaumoko2D to understand the effect cladding has upon the response of a structure. The 18 frame models included the three cladding configurations (mono panel, dual panel and fully clad), two cladding models types (quadrilateral and equivalent spring) and three connection hysteretic rules (long threaded rod, short threaded rod, slotted).

The clad frame models are compared to the bare frame model to investigate the cladding-structure interaction. Static push-over analyses showed that the inclusion of cladding increases the base shear by between 3 – 17% depending on the connection typology used. If a long-threaded rod or slotted connection is used, the increase in base shear was found to be less than 5%. However, if the slot length of the slotted connection is exceeded, or short threaded rod connections are used, an increase in base shear of between 14 – 17% can be expected. The inclusion of cladding was found to increase this stiffness of the frame by between 4 – 28%. Again, long threaded rod connections and slotted connections were found to have a minimal effect, increasing the stiffness by less than 7%. An increase in stiffness of 28% was found when short threaded rod connections were used.

The inclusion of cladding accounted for an increase in mass of the structural system of approximately 7%. Since both the mass and stiffness of the structure increased, it was found that the fundamental period of the structure was only slightly reduced; a 4% reduction in fundamental period was found for the inclusion of cladding with short threaded rod connections. The inclusion of cladding in the modal analysis of the structure resulted in the peak displacement reducing by 6 – 7% and the peak floor force increasing by 10 – 13%.

Since the use of seismic response history analyses play a major role in the performance-based assessment presented in this and subsequent chapters, selecting an appropriate representation of the seismic hazard is critical. Probabilistic seismic hazard analysis (PSHA) has been used to define the seismic hazard for this study since it has become the most unanimously adopted method by which seismic hazards are quantitatively assessed. Ground motion selection was subsequently performed to best represent the seismic hazard identified by PSHA using a generalised conditional intensity measure (GCIM) approach. This method was chosen as it allows an increased number of ground motion intensity measures to be considered in the ground motion selection.

A total of 24 frame model configurations with cladding were analysed to understand the effect cladding had upon the dynamic response of the case-study structure. Each of the 24 frame models was subjected to twenty ground motion records (ten earthquakes that include both orthogonal directions) at nine intensity levels.

Similarly to the static analyses, the inclusion of cladding causes an increase in base shear of between 2 – 12%. At low intensity levels, the difference is negligible. Minimal reductions in maximum and residual inter-storey drifts were observed for the clad frame cases. However, the percentage drop of such reductions can be misleading since often the difference is only a couple of millimetres which can be considered to be negligible. The cladding presence also has a negligible influence upon the structure's maximum floor accelerations, regardless of the connection type or earthquake intensity.

Investigation of the maximum lateral displacements demands observed in the cladding connection and cladding panel revealed that the sum of the dynamic displacement demand upon the individual components can exceed the inter-storey displacement demand of the structure. This result goes against the conventional approach that suggests the maximum inter-storey drift defines the maximum displacement demand upon the cladding. It was found that the displacement demand upon the cladding connection and cladding panel typically summed to between 140 – 160% that of the inter-storey frame displacement.

It was also found that the cladding connection acceleration varied from between 80 – 120% of the floor acceleration. This result was not highly dependent upon connection type, intensity level or floor height. This result suggests that the acceleration demand provided by Section 8 of NZS 1170.5 (2004) which multiplies the peak ground acceleration by an acceleration coefficient may be overly conservative for determining in-plane cladding acceleration demands. It should be noted that the accelerations measured were in-plane and typically Section 8 of NZS 1170.5 (2004) is used for determining out-of-plane demands so further research will be necessary to determine if a similar result is observed for out-of-plane behaviour.

Negligible difference was observed between the results of the two cladding model types used (quadrilateral and equivalent spring) which would suggest that both are suitable models for both static and dynamic analyses.

6.7 References

ASCE 31-03. (2003). Seismic Evaluation of Existing Buildings: American Society of Civil Engineers.

Bradley, B. A. (2009). *Structure Specific Probabilistic Seismic Risk Assessment.* Ph.D. Thesis, University of Canterbury, Christchurch, New Zealand.

Bradley, B. A. (2010a). A generalized conditional intensity measure approach and holistic ground-motion selection. *Earthquake Engineering & Structural Dynamics, 39*, 1321-1342.

Bradley, B. A. (2010b). NZ-Specific Pseudo-Spectral Acceleration Ground Motion Prediction Equations Based on Foreign Models: University of Canterbury.

Bradley, B. A., Dhakal, R. P., MacRae, G. A., & Cubrinovski, M. (2010). Prediction of spatially distributed seismic demands in specific structures: Structural response to loss estimation. *Earthquake Engineering & Structural Dynamics, 39*, 591 - 613.

Bull, D. K., & Brunsdon, D. (1998). *Examples of Concrete Structural Design to New Zealand Standards 3101*. Wellington, New Zealand: Cement & Concrete Association of New Zealand.

Carr, A. J. (2010). *Ruaumoko Programme for Inelastic Dynamic Analysis - User Manual*: Department of Civil Engineering, University of Canterbury, New Zealand.

Champion, C., & Liel, A. (2012). The effect of near-fault directivity on building seismic collapse risk. *Earthquake Engineering & Structural Dynamics, 42*(2).

Cornell, C. A. (1968). Engineering seismic risk analysis. *Bulletin of the Seismological Society of America, 58*(5), 1583-1606.

FEMA 450. (2003). NEHRP Recommended Provisions and Commentary for Seismic Regulations for New Buildings and Other Structures. Washington, DC., USA: Federal Emergency Management Agency.

Giberson, M. F. (1967). *The Response of Nonlinear Multi-Story Structures subjected to Earthquake Excitation.* Ph.D. Thesis, California Institute of Technology, Pasadena, CA., USA.

Goodno, B. J., Will, K. M., & Palsson, H. (1980). *Effect of cladding on building response to moderate ground motion*. Paper presented at the Seventh World Conference on Earthquake Engineering, Istanbul, Turkey.

Henry, R. M., & Roll, F. (1986). Cladding-Frame Interaction. *Journal of Structural Engineering, 112*(4), 815-834.

Hunt, J. P., & Stojadinovic, B. (2010). *Seismic Performance Assessment and Probabilistic Repair Cost Analysis of Precast Concrete Cladding Systems for Multistory Buildings*: Berkeley: Pacific Earthquake Engineering Research Center, University of California.

ISO 68-1. (1998). ISO General Purpose Screw Threads - Basic Profile - Part 1: Metric Screw Threads: International Organization for Standardization.

Kutner, M., Nachtsheim, C., Neter, J., & Li, W. (2005). *Applied Linear Statistical Models* (5th Edition ed.). New York, NY., USA: McGraw-Hill.

Mander, J. B., Priestley, M. J. N., & Park, R. (1988). Theoretical Stress-Strain Model for Confined Concrete. *ASCE Journal of Structural Engineering, 114*(8).

MBIE. (2011). Ammendment 11 to Compliance Document for New Zealand Building Code - Clause B1 - Structure. Wellington, New Zealand: Ministry of Business, Innovation and Employment.

Meyyappa, M., Palsson, H., & Craig, J. I. (1981). *Modal Parameter Estimation for a Highrise Building Using Ambient Response Data Taken During Construction.* Paper

presented at the 2nd Specialty Conference Dynamic Response of Structures: Experimentation, Observation, Prediction, and Control, New York, NY., USA.

Montejo, L. A., & Kowalsky, M. J. (2007). CUMBIA - Section and Member Response of Reinforced Concrete Members. Department of Civil, Construction and Enviromental Engineering, North Carolina State University.

NZS 1170.5. (2004). Structural Design Actions, Part 5: Earthquake Actions - New Zealand. Wellington: Standards New Zealand.

NZS 3101. (2006). Concrete Structure Standard - Part 1. Wellington: Standards New Zealand.

NZS 3404. (1997). Steel Structures Standard. Wellington: Standards New Zealand.

Otani, S., & Sake, A. (1974). A Computer Program for Inelastic Response of R/C Frames to Earthquakes. University of Illinois, IL., USA.

Pantoli, E., Wang, X., Chen, M., Hutchinson, T., Meacham, B., & Park, H. (2013). Shake Table Testing of a Full-Scale Five-Story Building: Performance of the Major Nonstructural Components - Egress and Facades *Structures Congress 2013* (pp. 1447-1459): ASCE.

Park, R., & Paulay, T. (1975). *Reinforced Concrete Structures*. New York, NY., USA: Wiley.

PCI. (1989). *Architectural Precast Concrete*. Chicago, IL., USA: PCI Architectural Precast Concrete Manual Committee.

PEER. (2010). Ground Motion Database Retrieved 20 November 2012, from http://peer.berkeley.edu/peer_ground_motion_database/

Prasad, B. K., Morgan, T. A., & Wienskowski, T. (2008). *Near Source Fault Effects on the Performance of Base-Isolated Hospital Building vs. a BRBF Hospital Building.* Paper presented at the Structural Engineers Association of California Convention, Big Island, H.I., USA.

SEAOC. (1995). Performance-based seismic engineering. Sacramento, CA: Structural Engineers Associate of California.

Serway, R. A., & Jewett, J. W. (2009). *Physics for Scientists and Engineers* (8 ed.): Cengage Learning.

Shahi, S. K. (2013). *A probabilistic framework to include the effects of near-fault directivity in seismic hazard assessment.* Ph.D. Thesis, Stanford University, CA., USA.

Shome, N., & Cornell, C. A. (1999). Probabilistic seismic demand analysis of nonlinear structures (Vol. Report No. RMS-35): Stanford University, CA., USA.

Shome, N., & Cornell, C. A. (2000). *Structural seismic demand analysis: Consideration of "Collapse".* Paper presented at the 8th ASCE Specialty Conference on Probabilistic Mechanics and Structural Reliability, 24-26 July, University of Notre Dame, South Bend, IN., USA.

Su, R. K. L., Chandler, A. M., Sheikh, M. N., & Lam, N. T. K. (2005). Influence of Non-Structural Components on Lateral Stiffness of Tall Buildings. *Structural Design of Tall and Special Buildings, 14*(2), 143-164.

Tonkin & Taylor Ltd. (2011). Christchurch Central City Geological Interpretative Report (Version 1.1 ed., Vol. 1): REP-CCC-INT.

Zareian, F., & Krawinkler, H. (2007). Assessment of probability of collapse and design for collapse safety. *Earthquake Engineering & Structural Dynamics, 36*(13), 1901-1914.

7 Quantifying Expected Damage of Multi-Storey Buildings with Heavy Cladding

7.1 Introduction

This chapter extends from the structural response predictions made in Chapter 6 to the performance assessment of traditional claddings in multi-storey buildings. A performance assessment is achieved by calculating the probability of exceeding a specified level of damage for a given ground motion intensity. The specified levels of damage for cladding are determined through experimental observations made in Chapter 4 and correspond to a qualitative description of damage. Both the cladding system components and the structural components are compared against specified demand levels to categorise each as being in a given performance level. In this way, performance levels provide a qualitative assessment of the level of damage by measuring qualitative demands. Performance levels thus provide the ability to determine the direct repair cost and the distribution of direct repair loss for a given level of ground motion.

7.2 Performance-Based Assessment

Performance-based engineering has become a standard norm for research, development and practice of earthquake engineering, particularly after the 1994 Northridge and 1995 Kobe earthquakes (SEAOC, 1995). Performance-based assessment provides a qualitative description of the likely level of damage to a certain level of seismic demand. The qualitative terms or descriptions used are intended to be meaningful to the general public and therefore employ basic terminology (i.e. Operational, Immediate Occupancy, Life Safety and Collapse Prevention). Each performance level is classified through appropriate technically-sound

engineering terms and parameters (Pampanin, 2005). These engineering parameters have to be able to assess the extent of damage (varying from negligible to minor, moderate and severe). Currently this is most commonly done using parameters that measure a structure or components maximum deformation (i.e. inter-storey drift or ductility) (Pampanin et al., 2002). The definition of appropriate engineering parameters to characterise each performance level represents the most critical and controversial phase of performance-based design. (Pampanin, 2005). These engineering parameters (commonly called performance or damage indicators) need to accurately reflect the level of damage in the structure after an earthquake.

This methodology of performance-based assessment can be applied for individual structural members, non-structural components as well as of the whole building system. Assessing the seismic performance of the structural members in addition to the cladding components is vital in order to compare the effect that cladding and its distribution has on the structural performance. Figure 7-1 provides a generic performance matrix with four different performance levels and design actions. The term 'performance level' has been used herein to describe the qualitative damage. This term is interchangeable with the commonly used term 'damage state'.

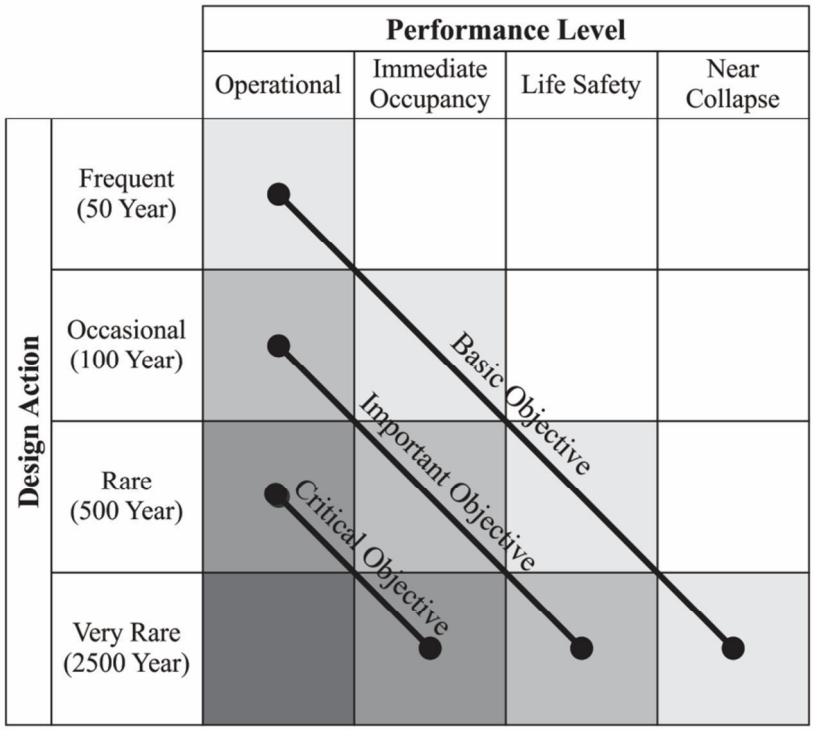

Figure 7-1: Seismic Performance Design Objective Matrix (SEAOC, 1995)

The non-structural performance levels suggested by FEMA P-58-1 (2012) are the following: Operational, Immediate Occupancy, Life Safety and Hazards Reduced. It is

important to distinguish that the level of structural and non-structural damage can be different and hence the structural and non-structural performance levels are not necessarily the same. FEMA P-58-1 (2012) provides a performance based design matrix that combines both structural and non-structural performance levels. This matrix is reproduced in Figure 7-2 along with descriptions for four global performance levels. The four global performance levels represent four recommended target combinations of structural and non-structural performance.

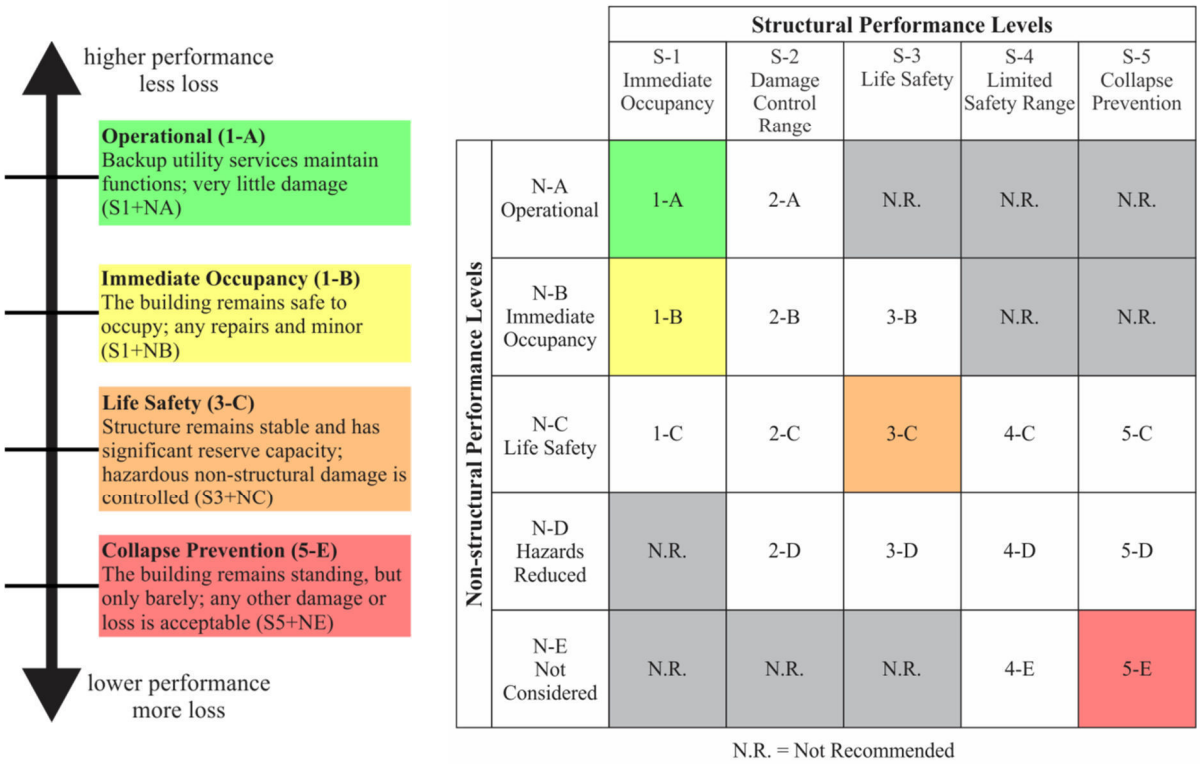

Figure 7-2: Post-earthquake structural and non-structural performance levels (FEMA P-58-1, 2012)

7.3 Performance Levels

The case-study structure introduced in Chapter 6 has been chosen to showcase the seismic performance of the structure and its claddings. A 2D model of the case-study structure was developed using the seismic response analysis program Ruaumoko2D (Carr, 2010). The case-study structure is based on the Red Book building (Bull & Brunsdon, 1998) which acts as a design example of the New Zealand Concrete Code (NZS 3101, 2006).

The structural and cladding performance levels of this case-study structure are identified in this section by use of acceptance criteria provided in literature and found by experimental testing.

7.3.1 Structural Performance

Structural damage is typically quantified by measuring the amount of inelastic deformation that occurs in the frame members. This unrecoverable deformation can be expressed directly in terms of strains, curvatures, rotations or elongations (FEMA P-58-1, 2012). As the building undergoes large lateral displacements, plastic hinges develop in the ends of the beam and column members. The amount of rotation that occurs in these plastic hinges, the plastic rotation, is used to indicate the amount of damage that the frame member has suffered. The maximum plastic rotation demands for beams and columns can be compared to the acceptance criteria provided in FEMA P-58-1 (2012), Table 6-7 (beams) and Table 6.8 (columns), shown below in Table 7-1.

Table 7-1: Acceptance criteria for reinforced concrete beams and columns (FEMA P-58-1, 2012)

Performance Level	Beam Plastic Rotation (rad)	Column Plastic Rotation (rad)
Operational	$\theta_p = 0$	$\theta_p = 0$
Immediate Occupancy	$\theta_p \leq 0.01$	$\theta_p \leq 0.005$
Life Safety	$\theta_p \leq 0.02$	$\theta_p \leq 0.015$
Collapse Prevention	$\theta_p \leq 0.025$	$\theta_p \leq 0.02$

For the numerical modelling of reinforced concrete, the curvature of beam and column members is the primary deformation measurement. The maximum curvature in a member can be related to the plastic rotation using equation (7-1).

$$\emptyset_m = \frac{\theta_p}{l_p} + \emptyset_y \qquad \textbf{(7-1)}$$

where

$\emptyset_m$ = Maximum curvature in member

θ_p = Plastic rotation

l_p = Equivalent length of plastic hinge

$\emptyset_y$ = Curvature at yielding

Because of the many uncertainties associated with the prediction of seismic performance, fragility functions have been developed to express the probability of exceeding the discrete damage limits as a function of the maximum member curvature. The development of the fragility functions was undertaken based on the standardised procedure documented by Porter et al. (2007).

Fragility functions are typically assumed to have lognormal distributions; thus their development involves estimation of the mean and standard deviation that uniquely define the lognormal distribution. The mean for each damage limit is taken as the maximum curvature of the member. These are computed for the case-study structure using Equation (7-1), the plastic rotation limits specified in Table 7-1 and assuming a plastic hinge length of 360 mm and 480 mm for the beams and columns respectively. A standard deviation of 0.4, typical of structural engineering applications is used for all damage limits (Bradley, 2010; Porter et al., 2007).

The fragility function defines the boundary between two performance levels, therefore four fragility functions, or damage limits have been defined for beam and column members; Damage Limit 1 (DL1) defines the transition from Operational to Immediate Occupancy performance levels, Damage Limit 2 (DL2) defines the transition from Immediate Occupancy to Life Safety performance levels, Damage Limit 3 (DL3) defines the transition from Life Safety to Collapse Prevention performance levels and Damage Limit 4 (DL4) defines the exceedance of the Collapse Prevention performance level. The exceedance of DL4 will be described herein as the Failure performance level. The fragility data for the structural members of the case-study building is presented in Table 7-2.

Table 7-2: Curvature damage limits for concrete beams and columns

		Beam Curvature (m^{-1})		Column Curvature (m^{-1})	
		Mean μ	**Standard Deviation σ**	**Mean μ**	**Standard Deviation σ**
Damage Limit	DL1	0.002	0.4	0.002	0.4
	DL2	0.030	0.4	0.012	0.4
	DL3	0.058	0.4	0.033	0.4
	DL4	0.071	0.4	0.044	0.4

The New Zealand Concrete Structures Standard (NZS 3101, 2006) specifies critical material strain limits in potential plastic hinge regions. The corresponding maximum allowable curvature the members are able to sustain can be calculated for the case study building. These were found to be 0.090 m^{-1} and 0.063 m^{-1} for the beams and columns respectively (Bull & Brunsdon, 1998). It can be seen that the damage limit for the Failure performance level is slightly conservative in comparison with the ultimate curvatures obtained from NZS 3101 (2006).

The numerical model incorporates strength degradation into the beams members' hysteretic behaviour that is based on the maximum curvature ductility reached. Strength degradation is initiated at a curvature ductility of 16.6 and decreases linearly to near zero at a curvature ductility of 46.3. These curvature ductilities are found using CUMBIA (Montejo & Kowalsky, 2007) which utilises the model for confined concrete proposed by (Mander et al., 1988).

The fragility functions (or curves) of each component are typically shown graphically using the cumulative probability functions of the log-normal distributions that have been defined for each damage limit (Mander, 1999). The fragility functions for the beam and column members are presented in Figure 7-3.

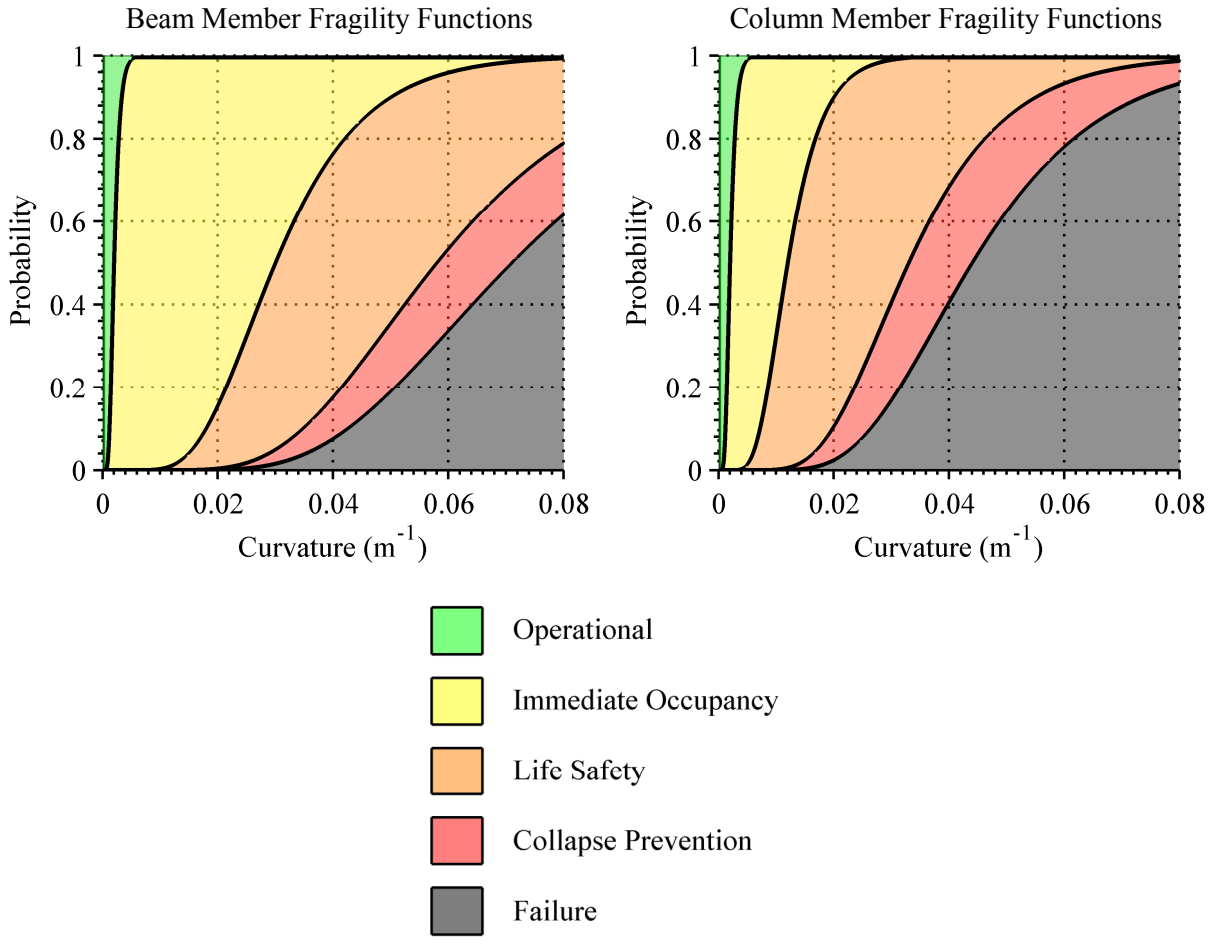

Figure 7-3: Fragility functions for concrete beams and columns

When shown graphically in this way the fragility functions present the probability of being in a given performance level as a function of the engineering demand parameter (EDP), in this case, curvature. The probability of being in the set of performance levels is collectively exhaustive (a member must be in one of the performance levels) and mutually

exclusive (a member cannot be in more than one performance level). Therefore, for a given level of EDP, the probability of being in a certain performance level is the difference between adjacent fragility functions. For example, at a curvature demand of 0.04 m^{-1}, a beam has a 0% probability of being deemed Operational, 24% Immediate Occupancy, 59% Life Safety, 10% Collapse Prevention and 7% Failure.

The distribution of the individual members structural performance is shown graphically using coloured circles at the ends of the beam and column members in Figure 7-4. Each coloured circle represents the performance level of the potential plastic hinge found at each member end. This is shown for a purely hypothetical case so that all of the different performance levels can be labelled.

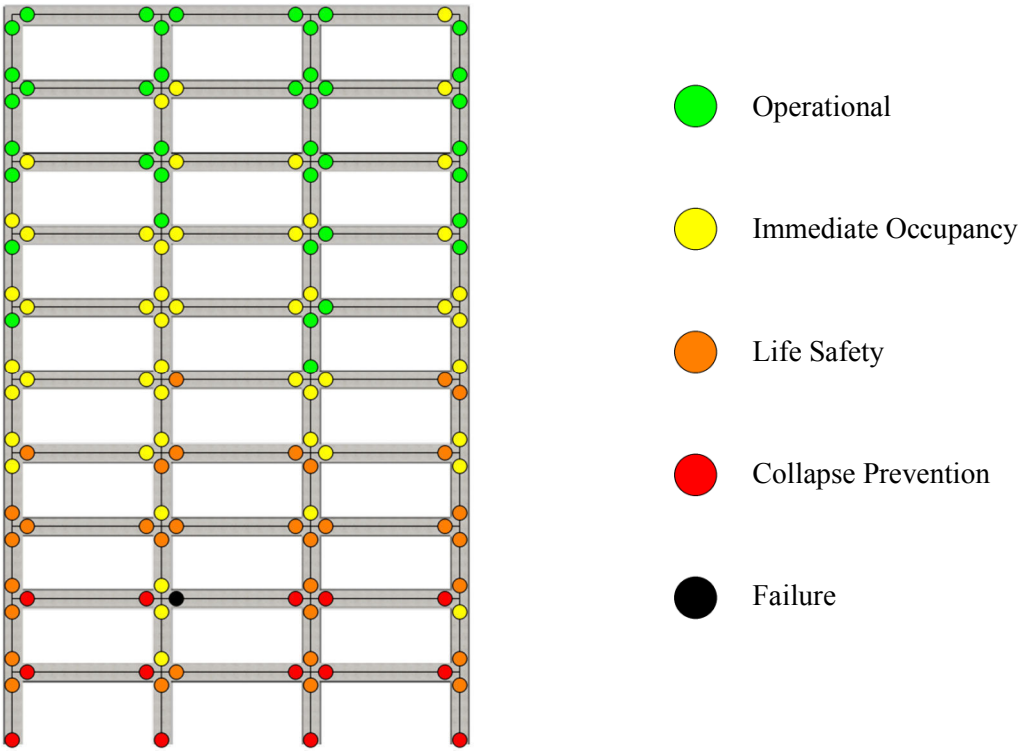

Figure 7-4: Graphical representation of structural performance limits

7.3.2 Cladding Performance

The performance of the cladding connections and cladding panels is determined individually according to the horizontal displacement demand on each component. The horizontal displacement demands are linked to performance levels by strain limits obtained using the Finite Element Models (FEM) verified in Chapter 5 and damage limits determined experimentally in Chapter 4.

The quantification of damage to the cladding system is done so in order to be consistent with the qualitative damage descriptions suggested in FEMA P-58-1 (2012). When considering non-structural performance, the structural performance level 'Collapse Prevention' is instead termed 'Hazards Reduced'. The Operational and Failure performance levels are also not described in FEMA P-58-1 (2012), however their descriptions can be easily identified by being at the ends of the damage spectrum. The Operational performance level corresponds to when the cladding remains undamaged and the Failure performance level corresponds to failure and possible disconnection of the cladding system. A summary of the criteria used for the performance levels of the cladding components tested is given in Table 7-3.

Table 7-3: Adopted cladding component Performance Levels

		Performance Level				
		Operational	Immediate Occupancy	Life Safety	Hazards Reduced	Failure
Cladding Element	Threaded Rod Connections	Undamaged; pre-yield	Connections yield; no observable damage	Visible cracking in connections	Severe cracking in connections; observable loss of cross-sectional area	Rupture of rod
	Slotted Connections	Undamaged; within slot capacity	Slot capacity exceeded; no observable damage	Visible damage to bolt and/or slot	Severe damage to connections	Rupture of bolt
	Cladding Panel	Undamaged; no visible cracks	Minor cracking; less than 0.3mm for SLS	Major cracking; crushing at connections	Some connection failure; no gross failure.	Disconnection of panel

7.3.2.1 Connections

Damage to cladding connections is most easily quantified by measuring the maximum lateral displacement that occurs in the connection. The lateral displacement in the connection is defined by the relative displacement between the cladding panel and the structure. Since the lateral displacement that defines the damage limit will be different for each connection it is necessary to provide a link between the local material damage and the lateral displacement

of the connection. It is proposed to use the strain in the connection as the measurement of the local material damage in the connection.

The same cladding connections as those investigated in earlier chapters have been included in this performance-based assessment; the long threaded rod, short threaded rod and slotted connections. Five performance levels have been identified for threaded rod connections and four for slotted connections. Therefore, four damage limits and fragility functions have been defined for threaded rod connections and three for slotted connections. Descriptions of the performance levels for threaded rod connections are given in Table 7-3. For slotted connection, even though the 'Failure' performance level has been defined, this performance level was not observed during experimental testing up to 3.5% drift so this performance level is not considered in the performance assessment of slotted connections.

7.3.2.1.1 Threaded Rod Damage Limits

Six different threaded rod configurations (three different lengths and two different diameters) were tested to determine their force displacement behaviour (refer to Section 6.2.2.1). The damage limits of each test were identified using the force-displacement data as well as visual observations made during testing.

The first damage limit (DL1) identifies the transition from Operation to Immediate Occupancy performance levels. DL1 was identified as the yield point of the connections and was determined from the experimental data.

Damage limit 2 (DL2) defines the transition from Immediate Occupancy to Life Safety and corresponded to when cracks were observed between the threads of the rods. This plastic deformation was observed around the ends of the rods and occurred parallel to the threads.

Damage limit 3 (DL3) defines the transition from Life Safety to Hazards Reduced performance level and was identified by either cracking perpendicular to the threads or noticeable prying open of cracks parallel to the threaded. The damage limit corresponded to a visual decrease in the cross-sectional area and thus significant reduction in the capacity of the rods.

Damage limit 4 (DL4) defines the transition beyond the Hazards Reduced performance level and corresponded to failure of the connections. A summary of the four damage limit displacements of the six rods tested is presented in Table 7-4.

Table 7-4: Damage limit displacements of threaded rods tested experimentally

	Rod Diameter	12 mm			20 mm		
	Rod Length	50 mm	150 mm	250 mm	50 mm	150 mm	250 mm
Damage Limit (mm)	DL1	0.6	2.2	4.6	0.5	1.2	3.4
	DL2	3.6	6.9	10.9	3.9	7.2	11.0
	DL3	15.9	29.4	45.7	14.6	30.3	43.0
	DL4	26.5	48.0	69.3	22.5	45.0	64.4

In order to determine the damage limits for other possible threaded rod connections of various lengths and diameters, it was necessary to define the damage limits above in terms of the strain in the rod. This was achieved using the finite element models (FEM) developed and analysed in Chapter 5 (refer to Section 5.2.3.1). The maximum strain in the FEM at the corresponding damage limit displacement was recorded for each of the damage limits and for each rod size tested. The maximum numerical strains at the corresponding displacements are presented in Figure 7-5.

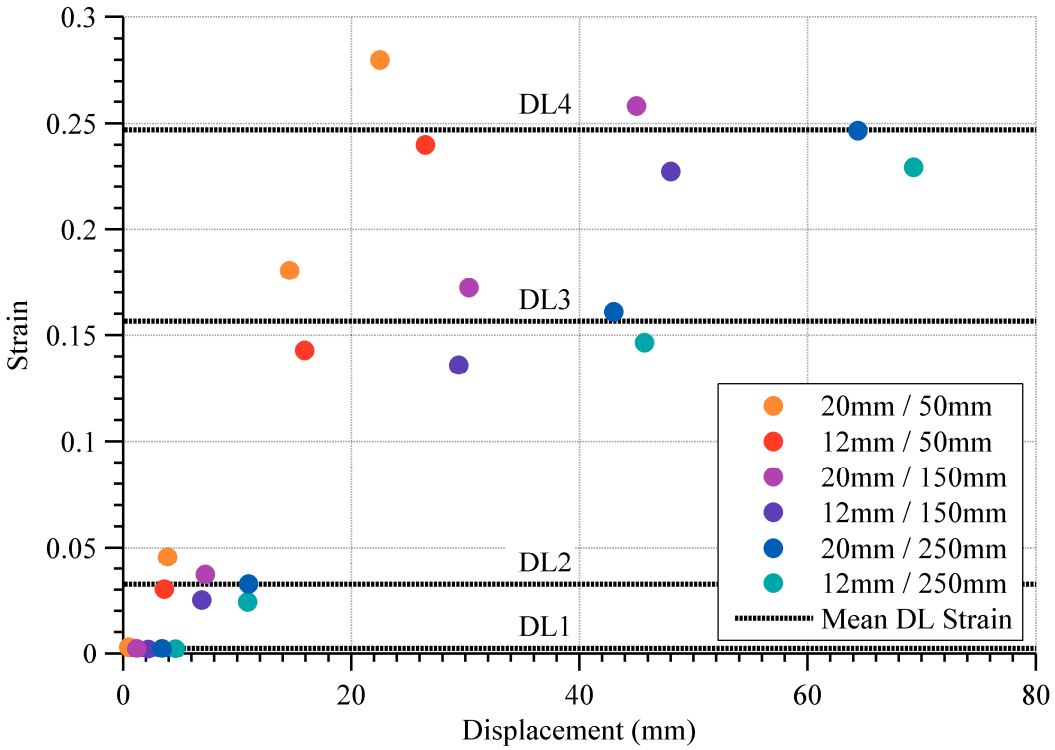

Figure 7-5: Maximum strain in threaded rod based on finite element analysis

It can be observed that the strains at each damage limit are reasonably consistent between the six rod sizes. The higher damage limits (DL3 and DL4) would be expected to

have a more scatter due to the measurements being more subjective, i.e. when cracking becomes 'severe'.

The average strain of the six rods is taken at each damage limit and these values are also presented as horizontal lines in Figure 7-5. These average strains are proposed as defining the damage limit strains for the threaded rods. The standard deviation of the strain data points was found to be range between 0.10 and 0.15. It was decided that greater variability was warranted due to the small amount of data, and hence a standard deviation of 0.20 was assigned for the connection fragility functions. The damage limit data for the threaded rods is provided in Table 7-5.

Table 7-5: Damage limit strains of threaded rods tested experimentally

		Mean μ	**Standard Deviation σ**
Damage Limit	DL1	0.002	0.2
	DL2	0.03	0.2
	DL3	0.16	0.2
	DL4	0.25	0.2

The strain limits presented in Table 7-5 are theoretically only applicable to the numerical model, hence it is useful to link these back to physical parameters to confirm their validity. Upon inspection, the mean strain values found are reasonably consistent with yield and rupture strains for mild steel (Pavlina & Van Tyne, 2008), thus confirming the FEM as a suitable numerical representation of the rods.

The damage limits of a range of rod sizes have been determined using the FEM parametric investigation undertaken in Section 6.2.3.1. The parametric investigation of the threaded rod connections involved varying the rod diameter and length. The diameters of threaded rods analyses were based on commercially available metric sizes. These included 12, 16, 20, 24 and 30 mm diameter rods. The threaded rod length was varied between 50 mm to 500 mm in 50 mm increments. In total, 50 numerical analyses were performed.

The maximum strain in the threaded rod was compared to the lateral displacement for each analysis. The displacement damage limits could therefore be determined for each of the four strain damage limits given in Table 7-5. The displacement damage limits for each of the four damage states are presented as charts in Figure 7-6 for the range of rod sizes analysed.

The displacement damage limits for threaded rods can subsequently be found using the charts in Figure 7-6. Rods of 24 mm diameter are required to resist the actions of the mono

panel and rods of 20 mm diameter are required to resist the actions of the dual panel. Two threaded rod lengths have been considered: 50 mm and 250 mm. The corresponding four damage limit displacements of these four rod sizes are presented in Table 7-6.

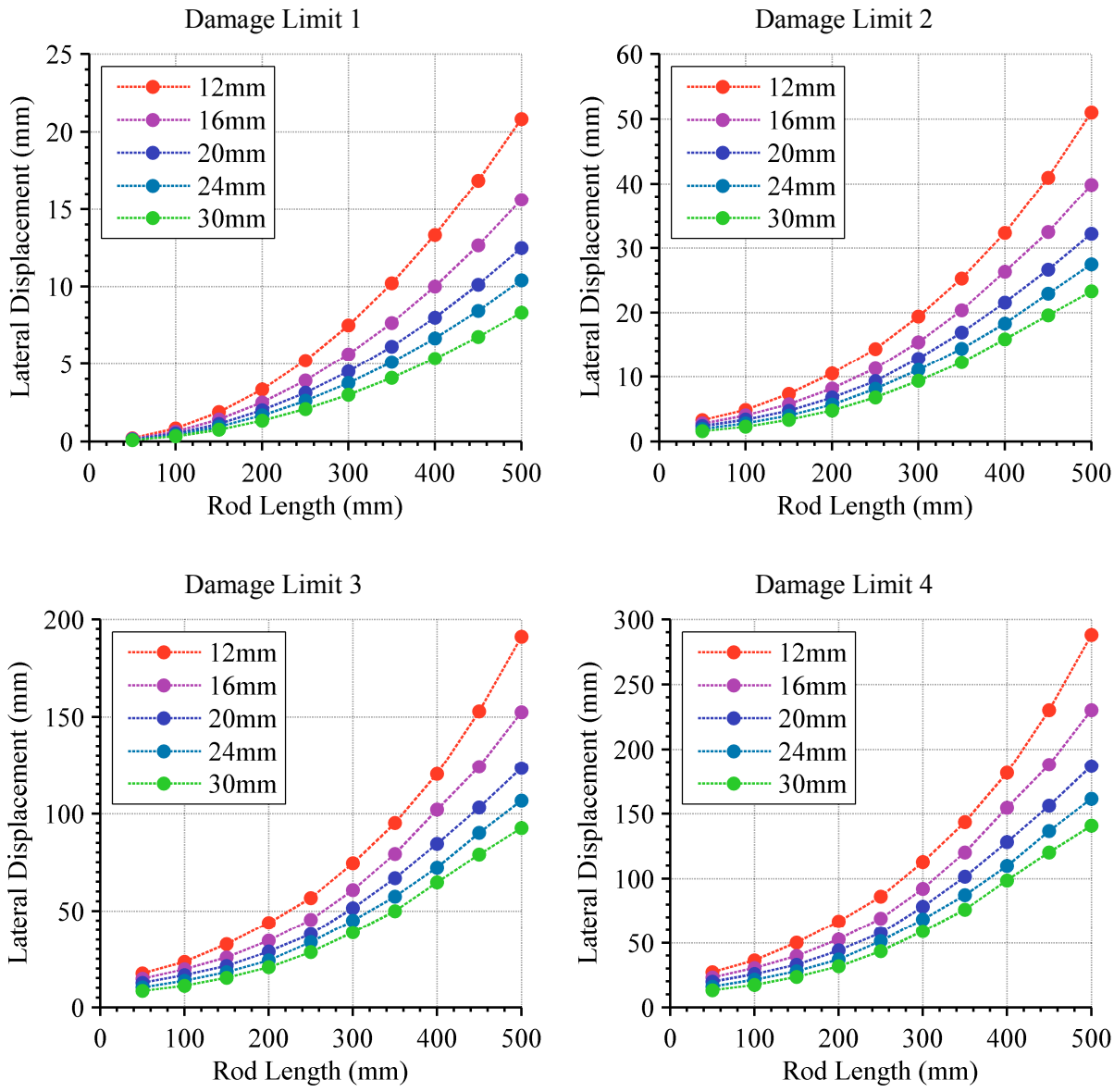

Figure 7-6: Displacement damage limit charts for threaded rods

The fragility functions of the four rod sizes are developed using the damage limits presented in Table 7-6, also assuming a standard deviation of 0.2. The fragility functions of the four rod sizes are shown in Figure 7-7 (note the lateral displacement axis varies between rod lengths).

Table 7-6: Damage limit displacements of case-study threaded rod connections

	Rod Diameter	20 mm		24 mm	
	Rod Length	50 mm	250 mm	50 mm	250 mm
Damage Limit (mm)	DL1	0.5	3.2	0.4	2.6
	DL2	2.3	9.3	1.9	8.1
	DL3	12.7	37.9	10.2	33.6
	DL4	19.8	57.7	16.0	51.4

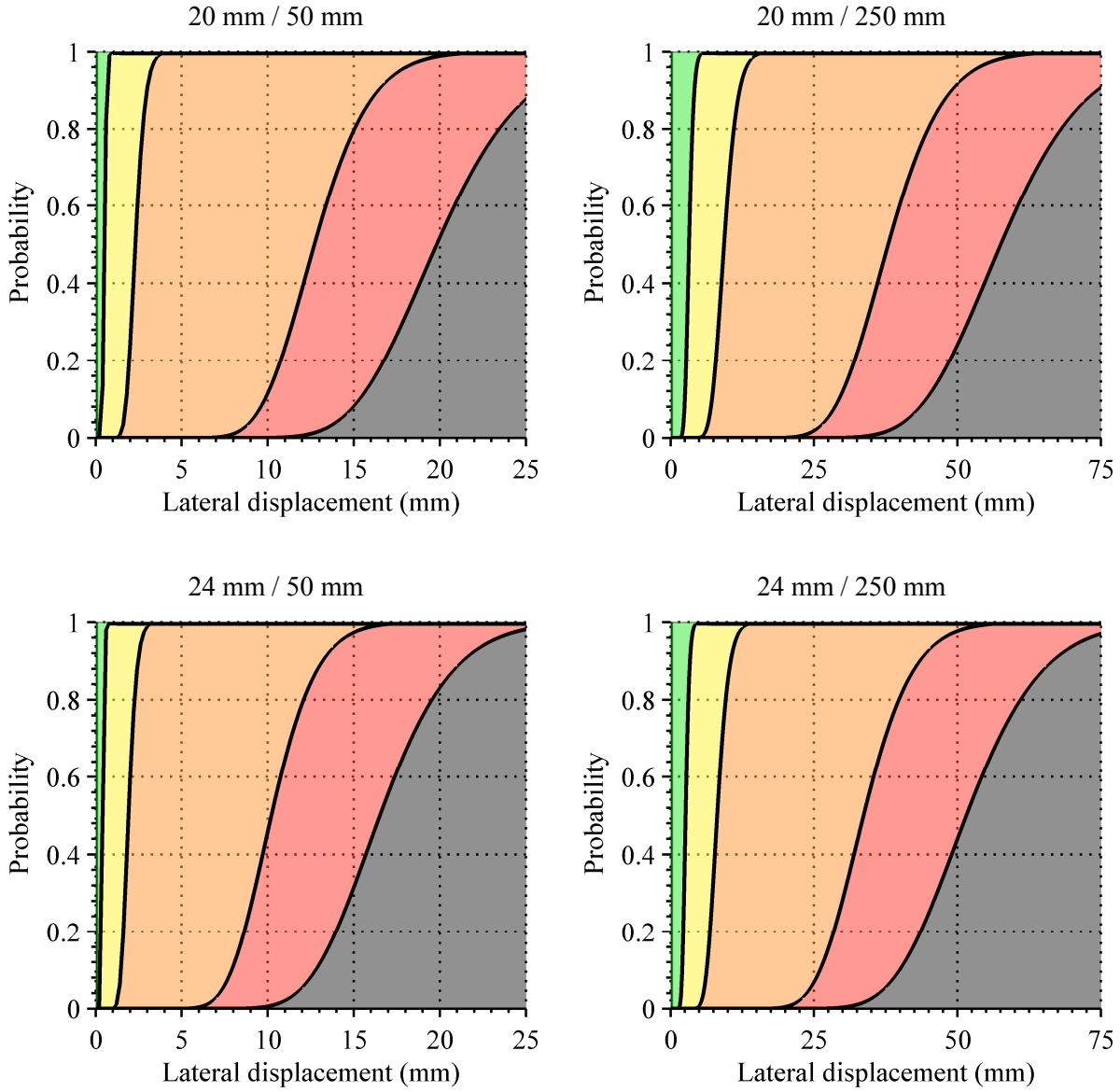

Figure 7-7: Fragility functions for case-study threaded rod connections

7.3.2.1.2 Slotted Connection Damage Limits

Both slotted connection models developed in Chapter 5 are included in the numerical response analyses. This includes the simplest slotted connection model of infinite slot length and the model of a restricted slot length. The infinite slotted connection requires the

definition of the friction force only. The finite slotted connection is deemed to have a slot length of ±25 mm. For a 20 mm bolt this would correspond to a 70 mm long slot. The displacement behaviour beyond the slot length is defined by the threaded rod connection model for a 24 mm diameter rod of 50 mm length. The three damage limit displacements for the slotted connection are presented in Table 7-7. A standard deviation of 0.2 has also been used to define the uncertainty of each damage limit. DL4 has not been considered since the Failure performance level was not determined during experimental testing.

Table 7-7: Damage limit displacements of slotted connections

		Mean μ	Standard Deviation σ
Damage Limit (mm)	DL1	25.0	0.2
	DL2	26.9	0.2
	DL3	35.2	0.2

The fragility functions of the slotted connections are developed using the damage limits presented in Table 7-7 and assume a standard deviation of 0.2. This assumes the same result found during experimental testing of the threaded rods. The uncertainty of DS1 would take into account the uncertainty of whether the bolt was originally located in the middle of the slot. The fragility functions of the slotted connection are presented in Figure 7-8.

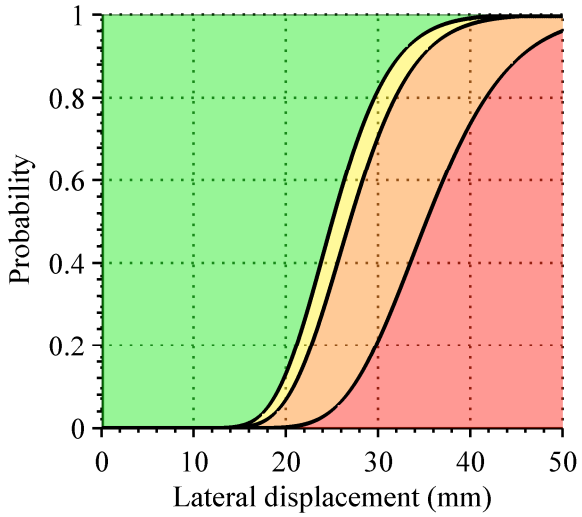

Figure 7-8: Fragility functions for case-study slotted connection

7.3.2.2 Panels

Damage to the cladding panels has been quantified by measuring the maximum in-plane shear deformation that occurs in the panel. The deformation in the panel is defined by

the relative horizontal displacement between the top and bottom of the panel. The displacements identified during experimental testing will be used to define the cladding panel damage limits of the case-study structure. Insufficient data currently exists to propose reliable damage limits based on cladding panel material and geometric properties. The ability to define such damage limits is inherently complex due to uncertainties due to different possible reinforcement configurations and concrete properties, consequently, it was decided that this was outside the scope of this research.

Three performance levels have been identified for the cladding panels. Therefore, two damage limits and fragility functions have been defined. DL1 corresponds to the first visible cracking of the panel. DL2 corresponds to when the maximum crack width for serviceability limit state criteria was exceeded. The New Zealand Concrete Structures Standard, NZS 3101 (2006) Table C2.1 recommends a maximum surface width cracks of 0.3 mm at serviceability limit state for reinforced concrete of exposure classification A2, B1 and B2.

No DL3 or DL4 has been assigned for the precast concrete panels since no damage to the panels was observed during the experimental testing that would have presented a hazard to pedestrians. The damage limits for the two precast concrete panel sizes are presented in Table 7-8.

A standard deviation of 0.4 was used to represent the significant uncertainty of the damage limits. The fragility functions of the two panel sizes are developed using these damage limits and are presented in Figure 7-9.

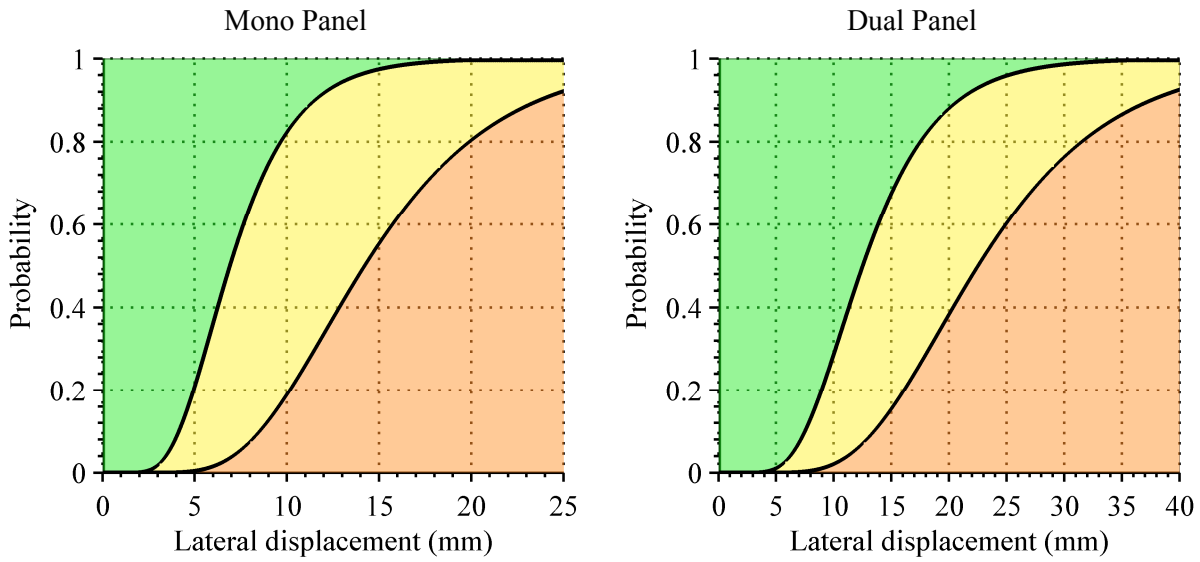

Figure 7-9: Fragility functions for case-study cladding panels

Table 7-8: Damage limit displacements of cladding panels

		Mono Panel		Dual Panel	
		Mean μ	Standard Deviation, σ	Mean μ	Standard Deviation, σ
Damage Limit (mm)	DL1	6.9	0.4	12.5	0.4
	DL2	12.2	0.4	22.5	0.4

7.3.2.3 Graphical Damage Distribution

The performance of the cladding connections and panels are shown graphically in Figure 7-4 for a purely hypothetical mono panel case. The bearing connections are shown in white as they as presumed to have been designed to remain undamaged. Where a connection is deemed to have failed (shown by a black triangle), a cross is also placed over the panel since the panel will have likely fallen from the structure so its performance is less important.

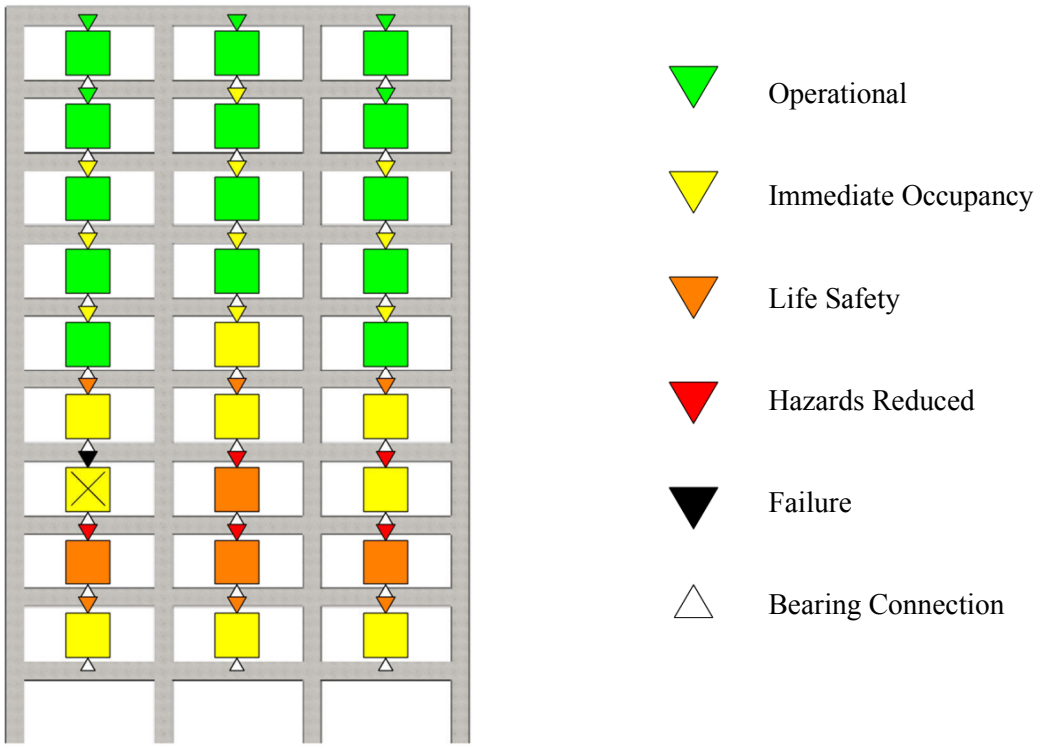

Figure 7-10: Graphical representation of cladding performance limits

7.4 Static Analyses

Adaptive non-linear push-over analyses were undertaken in the previous chapter and are included here to show how the displacement deformation of the structure relates to the quantifiable damage in the beam and column ends.

The initial load pattern used was that prescribed for the equivalent static method in NZS 1170.5 (2004). The pushover behaviour of the bare frame model up to 2.5% drift is presented in Figure 7-11. The frame drifts at which structural performance figures have been developed are also indicated in Figure 7-11 by vertical red dashed lines.

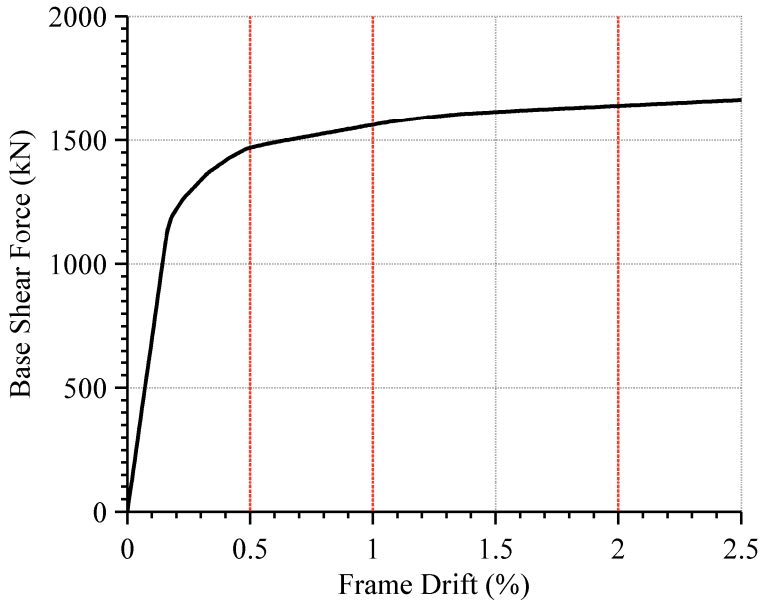

Figure 7-11: Pushover behaviour of bare frame (red drift correspond to limits of structural performance presented graphically in Figure 7-12)

The progressive development of plastic hinges and the increase in plastic rotation can be shown graphically using the structural performance acceptance criteria introduced in 7.3.1. The structural performance of the bare frame at 0.5%, 1.0%, and 2.0% drift are shown in Figure 7-12. It can be seen that at 0.5% drift, the beam ends in the first five floors have all yielded, resulting in some level of plastic rotation less than 0.01 radians, deeming them Immediate Occupancy performance level. At 1.0% drift, plastic hinging is activated at the base of all the columns and has increased to the sixth floor beams. The plastic rotation in the beams in the third and fourth floor has also increased so that the beams are now deemed to be in the Life Safety performance level. At a drift of 2.0%, the beams of the first, fourth and fifth floors are now all deemed to be in the Life Safety performance level. The plastic rotation in the third and fourth floors has exceeded the Life Safety damage limit and as such, the beams are deemed to be in the Collapse Prevention performance level. The overall strength of the frame increases monotonically up to 2.0% drift but can be observed to plateau at this level of deformation. It can also be seen that the columns remain elastic throughout the structure up to 2.0% drift with the exception of the column bases. This result is indicative of a moment-

resisting frame designed using capacity design principles to ensure that the columns are stronger than the beams (Park & Paulay, 1975).

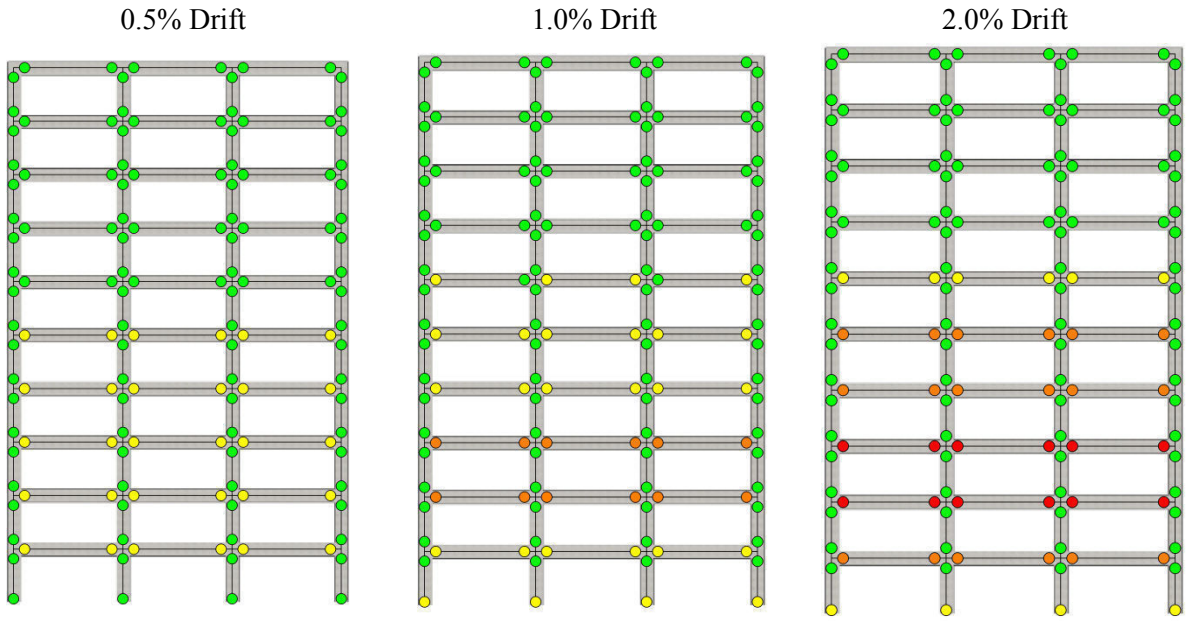

Figure 7-12: Structural performance of beam and column hinges during bare frame push-over analysis

7.5 Dynamic Analyses

The seismic performance of each structural and cladding component has been evaluated by comparing the maximum measured deformations to the performance levels identified in Section 7.3. The maximum measured deformations of the cladding and structure are found from the seismic response history analyses performed in Chapter 6.

7.5.1 Structural Performance

The structural performance to the seismic response analyses has been quantified according to the following engineering demand parameters (EDP): maximum beam and column curvature. This section explores how the inclusion of cladding in the structural model affects these two EDPs. The maximum curvature in each member is compared to the ground motion intensity (measured in terms of SA at 2.0 seconds).

The performance of the individual beam and column components can be identified by comparing the maximum member curvatures to the performance levels identified in Section 7.3.1. These performance levels are shown graphically in the subsequent figures by the colour codes defined previously and repeated in Figure 7-13 for convenience. The graphical limits are defined by the mean of each components fragility function.

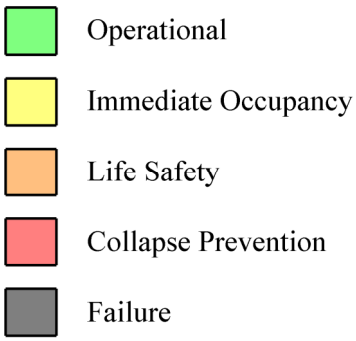

Figure 7-13: Structural performance level legend

7.5.1.1 Bare Frame Behaviour

The bare frame was subjected to each of the twenty ground motions at the nine intensity levels specified previously. The maximum beam curvature in the third and sixth floor was recorded for each ground motion and is presented in Figure 7-14 for the corresponding ground motion intensity. The different intensity levels can be identified by the nine vertical clusters of data points.

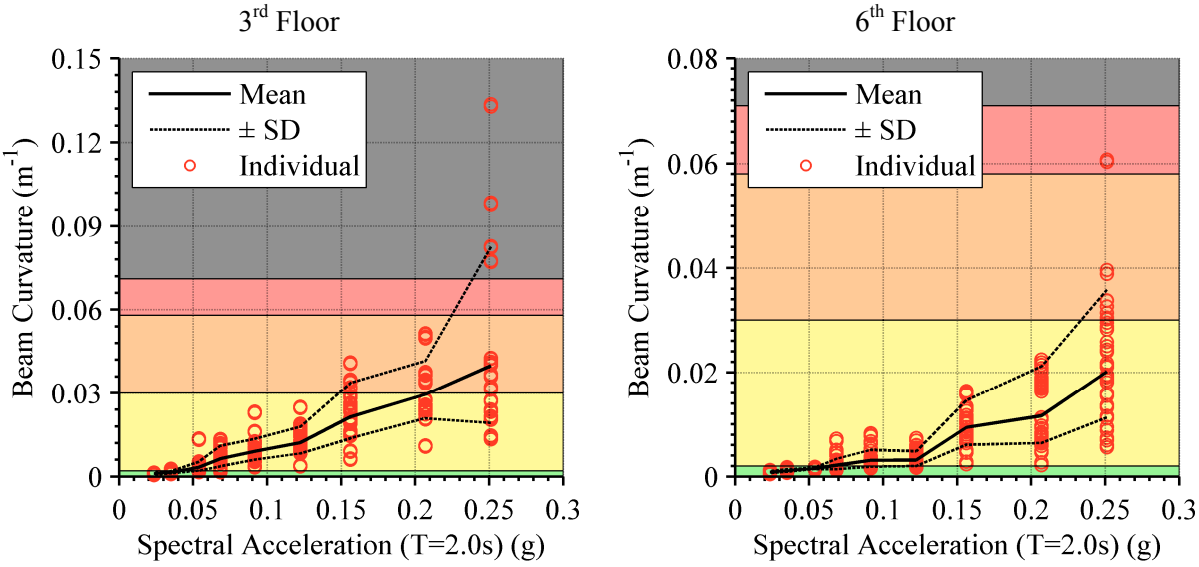

Figure 7-14: Maximum curvature of third floor (left) and sixth floor (right) beams at corresponding spectral acceleration demand for each ground motion

The mean and standard deviation of the maximum member curvatures are found at each intensity level using a lognormal distribution. These are shown using black lines in Figure 7-14. As would be expected, the mean of the maximum beam curvature increases with increasing earthquake intensity level for both floors. Although the general trend of the curvature increasing is the same for the third and sixth floor, the magnitudes of the beam curvatures in the sixth floor are lower than the third floor. This can be inferred by comparing

the data points in Figure 7-14 to the coloured performance levels. Therefore, it can be seen that the beams in the sixth floor are on average less damaged than the beams on the third floor.

In terms of the amount of damage to the beams, it can be seen that up to and including the 10% in 50 year event (SA = 0.122 g), the worst performance level obtained in the 20 ground motions is Immediate Occupancy. Referring back to Table 7-1, this corresponds to the beams having yielded but the plastic rotation being less than 0.01 radians.

At intensity levels greater than the 10% in 50 year event, several Life Safety cases of damage are observed in the third floor beams. However, up to and including the 2% in 50 year event (SA = 0.207 g), there are no cases of the maximum beam curvatures exceeding the Life Safety performance level.

At the strongest ground motion intensity considered, the 1% in 50 year event (SA = 0.251 g), it can be seen that several cases of probable failure exist in the third floor beams. As well as this, beam in the sixth floor also fall into the Collapse Prevention performance level.

Similarly to that for the beams, the maximum column curvatures in the first and third floor were recorded for each ground motion and are presented in Figure 7-15. Again, as expected, the maximum column curvature increases with increasing ground motion intensity. The damage can again be inferred by comparing the data points in Figure 7-15 to the coloured performance levels, which now correspond to the column performance levels identified in Section 7.3.1.

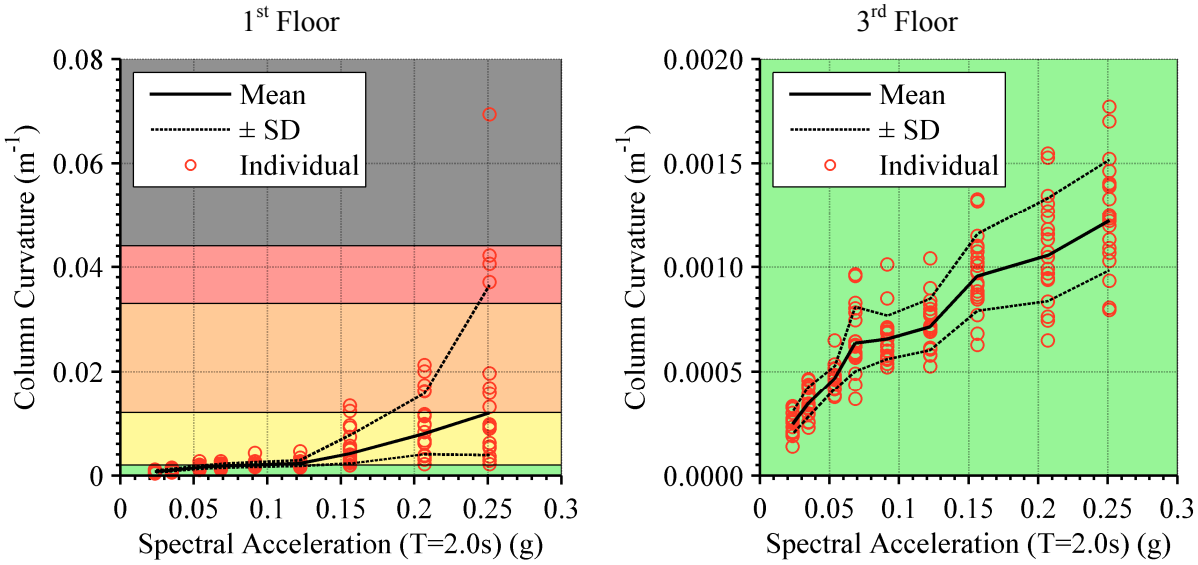

Figure 7-15: Maximum curvature of first floor (left) and third floor (right) columns at corresponding spectral acceleration demand for each ground motion

The major apparent difference between the performance of the beam and column members is the difference in performance between the first and third floor columns compared to the difference between the third and sixth floor beams. As illustrated in Figure 7-15 (right) the third floor columns fall inside the Operational performance level for all of the 180 response history analyses. In fact, upon inspection, none of the column members from the second floor upwards exceed the Operational performance level, i.e. they remain elastic and undamaged. This result is indicative of a moment-resisting frame designed using capacity design principles to ensure that the columns are stronger than the beams (Park & Paulay, 1975). When the structural performance of the first floor column is compared to the beam performance it can also be seen that less damage to the column base should be expected than that found in the beams.

The average distribution of structural damage to the bare frame is illustrated in Figure 7-16 for the three key intensity levels. It can be seen that on average the floors through the middle of the structure have all yielded for all three intensity levels. For the 2%/50 year intensity level it can be seen that significant damage to the beams in the third and fourth floors is expected. Also of interest is that the average level and distribution of damage in the 50%/50 year intensity level is virtually identical to that found for the push-over analysis at 0.5% drift (refer to Figure 7-12). The same is true when comparing the average level and distribution of damage in the 2%/50 year intensity level to the push-over performance at 2.0% drift.

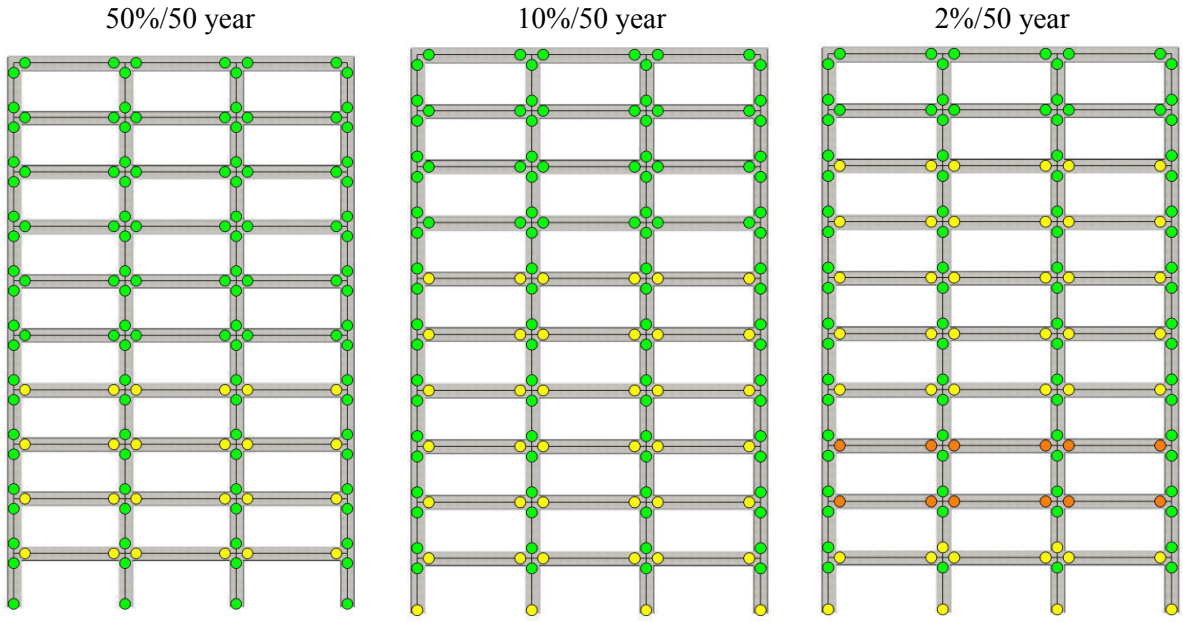

Figure 7-16: Structural performance of beam and column hinges during clad frame push-over analysis

The average distributions presented in Figure 7-16 can be expressed quantitatively as the proportion of damage to the structure. The proportion of damage (or performance) is found by counting the number of occurrences of each performance level throughout the structure for all 20 ground motion records and then dividing this by the number of members and number of ground motions. This proportion of damage is presented in Figure 7-17 and will herein be referred to as the total damage ratio.

The total damage ratio presented in Figure 7-17 shows that the number of beam members that are damaged throughout the structure increases as the ground motion intensity level increases. In comparison, the number of column members damaged does not increase at the same rate. This is due to the damage being isolated to the bottom floor columns.

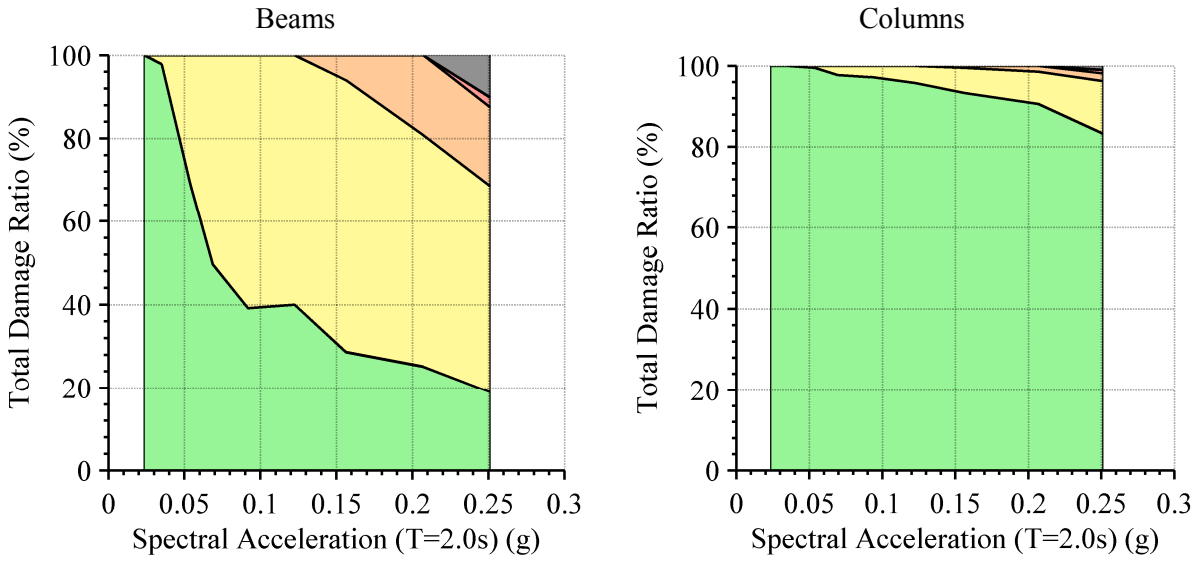

Figure 7-17: Total structural damage ratio in beams (left) and columns (right)

7.5.1.2 Clad Frame Performance

The effect cladding has upon the structural performance is found by comparing the maximum member curvatures of the clad and unclad frames. The mean of the maximum beam curvature in the third and sixth floor and column curvature in the first and third floor are used to compare the structural performance.

The maximum beam curvatures are presented in Figure 7-18 for the bare frame and the fully clad frame configuration for each of the connection types considered. It can be observed that all of the clad frame configurations reduce the maximum beam curvature in both floors of the structure presented here. This reduction in member curvatures agrees with the result found in Chapter 6 that the presence of cladding reduces inter-storey drifts. This is because member curvatures and frame deformation are intrinsically linked. The short threaded rod

connections have a greater influence in the sixth floor for stronger ground motion intensities. This result also agrees with that found in Chapter 6 where short threaded rods were observed to significantly reduce inter-storey drifts in the upper levels of the structure.

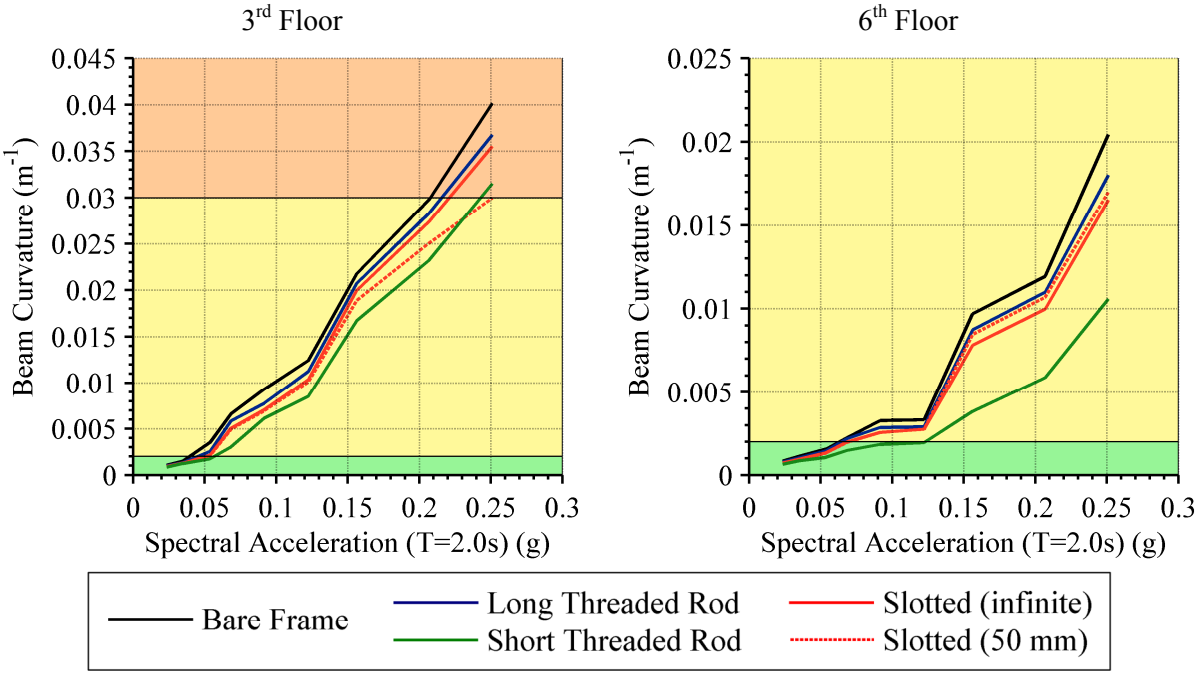

Figure 7-18: Effect of cladding upon maximum curvature of third floor (left) and sixth floor (right) beams at different earthquake intensity levels

Although the maximum beam member curvatures are slightly reduced, when comparing the clad and unclad beam curvatures to the expected performance levels it can be seen that the likely impact this reduction has on the expected performance is minimal. When inspecting the bare frame beam curvature, it the expected performance level for the majority of intensity levels in both the third and sixth floors is Immediate Occupancy. The expected performance level of the beams in the clad cases also appears to be Immediate Occupancy hence, it could be interpreted that the cladding's influence has no real impact upon the expected damage.

However, it must be remembered that the expected damage is based on probability and the transition from one performance level to the next is not defined by a discrete step, i.e. if the maximum beam curvature of a certain beam increases from 0.29 m^{-1} to 0.31 m^{-1} during an earthquake then the beam damage cannot be said to categorically go from being in the Immediate Occupancy performance level to in the Life Safety performance level. Rather, it can be said that the probability of the beam damage being in the Life Safety Performance level increases.

When the maximum beam curvature is found to be at the Life Safety performance level threshold (a maximum curvature of 0.03 m^{-1} that is depicted as the transition from yellow to

orange in Figure 7-18) the probability of the beam damage being either Operational or Immediate Occupancy is 50%. Likewise, the probability of the beam damage being deemed in the performance levels Life Safety, Collapse Prevention or Failure damage state is also 50%.

It is only with the explicit use of the fragility function that the individual percentage probability of each performance level can be computed for a given member curvature. Using the same example of a beam with maximum beam curvature of 0.03 m^{-1}, it can be found using the beam fragility function in Figure 7-3 that the probabilities of being in the Operational, Immediate Occupancy, Life Safety, Collapse Prevention and Failure performance levels are 0%, 50%, 45%, 3% and 2% respectively.

The structural performance level probabilities of the third floor beams for the different cladding connections are quantified and compared to those of the bare frame in Table 7-9. The probabilities are for the 2% in 50 year event (SA = 0.207 g) and are computed from the mean of the maximum beam curvature.

Table 7-9: 3rd floor beam performance in 2%/50 year event (mono panel)

	Operational	Immediate Occupancy	Life Safety	Collapse Prevention	Failure
Bare Frame	0.0%	49.7%	45.5%	3.3%	1.5%
Long Threaded Rod	0.0%	55.8%	40.6%	2.5%	1.1%
Slotted (infinite)	0.0%	59.0%	38.0%	2.1%	0.9%
Slotted (50 mm)	0.0%	67.2%	31.0%	1.3%	0.5%
Short Threaded Rod	0.0%	74.0%	24.9%	0.8%	0.3%

Referring back to Figure 7-18 it can be seen that the mean of the maximum beam curvature for both the unclad and clad frame configurations lie in the Immediate Occupancy performance level for the 2% in 50 year event. As mentioned previously, this result could be interpreted as the cladding having minimal impact upon the expected damage state. However, the performance level probabilities presented in Table 7-9 show that this interpretation is not true. The inclusion of cladding reduces the probability of the beam damage being deemed Life Safety level or worse by between 5 – 24%.

The maximum column curvatures are presented in Figure 7-19 for the bare frame and the fully clad frame configuration for each of the connection types considered. It can be observed that the influence of the cladding upon the maximum column curvatures is negligible. Since the performance of the bare frame column members in the third floor is

deemed Operational for all of the 180 ground motions, the reduction to the maximum column curvature observed in the third floor column does not equate to an improved performance.

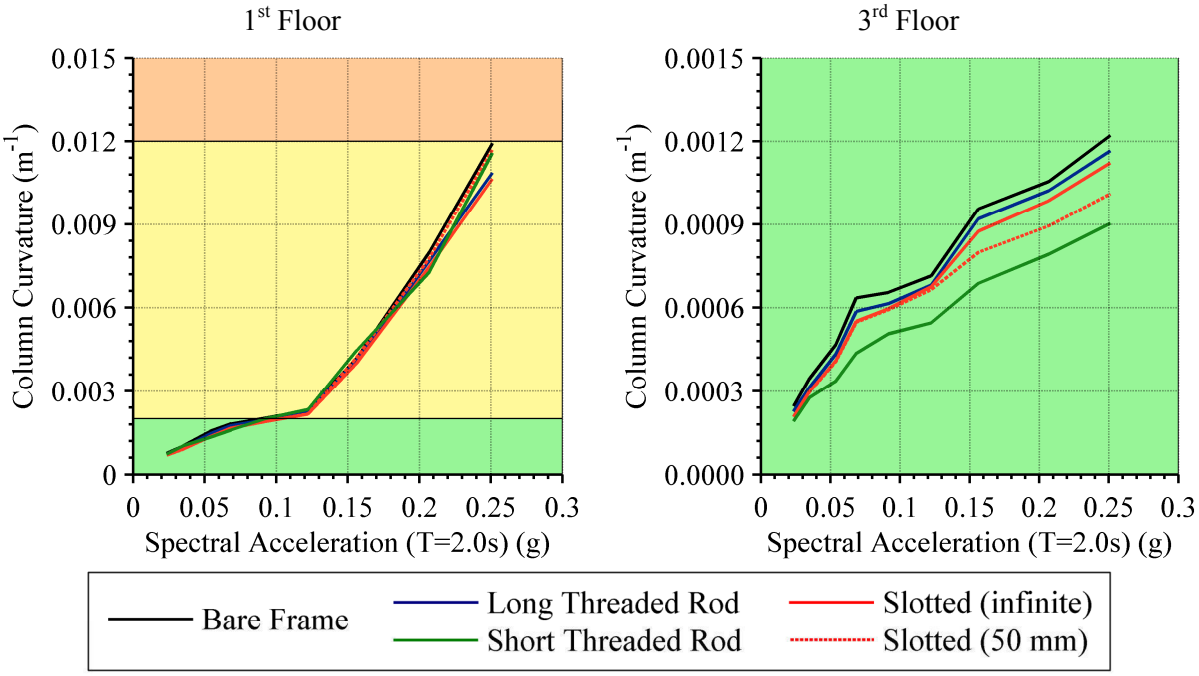

Figure 7-19: Effect of cladding upon maximum curvature of first floor (left) and third floor (right) columns at different earthquake intensity levels

The structural performance level probabilities of the first floor columns for different clad configurations are quantified and compared to those of the bare frame in Table 7-10. The probabilities are for the 2% in 50 year event (SA = 0.207 g) and are computed from the mean of the maximum column curvature.

Table 7-10: 1st floor column performance in 2%/50 year event

	Operational	Immediate Occupancy	Life Safety	Collapse Prevention	Failure
Bare Frame	0.0%	84.5%	15.5%	0.0%	0.0%
Long Threaded Rod	0.0%	86.8%	13.2%	0.0%	0.0%
Slotted (50 mm)	0.0%	88.3%	11.7%	0.0%	0.0%
Slotted (infinite)	0.0%	86.1%	13.9%	0.0%	0.0%
Short Threaded Rod	0.0%	89.5%	10.5%	0.0%	0.0%

It can be seen that the at the 2%/50 year intensity level, the damage to the first floor columns is expected to fall into either the Immediate Occupancy or Life Safety performance level, with approximately 85% likelihood of being deemed Immediate Occupancy. The cladding presence causes a small shift in improvement of the performance probabilities;

however the effect upon the columns is minimal in comparison with the effect upon the beam performance. It can also be seen that in general the performance of the columns is better than the beams, as expected due to the building being designed using capacity design principles (Bull & Brunsdon, 1998).

7.5.2 Cladding Performance

The cladding performance to the seismic response analyses has been quantified for both the cladding connections and the cladding panels. The connection performance is obtained using the maximum lateral connection displacement and the panel performance by the maximum in-plane panel displacement. This section explores the performance of the cladding systems when different cladding connections and panel configurations are used. The maximum displacement in each component is compared to the ground motion intensity (measured in terms of SA at 2.0 seconds).

The performance of the individual cladding components can be identified by comparing the maximum displacements to the performance levels identified in Section 7.3.2. The graphical limits are defined by the mean of each components fragility function. It should be noted that not all of the five possible performance levels exist for every cladding component.

The performance of the cladding connections is assessed at the third and sixth floor in order to compare the expected levels of damage to that of the beam members presented previously. It was also found in Chapter 6 that the third level experienced the largest inter-storey displacements and hence is where the worst damage should be expected. The cladding panel performance is assessed at the third floor only for each cladding system.

7.5.2.1 Long Threaded Rod

The seismic performance of the long threaded rod connections in the third and sixth floor of the mono panel cladding configuration (250 mm long – 24 mm diameter rods) are illustrated in Figure 7-20. The mean and standard deviation of the maximum connection displacement are found at each intensity level using a lognormal distribution. As would be expected, the mean of the maximum connection displacement increases with increasing earthquake intensity level for both floors. Also, on average, the connections are less damaged in the sixth floor than in the third floor.

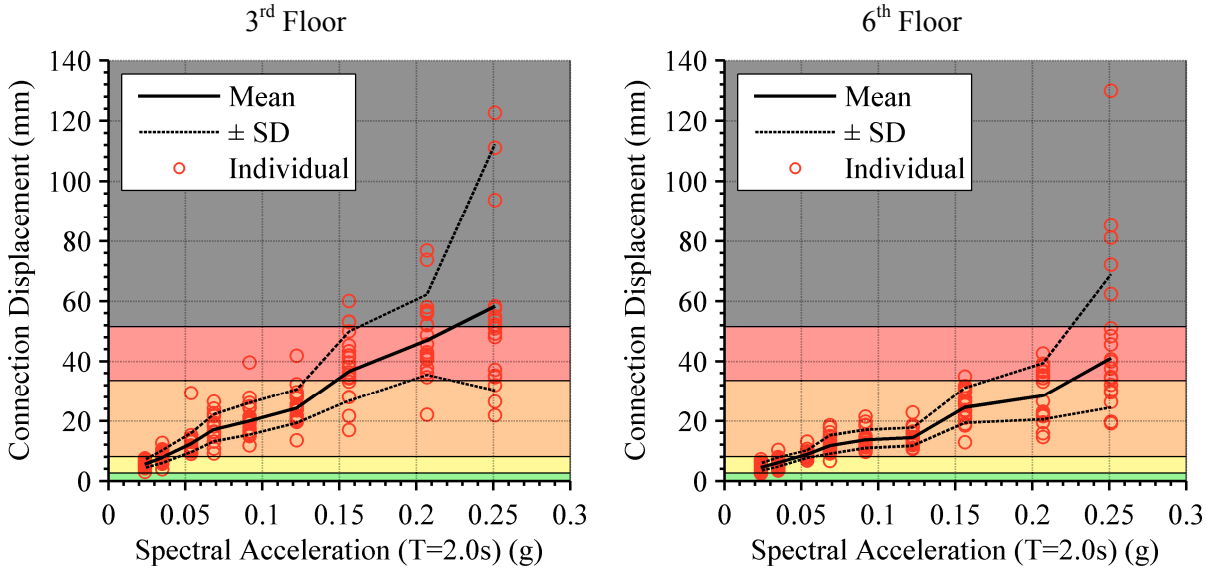

Figure 7-20: Maximum displacement of third floor (left) and sixth floor (right) 250mm/24mm cladding connections for mono panel system

By comparing the individual data points to the coloured performance levels in Figure 7-20 it can be seen that the likelihood of significant levels of damage is high; for all ground motions with a SA greater than 0.054 g (equivalent to the 50% in 50 year hazard level), the third floor connection displacements are all greater than the damage limit that defines the transition from Immediate Occupancy to Life Safety (8.1 mm).

The horizontal changes in coloured performance levels represent the mean of each fragility curve. Hence an individual data point exceeding the damage limit between Hazards Reduced and Failure does not guarantee failure but it can be said that the probability of failure for this connection is greater than 50%. The greater the maximum connection displacement is above this damage limit, the more probable that failure is. It can be seen in Figure 7-20 that cases of connection failure almost certainly exist at the strongest ground motion intensity considered, the 1% in 50 year event. Such cases exist in both the third and sixth floors of the structure. The mean of the maximum connection displacement in the third floor is above this damage limit; hence the probability of a connection failure at this intensity level is greater than 50%.

Similarly to that for the mono panel configuration, the seismic performance of the long threaded rod connections in the third and sixth floor of the dual panel cladding configuration are illustrated in Figure 7-21. It can be seen that the expected level of damage is very similar to that of the mono panel configuration; however a slightly better performance is observed in the dual panel system by comparing the mean of the maximum connection displacements with the coloured performance levels. This slightly better performance is a combination of

both the connection displacements being smaller in the dual panel system compared to the mono panel system as well as the damage limits being slightly higher for the dual panel connections. This is due to the dual panel connections having a diameter of 20 mm compared to the mono panel connections which have a diameter of 24 mm.

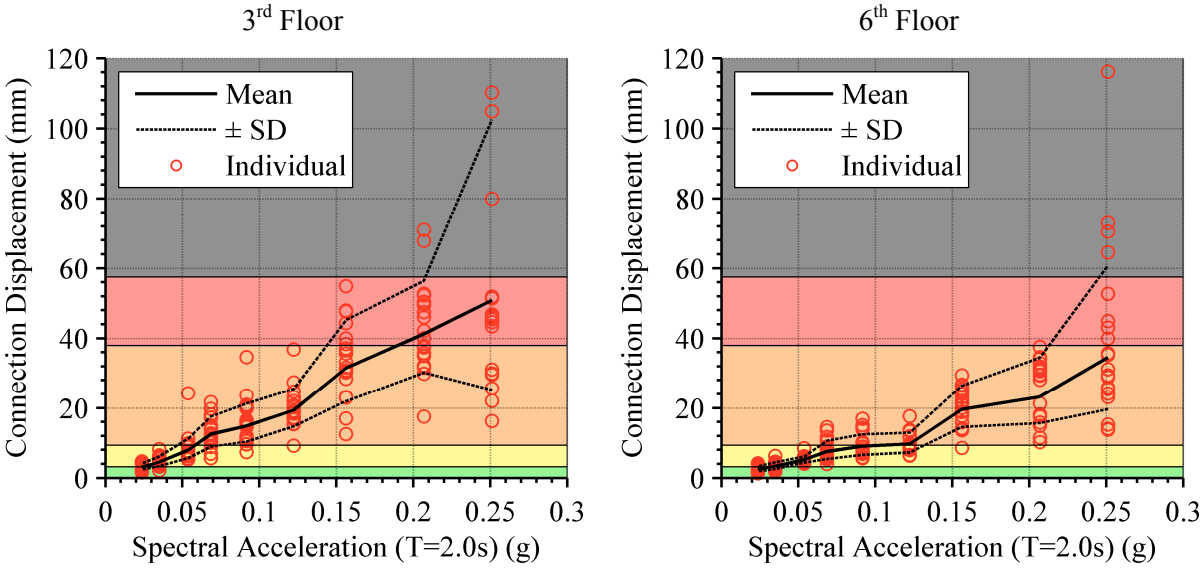

Figure 7-21: Maximum displacement of third floor (left) and sixth floor (right) 250mm/20mm cladding connections for dual panel system

The seismic performance of the third floor cladding panels when connected to the frame with long threaded rods is shown in Figure 7-22. The performance of the mono panel and dual panel configurations are shown by the maximum in-plane panel displacement undergone during each ground motion record.

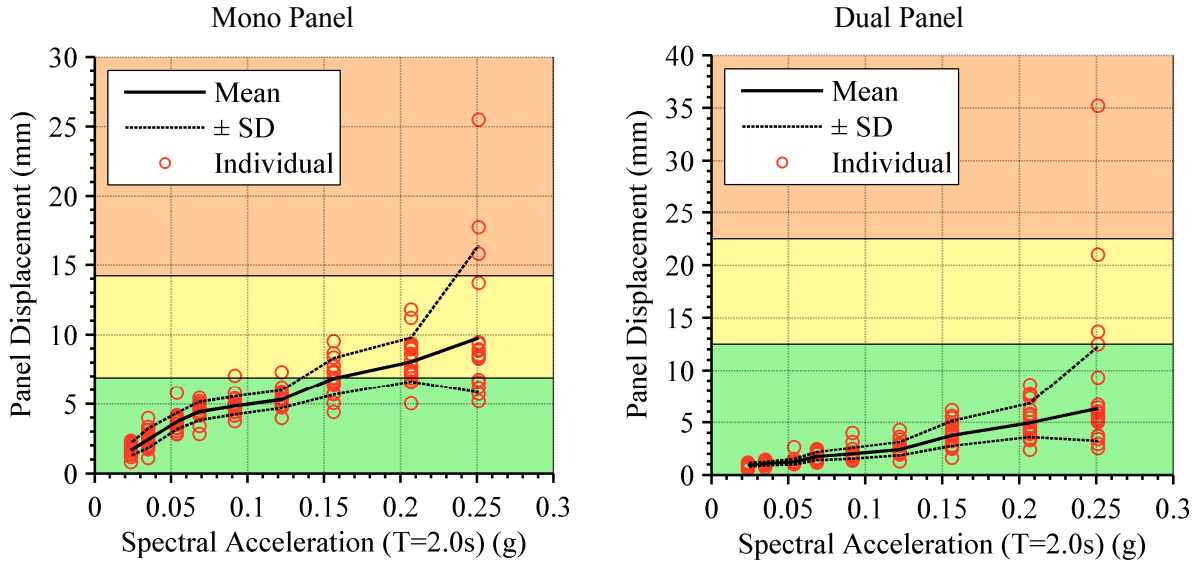

Figure 7-22: Maximum displacement of mono panel (left) and dual panel (right) cladding panels with long threaded rod connections

The mean and standard deviation of the maximum connection displacement are also presented. Only three performance levels have been defined for the cladding panels, with the highest amount of damage considered to be of Life Safety performance. It can be seen that on average, damage to the cladding panel is much less likely to occur than it is to the cladding connections presented previously. Damage to the dual panel system is also very unlikely for all of the ground motion intensities considered, with the exception of the strongest, 1%/50 year intensity level. At this ground motion intensity considered it can be seen that several cases occurred where the panel performance would have likely been considered Life Safety performance.

The average distribution of structural and cladding damage to the mono panel configuration frame is illustrated in Figure 7-23 for the three key intensity levels. The structural performance is virtually identical to that of the bare frame presented previously in Figure 7-16, however, the third and fourth floor beams are now deemed to be Immediate Occupancy the probability of Life Safety or greater damage shifts below 50% for the average 2%/50 year earthquake. The performance of the cladding panels is shown by the coloured squares. It can be seen that the panels remain undamaged in the 50%/50 year and 10%/50 year intensity levels. The cladding connection performance is shown by the coloured triangles above the cladding panels.

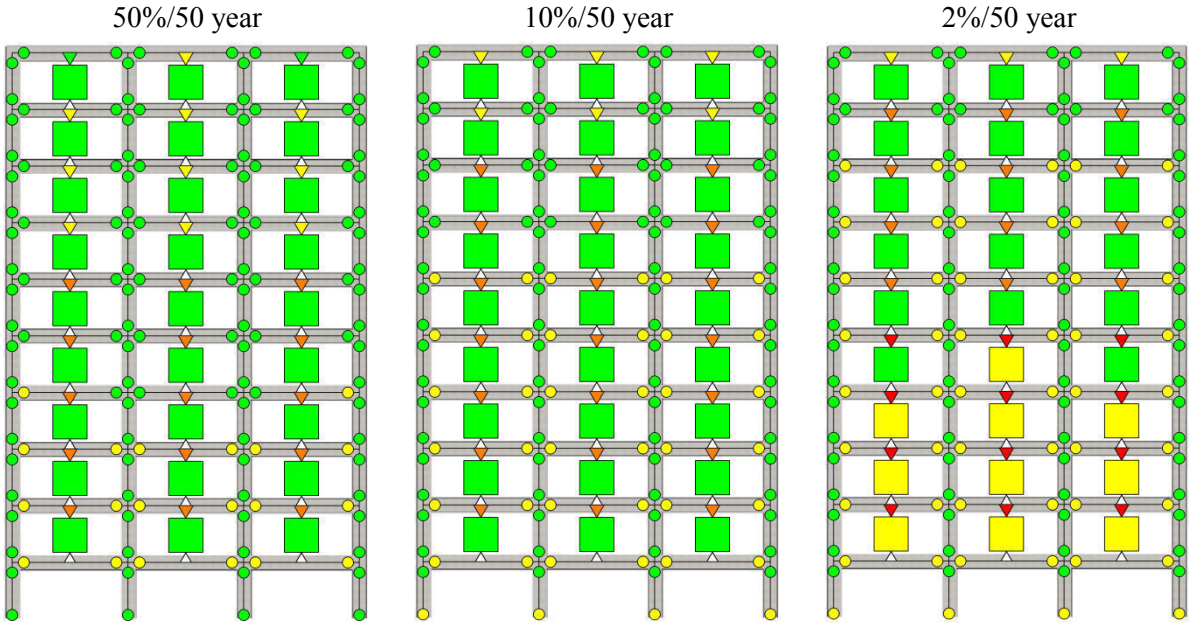

Figure 7-23: Structural and cladding performance with long threaded rod connections

The performance level probabilities of the third floor beams, long threaded rod connections and cladding panels are quantified in Table 7-11. The probabilities are for the

2% in 50 year event (SA = 0.207 g) and are computed from the mean of the maximum component deformations.

Table 7-11: 3rd floor long threaded rod system performance in 2%/50 year event

		Operational	Immediate Occupancy	Life Safety	Hazards Reduced	Failure
Mono Panel Configuration	**Beams**	0.0%	55.8%	40.6%	2.5%	1.1%
	Connection	0.0%	0.0%	4.7%	63.0%	32.3%
	Panel	35.0%	57.2%	7.8%	-	-
Dual Panel Configuration	**Beams**	0.0%	58.0%	38.8%	2.3%	0.9%
	Connection	0.0%	0.0%	33.5%	61.6%	4.9%
	Panel	99.0%	1.0%	0.0%	-	-

It can be seen that all of the components of the dual panel system have better performance probabilities than the mono panel system. The probability of connection failure is significantly reduced by the more flexible connection and the probability of damage to the panel is also virtually nil.

The most apparent difference in Table 7-11 is the significantly higher level of damage expected in the cladding connections compared to the structure for the same level of hazard. Most notably, the probability of failure in the connection is significantly greater than failure of the beams. This result is not irrational, as if the beams fails, then structural collapse may be imminent and the performance of other structural and non-structural components is irrelevant. Conversely, failure of the cladding connections will most likely have no effect upon the performance of the structure. Hence it is entirely practical to expect a lower probability of structural failure than cladding failure. However, the proportion of damage is much less practical. It could also be argued that the consequence of failure of a cladding connection also presents a significantly greater life-safety risk than failure of a beam in a capacity designed structure since significant redundancy in the latter almost certainly exists. The probability of the beams in the third floor being deemed Immediate Occupancy is 56% in a 2%/50 year event, whereas, the probability of cladding connections being in the same performance level is zero. This result tells us that there is a 56% chance that the structure will be able to be occupied without the need for structural repair, but that repair of the cladding is essentially a certainty.

The misalignment of the structural and cladding performance highlighted in Table 7-11 further reinforces the observations of recent earthquake events that were highlighted in

Chapters 1 and 2. As evident in the results presented in this chapter, with improved structural performance, this misalignment will likely become more apparent and the poor performance of cladding systems more readily exposed.

7.5.2.2 Slotted

The seismic performance of the 50 mm slotted connections in the third and sixth floor of the mono panel cladding configuration are illustrated in Figure 7-24. The mean and standard deviation of the maximum connection displacement are found at each intensity level using a lognormal distribution. In contrast to the five performance levels that exist for threaded rod connections, no Failure performance level has been defined for the slotted connections and hence only four performance levels exist. It can be seen in Figure 7-24 that the displacement at which a slotted connection remains in the Operational performance level is much greater than the threaded rod connections. Consequently, the level of damage expected in the slotted connections is on average less than that expected in threaded rod connections. As would be expected, the connections are less damaged in the sixth floor than in the third floor.

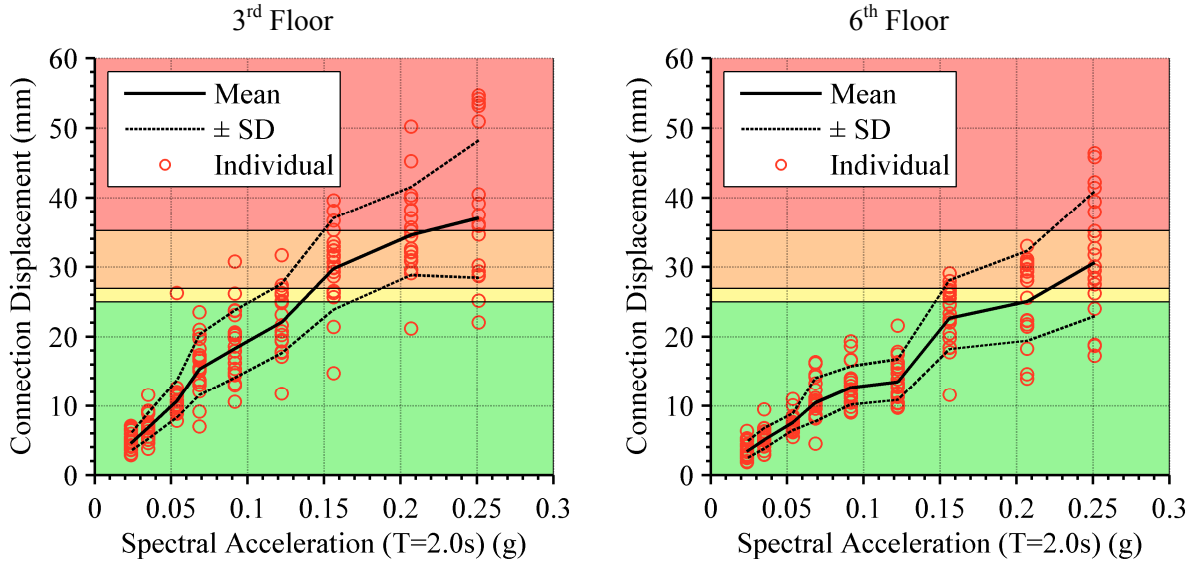

Figure 7-24: Maximum displacement of third floor (left) and sixth floor (right) slotted cladding connections for mono panel system

Similarly to that for the mono panel configuration, the seismic performance of the 50 mm slotted connections in the third and sixth floor of the dual panel cladding configuration are illustrated in Figure 7-25. In contrast to what was found for the long threaded rod connections, it can be observed that the expected level of damage is greater in the dual panel configuration compared to that of the mono panel configuration. The same connection

damage limits exist for both the mono panel and dual panel configurations, consequently, the greater displacements observed in the dual panel system equates to a greater expected level of damage.

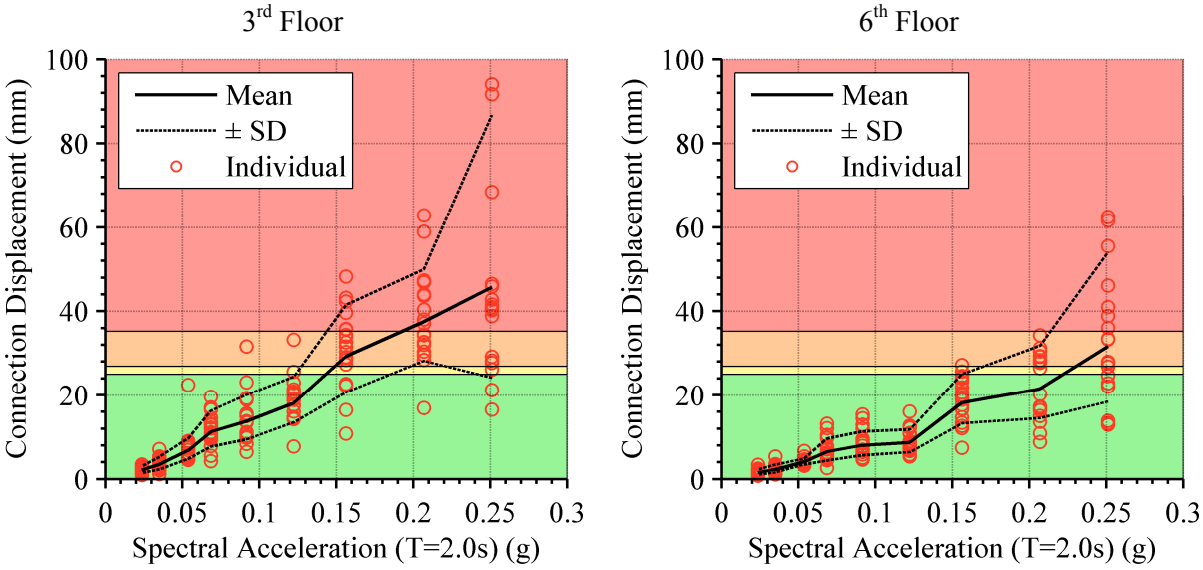

Figure 7-25: Maximum displacement of third floor (left) and sixth floor (right) slotted cladding connections for dual panel system

The seismic performance of the third floor cladding panels when connected to the frame with 50 mm slotted connections is shown in Figure 7-20. The performance of both the mono panel and dual panel configurations is shown.

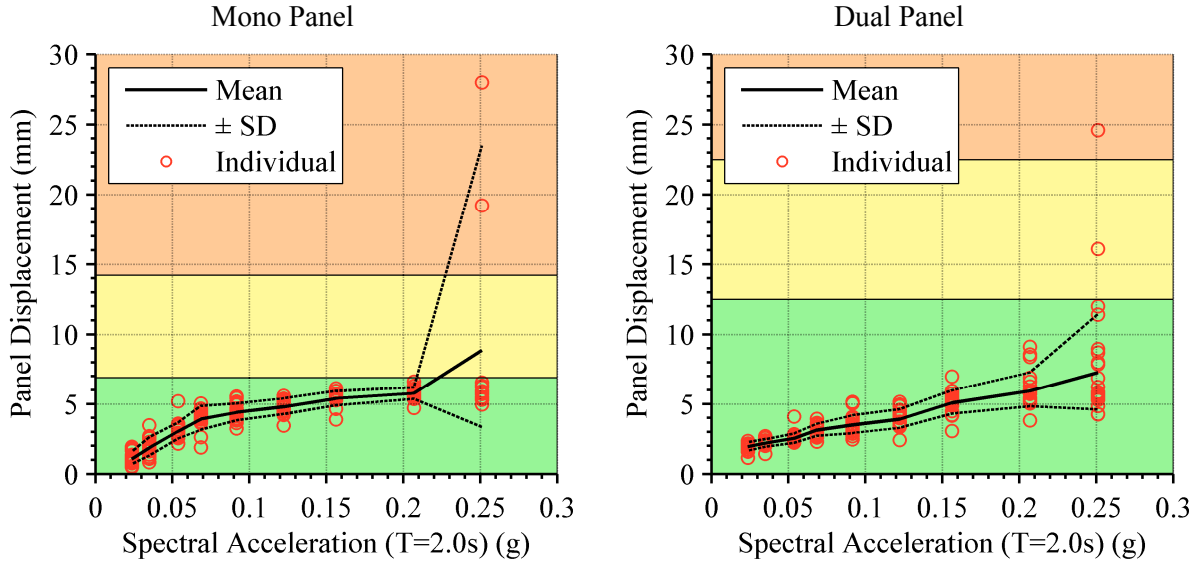

Figure 7-26: Maximum displacement of mono panel (left) and dual panel (right) cladding panels with slotted connections

Similar results are observed for the cladding panel performance to that of the long-threaded rod connections. This is expected since it was found in Chapter 6 that the majority

of in-plane panel deformation is due to the inertia of the panel rather than inter-storey induced deformation. Therefore, because both top connections provide very little in-plane resistance the performance of the panel is not strongly dependent upon the connection.

It can be seen in Figure 7-20 that for the strongest ground motion intensity considered, two ground motions exist that result in significantly greater than average panel displacements. These outliers exist also for the long threaded rod connections but the contrast between them and the average is not as apparent as it is for the slotted connections. The maximum panel displacement is very consistent for all other intensity levels. Upon inspection it is found that the panel displacement outliers also correspond to the two largest observed connection displacements, however, the reason for these large displacements is not clear.

The average distribution of structural and cladding damage to the mono panel configuration frame is illustrated in Figure 7-27 for the three key intensity levels. The performance of the cladding panels is on average deemed Operational for all three intensity levels. Clearly there is less damage expected to the cladding (both the connections and panels) when compared to that observed for the long threaded rod connections Figure 7-23. In general, it would appear that not only is the performance of the cladding better but also the performance of the structure and the cladding is in better alignment than that observed for the long threaded rod connections.

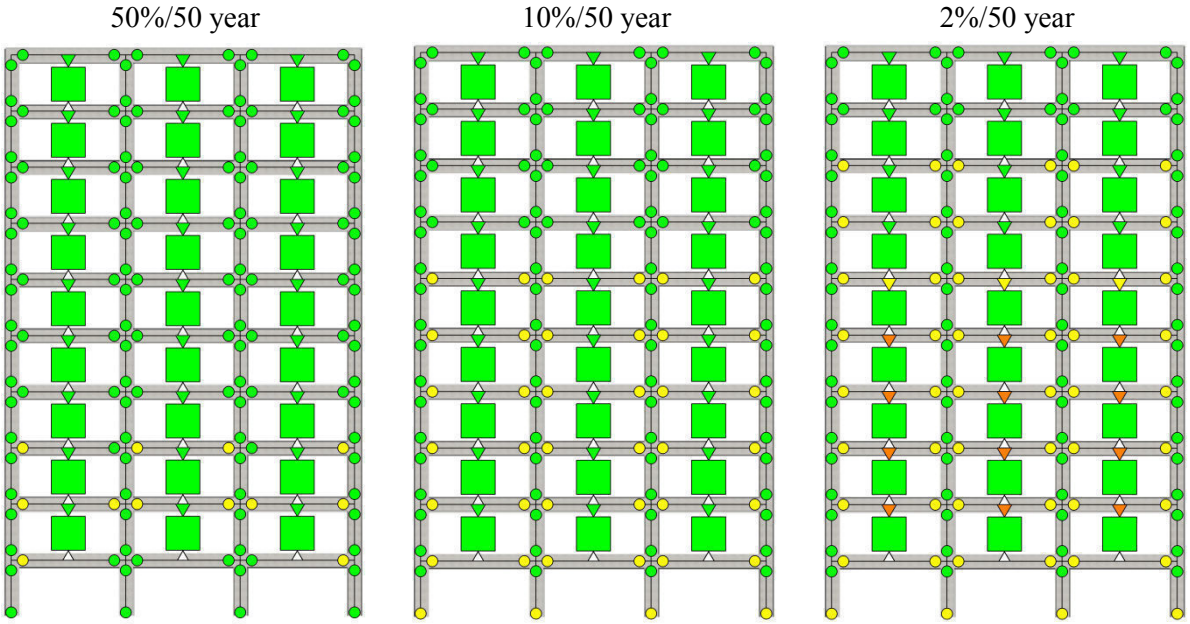

Figure 7-27: Structural and cladding performance with slotted connections

The performance level probabilities of the third floor beams, slotted connections and cladding panels are quantified in Table 7-12. The probabilities are for the 2% in 50 year event (SA = 0.207 g) and are computed from the mean of the maximum component deformations.

Table 7-12: 3rd floor slotted connection system performance in 2%/50 year event

		Operational	Immediate Occupancy	Life Safety	Hazards Reduced	Failure
Mono Panel Configuration	**Beams**	0.0%	67.2%	31.0%	1.3%	0.5%
	Connection	5.2%	5.2%	43.1%	46.5%	-
	Panel	67.4%	31.4%	1.2%	-	-
Dual Panel Configuration	**Beams**	0.0%	60.9%	36.4%	2.0%	0.7%
	Connection	2.1%	2.7%	32.7%	62.5%	-
	Panel	96.9%	3.1%	0.0%	-	-

Table 7-12 confirms that the slotted connections in the dual panel configuration have worse performance probabilities than the mono panel configuration. This is possibly attributed to the increased flexibility of the dual panels compared to the mono panels. However, the performance of the cladding panel in the dual panel system is reduced in the same way that was observed for the long threaded rod connection.

Although no Failure performance level is defined for the slotted connections it can be understood that failure cases can only exist for cases that have been deemed Hazards Reduced. The probability of the long threaded rod connections being deemed either Hazards Reduced or Failed was found to be 95.3% for the mono panel configuration and 68.5% for the dual panel configuration. The dual panel performance is similar but evidently the mono panel performance was significantly better when slotted connections were used.

7.5.2.3 Short Threaded Rod

The seismic performance of the short threaded rod connections in the third and sixth floor of the mono panel cladding configuration are illustrated in Figure 7-28. The mean and standard deviation of the maximum connection displacement are found at each intensity level using a lognormal distribution. It is immediately evident that the level of damage to the short threaded rod connections is significantly greater than both the long threaded rod connections and slotted connections. Failure of the connections is expected much sooner; there is a 50% chance of connection failure for the 10%/50 year intensity level (SA = 0.122 g) in the third

floor. As this intensity level is equivalent to the typical design level intensity for a structure, the failure of the cladding at this intensity would not be acceptable performance.

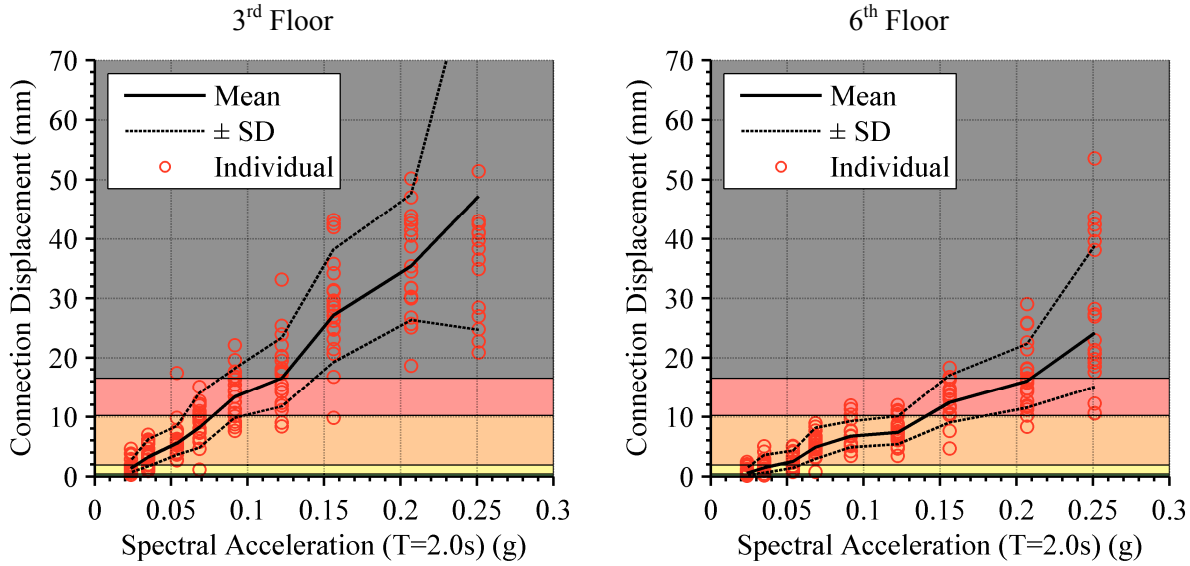

Figure 7-28: Maximum displacement of third floor (left) and sixth floor (right) 50mm/24mm cladding connections for mono panel system

The performance of the short threaded rod connections in the third and sixth floor of the dual panel cladding configuration are illustrated in Figure 7-29. Similarly to that for the long threaded rods, the expected level of damage to the dual panel configuration is very similar to that of the mono panel configuration; however a slightly better performance is observed in the dual panel system.

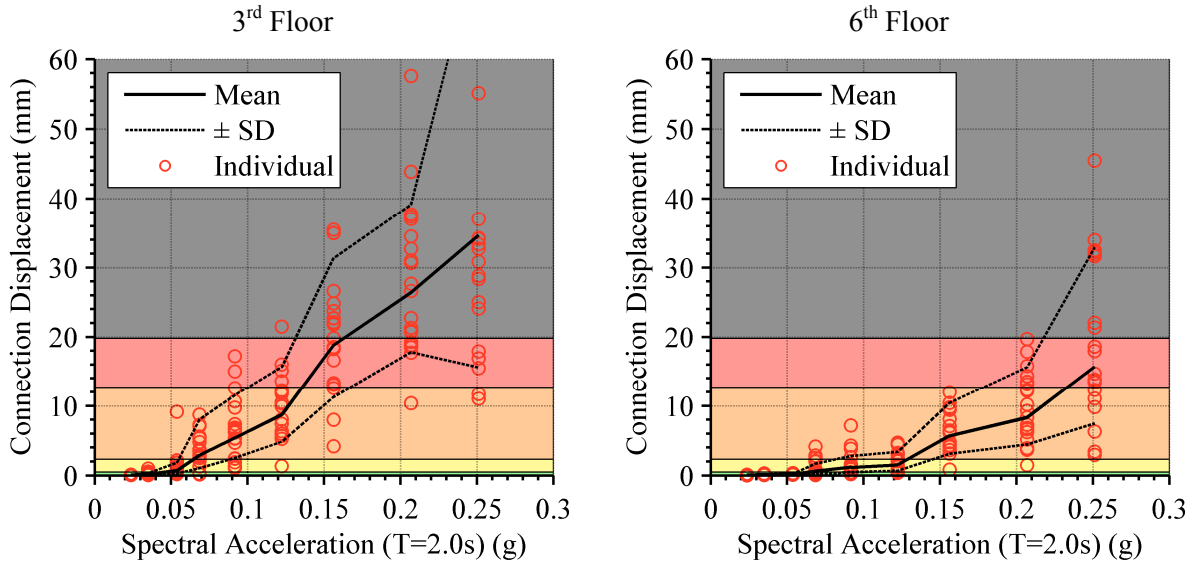

Figure 7-29: Maximum displacement of third floor (left) and sixth floor (right) 50mm/20mm cladding connections for dual panel system

This slight improvement in performance is likely due to the combination of both the connection displacements being smaller in the dual panel system compared to the mono panel system as well as the damage limits being slightly higher for the dual panel connections. In the dual panel configuration there is a 50% chance of connection failure in the third floor at a ground motion intensity of SA = 0.163 g. This is a 34% increase in SA compared to the same probability of failure in the mono panel configuration. The seismic performance of the third floor cladding panels when connected to the frame with short threaded rod connections is shown in Figure 7-30. The performance of both the mono panel and dual panel configurations is shown. The performance of the cladding panels is very similar to that observed when connected with the long threaded rod connections.

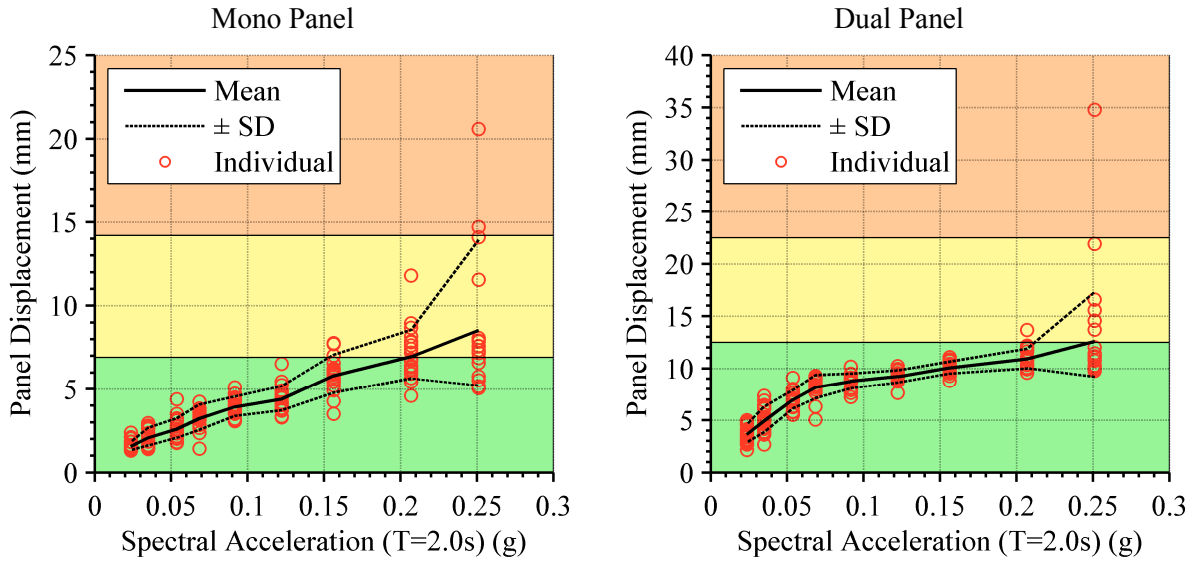

Figure 7-30: Maximum displacement of mono panel (left) and dual panel (right) cladding panels with short threaded rod connections

The average distribution of structural and cladding damage to the mono panel configuration frame is illustrated in Figure 7-31 for the three key intensity levels. The structural performance is virtually identical to that of the bare frame presented previously in Figure 7-16. Somewhat surprisingly, the panel performance is better for the short threaded rod connections compared to the long threaded rod connections (refer to Figure 7-23). However, this result is not significant since several of the short threaded rod connections are on average found to have failed at both the 10%/50 year and 2%/50 year intensity levels. The claddings in the bottom five floors all have a greater than 50% probability of failure during a 2%/50 year earthquake. Such failure could result in the disconnection of the cladding panel which poses a serious life-safety risk to pedestrians.

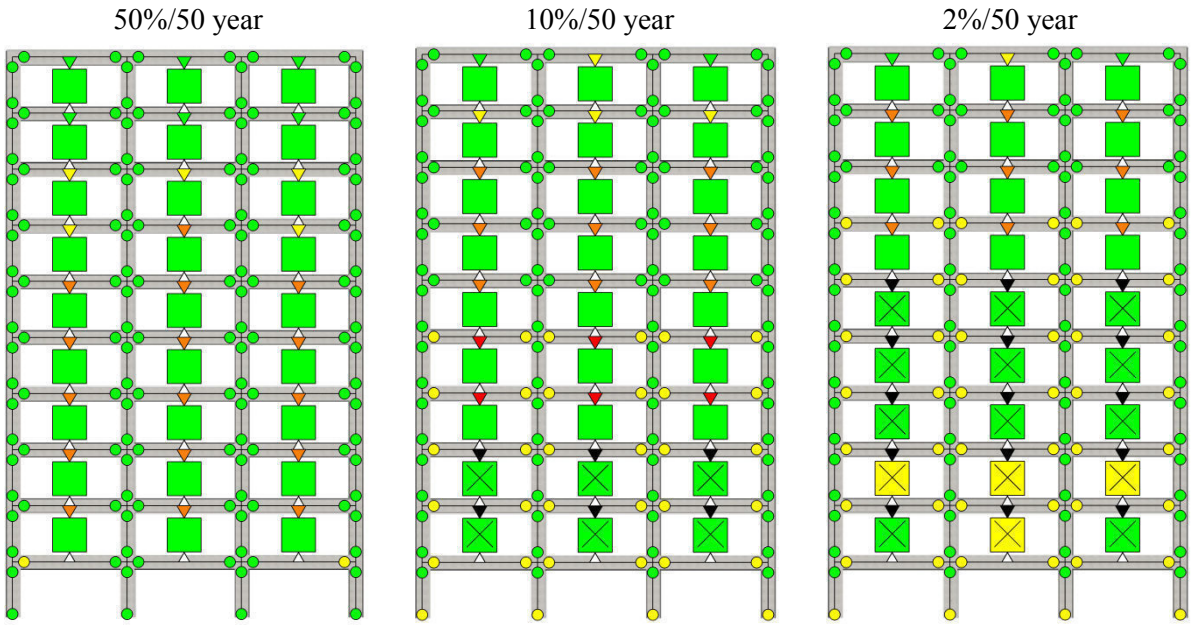

Figure 7-31: Structural and cladding performance with short threaded rod connections

The performance level probabilities of the third floor beams, short threaded rod connections and cladding panels are quantified in Table 7-13. The probabilities are for the 2% in 50 year event (SA = 0.207 g) and are computed from the mean of the maximum component deformations.

Table 7-13: 3rd floor short threaded rod system performance in 2%/50 year event

		Operational	Immediate Occupancy	Life Safety	Hazards Reduced	Failure
Mono Panel Configuration	**Beams**	0.0%	74.0%	24.9%	0.8%	0.3%
	Connection	0.0%	0.0%	0.0%	0.0%	100%
	Panel	49.3%	47.0%	3.7%	-	-
Dual Panel Configuration	**Beams**	0.0%	69.7%	28.8%	1.1%	0.4%
	Connection	0.0%	0.0%	0.0%	7.5%	92.5%
	Panel	63.4%	33.1%	3.5%	-	-

The presence of the cladding connected with short threaded rod connections improves the structural performance compared to the bare frame by the largest amount; the probability of beams being deemed Immediate Occupancy increases by 24.3% and 19.7% for the mono panel and dual panel configurations respectively.

However, the most noticeable result is the conclusive failure of the cladding connections at this ground motion intensity. The maximum connection displacements in the third floor are so large that the short threaded rod connections are deemed to be virtually

guaranteed to fail in both the mono panel and dual panel configuration. Clearly such a result would not be acceptable and nor would it be remotely consistent with the structural performance.

The total damage ratio of the three connection types and cladding panel (mono panel) is presented in Figure 7-17. It can be seen that the damage to the cladding connections, the threaded rods in particular, occurs throughout the structure. This result shows that the damage is not limited to only the middle floors where the maximum inter-storey drifts are found. It is also clearly evident that the long threaded rod and short threaded rod connections are expected to perform much more poorly than the slotted connections and cladding panel.

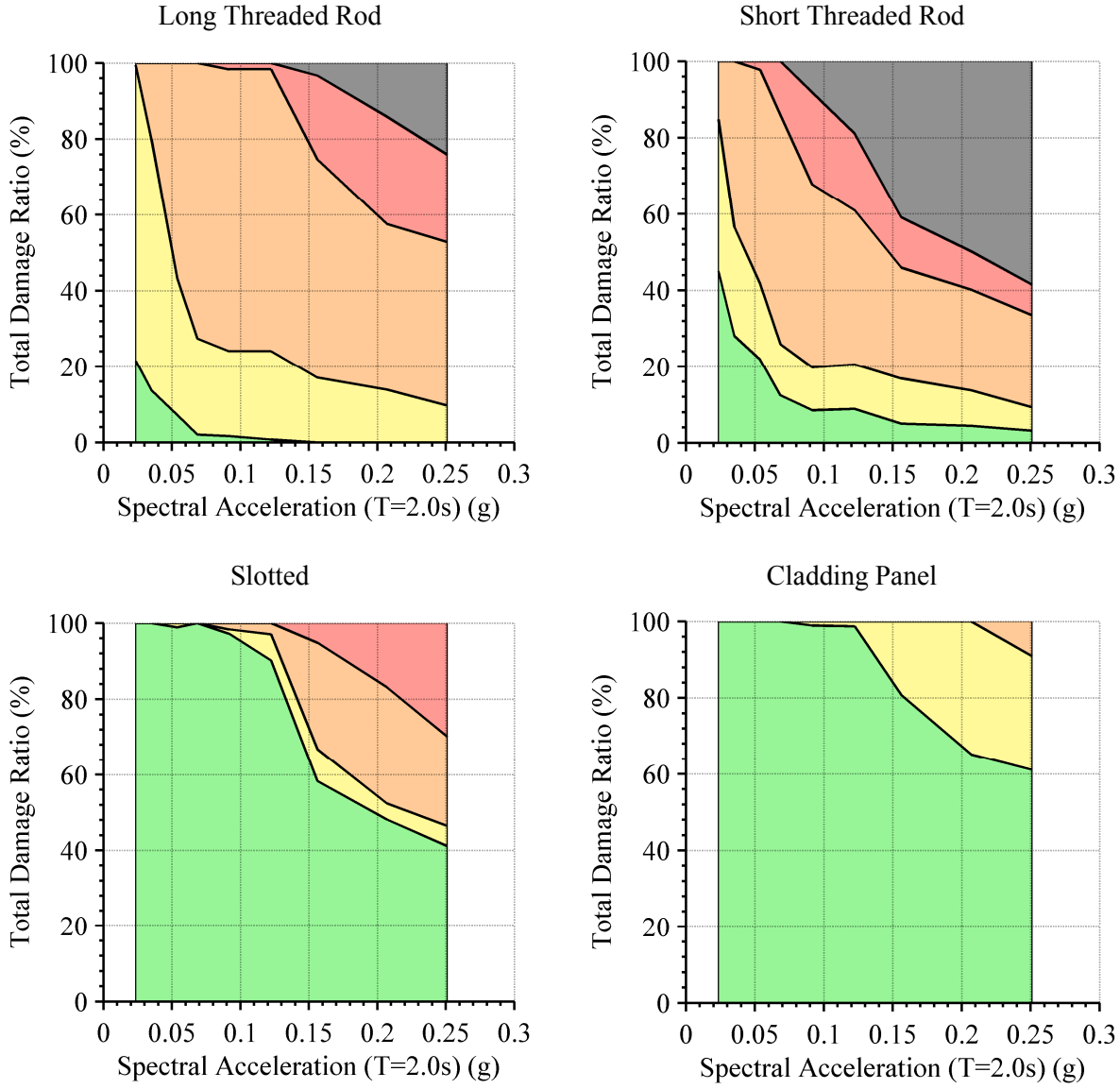

Figure 7-32: Total cladding damage ratio in long threaded rod connections (top left), short threaded rod connections (top right), slotted connections (bottom left) and cladding panels (bottom right)

7.6 Seismic Demand Hazard

The seismic demand hazard is a useful metric in quantifying the seismic performance of a structure because it accounts for both the likelihood of various levels of ground shaking at a site and the relationship between ground shaking and seismic response, including its uncertainty (Bradley, 2012).

The seismic demand hazard provides the probability of an EDP exceeding a specific level of seismic demand. As opposed to an intensity-based assessment (like that presented previously) that considers the seismic demand at a single intensity level, the seismic demand hazard combines the expected seismic demand from a range of possible intensity levels. Also, the seismic demand hazard is not dependent upon the selection of a conditioning intensity measure (here spectral acceleration has been used) like intensity-based assessment is (Bradley, 2013). The seismic demand hazard is therefore defined as the integral of the probability of the EDP exceeding a given demand for a given intensity measure multiplied by the incremental probability of that intensity measure occurring, as shown in Equation (7-2).

$$\lambda_{EDP} = \int_0^{\infty} P_{EDP|IM}(edp|im) \left| \frac{d\lambda_{IM}(im)}{dIM} \right| dIM \qquad \textbf{(7-2)}$$

where

$P_{EDP|IM}(edp|im)$ = Probability of the EDP exceeding a given demand for a given intensity measure

$\frac{d\lambda_{IM}(im)}{dIM}$ = Incremental probability of a given intensity measure

The steps used to determine the seismic demand hazard for a certain EDP are summarised below:

1. Perform seismic response analyses at various intensity levels
2. Obtain a lognormal probability density function of the individual seismic responses for a single intensity level.
3. Compute the probability of the EDP exceeding a given demand using this probability density function.
4. Multiply the probability from step 3 by the incremental probability of that intensity level occurring. This is obtained directly from the seismic hazard curve.
5. Repeat steps 2-4 for each intensity level considered

6. Sum the result from each intensity level

The process of obtaining the seismic demand hazard curve from the individual seismic response is depicted graphically in Figure 7-33.

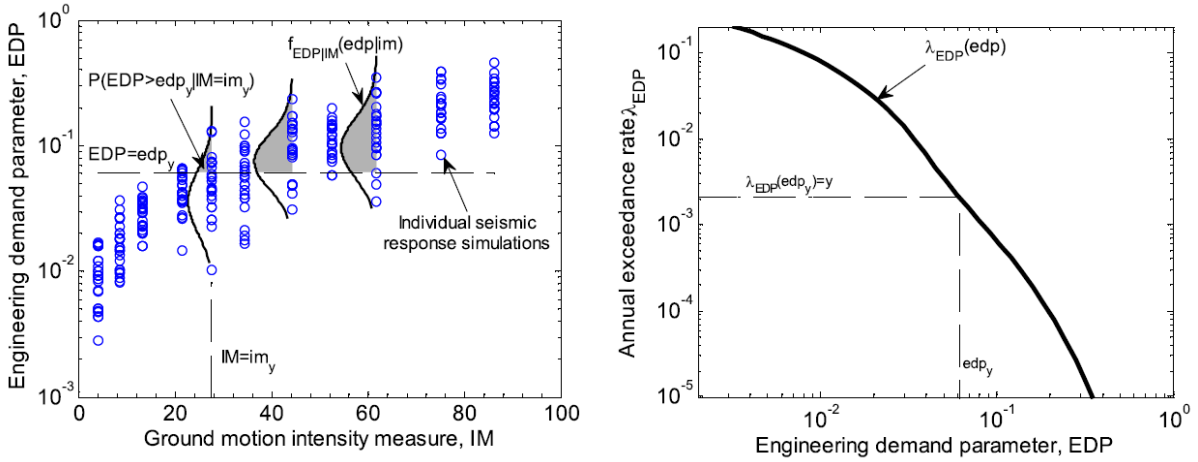

Figure 7-33: Distribution of seismic demand conditional on various intensity measure values (left) and the computed seismic demand hazard (right) (Bradley, 2013)

7.6.1 Structural Demand Hazard

The seismic demand hazard for the structural response has been quantified by the beam and column curvature demands found using the analyses performed in the previous section. The individual responses have been used to obtain the lognormal probability distributions at each intensity level which account for the variability in response due to complex ground motions.

The beam and column curvature demand hazard curves are presented in terms of the annual frequency of exceedance. The annual frequency of exceedance is equivalent to the reciprocal of the return period and has been presented in this section in a logarithmic scale. The member curvatures are presented in linear scale.

The demand hazard curves are presented for the every second floor of the structure in order to gain an appreciation of the performance throughout the structure and the effect the cladding presence has upon the structural performance.

7.6.1.1 Bare Frame

The seismic demand hazard curves for the beam and column curvatures are presented in Figure 7-34. For clarity, the curves for the member curvatures are only shown for odd floors. Using the structural damage limits defined previously, Figure 7-34 illustrates the annual rate

of the beams in each floor exceeding these damage limits. The demand hazard curves can be interpreted by considering that the higher the damage limit exceedance value, the more vulnerable and thus more likely a member is to be damaged in the structures lifetime. Since the seismic demand hazard takes into account all of the likely hazards facing the structure, the curves presented in Figure 7-34 represent the hazard facing the members over the structure's lifetime. Therefore, over the lifetime of the case-study structure it can be seen that the third floor beams are more likely to be more heavily damaged than those on any other floor. It should be noted that the analyses performed included hazards that ranged from 1% in 50 year likelihood to 50% in 50 years likelihood. Hazards certainly exist outside this range, however they have not been considered as it is believed they would not strongly affect the results presented. This is due to the hazards outside this range either being too weak to cause damage or being too rare to have meaningful results.

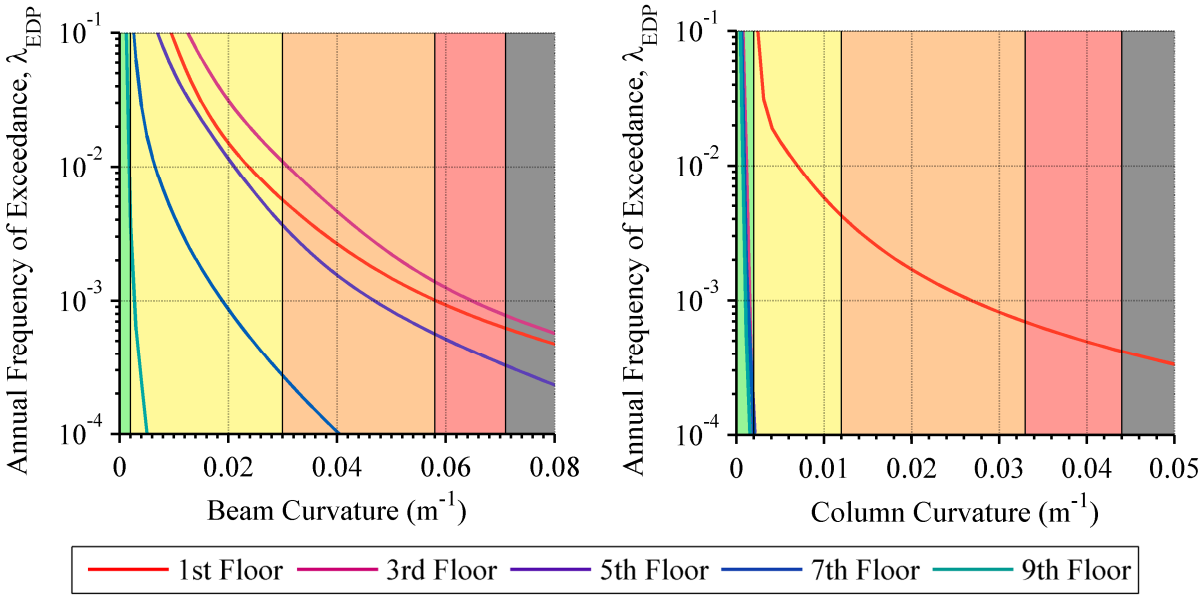

Figure 7-34: Bare frame beam (left) and column (right) demand hazard curves

Also shown in Figure 7-34 is the strong contrast in expected damage to the first floor columns compared to the rest of the columns. Clearly, the performance of the columns in the first floor is the only column performance that is of importance over the structure's lifetime. It is also possible to compare across between the beam and column demand hazard curves to appreciate for a given annual frequency of exceedance, what the expected performance of the beams in the different levels is and what the performance of the first floor columns is. For example, for an annual frequency of exceedance of 10^{-3} (1000 year return period), the third floor beams are expected to be in the Collapse Prevention performance level, the first and

fifth floor beams are expected to be in the Life Safety performance level, as are the first floor columns, and the seventh and ninth floor beams are expected to be deemed in the Immediate Occupancy performance level.

The annual rate of exceeding each of the member curvature damage limits can be interpolated from Figure 7-34. These values provide a useful way of comparing the vulnerability of various structural and non-structural components in a way that does not require an understanding of intensity measures (e.g. spectral acceleration) or of the engineering demand parameter used to quantify the damage (e.g. curvature). Presented in Table 7-14 are the return periods (reciprocal of annual frequency of exceedance) of exceeding each of the structural damage limits. These values are presented according to floor level and are only presented for floors where meaningful values exist, i.e. the return period on DL4 being exceeded in the seventh floor is 10,000 years so is not a meaningful result.

Table 7-14: Bare frame structural damage limit return period (years)

	Return Period DL1	**Return Period DL2**	**Return Period DL3**	**Return Period DL4**
1st Floor Beam	1	180	990	1600
3rd Floor Beam	1	90	720	1300
5th Floor Beam	2	280	1800	3100
1st Floor Column	3	240	1400	2400

It can be seen that the lowest return period for a ground motion that could lead to possible collapse of the structure is 1300 years. This is defined by the return period at which DL4 is first exceeded, which occurs first in the third floor beams. It is expected that a ground motion with a return period of 2400 years may result in the failure of the first floor column. It can also be seen in Table 7-14 that the return period for exceeding DL1 for all of components in is only 1 – 3 years. This result tells us that it is essentially guaranteed that the structure will surpass this damage limit in its lifetime.

Another possible way of representing the annual rates at which each damage limit is exceeded is achieved by converting the rates into the probability of exceeding the damage limit in 50 years, as shown in Table 7-15. This is often how the seismic hazard is communicated (as it has been here) so it is useful comparison. It can be seen that the probability of exceeding DL1 is 100% in 50 years. The probability of exceeding DL2 in a 50 year period is 42% in the third floor beams. The probability of failure in 50 years is around 2 – 4% which is approximately equivalent to the maximum considered design earthquake

which is often taken as the hazard with a probability of exceedance of 2% in 50 years (McGuire, 2008).

Table 7-15: Bare frame structural damage probability of exceedance (PoE) in 50 years

	PoE DL1	PoE DL2	PoE DL3	PoE DL4
1st Floor Beam	100%	25%	5%	3%
3rd Floor Beam	100%	42%	7%	4%
5th Floor Beam	100%	17%	3%	2%
1st Floor Column	100%	19%	3%	2%

7.6.1.2 Clad Frame

A comparison between the clad and unclad seismic demand hazard curves for the beam and columns curvatures is presented in the following figures for each of the three connection types investigated. Figure 7-35 illustrates the influence of the cladding upon the structural performance when connected with long threaded rod connections. It can be seen that the level of demand expected to the structural components is reduced by the presence of the cladding; however the difference is not significant. The influence of the cladding is reasonably consistent although it can be seen the member demands are reduced proportionately more for less frequent events.

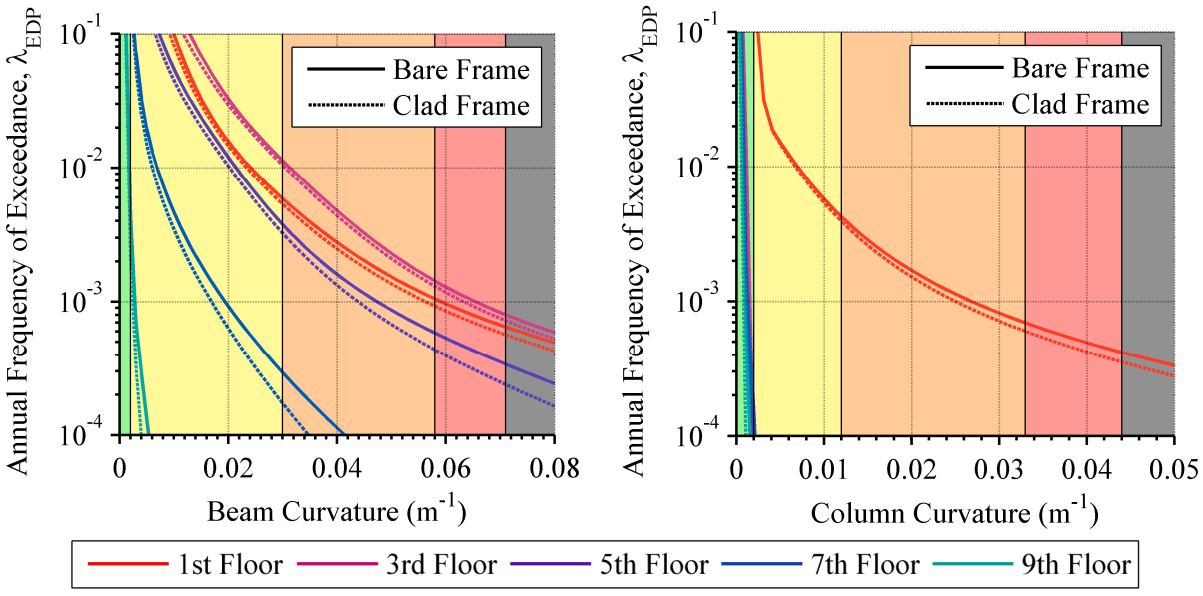

Figure 7-35: Comparison of bare and clad frame beam (left) and column (right) demand hazard curves for long threaded rod connections

The influence of the cladding when connected to the structure with slotted connections is presented in Figure 7-36. It can be seen that the slotted connections significantly reduce the

expected demands in the beams of the third and fifth floor (shown as indigo and violet respectively). The cladding also reduces these demands proportionately more for less frequent earthquake hazards. This would be expected since the connections have minimal influence upon the structure's response unless large structural deformations occur and hence the displacement demand upon the connection exceeds the slot capacity. The slotted cladding connections have no effect upon the expected column performance nor upon the expected beam performance in the upper floors.

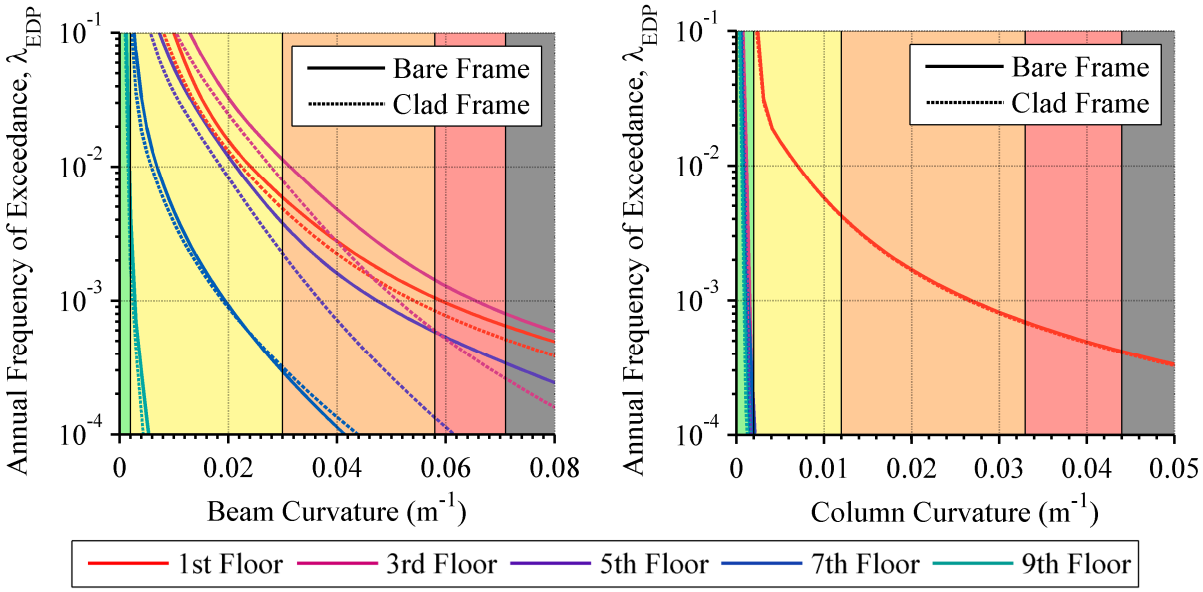

Figure 7-36: Comparison of bare and clad frame beam (left) and column (right) demand hazard curves for slotted connections

The influence of the cladding when connected to the structure with short threaded rod connections is presented in Figure 7-37. It can be seen that the annual rate at which each structural damage state is exceeded is reduced for all of the structural members of the clad frame. This reduction is reasonably consistent which indicated that the cladding reduces the structural demands for both frequent and infrequent earthquake hazards. As opposed to the slotted connections which were found to reduce the beam demands in the lower floors, the short threaded rod connections are found to cause a significant reduction in the expected beam demands in the mid to upper floor beams (shown as violet and blue).

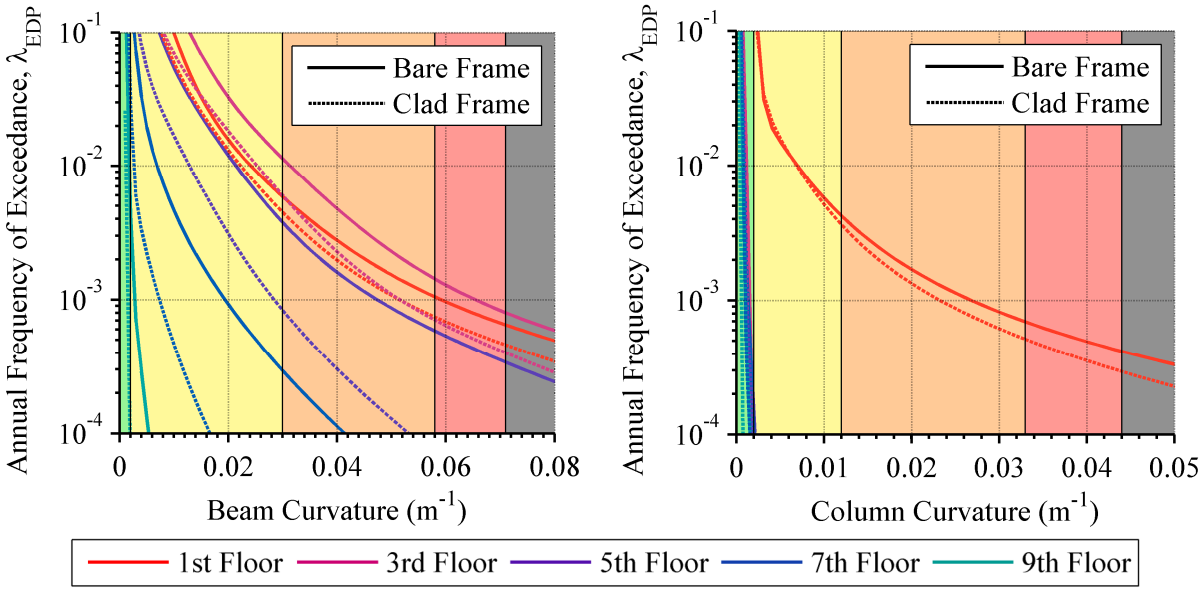

Figure 7-37: Comparison of bare and clad frame beam (left) and column (right) demand hazard curves for short threaded rod connections

The effect the cladding has upon the structure's expected life-time performance can be understood by comparing the annual rate at which each structural damage limit is exceeded in the clad frame and bare frame. The third floor beams and first floor columns have been identified as the key structural performance indicators; hence the return periods that these members exceed the member curvature damage limits have been compared in Table 7-16 and Table 7-17. The return period that the third floor beam curvatures are expected to exceed each of the damage limits is presented in Table 7-16 for the bare frame and clad frames. The clad frames include each of the three connection types in the mono panel configuration. It can be seen that the effect of the long threaded rod connection is negligible upon the structure's expected performance. The return periods of DL3 and DL4 for the slotted and short threaded rod connections systems are significantly greater than those of the bare frame, hence it can be concluded that the probability of the structure suffering heavy damage or failing with these cladding systems attached is reduced.

Table 7-16: Structural damage limit return period (years) in third floor beams

	Return Period DL1	Return Period DL2	Return Period DL3	Return Period DL4
Bare Frame	1	90	720	1300
Long Threaded Rod	1	100	770	1400
Slotted	1	130	1700	3800
Short Threaded Rod	2	170	1400	2500

The return period that the first floor column curvatures are expected to exceed each of the damage limits is presented in Table 7-17 for the bare frame and clad frames. It can be seen that the influence of the cladding upon the expected column performance is not as significant as it is upon the beam performance. The short threaded rod connections are found to reduce the likelihood of damage the most, but the overall impact upon the column performance is minimal.

Table 7-17: Structural damage limit return period (years) in first floor columns

	Return Period DL1	Return Period DL2	Return Period DL3	Return Period DL4
Bare Frame	3	240	1400	2400
Long Threaded Rod	4	260	1700	2800
Slotted	4	240	1400	2400
Short Threaded Rod	4	270	1900	3400

7.6.2 Cladding Demand Hazard

The seismic demand hazard for the cladding response has been quantified by the cladding connection and panel displacement demands found using the analyses performed in the previous section. The displacement demand hazard curves are presented in terms of the annual frequency of exceedance similarly to those presented previously. It should be noted that the scale of the annual frequency axis has been increased compared to the figures presented previously of the structural demand hazard curves.

The demand hazard curves are presented for the every second floor of the structure in order to gain an appreciation of the cladding performance throughout the structure. The performance of each of the three connection types investigated is shown for both the mono panel and dual panel configuration. The performance of the cladding in both panel configurations is also presented.

7.6.2.1 Long Threaded Rod

The performance of the long threaded rod connections is illustrated in the seismic demand hazards curves of Figure 7-38. It can be seen that there is a consistent trend of performance between the mono panel and dual panel configurations; however, as identified previously, a greater level of damage to the connections in the mono panel configuration is expected for the same ground motion annual frequency of exceedance. The expected damage to the cladding connections is critical for both the first and third floors of the structure (shown

as red and violet, respectively). This is in contrast to the structural demands in the third floor beams consistently being more critical than those in the first floor. The annual frequency that the connection deformations are expected to be either Hazards Reduced or Failure is clearly significantly higher, i.e. more likely to occur, compared to that of the structural members.

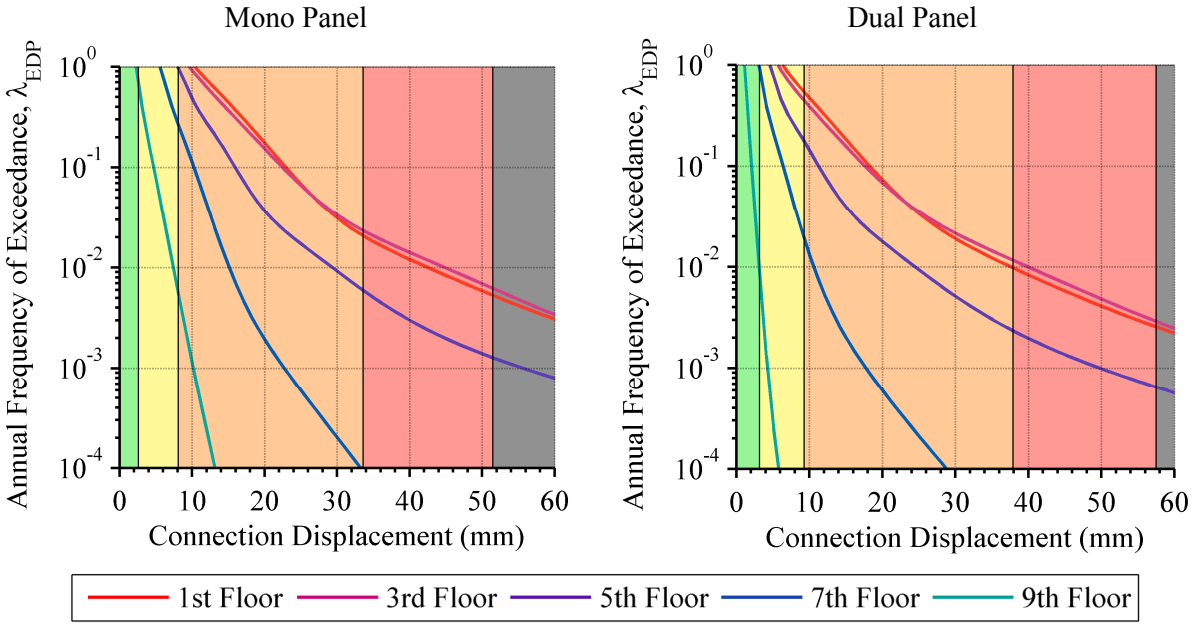

Figure 7-38: Long threaded rod connection demand hazard curves for mono panel (left) and dual panel (right)

The annual rate of the connection damage limits being exceeded can be interpolated from Figure 7-38. The first, third and fifth floor levels have been used to illustrate the distribution in expected cladding damage. The return period that the long threaded rod cladding connection displacements are expected to exceed each of the damage limits is presented in Table 7-18 for the mono panel and dual panel configuration.

Table 7-18: Long threaded rod connection damage limit return period (years)

		Return Period DL1	Return Period DL2	Return Period DL3	Return Period DL4
Mono Panel Configuration	**1st Floor**	1	1	45	190
	3rd Floor	1	1	43	160
	5th Floor	1	1	170	790
Dual Panel Configuration	**1st Floor**	1	2	100	390
	3rd Floor	1	2	90	340
	5th Floor	1	6	430	1500

Similarly to that presented previously for the expected return period of the first structural damage limit (DL1) being exceeded, the expected return period of both DL1 and DL2 being exceeded is so small it essentially guarantees these limits will be exceeded over

the structure's lifetime. It is also apparent that the return period of failure being expected (DL4 being exceeded) is well below that of the structure; the greatest risk being to the third floor connections in the mono panel having a 27% chance of failure in 50 years (equivalent to a return period of 160 years).

7.6.2.2 Slotted

The performance of the slotted connections is illustrated in the seismic demand hazards curves of Figure 7-39. It can be seen that the same trends in performance are evident in the slotted connections as identified earlier for the long threaded rod connections. That is, there is a consistent performance between the mono panel and dual panel configurations; and the expected damage to the cladding connections is critical for both the first and third floors of the structure (shown as red and violet, respectively). It is evident that the annual frequency that the slotted connections are expected to exceed each of the damage limits is much less than that of the long threaded rod connections. In particular, the annual frequency that the connection performance is expected to remain Operational is not trivial like it is for the threaded rod connections.

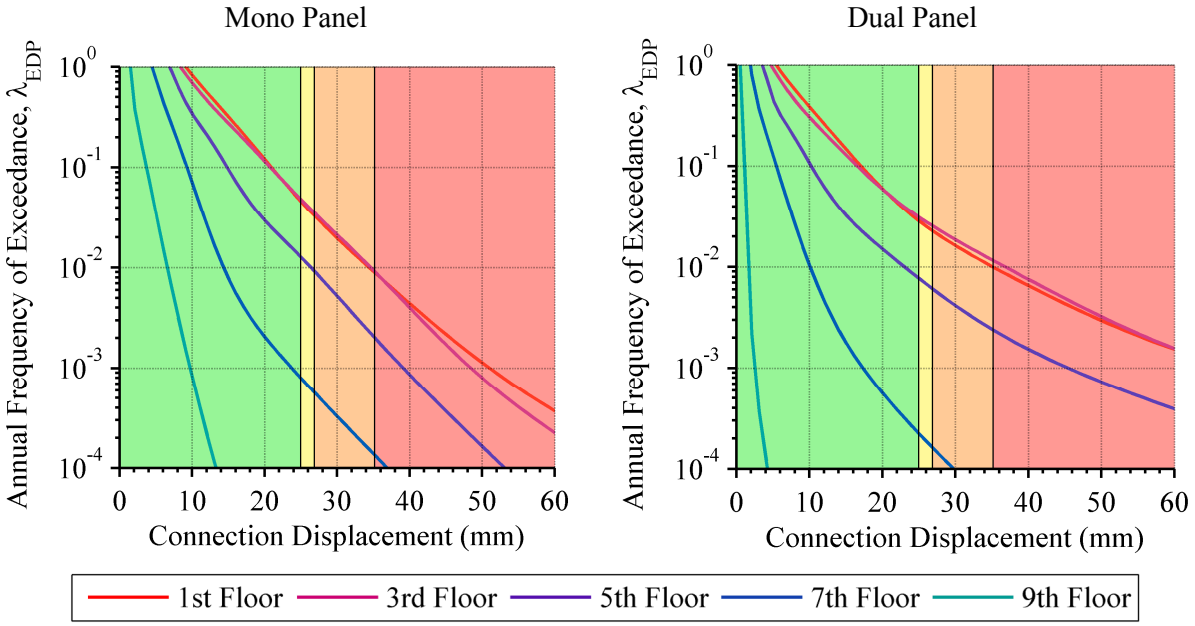

Figure 7-39: Slotted connection demand hazard curves for mono panel (left) and dual panel (right)

The return period that the slotted cladding connection displacements are expected to exceed each of the damage limits is presented in Table 7-19 for the mono panel and dual panel configuration. As mentioned previously, the return period of exceeding DL1 and DL2 is not trivial for slotted connections; consequently, the probability of the connections

suffering minor damage is not a near certainty like it is for the threaded rod connections. The probability of exceeding DL2 in the third floor connections of the mono panel configuration is found to be 84% in 50 years. The probability of exceeding DL3 and being deemed Hazards Reduced in a 50 year period is found to be 37%. For long threaded rod connections, the equivalent probability is 69%.

Table 7-19: Slotted connection damage limit return period (years)

		Return Period DL1	Return Period DL2	Return Period DL3
Mono Panel Configuration	**1st Floor**	22	30	110
	3rd Floor	21	28	110
	5th Floor	78	110	500
Dual Panel Configuration	**1st Floor**	35	44	100
	3rd Floor	32	40	86
	5th Floor	130	170	420

7.6.2.3 Short Threaded Rod

The performance of the short threaded rod connections is illustrated in the seismic demand hazards curves of Figure 7-40.

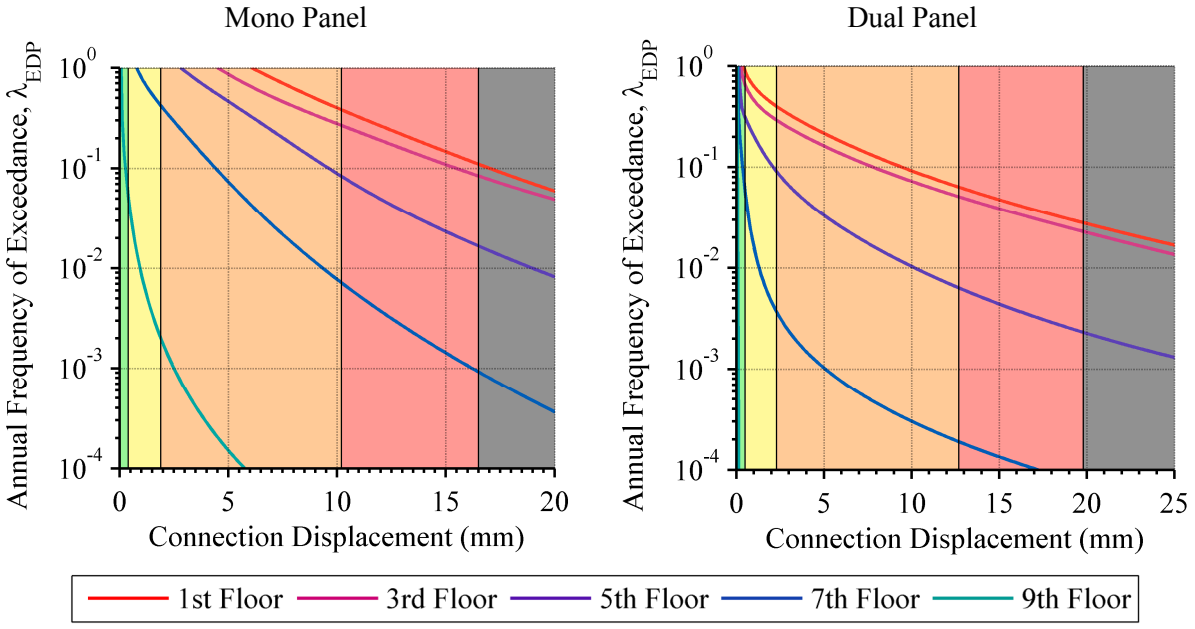

Figure 7-40: Short threaded rod connection demand hazard curves for mono panel (left) and dual panel (right)

Immediately evident is the higher frequency at which the damage limits are exceeded by the short threaded rod connections in comparison to both of the other connections investigated, as well as the structural members. The connections of the mono panel

configuration are also markedly more likely to exceed each damage state than those of the dual panel configuration.

The return period that the short threaded rod connection displacements are expected to exceed each of the damage limits is presented in Table 7-20 for the mono panel and dual panel configuration. In accordance with the demand hazard curves presented in Figure 7-40, the expected return period of exceeding DL4 is significantly less than that of the other connections investigated, as well as the structural members. The probability of exceeding DL4 in the third floor connections of the mono panel configuration is found to be 98% in 50 years. The probability of exceeding DL4 in the dual panel configuration is 75%, a better result but clearly the performance of both systems is unacceptable.

Table 7-20: Short threaded rod connection damage limit return period (years)

		Return Period DL1	Return Period DL2	Return Period DL3	Return Period DL4
Mono Panel Configuration	**1st Floor**	1	1	3	9
	3rd Floor	1	1	3	12
	5th Floor	1	1	12	23
Dual Panel Configuration	**1st Floor**	1	3	16	36
	3rd Floor	2	3	20	44
	5th Floor	3	11	160	430

7.6.2.4 Panel

The performance of the cladding panels is illustrated in the seismic demand hazards curves of Figure 7-41. The mono panel and dual panel performance has been found for the long threaded rod connections. As presented in Section 7.5.2, the performance of the cladding is not strongly dependent upon the connection type; the worst performance was found to be when the long threaded rod connection were used. Figure 7-41 clearly shows that the more flexible dual panel is much less likely to suffer damage than the mono panel. As opposed to the connection performance, the difference in expected panel performance between floors is not as large. It can also be seen that the panels from the fifth floor upwards are essentially guaranteed to remain undamaged regardless of the intensity of ground motion.

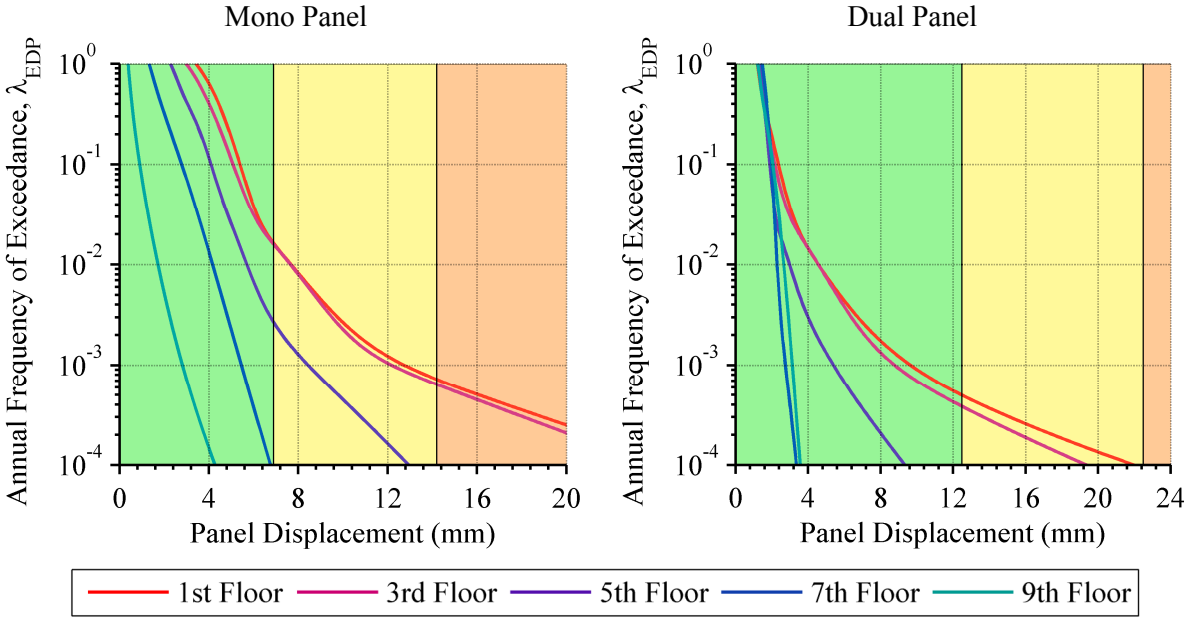

Figure 7-41: Cladding panel demand hazard curves for mono panel (left) and dual panel (right)

The return periods that the two panel sizes are expected to exceed each of the damage limits is presented in Table 7-21. Evidently, only the mono panels in the lower floors of the structure have any realistic probability of being damaged. The probability of any damage to the dual panel systems is trivial.

Table 7-21: Cladding panel damage limit return period (years)

		Return Period DL1	Return Period DL2
Mono Panel	**1st Floor**	62	1400
	3rd Floor	63	1600
	5th Floor	370	19000
Dual Panel	**1st Floor**	2000	11000
	3rd Floor	2600	17000
	5th Floor	51000	4300000

7.7 Conclusions

The expected damage to both the structure and cladding has been quantified in this chapter using a performance-based assessment methodology. This methodology calculates the probability of exceeding a specified level of demand which corresponds to a qualitative level of damage. These levels of demand have been determined from literature (for structural damage limits) or from experimental testing presented in previous chapters (for cladding damage limits). Structural damage is typically quantified by measuring the amount of inelastic deformation that occurs in the frame members. For this investigation, this inelastic

deformation was measured by the amount of rotation that occurs in the plastic hinges of the beam and column ends. The performance of the cladding connections and cladding panels was determined according to the horizontal displacement demand upon each component.

The structural performance of the bare frame was first quantified in order to provide a base-line for comparison against when the effect of cladding was included. The results for the bare frame showed damage typical for a ductile reinforced concrete moment frame structure. The structural damage was in accordance with the development of a beam-sway mechanism, with a concentration of damage around the lower level beams. This was likely a result of the vertical uniformity of the structure.

It was observed that all of the clad frame configurations reduced the expected quantity of structural damage for the same seismic demand. This reduction agrees with the result found in Chapter 6 that the presence of cladding reduces inter-storey drifts. This is because beam and column curvatures are intrinsically linked to frame deformation. The short threaded rod connections had the greatest influence in reducing structural damage. The inclusion of cladding reduces the probability of the beam damage being deemed Life Safety level or worse in a 2%/50 year seismic event by between 5 – 24%. The cladding presence causes a small shift in improvement of the column performance; however the effect upon the columns is minimal in comparison with the effect upon the beam performance.

The expected damage to the cladding components showed that significantly higher levels of damage are expected in the cladding connections compared to the structure for the same level of hazard. Most notably, the probability of failure in the connection is significantly greater than failure of the beams. This result is not irrational, as if the beams fail, then structural collapse may be imminent and the performance of other structural and non-structural components is irrelevant. Conversely, failure of the cladding connections will most likely have no effect upon the performance of the structure. Hence it is entirely practical to expect a lower probability of structural failure than cladding failure. However, the proportion of damage is much less practical. For example, the probability of the beams in the third floor being deemed Immediate Occupancy is 56% for a 2% in 50 year seismic event, whereas, the probability of the cladding connections being in the same performance level is zero. This result tells us that there is a 56% chance that the structure will be able to be occupied without the need for structural repair, but that repair of the cladding will essentially be a certainty.

The expected structural and cladding damage was also quantified by seismic demand hazard which accounts for both the likelihood of various levels of ground shaking at a site and the relationship between ground shaking and seismic response, including its uncertainty. The seismic demand hazard therefore provides the overall probability of exceeding a certain level of damage rather than considering only the damage at a single intensity level.

This metric showed that the effect of cladding with long threaded rod connection is negligible upon the structure's expected performance. However, the return periods of exceeding DL3 and DL4 for the slotted and short threaded rod connections systems are significantly greater than those of the bare frame, hence it can be concluded that the probability of the structure suffering heavy damage or failing with these cladding systems attached is almost halved. However, the short threaded rod connections are deemed to be virtually guaranteed to fail at this level of demand. Clearly such a result would not be acceptable and nor would it be remotely consistent with the improvement in structural performance. The probability of the third floor slotted connections being heavily damaged and hence requiring repair in a 50 year period was found to be 37%. For the long threaded rod connections, the equivalent probability is 69%.

The definitions of the performance levels presented in this chapter are also linked to different repair requirements. These repair requirements have repair costs and repair time associated with each performance level. The results from this chapter will be used in Chapter 11 to determine repair costs, repair time and casualties as part of a probabilistic seismic loss assessment.

7.8 References

Bradley, B. A. (2010). Epistemic Uncertainties in Component Fragility Functions. Earthquake Spectra, 26(1), 41-62.

Bradley, B. A. (2012). The seismic demand hazard and importance of the conditioning intensity measure. Earthquake Engineering & Structural Dynamics, 41(11), 1417-1437.

Bradley, B. A. (2013). A comparison of intensity-based demand distributions and the seismic demand hazard for seismic performance assessment. Earthquake Engineering & Structural Dynamics, (in press).

Bull, D. K., & Brunsdon, D. (1998). Examples of Concrete Structural Design to New Zealand Standards 3101. Wellington, New Zealand: Cement & Concrete Association of New Zealand.

Carr, A. J. (2010). Ruaumoko Programme for Inelastic Dynamic Analysis - User Manual: Department of Civil Engineering, University of Canterbury, New Zealand.

FEMA P-58-1. (2012). Seismic Performance Assessment of Buildings Volume 1 - Methodology. Washington, DC., USA: Federal Emergency Management Agency.

Mander, J. B. (1999). Fragility Curve Development for Assessing the Seismic Vulnerability of Highway Bridges Research Progress and Accomplishments: 1997 -1999. Buffalo, NY., USA: Multidisciplinary Centre for Earthquake Engineering Research (MCEER).

Mander, J. B., Priestley, M. J. N., & Park, R. (1988). Theoretical Stress-Strain Model for Confined Concrete. ASCE Journal of Structural Engineering, 114(8).

McGuire, R. (2008). Probabilistic seismic hazard analysis: Early history. Bulletin of the Seismological Society of America, 37(3), 329-338.

Montejo, L. A., & Kowalsky, M. J. (2007). CUMBIA - Section and Member Response of Reinforced Concrete Members. Department of Civil, Construction and Enviromental Engineering, North Carolina State University.

NZS 1170.5. (2004). Structural Design Actions, Part 5: Earthquake Actions - New Zealand. Wellington: Standards New Zealand.

NZS 3101. (2006). Concrete Structure Standard - Part 1. Wellington: Standards New Zealand.

Pampanin, S. (2005). Emerging Solutions for High Seismic Performance of Precast/Prestressed Concrete Buildings. Journal of Advanced Concrete Technology, 3(2), 207-223.

Pampanin, S., Christopoulos, C., & Priestley, M. J. N. (2002). Residual deformations in the performance-based seismic assessment of frame structures. Pavia, Italy: IUSS Press.

Park, R., & Paulay, T. (1975). Reinforced Concrete Structures. New York, NY., USA: Wiley.

Pavlina, E. J., & Van Tyne, C. J. (2008). Correlation of Yield Strength and Tensile Strength with Hardness for Steels. Journal of Materials Engineering and Performance, 17(6), 888 - 893.

Porter, K. A., Kennedy, R., & Bachman, R. (2007). Creating Fragility Functions for Performance-Based Earthquake Engineering. Earthquake Spectra, 23(2), 471-489.

SEAOC. (1995). Performance-based seismic engineering. Sacramento, CA: Structural Engineers Associate of California.

8 Experimental Testing of Innovative Cladding Systems

8.1 Introduction

This chapter presents the experimental investigation into the development of low-damage, innovative cladding connections. The experimental campaign comprises both component and full scale testing of U-shaped flexural plates (UFP) to determine their suitability as a possible innovative cladding connection. The full-scale testing replicates that used for testing of traditional cladding connections in Chapter 4. This comprises a single-storey; single-bay portion of a reinforced concrete (RC) frame building clad with precast concrete cladding. The cladding-frame system is tested under uni-directional quasi-static cyclic loading. The cyclic response of the cladding-structure system is compared to a benchmark test of the frame without any cladding present. The testing aims to investigate the performance of the cladding system when innovative cladding connections are used and to explore the cladding connections ability to provide additional passive energy dissipation to the structure.

8.2 Background

The concepts and philosophy behind the use of innovative cladding connections is briefly presented here. Previous testing and design equations of the proposed connection components are also presented.

The fundamental requirement for an innovative connection is that it is low-damage, i.e. able to withstand multiple seismic events without the need for repair or replacement. It is also vital that the connection is cost comparable to a traditional cladding connection and is flexible and simple in its design and implementation. Furthermore, it is also desirable for the

connection to be able to provide some additional positive value to the seismic performance of the structure.

These factors are considered fundamental in order to provide the encouragement for practitioners to adopt new technology. This is because the use of any new technology requires additional time and resources to implement, when compared to an existing technology.

The possible positive value explored for the innovative connection presented in this chapter is the ability to passively dissipate seismic energy. For further information on innovative connections and the use of cladding to passively dissipate seismic energy refer to Chapter 2.

8.2.1 Philosophy of Innovative Connections

A building fully clad in precast concrete cladding presents an increase of approximately 20-30% in the inertial mass of a multi-storey building (Pall, 1989). This increased mass means increased seismic forces during earthquake excitation. However, unlike other decorative type curtain walls, precast concrete claddings have inherent strength and stiffness that is typically ignored. Current design philosophies attempt to isolate cladding from interacting with the frame during deformations due to wind and earthquake loading (Arnold, 1990). Bolted connections with slotted or oversized holes are commonly used to isolate panels as well as accommodate erection tolerances. However, recent studies have outlined how even when attempts to isolate the cladding are made, precast concrete cladding can still increase the overall stiffness of a structure, as shown in Chapter 6 as well as previous research (Goodno & Craig, 1989; Hunt & Stojadinovic, 2010; McMullin et al., 2012).

Instead of attempting to simply isolate the structure-panel interaction, it is proposed to take advantage of it to dissipate energy. By doing so, the deformations of the main structure can also be reduced, preventing damage in both structural and non-structural components. Controlling the cladding participation requires the development of an innovative connection that has high ductility and damping qualities that results in high energy dissipation without failure during moderate or strong earthquakes (Pinelli et al., 1993). By using cladding connections to passively dissipate earthquake energy, significant advantages can be achieved over conventional designs. The energy dissipation and damping can be distributed evenly over the height of the building and due to the increased damping, the overall response of the building is reduced and hence damage to non-structural elements and contents can be avoided

(Goodno, 1983) It is also desirable for the additional damping from the cladding connections to be activated at SLS level demands where the elastic damping in the structure is low. This will be highly dependent upon the stiffness of the connection.

Such a cladding connection must also be simple to design, highly robust and limit the forces transmitted into the panel. As well as this they must be cost comparable to current cladding connections so that industry is more likely to adopt them. This chapter explores experimentally the possibility of using U-shaped flexural plates (UFPs) as such an advanced cladding connection.

8.2.2 U-Shaped Flexural Plate Dissipators

U-Shaped flexural plates (UFPs) are formed by heating mild steel plates and bending a section around a fixed radius to form a 'U' shape. Initially proposed by Kelly et al. (1972), the basic concept of a UFPs dissipation mechanism is shown in Figure 8-1. UFPs are a form of flexural dissipator which utilise the post-yield ductility of steel to dissipate energy. When one side of the UFP is subjected to a displacement relative to the other side, the semi-circular section rolls along the plate and work is done at the two points where the radius of curvature is changed from straight to curved and vice versa. Thus the yielding point of the plate moves back and forth along the plate.

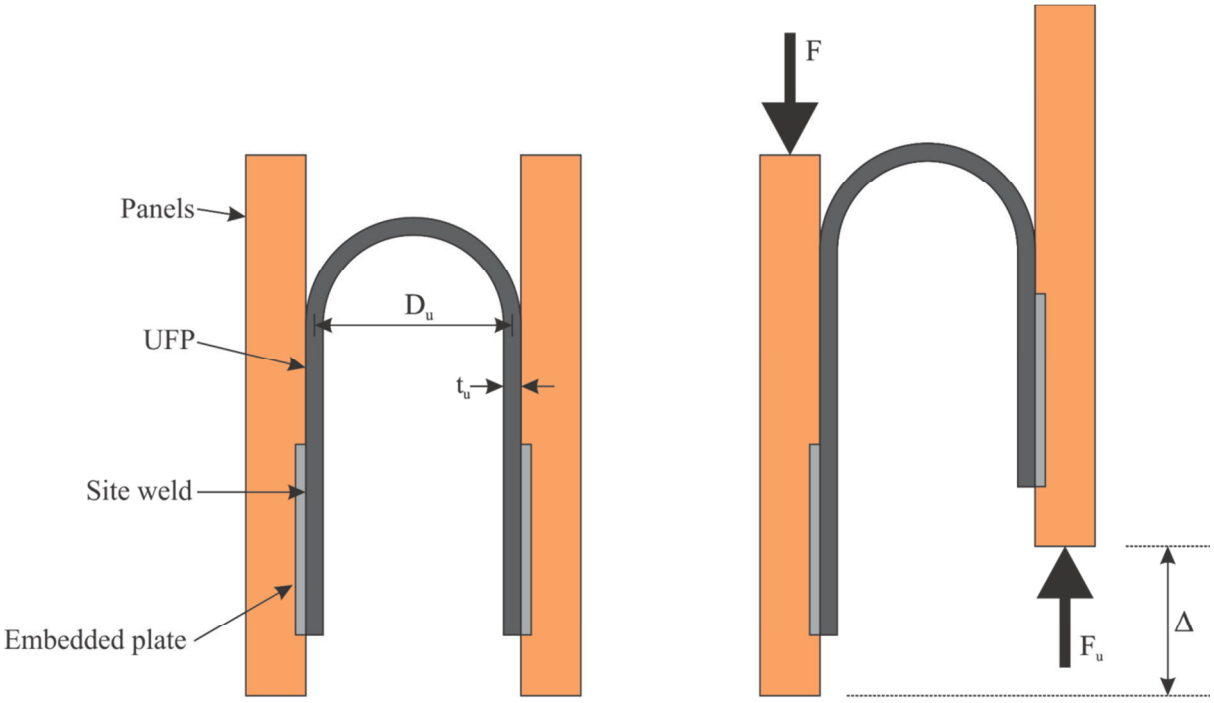

Figure 8-1: Coupling mechanism of a U-Shaped Flexural Plate (UFP)

UFPs can be designed for a large range of possible displacements and force levels by varying the plate thickness, width and radius. The design considers the displacement stroke such that the amount of steel that is deformed during loading is limited. This ensures the maximum strain is kept low enough to ensure that a specified lifetime (in terms of low-cycle fatigue) is achieved. UFPs have successfully been tested and implemented in several structural dissipation applications, more recently as a device between coupled precast concrete or timber shear walls, like those shown in Figure 8-2.

Figure 8-2: Application of UFP devices between concrete PRESSS walls (Southern Cross Building, Christchurch) and timber Pres-Lam walls (NMIT Building, Nelson) (Iqbal et al., 2007)

8.3 Connection Design

One of the main attractive features of a UFP is that the maximum strain within the steel remains constant during positive and negative displacements. This is due to the inelastic deformation moving along the steel plate. The constant strain demand is related to the radius of the UFP and the thickness of the plate by Equation (8-1).

$$\varepsilon_{max} = \frac{t_u}{D_u} \qquad \textbf{(8-1)}$$

where

ε_{max} = Maximum strain

t_u = Thickness of UFP plate

D_u = Diameter of UFP bend

It should be noted that the diameter used in Equation (8-1), D_u, is defined as the diameter to the centre of the plate, as shown in Figure 8-1.

Since there is no term related to displacement in Equation (8-1), theoretically, the strain in the connection is not dependent upon the maximum displacement of the UFP. The maximum displacement is instead governed by the connection detail and is limited by cyclic fatigue criteria. The cyclic fatigue criteria was found by Kelly et al. (1972) to be defined by the relationship between the maximum strain defined by Equation (8-1) and the normalised UFP displacement (stroke). The normalised displacement is defined as the UFP displacement divided by the UFP radius. The dependable number of cycles can be determined from the intersection of these two parameters and is presented in the following section in Figure 8-6. Tests carried out on UFPs under reversed cyclic loading showed that the mode of failure is characterised by a localised kinking of the plate, followed rapidly by a complete transverse fracture (Iqbal et al., 2007; Kelly et al., 1972). The plastic force, which defines when the entire section of UFP has yielded, of a single UFP is given by Equation (8-2). Further analytical derivation is provided in Chapter 9 for the development of modelling parameters.

$$F_p = f_y \frac{b_u t_u^2}{2D_u} \qquad \textbf{(8-2)}$$

where

F_p = Plastic force of UFP

f_y = Yield stress of UFP

b_u = Width of UFP

Tests have shown that the maximum force in a UFP device exceeds the plastic force given by Equation (8-2) due to strain hardening of the steel (Bauschinger effect). Stressed are typically in the order of 145 – 215% that of the yield stress obtained from direct tension. (Kelly et al., 1972; Pampanin et al., 2010).

8.3.1 Cladding Connection Application

Applying the UFP as a cladding connection requires slightly different considerations to that of the structural applications it was originally intended for. Firstly, in most structural applications the UFP is desired to provide large forces over a relatively short stroke; whereas as a cladding connection, the UFP is required to provide relatively small forces over a large stroke. To ensure the force provided by the UFP does not increase significantly beyond the

yield strength, it is necessary to ensure the maximum strain in the steel is kept to a minimum. This ensures that large overstrength does not develop in the steel. As seen in Equation (8-1), the maximum strain is dependent upon the thickness of the plate and the diameter of the bend. Therefore, the use of UFPs as a cladding connection requires the thickness of the plate to be kept small relative to the diameter. This is easily achievable since it is desirable for the UFP to have a large bend diameter. A large bend diameter provides the ability to have a long stroke without risk of failure (Kelly et al., 1972). Thus the design of a suitable UFP is relatively straight forward, relying on the definition of a maximum desired stroke and maximum desired force. The width of the UFP also provides an additional variable that can be altered to fine tune the expected force in the UFP.

Another considerations that is required to ensure the UFP behaves as intended is to ensure that the UFP bending is constrained laterally. This is required so that the bending moves along the plate length and is not fixed in one location. Figure 8-3 illustrated the behaviour of a UFP when the bending is constrained (left) and when it is not (right).

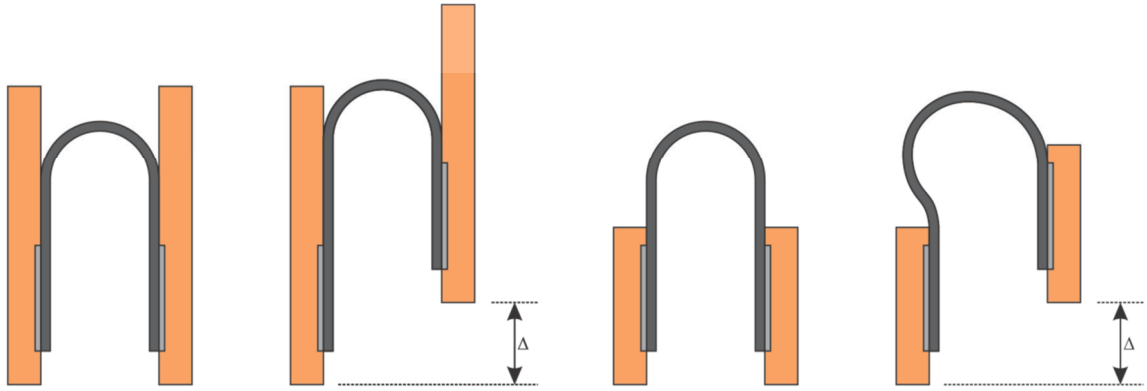

Figure 8-3: Properly constrained UFP (left) compared with unconstrained UFP (right)

It can be seen that when the plate is not restrained laterally, the plate is induced into bending outwards, causing localised bending stresses to occur around the end of the plate restraints. Since the bending does not move around the plate, the maximum strains in the UFP increase substantially. This results in the resisting force increasing also and giving rise to possible premature failure. This behaviour was observed experimentally and numerically and will be discussed more in the relevant sections.

The final consideration that is necessary when applying UFPs as a cladding connection is to ensure the UFP meets the out-of-plane requirements of a cladding connection. The ability to accommodate lateral displacement without damage is important, but first and foremost, a cladding connection must be able to resist the out-of-plane loads due to

earthquake excitation. In order to achieve this requirement, it was proposed to house the UFP inside a rectangular hollow section (RHS) with a slotted hole, as shown in Figure 8-4. This effectively combined the UFP connection with a traditional slotted connection.

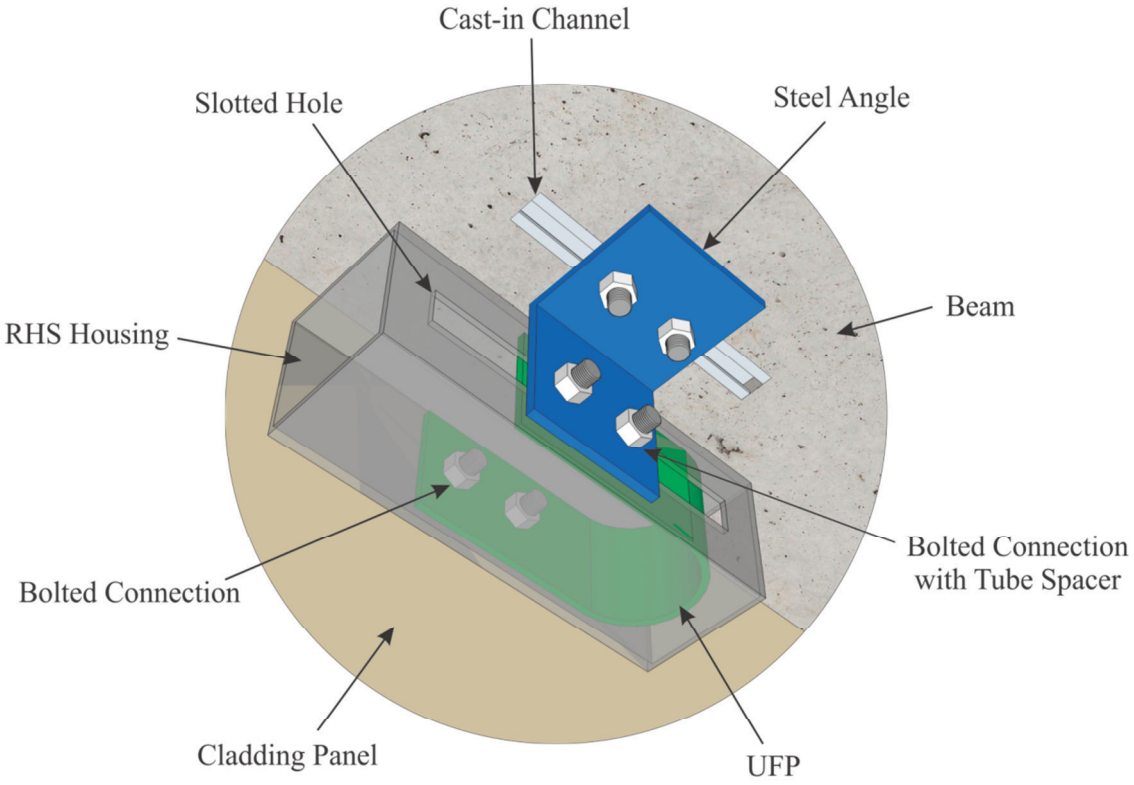

Figure 8-4: UFP connection housing

By providing the UFP with housing, the behaviour of the UFP was found to be significantly more consistent with the ideal case illustrated in Figure 8-3 (left). The RHS housing also ensures that the necessary out-of-plane capacity is provided. Albeit very unlikely, if the UFP was then to fail, the connection would still provide out-of-plane resistance. The connection would become effectively revert to being a slotted connection until the UFP was replaced.

8.3.2 UFP Design

One size of UFP was fabricated for use as a cladding connection. The magnitude of force transferred into the cladding panel could be altered by the number of UFP connections used. The maximum relative displacement between the cladding and frame was chosen as 105 mm; corresponding to the maximum possible displacement of the full-scale test rig. Certain aspects of the possible UFP geometry were constrained by the possible materials and machinery available; the plate thickness and width was restricted to the standard metric sizes

available; the bend diameter was restricted by the roller sizes available to the fabricator. A local Christchurch company, Bellamy and East Spring Makers, was used to fabricate the UFPs. The largest bend diameter they could provide had an inner diameter of 120 mm. As a large thickness to diameter was desired, this large diameter was chosen. In order to obtain the design force of approximately 10 kN, a plate size of 120 x 8 mm was selected. This gave a plastic force of 9.6 kN as given by Equation (8-3). A nominal yield strength of 320 MPa (AS/NZS 3678, 1996) has been assumed for the 8 mm plate.

$$F_y = f_y \frac{b_u t_u^2}{2D_u} = 320 \times \frac{120 \times 8^2}{2 \times 128} = 9.6\ kN \qquad \textbf{(8-3)}$$

The dimensions of the final UFP design are illustrated in Figure 8-5 along with one of the specimens before testing. Fabrication tolerances were found to be within ± 2 mm. The maximum stroke and bend diameter defined the length of plate required. A 100 mm straight length between the end of the bend and the bolt fixings was provided to ensure the bend would remain constant (refer to Figure 8-3). Two 16 mm holes were drilled into the straight region of the plate so the UFP could be bolted into place. Previous testing by Iqbal et al. (2007) made use of welded fixings; however, bolted fixings were chosen due to the desire of the connections to be easily installed and replaceable/removable. The original testing of UFPs by Kelly et al. (1972) made use of bolted fixings.

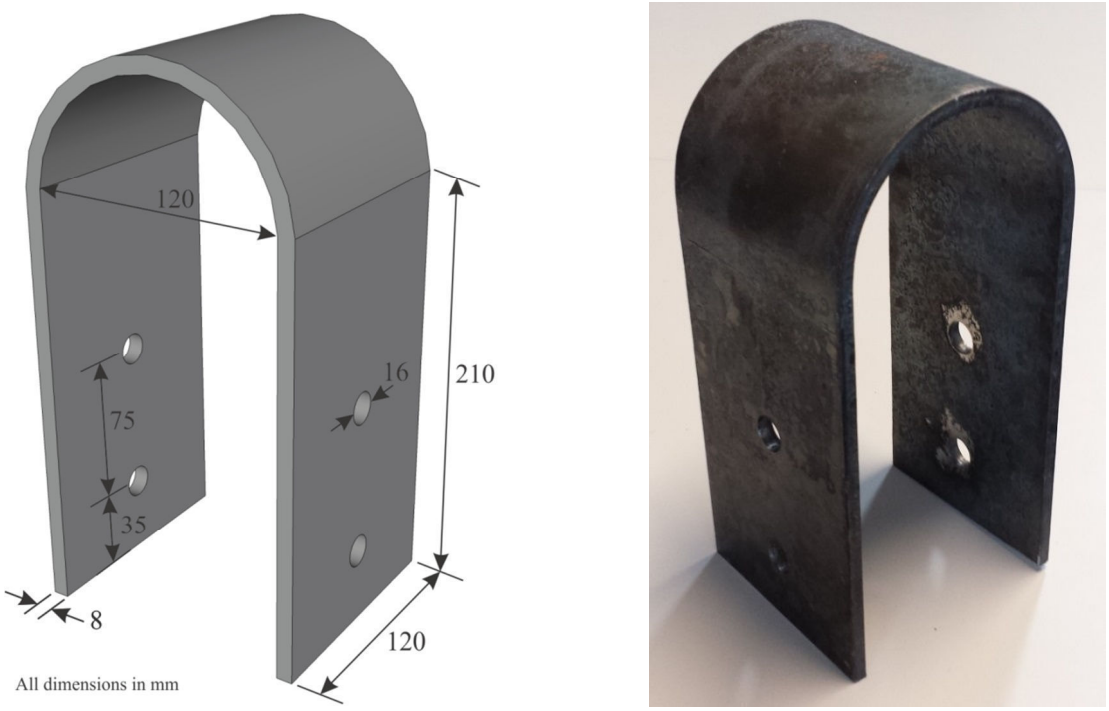

Figure 8-5: Dimensions of UFPs tested (left) and photograph of UFP prior to testing (right)

The maximum strain in the plate, as defined by Equation (8-1) as the ratio of the thickness of the plate and the diameter of the bend of the UFP was found to be 6.3%. The normalised stroke, obtained by dividing the maximum stroke of 105 mm by the bend radius of 64 mm, is 1.64; hence the expected cycles to failure of the UFP can be defined using the data from Kelly et al. (1972) and is shown in Figure 8-6. Evidently, no data exists for UFPs in this region of low strain and low normalised stroke, so the only conclusion is that a minimum of 150 cycles (at the maximum stroke) would be expected to lead to failure of the UFP. However, going by the trend of the results, it would be expected that the UFP could undergo more than 150 cycles before failure. Of course it is also highly unlikely that the UFP would ever be subjected to such a high number of large stroke displacements. It is much more likely to undergo a large number of low displacement cycles. A maximum stroke of 105 mm was chosen as it represented the maximum possible connection displacement when the test-frame was at 3.5% drift. Further research into the medium to high-cycle fatigue performance of UFPs is required.

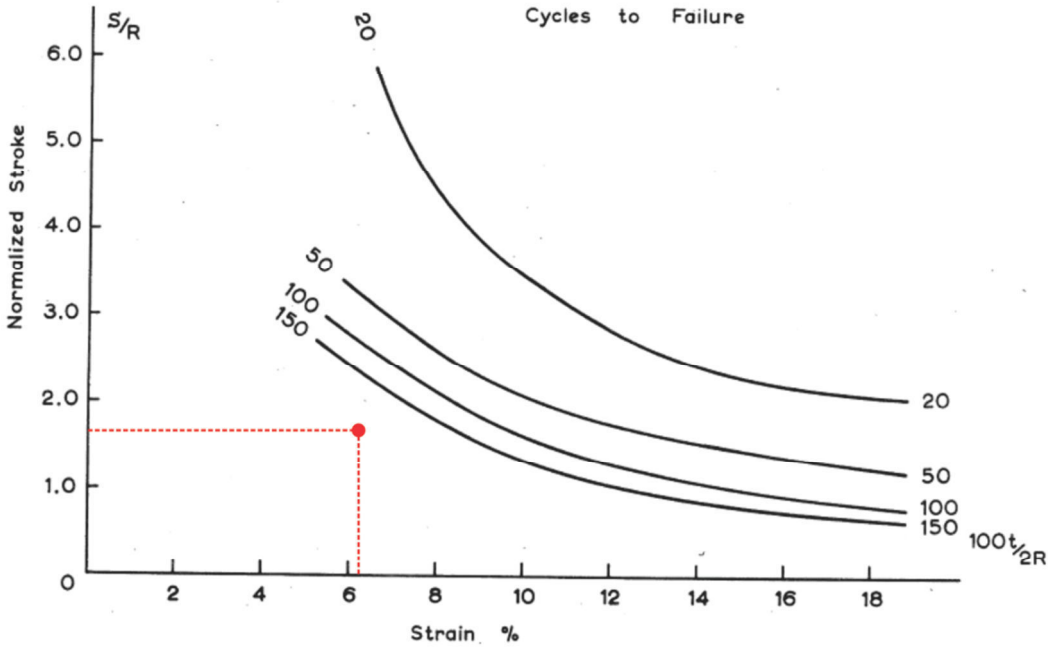

Figure 8-6: Number of cycles to failure (Kelly et al., 1972)

8.4 Connection Testing

In order to characterise the behaviour of the UFPs connections, a series of tests were performed using an Instron Materials Testing Machine. A displacement controlled loading protocol was used to undertake the quasi-static, cyclic loading. The quasi-static loading

regime consisted of three cycles at each displacement level, with the maximum displacement being ±82.5 mm (equivalent to 2.75% drift of the full-scale test frame). The loading rate was varied between 0.5 mm/sec up to 5 mm/sec according to the magnitude of the displacement cycle. The procedure defining the loading protocol was adopted from the ACI recommendations (ACI - 374.1R, 2005).

Two UFPs were tested in parallel in order for the loading to be symmetric. This was done to prevent a moment being applied to the loading apparatus and load cell. The UFPs were tested both by themselves and inside the RHS housing. The testing setup of the UFPs inside the RHS housing is illustrated in Figure 8-7. The setup consisted of the two RHS housing being fixed to a base platform with a gap in between. A smaller RHS section (referred to herein as the loading RHS) was attached to the loading actuator of the Instron testing machine and was driven up and down between the two larger RHS sections in order to impose the displacement demand upon the UFPs. A 50 kN load cell was attached to the top of the loading RHS to record the load and a linear potentiometer on the side of the Instron was used to record the vertical displacement.

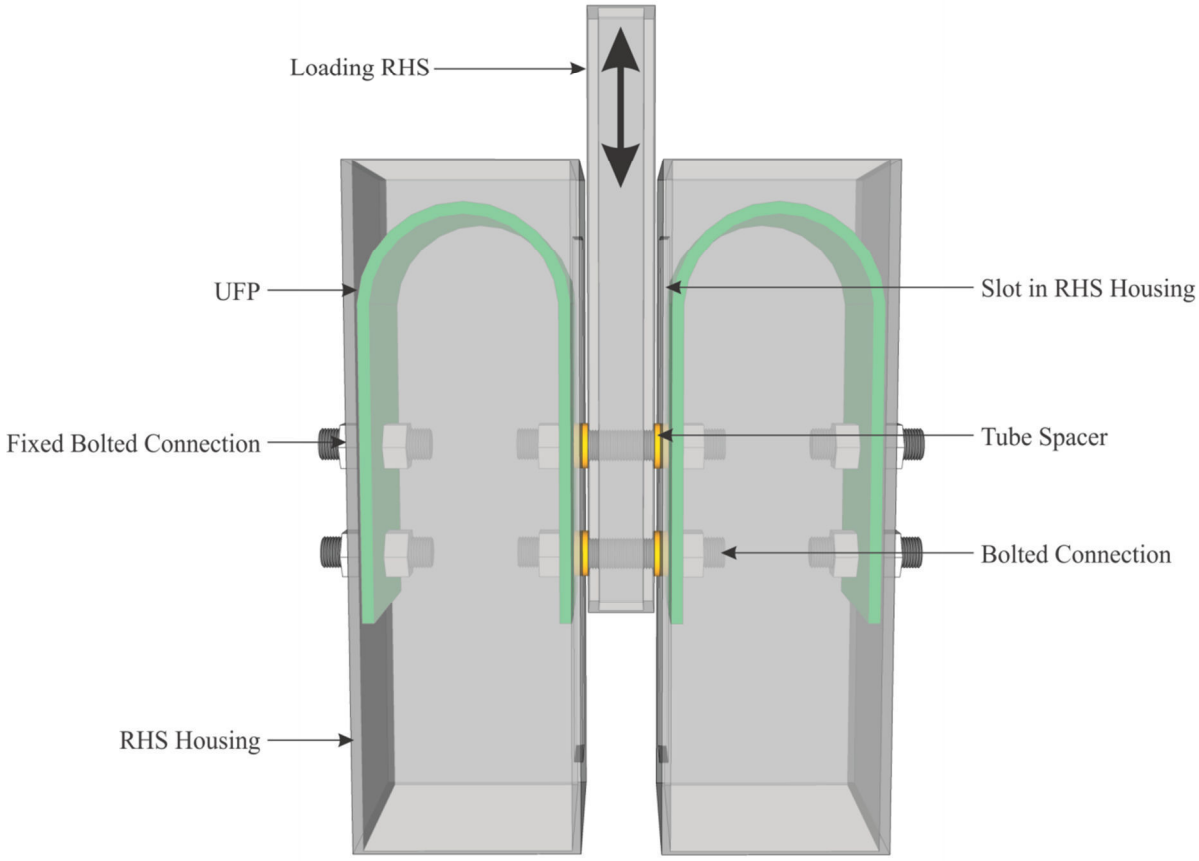

Figure 8-7: UFP component testing setup with housing

As shown in Figure 8-7, the UFPs were fixed to the inside the housing by two 16 mm bolts on the outer face. On the inside face the housing was slotted to allow the bolts on this side of the UFP to move up and down. The UFPs were bolted firmly against the loading RHS using a tube spacer to ensure that they were not pressed against the inside of the housing.

When tested without the housing, the UFPs were bolted directly to the loading RHS. The housing was still used as the support for the UFPs but was cut away on the inside so that there was no sliding surface. Photographs of both test setups are shown in Figure 8-8 along with photos of the UFPs at the maximum imposed displacement of 82.5 mm.

Figure 8-8: UFP component testing with housing (top left) without housing (top right), flaking of steel at maximum upward stroke (bottom left), deformed shape at maximum upward stroke (bottom right)

8.4.1 Results

The hysteretic behaviour of two of the tests performed is shown in Figure 8-9. The force recorded by the load cell has been halved so the force shown in the force provided by a single UFP. The left figure shows the force displacement behaviour of a UFP housed inside the slotted RHS (refer to Figure 8-8 (left)) and the right figure shows the behaviour of a UFP attached directly to the loading RHS, i.e. without any housing (refer to Figure 8-8 (right)). It can be seen that the behaviour of the two systems is virtually identical. The maximum force of the housed UFP is slightly larger in the housing and also slightly less consistent than when not in the housing. This is likely due to friction between the UFP and housing.

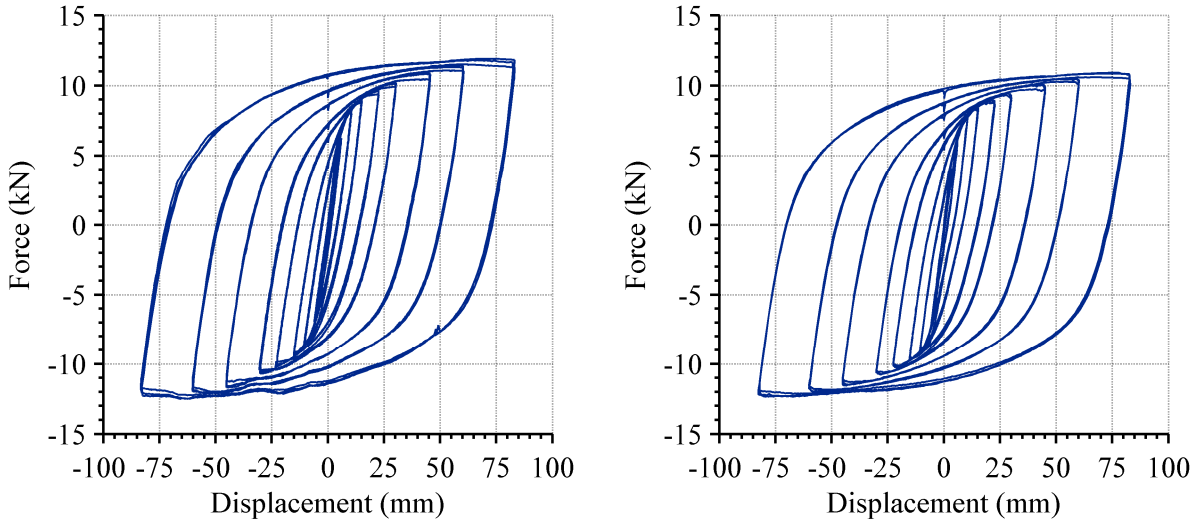

Figure 8-9: Force displacement hysteretic behaviour of housed (left) and unhoused (right) UFP

The yield force was found to be approximately 6 kN and yield displacement approximately 7 mm. Therefore the UFPs were tested to a displacement ductility of approximately 10. It can be seen that the UFPs produce a stable hysteretic loop with the maximum force in a single UFP of approximately 12.5 kN. This is greater than the design force of 9.6 kN due to strain hardening in the steel (Bauschinger effect).

The overstrength ratio between the design force and maximum force is 130%. This is lower than that suggested by Kelly et al. (1972) who found that overstrength can be in the order of 145 – 215% greater than the theoretical plastic design force. However, the tests performed by Kelly et al. (1972) subjected the UFPs to high strokes relative to their radius. This resulted in high strains and large overstrength values and consequently a relatively low number of cycles to failure. The UFPs tested here have a considerably lower stroke to radius

ratio; hence the maximum strains and overstrength are lower. A proposed definition of the overstrength factor for UFPs is presented in Chapter 9 using finite element analyses.

The shape of the UFPs was found to not change significantly during testing. Shown in Figure 8-10 (left) are two UFPs: the one of the left has not been tested and the one of the right has been. From this figure it is difficult to distinguish any difference between the two. However, on close inspection, the bend at the top of the UFP was observed to alter slightly. An amplified (not to scale) representation of the bend shape at the top of the UFP is illustrated in Figure 8-10 (right). It was found that the bend diameter formed a smaller radius region around the tip. This feature was only pronounced after the largest stroke cycle.

Figure 8-10: Photograph of deformed shape of untested UFP (left) and UFP after testing, with exagerated shapes shown (right)

Because of this change in shape it can be seen how multiple large stroke displacements would evidently produce strains higher than those initially designed for and consequently possible failure of the UFP. The hysteretic behaviour shown in Figure 8-9 does not suggest failure is imminent since there is no decrease in strength. One of the UFP tests concluded with twenty cycles at maximum stroke and no drop in strength was evident nor was any sign of imminent failure observed. This result confirms that the behaviour of UFPs is highly reliable and robust, especially when the maximum strain is limited (in this case less than 6%).

8.5 Full-Scale System Testing

The full-scale, single-bay, single storey frame subassembly introduced in Chapter 4 was used to test precast concrete cladding systems utilising UFP connections. The implementation of UFPs as cladding connections is presented in this section.

8.5.1 Experimental Sub-assembly

A short summary of the full scale experimental sub-assembly used for testing is presented here, for more information refer to Chapter 4. The experimental sub-assembly testing frame represents a portion of a reinforced concrete moment resisting frame. The beam and column members were individually cast and the beam-column connections utilise Precast Seismic Structural System (PRESSS) technology which allows the frame to be tested repeatedly to high drift levels with different claddings without sustaining significant structural damage (Priestley et al., 1999). The experimental sub-assembly test frame was constructed at full-scale so that real-size connections and cladding components could be used. The inter-storey height was 3.0 m and bay spacing was 3.8 m, as shown in Figure 8-11.

The frame is subjected to increasing levels of drift using a hydraulic jack attached to the top of the west column. The testing regime was that of a simple racking test. A racking test is the typical experimental testing procedure used to test the seismic performance of cladding (AS/NZS 4284, 2008). A racking test aims to replicate the relative inter-storey displacements observed during an earthquake. This cyclic, quasi-static loading enables deformation limits to be established using damage observations (Wang, 1987). The quasi-static loading regime consisted of three cycles at each specified drift ratio. The procedure defining the loading protocol was adopted from the ACI recommendations (ACI - 374.1R, 2005).

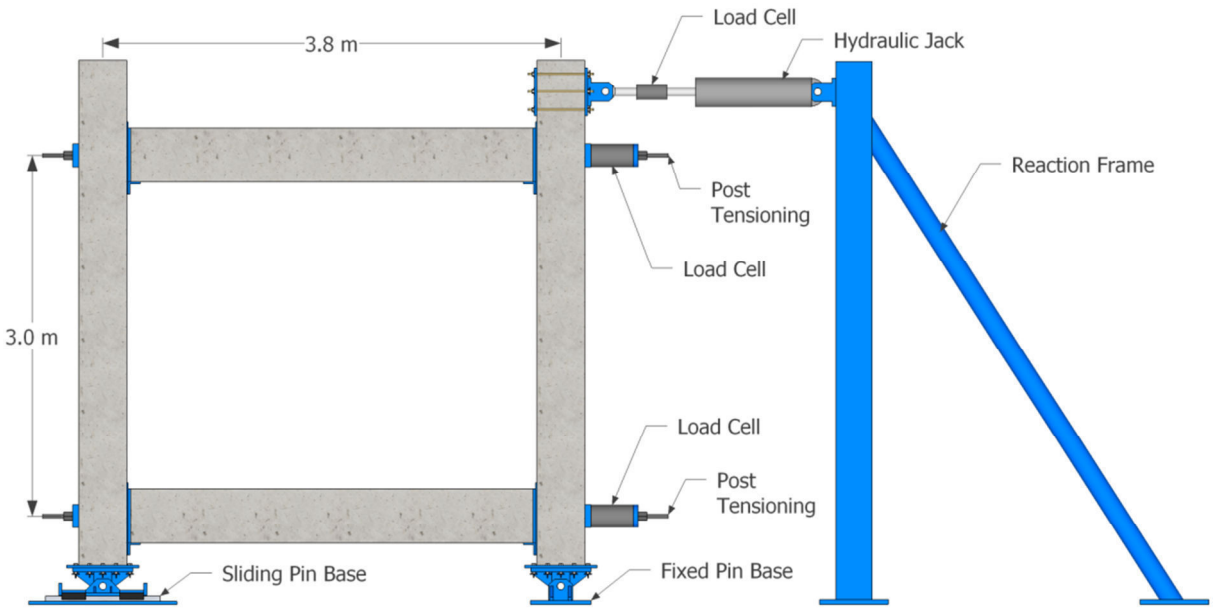

Figure 8-11: Experimental test set-up including loading apparatus

Two sizes of precast concrete panels were tested. One size was a full-bay, single-storey panel and the other a half-bay, single storey. Both panels have central, single opening for which a normally would normally be located. The panels were 120 mm thick and contained a single layer of reinforcement.

8.5.2 Cladding Connections

The precast concrete panels were attached to the frame using two different connection types: bearing connections and UFP connections. The bearing connections located at the base of the panels, and the UFP connections were located at the top of the panel as shown in Figure 8-12.

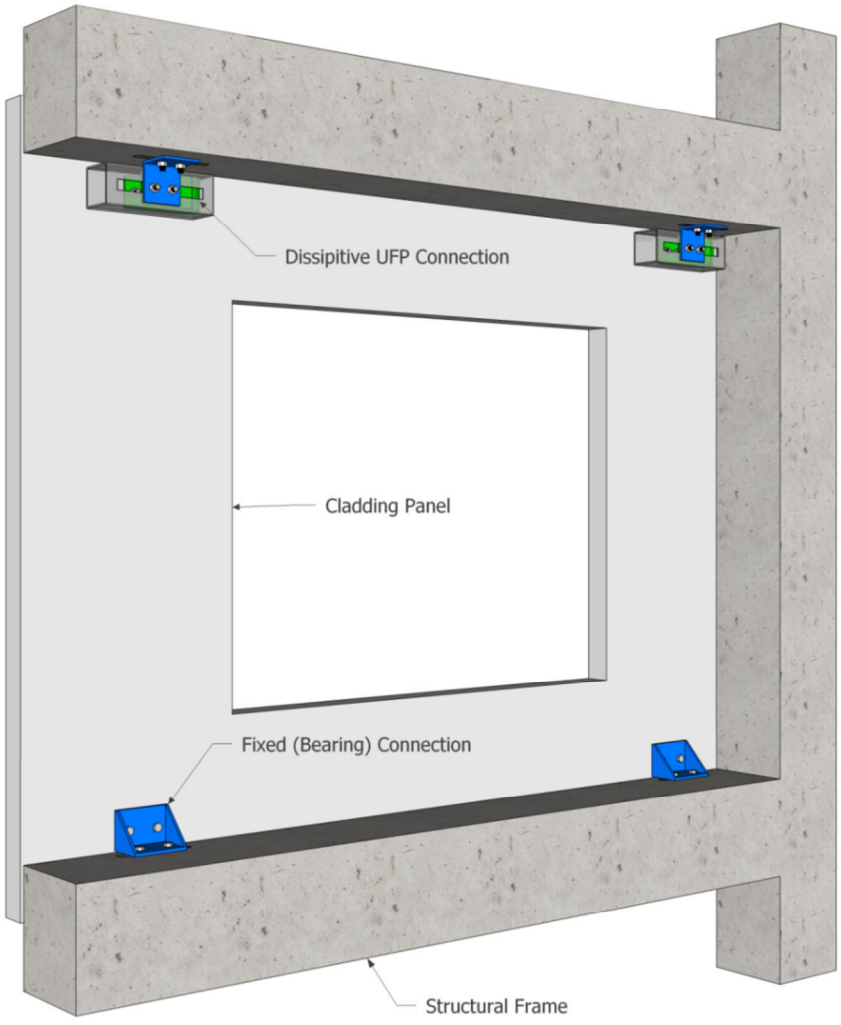

Figure 8-12: Cladding panel setup with connection types and locations

The bearing connections carry the gravity load of the panel back to the frame. These connections are metal angles securely bolted into place using anchors cast into the panel and frame and are located at the base of the panel. The bearing connection is not able to

accommodate movement between the panel and frame as it is a fixed connection between the panel and the frame.

The UFP connections are located at the top of the panel. They must be able to resist out-of-plane forces due to wind and earthquake loading as well as be able to accommodate in-plane relative movement between the frame and the cladding panel during earthquake induced movement. It is the relative movement between the panel and frame which activates the UFPs and dissipates earthquake energy.

The UFP connections were bolted to the underside of the top beams using 300 mm long t-channels that were cast into the concrete. The connection to the panels made use of the 10 mm thick steel plates secured to the panel with four cast-in ferrule anchors.

Different configurations of UFP connections were tested; including housed and un-housed UFPs as well as the UFPs in different orientations, as shown in Figure 8-13.

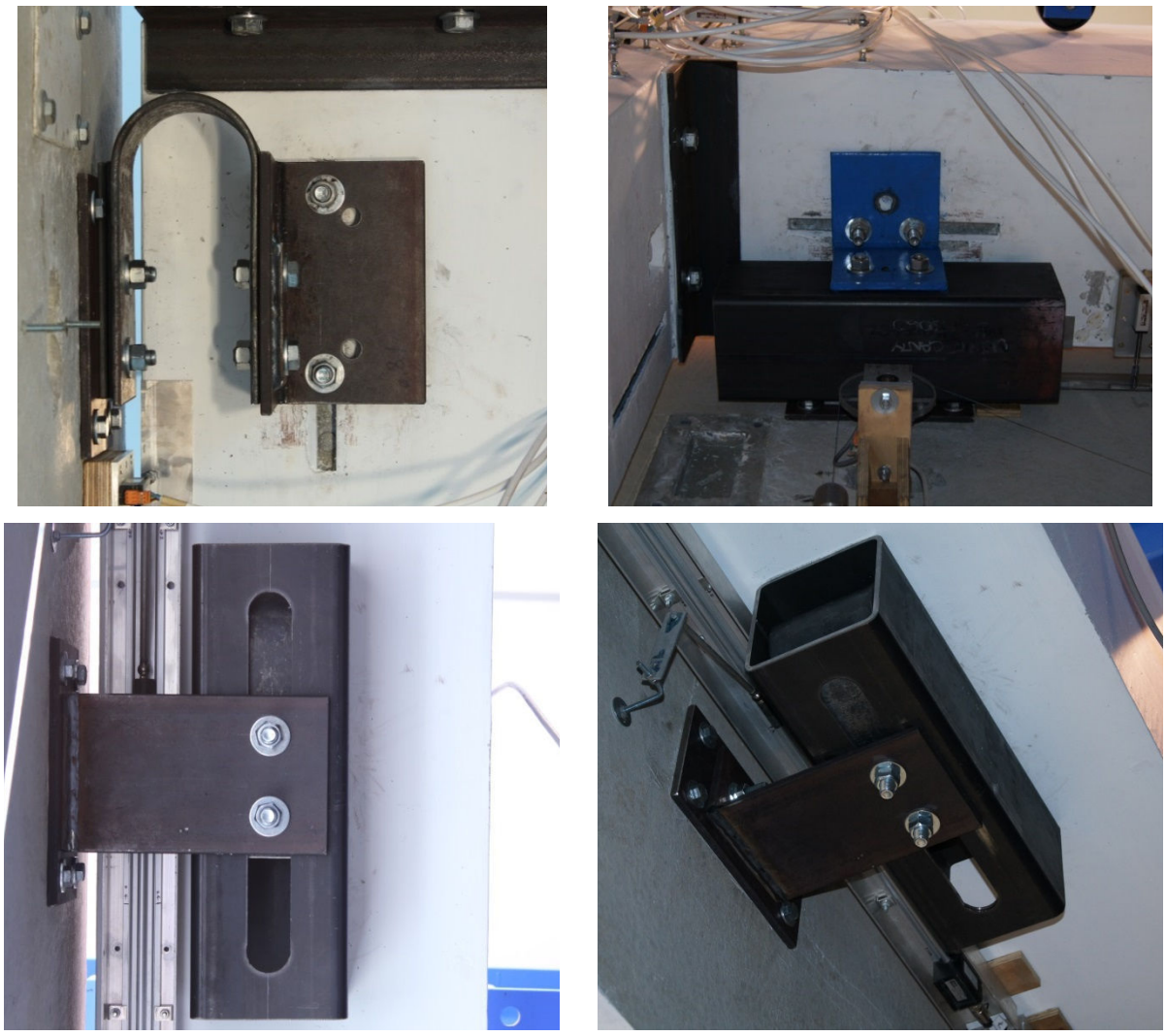

Figure 8-13: Photographs of different UFP connection configurations tested: configuration 1 -unhoused (top left), configuration 2 - housed (top right), configuration 3 - housed (bottom left and bottom right)

The aim of testing different configurations and orientations was to determine if an optimal configuration existed, as well as to discover possible drawbacks from using the connections. The un-housed UFPs were also tested in combination with slotted connections so that out-of-plane restraint requirements were met. A full description of the systems tested is presented in the following section.

8.5.3 Details of Specimens

A total of nine full-scale cladding systems were tested with UFP connections. Due to the ductile nature of the connection, each configuration was only tested once. Testing utilised both panel sizes as well as the inclusion of the slotted connections tested in Chapter 4. Of the nine different tests performed, a total of four different UFP configurations were possible. Each configuration varied the location of the sliding interface and the orientation of the UFP, as shown in Figure 8-14.

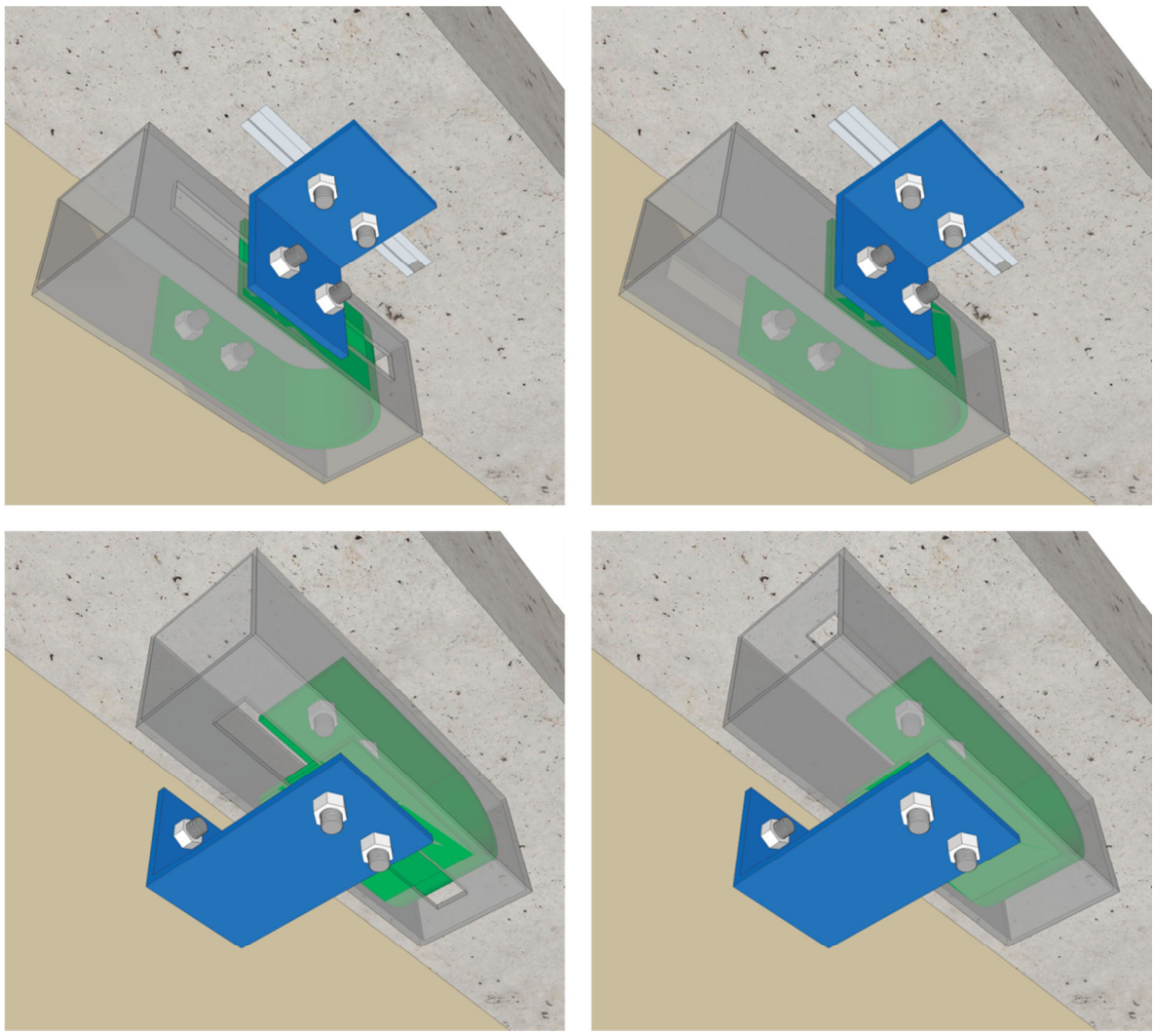

Figure 8-14: UFP configuration 1 (top left), 2 (top right), 3 (bottom left) and 4 (bottom right)

Configuration 1 corresponds to the RHS housing being fixed to the panel with the slot facing outwards with the movement occurring between this outside face of the housing and the metal angle on the underside of the beam.

Configuration 2 is similar to Configuration 2; however, the housing is flipped so that the sliding movement occurs between the housing and the panel.

Configuration 3 corresponds to the RHS housing being fixed to the underside of the beam with the slot facing outwards and the movement occurring between this outside face of the housing and the L-shaped metal angle connected to the panel.

Configuration 4 is similar to Configuration 3; however, the housing is flipped so that the sliding movement occurs between the housing and the underside of the beam.

The UFPs were removed and replaced following all but one of the tests (Test MP-UFP5). All of the systems tested had the UFP connections attached to the underside of the beam. The two first tests were performed up to the 1.5% drift cycle because of movement allowance restrictions which will be expanded upon in the following section. The subsequent seven tests were performed up to the maximum drift cycle of 3.5%. The nine different tests are summarised in Table 8-1.

Table 8-1: UFP connection tests

Test ID	Panel Size	Number	Housed	Configuration	Details
MP-UFP1	Mono Panel	2	No	1	2 UFPs
MP-UFP2	Mono Panel	2	No	1	2 UFPs + 2 Slotted
MP-UFP3	Mono Panel	2	Yes	1	2 Housed UFPs
MP-UFP4	Mono Panel	4	Yes	1	4 Housed UFPs
MP-UFP5	Mono Panel	2	Yes	2	2 Housed UFPs
MP-UFP6	Mono Panel	2	Yes	3	2 Housed UFPs
MP-UFP7	Mono Panel	2	Yes	4	2 Housed UFPs
DP-UFP1	Dual Panel	2	Yes	1	2 Housed UFPs
DP-UFP2	Dual Panel	4	Yes	1	4 Housed UFPs

The 30 UFPs used for all tests were fabricated out of 8 mm thick, 120 mm wide Grade 300 steel plate. The fabricator of the UFPs was a local spring maker who heated the plates prior to bending. Each UFP was bent around a fixed diameter of 120 mm. The cost for the steel and to fabricate each UFP was NZ$32.66 excluding goods and services tax (GST).

8.6 Test Results

The key test results of the nine tests are presented in this section. The response of the clad frame is compared to the bare frame response of the test frame. The bare frame response

was established by undertaking three consecutive tests without any cladding attached (refer to Section 5.6.1 for further information on the bare frame response). This ensured a repeatable behaviour in the frame was established. In this way, the interaction of the cladding with the bare frame could be accurately determined.

The results of the nine tests are presented in the order they were performed and are grouped according to the panel type used for testing (mono panel or dual panel).

8.6.1 Mono Panel Tests

The force-displacement behaviour of the frame-cladding system during test MP-UFP1 is illustrated in Figure 8-15 (left). This test consisted of only the UFPs at the top and was performed up to 1.5% drift. When the behaviour of the frame-cladding system is contrast with behaviour of the bare frame alone it can be seen that the UFP connections are increasing the strength and stiffness of the system while also adding hysteretic behaviour.

The force difference between test MP-UFP1 and the bare frame test can be computed and is shown below in Figure 8-15 (right). It can be observed that the cladding adds a maximum of approximately 20 kN to the bare frame system.

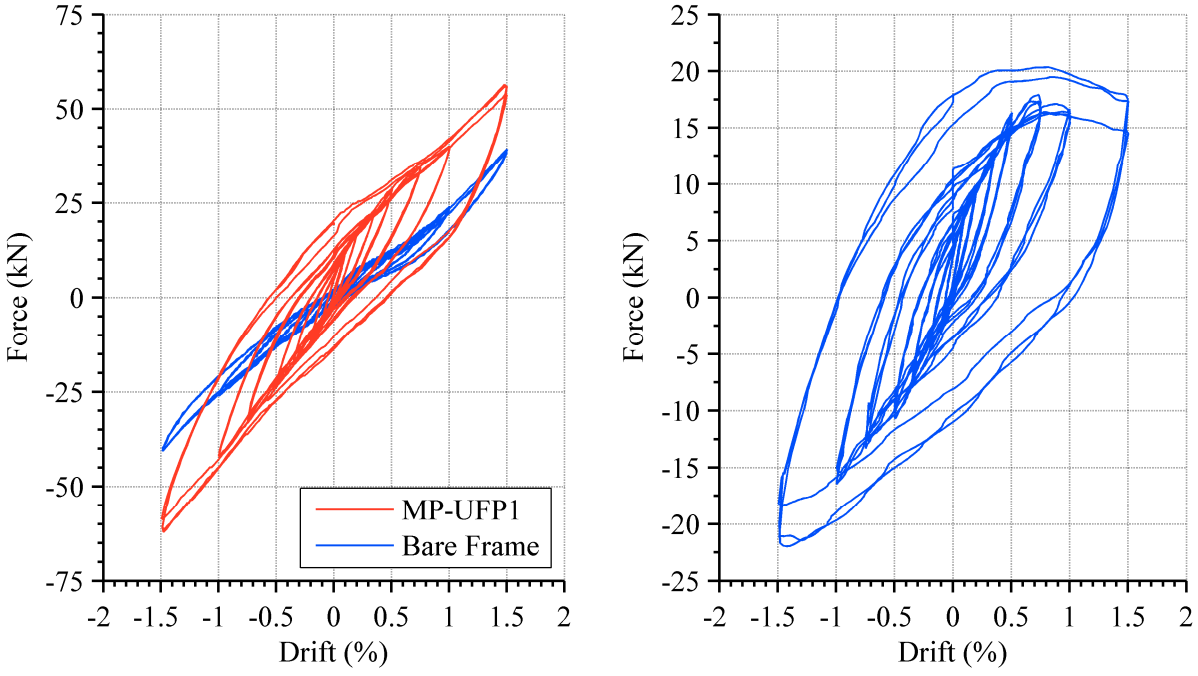

Figure 8-15: Force-drift behaviour (left) and difference between clad and unclad frame (right) for UFP connection test specimen MP-UFP1

The test had to be stopped after the 1.5% drift cycle due to the out-of-plane movement of the panel being unacceptable. Figure 8-16 shows the distortion to the UFP that occurred during testing as well as the final shape of the UFPs when removed.

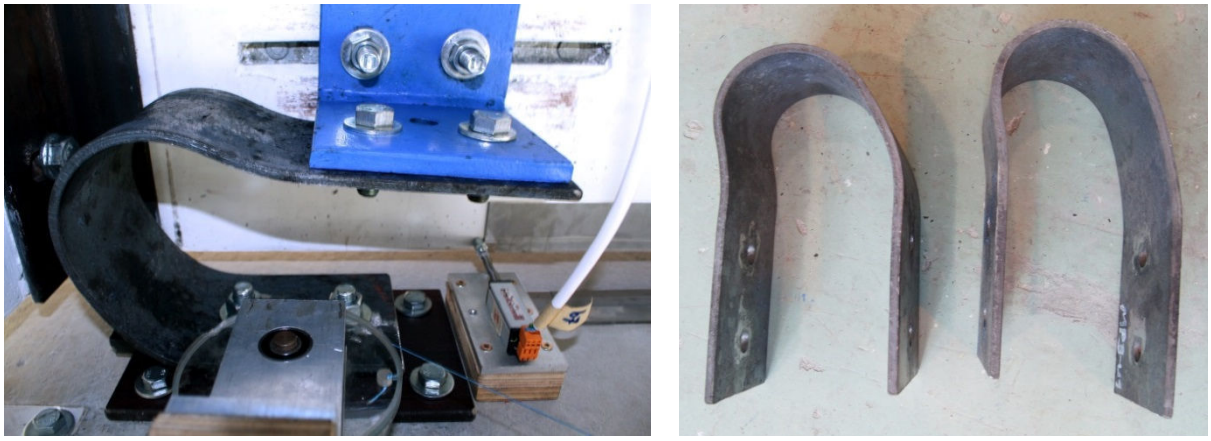

Figure 8-16: Distortion of unconstrained UFP during test MP-UFP1 (left) and final shape of UFPs after testing (right)

The two parallel ends of the UFPs moved apart during the cyclic testing causing the panel to move approximately 25 mm outwards. This caused the panel to come to rest on the out-of-plane safety support. Clearly, without additional out-of-plane restraint, the use of UFPs as a cladding connection is unsuitable due to this unstable out-of-plane behaviour. Thereafter, the steel angles were altered to properly restrain the UFPs so that the deformation was more symmetric (refer to Figure 8-3).

The force-displacement behaviour of the frame-cladding system during test MP-UFP2 is illustrated in Figure 8-17 (left). This test again consisted of two UFPs at the top and was performed up to 1.5% drift.

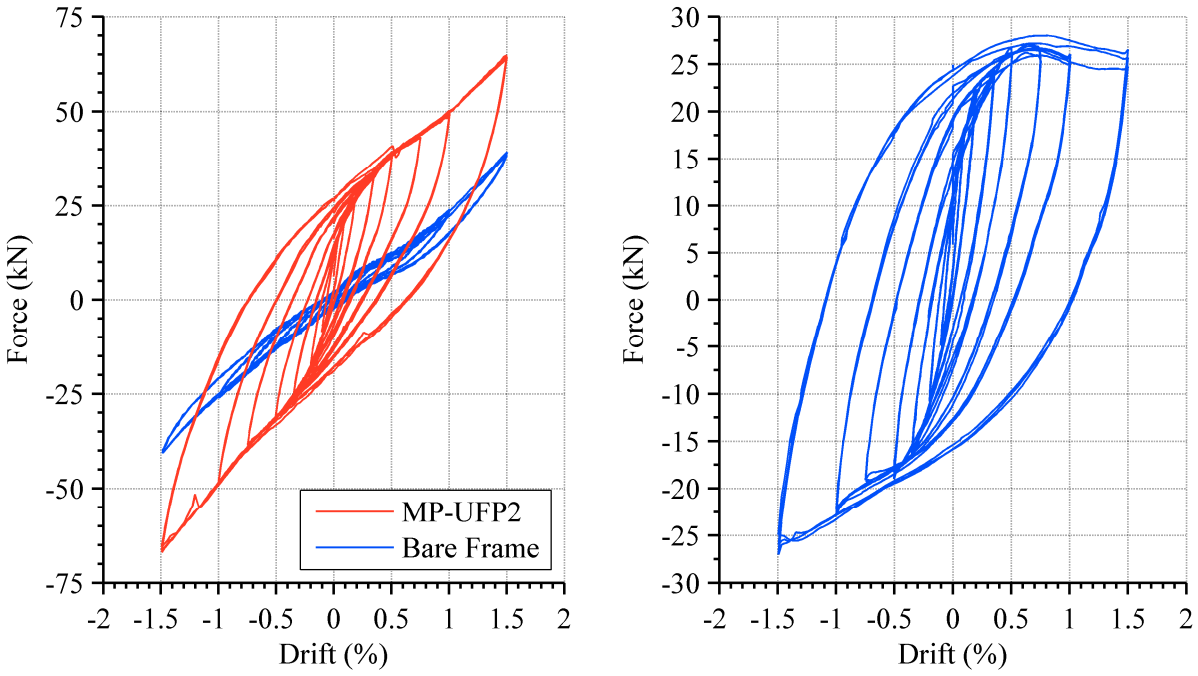

Figure 8-17: Force-drift behaviour (left) and difference between clad and unclad frame (right) for UFP connection test specimen MP-UFP2

This test was different to MP-UFP1 because additional slotted connections were attached to the top of the panel to provide out-of-plane restraint. It can be observed that the cyclic behaviour was much more stable during this test. The force in the cladding system increases compared to MP-UFP1, as shown in Figure 8-17 (right). This is likely attributed to the confinement of the UFPs as well as some level of friction in the slotted connections. Consequently, it can be seen that a greater level of dissipation was also occurring.

Since the UFPs were properly restrained, test MP-UFP2 did not have the same problems with distortion as MP-UF1. The final shape of the UFPs can be seen in Figure 8-18. It is evident that the UFPs are slightly out-of-shape, with the deformed shape resembling that depicted in Figure 8-10 with a slight narrowing of the bend radius. The amount of permanent deformation observed was definitely more visible for this connection detail as opposed to when the UFPs were contained in the RHS housing during component testing (and during latter system tests).

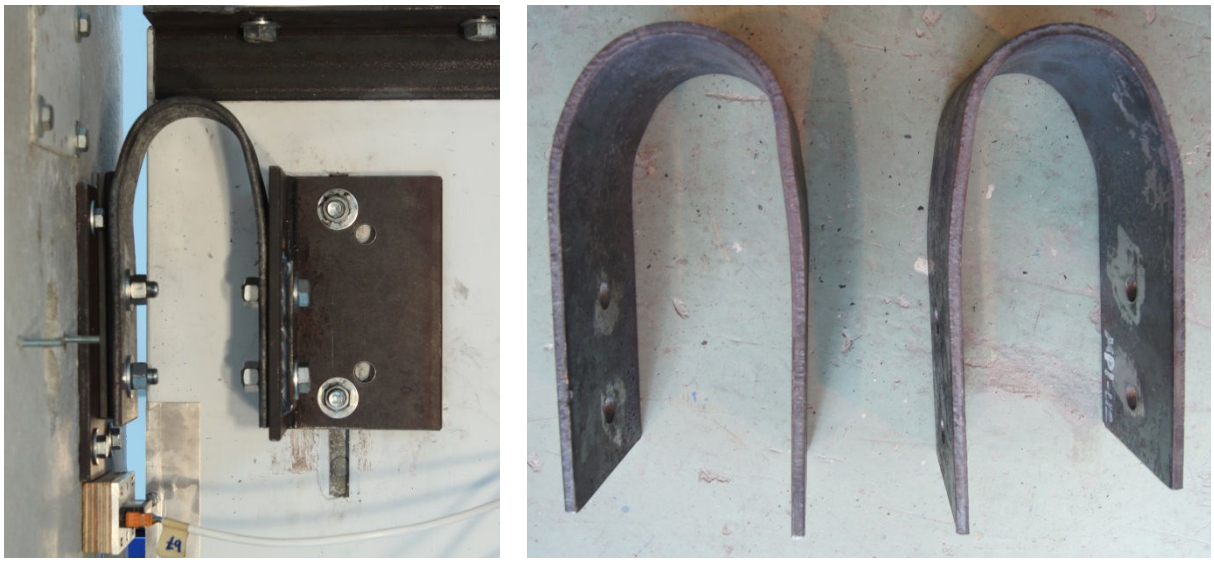

Figure 8-18: Deformed shape of constrained UFP during test MP-UFP2 (left) and final shape of UFPs after testing (right)

The force-displacement behaviour of the frame-cladding system during test MP-UFP3 is illustrated in Figure 8-19 (left). This test was the first test to include the RHS housing of the UFP connections. Again, two UFP connections were used. The orientation of the UFP connection housing was that of 'Configuration 1', shown previously in Figure 8-14. The slots in the housing were long enough so that the test could be performed up to 3.5% drift.

The cyclic behaviour of the system is very stable; it is very hard to distinguish any difference between the three cycles at each drift level in Figure 8-19 (left). The UFP connections clearly add a significant amount of dissipation compared to the bare frame. The

force in the system is larger compared to both MP-UFP1 and MP-UFP2, as shown in Figure 8-19 (right). This is likely attributed to additional friction from the UFP being inside the housing as well as the confinement of the UFPs as well as increased strain hardening of the steel. It can be seen that during the 1.5% drift cycle the maximum force is actually lower than that found during test MP-UFP2. Hence it would appear that the friction from the UFP housing is similar or less influential than that of a typical slotted connection.

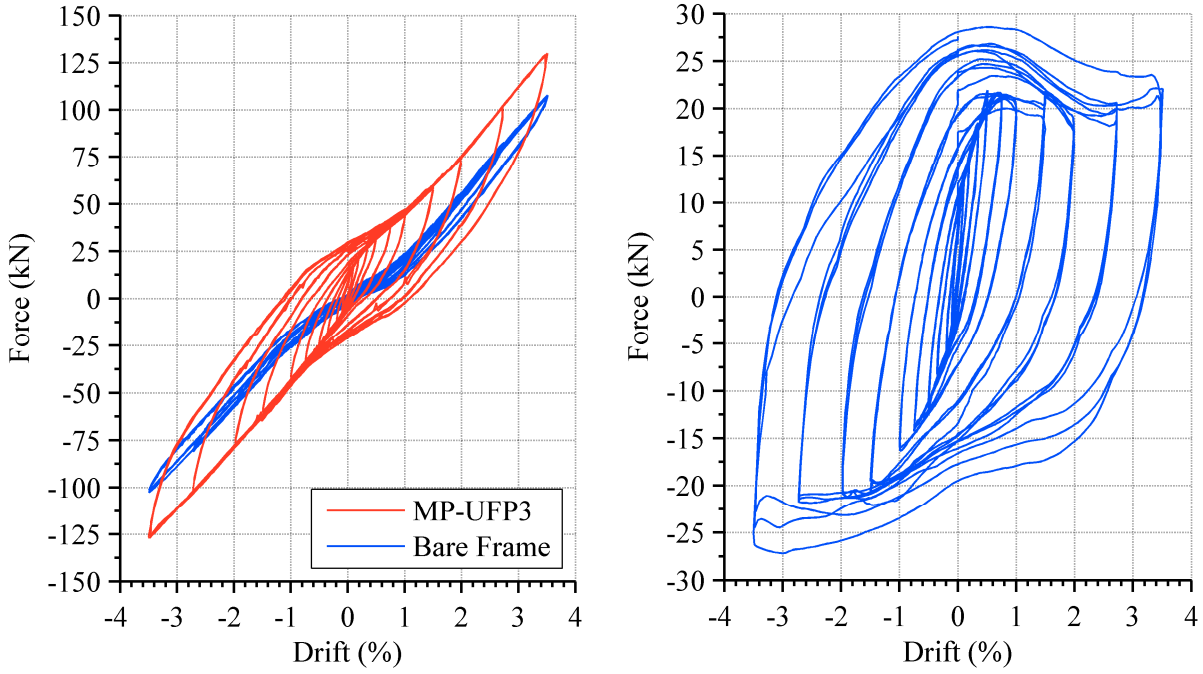

Figure 8-19: Force-drift behaviour (left) and difference between clad and unclad frame (right) for UFP connection test specimen MP-UFP3

There is no strength or stiffness degradation through the higher cycles to suggest damage is occurring in either the cladding panel or the frame. Inspection of the panel during testing confirmed that no cracking had occurred to the panel. The UFP connections did not show any signs of fatigue and retained their shape after being tested to large drifts. The permanent deformation of the UFPs after being tested was significantly reduced when the housing was used. It can be seen in Figure 8-20 that the shape is very similar to that of an untested UFP.

When a new UFP was put into the RHS housing, a 2 mm clearance between the UFP and the inside of the housing would be present. After being tested, this gap would no longer be present, with the UFP pressing against the inside of the RHS. However, the UFP was always able to be easily removed by hand.

Figure 8-20: UFP being placed inside RHS housing (left) and untested UFP shape compared with tested UFP shape (right)

As introduced earlier, the effect of the housing is to properly constrain the UFP so that the yield point moves back and forth along the plate as the radius of curvature of the plate is changed from straight to curved and vice versa. When constrained properly, as shown in Figure 8-21 (top), a significant portion of the region of the UFP is forced to yield. This is due to different regions of the plate yielding as the displacement is cycled in each direction.

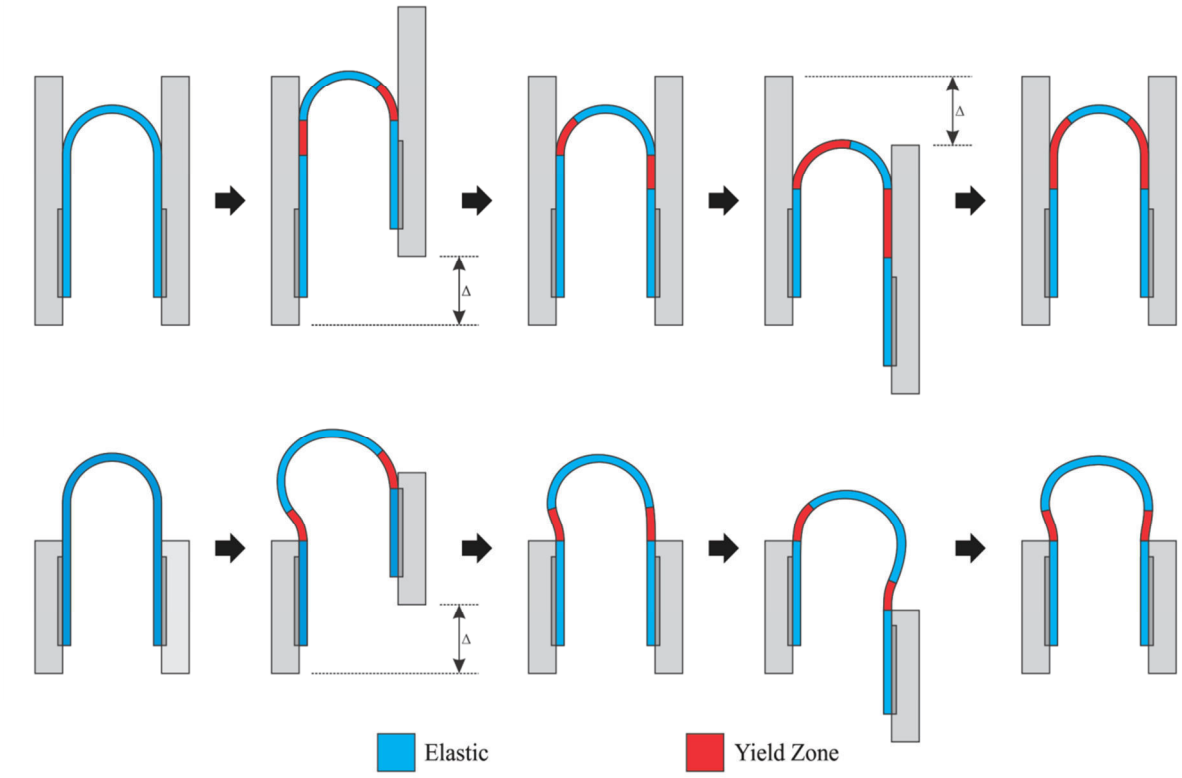

Figure 8-21: Comparison of yielding zone in constrained UFP (top) and unconstrained UFP (bottom)

Conversely, the yield point of a poorly constrained UFP will not move back and forth in the same way, as shown in Figure 8-21 (bottom). Instead, the UFP will bend

asymmetrically, concentrating the yield zone at the region above the UFP restraints. Consequently, the final deformed shape has a larger radius and was often found to be asymmetrical, believed to be due to the initial loading direction.

Since the UFP is inclined to bend outwards if not restrained, as illustrated in Figure 8-21 (bottom), a lateral force must be present to prevent this from occurring. This force is quantified with Finite Element Analyses in the following chapter. It is possible that this lateral force would cause the friction force between the UFP and housing to increase. Since the UFPs were able to be removed by hand following testing it is not believed the lateral forces generated are large enough to develop significant friction forces.

The force-displacement behaviour of the frame-cladding system during test MP-UFP4 is illustrated in Figure 8-22 (left). This test made use of four UFP connections in the same configuration as the previous three tests. The additional connections were located near the centre at the top of the panel and were of the same configuration of the previous connections.

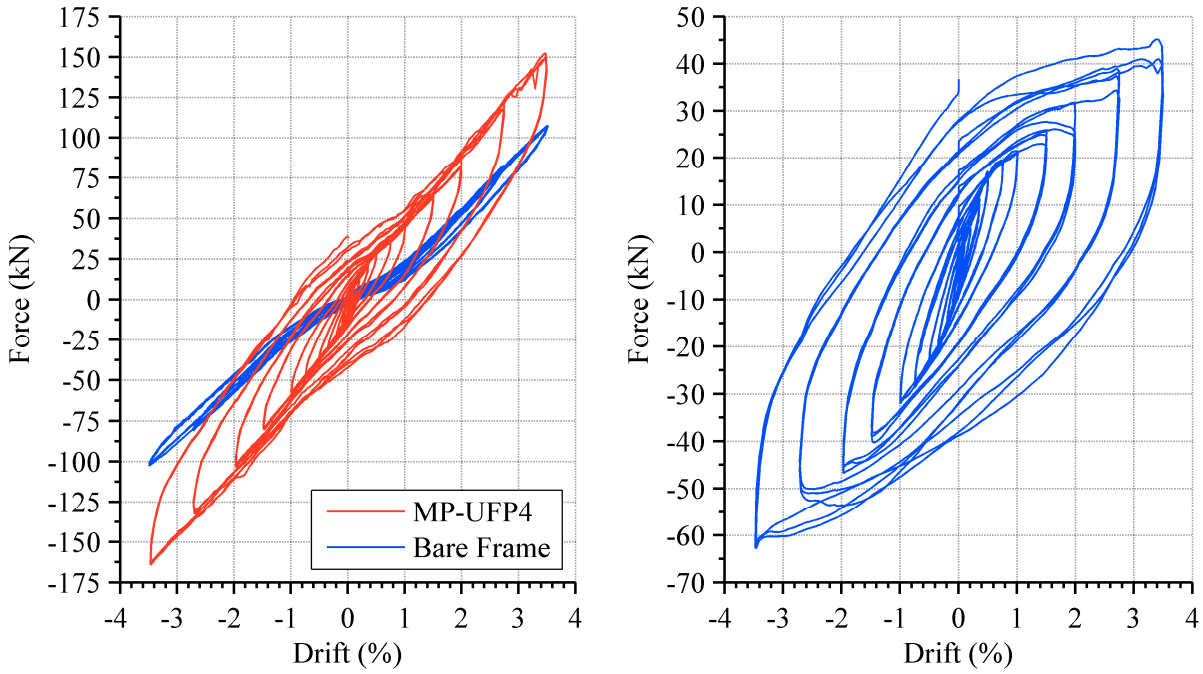

Figure 8-22: Force-drift behaviour (left) and difference between clad and unclad frame (right) for UFP connection test specimen MP-UFP4

As shown in Figure 8-22 (right), the four UFP connections transfer up to 60 kN of force into the panel. The panel had already been tested with the traditional connections prior to testing the UFP connections. Consequently, it was not possible to tell if this magnitude of force would crack the panel since it was already cracked from this previous testing. However, the previous testing found that the panel first cracked when the lateral force exceeded 33 kN

and these cracks exceeded serviceability limit state when the force reached 39 kN. It can therefore be presumed that if an undamaged panel was tested then it would have cracked when tested with the four UFP connections. This would not be a satisfactory outcome for the connection to be deemed low-damage.

The following tests investigated the effect the orientation of the UFP connections has upon the cyclic response. For details of each configuration, refer to Figure 8-14. The orientation of the UFP in Configuration 2 was the same as that in Configuration 1 but the sliding interface was flipped so that it was between the panel and the connection. The response of Configuration 2 was found to be virtually identical to that of Configuration 1 so is not presented here.

The orientation of the UFP was rotated 90 degrees for Configuration 3 and 4. Configuration 3 consisted of the UFP being fixed to the underside of the beam with the slotted interface between the opposite side of the RHS housing and a steel angle attached to the panel, as shown in Figure 8-24. Test MP-UFP6 has two UFP connections in this configuration. The force-displacement behaviour of the frame-cladding system is illustrated in Figure 8-23 (left).

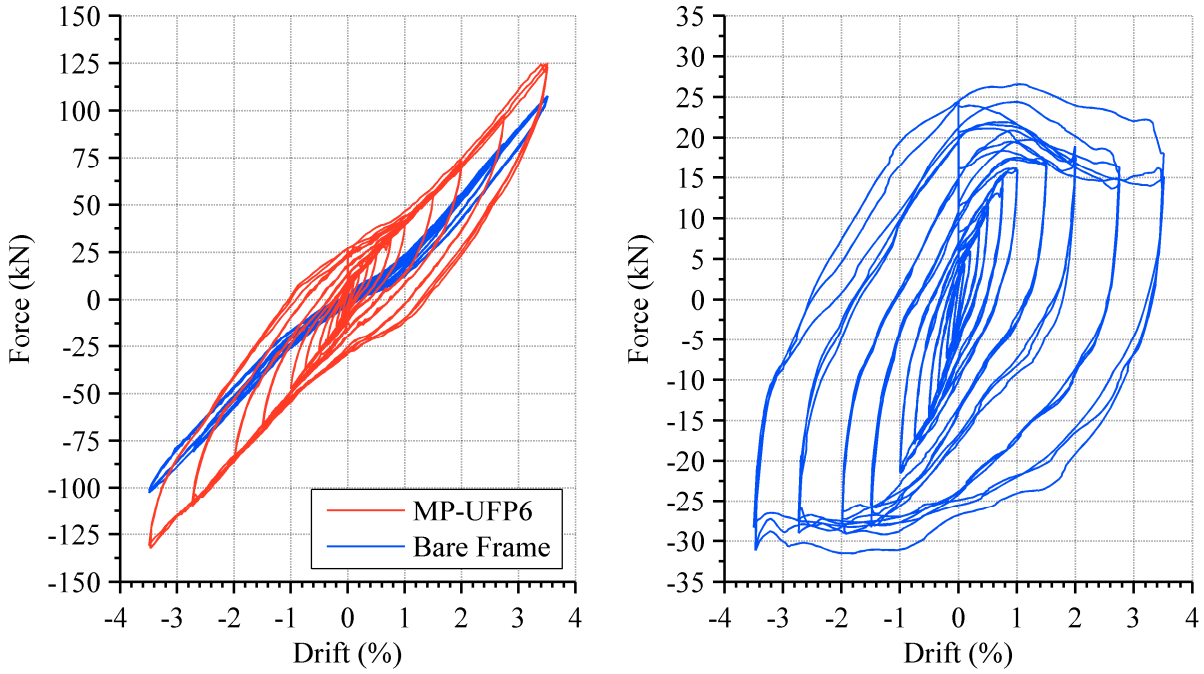

Figure 8-23: Force-drift behaviour (left) and difference between clad and unclad frame (right) for UFP connection test specimen MP-UFP6

The hysteretic behaviour of the connection in this configuration is again reasonably stable, however, it can be seen in Figure 8-23 (right) that the magnitude of the force

transferred into the panel in this configuration is greater than that of Configuration 1 (refer to test MP-UFP3 shown in Figure 8-19). This additional force could be due to a number of possible factors. Firstly, a small amount of burnishing and galling was observed to both the interior and the exterior of the RHS housing due to the steel on steel friction of the connection. This can be seen as the shiny region in Figure 8-24 (left).

The additional force is also possible due to the UFP twisting slightly. The UFP connection twisted due to the larger eccentricity of the force acting through the connection. This eccentricity caused a larger moment to be applied to the UFP and due to a small amount of flex in the longer steel angle and in the connection to the underside of the beam; the UFP was able to rotate slightly, as shown by comparing the two photographs shown in Figure 8-24.

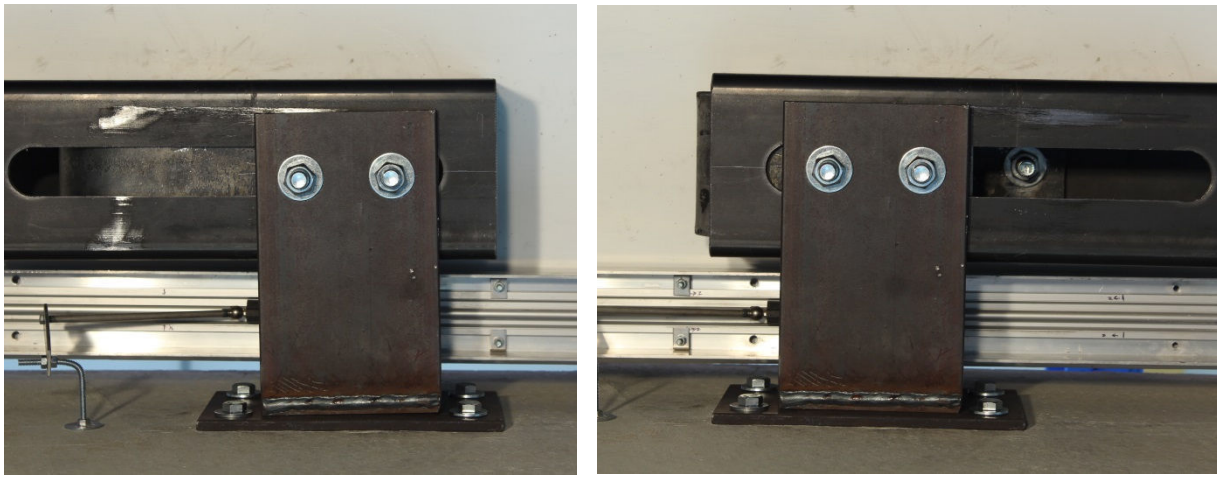

Figure 8-24: Rotation and friction burnishing of UFP connection elements in Configuration 3

The orientation of the UFP in Configuration 4 was the same as that in Configuration 3 but the sliding interface was flipped so that it was between the connection and the underside of the beam. The response of Configuration 4 was found to be very similar to that of Configuration 3 so is not presented here.

8.6.2 Dual Panel Tests

Two tests of the dual panels were performed using UFP connections. The two tests utilised Configuration 1 where the UFP connections are fixed to the panel. The first dual panel system consisted of each panel being connected to the frame with one UFP connection and one slotted connection. Because of the smaller width of the panel, the maximum number of connections possible on each dual panel is two, compared to the wider mono panel which can accommodate four connections. Therefore, the connections had to be asymmetrical when

only one UFP connection was used. The UFP connection was placed in the corner of each panel closest to the beam-column joint and the slotted connection placed in the centrally located connection.

The force-displacement behaviour of the frame-cladding system during test DP-UFP1 is illustrated in Figure 8-25 (left). It can be seen that the cyclic behaviour of the system is very stable. The overall behaviour is very similar to that of MP-UFP3 where two UFP connections were also used in the same configuration. The force in the cladding system, as shown in Figure 8-25 (right), is also very similar.

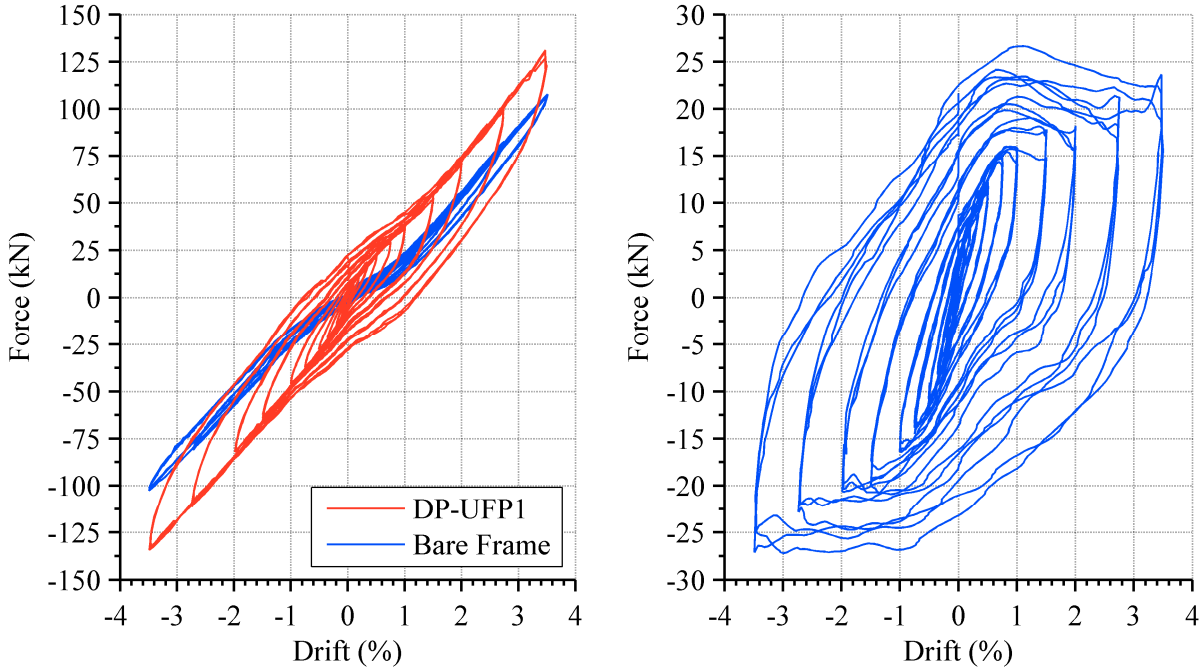

Figure 8-25: Force-drift behaviour (left) and difference between clad and unclad frame (right) for UFP connection test specimen DP-UFP1

The force-displacement behaviour of the frame-cladding system during test DP-UFP2 is illustrated in Figure 8-26 (left). This test consisted of two UFP connections at the top of each panel, for a total of four UFP connections. It can be seen that significantly more force is transferred into the panel and as such, damage to the panel is observed during the 1.0% drift cycle and subsequent larger cycles.

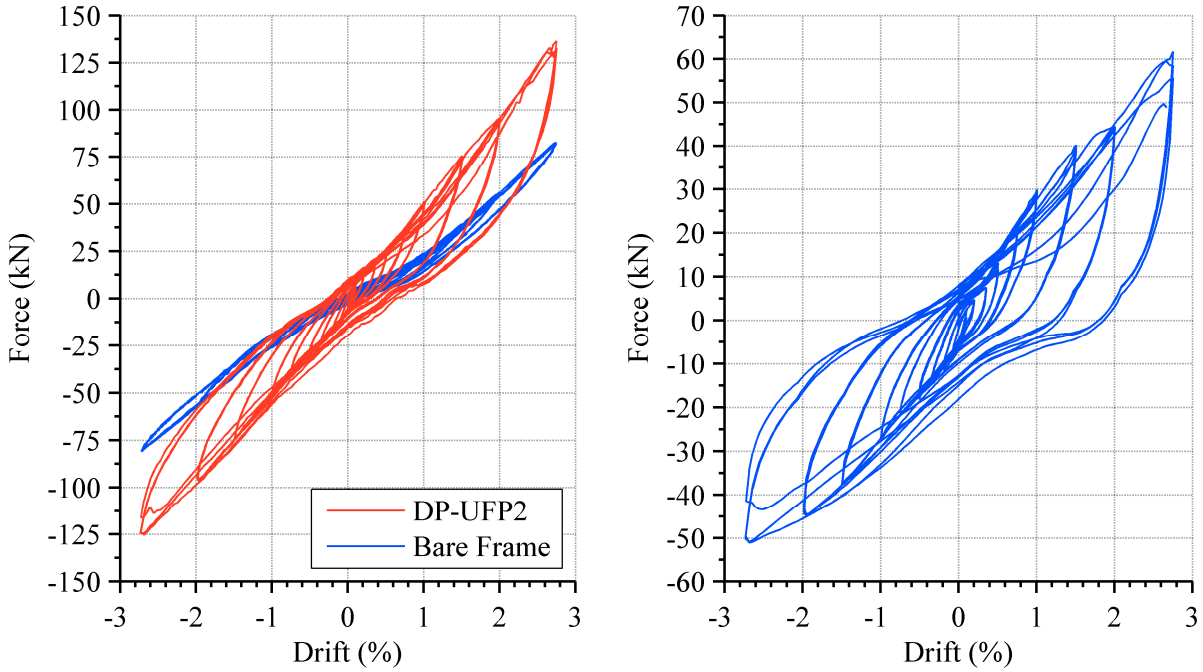

Figure 8-26: Force-drift behaviour (left) and difference between clad and unclad frame (right) for UFP connection test specimen DP-UFP2

The drop in strength and stiffness of the cladding is clearly visible in the 2.75% drift cycle due to cracks forming in the panel. The test was stopped before the largest drift cycle of 3.5% drift due to safety concerns due to the significant cracking observed around the weight bearing connections, as shown in Figure 8-27. The cause of the cracking was not fully understood and was not included as a damage state in the quantification of damage that follows due to this. It is possible that the amount of shear force transferred through the UFPs was too great for the bearing connections, or that the large deformation of the panel and the large moment at the connection was the cause of the cracking.

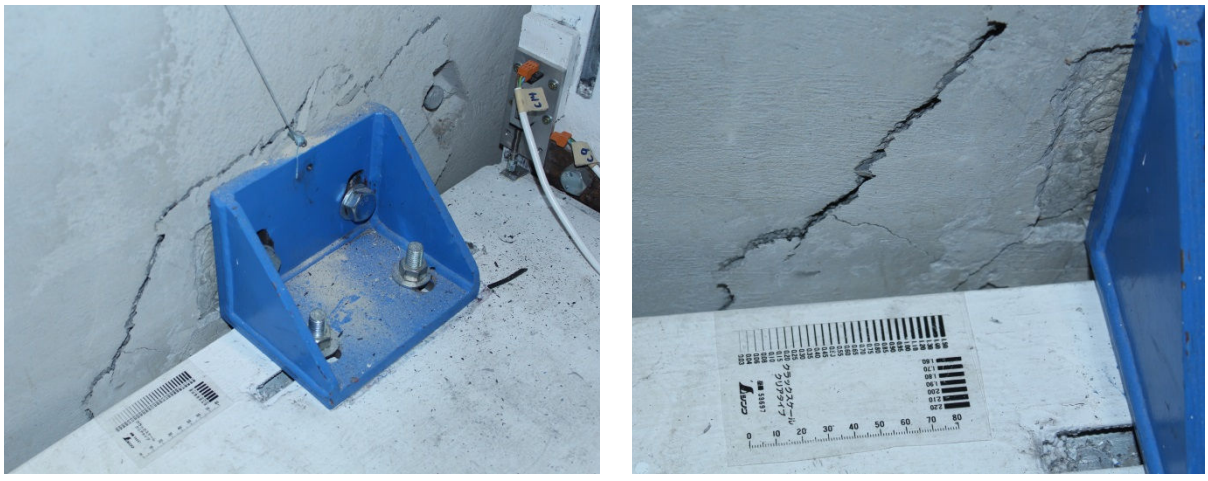

Figure 8-27: Damage to panel bearing connection during test DP-UFP2

8.7 Experimental Outputs

For modelling purposes as well as for defining damage states it is necessary to know several key experimental output parameters of the UFP connections tested. The following parameters are presented below in Table 8-2.: initial stiffness, yield force, yield displacement and maximum force. These values have been interpolated from the component testing and represent values for a single connection.

Table 8-2: Single UFP cladding connection modelling parameters

Initial Stiffness	1100 kN/m
Yield Force	6.4 kN
Yield Displacement	6 mm
Maximum Force	12.5 kN

8.8 Conclusions

Innovative cladding panel connections were experimentally tested in order to investigate their potential as low-damage connections that can also provide additional positive value to the seismic performance of the structure. The fundamental requirement for the innovate connections is that they are low-damage, i.e. able to withstand multiple seismic events without the need for repair or replacement. It is also vital that the connection is cost comparable to a traditional cladding connection and is flexible and simple in its design and implementation. Furthermore, it is also desirable for the connection to be able to provide a positive value to the seismic performance of the structure. The ability to passively dissipate seismic energy was used as the metric to qualify this.

The U-shaped flexural plate (UFP) was selected to determine its suitability as a possible innovative cladding connection. Initially proposed by Kelly et al. (1972), UFPs are a form of flexural dissipator which utilise the post-yield ductility of steel to dissipate energy. They are typically designed for small displacements (less than 50 mm) and high forces (greater than 50 kN). For the UFP to be a suitable low-damage connection it was necessary for it to withstand large displacements while transferring a small amount of force (less than 20 kN). Consequently, it was necessary to undertake component testing of UFPs due to the different geometry of the UFPs proposed to those tested previously.

Component testing subjected the UFPs to a maximum displacement of ±82.5 mm. It was found that the UFPs produced a stable hysteretic loop with the maximum force in a single UFP of approximately 12.5 kN. This maximum force was equivalent to 130% of the

design force, achieved when the full section has yielded. The UFP was tested to a displacement ductility of approximately 10 and the shape was found to not change significantly during testing.

Full-scale testing was subsequently carried out which utilised the UFP as the top connection between precast concrete cladding panels and the test-frame structure. A total of nine different tests were performed, with a total of four different connection configurations trialled in order to determine the best performing configuration.

It was found that each UFP would add a maximum lateral resistance of 10 – 15 kN to the overall system. It appeared that the force was greater in some connection configurations due to the eccentricity of the connection increasing the amount of friction in the connection. It was also found that the most suitable method for creating a stable hysteretic connection, while also providing adequate out-of-plane resistance was to house the UFP inside a slotted SHS section. The housing ensured that the UFP was properly constrained and did not allow any out-of-plane movement.

The experimental component and full-scale system testing confirmed that UFPs are suitable as innovative, low-damage cladding connections. Referring back to the aspects required of an innovative cladding connection, it was found that UFPs were inexpensive and straightforward to fabricate, produce reliable and stable hysteretic behaviour, provide flexibility in their design and implementation, and are able to withstand large displacements while transferring small force into the cladding.

The testing did show that care has to be taken to ensure the cladding panel and fixings are able to transfer the force from the UFP connection. The use of two UFP connections per small sized panel resulted in a significant amount of damage to the fixing between the bearing connection and the cladding panel. Likewise, if four connections were used for the large sized panel, the force transfer would have likely resulted in cracking to the panel. It is therefore recommended that a significant degree of conservatism be taken when the designer intends for the cladding to contribute to the lateral resistance of the structural system, particularly if seeking a low-damage outcome.

The following chapter aims to supplement the outcomes found in this experimental chapter by providing additional design information, including the stiffness and overstrength factor so that a designer can more accurately and reliably predict the non-linear behaviour of UFPs. Finally, Chapter 10 and Chapter 11 explore the final aspect of innovative connections; whether they provide a positive value to the seismic performance of the structure.

8.9 References

ACI - 374.1R. (2005). Acceptance Criteria for Moment Frames Based on Structural Testing and Commentary: American Concrete Institute.

Arnold, C. (1990). Architectural Precast Cladding *Cladding Design: Recent Architectural Trends and Their Impact on Seismic Design* (pp. 29-30). Chicago, IL., USA.

AS/NZS 3678. (1996). Structural steel - Hot-rolled plates, floorplates and slabs. Wellington: Standards New Zealand.

AS/NZS 4284. (2008). Testing of Building Facades. Wellington: Standards New Zealand.

Goodno, B. J. (1983). *Cladding-structure interaction in highrise buildings*: Schools of Civil and Aerospace Engineering, Georgia Inst. of Technology, Atlanta.

Goodno, B. J., & Craig, J. I. (1989). *Historical Overview of Studies on the Contribution of Cladding to Lateral Resistance of Buildings*. Paper presented at the Architectural Precast Concrete Cladding - Its Contribution to Lateral Resistance of Buildings, Chicago, IL., USA.

Hunt, J. P., & Stojadinovic, B. (2010). *Seismic Performance Assessment and Probabilistic Repair Cost Analysis of Precast Concrete Cladding Systems for Multistory Buildings*: Berkeley: Pacific Earthquake Engineering Research Center, University of California.

Iqbal, A., Pampanin, S., Buchanan, A. H., & Palermo, A. (2007). *Improved Seismic Performance of LVL Post-tensioned Walls Coupled with UFP devices*. Paper presented at the 8th Pacific Conference on Earthquake Engineering, Singapore.

Kelly, J. M., Skinner, R. I., & Heine, A. J. (1972). Mechanisms of Energy Absorption in Special Devices for use in Earthquake Resistant Structures. *Bulletin of the New Zealand Society for Earthquake Engineering, 5*(3).

McMullin, K., Ortiz, M., Patel, L., Yarra, S., Kishimoto, T., Stewart, C., & Steed, B. (2012). *Response of Exterior Precast Concrete Cladding Panels in NEES-TIPS/NEESGC/ E-Defense Tests on a Full Scale 5-Story Building*. Paper presented at the Structures Congress 2012, Chicago, IL., USA.

Pall, A. S. (1989). *Friction Damped Connections for Precast Concrete Cladding*. Paper presented at the Architectural Precast Concrete Cladding - Its Contribution to Lateral Resistance of Buildings, Chicago, IL., USA.

Pampanin, S., Marriott, D., & Palermo, A. (2010). PRESSS Design Handbook. Auckland, New Zealand: New Zealand Concrete Society, NZCS.

Pinelli, J. P., Craig, J. I., Goodno, B. J., & Hsu, C. C. (1993). Passive control of building response using energy dissipating cladding connections. *Earthquake Spectra, 9*(3), 529-546.

Priestley, M. J. N., Sritharan, S., Conley, J., & Pampanin, S. (1999). Preliminary Results and Conclusions from the PRESSS Five-Story Precast Concrete Test Building. *PCI Journal, 44*(6).

Wang, M. L. (1987). Cladding performance on a full-scale test frame. *Earthquake Spectra, 3*(1), 119-173.

9 Development of Numerical Models for Innovative Cladding

9.1 Introduction

This chapter presents the development of modelling techniques for innovative cladding systems. Analytical derivations based on fundamental engineering principles are first used as a framework to determine key modelling parameters. These analytical derivations are compared against experimental results and used to develop finite element models. The finite element models are verified using experimental results of the innovative cladding systems investigated in Chapter 8. Once verified, a series of parametric analyses are undertaken to characterise the behaviour of cladding components when certain geometric parameters are varied. Using the combination of experimental, analytical and numerical results, methods to determine the key modelling parameters of cladding components are presented.

These modelling parameters are used to develop local lumped plasticity cladding models that can be easily incorporated into frame analyses. Finally, these simplified cladding models are compared to the experimental results obtained in Chapter 8 to examine their suitability.

9.2 Cladding Component Characterisation

The cladding systems to be characterised consist of those that utilise the U-Shaped flexural plate (UFP) connections tested experimentally in Chapter 8. Since the cladding panel has already been characterised in Chapter 5, this section will focus on the characterisation of the UFP in order to implement the connection into a simplified two component cladding model.

The characterisation of the UFP connection is based upon the combination of analytical derivation, experimental testing and numerical modelling. The combination of these three tools provides a robust process for deriving reliable modelling parameters for the UFP connections. These parameters include the yield force, yield displacement, initial stiffness and post-yield behaviour.

The process used to characterise the UFPs is as follows:

1. The analytical derivation of key parameters is compared against the observed experimental behaviour to ascertain the suitability of these formulae
2. A numerical finite element model of the UFPs tested experimentally is developed and calibrated against the experimental behaviour
3. A parametric investigation is performed using the calibrated numerical model to find a range of possible UFP performance
4. The key parameters from the numerical modelling response is found using non-linear regression
5. Combinations of analytical and empirical formulae are proposed using the key modelling parameter outputs.

9.2.1 Analytical and Experimental Comparison

The key parameters that can be derived analytically for UFP connections are the maximum strain and yield force. The maximum strain is of interest in order to determine the low-cycle fatigue characteristics of the UFPs. Accurately determining the yield force is also important since this determines the magnitude of the force transferred into the cladding panel.

The maximum strain in a UFP can be determined analytically by considering that the maximum deformation of the plate will be in going from straight to curved or vice-versa. Since the radius of the curved section is fixed, it is possible to derive the strain that occurs in the plate from making this transition. Considering a small region of the straight section of UFP, as illustrated by the square region in blue in Figure 9-1, it can be seen that when going from the straight to curved section of the plate, the blue region must deform. Around the outside edge of the UFP the plate must extend by Δy, indicated by the light blue region, and around the inside edge, the plate must compress by Δy, indicated by the dark blue region.

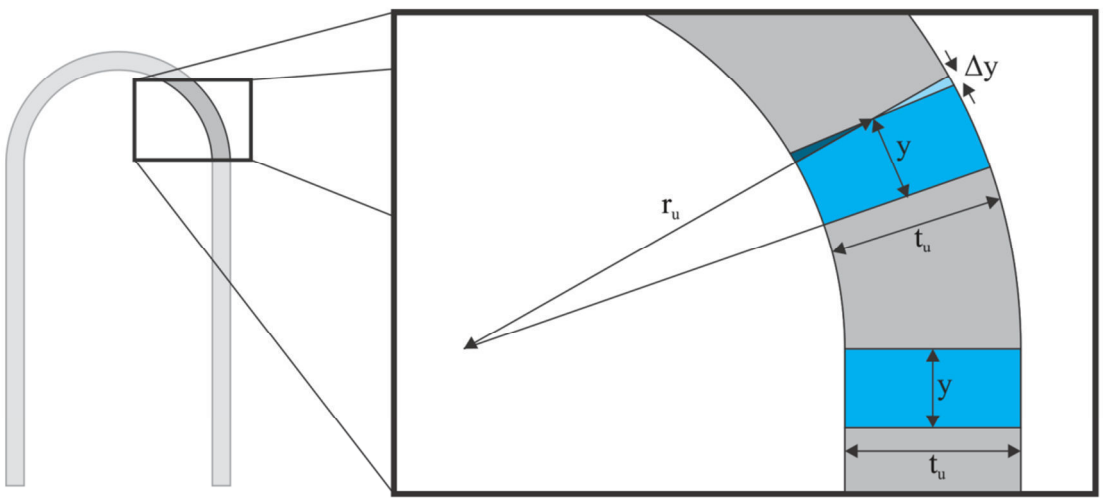

Figure 9-1: Maximum UFP strain derivation

Making use of the geometry shown in Figure 9-1, the following relationship can be derived:

$$\frac{y}{r_u} = \frac{2\Delta y}{t_u} \tag{9-1}$$

where

y = Length of region of UFP

r_u = Radius of UFP bend

Δy = Change in length of region of UFP

t_u = Thickness of UFP

The maximum strain demand is therefore defined by the change in length of the region considered divided by the length of and is given by Equation (9-2).

$$\frac{y}{\Delta y} = \frac{t_u}{2r_u} = \varepsilon_{max} \tag{9-2}$$

Therefore, the maximum strain expected in the UFP is:

$$\varepsilon_{max} = \frac{8\ mm}{2 \times 64\ mm} = 6.25\% \tag{9-3}$$

The actual strain in the UFP was measured in three different locations on both UFPs during component testing. The strain was measured using high cycle strain gauges that were located on the sides and top of the UFPs as shown in Figure 9-2. The strain gauges on the

sides were located on the inside face of each UFP and the strain gauges on the top were located on the outside face.

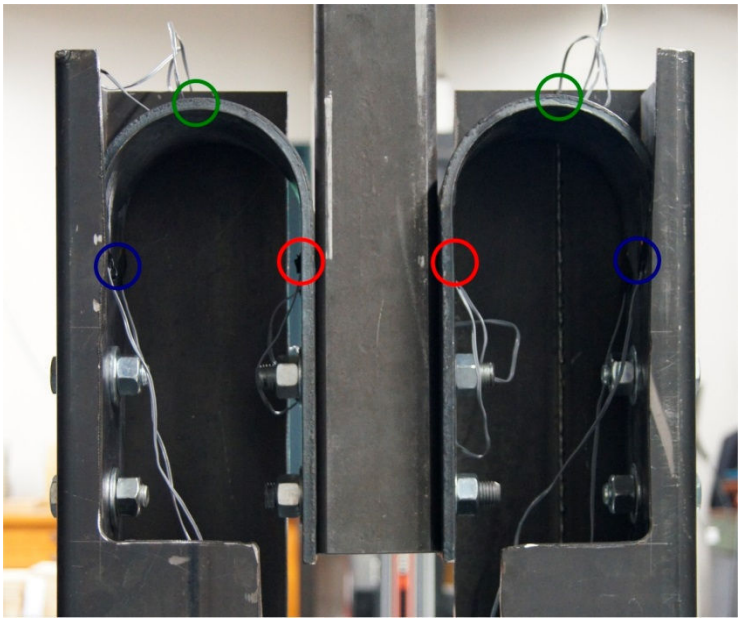

Figure 9-2: Strain gauge locations (blue – fixed face, red – moving face, green – top face)

The strain gauges on the side were located at the region where the UFP transitions from straight to curved and hence are expected to be subjected to the largest strains. The strain gauges at the top should theoretically be in a region where the curvature does not change and hence should not record significant strains. Two strain gauges were attached at each location. The strain from the six strain gauges is shown in Figure 9-4 for both UFPs when housed.

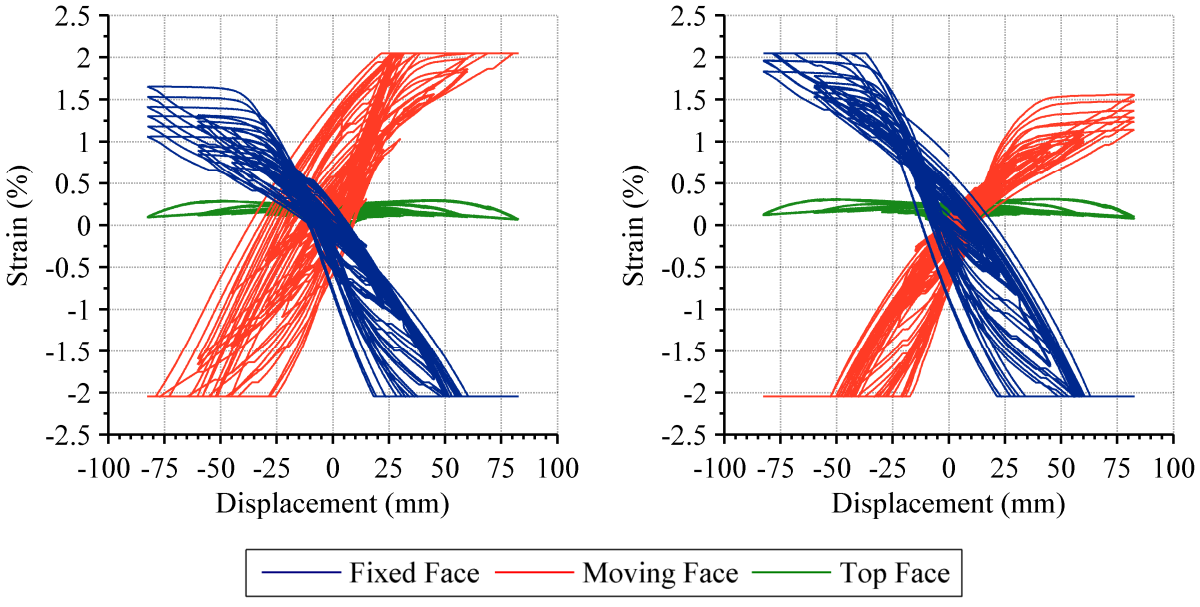

Figure 9-3: Housed UFP test strain data

The data recorder was only able to record strains up to 2.0%, hence any strains greater than this were not captured. However, even without this data, it is possible to see that the recorded strains were likely to be significantly less than that of 6.3%, the maximum strain predicted by Equation (9-3). Up until and including the 1.5% drift cycle, which corresponds to ±45 mm of vertical displacement, the maximum strain was 1.7%, i.e. none of the strain gauges had reached their limit. It can be seen that the strain in the sides of the UFPs was very symmetrical, and that the strain in the top of the UFP was minor, as would be expected. The strain in the top of the UFP in fact indicated that this region of the plate yielded during the 0.75% drift cycle (22.5 mm displacement). This indicates that the UFP yield surface is likely distributed further around the UFP than that determined theoretically.

The strain from the six strain gauges on each UFP is shown in Figure 9-4 when the UFPs are not housed. It can be seen that a similar result is observed to that when the UFP was housed.

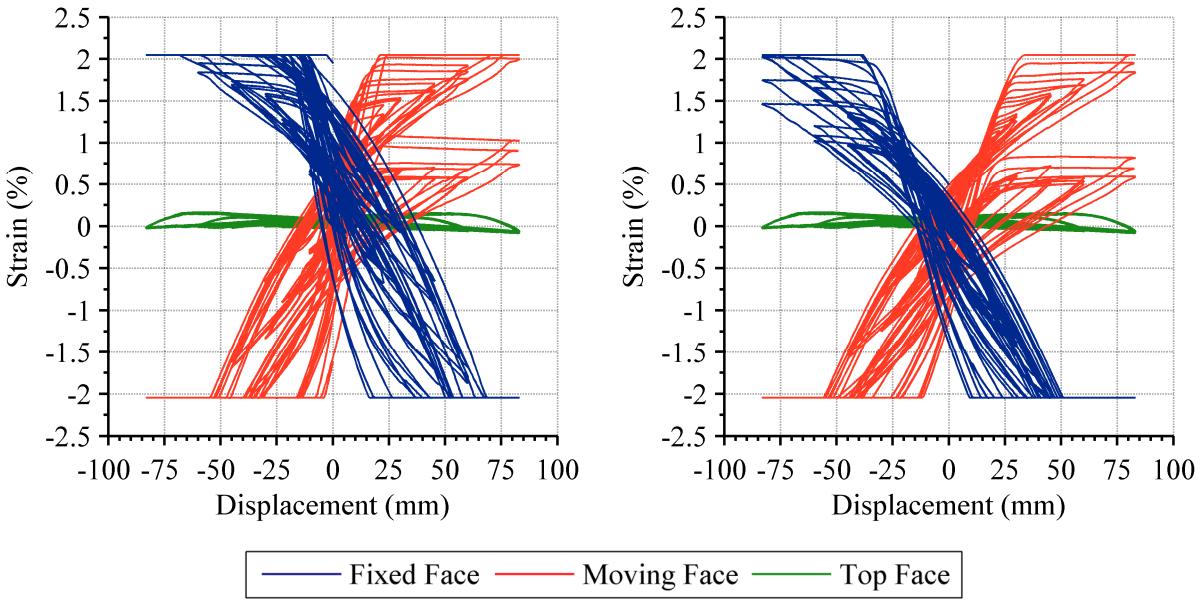

Figure 9-4: Un-housed UFP test strain data

The yield force of a UFP can be derived analytically by relating the coupling shear of the UFP to the yield moment. The yield moment of the UFP is given by Equation (9-4), which defines the moment when outermost fibre of the UFP section yields. The plastic force of a UFP is derived similarly, using the plastic moment which is given by (9-5) and defines when the s the entire region of a rectangular section has surpassed yield.

$$M_y = f_y S_u = f_y \frac{b_u t_u^2}{6} \quad \textbf{(9-4)}$$

$$M_p = f_y Z_u = f_y \frac{b_u t_u^2}{4} \quad \textbf{(9-5)}$$

where

M_y = Yield moment

M_p = Plastic moment

f_y = Yield stress of UFP steel

S_u = Elastic section modulus of UFP

Z_u = Plastic section modulus of UFP

b_u = Width of UFP section

As shown in Figure 9-5, the plastic moment can be related to the coupling shear, which is equivalent to the yield force of the UFP.

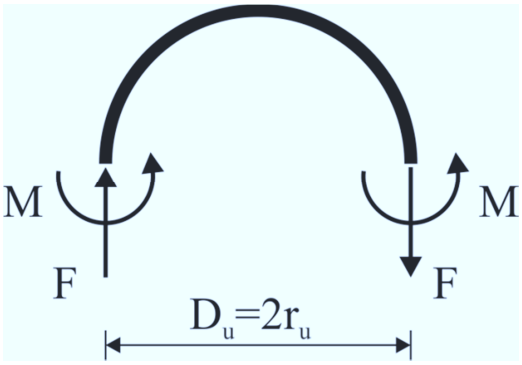

Figure 9-5: Plastic moment and coupling shear of UFP, reproduced from Pampanin et al. (2010)

The yield force of a UFP can therefore be defined by Equation (9-6).

$$F_y = \frac{2M_y}{D_u} \quad \textbf{(9-6)}$$

where

F = Force in UFP

D_u = Diameter of UFP bend

Combining Equation (9-4) and (9-6) provides the yield force in terms of the geometry of the plate and yield stress.

$$F_y = f_y \frac{b_u t_u^2}{3D_u} \quad \textbf{(9-7)}$$

Similarly, combining Equation (9-5) and (9-6) provides the plastic force in terms of the geometry of the plate and yield stress.

$$F_p = f_y \frac{b_u t_u^2}{2D_u} \tag{9-8}$$

The yield and plastic force of the UFPs tested can therefore be calculated to be 6.4 kN and 9.6 kN, respectively, assuming the nominal yield strength of the 8 mm plate is 320 MPa (AS/NZS 3678, 1996). These forces are compared against the hysteretic behaviour of the two component tests performed in Figure 9-6. The force recorded by the load cell has been halved so the force shown in the force provided by a single UFP. The left figure shows the force displacement behaviour of a UFP housed inside the slotted RHS (refer to Figure 9-6 (left)) and the right figure shows the behaviour of a UFP attached directly to the loading RHS, i.e. without any housing (refer to Figure 9-6 (right)). The definition of the point where the UFP is fully yielded is ambiguous, due to the gradual change in stiffness that occurs as different regions transition through the yielded states.

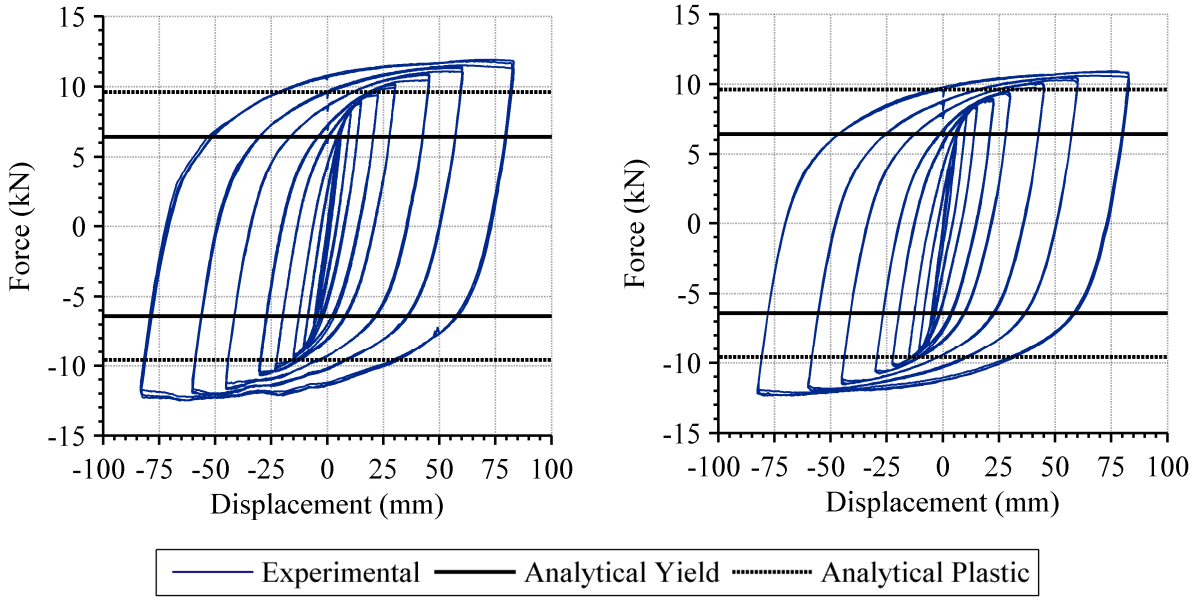

Figure 9-6: Comparison of analytical derived yield and plastic force values to experimental UFP tests

It is clear that the analytical plastic force underestimates the maximum force so clearly a level of over-strength due to strain hardening is evident. It can be seen that the maximum force in a single UFP is approximately 12.5 kN. Depending on what analytical solution is compared to, this either gives an overstrength factor of 130% or 195%. Quantifying the over-strength is critical in order to implement UFPs as a cladding connection to ensure that the maximum force in the UFP does not exceed the capacity of the cladding panel. Typically

overstrength is calculated from first yield; in this case the overstrength is 195%. However, due to the cyclic nature of the UFP, Kelly et al. (1972) suggested that using the 'first yield' is not a useful metric since the force will undoubtedly exceed this value, so instead compared the overstrength to the 'fully yielded' force. The 'fully yielded' force has here been termed the 'plastic force'.

The yield displacement of a UFP can be determined analytically using energy methods, otherwise known as Castigliano's Second Theorem. This method finds the deflection from the partial derivative of the strain energy determined by the loads applied. For the UFP we are only considering bending loads since there is no torsional component and the axial deformation will be negligible. The general equation for Castigliano's Theorem is given by Equation (9-9).

$$\Delta = \frac{\partial U}{\partial F} \tag{9-9}$$

where

Δ = Displacement
U = Strain energy
F = Applied load

The strain energy due to bending is found by taking the integral of the moment squared as given in Equation (9-10)

$$U = \int_0^L \frac{M^2(x)}{2EI} dx \tag{9-10}$$

where

$M(x)$ = Moment function
E = Elastic modulus
I = Moment of inertia

The moment function in the bent region of the UFP due to loading at one end is best defined using the polar coordinates R and θ, as shown in Figure 9-7.

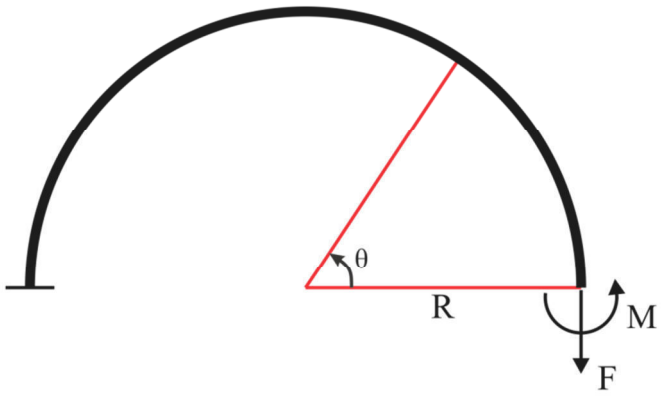

Figure 9-7: Derivation of polar moment function in UFP

The moment in terms of theta can be defined by Equation (9-11).

$$M(\theta) = Fr_u(1 - \cos\theta) + Fr_u \qquad \textbf{(9-11)}$$

where

r_u = Radius of U

θ = Rotation from point of loading

Combining Equations (9-9), (9-10) and (9-11), gives Equation (9-12) which defines the displacement at the end of the UFP due to the loading conditions shown in Figure 9-7. Note that the substitution of the integral operator includes an additional radius term, i.e. $dx=Rd\theta$ and that the integral is now from zero to pi.

$$\Delta = \int_0^{\pi} \frac{\partial}{\partial F} \frac{[Fr_u(1 - \cos\theta) + Fr_u]^2}{2EI} r_u d\theta \qquad \textbf{(9-12)}$$

Expanding the differential gives:

$$\Delta = \int_0^{\pi} \frac{\partial}{\partial F} \frac{4F^2{r_u}^3 - 4F^2{r_u}^3\cos\theta + F^2{r_u}^3\cos^2\theta}{2EI} d\theta \qquad \textbf{(9-13)}$$

Taking the partial derivative with respect to F, collecting the constants and moving them outside the integral:

$$\Delta = \frac{F{r_u}^3}{EI} \int_0^{\pi} 4 - 4\cos\theta + \cos^2\theta \, d\theta \qquad \textbf{(9-14)}$$

Integrating with respect to theta:

$$\Delta = \frac{F{r_u}^3}{EI}\left[4\theta - 4\sin\theta + \frac{\theta}{2} + \frac{\sin 2\theta}{4}\right]_0^{\pi} \quad \textbf{(9-15)}$$

Substituting in the integral limits:

$$\Delta = \frac{F{r_u}^3}{EI}\left[4\pi - 0 + \frac{\pi}{2} + 0\right] \quad \textbf{(9-16)}$$

Simplifying and multiplying by two to account for the loading at the opposite end:

$$\Delta = \frac{9\pi F{r_u}^3}{2EI} \quad \textbf{(9-17)}$$

Or, in terms of the UFP geometry by making the appropriate substitution for the moment of inertia and radius:

$$\Delta_p = \frac{27\pi F{D_u}^3}{16Eb_u t_u^3} \quad \textbf{(9-18)}$$

The initial stiffness can thus be defined as:

$$k_0 = \frac{16Eb_u}{27\pi}\left(\frac{t_u}{D_u}\right)^3 \quad \textbf{(9-19)}$$

9.2.2 Finite Element Modelling

The ABAQUS finite element programme (ABAQUS Inc., 2011) was used to model the force-displacement behaviour of the UFPs. A Finite Element Model (FEM) of the UFPs tested experimentally was developed and validated against the experimental data by modifying the material properties.

A 3D deformable solid made up of 2.5 mm tetrahedral mesh elements was used to model the UFPs. The geometry of the model was that of the UFP tested experimentally, a 120 x 8 mm plate with a bend diameter of 120 mm. The steel material was modelled using a plastic isotropic yield model with (combined) cyclic hardening.

The mesh arrangement of the UFP is shown in Figure 9-8 (top left). The UFP was first modelled without any additional restraint, with the boundary conditions comprising a fixed surface on one end of the plate and a moving surface on the other, as shown Figure 9-8 (top

right). It can be seen in Figure 9-8 (bottom) that the deformed shape becomes asymmetric with these boundary conditions. The deformed shape of the UFP corresponds to a downwards movement of 30 mm of the right hand end of the plate. This deformed shape was observed experimentally during the systems testing when the UFP was not well restrained. The maximum principal stresses are superimposed onto the deformed shape in Figure 9-8 (bottom). It can be seen how the maximum stresses occur on the edge of the plate in the regions that were previously straight but are now curved.

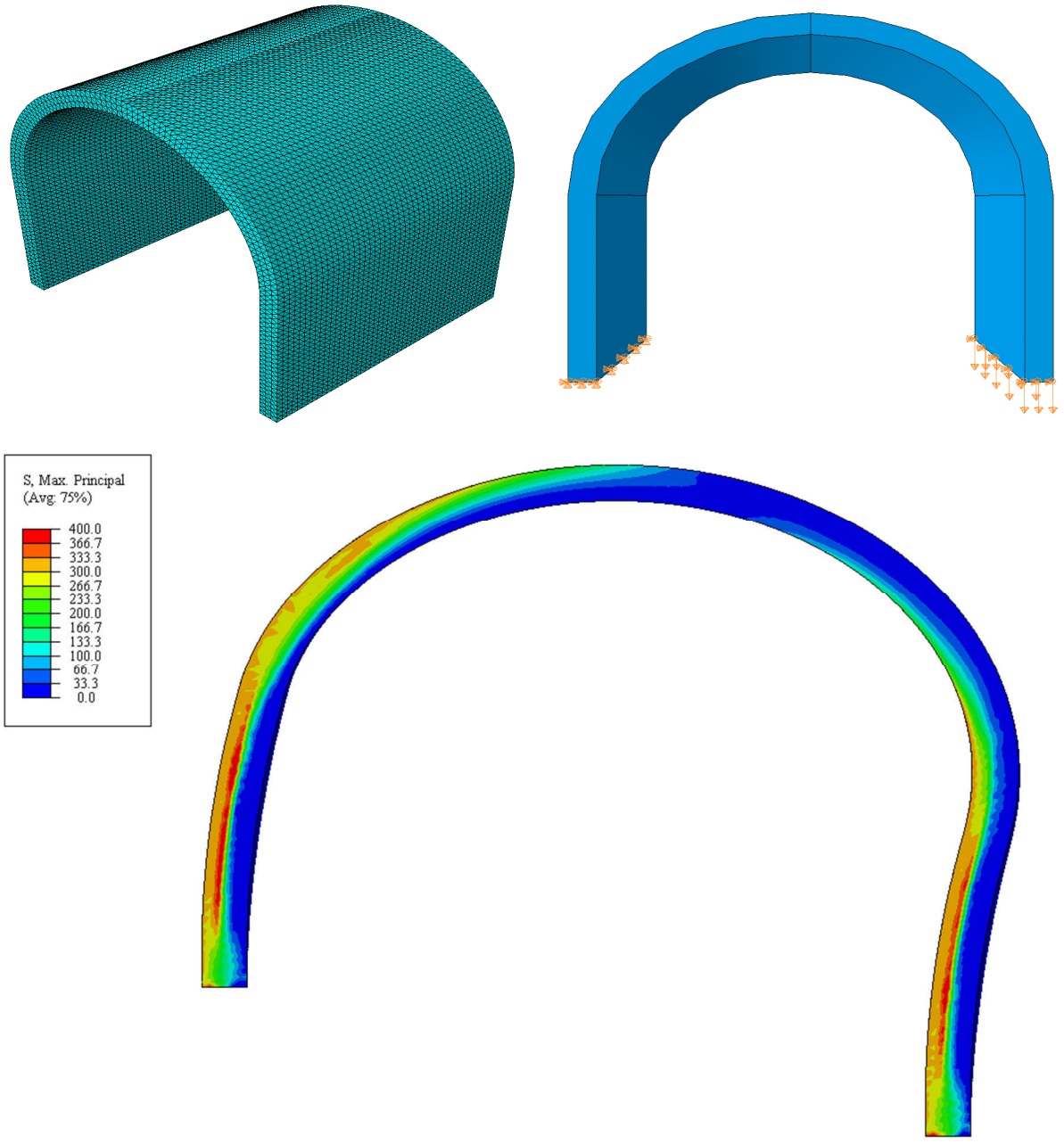

Figure 9-8: Finite element mesh (top left), boundary conditions (top right) and maximum principal stress distribution on deformed shape (bottom) for unrestrained UFP analyses

The deformed shape of the FEM matches the deformed shape of an un-housed UFP well; however, modelling the behaviour of a housed UFP was essential since this represents the most likely application. Modelling the UFP in the housing required the FEM to be properly constrained; therefore additional boundary conditions were required. This was achieved by using additional rigid body blocks on either side of the UFP. These blocks were assigned the same boundary conditions of the UFP, with one being kept fixed with the fixed side of the UFP, and the other moving vertically with the moving side of the UFP.

The interaction between the UFP and the blocks was defined by a surface to surface 'contact interaction'. The master surface was defined as the side of the rigid block with the slave surface being defined as the corresponding side of the UFP. The surface to surface contact requires the definition of the normal and tangential behaviour between the two components. The tangential behaviour was assumed to be frictionless since the block was moving with the UFP and hence no friction should be present. The normal behaviour was defined as 'hard contact' that allowed separation after contact. The mesh of the blocks was defined using 2.5 mm hexagonal structured elements.

The mesh arrangement of the UFP with the block restraints is shown in Figure 9-9 (top left). The boundary conditions of the UFP with the blocks is shown in Figure 9-9 (top right) along with the contact interaction. The deformed shape of the UFP after the right hand end has been displaced 30 mm downwards is presented in Figure 9-9 (bottom). It can be seen that the deformed shape of the UFP with the block restraints is much more symmetrical, as shown in compared to the UFP when no restraints are present. The maximum principal stresses are also superimposed onto the deformed shape in Figure 9-9 (bottom). It can be seen how the maximum stresses occur across a similar area as the un-restrained UFP but are clearly better distributed. This can be interpreted by the lack of any visible concentration of red stress contours in Figure 9-9 (bottom) compared to those present in Figure 9-8 (bottom).

The FEM was run using the same displacement cycles as testing however only a single cycle was applied at each displacement level. The elastic material properties of the FEM were based on typical steel properties, with the elastic modulus of the FEM material set at 200 GPa and Poisson's ratio set at 0.3. The yield stress was also set as 320 MPa, the nominal yield stress of an 8 mm hot rolled plate (AS/NZS 3678, 1996). The behaviour of the UFP was calibrated by altering the post-yield plastic material properties. Combined cyclic hardening with a Q-infinity of 120 MPa and Hardening Parameter of 4.5 was found to best match the experimental post-yielding behaviour. The Q-infinity parameter represents the additional

stress the material can reach beyond yield, which would in this case be 440 MPa. The Hardening Parameter is a measure of the rate at which this maximum stress is reached post-yield.

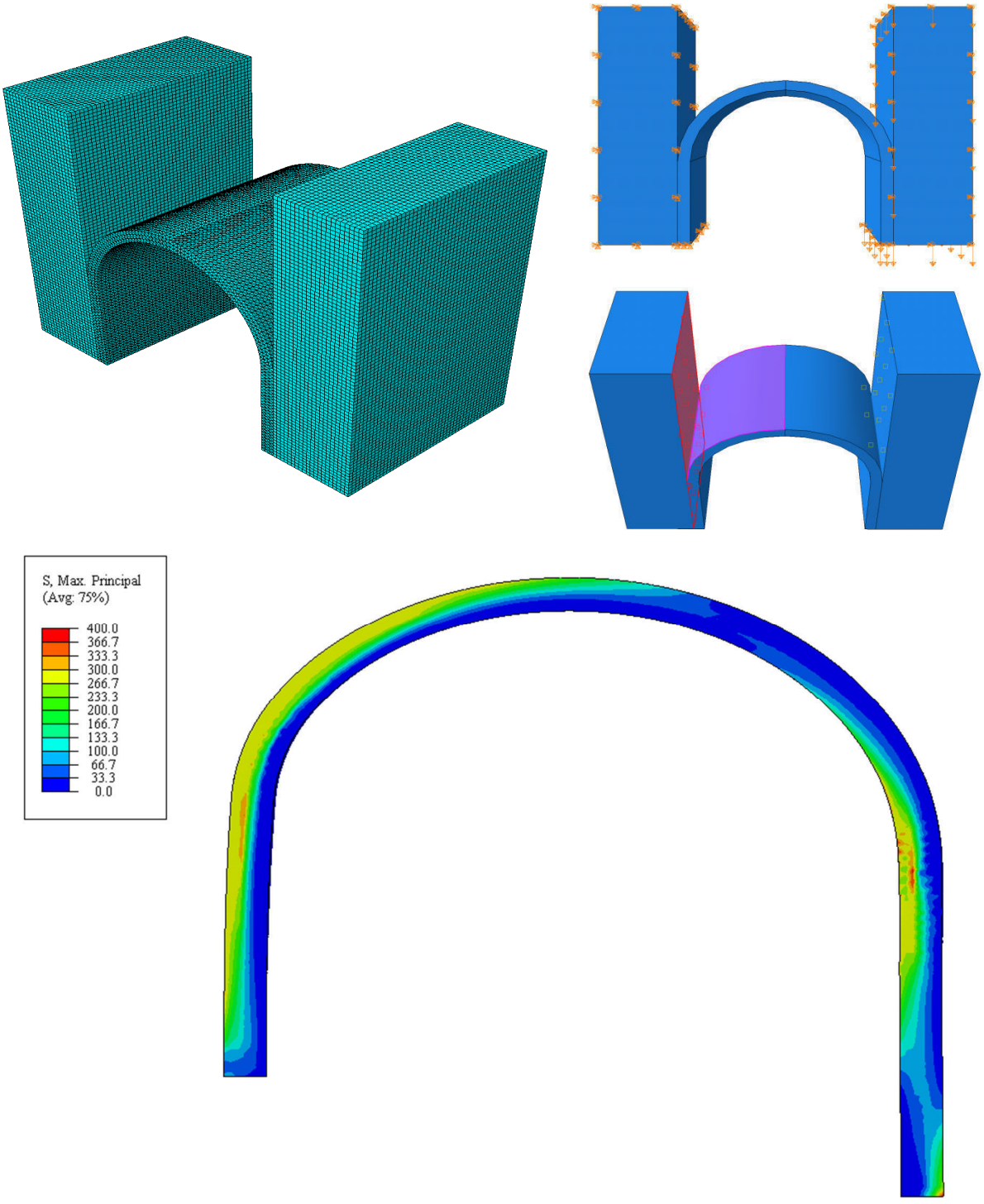

Figure 9-9: Finite element mesh (top left), boundary conditions and contact interaction (top right), and maximum principal stress distribution on deformed shape (bottom) for restrained UFP analyses

A contour plot of the stress distribution in the UFP is shown in Figure 9-10 for the restrained UFP after being subjected to the cyclic loading. The maximum principal stresses are shown. The contour plot shows how the plate yields in the region where the curvature of the plate changes from straight to curved. It can also be seen how the maximum stresses occur on the outer faces of the plate, analogous to the theory presented in Figure 9-1.

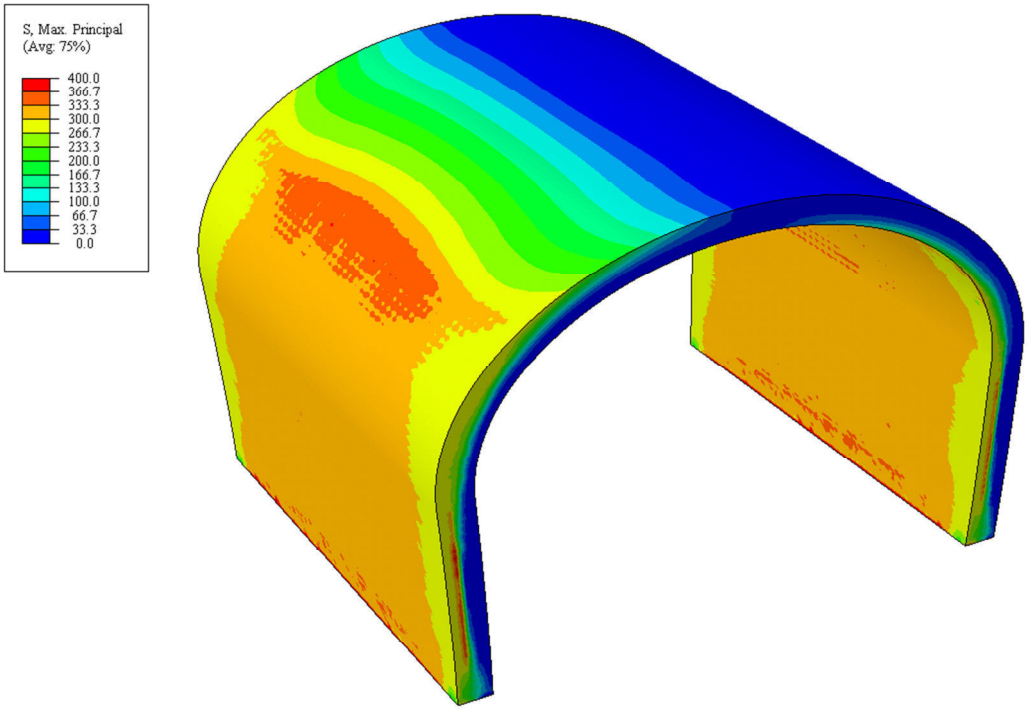

Figure 9-10: Maximum principal stress distribution on outer face of restrained UFP

The numerical force-displacement behaviour of the UFP is shown in Figure 9-11 along with the experimental behaviour of both UFPs tested (housed and un-housed). The analytically predicted yield force is also shown. The numerical model evidently models the cyclic behaviour of the UFPs very well, capturing the yielding of the plates and the post-yield behaviour very accurately. The post-yield material properties were matched primarily against the un-housed UFP since this essentially the experimental system that the model represents. The maximum force matches the experimental data well but it can be seen in Figure 9-11 that the FEM did not accurately capture the Bauschinger effect in the steel. Consequently, the numerical hysteresis has a slightly greater area than that of the experimental results. Modelling the non-linear behaviour of steel usually involves some sort of trade-off in accuracy. For this situation, the most important aspect of the modelling was to accurately capture the backbone curve. This model accurately achieved this, with the trade-off being an introduction of some inaccuracy in the unloading, however, this inaccuracy is not believed to be of particularly high importance.

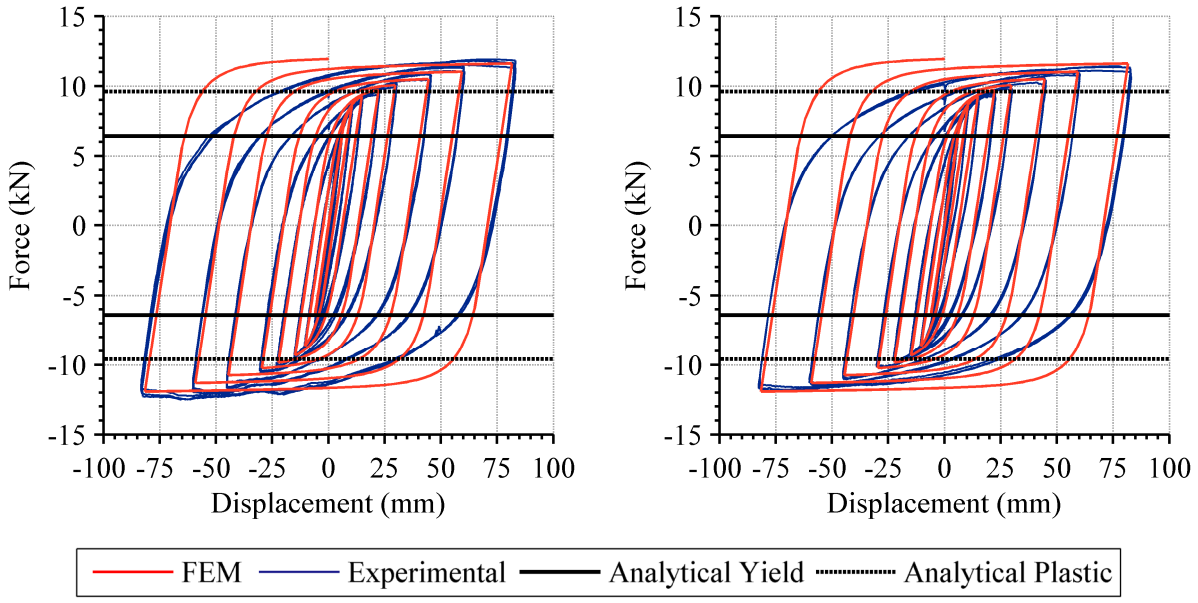

Figure 9-11: Force-displacement comparison of experimental, analytical and finite element modelling of housed UFP (left) and un-housed UFP (right)

As well as the cyclic analyses, monotonic analyses were also performed on the UFPs. Monotonic analyses will form the basis for the parametric investigation in the following section. The monotonic force-displacement behaviour of the same FEM used for the cyclic analyses is shown in Figure 9-12 along with the cyclic FEM behaviour and the experimental behaviour of both UFPs tested (housed and un-housed). It can be seen that the monotonic behaviour has the same initial stiffness and yield point as the cyclic tests but does not generate the same level of overstrength due to the lack of cyclic hardening.

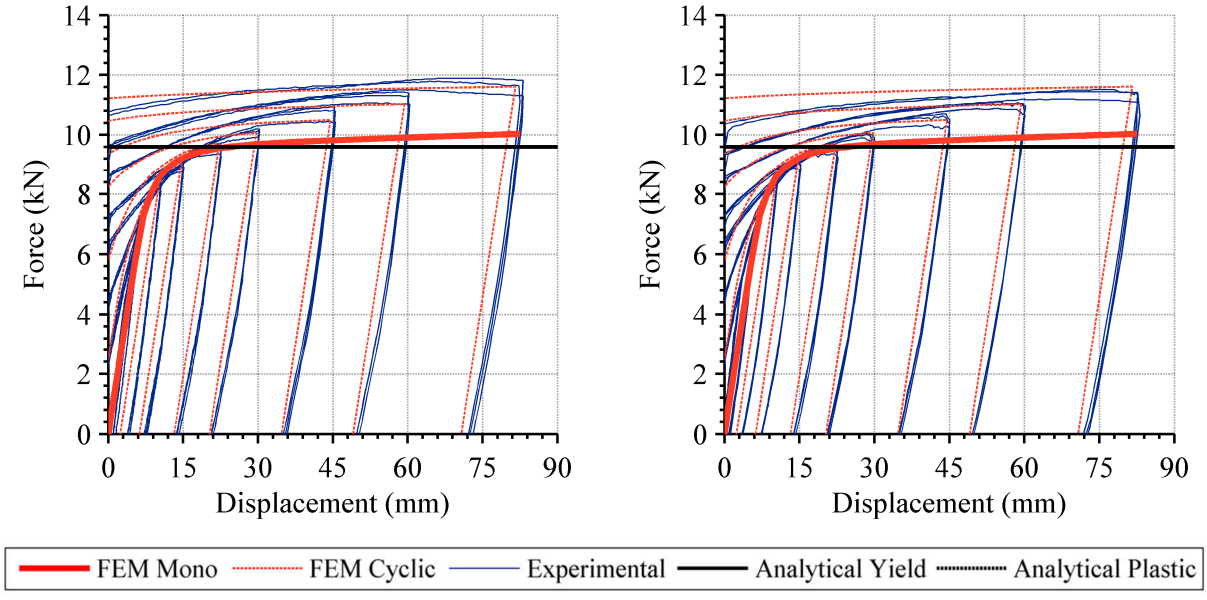

Figure 9-12: Monotonic finite element model force displacement comparison with cyclic results of housed UFP (left) and un-housed UFP (right)

9.2.3 Non-Linear Regression

The yield force, initial stiffness, yield displacement and post-yield stiffness of the UFP model are determined in this section using the monotonic response of the finite element model (FEM) analysis. The decision on whether to determine the UFP parameters based on the monotonic response or the cyclic backbone response is again a trade-off in terms of accuracy and conservatism. The monotonic response underestimates the peak forces attainable by the UFP, and consequently the equivalent displacements predicted are larger for the same force. However, if the cyclic backbone were to be used as the basis of the non-linear behaviour, the peak forces would be overestimated and the equivalent displacements under-predicted. This is due to the cyclic response relying upon repetitive reverse cycling in order to develop the larger forces attributed to cyclic hardening. It was decided to use the monotonic response for defining the non-linear behaviour since this was deemed the most appropriate for not over-estimating expected forces or underestimating expected displacements.

The non-linear behaviour is approximated with the non-linear Ramberg-Osgood hysteretic rule (Ramberg & Osgood, 1943). The Ramberg-Osgood hysteresis is suited for representing steel behaviour since it shows a smooth elastic-plastic transition. The Ramberg–Osgood hysteresis that relates force and displacement is given by Equation (9-20). It can be seen that the hysteretic rule requires the definition of just three parameters: the initial stiffness, k_0, yield force, F_y, and R factor. It should be noted that the R factor used to define the Ramberg-Osgood hysteresis is not analogous to the R factor used to define a bi-linear relationship where it is a percentage of initial stiffness. For the Ramberg-Osgood function, the larger the R factor value, the closer the post-yielding behaviour is to being perfectly plastic (Kaldjian & Fan, 1967).

$$\delta = \frac{F}{k_0}\left[1 + \left(\frac{F}{F_y}\right)^{(R-1)}\right] \qquad \textbf{(9-20)}$$

where

δ = Displacement

F = Force

k_0 = Initial stiffness

F_y = Yield force

R = R factor

A Ramberg-Osgood function is fitted to the monotonic FEM analysis using a MATLAB regression function that estimates the function coefficients using an iterative least squares estimation (MathWorks Inc., 2011). The initial stiffness can be extracted directly from the numerical data, leaving only the yield force and R factor to require fitting. Figure 9-13 shows the Ramberg-Osgood function that has been fitted to the numerical data of the monotonic UFP analysis of the UFP. It can be seen that the Ramberg-Osgood function is an excellent representation of the behaviour.

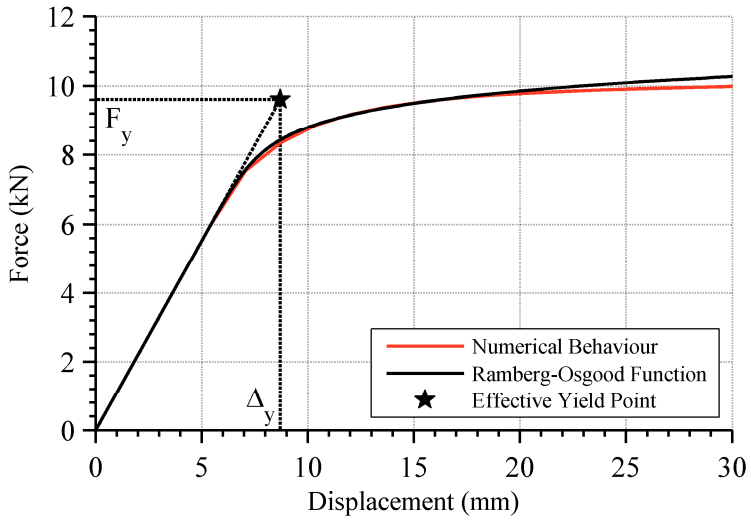

Yield Force, F_y (kN)	9.7
Yield Displacement, Δ_y (mm)	8.8
Initial Stiffness, k_i (kN/mm)	1.1
R factor	11.9

Figure 9-13: Curve fitting of Ramberg and Osgood (1943) function to numerical behaviour obtained by finite element analyses (left) with parameters (right)

The numerically obtained 'effective' yield force, yield displacement, initial stiffness and R factor are presented in the right of Figure 9-13. The effective yield force of 9.7 kN obtained by curve fitting the Ramberg-Osgood function is very similar to the plastic force given analytically by Equation (9-8) of 9.6 kN. This difference arises because the yield constant of the Ramberg-Osgood function is not defined by the 'first yield' point. Rather it is determined by a 'yield offset', as shown in Figure 9-13 (left). The definition of the 'effective' yield force and the plastic (fully yielded) force is very similar and hence this 'effective' yield force will be subsequently considered to be equivalent to the 'fully yielded' yield force.

9.2.4 Parametric Investigation

A parametric investigation of the UFPs has been performed using the FEM developed from the experimental results. The parametric investigation of the UFPs involves varying the plate thickness and bend diameter and examining how these parameters affect the yield force (fully yielded), yield displacement, initial stiffness and R factor. A Ramberg-Osgood function

is fitted to each numerical analysis in order to define the aforementioned parameters. Each numerical analysis consists of a monotonic loading to produce a force-displacement plot similar to that shown in Figure 9-13.

The plate thickness of the UFPs was varied based on commercially available metric sizes. These included 5, 6, 8, 10 and 12 mm thick plates. A standard plate width of 100 mm was used. Equation (9-7) demonstrates that the plate width has a linear relationship with the force in the plate and therefore the results are effectively all per 100 mm of plate width. The inner diameter, D_i, of the UFP was varied from 60 mm to 120 mm in 20 mm increments. The nominal diameter, D_u, is equal to the inside diameter, D_i, plus the plate thickness, t_u. In total, 20 numerical analyses were performed.

The yield force and yield displacement are presented in Figure 9-15 for the 20 numerical analyses. The results are presented for the various plate sizes and diameters. The different colours correspond to the five plate sizes considered, with the diameter of the UFP being plotted along the x-axis. As expected, Figure 9-15 shows that the yield force is larger for thicker plate sizes and an inverse relationship exists between the diameter and the yield force, such that as the diameter gets larger, the yield force decreases. There is also an evident trend in the yield displacements, with the thicker plates and smaller diameters having a lower yield displacement.

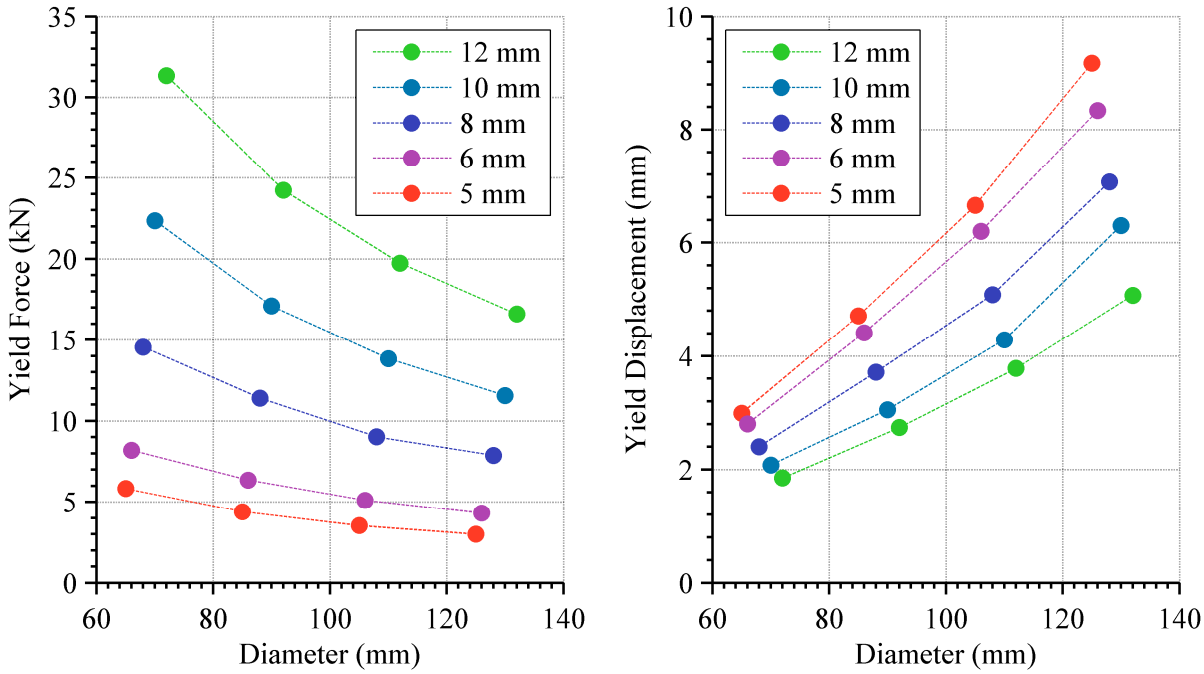

Figure 9-14: Results of finite element parametric analysis: yield force (left), yield displacement (right)

The initial stiffness of the UFPs is presented in Figure 9-15 along with the Ramberg-Osgood R factors obtained via the non-linear regression. As would be expected, a larger initial stiffness was observed in the thicker and smaller diameter UFPs. The R factor values are a bit erratic, varying between 6 and 18. There is a trend of smaller R factors for larger diameter, as well as for thinner plates. Since the force in the UFP eventually reaches a flat plateau, it makes physical sense for the R factor to be greater when the initial stiffness is higher (the greater the R factor, the closer to bi-linear the relationship is). The relationship between the geometric ratio and overstrength ratio will be developed upon later in this section.

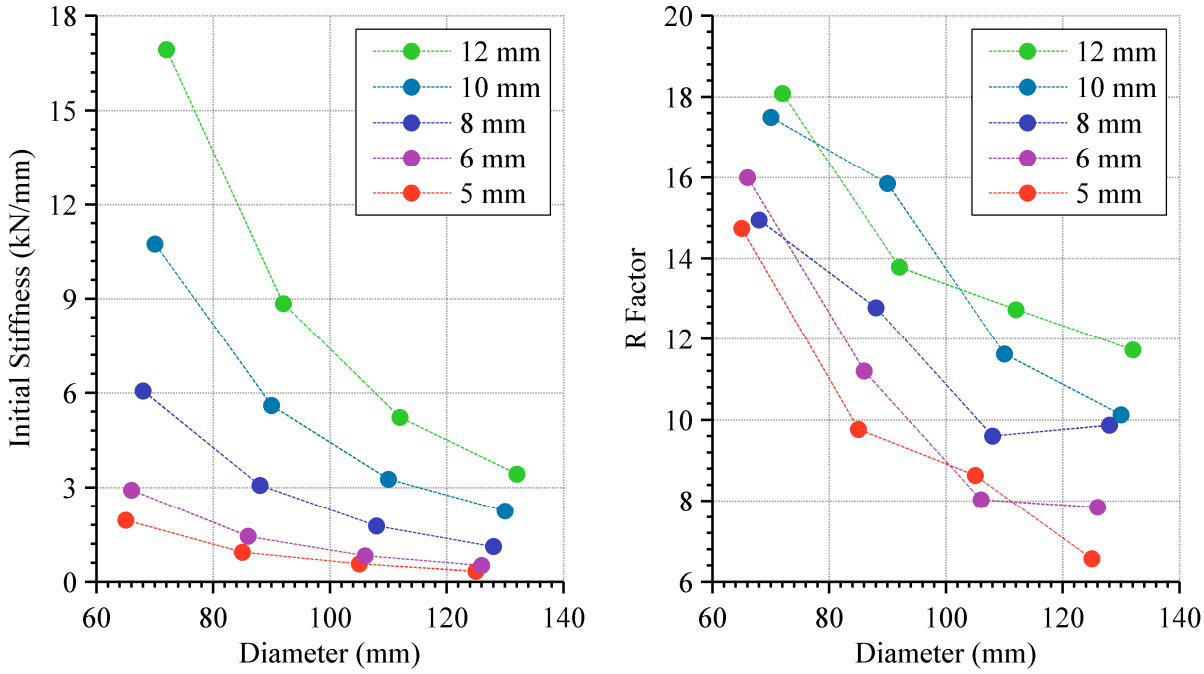

Figure 9-15: Results of finite element parametric analysis: initial stiffness (left) and R factor (right)

The yield force values obtained from the numerical FEM are compared in Figure 9-16 against the fully yielded values obtained from the experimental testing and those derived analytically by Equation (9-8). It can be seen that the fully yielded analytical solution very accurately predicts the yield force of the FEM for the UFP sizes considered as well as that of the UFP tested experimentally. The experimental data point has been linearly adjusted in this and subsequent figures to represent a UFP with a plate with of 100 mm instead of 120 mm. The analytical solutions very slightly overestimate the yield force however this is likely attributed to the method of defining the yield point using the non-linear regression.

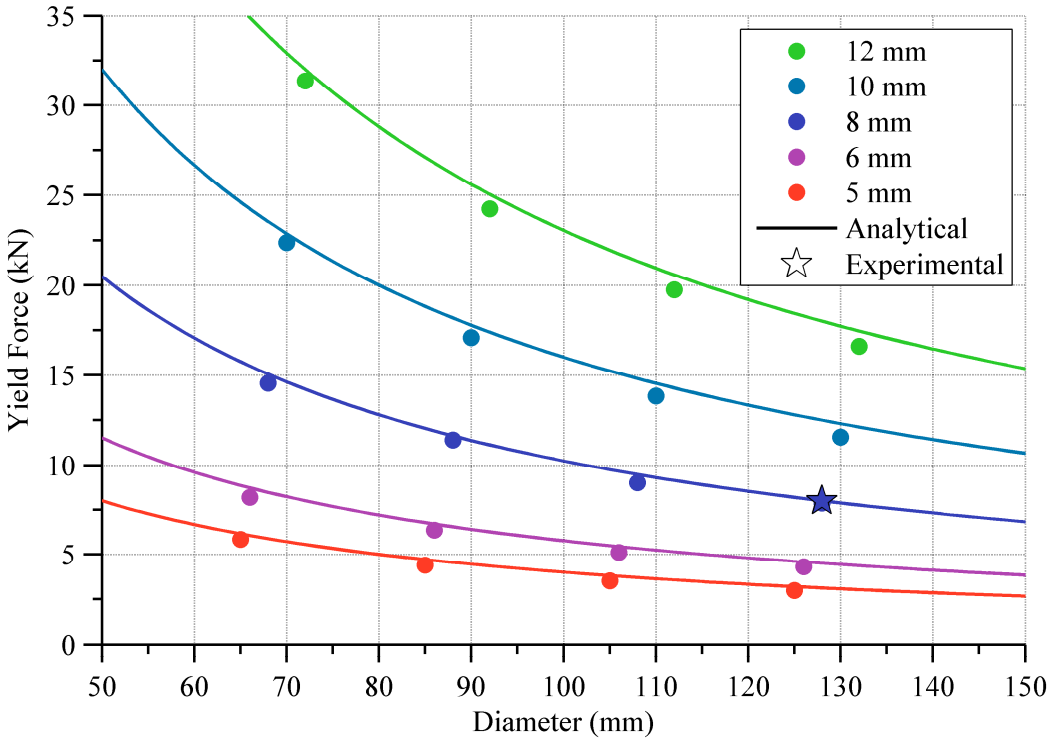

Figure 9-16: Comparison of yield force values obtained experimentally, analytically and numerically

The analytical yield displacement calculated using Equation (9-18) is shown in Figure 9-17 along with the data points from the numerical FEA and the experimental testing.

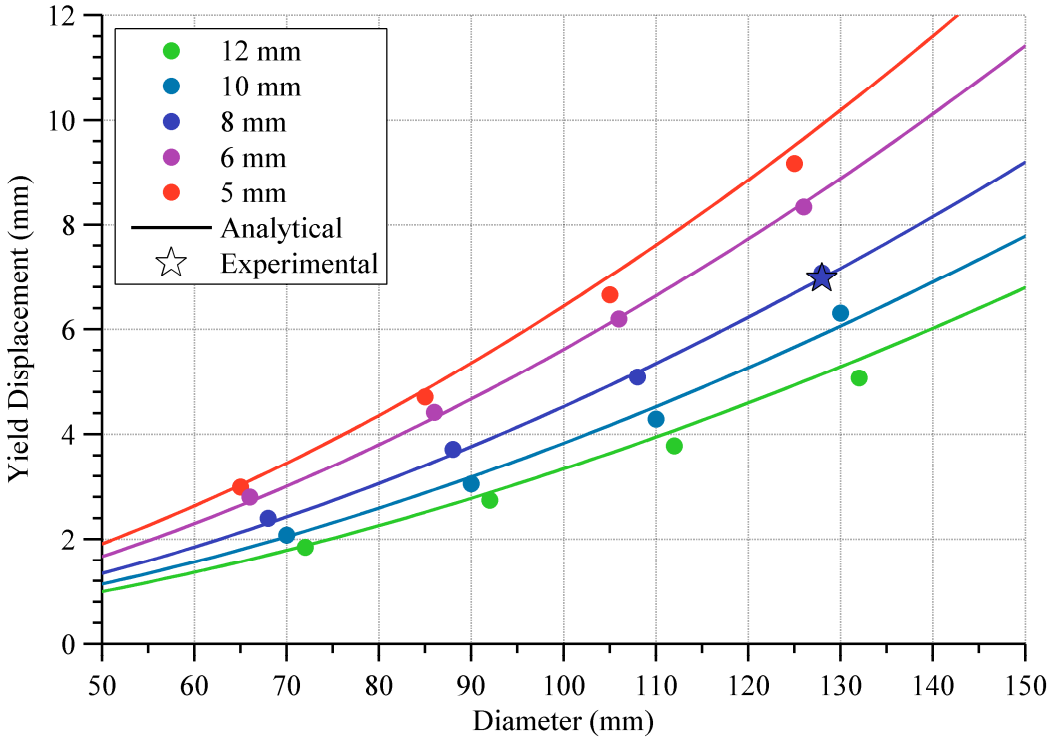

Figure 9-17: Comparison of yield displacement obtained experimentally, analytically and numerically

The experimental data point has been linearly adjusted to represent a UFP with a plate with of 100 mm instead of 120 mm. It can be seen that the analytical solution for the yield displacements fits the data well, with the analytical solutions slightly overestimating the observed yield displacements. This is likely attributed to the method of defining the yield point which also saw a slight over-estimation.

The analytical solution for the initial stiffness has been found using Equation (9-19) and is presented in Figure 9-18 along with the 20 FEM analyses and experimental data point. For simplicity, the data has been presented in non-dimensionalised form. The plate thickness, t_u, has been non-dimensionalised by the bend diameter, D_u. This dimensionless value shall herein be referred to as the 'geometric ratio'.

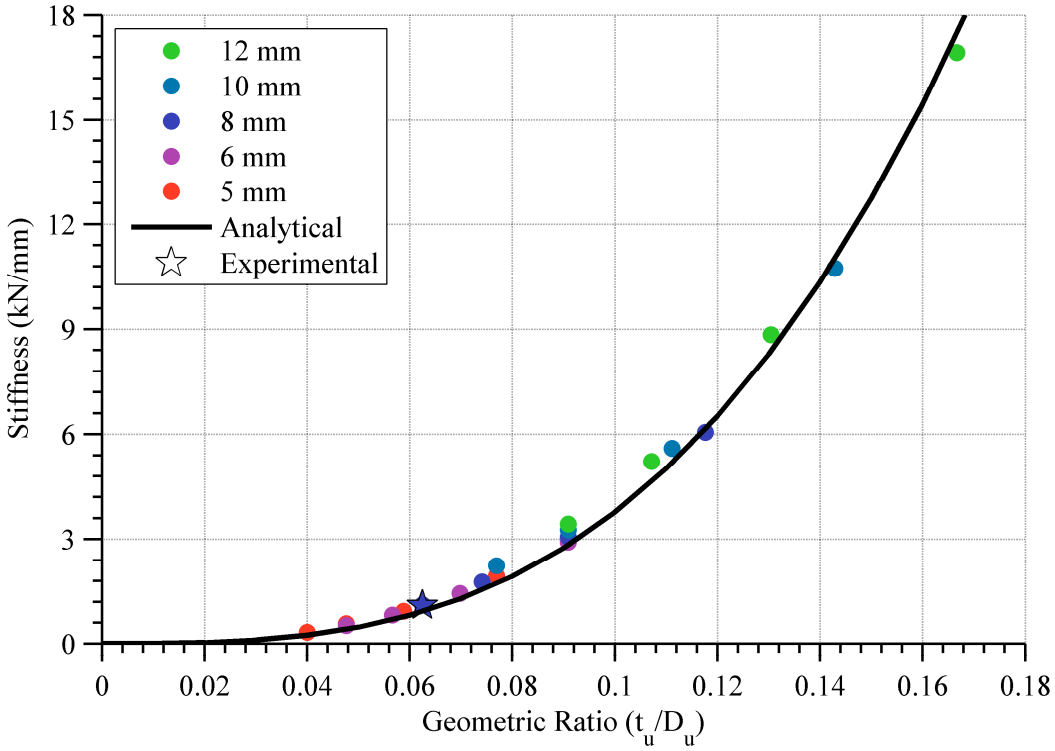

Figure 9-18: Comparison of initial stiffness values obtained experimentally, analytically and numerically

It can be seen that when presented against the geometric ratio, the stiffness data points follow a single curve. The analytical function fits the numerical data points and the single experimental data point extremely well.

Since the geometric ratio condenses the data down to a single variable, it allows for further refinement in the characterisation of the post-yield behaviour. Firstly, an empirical relationship has been proposed to define the R factor in terms of the geometric ratio. Shown in Figure 9-19 are the R factors of the numerical analyses plotted against their corresponding geometric ratio. It can be seen that the R factor shows a trend of being larger for greater

geometric ratios. This trend appears to flatten out for greater geometric ratios, suggesting a logarithmic function would be a good fit to approximate the data. A logarithmic function is fitted to the data using an iterative approach to minimise the squares of the difference between the function and data points and is shown in Figure 9-19.

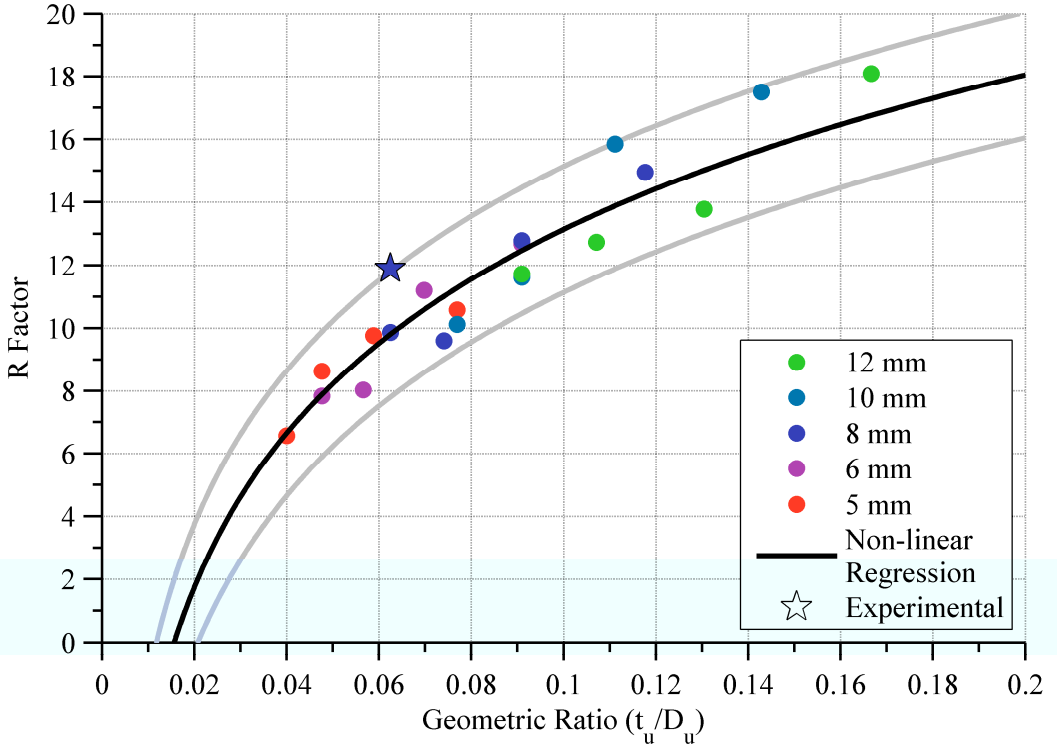

Figure 9-19: R factor values of Ramberg and Osgood (1943) function when fitted to numerical results

The fitted logarithmic function is given by Equation (9-21). Obviously this relationship is only applicable for the geometric ratios considered here (between 0.04 and 0.18). Also shown in Figure 9-19 is the logarithmic function shifted up and down by 2.0. This represents a shift in the constant of Equation (9-21) and has been shown in order to present an upper and lower bound for the R factor.

$$R = 7.1 \ln\left(\frac{t_u}{D_u}\right) + 29.5 \qquad \textbf{(9-21)}$$

where

R = R factor

Since the R factor is critical in determining the peak force and peak displacement of the UFP, a thorough design of a UFP may require the use of an upper and lower bound R factor. In this way the maximum probable force provided by the UFP can be established by use of the lower bound R factor, given by Equation (9-22). Likewise, the minimum probable force

and hence the maximum probable displacement is obtained by use of the upper bound R factor, given by Equation (9-23).

$$R = 7.1 \ln\left(\frac{t_u}{D_u}\right) + 27.5 \quad \textbf{(9-22)}$$

$$R = 7.1 \ln\left(\frac{t_u}{D_u}\right) + 31.5 \quad \textbf{(9-23)}$$

The second method used to characterise the post-yield behaviour is that shown in Figure 9-20. This method calculates the overstrength force using the Ramberg-Osgood equation for different levels of displacement ductility, μ_Δ, of the UFP. The overstrength ratio is then presented in terms of the displacement ductility and the geometric ratio. As has been the case for previous measures of post-yield behaviour, these results also quite erratic. However, there is an evident trend of a higher overstrength ratio for lower geometric ratio, and as would be expected, higher overstrength ratio for greater displacement ductility.

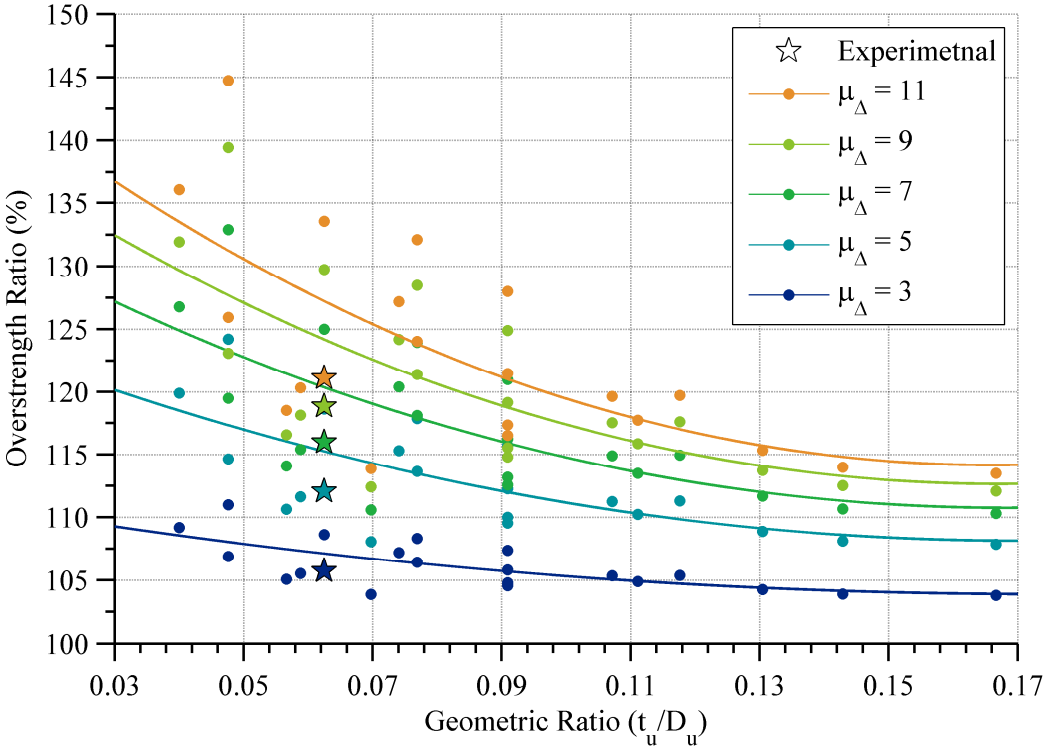

Figure 9-20: Comparison of initial stiffness values obtained experimentally, analytically and numerically

It is envisaged that Figure 9-20 would serve as a useful preliminary design tool in order to anticipate the level of overstrength expected for a chosen UFP geometry and ductility demand. It is then recommended that the empirical R factor relationship given by Equation (9-21) is used to better quantify the expected overstrength forces in a UFP.

9.2.5 Summary of Recommended Modelling Parameters

Using the combination of experimental, analytical and numerical results, the yield force (representing the full yield of the section), yield displacement, initial stiffness and Ramberg-Osgood R factor required for modelling UFP connections are given in Equations (9-8), (9-19) and (9-21) respectively.

$$F_p = f_y \frac{b_u t_u^2}{2D_u} \quad \textbf{(9-8)}$$

$$\Delta_p = \frac{27\pi F {D_u}^3}{16 E b_u t_u^3} \quad \textbf{(9-24)}$$

$$k_0 = \frac{16 E b_u}{27\pi}\left(\frac{t_u}{D_u}\right)^3 \quad \textbf{(9-19)}$$

$$R = 7.1 \ln\left(\frac{t_u}{D_u}\right) + 29.5 \quad \textbf{(9-21)}$$

where

b_u = Width of UFP plate section

t_u = Thickness of UFP plate section

D_u = Diameter of UFP bend

E = Elastic modulus

f_y = Yield stress of UFP

9.3 Cladding Model Verification

The two cladding models (quadrilateral and equivalent spring) developed in Chapter 5 are incorporated here for the use of developing and verifying numerical models for innovative cladding systems. The innovative cladding systems tested experimentally in Chapter 8 represent the basis for the cladding systems being modelled. The parameters used to represent the cladding panel are those developed in Chapter 5 and the parameters used to represent the UFP connections are those presented in this chapter.

A representation of the two models is shown in Figure 9-21. The top cladding connection is represented by a horizontal linear spring element that links the panel to the beam and this is where the UFP connections are implemented, refer to Section 6.4 for further information on the cladding model.

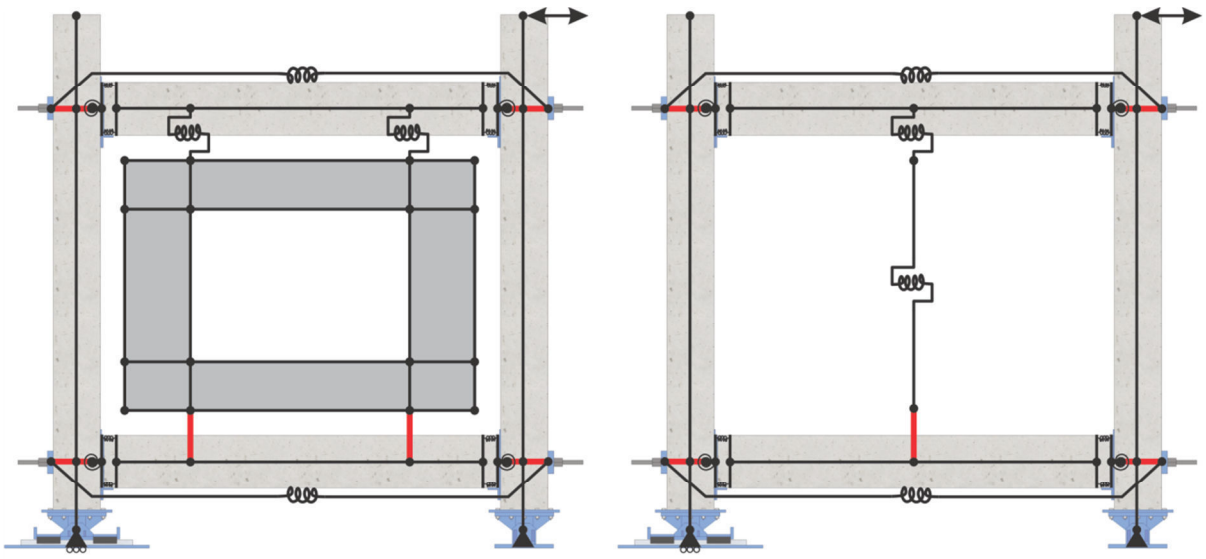

Figure 9-21: Quadrilateral (left) and equivalent spring (right) cladding model incorporated in test frame

This section compares the force-displacement response of the numerical cladding models against the observed experimental response in order to verify the validity of the models. To compare the force-displacement response of the numerical models with the experimental response the models were subjected to the same displacement controlled loading protocol that was used during experimental testing. The force-displacement response of the numerical bare frame is subtracted from the overall numerical frame response to display the force-displacement contribution of the cladding system for each connection type modelled.

A total of four numerical models have been developed for verification. The models include representations of cladding systems with both two UFP and four UFP connections, utilising both cladding model types (quadrilateral and equivalent spring). The experimental tests that represent the two UFP and four UFP cladding systems are MP-UFP3 and MP-UFP4, as presented in Chapter 8. These tests are performed up to 3.5% drift and make use of the RHS housing to properly restrain the UFP connections.

9.3.1 Experimental UFP Connections

A quadrilateral and an equivalent spring model have been developed using the recommended modelling parameters presented in Section 9.2.5. Both models represent the UFP connections with linear spring elements. The amount of force transferred through the cladding system being dictated by the hysteretic behaviour of these springs. The non-linear behaviour of the connection springs for both models was represented using the Bounded

Ramberg-Osgood hysteretic rule. The bounded version of the Ramberg-Osgood hysteretic rule produces a modified loop on small cycle reloading. This is necessary for cycle loading since the original version of the hysteretic rule tends to exhibit un-realistic forces if the loop reverses and has not moved very far from the back-bone curve (Carr, 2008).

The yield force, initial stiffness and R factor for the UFPs using Ramberg-Osgood are given in Equations (9-7), (9-19) and (9-21) respectively.

$$F_y = f_y \frac{b_u t_u^2}{2D_u} = 320 \times \frac{120 \times 8^2}{2 \times 128} = 9.6\ kN \quad \textbf{(9-7)}$$

$$k_0 = \frac{16 E b_u}{27\pi}\left(\frac{t_u}{D_u}\right)^3$$

$$k_0 = \frac{16 \times 200{,}000 \times 120}{27\pi}\left(\frac{8}{128}\right)^3 = 1.1\ kN/mm \quad \textbf{(9-19)}$$

$$R = 7.1 \ln\left(\frac{t_u}{D_u}\right) + 29.5$$

$$R = 7.1 \ln\left(\frac{8}{128}\right) + 29.5 = 9.8 \quad \textbf{(9-21)}$$

The R factor has been found using the equation derived that best fits the numerical data. There was no strength degradation incorporated into the definition of hysteretic behaviour so the connection has an infinite ductility. This is considered appropriate considering the equivalent displacement demand did not result in any failure during testing.

The cladding panel was represented in the quadrilateral model using the geometry of the panel and an elastic modulus of 35 GPa (the elastic modulus of the panel concrete tested experimentally). The stiffness of the spring model was defined as 4800 kN/m.

9.3.2 Quadrilateral Model

The force-displacement response of the quadrilateral cladding model compared with the experimental response of test MP-UFP3 is illustrated in Figure 9-22. The experimental system consists of two housed UFP connections. It can be observed that the numerical model accurately reproduces the cyclic response of the cladding system. The only notable inaccuracy of the mode concerns the unloading strength and stiffness, particularly during larger cycles. This minor inaccuracy in capturing the unloading strength and stiffness can be traced back to difficulty in calibrating a numerical model that accurately captures the unloading and re-loading characteristics. However, the model very accurately captures the

peak forces in the system. Also shown in Figure 9-22 is the force-displacement contribution from the cladding system and the parameters of the hysteretic rule for an individual connection.

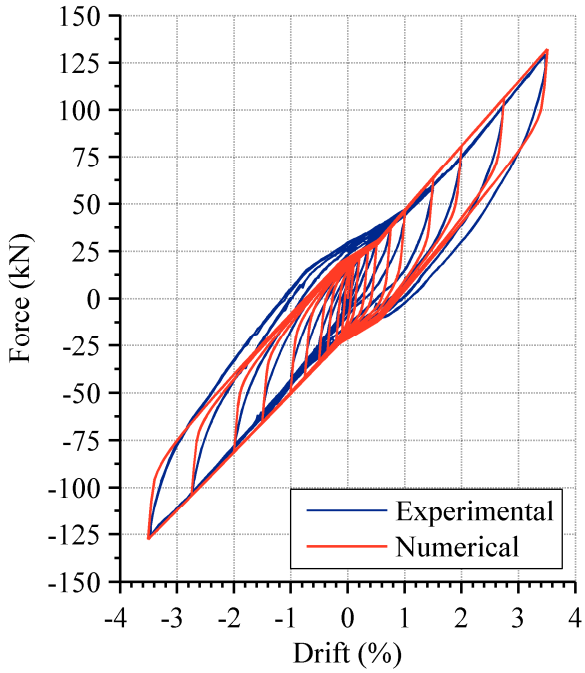

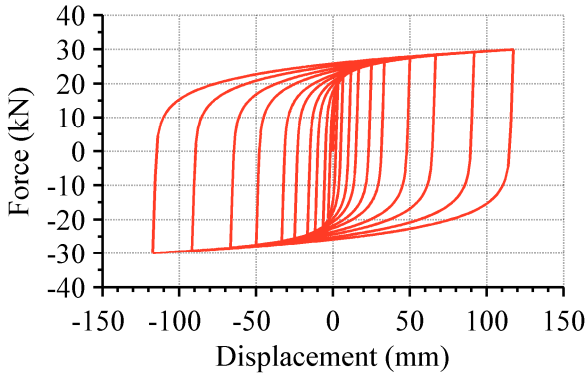

Model Type	Quadrilateral
Hysteretic Rule	Bounded Ramberg-Osgood
Initial Stiffness	1.1 kN/mm
Yield Force	9.6 kN
R factor	9.8

Figure 9-22: UFP cladding model (quadrilateral) compared with experimental results of test MP-UFP3

The force-displacement response of the quadrilateral cladding model compared with the experimental response of test MP-UFP4 is illustrated in Figure 9-23. The experimental system consists of four housed UFP connections. It can be seen that the model does not match the experimental behaviour as well as in the previous case. The model over-estimates the strength and stiffness of the cladding system, more so in the positive direction than the negative. It would appear that the experimental cladding panel is accommodating a greater proportion of the movement than that of the cladding panel in the model, leading to lower forces in the connections. This is analogous to the panel having a non-linear response. Such a response would be likely at the force levels observed (approximately 40 kN) since this is when cracking was observed during testing of short threaded rod connections in Chapter 4. Where the model of two UFP connections slightly underestimates the observed hysteretic response, it is evident in Figure 9-23 that the model of four UFPs overestimates the hysteretic response. Also shown in Figure 9-23 is the force-displacement contribution from the cladding system and the parameters of the hysteretic rule for an individual connection.

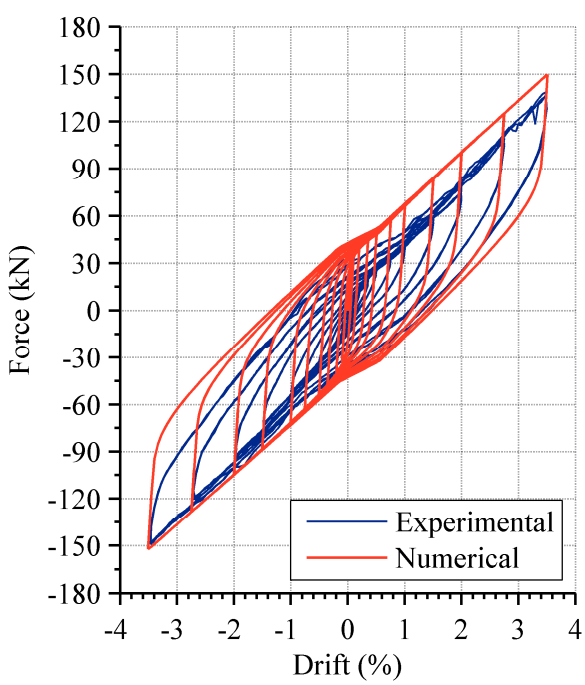

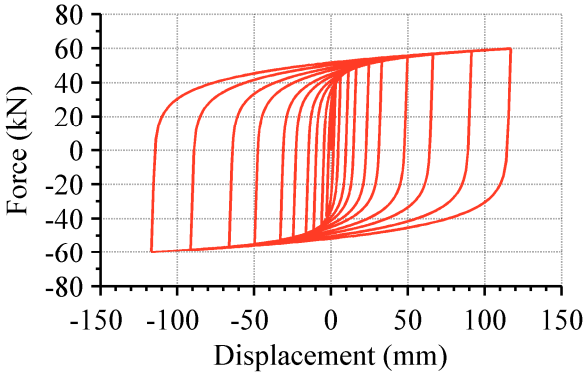

Model Type	Quadrilateral
Hysteretic Rule	Bounded Ramberg-Osgood
Initial Stiffness	2.2 kN/mm
Yield Force	19.2 kN
R factor	9.8

Figure 9-23: UFP cladding model (quadrilateral) compared with experimental results of test MP-UFP4

9.3.3 Equivalent Spring Model

The force-displacement response of the equivalent spring cladding model compared with the experimental response of test MP-UFP3 is illustrated in Figure 9-24.

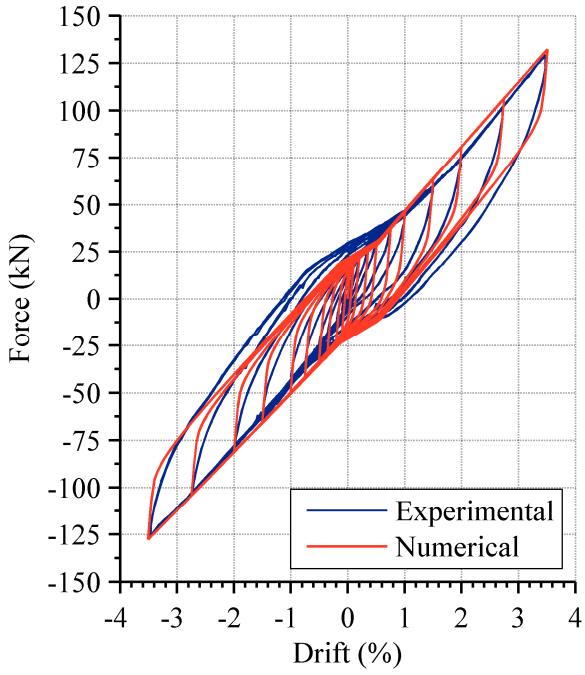

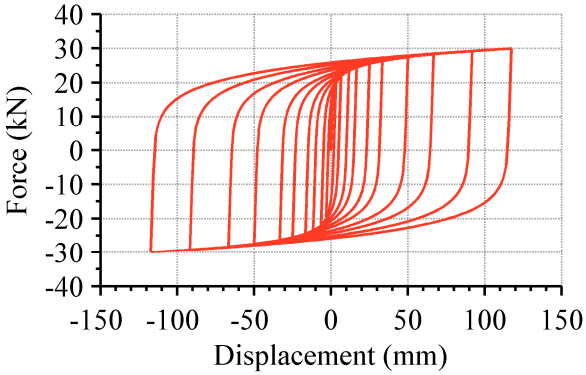

Model Type	Equivalent Spring
Hysteretic Rule	Bounded Ramberg-Osgood
Initial Stiffness	2.2 kN/mm
Yield Force	19.2 kN
R factor	9.8

Figure 9-24: UFP cladding model (equivalent spring) compared with experimental results of test MP-UFP3

The single connection spring of the model was assigned double the stiffness and yield force to make it equivalent to two connection springs being in parallel. It can be observed that the behaviour of the model is virtually identical to that of the quadrilateral model presented in Figure 9-22. Also shown in Figure 9-24 is the force-displacement contribution from the cladding system and the parameters of the hysteretic rule for the equivalent spring connection.

The force-displacement response of the quadrilateral cladding model compared with the experimental response of test MP-UFP4 is illustrated in Figure 9-25.

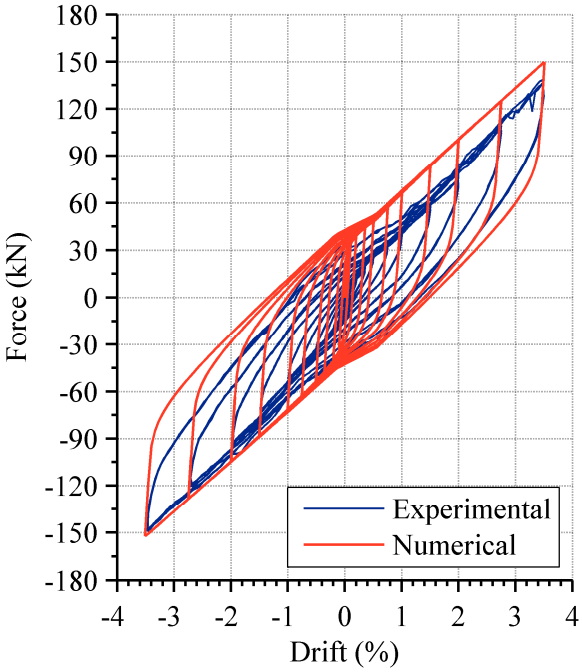

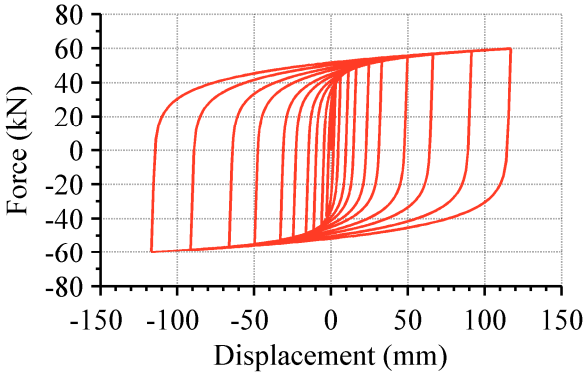

Model Type	Equivalent Spring
Hysteretic Rule	Bounded Ramberg-Osgood
Initial Stiffness	4.4 kN/mm
Yield Force	38.4 kN
R factor	9.8

Figure 9-25: UFP cladding model (spring) compared with experimental results of test MP-UFP4

The experimental system consists of four housed UFP connections. It can again be observed that the behaviour of the model is virtually identical to that of the quadrilateral model presented in Figure 9-23 and hence the model overestimates the hysteretic response. Also shown in Figure 9-25 is the force-displacement contribution from the cladding system and the parameters of the hysteretic rule for the spring connection.

9.4 Conclusions

This chapter presented the development of modelling techniques for innovative cladding systems. This follows on from the previous chapter where experimental testing was undertaken. The results of the experimental testing showed that UFPs were low-cost and straightforward to fabricate, produced reliable and stable hysteretic behaviour, provided

flexibility in their design and implementation, and were able to withstand large displacements while transferring small force into the cladding.

This chapter focussed on providing the tools so that the connections are simple to design and model. It was found the analytical derivations very accurately predicted the initial yield and initial stiffness of UFPs. Finite element models were calibrated against the cyclic experimental behaviour of UFPs and a subsequent parametric analysis was undertaken to expand the experimental dataset to include UFPs of varying geometry. The elastic results of this parametric analysis also matched the analytical solutions extremely well, further confirming their suitability.

Non-linear parameters based on the Ramberg-Osgood function were proposed to develop a model for UFPs. The force-displacement results of the numerical models were compared against the experimental behaviour for the different UFP cladding connection configurations tested. An excellent fit was observed for the lateral resistance provided by the cladding systems that included two UFP connections. The numerical models slightly overestimated the lateral resistance of the cladding systems with four UFP connections, likely due to the actual cladding panel being able to accommodate a greater proportion of the movement than that of the cladding panel in the model. In general, it can be concluded that the numerical model developed of UFPs does accurately represent their behaviour when implemented as an innovative cladding connection.

9.5 References

ABAQUS Inc. (2011). Abaqus FEA: Providence, RI., USA.

AS/NZS 3678. (1996). Structural steel - Hot-rolled plates, floorplates and slabs. Wellington: Standards New Zealand.

Carr, A. J. (2008). *Ruaumoko Programme for Inelastic Dynamic Analysis - Appendices*: Department of Civil Engineering, University of Canterbury, New Zealand.

Kaldjian, M. J., & Fan, W. R. S. (1967). Earthquake Response of a Ramberg-Osgood Structure. Industry Program of the College of Engineering: The University of Michigan.

Kelly, J. M., Skinner, R. I., & Heine, A. J. (1972). Mechanisms of Energy Absorption in Special Devices for use in Earthquake Resistant Structures. *Bulletin of the New Zealand Society for Earthquake Engineering, 5*(3).

MathWorks Inc. (2011). MATLAB 7.11. Natick, MA., USA.

Pampanin, S., Marriott, D., & Palermo, A. (2010). PRESSS Design Handbook. Auckland, New Zealand: New Zealand Concrete Society, NZCS.

Ramberg, W., & Osgood, W. R. (1943). Description of stress-strain curves by three parameters (Version Technical Note No. 902). Washington, DC.,USA: National Advisory Committee for Aeronatics.

10 Seismic Response and Expected Damage of Multi-Storey Buildings with Innovative Cladding

10.1 Introduction

This chapter presents the seismic response and corresponding performance assessment of multi-storey buildings with innovative cladding. The innovative cladding system utilises U-Shaped Flexural Plates (UFPs) as a passive energy dissipation device. The innovative cladding is incorporated into a case-study building using the cladding models developed and verified in Chapter 9. Numerical analyses of the case-study building are performed to assess the effect that the innovative cladding has upon the seismic response. The numerical analyses performed include modal analyses, non-linear adaptive pushover analyses, and non-linear dynamic seismic response (time-history) analyses.

The seismic response from these analyses is used to assess the expected performance of the structure and cladding. This is achieved by calculating the probability of exceeding a specified level of damage for a given ground motion intensity. This performance assessment is undertaken considering both the structural and cladding performance. Finally, a quantitative assessment of whether the innovative cladding connections have an effect upon the seismic response and thus damage level to the case-study structure is presented. The potential repair cost savings of such effects will be explored in the following chapter.

10.2 Cladding-Structure Model

The case-study structure introduced in Chapter 6 has been chosen to showcase the influence the innovative cladding has upon the structural behaviour. The 2D model was developed using the seismic response analysis program Ruaumoko2D (Carr, 2010). The

structure is based on the Red Book building (Bull & Brunsdon, 1998) which acts as a design example of the New Zealand Concrete Code (NZS 3101, 2006). The primary lateral load carrying system consists of perimeter moment resisting frames which are three bays long. The bottom floor has a storey height of 4 m while the upper floors have a storey height of 3.6 m.

The structure was modelled using a lumped mass model and non-linear frame elements that utilise the Giberson One Component Beam model (Giberson, 1967). The non-linear behaviour was based on the modified Takeda hysteresis (Otani & Sake, 1974), with the appropriate section properties determined using section modelling programme CUMBIA (Montejo & Kowalsky, 2007). The column members also were defined a moment-axial yield interaction surface to account for the effect axial load has on the moment capacity (Park & Paulay, 1975). The beam-column-joint regions of the frame were assumed to be rigid.

10.2.1 Innovative Cladding System Models

The UFP cladding systems have been incorporated into the case-study structure model utilising the mono panel cladding configuration only. The mono panel configuration cladding model includes a single storey height panel in each bay and in every floor except the ground floor, as illustrated in Figure 10-1. Only one cladding configuration was analysed with the UFP cladding system since the comparison between configurations was undertaken in Chapter 6.

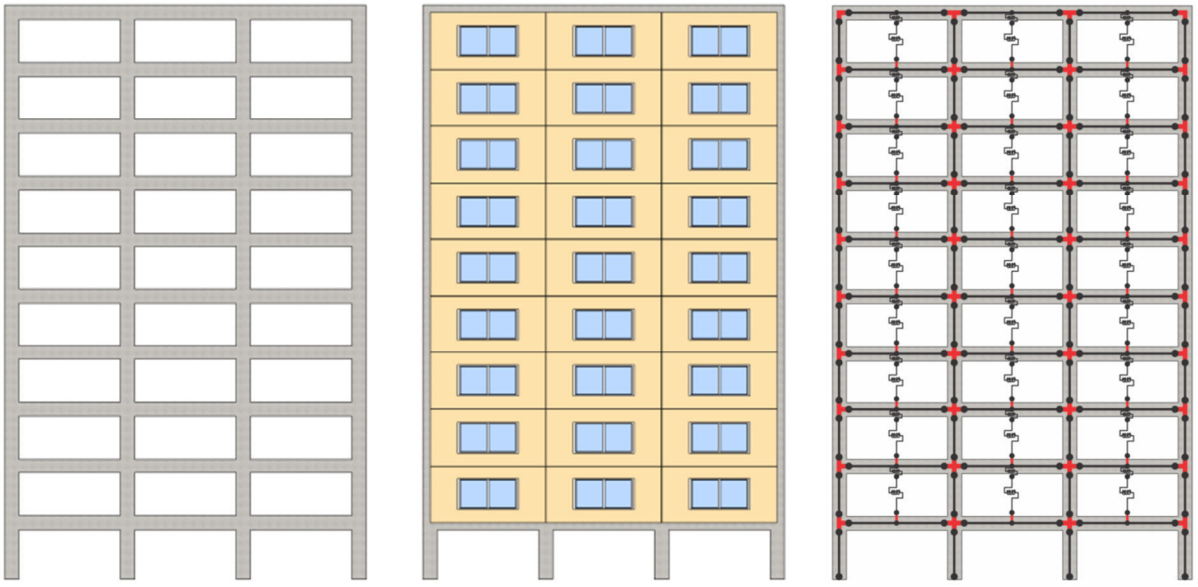

Figure 10-1: Bare frame of case-study structure (left), mono panel cladding configuration (centre) and lumped plasticity model including equivalent spring cladding panel model (right)

The prototype clad building models presented in Figure 10-1 were implemented in Ruaumoko2D (Carr, 2010) using only the equivalent spring cladding models developed in Chapter 9. The implementation of the equivalent spring model into the frame structure was chosen since it represents the simplest and the computationally least expensive inclusion of a cladding model. The outputs of the equivalent spring cladding model were also shown in Chapter 6 to be very similar to that of the quadrilateral cladding model. The equivalent spring model consists of a single spring for the cladding panel, a single rigid base connection and a single spring to represent the UFP connection. A visual representation of the equivalent spring model implemented in the mono panel configuration is shown in Figure 10-1.

10.2.2 Design of UFP Connection Systems

The development of the cladding models for the case study structure requires the definition of the UFP connection parameters, with the panel parameters being the same as those used previously. A UFP connection design is necessary in order to define the UFP connection parameters. The key design constraints for the UFP design are the maximum stroke and the maximum design force.

The maximum stroke is defined as the maximum relative displacement expected between the top of the cladding and the structure. For this design, the maximum relative displacement has been chosen using the information gained from the seismic response analyses performed in Chapter 6. The analyses found that for a 2% in 50 year intensity level earthquake, the maximum relative displacement observed was 77 mm. Of the 20 ground motion analyses undertaken at this intensity level, the average maximum was 47 mm. A maximum relative displacement of 80 mm has been chosen for the UFP design. This displacement is analogous to a maximum inter-storey drift of 2.2%. This relative displacement has to be accommodated by lateral deformation of both the cladding panel and cladding connection.

The maximum design force is limited by the amount of force that can be transferred through the panel while ensuring the risk of damage to the panel is low. Assuming the cladding panel damage is directly proportional to the lateral displacement of the panel, a level of panel displacement that is deemed to carry an acceptable level of risk can be chosen using the fragility function developed in Chapter 7. The force corresponding to this panel displacement can be found by knowing the stiffness of the panel.

Two possible panel displacements and hence two possible UFP connection designs are herein considered. The intention of the first design is to ensure that the probability of any possible damage to the cladding panel is kept to an absolute minimum. The second is done with the intention that some risk of damage to the cladding panel is acceptable in a significant earthquake but failure is avoided. The first option will herein be referred to as the Low-Damage (LD) design and the second as the Damage-Reduction (DR) design. The second option is predominantly focussed on providing a mechanism that significantly reduces the expected damage to the structure while accepting that damage to the cladding may be a consequence. Such a design philosophy may be used as a retrofit solution for a structure that is deemed to be under-capacity and as such, the desire is to provide additional strength and stiffness is the main focus.

Referring to the fragility function presented in Figure 10-2, a design panel displacement of 2.0 mm has been chosen for the low-damage design and a panel displacement of 5.0 mm has been chosen for the damage-reduction design. As, illustrated in the fragility function in Figure 10-2, the low-damage design panel displacement provides a 100% probability of the panel remaining in the Operational performance level. The damage-reduction design panel displacement provides a 79% probability of the performance being Operational and 21% probability of the performance being deemed Immediate Occupancy. At this panel displacement, the probability of exceeding Immediate Occupancy is 0.4%, thus the likelihood of significant damage has been kept to a minimum.

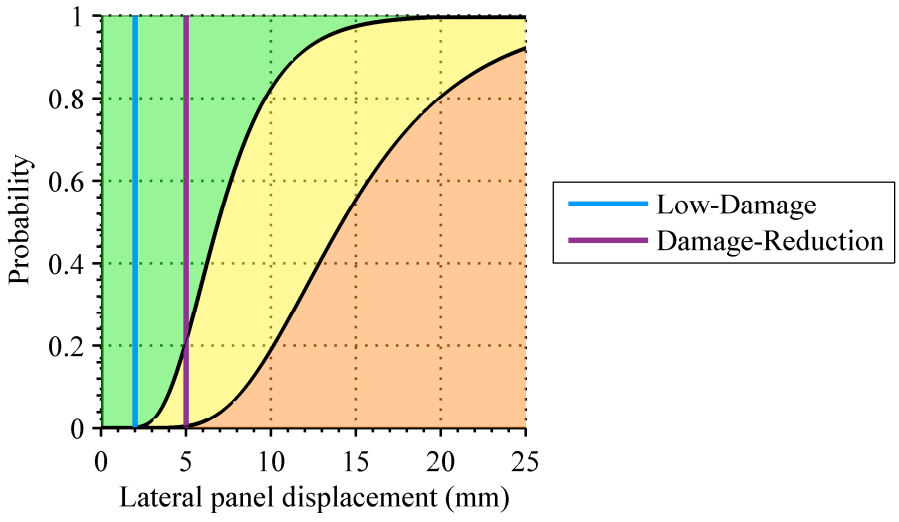

Figure 10-2: Fragility function of cladding panel including design panel displacement limit of two proposed design philosophies

The force developed in the panel corresponding to the panel displacement of the two designs is found using the stiffness of the panel, as given by Equation (10-1) and (10-2) for the respective designs.

With the maximum design force and maximum stroke determined, it is possible to choose the dimensions of the UFP that satisfy these constraints. The maximum stroke is required in order to determine the cyclic fatigue performance of the design, with the aim to keep the maximum strain to a minimum. The design therefore aims to minimise the ratio of plate thickness to bend diameter.

$$F_{p1} = k_p \Delta_{p1} = 23.3 \times 2.0 = 46.6\ kN \quad \textbf{(10-1)}$$

$$F_{p2} = k_p \Delta_{p2} = 23.3 \times 5.0 = 116.5\ kN \quad \textbf{(10-2)}$$

where

F_{pi} = Maximum panel force

k_p = In-plane cladding panel stiffness

Δ_{pi} = Maximum panel displacement

For the low-damage design, a plate size of 100 x 12 mm was selected with an inner bend radius of 120 mm. The nominal UFP diameter is thus 132 mm. This size UFP would require the use of 150 x 150 RHS housing. The key modelling parameters of the UFPs are calculated using the relationships derived in Chapter 9. The yield force, initial stiffness and Ramberg-Osgood R factor are given in Equations (10-3), (10-4) and (10-5) respectively. Note the nominal yield strength of an 10 mm plate is 310 MPa (AS/NZS 3678, 1996).

$$F_y = f_y \frac{b_u t_u^2}{2D_u} = 310 \times \frac{100 \times 12^2}{2 \times 132} = 16.9\ kN \quad \textbf{(10-3)}$$

$$k_0 = 2350 \left(\frac{t_u}{D_u}\right)^{2.75} \quad \textbf{(10-4)}$$

$$k_0 = 2350 \times \left(\frac{12}{132}\right)^{2.75} = 3.2\ kN/mm$$

$$R = 7.1 \ln\left(\frac{t_u}{D_u}\right) + 29.5 \quad \textbf{(10-5)}$$

$$R = 7.1 \ln\left(\frac{12}{132}\right) + 29.5 = 12.5$$

where

F_y = Yield force of UFP

f_y = Yield stress of UFP plate

b_u = Width of UFP plate

t_u = Thickness of UFP plate

D_u = Diameter of UFP bend

The UFP dimensions were chosen using an iterative process which requires the calculation of the maximum expected force in the UFP at the maximum stroke. The iterative process requires the following steps:

1. Select UFP geometry with lowest geometric ratio that maximises the yield force
2. Calculate modelling parameters of geometry selected
3. Calculate the force at maximum stroke using Ramberg-Osgood relationship
4. Check that the force is less than the maximum allowable force in the panel, if not, alter geometry and repeat Steps 1-3 until geometry is optimised.
5. Check a suitable RHS section exists for the UFP dimensions, if not repeat Steps 1-4

The force-displacement behaviour of the chosen UFP geometry is illustrated in Figure 10-3. The behaviour is also shown when the R factor of the Ramberg-Osgood relationship is varied by ± 2.0. This range encapsulates the range of R factors observed during the numerical analyses. Also shown in Figure 10-3 is half of the maximum allowable force in the panel (since two connections are used). It can be seen that the expected force in the UFP is always less than that of the maximum allowable force in the panel.

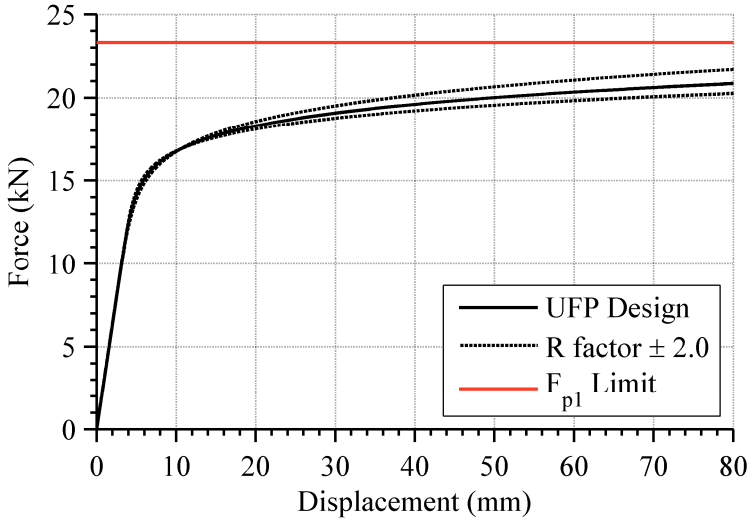

Figure 10-3: Force-displacement behaviour of chosen UFP including cladding panel force limit

For the damage-reduction design, it was decided to use the same UFP design and include four of the UFP cladding connections. For a panel displacement of 5.0 mm, the corresponding panel force is 116.5 kN. When four connections are used, the maximum allowable horizontal force in the panel per connection is 29 kN, hence this configuration is within the force limit shown in Figure 10-3.

The maximum strain in the plate, ε_{max}, defined as the ratio of the thickness and the diameter of the UFP bend given in Equation (10-6) was found to be 9.1%.

$$\varepsilon_{max} = \frac{t_u}{D_u} = \frac{12}{132} = 9.1\% \qquad \textbf{(10-6)}$$

where

ε_{max} = Maximum strain

The maximum stroke of 80 mm when normalised by the bend radius, gives a normalised stroke of 1.21; hence the expected cycles to failure of the UFP can be defined using the data from Kelly et al. (1972) and is shown in Figure 10-4. Evidently, no data exists for UFPs in this region of low strain and low normalised stroke, so the only conclusion is that a minimum of 150 cycles (of the maximum stroke) would be expected to lead to failure of the UFP. However, going by the trend of the results, it would be expected that the UFP could undergo more than 150 cycles before failure. Of course it is also highly unlikely that the UFP would ever be subjected to such a high number of large stroke displacements. It is much more likely to undergo a large number of low displacement cycles.

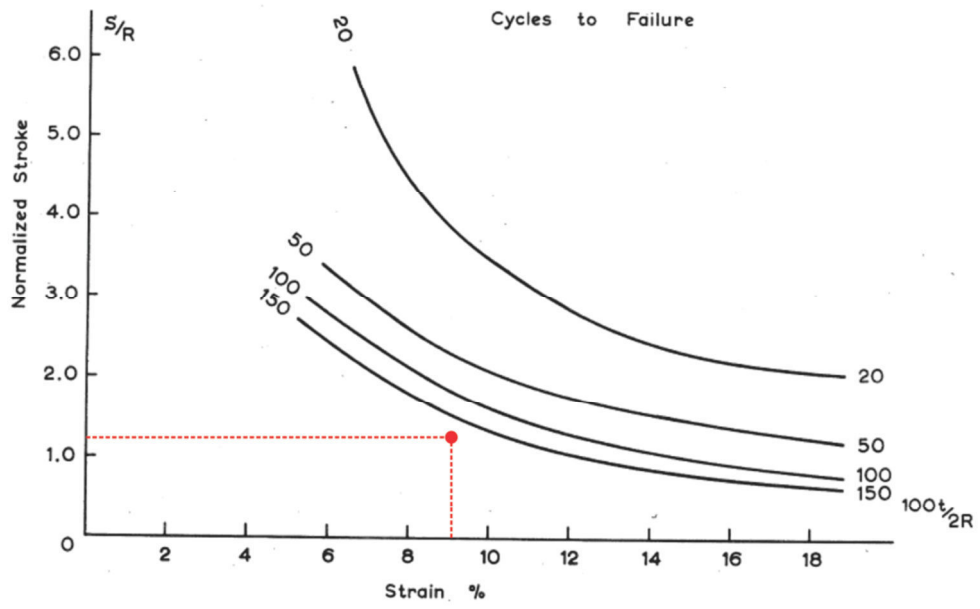

Figure 10-4: Number of cycles to failure (Kelly et al., 1972)

10.3 Static Analyses

Adaptive non-linear push-over analyses were undertaken to show the difference in stiffness and strength between the bare frame and the innovative cladding frame models. An adaptive pushover is a succession of incremental static analysis performed by subjecting the frame to a lateral load pattern that is adapted as the structure deforms. The initial load pattern used was that prescribed for the equivalent static method in NZS 1170.5 (2004).

Pushover analyses were performed up to a maximum frame drift of 2.0% for the bare frame and clad frame models. The two innovative clad frame models consist of the low-damage (LD) UFP connection design and the damage-reduction (DR) connection design. Both connection systems are incorporated in the mono panel configuration. The force-drift response is shown in Figure 10-5. The behaviour of the three frame systems up to 0.2% is shown in Figure 10-5 (left) in order to compare the initial stiffness and yield point of the systems. The initial stiffness of the bare frame is 19.2 kN/mm. The inclusion of the low-damage UFP cladding system increases this stiffness by 22% and the damage-reduction system increases the stiffness by 32%. It can also be seen that the bare frame remains elastic up to a drift of 0.16%, or a corresponding top displacement of 58 mm. The initial yield point of the clad frames occurs slightly earlier, at a drift of approximately 0.14 – 0.15%.

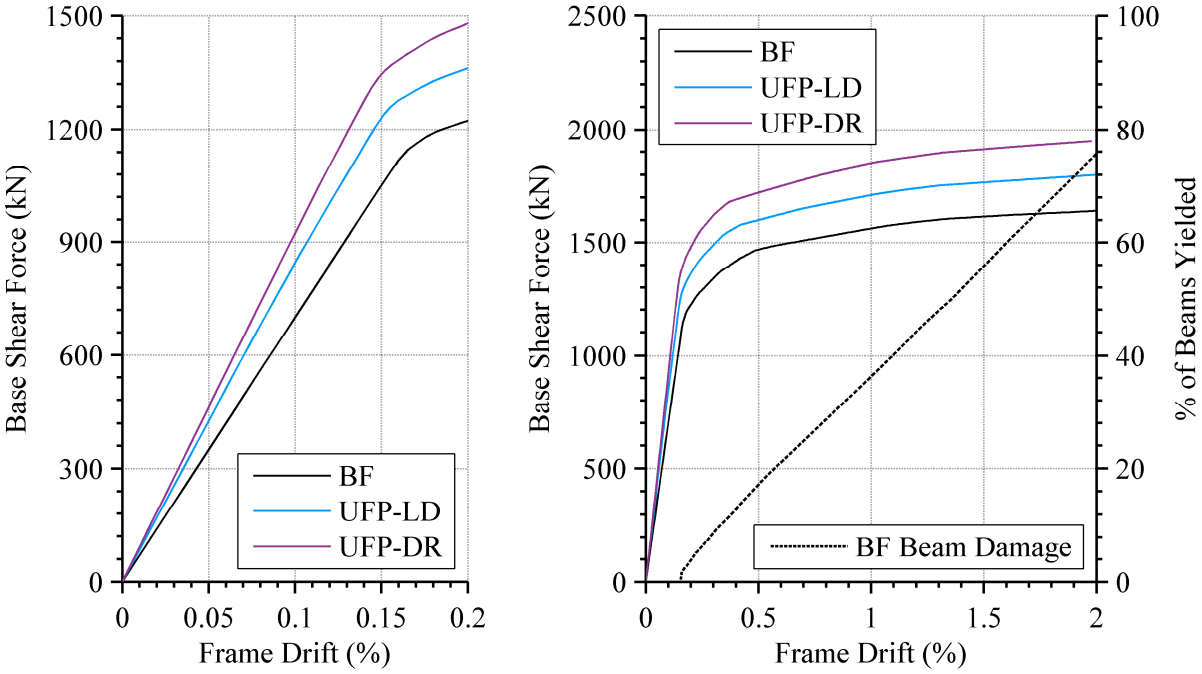

Figure 10-5: Initial (left) and complete (right) pushover behaviour for different UFP frame configurations

The full pushover behaviour of the different frame systems up to 2.0% frame drift is also shown in Figure 10-5 (right). At 0.5% frame drift, the bare frame has a base shear force

of 1470 kN. The inclusion of the low-damage UFP cladding system increases the base shear force by 9% and the damage-reduction system increases the base shear force by 17%. This percentage increase is reasonably constant after yield since the force contribution from the UFP connections flattens out quickly once yielded.

10.4 Dynamic Analyses

The dynamic behaviour of the case-study structure with and without cladding is explored in this section through numerical analyses. The numerical analyses include a modal response spectrum analysis as well as non-linear time-history analyses (seismic response analyses) using the earthquake ground motions selected previously in Chapter 6.

10.4.1 Modal Response

A modal response spectrum analysis was undertaken on each of the numerical building models to investigate how the inclusion of the UFP cladding systems affects the dynamic response. The modal response is undertaken using the first four modes of free vibration in the structure considering an elastic site spectra for horizontal loading obtained from the New Zealand Standard for earthquake actions (NZS 1170.5, 2004). A seismic hazard of Z = 0.22, corresponding to the building being located in Christchurch prior to the increase in seismic hazard post September 2010 (MBIE, 2011), soil type D (Tonkin & Taylor Ltd., 2011) and annual probability of exceedance of 1/1000 (R_s = 1.3) are considered.

It was found through the modal response analyses performed in Chapter 6 that the first mode dominates the lateral displacement of the building; however, the higher modes provide a contribution to the peak floor force throughout the building, particularly to the top two floors of the building.

The interstorey displacements and peak forces of each mode are combined by carrying out a square root of the sum of the squares (SRSS) at each level of the structure. The SRSS envelopes of the frame displacements and peak floor forces in the bare frame model are compared with the clad frame models in Figure 10-6.

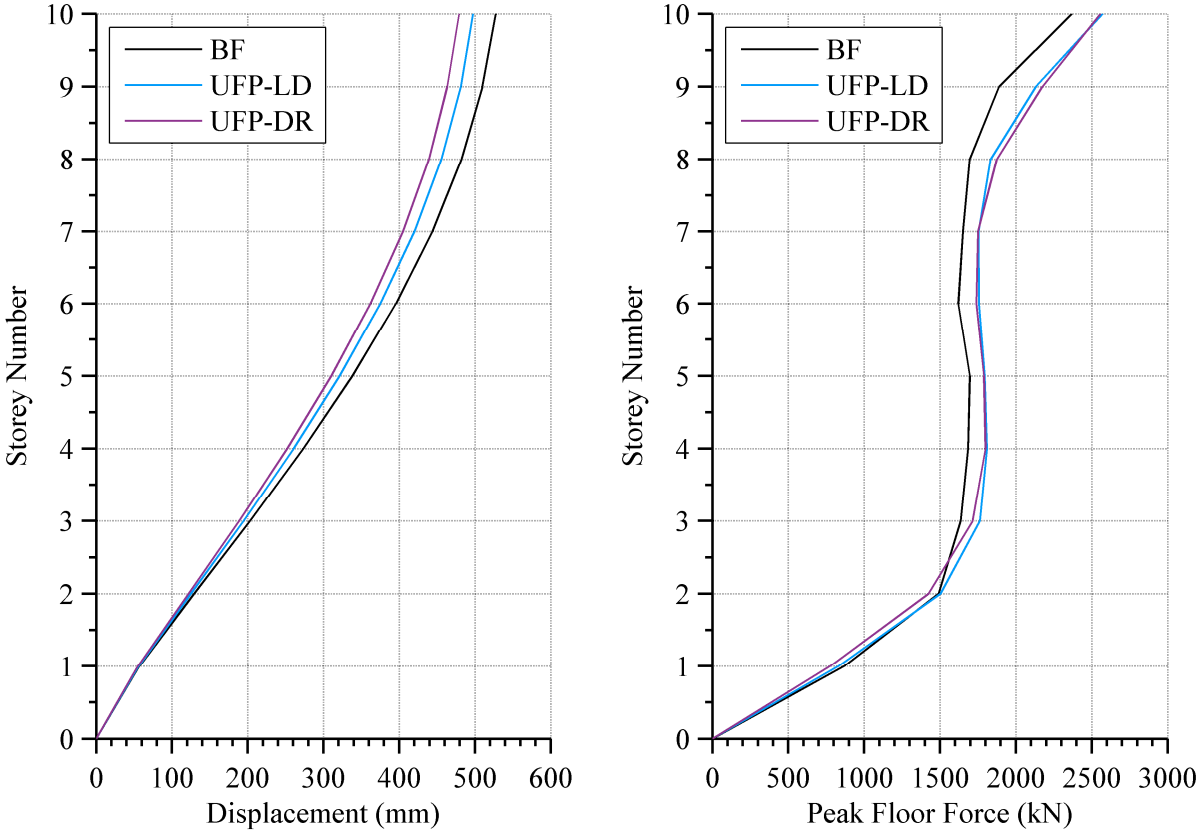

Figure 10-6: Displacement profile (left) and peak floor force profile (right) for different UFP frame configurations

It can be observed in Figure 10-6 that there is a reduction in the maximum displacements and increase in peak floor force due to the presence of the cladding. The difference in result appears very similar to that observed for modal analyses performed on the traditional cladding systems in Chapter 6. The displacement at the top of the bare frame was found to be 530 mm for this seismic hazard, equivalent to 1.45% frame drift. This is reduced by 6 – 10% when the cladding is included, with the damage-reduction system having the greater influence of the two configurations. The peak floor force in the bare frame was found to be 2370 kN. This maximum force increases by 8 – 9% when the cladding is included. It can also be seen in Figure 10-6 that this increase is apparent throughout the structure and not just at the top, as is the case for the increase in displacement profile. The two UFP cladding systems contribute approximately the same increase to the peak floor force. A summary of the periods for the first four modes for each of the frame systems is presented in Table 10-1. Similarly to the results found in Chapter 6 where the traditional cladding connections were found to cause at most a 9% reduction in the fundamental period, the innovative connections also result in a maximum reduction in the fundamental period of 9%.

Table 10-1: Period of first four modes for different UFP frame configurations

Mode	Bare Frame	Low Damage Claddings	Damage Reduction Claddings
1	1.97 s	1.86 s	1.79 s
2	0.63 s	0.60 s	0.58 s
3	0.35 s	0.34 s	0.33 s
4	0.23 s	0.22 s	0.22 s

10.4.2 Seismic Hazard and Ground Motions

The ground motion selection has been performed using a generalised conditional intensity measure (GCIM) approach (Bradley, 2010). The ground motions have been selected to best represent the seismic hazard identified by probabilistic seismic hazard analysis (PSHA) (Cornell, 1968). The seismic hazard is based on a site in Christchurch, New Zealand prior to the knowledge of the fault systems that caused the 2010 Darfield and subsequent Canterbury earthquakes. GNS Science quantified the change in seismic hazard due to the discovery of these faults as being a 37% increase.

The same seismic hazard and thus the same ground motions used to perform the response history analyses in Chapter 6 have been used here. Thus, it is possible to later compare the response and performance between traditional and innovative systems. Nine earthquake intensity levels have been considered to represent the seismic hazard, repeated here in Table 10-2 for convenience.

Table 10-2: Spectral acceleration seismic hazard data for Christchurch, New Zealand

IM Level	SA (g)	Probability of Exceedance in 50 Years	Annual Rate of Exceedance	Return Period (years)
1	0.024	90%	4.50×10^{-2}	22
2	0.035	75%	2.73×10^{-2}	37
3	0.054	50%	1.38×10^{-2}	73
4	0.059	35%	8.58×10^{-3}	117
5	0.092	20%	4.45×10^{-3}	225
6	0.122	10%	2.10×10^{-3}	475
7	0.156	5%	1.03×10^{-3}	975
8	0.207	2%	4.04×10^{-4}	2475
9	0.251	1%	2.01×10^{-4}	4975

10.4.3 Structural Response

The structural response to the seismic response analyses has been quantified according to the following engineering demand parameters (EDP): maximum base shear force, maximum inter-storey drift, residual inter-storey drift and peak floor acceleration. This

section explores how the inclusion of cladding in the structural model affects these EDPs. Quantifying the structural performance (in terms of damage) to the structure is explored in Section 10.5 onwards.

Each of the UFP cladding models was subjected to twenty ground motion records (ten earthquakes that include both orthogonal directions) at each of the nine intensity levels. The maximum base shear for each ground motion was recorded and the mean for each of the intensity levels calculated using a lognormal distribution. The lognormal distribution is used since the EDPs are the multiplicative product of many independent variables, e.g. stiffness, mass, acceleration. Since the EDPs represent absolute values the lognormal distribution is also useful since it does not allow negative data, unlike a normal distribution.

The mean base shear of the bare frame is compared against those obtained for the clad frames for each of the four connection types in Figure 10-7. It can be observed that both UFP cladding systems cause an increase in the maximum base shear of the structure. As would be expected, the damage-reduction system causes the greater increase due to it providing the greater increase in stiffness.

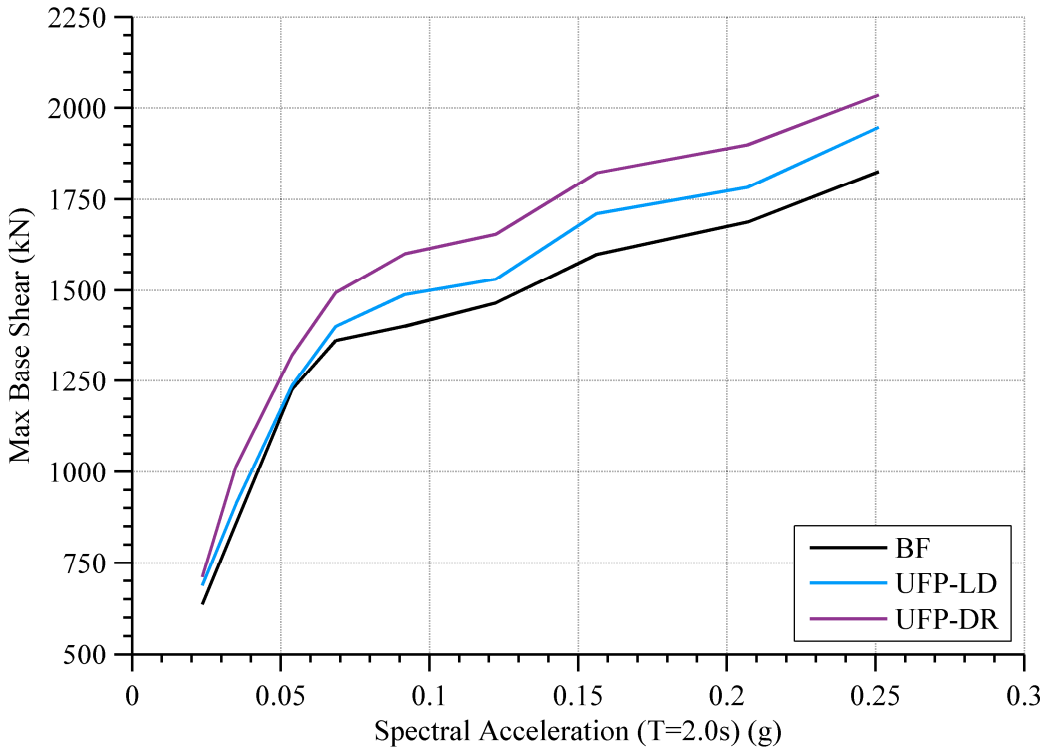

Figure 10-7: Effect of UFP cladding upon maximum base shear at different earthquake intensity levels

The mean of the maximum base shears are presented in Table 10-3 for comparison purposes. The damage-reduction system increases the base shear on average by between 8 –

13% across the range of seismic hazard considered. The low-damage system also increases the base shear across all seismic hazards, but by a maximum of 6%.

Table 10-3: Mean of maximum base shear for different UFP systems

	50%/50 Year	10%/50 Year	2%/50 Year
Bare Frame	1225 kN	1465 kN	1688 kN
UFP Low Damage	1236 kN	1532 kN	1783 kN
UFP Damage Reduction	1321 kN	1655 kN	1899 kN

The inter-storey drift envelopes for the two UFP cladding systems at the three key intensity levels are presented in Figure 10-8. The inter-storey drift envelopes are the mean of the maximum inter-storey drifts recorded for all analyses of that system at the corresponding earthquake intensity. These envelopes are compared to the bare frame envelope obtained previously.

It can be seen that both of the UFP connection types reduce the maximum inter-storey drift throughout the entire height of the structure, with the damage-reduction system having the greater influence. The inter-storey drifts are reduced consistently across the different intensity levels and the different floors of the structure, with the exception of the first floor where a negligible difference is observed.

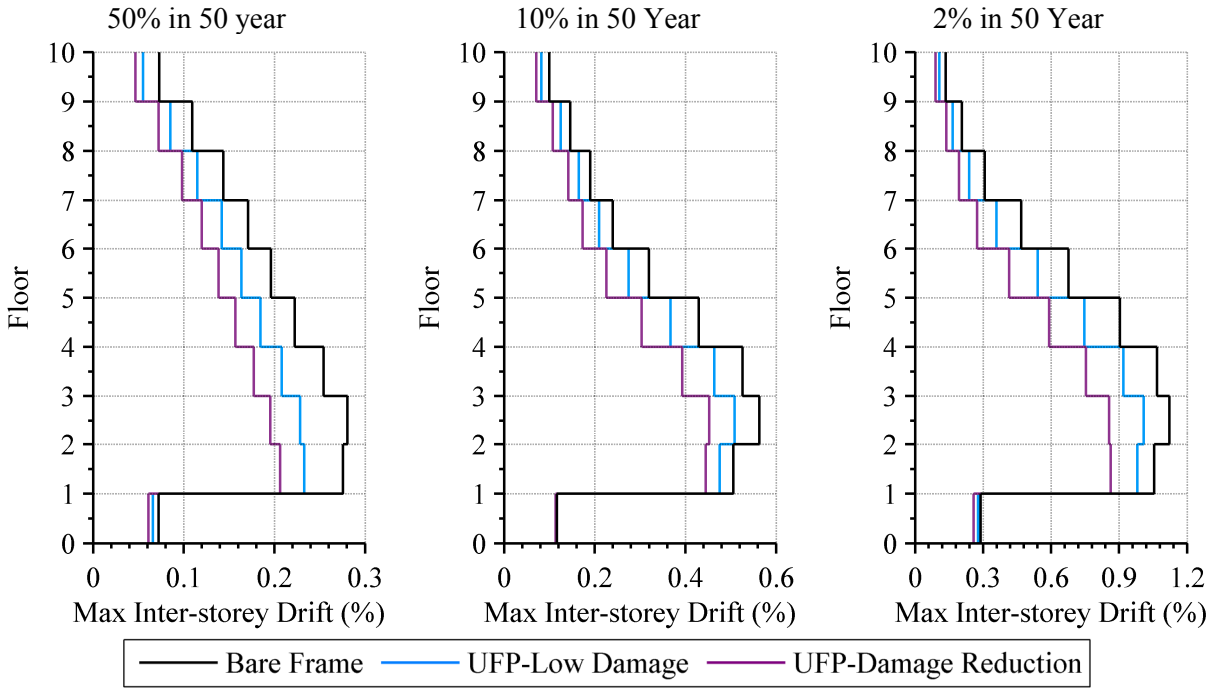

Figure 10-8: Effect of UFP cladding upon maximum inter-storey drift envelopes

he mean of the maximum inter-storey drifts at the third and 6th floor at all nine intensity levels are presented for the two UFP clad frames in Figure 10-9. The inter-storey drifts of the bare-frame are also presented for comparison. The intensity measure is defined by the spectral acceleration at two seconds. The proportion that the cladding reduces the maximum inter-storey drift is fairly consistent across all intensity levels for both floors presented. The low-damage system reduces the maximum interstorey displacement by between 6 – 18%. The damage-reduction system reduces the maximum interstorey displacement by between 18 – 30%.

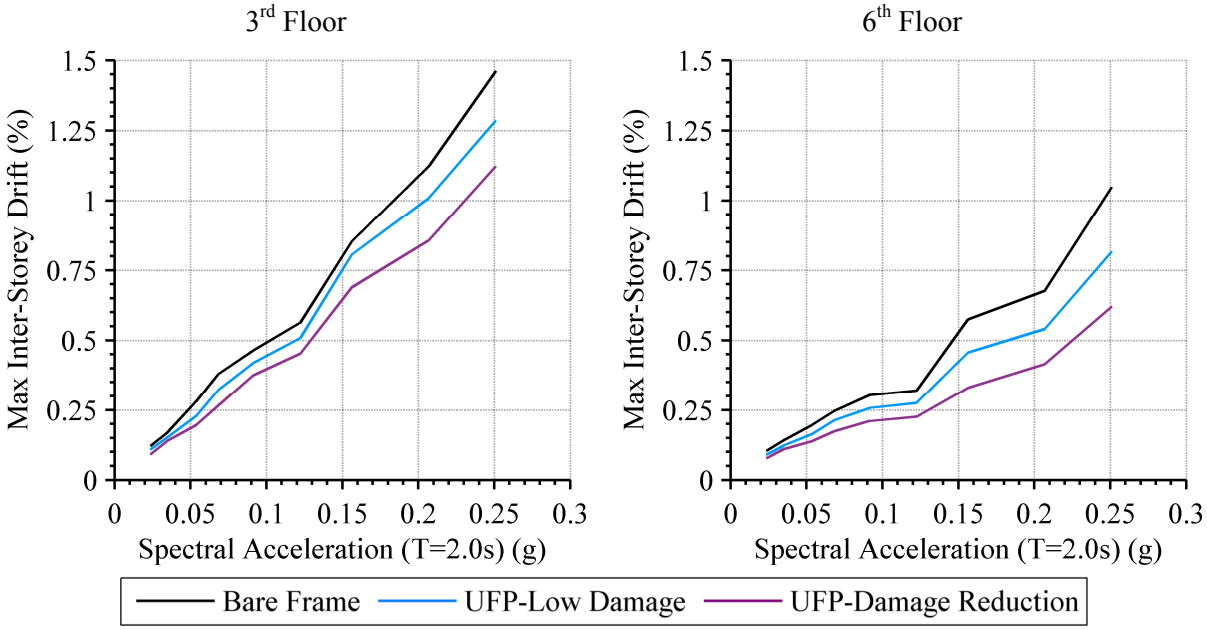

Figure 10-9: Effect of UFP cladding upon maximum inter-storey drift at different earthquake intensity

It is useful to know whether the above reductions in inter-storey drift are purely due to the structure being stiffened by the cladding system, or whether the UFPs are providing additional damping. One way to examine this is to analyse the energy within a structure during a time-history analysis. The energy delivered to a structure by an earthquake must be consumed or stored within the structure. How the energy is consumed or stored can be broken down into the following energy forms: kinetic energy, elastic strain energy, viscous damped energy, and plastic strain energy (Soong & Dargush, 1997). The first two forms of energy can be considered as short term energy storage and the latter two forms as the main mechanisms that energy is dissipated. Energy dissipated through plastic strain energy in a building is a result of some sort of permanent damage, i.e. yielding or cracking. If the plastic strain energy (or hysteretic energy) in the structure is reduced, this means that damage to the structure is reduced also. In order for this to happen, energy must be dissipated by other means.

Figure 10-10 shows the energy response of case-study building to the Superstition Hills (1987) earthquake record, scaled to the 10%/50 year seismic hazard. The bare frame energy response is shown in Figure 10-10 (left) and the frame when clad with the UFP damage reduction cladding system is shown in Figure 10-10 (right). It can be seen that the amount of viscous damped energy is nearly identical whether the building is clad or not. However, the amount of energy dissipated by damage to the structure drops by 48%. It can be seen that some of this energy is instead consumed by the UFP devices. It can also be seen that the total input energy decreases when the structure is clad with the UFP cladding system. This is likely attributed to the change in stiffness affecting how the structure responds to the ground motion. How this affects the total input energy will depend upon the characteristics of the earthquake ground motion.

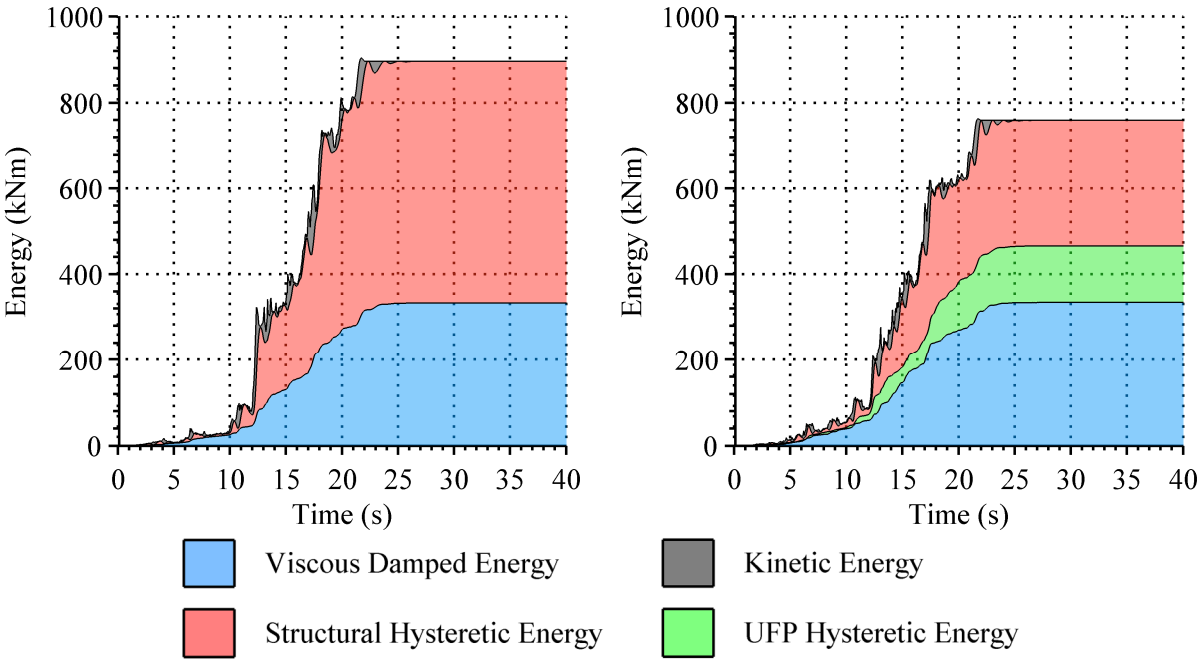

Figure 10-10: Example of energy response for bare frame (left) and building clad with UFP damage reduction cladding system (right) for Superstition Hills (1987) ground motion record scaled to 10%/50 year seismic hazard

This research does not consider energy analysis any further, as it is beyond the scope of this thesis. However, these preliminary results indicate that the additional hysteretic damping provided by UFP cladding connections can significantly reduce the total structural hysteretic energy demands upon a structure. As mentioned above, this reduction equates to a reduction in structural damage. Further research is necessary in order to quantify to what extent these reductions in hysteretic energy equate to damage reduction.

The residual inter-storey drift envelopes for the two UFP cladding systems at the three key intensity levels are presented in Figure 10-11. These envelopes are compared to the bare frame envelope obtained previously.

It can be seen that the residual drift is reduced throughout the structure for the 50%/50 year intensity level. Such reductions are negligible since the drifts are so small at this level (less than 1.0 mm). At greater earthquake intensities, a reduction in the residual drift is not evident, thus similarly to the traditional connection, the UFP connections do not appear to have any impact upon the residual displacements of the structure. Similarly negligible residual displacements were found for the cladding components, indicating that even though the UFP is not a self-centering system, the connections are unlikely to result in residual deformations that would compromise the weather tightness of the structure.

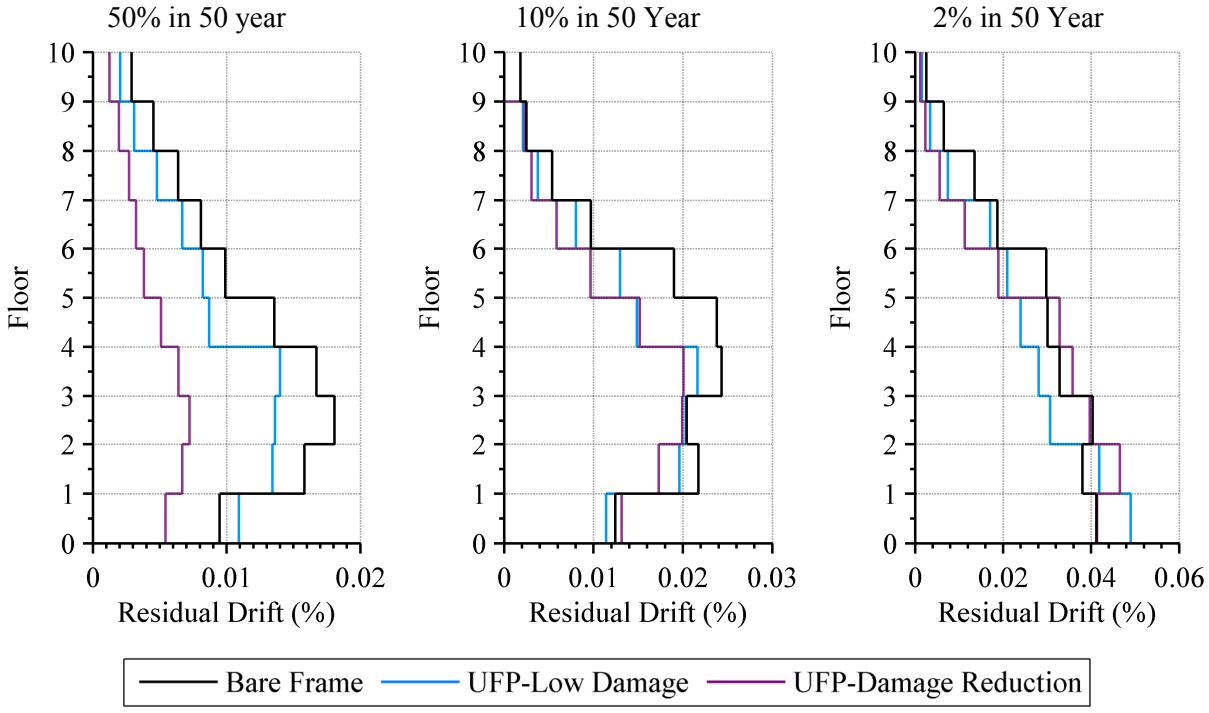

Figure 10-11: Effect of UFP cladding upon residual inter-storey drift envelopes

The lack of a discernible trend in the influence cladding has upon the residual drift is further illustrated in Figure 10-12. The figure shows the residual drifts of the clad frames compared to the bare frame at the first and third floor for the nine intensity levels. At some intensity levels the cladding presence has a positive effect upon the residual drift and others a negative effect. In all cases the effect is minimal and corresponds to less than 5 mm difference from the bare frame behaviour.

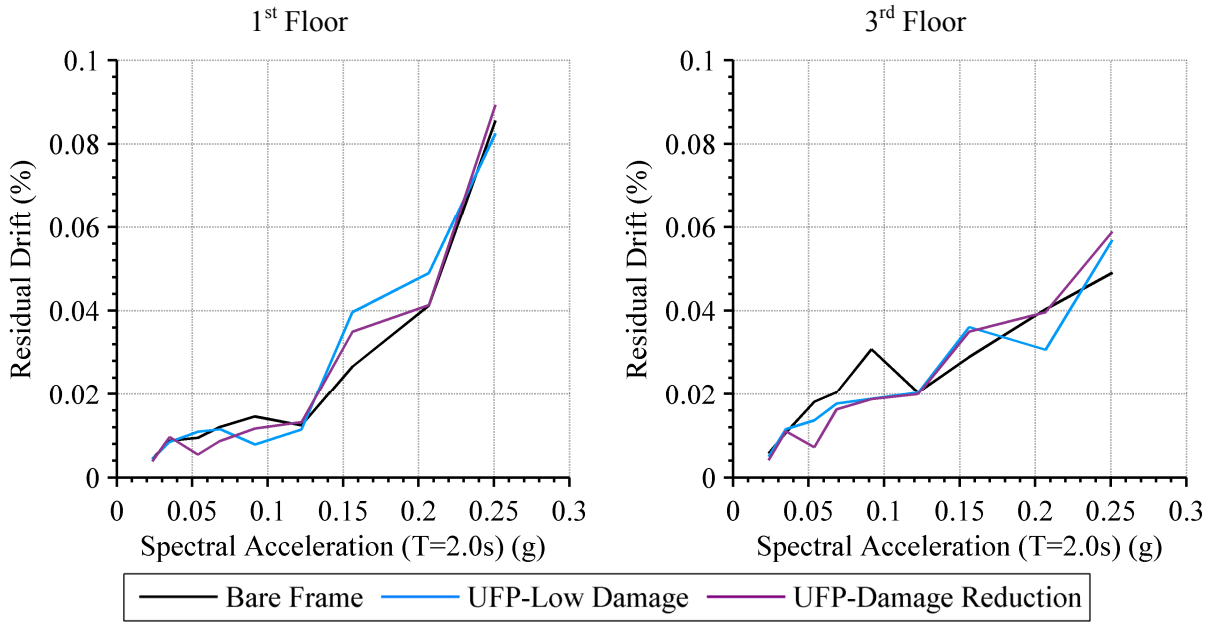

Figure 10-12: Effect of UFP cladding upon residual inter-storey drift at different earthquake intensity

The maximum mean floor acceleration envelopes for the two UFP cladding systems at the three key intensity levels are presented in Figure 10-13. These envelopes are compared to the bare frame envelope obtained previously.

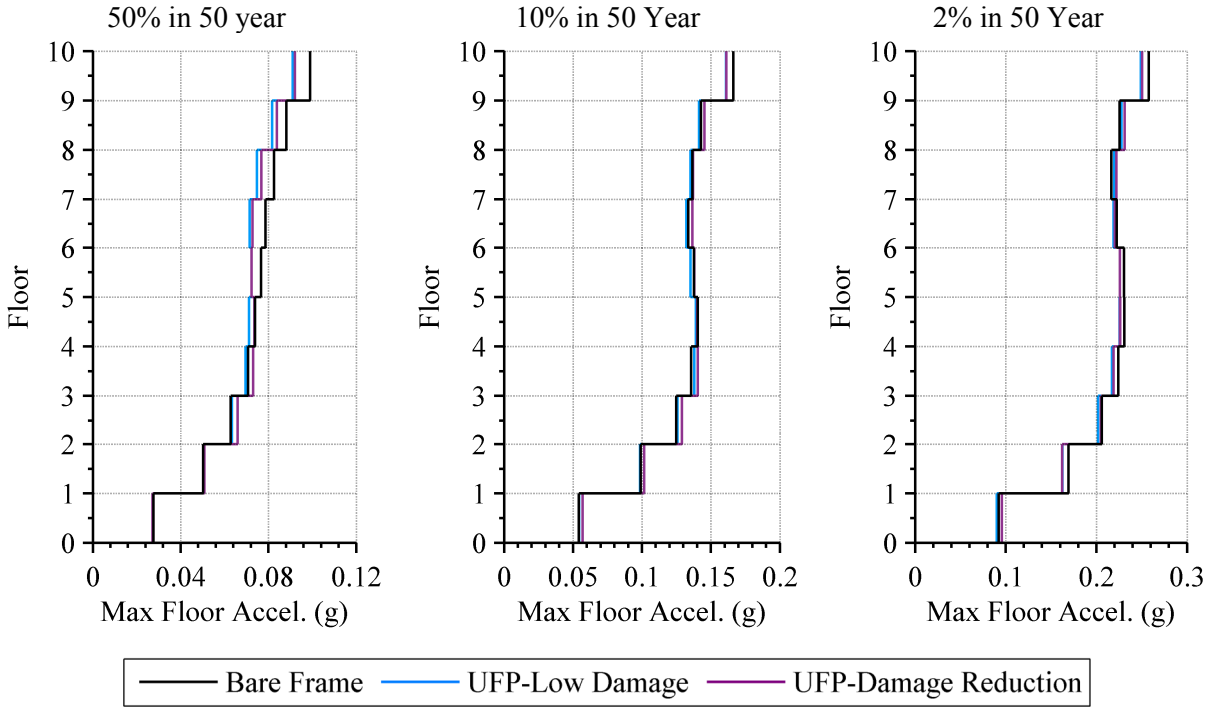

Figure 10-13: Effect of UFP cladding upon maximum floor acceleration envelopes

Figure 10-14 portrays the mean maximum floor accelerations of the third and tenth floor of the clad frames compared to the bare frame at the nine intensity levels.

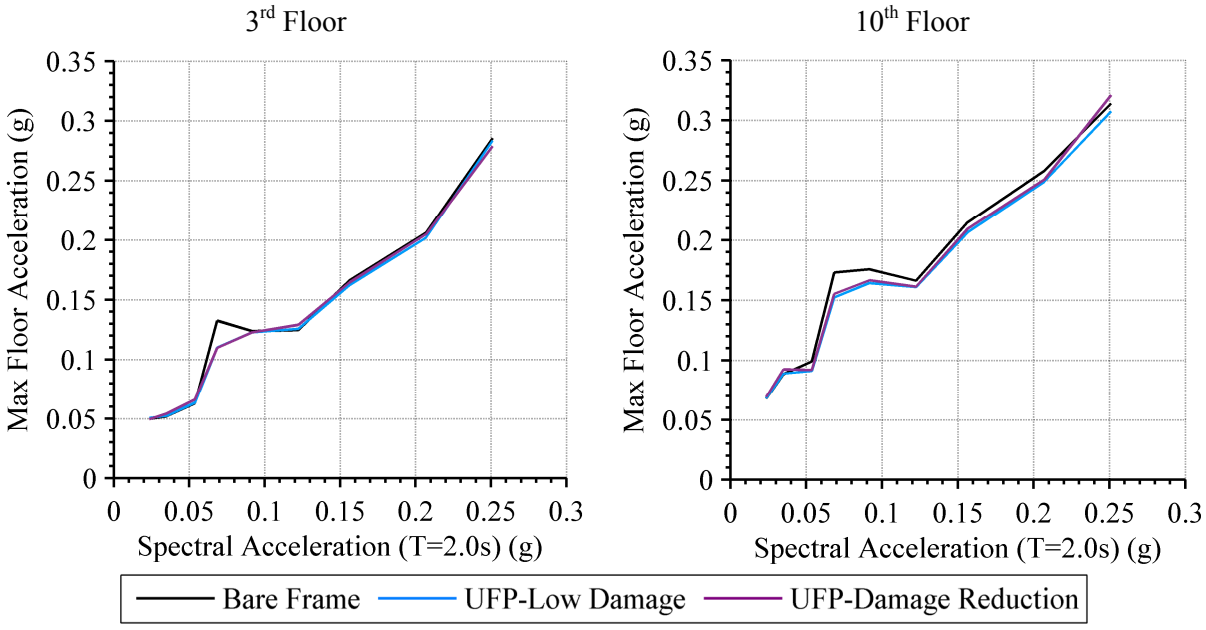

Figure 10-14: Effect of UFP cladding upon maximum floor acceleration at different earthquake intensity

Evidently, the innovative cladding systems have a very minimal influence upon the structure's maximum floor accelerations, regardless of the floor height or earthquake intensity.

10.4.4 Cladding Response

The engineering demand parameters (EDPs) used to quantify the cladding performance during the overall systems seismic response are the maximum lateral connection displacement, the maximum lateral panel displacement and the maximum connection acceleration. The maximum connection acceleration is analogous to the maximum acceleration at the top of the cladding panel. As mentioned previously, the residual connection / panel displacements were found to be negligible so have not been presented.

10.4.4.1 *Cladding Displacements*

The mean envelopes of maximum connection displacement and maximum inter-storey frame displacement are presented in Figure 10-15 for the two UFP connection configurations when subjected to the 2% in 50 year intensity level. The displacement in the connection is defined by the relative displacement between the top of the cladding panel and the structure. The frame displacement is defined by the displacement between floors (interstorey displacement).

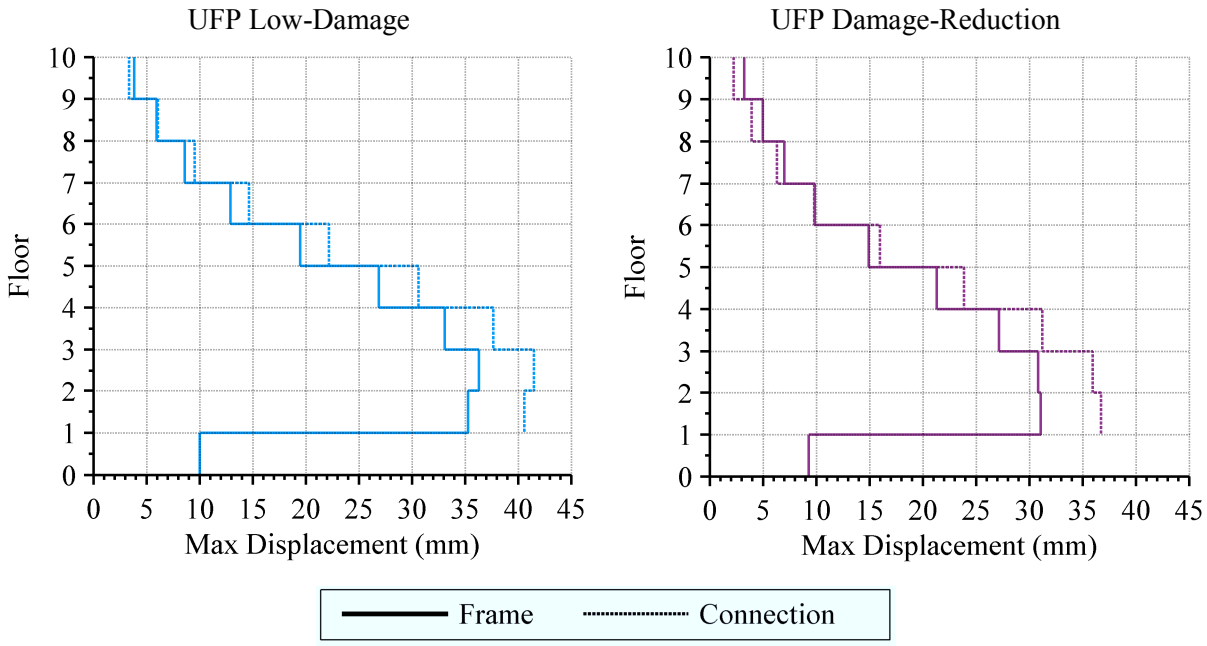

Figure 10-15: Maximum cladding connection displacement envelope compared with inter-storey frame displacement envelope for different UFP cladding systems at 2%/50 year intensity level

It can be seen that the maximum connection displacement is reasonably consistent with the maximum frame displacement. The greatest connection displacements occur around the third floor of the structure. The ratio between the connection and frame displacement also appears to be greatest in these lower floors. This ratio between connection displacement and frame inter-storey displacement is approximately 1.15. It can also be seen that the absolute frame and connection displacements of the low-damage system are greater than that of the damage-reduction system.

The mean maximum displacement of each of the connection types at the third and sixth floor is presented in Figure 10-16 for the nine different earthquake intensity levels. The connection displacement demand increases approximately linearly with increasing spectral acceleration hazard. On average, the connection displacements are less in the sixth floor than the third floor, in agreement with the envelopes presented in Figure 10-15.

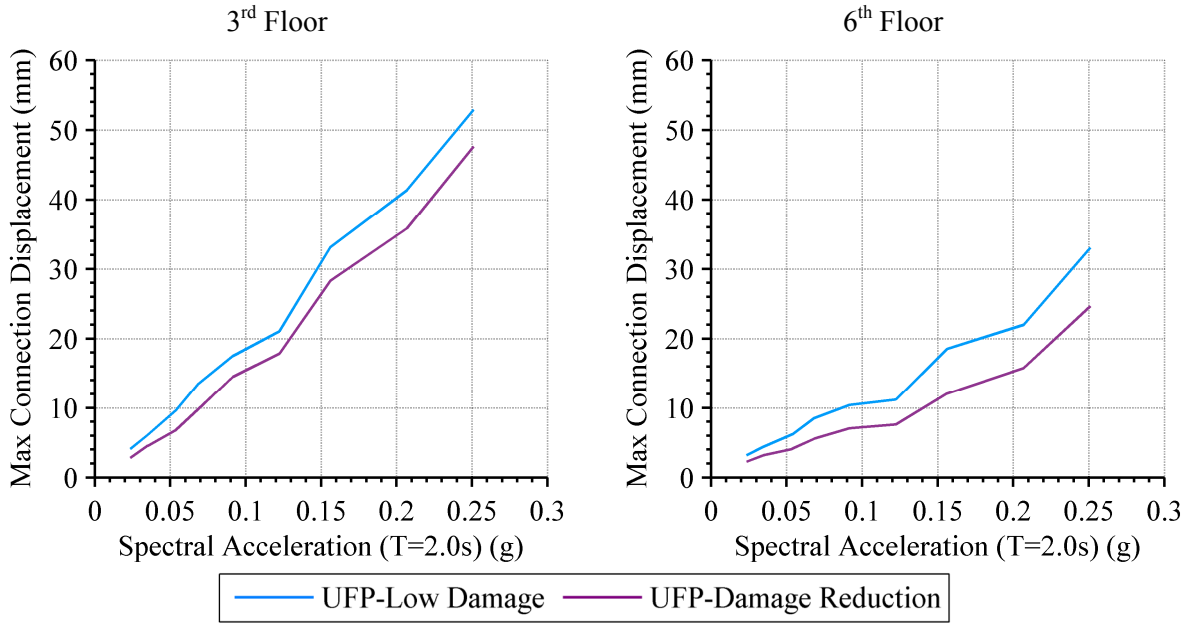

Figure 10-16: Maximum UFP connection displacement at different earthquake intensity levels

The mean envelopes of maximum panel displacement and maximum inter-storey frame displacement are presented in Figure 10-17 for the two UFP connection configurations when subjected to the 2% in 50 year intensity level. The displacement in the panel is defined by the relative displacement between the top and bottom of the panel's connections. The panel displacement follows the same trends as those observed for the frame and the connections, with the largest displacements occurring in the bottom levels of the structure. The magnitudes of the maximum panel displacements are similar between the two UFP configurations.

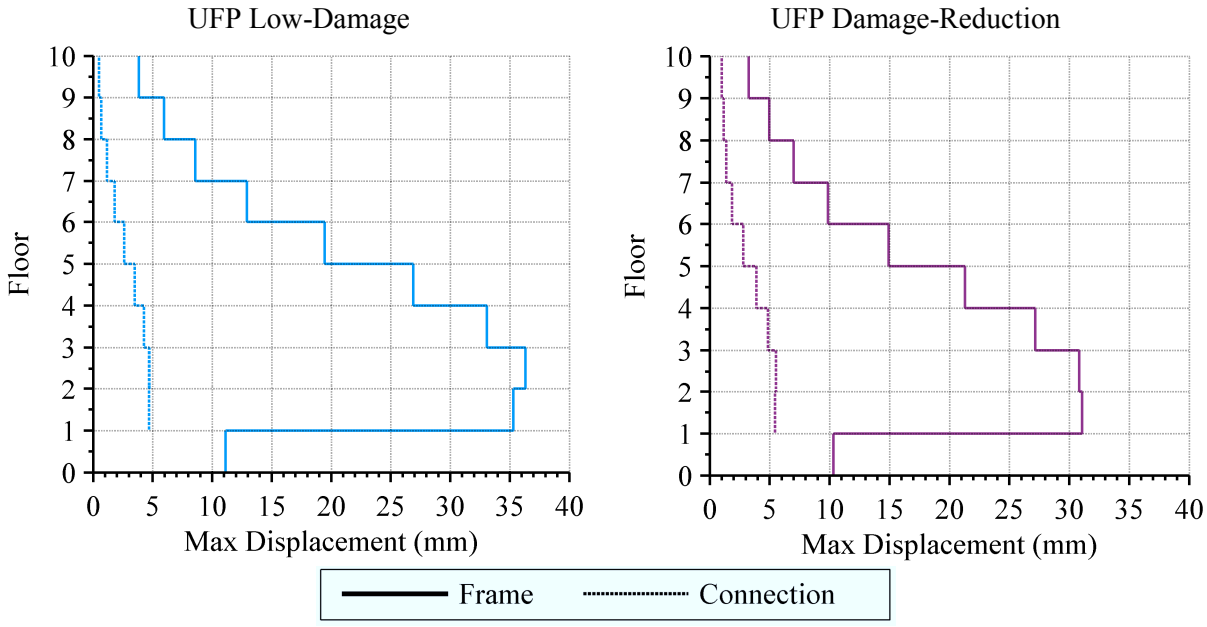

Figure 10-17: Maximum panel displacement envelope compared with inter-storey frame displacement envelope for different UFP cladding systems at 2%/50 year intensity level

The maximum panel displacement at the third and sixth floor is presented in Figure 10-18 for the two UFP connection configurations. Similarly to the connection displacement, the panel displacement demand increases approximately linearly with increasing spectral acceleration hazard. However, a slightly larger panel displacement demand is observed in the third floor of the damage-reduction system. This difference is evident for larger spectral accelerations only.

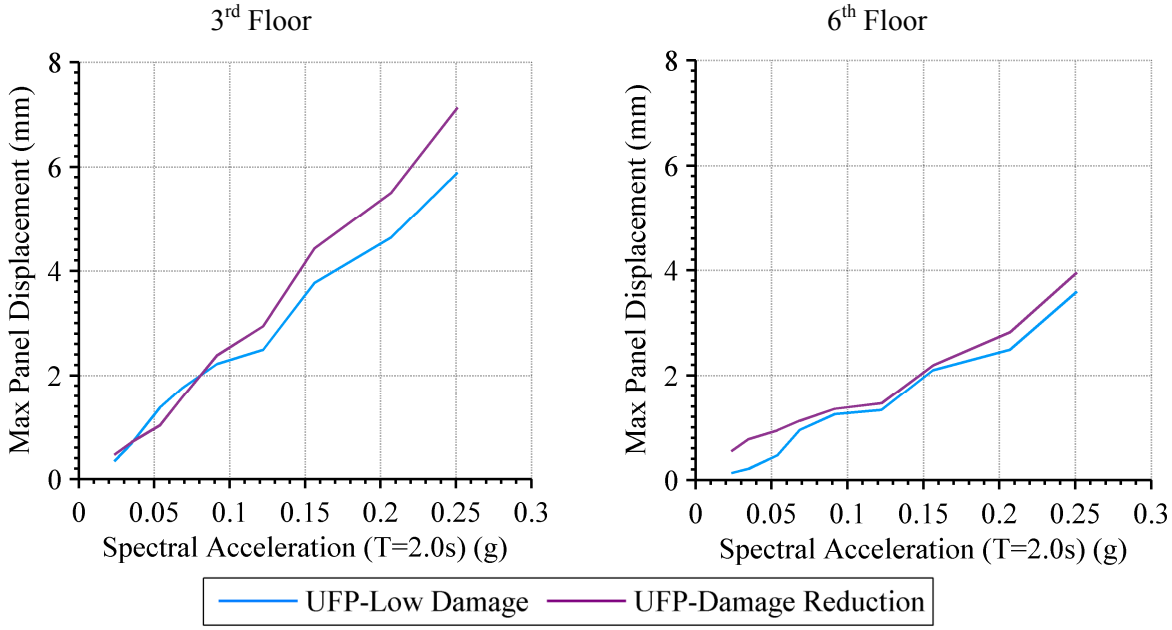

Figure 10-18: Maximum panel displacement at different earthquake intensity levels

This result shows that the connection configuration only has a minor influence upon the panel displacement demand. As found during the numerical investigation into the seismic response of traditional cladding connections, the dynamic properties of the panel appear to be the major factor in determining the in-plane response of the cladding panel. Thus, designing the UFP connections according to the maximum static force that the panel can withstand does not ensure that the panel displacement is restricted and hence damage to the panel is avoided.

The ratio of the connection and panel displacements relative to the frame displacement in presented in Figure 10-19. These are presented for the 2% in 50 year intensity level ground motion. It can be observed that the sum of the displacement ratio exceeds 1.0 (the frame displacement) throughout the structure for both connection configurations. The ratios consistently sum to approximately 125% of the frame displacement.

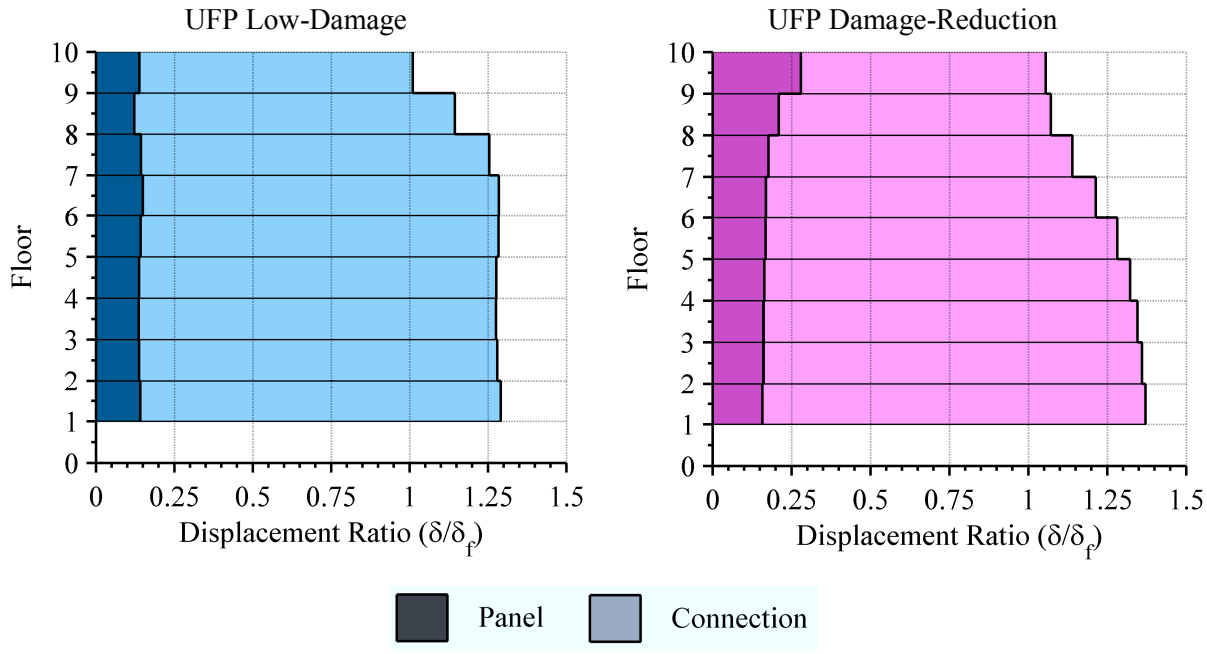

Figure 10-19: Connection and panel displacement ratios for different UFP cladding systems at 2%/50 year intensity level

Presented in Figure 10-20 are the displacement ratios of the connection and panel for the nine intensity levels investigated. The displacement ratio at each intensity level is taken as the average of the ten floors. The displacement ratio of the cladding panel in the Low Damage system is clearly lower than that of the Damage Reduction system. From this analysis 1.25 – 1.30 can thus be considered a reasonable amplification factor of the inter-storey drift to be used to design the cladding system displacement.

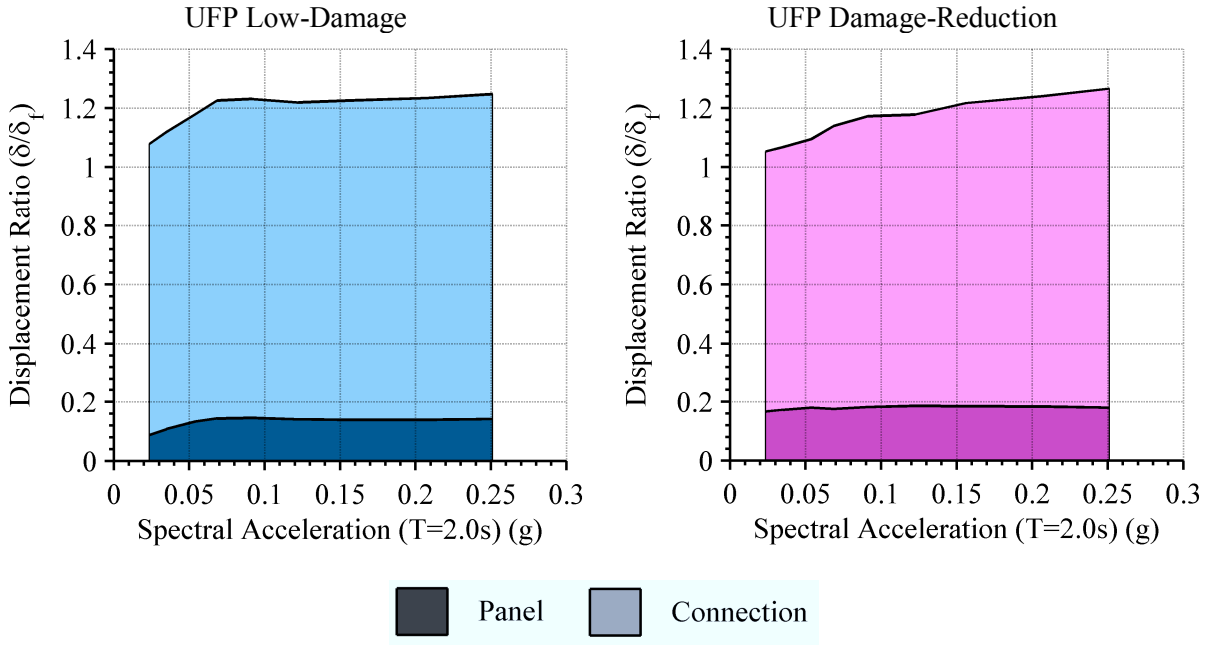

Figure 10-20: Connection and panel displacement ratios of UFP cladding system at different earthquake intensity levels

This amplification in the sum of the maximum cladding displacements is less for the UFP connections than that found for the traditional systems analysed in Chapter 6; the displacement ratios summed to between 140 – 160% of the inter-storey frame displacement for the traditional connections. This is possible due to the significantly greater stiffness provided by the UFP cladding connections suppressing the dynamic amplification of the cladding panel.

10.4.4.2 *Cladding Accelerations*

The lateral acceleration at the top of the cladding panel during each response history analysis was recorded to determine the maximum acceleration (and force) the cladding connection was subjected to. The means of the maximum connection and floor accelerations are presented in Figure 10-21 for the two UFP connection configurations when subjected to the 2% in 50 year intensity level. The connection acceleration envelopes are of a similar shape to the floor acceleration envelopes; with the maximum connection accelerations are slightly greater than floor accelerations in some floors and slightly less in others. It can also be seen that the two connection configurations produce nearly identical maximum accelerations.

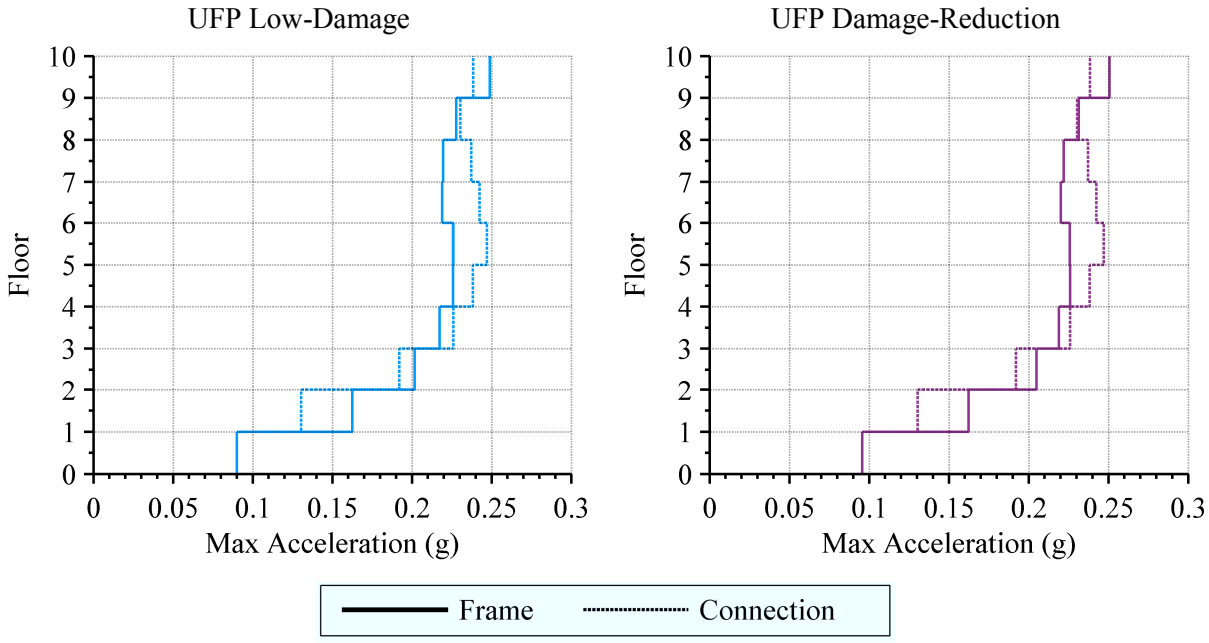

Figure 10-21: Maximum cladding connection acceleration envelope compared with maximum floor acceleration envelope for different UFP cladding systems at 2%/50 year intensity level

The maximum connection accelerations occurred around the top five floors of the structure. The mean of the maximum connection accelerations in the third and tenth floor of the structure are presented in Figure 10-22 for the nine different earthquake intensity levels. It

can be seen that the difference in connection displacement between the two connection configurations is negligible.

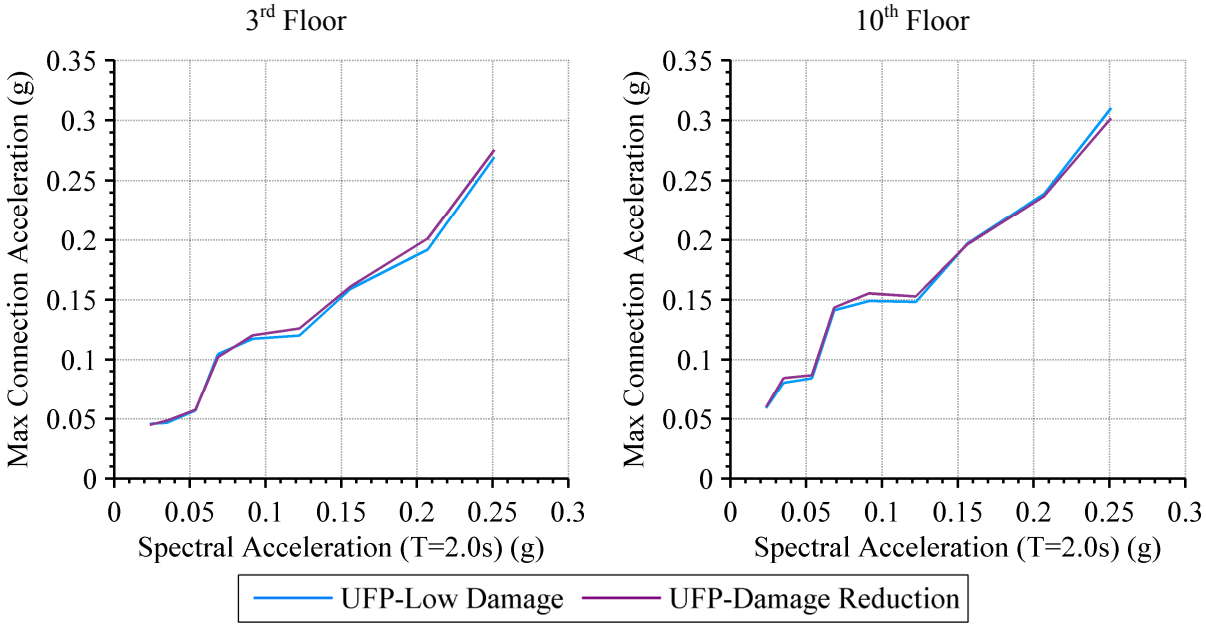

Figure 10-22: Maximum connection acceleration at different earthquake intensity levels

10.5 Structural Performance

The seismic performance of the case-study structure under the numerical analyses is assessed by monitoring the maximum member curvatures. As was introduced in Chapter 7, the maximum curvature of the beam and column members has been used to quantify the amount of inelastic deformation that occurs in the frame members. The influence of the UFP cladding connections upon the structural performance is found by comparing the maximum member curvatures of the clad and unclad frames. Refer to Section 8.3.1 for further information on the fragility functions for the beam and column members.

The maximum beam curvatures of the third and sixth floor are presented in Figure 10-23 for the bare frame and for each of the two UFP connection configurations. The third floor represents the region of the structure where inter-storey drifts were found to be largest and hence is where the largest beam curvatures and observed. It can be observed that both the low-damage and damage-reduction connection configurations reduce the maximum beam curvatures in both floors of the structure presented here.

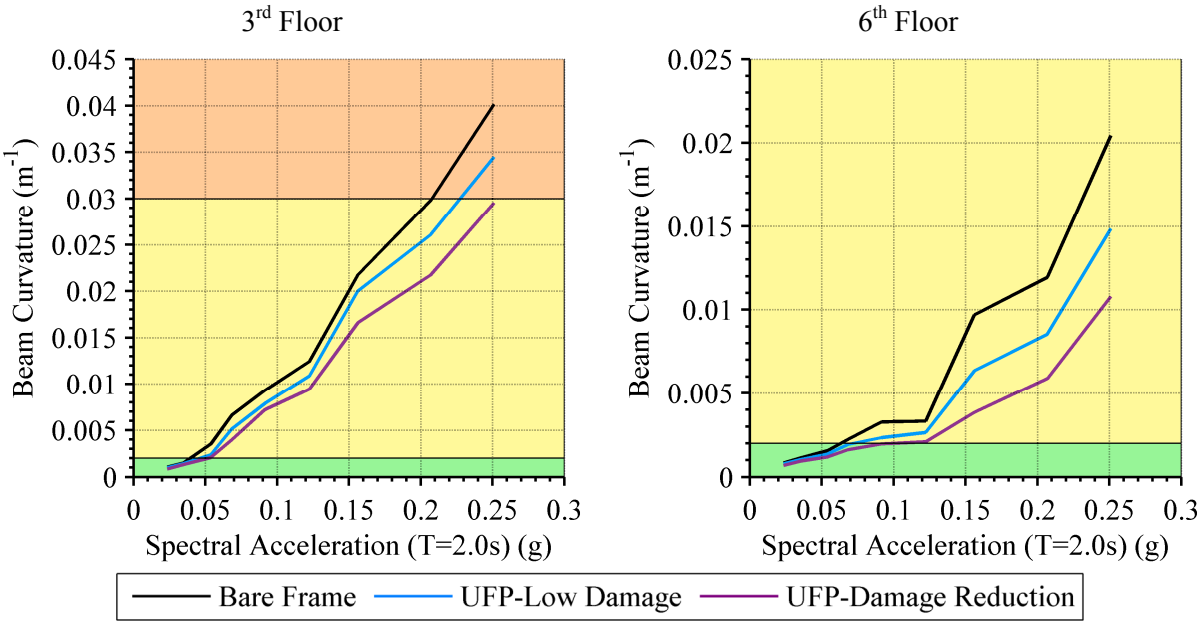

Figure 10-23: Effect of UFP cladding systems upon maximum curvature of third floor (left) and sixth floor (right) beams at different earthquake intensity levels

The impact that the UFP cladding systems have upon the structural performance can be quantified with the use of the fragility functions. The structural performance level probabilities of the third floor beams for the two UFP connection configurations are quantified and compared to those of the bare frame in Table 10-4. The probabilities are for the 2% in 50 year event (SA = 0.207 g) and are computed from the mean of the maximum beam curvature.

Table 10-4: 3rd floor beam performance in 2%/50 year event

	Operational	Immediate Occupancy	Life Safety	Collapse Prevention	Failure
Bare Frame	0.0%	49.7%	45.5%	3.3%	1.5%
UFP Low Damage	0.0%	63.6%	34.1%	1.7%	0.6%
UFP Damage Reduction	0.0%	79.1%	20.2%	0.5%	0.2%

It can be seen that the utilisation of the low-damage UFP cladding connection reduces the probability of the beam damage exceeding the Life Safety limit state or worse by 14%. For the damage-reduction cladding connections this probability reduces by 29%. The damage-reduction system evidently causes a significant improvement in the seismic structural performance.

The maximum column curvatures are presented in Figure 10-24 for the bare frame and for each of the two UFP connection configurations. It can be observed that the damage-

reduction cladding system has a very minor detrimental impact upon the performance of the first floor columns. Evidently, the increased stiffness of the upper nine floors due to the presence of the places an increased deformation demand upon the first floor columns. The impact of the low-damage cladding system upon the column performance is negligible.

Due to the additional stiffness provided by the cladding systems over the top nine floors, the deformation demand upon the columns is reduced throughout the rest of the structure. This is shown by the reduced maximum column curvatures found in the third floor, as shown in Figure 10-24. In reality, this reduction does not correspond to an improved performance since elastic behaviour is essentially guaranteed regardless of cladding connection type.

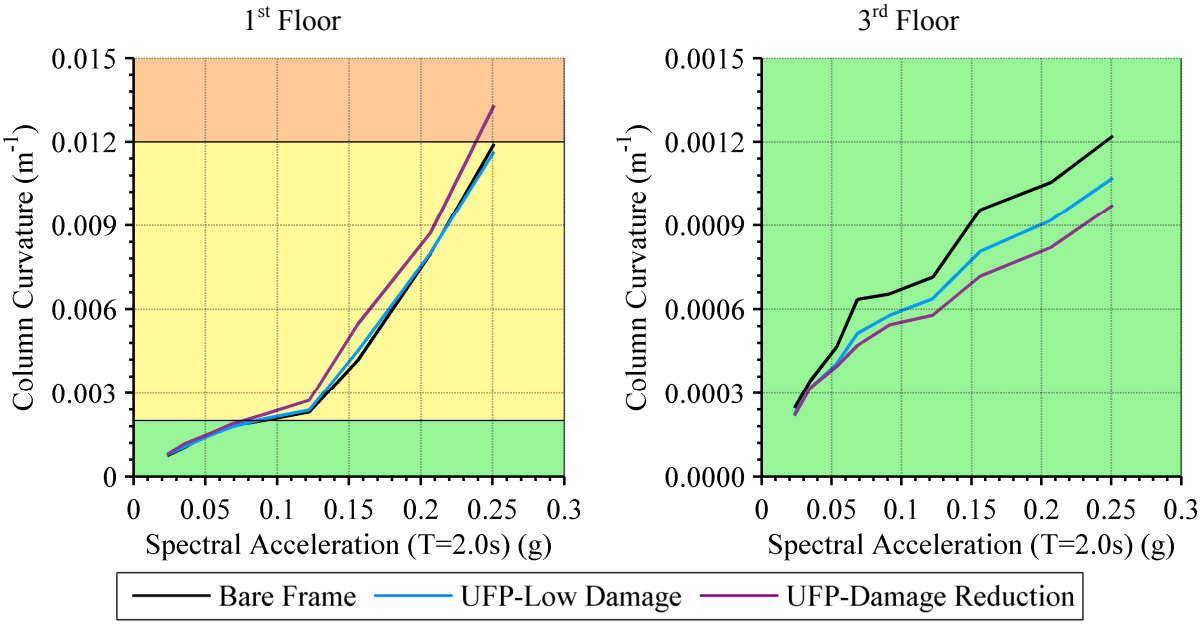

Figure 10-24: Effect of UFP cladding systems upon maximum curvature of first floor (left) and third floor (right) columns at different earthquake intensity levels

The structural performance level probabilities of the first floor columns for two UFP connection configurations are quantified and compared to those of the bare frame in Table 10-5. The probabilities are for the 2% in 50 year event (SA = 0.207 g) and are computed from the mean of the maximum column curvature.

Table 10-5: 1st floor column performance in 2%/50 year event

	Operational	Immediate Occupancy	Life Safety	Collapse Prevention	Failure
Bare Frame	0.0%	84.5%	15.5%	0.0%	0.0%
UFP Low Damage	0.0%	84.4%	15.6%	0.0%	0.0%
UFP Damage Reduction	0.0%	78.9%	21.1%	0.0%	0.0%

It can be seen that the at the 2%/50 year intensity level, the damage to the first floor columns is expected to fall into either the Immediate Occupancy or Life Safety performance level, with approximately 85% likelihood of being deemed Immediate Occupancy. As illustrated in Figure 10-24, the cladding presence has small negative effect upon the performance of the first floor columns. Although this impact is minimal for this building, it is a critical consideration if the column performance was of concern.

The use of innovative cladding connections as a retrofit solution for under-capacity buildings requires an assurance that the structure meets capacity design requirements, that is, the columns are stronger than the beams. Otherwise, the effect of the building being stiffened can lead to a detrimental performance in the lower columns and the risk of a soft-storey (Nagae et al., 2006). This is more applicable to the situation of the mono panel frame where the entire structure is clad except the bottom floor. Conversely, it is evident that the participation of the cladding can have a positive effect upon the column performance if present at the floor of concern. This is shown by the reduced column curvature demand throughout the nine floors of the structure where cladding was present.

10.5.1 Cladding Performance

The cladding performance to the seismic response analyses has been quantified for both the UFP connections and the cladding panels. Definitions of the Damage Limits for UFPs are introduced here using experimental observations. Therefore the performance of the UFPs is obtained using the maximum lateral displacement of the top connection, with the panel performance being determined by the maximum in-plane panel displacement. The maximum displacement in each component is compared to the ground motion intensity (measured in terms of SA at 2.0 seconds).

10.5.1.1 *UFP Damage Limits*

Two damage limits have been used to assess the performance of UFPs. The first damage limit (DL1) identifies the transition from Operation to Immediate Occupancy performance levels. DL1 was identified as the yield point of the UFP and was determined from using the analytical solution. Damage limit 2 (DL2) defines the transition from the Immediate Occupancy performance level to Life Safety. DL2 was identified by the maximum relative displacement of the UFP connection. The transition to the Life Safety performance level is more related to the exceedance of the slot allowance of the connection than the risk of UFP failure. This is since it is expected that the UFP can exceed this maximum displacement without failure, however, the detailing of the connection may prevent the maximum displacement being exceeded, possibly leading to brittle failure mechanisms, hence the Life Safety performance level.

The two damage limit displacements for the UFP connection used are presented in Figure 10-25 along with the fragility functions shown using the typical cumulative log-normal distributions. A standard deviation, σ, of 0.2 has been chosen to represent the level of uncertainty surrounding these two damage limits.

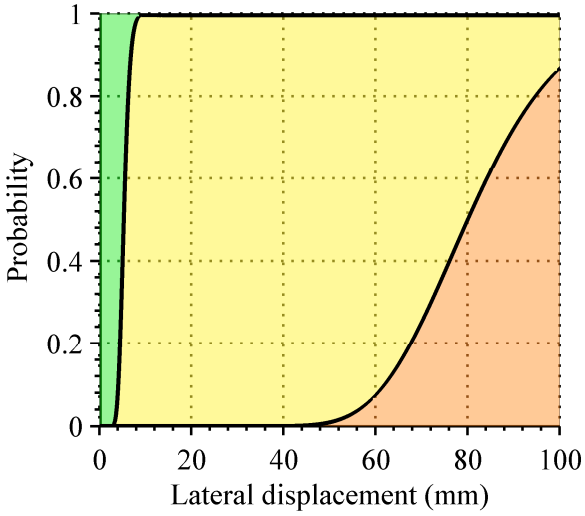

		Mean μ	Standard Deviation σ
Damage Limit (mm)	DL1	5.3	0.2
	DL2	80	0.2

Figure 10-25: UFP fragility function (left) and damage limit data (right)

The performance of the cladding components is assessed at the third and sixth floor in order to compare the expected levels of damage to that of the beam members presented previously. The third level also experienced the largest inter-storey displacements and hence is where the worst damage should be expected.

10.5.1.2 *UFP Connection Performance*

The maximum connection displacements in the third floor from each of the twenty seismic response history analyses performed at the nine intensity levels specified is presented in Figure 10-26. The nine intensity levels can be identified by the vertical clusters of individual data points.

The mean and standard deviation of the maximum connection displacement is found at each intensity level using a lognormal distribution. It can be seen that the maximum connection displacements, and hence the expected performance of the connections is virtually identical for the two UFP connection systems. In all but the 1%/50 year intensity level, the expected performance level of the UFPs can be seen to be Immediate Occupancy. This result shows that the UFPs are being activated in low to high seismicity events since the Immediate Occupancy performance level corresponds to the UFPs yielding. Hence the UFP connections are acting to passively dissipate earthquake energy over a wide range of intensities. Few cases exist where the maximum displacement demand upon the connection is beyond the limit of DL2, and these events only occur during 1%/50 year ground motions. At this earthquake intensity, Life Safety performance is an acceptable outcome that is in alignment with the structural performance outcomes.

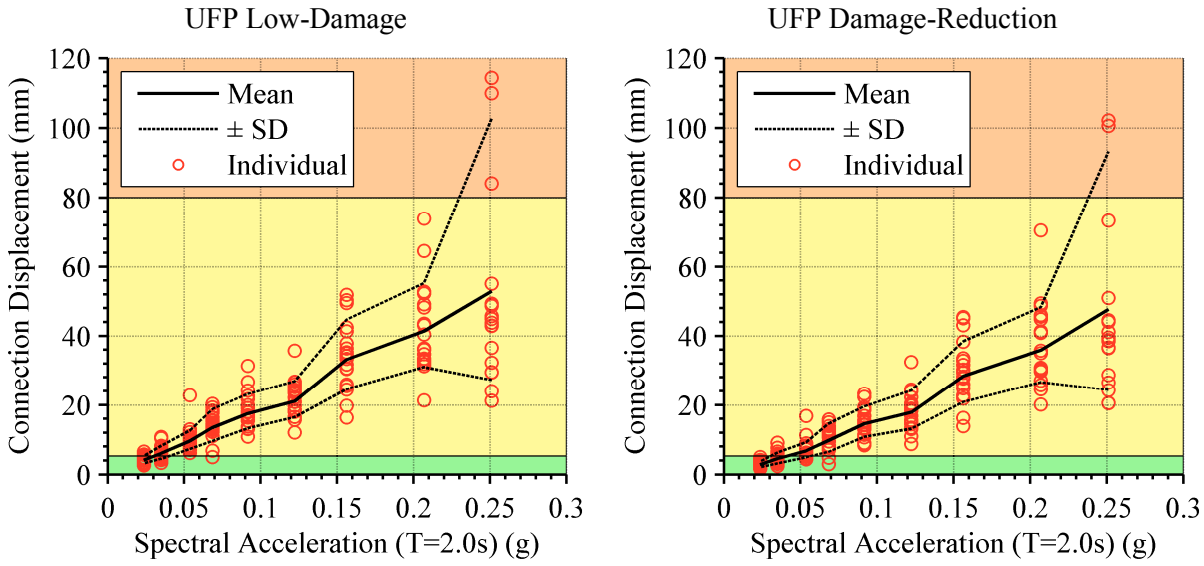

Figure 10-26: Maximum displacement of third floor connection for UFP cladding systems

The maximum connection displacements in the sixth floor are presented in Figure 10-27. In comparison to the third floor, it can be seen that the UFPs are not as likely to be activated in low-seismicity events, however, are virtually guaranteed to be activated in

medium – high seismicity events. The probability of exceeding DL2 is also negligible in the sixth floor.

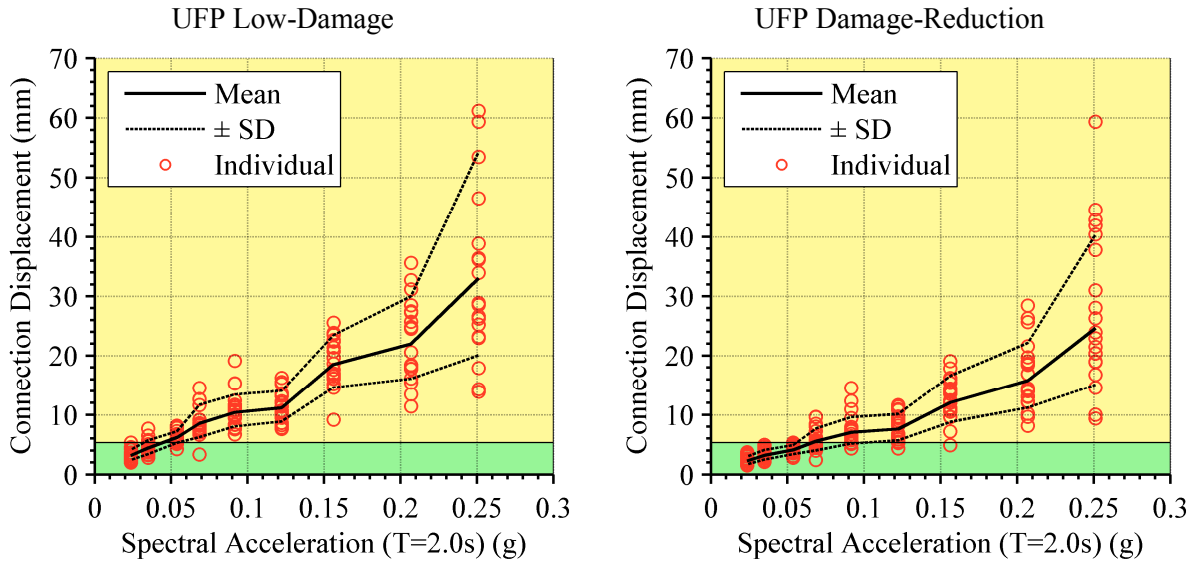

Figure 10-27: Maximum displacement of sixth floor connection for UFP cladding systems

10.5.1.3 *Cladding Panel Performance*

The seismic performance of the third floor cladding panels when connected to the frame with the two UFP connection configurations are shown in Figure 10-28. Only three performance levels have been defined for the cladding panels, with the highest amount of damage considered to be of Life Safety performance.

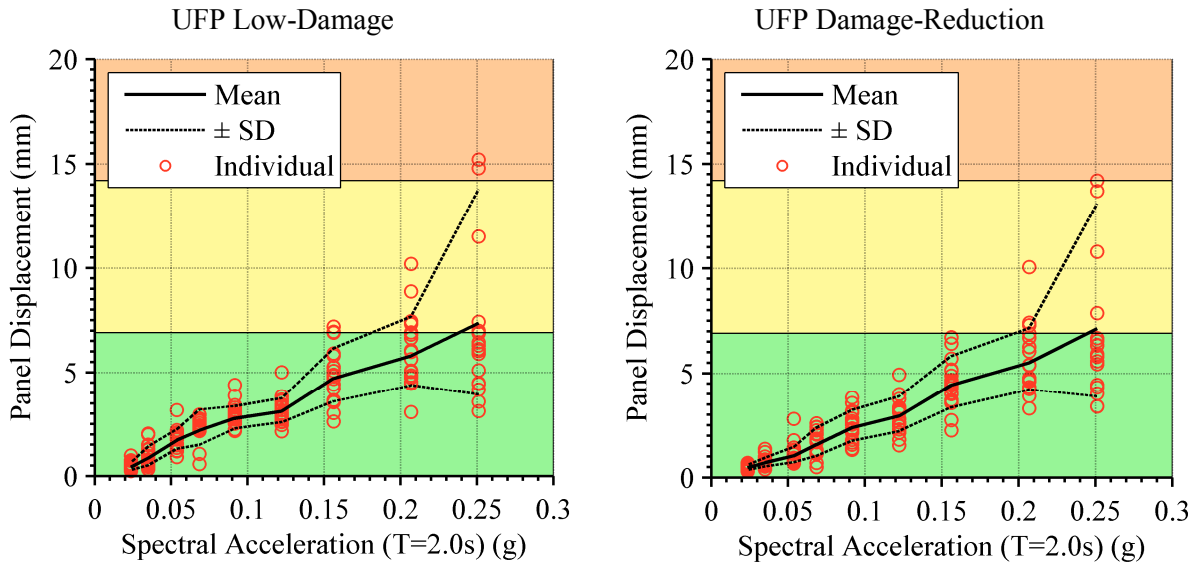

Figure 10-28: Maximum displacement of third floor cladding panel for UFP cladding systems

It can be seen that the maximum panel displacements, and hence the damage expected to the panel is virtually identical for the two UFP connection systems; slightly less damage is

expected in the low-damage system. The cladding panels are expected to be completely undamaged up to and including the 10%/50 year intensity level. Damage that is categorised as being in the Life Safety performance level is unlikely, except during the 1%/50 year intensity level.

The seismic performance of the sixth floor cladding panels when connected to the frame with the two UFP connection configurations are shown in Figure 10-29. It can be seen that the panels in this level of the structure are expected to remain undamaged for all but the 1%/50 year intensity level.

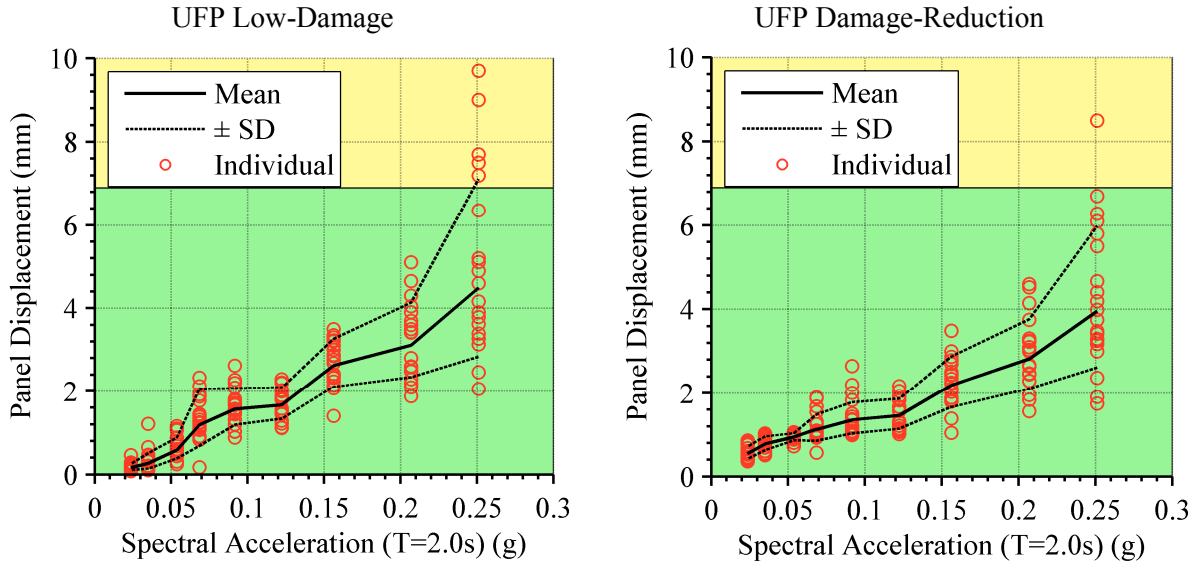

Figure 10-29: Maximum displacement of sixth floor cladding panel for UFP cladding systems

The average distribution of structural and cladding damage to the UFP low-damage system is illustrated in Figure 10-30 for the three key intensity levels. The performance of the damage-reduction system is very comparable to that of the low-damage system, as presented throughout this section.

The average structural performance is improved slightly compared to that of the bare frame; with the third and fourth floor beams being categorised as Immediate Occupancy instead of Life Safety for the 2%/50 year earthquake. The performance of the cladding panels is shown by the coloured squares. It can be seen that the panels on average remain undamaged for all intensity levels. The cladding connection performance is shown by the coloured triangles above the cladding panels and it can be seen that these are on average categorised as Immediate Occupancy performance level. This corresponds to the connections having yielded, as hence the cladding system has been activated to passively dissipate earthquake energy, but have not been damaged in any considerable way.

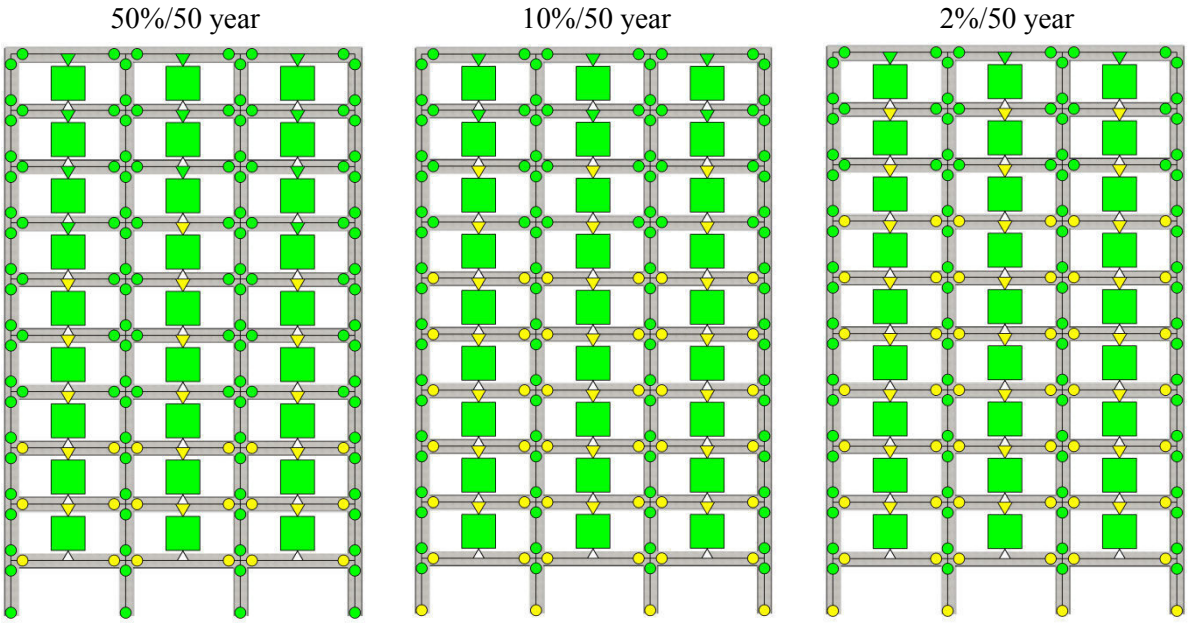

Figure 10-30: Structural and cladding performance with low-damage UFP cladding system

The performance level probabilities of the third floor beams, UFP connections and cladding panels are quantified in Table 10-6. The probabilities are for the 2% in 50 year event (SA = 0.207 g) and are computed from the mean of the maximum component deformations.

Table 10-6: 3rd floor UFP cladding system performance in 2%/50 year event

		Operational	Immediate Occupancy	Life Safety	Hazards Reduced	Failure
UFP Low-Damage	**Beams**	0.0%	63.6%	34.1%	1.7%	0.6%
	Connection	0.0%	99.9%	0.1%	-	-
	Panel	84.0%	15.8%	0.2%	-	-
UFP Damage-Reduction	**Beams**	0.0%	79.1%	20.2%	0.5%	0.2%
	Connection	0.0%	100.0%	0.0%	-	-
	Panel	71.5%	27.6%	0.9%	-	-

It can be seen that the expected performance of the cladding systems is significantly better than that of the structure. This result is the opposite of that found in Chapter 7 where the expected performance of the cladding was considerably worse than that of the structure. Thus, not only have the innovative cladding connections improved the performance of the structure, but they have done so while ensuring the probability of damage to the cladding connection and panel is kept to a minimum.

The performance of the connections along with the robustness of the UFP means that the replacement of the connection is unlikely to be required during the buildings service life, even if subjected to multiple significant earthquake events, like that experienced during the Canterbury earthquake sequence.

10.6 Seismic Demand Hazard

The seismic demand hazard quantifies the seismic performance of a structure according to the likelihood of a level of ground shaking at a site and the relationship between the ground shaking and seismic response (Bradley, 2012).

The seismic demand hazard provides the probability of an EDP exceeding a specific level of seismic demand. As opposed to an intensity-based assessment (like that presented previously) that considers the seismic demand at a single intensity level, the seismic demand hazard combines the expected seismic demand from a range of possible intensity levels.

The seismic demand hazard for the structural response has been quantified by the beam and column curvature demands found using the seismic response analyses presented in this chapter. The beam and column curvature demand hazard curves are presented in terms of the annual frequency of exceedance. The annual frequency of exceedance is equivalent to the reciprocal of the return period and has been presented in this section in a logarithmic scale. The member curvatures are presented in linear scale.

10.6.1 Structural Performance

The seismic demand hazard curves for the beam and column curvatures of the innovative connections are presented in this section. The seismic demand hazard curves are shown for both the clad frame and the bare frame in order to gain an appreciation of the effect the cladding presence has upon the structural performance. For clarity, the curves for the member curvatures are only shown for odd floors.

Using the structural damage limits defined previously, Figure 10-31 illustrates the annual rate of the structural members exceeding these damage limits when utilising the low-damage UFP connection. The demand hazard curves can be interpreted by considering that the higher the damage limit exceedance value, the more vulnerable and thus more likely a member is to be damaged in the structures lifetime.

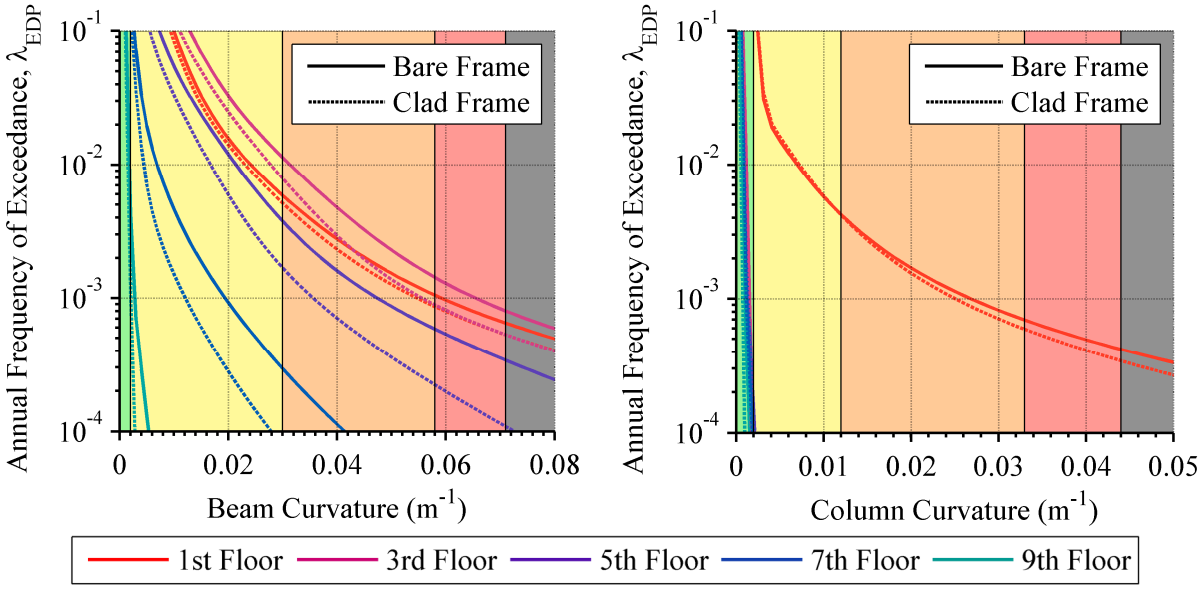

Figure 10-31: Comparison of bare and clad frame beam (left) and column (right) demand hazard curves for low-damage UFP cladding sytem

It can be seen in Figure 10-31 that the low-damage cladding system has a positive effect the structural performance of all of the structural members. The magnitude of this effect is much more significant in the beams of the third floor and above. Clearly, the performance of the columns in the first floor is the only column performance that is of importance over the structure's lifetime and it can be seen that the effect of the cladding upon the column performance is negligible. The influence of the cladding is reasonably consistent although it can be seen the member demands are reduced proportionately more for less frequent events.

A comparison between the clad and unclad seismic demand hazard curves is presented in Figure 10-32 for the damage-reduction UFP cladding system. It can be seen that the level of demand expected to the beams is significantly reduced by the presence of the damage-reduction cladding system. When compared to the performance of the low-damage clad system in Figure 10-31, the damage-reduction system has a more substantial impact upon improving the expected seismic performance of the structural system; however, it can also be seen that the expected performance of the columns is slightly reduced. This is likely due to the added stiffness of the structure resulting in increased demands upon this first floor.

The effect the cladding has upon the structure's expected life-time performance can be understood by comparing the annual rate at which each structural damage limit is exceeded in the clad frame and bare frame. The third floor beams and first floor columns have been identified as the key structural performance indicators; hence the return periods that these

members exceed the member curvature damage limits have been compared in Table 10-7 and Table 10-8.

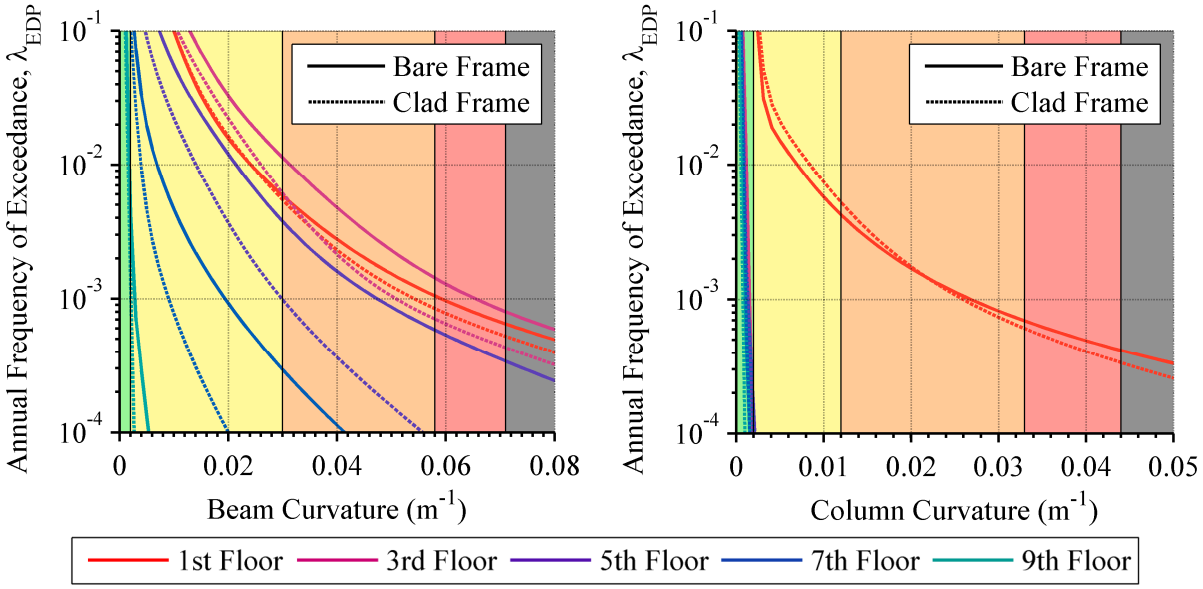

Figure 10-32: Comparison of bare and clad frame beam (left) and column (right) demand hazard curves for damage-reduction UFP cladding sytem

The return period that the third floor beam curvatures are expected to exceed each of the damage limits is presented in Table 10-7 for the bare frame and clad frames. The clad frames include the two UFP cladding systems. Both systems increase the expected return period that each of the Damage Limits, with the damage-reduction system having the more significant impact. The return periods of DL3 and DL4 for the damage-reduction UFP connection configuration is almost double that of the bare frame.

Table 10-7: Structural damage limit return period (years) in third floor beams

	Return Period DL1	Return Period DL2	Return Period DL3	Return Period DL4
Bare Frame	1	90	720	1300
UFP Low Damage	1	130	1100	1900
UFP Damage Reduction	1	160	1400	2300

The return period that the first floor column curvatures are expected to exceed each of the damage limits is presented in Table 10-8 for the bare frame and clad frames. It can be seen that the influence of the cladding upon the expected column performance is not as significant as it is upon the beam performance. The low-damage connection configuration has a minimal impact and the damage-reduction connection configuration has a negative impact

upon the expected return period of the first two damage limits, but the overall impact upon the column performance is minimal.

Table 10-8: Structural damage limit return period (years) in first floor columns

	Return Period DL1	Return Period DL2	Return Period DL3	Return Period DL4
Bare Frame	3	240	1400	2400
UFP Low-Damage	3	240	1700	3000
UFP Damage-Reduction	2	190	1600	3000

10.6.2 Connection Performance

The performance of the UFP connections in the two configurations is illustrated in the seismic demand hazards curves of Figure 10-33. There is a consistent performance between the two configurations; with the expected damage to the cladding connections of the first and third floors being the only result of importance (shown as red and violet, respectively). It is evident that the performance of the connections is better than that of the structure for the same annual frequency of exceedance, as presented previously in Figure 10-31 and Figure 10-32. The connection performance is expected to be categorised as Immediate Occupancy for seismic hazards.

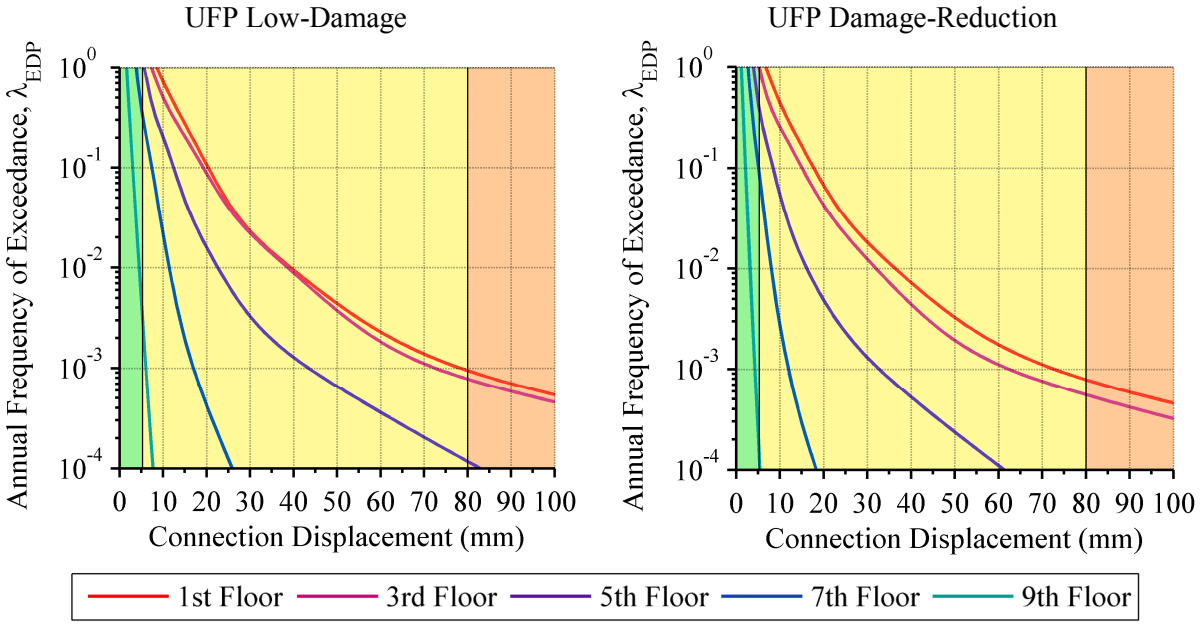

Figure 10-33: UFP connection demand hazard curves

The return period that the innovative connections are expected to exceed each of the damage limits is presented in Table 10-9. This result shows that the connections are very likely activated (exceeding DL1) for most earthquake intensities and that the probability of

them having any significant damage (exceeding DL2) is only likely in rare earthquakes that will also result in significant structural damage. The probability of exceeding DL2 in the third floor connections is 4% in 50 years for the low-damage connections and 3% in 50 years for the damage-reduction connections.

Table 10-9: UFP connection damage limit return period (years)

		Return Period DL1	Return Period DL2
UFP Low-Damage	**1st Floor**	1	1100
	3rd Floor	1	1300
	5th Floor	1	8500
UFP Damage-Reduction	**1st Floor**	1	1300
	3rd Floor	1	1800
	5th Floor	3	38000

10.6.3 Panel Performance

The performance of the cladding panels when utilising the innovative cladding connections is illustrated in the seismic demand hazards curves of Figure 10-34. As identified previously, the performance of the cladding panel is not strongly dependent upon the connection type and hence, the expected panel performance of the two systems is very similar throughout the structure. It can also be seen that the panels from the fifth floor upwards are essentially guaranteed to remain undamaged regardless of the intensity of ground motion.

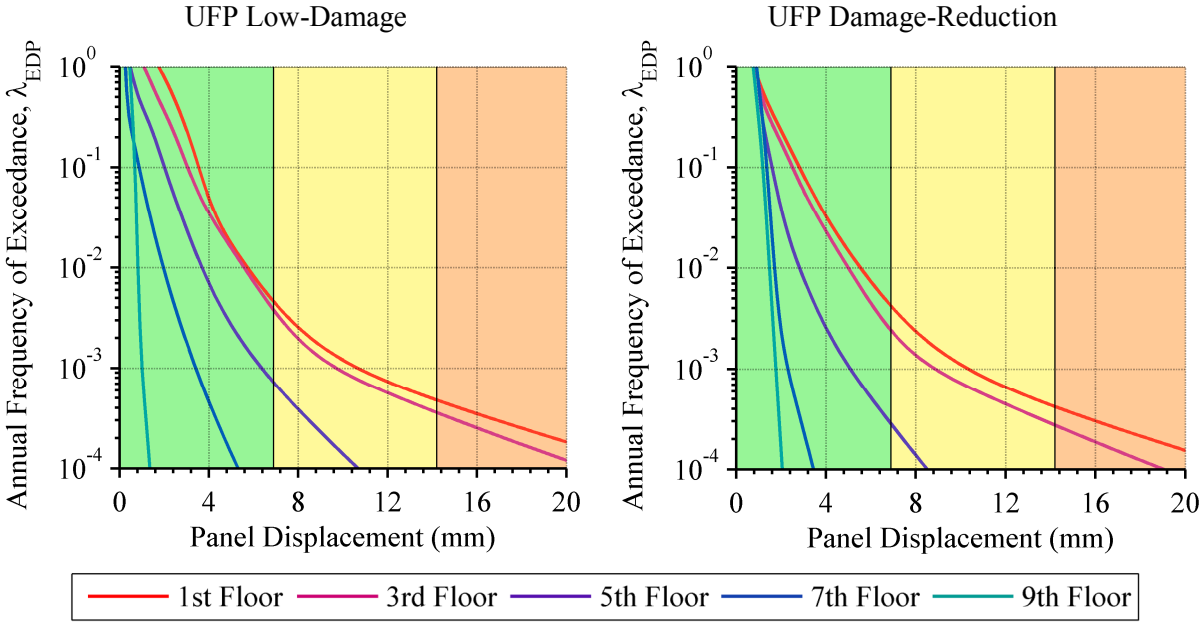

Figure 10-34: Cladding panel demand hazard curves for UFP cladding systems

The return periods that the panels are expected to exceed each of the damage limits is presented in Table 10-10. Evidently, the probability of the panel damage exceeding DL2 is 2% in 50 years or less.

Table 10-10: Cladding panel damage limit return period (years)

		Return Period DL1	Return Period DL2
UFP Low Damage	**1st Floor**	220	2100
	3rd Floor	260	2800
	5th Floor	1400	51000
UFP Damage Reduction	**1st Floor**	240	2400
	3rd Floor	400	3600
	5th Floor	3500	320000

10.7 Conclusions

In Chapter 8, the following requirements were proposed for a cladding connection to be deemed an innovative connection:

- Low-damage, i.e. able to withstand multiple seismic events without the need for repair or replacement;
- Cost comparable to a traditional cladding connection;
- Flexible and simple in its design and implementation;
- Able to provide a positive value (in terms of enhanced performance) to the structure.

The previous two chapters have shown that the UFP cladding connection meets all of the above requirements, with the exception of the final point. This chapter aimed to address this final point by presenting the seismic response and corresponding performance of multi-storey buildings that include innovative cladding systems. This was achieved through the analysis of numerical models that incorporate the passive energy dissipating cladding system developed and verified in Chapters 8 and 9.

Two theoretical innovative cladding systems were designed. These were labelled the low-damage design and a damage-reduction design. The intention of the first design was to ensure that the probability of any possible damage to the cladding panel was kept to an absolute minimum. The second design was made with the intention that some damage to the cladding panel was acceptable in a significant earthquake but failure was avoided. The difference in the two design philosophies was based upon targeting different maximum lateral displacements in the cladding panel. These maximum lateral panel displacements

were selected based on the cladding panel fragility function developed in Chapter 7. The equivalent lateral force in the cladding panel was found using the cladding panel stiffness. The UFPs were subsequently designed to ensure that this maximum force was not exceeded.

Static analyses showed that the inclusion of the low-damage UFP cladding system increased the stiffness of the case-study building by 22% and the damage-reduction system increased the stiffness by 32%. The initial yield point of the clad frames occurred slightly earlier, at a drift of approximately 0.14 – 0.15% compared to 0.16% in the bare-frame. Similarly to the results found in Chapter 6 where the traditional cladding connections were found to cause at most a 9% reduction in the fundamental period, the innovative connections also resulted in a maximum reduction in the fundamental period of 9%.

Dynamic analyses showed that the inclusion of the damage-reduction cladding system increased the base shear on average 8 – 13% across the range of seismic hazards considered. The low-damage system also increases the base shear across all seismic hazards, but by a maximum of 6%. Both of the UFP connection types reduced the maximum inter-storey drift throughout the entire height of the structure; with the damage-reduction system having the greater influence, reducing the inter-storey drift by between 18 – 30%. Similarly to that found for traditional connections, the innovative connections had a very minimal influence upon the structure's maximum floor accelerations and residual drifts.

The reduction in inter-storey drift did translate to an improvement in structural performance when the expected damage was quantified. The low-damage UFP cladding connection reduced the probability of beam damage being deemed Life Safety level or worse by 14% for a 2%/50 year seismic event. The damage-reduction cladding connections reduced this probability by 29%. The damage-reduction system evidently causes a significant improvement in the structural performance as was the intention of the connection design.

This improvement in structural performance is further confirmed from the derivation of seismic demand hazard curves. The expected return period of the third floor beams exceeding the Life Safety performance level almost doubles when damage-reduction cladding is added to the bare frame system.

The maximum panel displacement results found that the expected damage to the cladding panel was virtually identical for both of the UFP design philosophies. This result was in conflict with the different design philosophy for each connection system. As was found in Chapter 7, this result suggests that the cladding connection alone does not dictate the performance of the cladding panel.

Finally, the analyses showed that the use of innovative cladding connections must be applied with care, due to the stiffening effect of the cladding possibly leading to undesired damage mechanisms, such as soft-storeys.

10.8 References

AS/NZS 3678. (1996). Structural steel - Hot-rolled plates, floorplates and slabs. Wellington: Standards New Zealand.

Bradley, B. A. (2010). A generalized conditional intensity measure approach and holistic ground-motion selection. *Earthquake Engineering & Structural Dynamics, 39*, 1321-1342.

Bradley, B. A. (2012). The seismic demand hazard and importance of the conditioning intensity measure. *Earthquake Engineering & Structural Dynamics, 41*(11), 1417-1437.

Bull, D. K., & Brunsdon, D. (1998). *Examples of Concrete Structural Design to New Zealand Standards 3101*. Wellington, New Zealand: Cement & Concrete Association of New Zealand.

Carr, A. J. (2010). *Ruaumoko Programme for Inelastic Dynamic Analysis - User Manual*: Department of Civil Engineering, University of Canterbury, New Zealand.

Cornell, C. A. (1968). Engineering seismic risk analysis. *Bulletin of the Seismological Society of America, 58*(5), 1583-1606.

Giberson, M. F. (1967). *The Response of Nonlinear Multi-Story Structures subjected to Earthquake Excitation.* Ph.D. Thesis, California Institute of Technology, Pasadena, CA., USA.

Kelly, J. M., Skinner, R. I., & Heine, A. J. (1972). Mechanisms of Energy Absorption in Special Devices for use in Earthquake Resistant Structures. *Bulletin of the New Zealand Society for Earthquake Engineering, 5*(3).

MBIE. (2011). Ammendment 11 to Compliance Document for New Zealand Building Code - Clause B1 - Structure. Wellington, New Zealand: Ministry of Business, Innovation and Employment.

Montejo, L. A., & Kowalsky, M. J. (2007). CUMBIA - Section and Member Response of Reinforced Concrete Members. Department of Civil, Construction and Enviromental Engineering, North Carolina State University.

Nagae, T., Suita, K., & Nakashima, M. (2006). Seismic Performance of Reinforced Concrete Buildings with Yielding Soft First Stories. *Journal of Structural and Construction Engineering*(610), 123-130.

NZS 1170.5. (2004). Structural Design Actions, Part 5: Earthquake Actions - New Zealand. Wellington: Standards New Zealand.

NZS 3101. (2006). Concrete Structure Standard - Part 1. Wellington: Standards New Zealand.

Otani, S., & Sake, A. (1974). A Computer Program for Inelastic Response of R/C Frames to Earthquakes. University of Illinois, IL., USA.

Park, R., & Paulay, T. (1975). *Reinforced Concrete Structures*. New York, NY., USA: Wiley.

Soong, T. T., & Dargush, G. F. (1997). *Passive Energy Dissipation Systems in Structural Engineering*. New York, NY., USA: Wiley.

Tonkin & Taylor Ltd. (2011). Christchurch Central City Geological Interpretative Report (Version 1.1 ed., Vol. 1): REP-CCC-INT.

11 Probabilistic Seismic Loss Assessment of Traditional and Innovative Cladding

11.1 Introduction

This chapter describes the probabilistic seismic performance of both traditional and innovative cladding systems in terms of repair costs, repair time and casualties. The methodology and procedures used are based on seismic performance assessment of building methodology developed by FEMA P-58-1 (2012) as part of the Pacific Earthquake Engineering Research Centre (PEER) framework for performance based earthquake engineering. The PEER framework applies the total probability theorem to predict earthquake consequences in terms of casualties, repair costs, and repair time (Moehle & Deierlein, 2004).

The loss assessment utilises the seismic performance and damage quantification of traditional and innovate claddings presented in Section 2 and 3 respectively. Estimates of potential repair costs and repair time are found using the cladding fragility functions developed previously when combined with loss consequence functions. Loss consequence functions provide estimates of the repair costs and repair times associated with each damage state. These have been developed using data gathered from a combination of sources, including post-earthquake repair data. The casualty loss assessment is developed based on a novel approach to define an expected pedestrian population that is at risk to cladding collapse. The explicit loss consequences (casualties, repair cost and repair time) may be viewed as ultimate measures of seismic performance for decision making (Bradley, 2009).

11.2 Background

Probabilistic seismic loss assessment (PSLA) can be defined as the final product of the formal performance based seismic design process for design of new buildings, or seismic

upgrade of existing buildings. PLSA expresses the expected performance in terms of tangible outcomes, namely cost, time and casualties.

Under the PEER framework, earthquake performance is computed as a multi-level integral of the probability of incurring earthquake effects of differing intensity, over all intensities; the probability of experiencing building response (drifts, accelerations, component demands) of different levels, given an intensity of shaking; the probability of incurring damage of different types, given building response; and the probability of casualties, repair costs and repair time given that damage occurs (FEMA P-58-1, 2012).

Understandably, the several layers of complexity provided by each level of integration give rise to significant uncertainties. Performance assessment is here limited to the consideration of consequences that occur as a direct result of damage to cladding. Casualty consequences have been considered; however, the results utilise a newly proposed method that considers the risk to a theoretical footpath population. Consequently, the casualty consequences presented in this chapter have a large amount of uncertainty.

Damage to cladding can also lead to numerous secondary consequences, both inside and outside the building envelope. The most important secondary consequence of cladding damage is a loss of weather tightness. If minor cladding damage results in a leaky building and water damage occurs as a result of water infiltration, it is feasible that the cost to repair the water damage may outweigh the cost to repair the minor cladding damage. Development of models to assess these additional impacts is possible, but beyond the scope of this research.

If the consequence of a secondary effect such as water damage is such that it could result in a more significant loss than those associated with the cladding damage itself, e.g. a warehouse containing important documents, then the engineer conducting the seismic performance assessment should, as a minimum, qualitatively evaluate these other effects, and, if judged significant, report appropriate limitations to decision-makers (FEMA P-58-1, 2012).

It should be recognised that seismic loss assessment, by its nature, is never completely accurate. The actual earthquake event will never be the same as that expressed by the hazard model; the actual structure will never behave exactly like the numerical model; the damage will never be exactly that determined from fragility curves and the repair cost will never be exactly that determined from loss functions. With such high uncertainty, the usefulness of a seismic loss assessment is determined by the way it is used. Rather than being used as a tool

to obtain a single cost figure, the results are more useful as decision making tools by presenting trends or giving 'ballpark' costs. For example, if the cladding damage is going to lead to costs of approximately $1 mil then a decision can be made whether a retrofit is worthwhile relative to this cost. Likewise, if the loss assessment shows that the cladding in the bottom of the structure is contributing towards the majority of this cost then a decision can be made to only retrofit the cladding in this region. In this way, seismic loss assessments are a valuable decision making tool in communicating risk and consequences to those outside the engineering community.

11.3 Loss Consequences

Loss consequence functions are relationships that indicate the potential distribution of losses as a function of damage state. Consequence functions translate damage into potential repair and replacement costs, repair time, casualties, and other possible impacts (FEMA P-58-1, 2012). This is also commonly referred to as the three D's (Damage, Death and Downtime). For each of the cladding performance levels (damage states) introduced in previous chapters, repair descriptions are proposed that provide information on repair actions, materials, and quantities necessary to develop repair cost and repair time consequences. Casualty estimation was separately based upon the failure performance level and the affected area over which the falling cladding hazards would exist.

Consequence functions for the repair cost and repair time of each performance level have been developed based on repair data obtained after the Canterbury earthquakes in combination with discussions with professionals including contractors, quantity surveyors, and engineering consultants. At least three quotes were obtained from three different sources in order to find the average cost, defined here as the 'best estimate'. The costs are in New Zealand dollars and were obtained during 2012 and 2013. As such, the costs include contractor pricing strategies and construction cost escalation due to the post-earthquake environment. No attempt has been made here to distinguish between the repair costs of a typical construction environment compared to that in the post-earthquake environment since it is believed the latter is the most accurate representation of the post-disaster market.

11.3.1 Cladding Repair

Cladding repair includes all necessary construction activities to return the damaged cladding to its pre-earthquake condition. These construction activities, herein referred to as

repair actions, assume that the repair or replacement is 'like-for-like', i.e. that the condition of the repaired components are equivalent to that of the original components. Repair costs and repair time are found for each performance level and include all the activities a contractor would implement to conduct a repair, such as:

- Temporary relocation and protection of building contents
- Removal and reinstallation of covering elements
- Repair of component
- Clean-up
- Staging and access

11.3.2 Cladding Component Performance Levels

Cladding repair is considered based upon the individual components that have been the subject of the previous two sections, namely the cladding connection and the cladding panel. A loss assessment is presented here that considers both traditional and innovative cladding connections. Therefore, the cladding components considered consist of threaded rod connections, slotted connections, UFP connections and precast cladding panels. A description of the performance levels for each of these components is presented in Table 11-1 for convenience.

Table 11-1: Cladding component Performance Levels adapted from FEMA P-58-1 (2012)

		Performance Level				
		Operational	Immediate Occupancy	Life Safety	Hazards Reduced	Failure
Cladding Element	Cladding Panel	Undamaged; no visible cracks	Minor cracking; less than 0.3mm for SLS	Major cracking; crushing at connections	Not considered	Not considered
	Threaded Rod Connections	Undamaged; pre-yield	Connections yield; no observable damage	Visible cracking in connections	Severe cracking in connections; observable loss of cross-sectional area	Rupture of rod and disconnection of panel
	Slotted Connections	Undamaged; within slot capacity	Slot capacity exceeded; no observable damage	Visible damage to bolt and/or slot	Severe damage to connections	Not considered
	UFP Connections	Undamaged; pre-yield	Connections yield; no observable damage	Connection capacity reached; visible damage	Not considered	Not considered

The performance levels described include only those considered in the numerical analyses of previous sections. Note that the performance levels of long and short threaded rod connections are identical so are presented in Table 11-1 under the combined heading: 'Threaded Rod Connections'.

11.3.3 Repair Actions

Repair strategies are required in order to approximate the likely repair costs. It is therefore necessary to determine the key repair actions that must be undertaken to conduct the repair work. The repair actions have been gathered for each of the cladding components from discussion with contractors about repair and inspection work undertaken in Christchurch. The repair actions for each performance level are presented in the following tables and are grouped according to cladding component. Table 11-2 presents the repair actions required for precast concrete cladding panels and Table 11-3 presents the repair actions required for cladding connections.

Table 11-2: Precast concrete cladding panel repair actions

Performance Level	Repair Description	Repair Actions
Operational	None	· None
Immediate Occupancy	Cosmetic repair	· Erect and remove scaffolding or other work platform · Paint over cracked area
Life Safety	Epoxy injection and concrete patching	· Erect and remove scaffolding or other work platform · Remove loose concrete spall and patch spalled regions · Epoxy inject cracks · Plaster and skim repaired area · Paint repaired area

Table 11-3: Cladding connection repair actions

Performance Level	Repair Description	Repair Actions
Operational	None	· None
Immediate Occupancy	Inspect connections	· Remove, protect and reinstall contents adjacent to damaged area · Remove and re-instate internal linings and any services that obstruct access to connections · Inspect connections for damage

Life Safety	Repair/replace connections	· Remove, protect and reinstall contents adjacent to damaged area · Remove and re-instate internal linings and any services that obstruct access to connections · Replace connections or repair where possible
Hazards Reduced	Install new connections	· Remove, protect and reinstall contents adjacent to damaged area · Remove and re-instate internal linings and any services that obstruct access to connections · Drill panel and fix epoxy anchor for new connection · Install new connection to structure
Failure	Replace connections and cladding	· Remove, protect and reinstall contents adjacent to damaged area · Remove and re-instate internal linings and any services that obstruct access to connections · Erect and remove scaffolding or other work platform · Crane in and mount new cladding panel · Install new connections to structure

11.4 Repair Costs

The term repair cost is used herein to represent the direct losses associated with the cost of earthquake-induced cladding damage. Repair costs include all necessary construction activities to return the damaged cladding to its pre-earthquake condition according to each of the repair actions presented previously. The repair actions are grouped according to cladding panel repair action costs in Table 11-4 and connection repair action costs in Table 11-5. The quantity and units of measurement are based on repair to a single cladding panel that is 26.5 m^2 with two cladding connections (this is equivalent to the mono panel system modelled in previous chapters). The uncertainty in cost has been represented by presenting the best estimate, which represented the 50^{th} percentile cost, as well as the low and high estimate, which represent the 10^{th} and 90^{th} percentiles.

Table 11-4: Cladding panel repair action costs

Repair action	Quantity	Unit	Rate	Best estimate	Low estimate	High estimate
Erect and remove scaffolding or other work platform	50	m^2	$5	$250	$150	$420
Remove loose concrete spall	4	m^2	$90	$360	$240	$540

Patch spalled regions with grout or dry pack	4	m^2	$90	$360	$240	$540
Epoxy inject cracks	250	m	$10	$2500	$1200	$5200
Plaster and skim repaired area	12	m^2	$6	$70	$50	$100
Paint repaired area	26	m^2	$4	$100	$70	$140
Immediate Occupancy	Per panel			$350	$220	$560
	Per m^2			$13.20	$8.30	$21.10
Life Safety	Per panel			$3,640	$1,950	$6,940
	Per m^2			$137.40	$73.60	$261.90

Table 11-5: Cladding connection repair action costs

Repair action	Quantity	Unit	Rate	Best estimate	Low estimate	High estimate
Remove, protect and reinstall contents adjacent to damaged area	1	ea.	$300	$300	$150	$600
Remove and re-instate internal linings and any services that obstruct access to connections	1	ea.	$600	$600	$300	$1200
Inspect connections for damage	1	ea.	$120	$120	$80	$180
Replace connections or repair where possible	2	ea.	$300	$600	$300	$1200
Drill panel and fix epoxy anchor for new connection	2	ea	$800	$1600	$800	$3200
Install new connection to structure	2	ea	$1200	$2400	$1200	$4800
Erect and remove scaffolding or other work platform	50	m^2	$5	$250	$150	$420
Crane in and mount new cladding panel	1	day	$7000	$7000	$3500	$14000
Immediate Occupancy	Per panel			$1,020	$530	$1,980
	Per m^2			$38.50	$20.00	$74.70
Life Safety	Per panel			$1,500	$750	$3,000
	Per m^2			$56.60	$28.30	$113.20
Hazards Reduced	Per panel			$4,900	$2450	$9800
	Per m^2			$184.90	$92.50	$369.80
Failure	Per panel			$10,300	$5,150	$20,600
	Per m^2			$388.70	$194.30	$777.40

The uncertainty in repair cost can be represented as a log-normal distribution for each performance level. When shown as cumulative distributions, these are often referred to as loss functions (Bradley et al., 2009), however, will be herein referred to as repair cost functions. The repair cost functions are analogous to the fragility curves for the connection performance levels. The repair cost functions for the four performance levels of connections are presented in Figure 11-1.

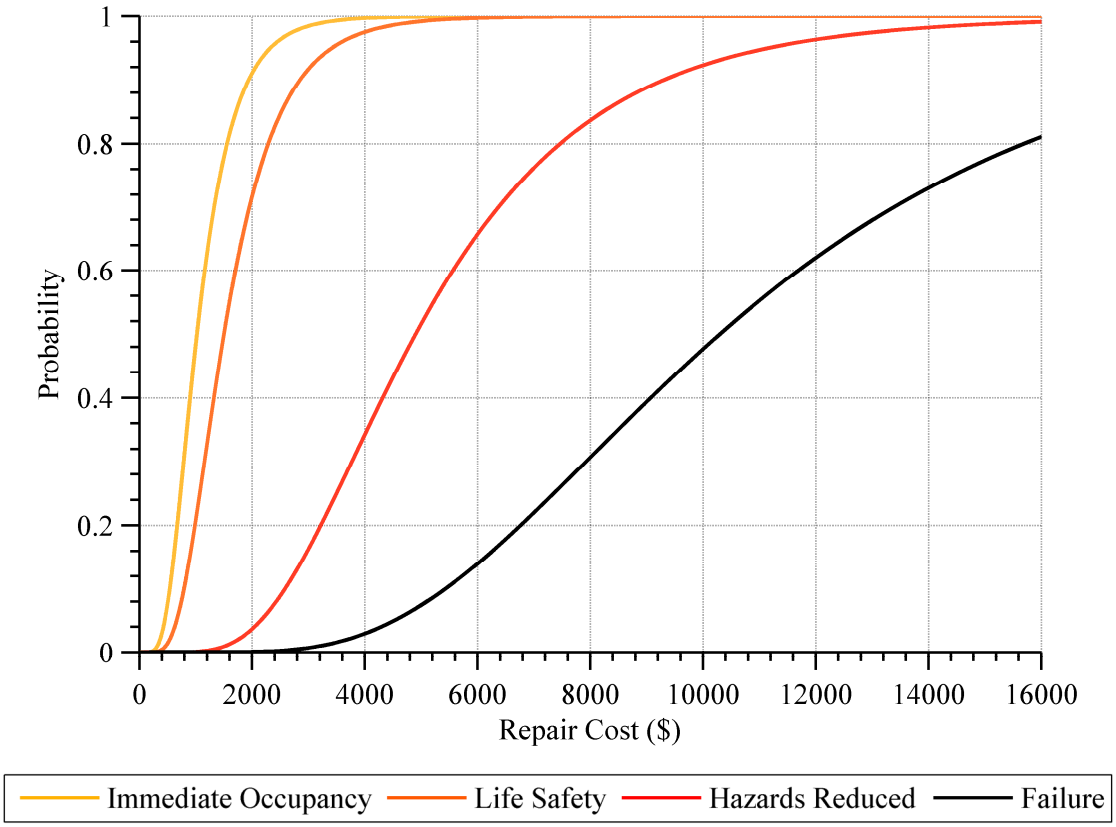

Figure 11-1: Cladding connection repair cost functions

Evidently, a significant amount of uncertainty exists for all of the repair cost functions. This uncertainty is especially evident for the failure performance level, as would be expected due to the complicated repairs that are associated with this outcome.

11.4.1 Expected Repair Cost

The expected repair cost for a given demand can be found by summing the mean repair cost for each performance level, multiplied by the probability of achieving that performance level for a given demand, as given by Equation (11-1). The standard deviation of the repair cost for a given demand is given by Equation (11-2) (Bradley et al., 2009). For the cladding

components, the demand is measured in terms of the maximum lateral displacement (of either the connection or panel component).

$$\mu_{RC|MLD} = \sum_{i}^{N_{DS}} \mu_{RC|DS_i} \times P_{DS_i|MLD} \quad \textbf{(11-1)}$$

$$\sigma^2_{RC|MLD} = \sum_{i}^{N_{DS}} \left[\mu^2_{RC|DS_i} + \sigma^2_{RC|DS_i}\right] \times P_{DS_i|MLD} - \mu^2_{RC|MLD} \quad \textbf{(11-2)}$$

where

$\mu_{RC|MLD}$ = Mean repair cost given maximum lateral displacement

$\mu_{RC|DS_i}$ = Mean repair cost given damage state

$P_{DS_i|MLD}$ = Probability of damage state given maximum lateral displacement

$\sigma_{RC|MLD}$ = Standard deviation of repair cost given maximum lateral displacement

$\sigma_{RC|DS_i}$ = Standard deviation of repair cost given damage state

Shown in Figure 11-2 and Figure 11-3 are the expected repair costs of each of the cladding components according to maximum lateral displacement. The cladding connection repair costs are firstly shown in Figure 11-2 for the long threaded rod, short threaded rod, slotted and UFP connection types. The repair costs include all of the possible performance levels and their corresponding repair actions and are presented considering the maximum unit repair costs, i.e. no economy of scale is taken into account. The mean repair cost in each figure is shown by the black line and the 16th and 84th percentile repair costs are shown by the grey shaded region.

The repair cost of the short threaded rods escalates the fastest of the cladding connections, with the long threaded rods eventually reaching the maximum costs associated with failure like that of the short threaded rods. Since no failure performance level has been considered for the slotted connections or UFP connections it can be seen that the maximum costs are much less for these connections than those associated with the threaded rod connections. It can also be seen that because damage does not occur in the UFP connections until large displacements occur, the unit repair cost is nil until approximately 50 mm

maximum lateral displacement and only increases. The uncertainty of repair costs also grows as the cost increases, shown by the grey region increasing in range with greater costs.

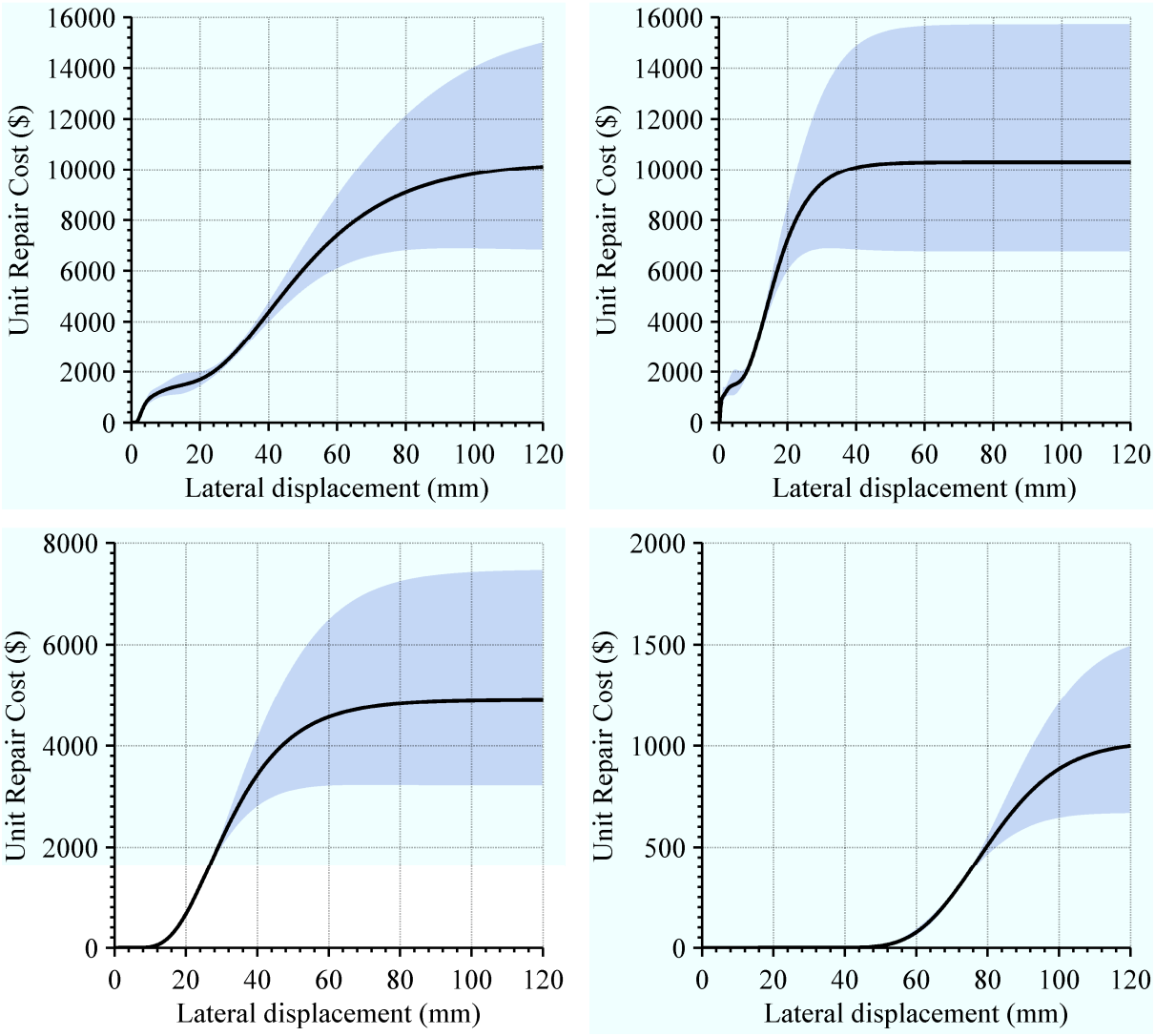

Figure 11-2: Expected repair cost for each cladding connection: long threaded rod (top left), short threaded rod (top right), slotted connection (bottom left) and UFP (bottom right)

The cladding panel repair cost is shown in Figure 11-3. The repair cost includes the two performance levels considered for the cladding panel (Immediate Occupancy and Life Safety) and their corresponding repair actions. Like that for the connections, the cladding panel repair cost is also presented considering the maximum unit repair costs.

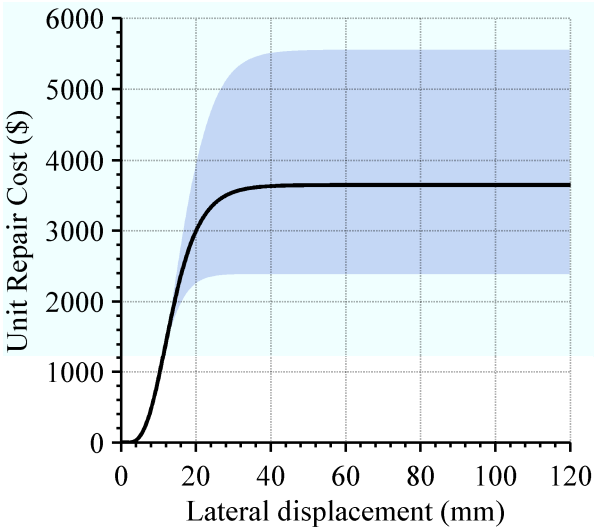

Figure 11-3: Expected repair cost for cladding panel

Since repair costs have been considered for performance levels corresponding to Hazards Reduced or Failure it can be seen that the maximum expected repair costs for the cladding panel do not increase after 40 mm lateral displacement. Also, as expected, the maximum unit repair cost that is obtained is $3,640, as defined by the repair cost consequence function. The maximum repair cost for the cladding panel is less than the maximum repair cost of the cladding connection due to the consideration of the cladding connection failure performance level that includes full replacement of the panel.

The mean unit repair costs of all of the cladding components considered are presented in Figure 11-4 for comparison purposes. Similarly to a fragility function, these functions are useful since they are general relationships that are true regardless of where the component is located. They are therefore independent of structural system or location of the structure. Unlike fragility functions the unit repair cost functions are dependent upon the country and time that they were developed in, with these repair cost functions given in New Zealand dollars during 2012 and 2013. However, the shape of the repair cost functions will remain consistent, making it possible to adjust the curves to account for inflation or changes in currency using appropriate price indexes.

Presenting the repair costs in terms of the demand parameter is useful in observing and comparing the expected seismic performance of various components. However, it is also desirable to be able to determine the expected repair costs when the demand upon the component is defined by the structure. This is achieved by combining the repair cost relationship with the seismic response relationship for a particular location in the structure. The result defines the repair cost as a function of the ground motion intensity.

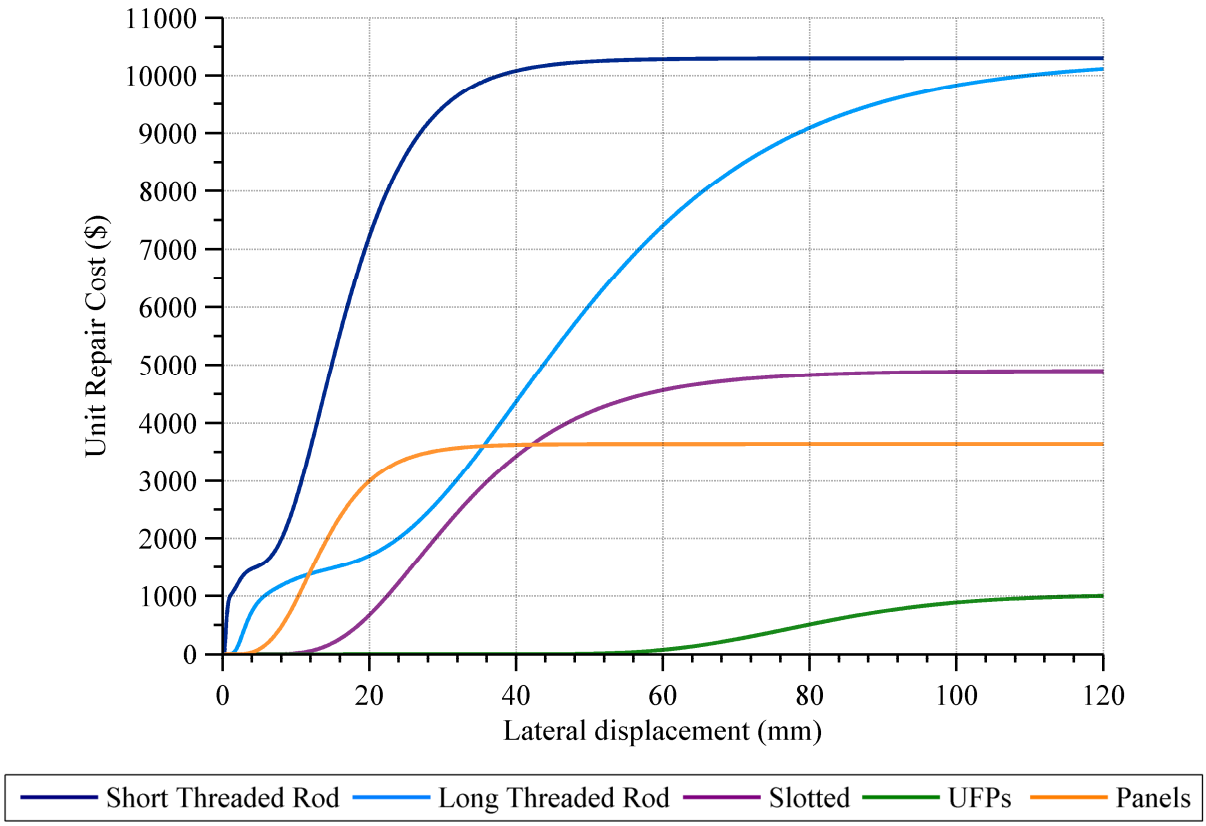

Figure 11-4: Comparison of mean unit repair cost for cladding components

The repair cost when defined by ground motion intensity is calculated by multiplying the mean repair cost given a maximum lateral displacement by the probability of that displacement occurring, given a level of ground motion intensity, and then integrating over all possible displacement demands for that ground motion intensity. The mean and standard deviation are given by Equation (11-3) and (11-4), respectively. Statistical derivation is not presented here, for more information refer to Bradley et al. (2009).

$$\mu_{RC|IM} = \int \mu_{RC|MLD} \times f_{MLD|IM}\, dMLD \qquad \textbf{(11-3)}$$

$$\sigma^2_{RC|IM} = \int \left[\mu^2_{RC|MLD} + \sigma^2_{RC|MLD}\right] \times f_{MLD|IM}\, dMLD - \mu^2_{RC|IM} \qquad \textbf{(11-4)}$$

where

$\mu_{RC|IM}$ = Mean repair cost given ground motion intensity

$f_{MLD|IM}$ = Probability density function of maximum lateral displacement given intensity measure (seismic response relationship)

$\sigma_{RC|IM}$ = Standard deviation of repair cost given ground motion intensity

When the repair costs are defined in terms of ground motion intensity, the specific location of the component in the structure needs to be defined. This means the relationship is

defined for a particular component in a particular location in the structure. This is required because the expected level of demand will vary throughout the structure. For example, the expected displacement demand upon the cladding components will be greater in the lower floors compared to the top floors since in general, greater displacements were found to occur in the lower floors. These relationships between ground motion intensity and maximum demand, in this case, maximum lateral (panel or connection) displacement, are called seismic response relationships. The seismic response relationship defines the probability density function of the expected maximum lateral displacement for a given ground motion intensity. These have been determined previously for the case study building as part of the numerical analyses performed in Ruaumoko 2D (Carr, 2010) and presented in earlier chapters. The repair cost functions of the four connection types are presented in Figure 11-5.

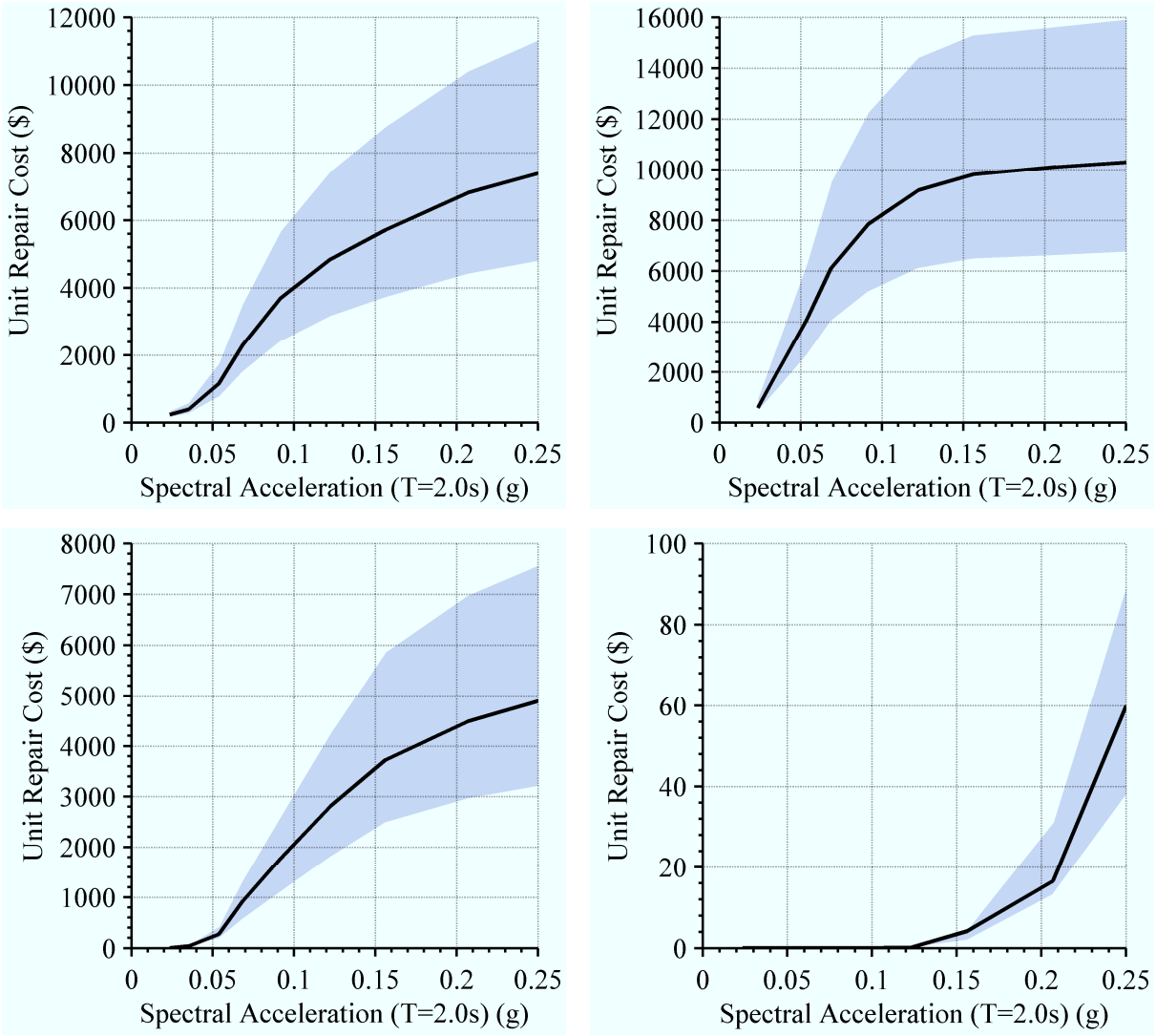

Figure 11-5: Expected repair cost for third floor cladding connection: long threaded rod (top left), short threaded rod (top right), slotted connection (bottom left) and UFP (bottom right)

The ground motion intensity is presented in terms of the spectral acceleration at a period of two seconds (the fundamental period of the case study structure, as determined in Chapter 6). The repair cost functions are based on the seismic response functions of the third floor connections of the case study building analysed in previous chapters. As presented earlier, this region was found to be the floor where interstorey displacements were greatest and hence where unit repair costs are greatest also. The mean repair cost in each figure is shown by the black line and the 16th and 84th percentile repair costs are shown by the grey shaded region. The repair cost functions of the cladding panel are presented for each of the four connections in Figure 11-6.

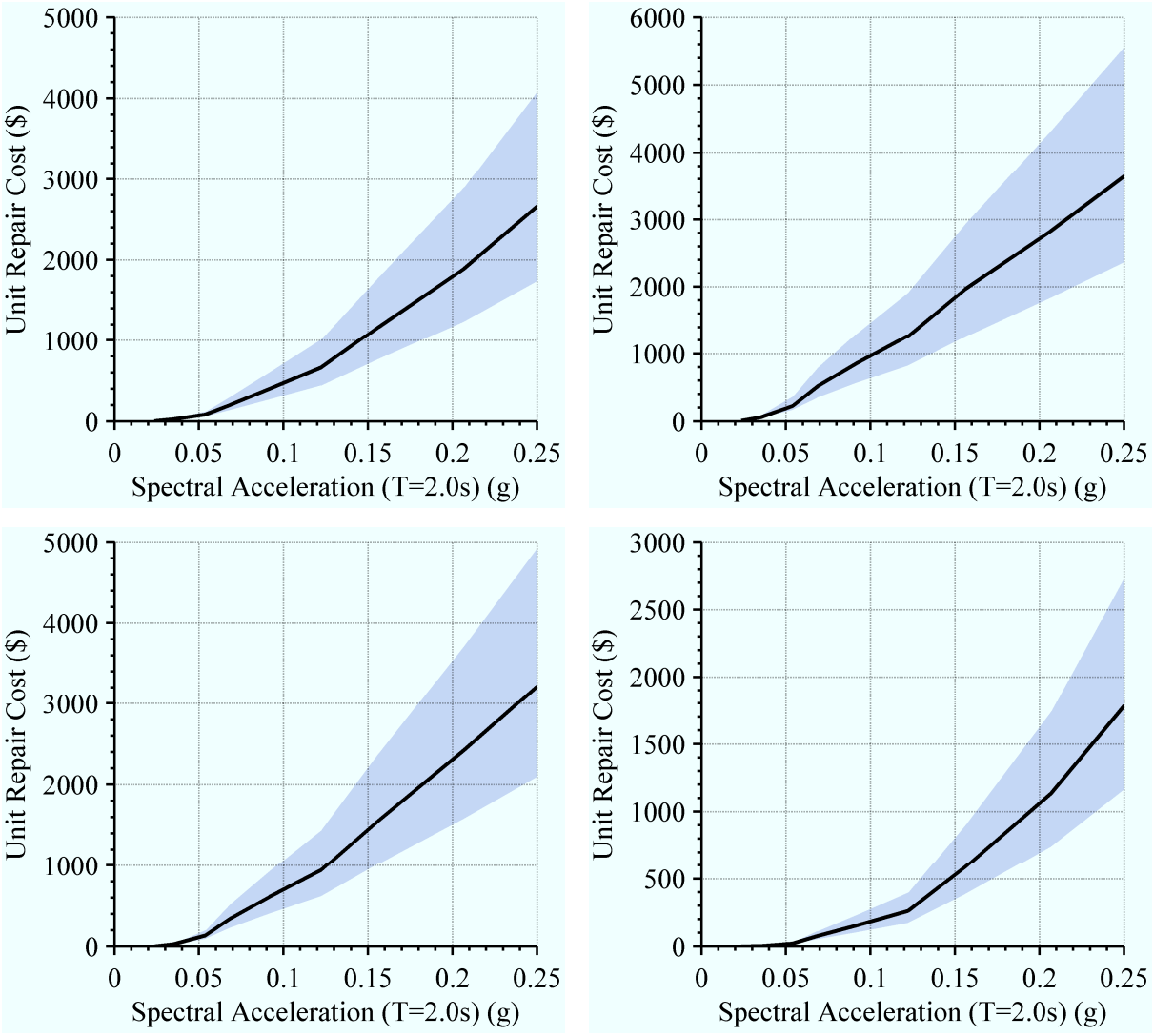

Figure 11-6: Expected repair cost for third floor cladding panel with different connection: long threaded rod (top left), short threaded rod (top right), slotted connection (bottom left) and UFP (bottom right)

The repair cost functions are based on the seismic response functions of the third floor cladding panels of the case study building analysed in previous chapters. Different cladding

panel repair cost functions are required for each connection type since when presented in terms of ground motion intensity, the cladding panel damage is dependent upon the connection type used as well as the location of the cladding panels. The mean repair cost in each figure is shown by the black line and the 16th and 84th percentile repair costs are shown by the grey shaded region.

The mean connection and panel repair costs for the four cladding connections are shown in Figure 11-7. It can be seen that the expected connection repair costs of the short threaded rods are greatest for all levels of spectral acceleration considered. The repair cost also begins to plateau as the probability of connection failure becomes almost certain. The general shape of the expected cost function is the same for the other connection types also, with the expected cost of the long threaded rod connections being on average 47% of that of the short threaded rod connections. The expected repair cost of the slotted connections was on average 23% that of the short threaded rod connections. It can also be seen that the expected repair cost associated with the UFP connections is virtually negligible for all of the levels of spectral acceleration considered.

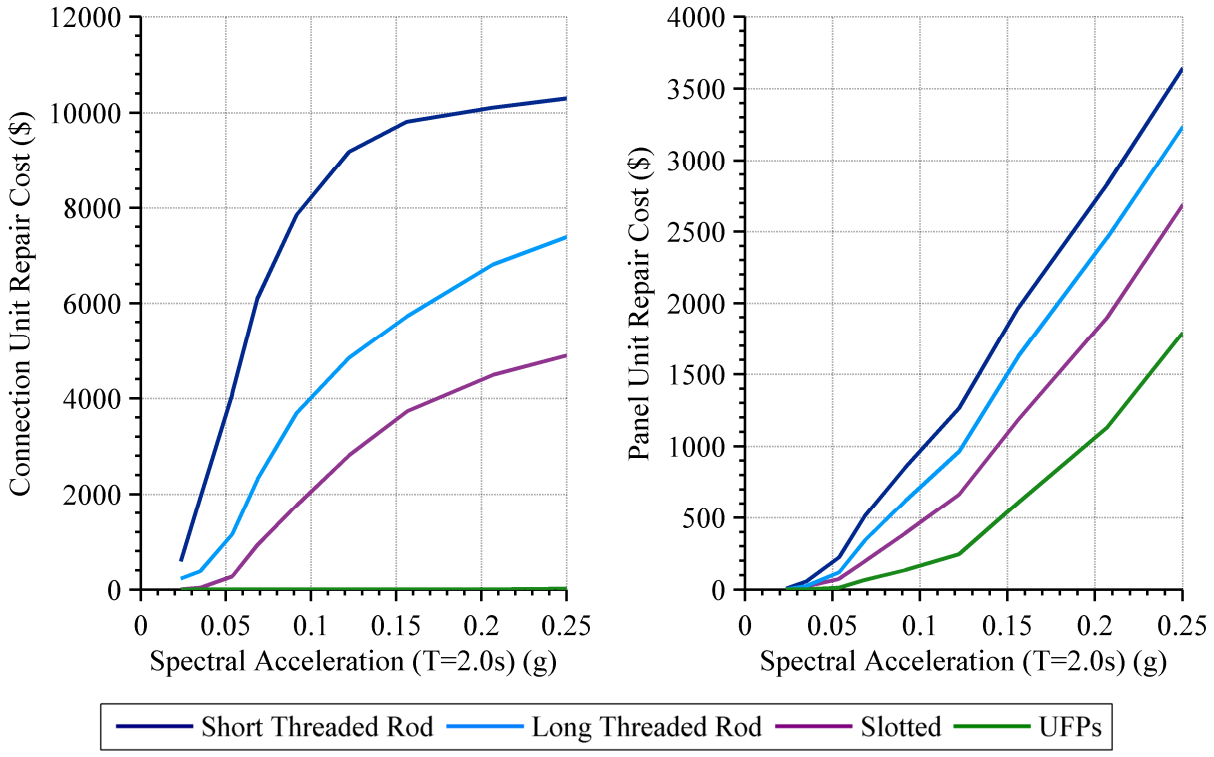

Figure 11-7: Comparison of mean connection (left) and panel (right) repair cost for the four cladding connections

When considering the repair costs of the cladding panel, it can be seen that the repair cost is relatively similar between connection types. As was the case for the connection repair

costs, the repair costs of the cladding panel when connected to the structure with short threaded rods is greatest for all levels of spectral acceleration considered. The panel repair costs when connected with long threaded rod connections are on average 66% of that when connected with short threaded rods. The panel repair costs when connected with slotted connections are on average 48% of that when connected with short threaded rods. Finally, the panel repair costs when connected with UFP connections are on average 20% of that when connected with short threaded rods.

11.4.2 Repair Cost Consequence Functions

The repair cost consequence function builds upon the unit repair costs obtained in the previous section to include consideration of economies of scale and efficiencies in construction operations. When a large quantity of the same type of work is necessary, contractor mobilisation, demobilisation, and overhead costs can be spread over a larger volume of work, resulting in reduced unit rates. A typical consequence function taken from FEMA P-58-1 (2012) for repair cost is illustrated in Figure 11-8.

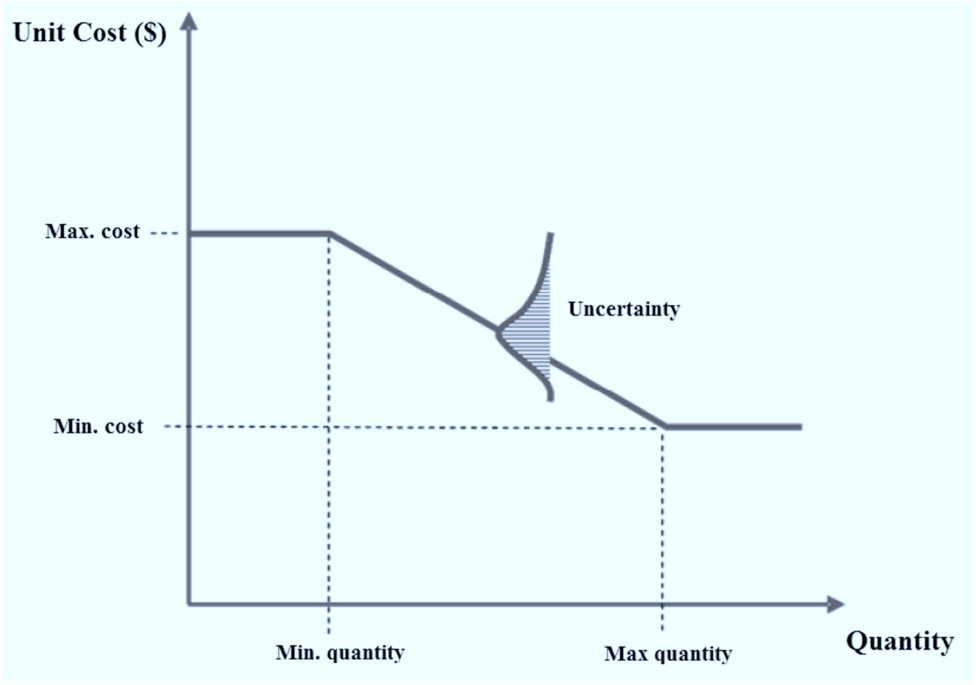

Figure 11-8: Typical consequence function for repair cost (FEMA P-58-1, 2012)

For each performance level, repair costs are described using the following parameters:

- **Minimum quantity:** Quantity of repair actions of a given type, below which there is no discount reflecting economies of scale or efficiencies in operation.

- **Maximum quantity:** Quantity of repair work, above which no further economies of scale or efficiencies in operation are attainable.
- **Minimum cost:** The unit cost to perform a repair action, considering all possible economies of scale and efficiencies in operation.
- **Maximum cost:** The unit cost to perform a repair action, excluding any economies of scale or efficiencies in operation.

At each point along the consequence function, the uncertainty in cost is represented by a distribution of potential repair costs. As presented earlier in Figure 11-1, the dispersion of the lognormal distribution used to represent the uncertainty in cost is based on the best, low and high estimates found for the repair action costs.

The repair consequence data for cladding panels and cladding connections are presented in Table 11-6 and Table 11-7, respectively. The quantity and units of measurement are based on repair to a single cladding panel that is 26.5 m^2 with two cladding connections. The best estimates of the repair action costs have been selected to represent the maximum unit costs of the consequence functions. This was decided since the best estimate data was obtained without considering economies of scale in repair. The minimum unit costs were chosen using economies of scale as similar activities in PACT (FEMA P-58-1, 2012). This economy of scale is largely representative of the costs associated with the temporary works as opposed to the cost of the repair work itself, e.g. the costs of erecting scaffolding are similar whether for a single damaged panel of for 20+ damaged panels. A check was also made to ensure the minimum unit cost was at least equal to the lower bound cost estimate.

Table 11-6: Cladding panel repair cost consequence data

	Quantity		Unit Repair Cost	
Performance Level	Min	Max	Min	Max
Immediate Occupancy	4	40	$200	$350
Life Safety	4	40	$2,580	$3,640

Table 11-7: Cladding connection repair cost consequence data

	Quantity		Unit Repair Cost	
Performance Level	Min	Max	Min	Max
Immediate Occupancy	5	25	$820	$1,020
Life Safety	5	25	$1,090	$1,500
Hazards Reduced	5	25	$3,350	$4,900
Failure	5	25	$6,200	$10,300

The repair cost consequences for each of the performance levels of the cladding panels and connections are presented graphically in Figure 11-9.

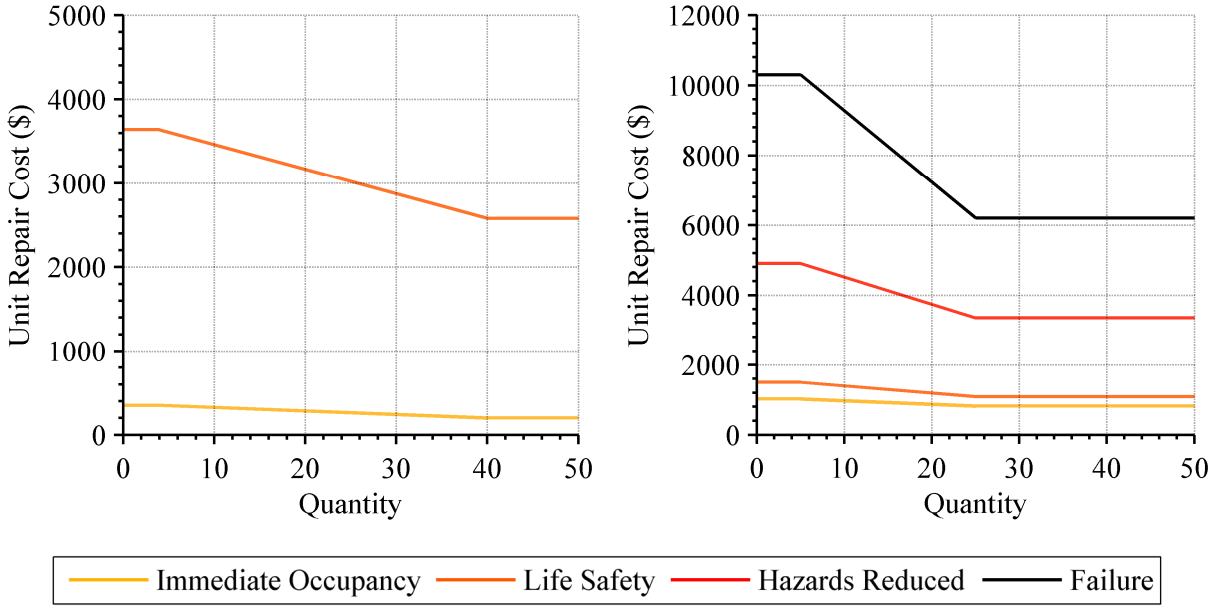

Figure 11-9: Repair cost consequence function for precast panels (left) and cladding connections (right)

11.4.3 Total Repair Cost

The expected repair costs for the entire extent of cladding damage throughout the structure can be calculated using the same approach as that used to develop the repair costs in Section 11.4.1 and summing the costs throughout the structure. At this step it is also necessary to consider the consequence functions presented in Section 11.4.2 to account for economies of scale in repairing multiple connections.

Another factor that needs to be included when summing the repair cost throughout the structure is the consideration of where in the structure the repairs are taking place. Since cladding repair typically takes place on the exterior of the structure, the cost of accessing the damaged area has a significant impact upon the repair costs. For example, it is more difficult, and, hence, more costly to repair cladding damage on the tenth floor than on the first floor. A height adjustment factor is proposed here that increases the repair cost according to the floor that damage occurs. The height adjustment factor is equivalent to a 5% increase from the base repair cost for each floor above ground level, as given by (11-5) and presented graphically in Figure 11-10.

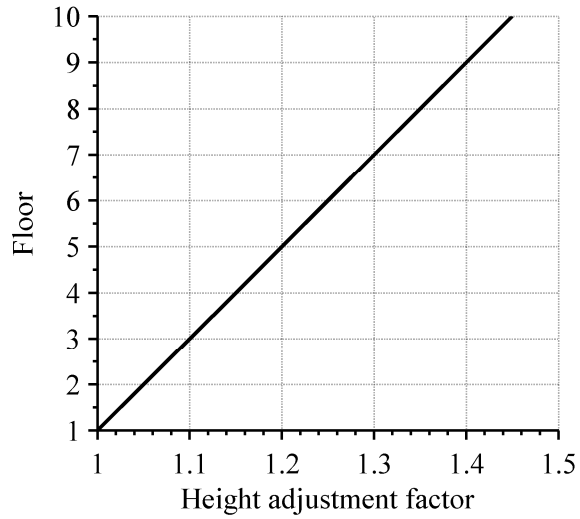

$$HAF = 1 + n_f \times 0.05 \quad \textbf{(11-5)}$$

where

HAF = Height adjustment factor

n_f = Number of floors above ground level

Figure 11-10: Height adjustment factor

The total repair costs sum both the connection and panel repair costs throughout the structure. Shown in Figure 11-11 Figure 11-12 are the total repair costs for each of the four connection types. The contribution to the total cost from the panel and connection repair is shown by the different shaded regions, with the panel contribution being the lower, dark coloured region and the connection contribution being the upper, lighter coloured region.

It can be seen that the connection repair costs make up the majority of the costs for the threaded rod connections. The total repair costs for slotted connections are evenly split between connection and panel repair costs and the total repair costs for UFP connections are essentially the panel repair cost only.

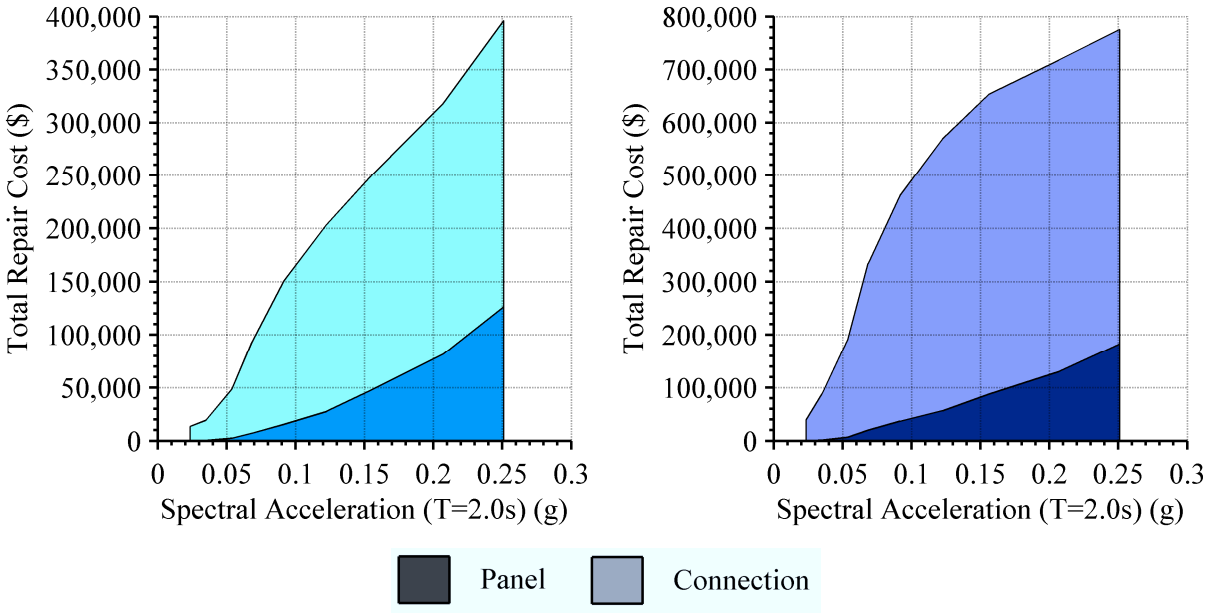

Figure 11-11: Total repair cost of long threaded rod (left) and short threaded rod (right) cladding systems

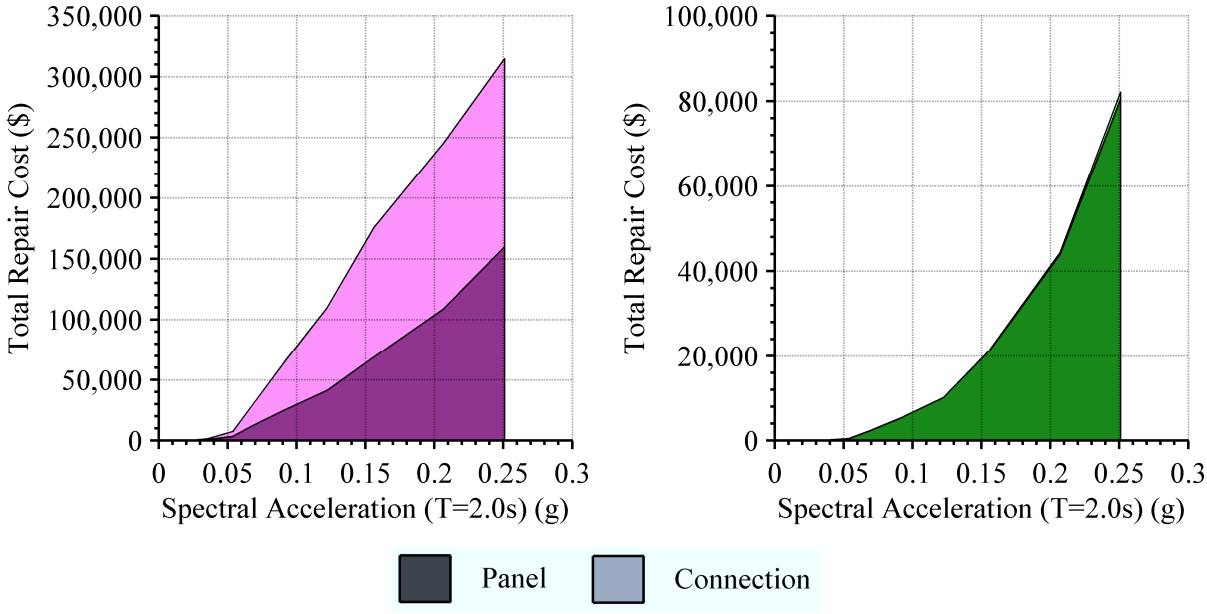

Figure 11-12: Total repair cost of slotted connection (left) and UFP (right) cladding systems

The total repair costs for each of the four connections (including connection and panel costs) are shown for comparison in Figure 11-13. Evidently, the expected repair costs for cladding damage to short threaded rod connections are significantly more than any of the other connection types.

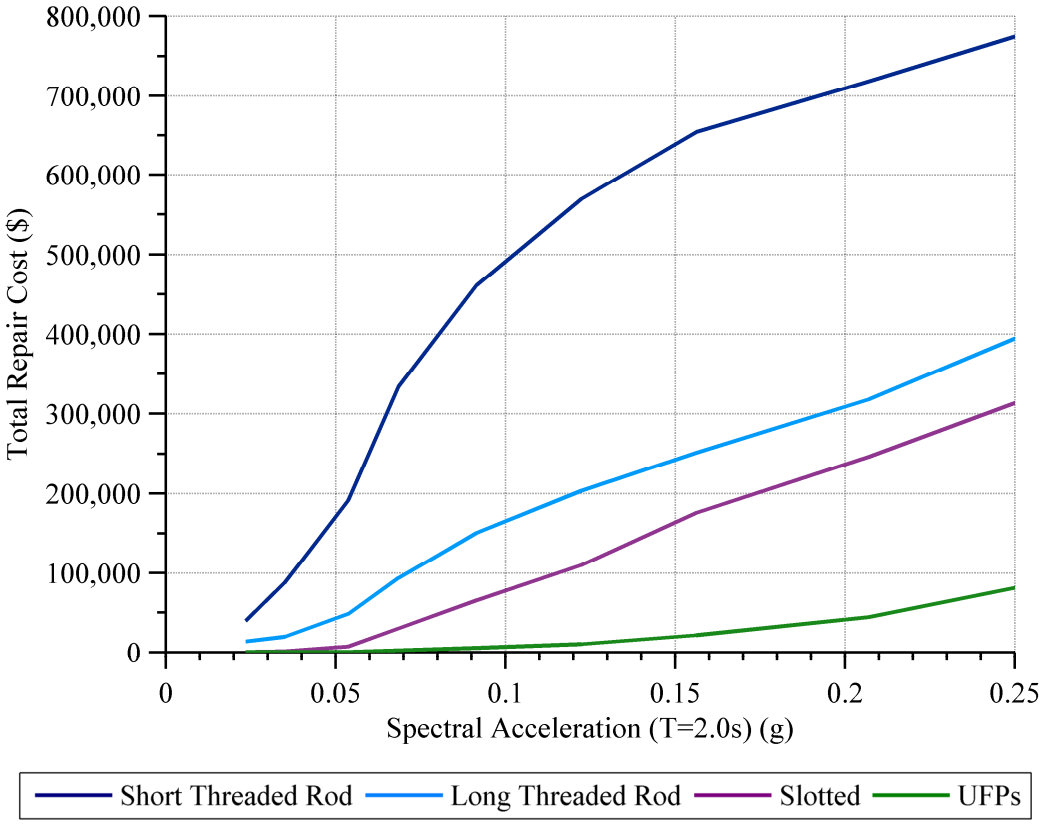

Figure 11-13: Comparison of total repair cost for the four cladding systems

11.4.4 Repair Cost Hazard

The repair cost hazard represents the final product of a probabilistic seismic loss assessment (PSLA) and represents the culmination of each of the previous steps to present the repair costs in terms of annual probability of exceedance. The repair cost hazard is calculated based on the likelihood of various levels of ground shaking at a site, the relationship between the ground shaking and the seismic response, the relationship between the seismic response and the cladding performance, the relationship between the cladding performance and the cladding repairs and finally the relationship between the cladding repairs and the repair cost. The repair cost hazard is similar to the seismic demand hazard, introduced in Chapter 7, in which it is not an intensity-based assessment that considers the repair cost at a single intensity level; rather it combines the expected repair cost from a range of possible intensity levels. The repair cost hazard is therefore defined as the integral of the probability of repair cost for a given intensity measure multiplied by the incremental probability of that intensity measure occurring, as shown by Equation (11-6).

$$\lambda_{RC} = \int_0^{\infty} P_{RC|IM}(rc|im) \left| \frac{d\lambda_{IM}(im)}{dIM} \right| dIM \qquad \textbf{(11-6)}$$

where

λ_{RC} = Annual frequency of exceedance of repair cost

$P_{RC|IM}(rc|im)$ = Probability of repair cost for a given intensity measure

$\frac{d\lambda_{IM}(im)}{dIM}$ = Incremental probability of a given intensity measure

The repair cost hazard curves are presented in terms of the annual frequency of exceedance for each of the four connection types considered. The annual frequency of exceedance is equivalent to the reciprocal of the return period and has been presented here in logarithmic scale. The total repair cost is presented in linear scale. Shown in Figure 11-14 are the total repair cost hazard curves for each of the four cladding connection types considered.

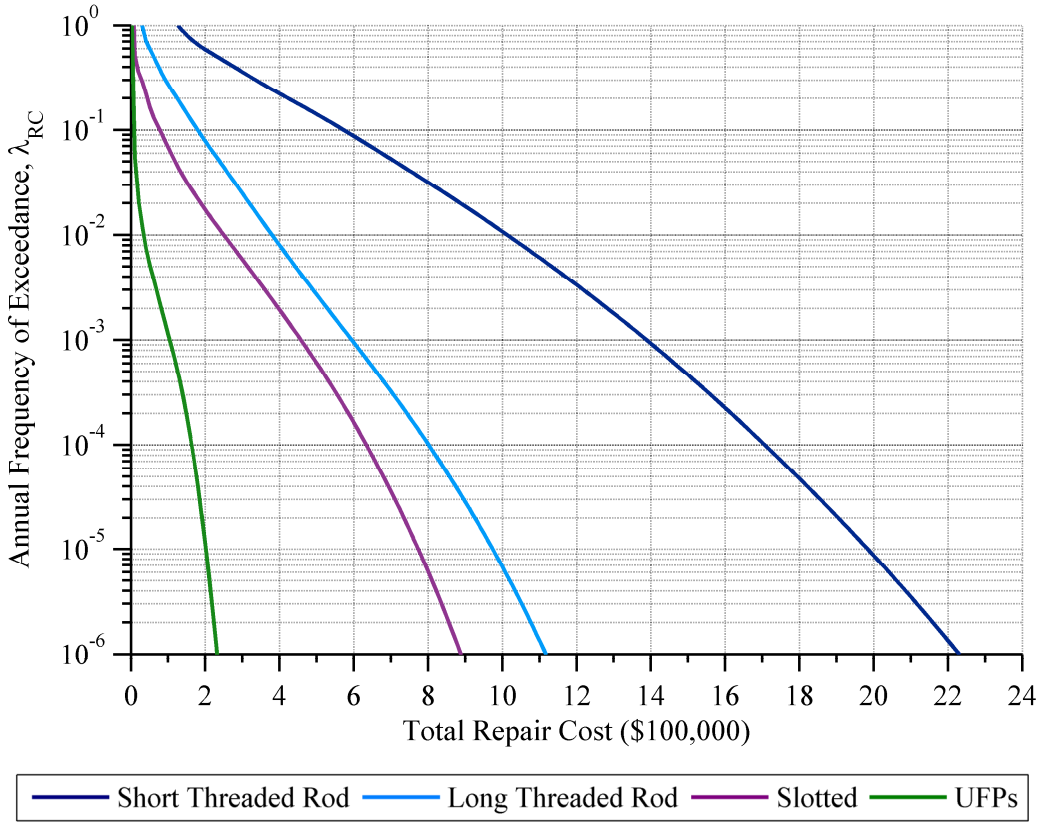

Figure 11-14: Comparison of repair cost hazard curves for four cladding connections

Similarly to when the total repair cost was found for various levels of spectral acceleration, the expected repair cost for a building clad with short threaded rod connections is significantly greater than that of the other connection typologies. The long threaded rod and slotted connections have similar expected total repair costs, with the total cost for long threaded rods being slightly greater. The total expected repair cost for cladding system utilising UFP connections is not zero but is significantly less than that of the other connection types. The total expected repair costs at 50%, 10% and 2% probability of exceedance in 50 years are presented in Table 11-8.

Table 11-8: Expected cladding total repair costs

	Probability of Exceedance in 50 years		
Connection Type	**50%**	**10%**	**2%**
Long Threaded Rod	$350,000	$520,000	$680,000
Short Threaded Rod	$960,000	$1,270,000	$1,520,000
Slotted	$220,000	$390,000	$530,000
UFP	$30,000	$80,000	$130,000

11.5 Repair Time

After an earthquake, the cost of repairing damage will not be the only loss suffered by building stakeholders. Undertaking the repair actions necessary to return the cladding to its undamaged state will also cause business interruption as well as the possibility of building closure as a safety precaution. This type of loss is often referred to as downtime, however, the use of the term 'downtime' has been avoided here as this describes the greater period of time between the occurrence of a seismic event and the completion of the building repair effort.

There are various factors that can affect building downtime: building inspection, damage assessment, finance planning, architect/engineering consultations, a possible competitive bidding process, and the repair effort needed to return a building back to its undamaged state (Comerio & Stallmeyer, 2002). This study focusses solely on the final aspect: the repair time needed to return the cladding back to its undamaged state. This portion of downtime is often referred to as the rational component (Mitrani-Reiser, 2007), and although seemingly straightforward, this repair effort is still highly variable depending on the repair scheme and will vary from one owner to another.

The remaining portion of building downtime is difficult to model because it is highly dependent on irrational components, which include financing, relocation of functions, human resources, and economic and regulatory uncertainty (Comerio, 2006).

This study does not aim to capture these aspects since these irrational components are strongly dependent upon not only the cladding damage, but the entire extent of damage throughout the building. Since it is highly unlikely that a building will experience cladding damage only, any attempt to quantify the irrational component of downtime will be flawed. As well as this, the actual time that a building will be unusable following an earthquake is very difficult to determine. Factors that can affect the length of time for building re-occupancy include:

- Who is responsible for performing repairs (e.g., owner or tenants);
- Financial resources available to the party responsible for performing repairs;
- Availability of design professionals to assess the condition of the building and design repair actions;
- Availability of contractors and availability of equipment and materials necessary to perform repairs;

- The time it takes to procure specialised equipment (i.e., long lead time) and materials for a specific building or occupancy;
- Whether or not the building will remain in service during repairs, which limits repair work to unoccupied areas, versus remaining vacant to provide complete access for conducting repairs on a building-wide basis;
- Whether or not the building has been posted with an unsafe placard, and the length of time necessary to convince a building official that it is safe to conduct repair operations within the building;

It is necessary to take the above factors into account when calculating the downtime of a building following an earthquake. However, as stated previously, the aim of this study is not to calculate the expected downtime, rather it is to calculate more accurately the repair time associated with cladding damage. This information can then be used by others to more accurately quantify the actual overall downtime, which at present, is extremely difficult to do. Krawinkler and Miranda (2004) summarised the challenge facing estimating downtime as follows:

"The basic difficulties in quantifying length of downtime are great uncertainties associated with the availability of labour, materials, and capital following a major seismic event, and difficulties relating quantifiable damage and the needs for repair with loss of function. Even if downtime could be quantified with confidence, the associated losses will be highly uncertain and strongly case and scenario specific. Estimation of downtime losses is and will remain perhaps the biggest challenge of seismic performance assessment and risk management."

The term repair time is used herein to represent the length of time necessary by a team of workers to conduct repair actions described in Section 11.3.3 for earthquake-induced cladding damage. These repair actions have been identified as all of the activities necessary to return the damaged cladding to its pre-earthquake conditions for each of the cladding component performance levels identified in Section 11.3.2. The repair actions are assumed to occur in sequential order, that is, 'Action B' cannot start until 'Action A' is complete. This is not to say that multiple areas cannot be repaired simultaneously if more labour is available, which will be expanded upon later when the total repair time for all cladding damage is calculated. It is important to note that the repair time does not represent man-hours but rather the time taken for the most suited number of workers to perform the repair action.

The repair times are grouped according to cladding panel repair times in Table 11-9 and connection repair times in Table 11-10. The time (given in days) is based on the time to repair a single cladding panel that is 26.5 m^2 with two cladding connections (this is equivalent to the mono panel system modelled in previous chapters). The uncertainty in time has been represented by presenting the best estimate, which represented the 50th percentile cost, as well as the low and high estimate, which represent the 10th and 90th percentiles.

Table 11-9: Cladding panel repair action times

Repair action		Unit	Best estimate	Low estimate	High estimate
Erect and remove scaffolding or other work platform		days	1.5	0.75	3.0
Remove loose concrete spall		days	0.5	0.25	1.0
Patch spalled regions with grout or dry pack		days	1.0	0.25	2.0
Epoxy inject cracks		days	2.0	1.0	4.0
Plaster and skim repaired area		days	0.5	0.25	1.0
Paint repaired area		days	0.5	0.25	1.0
Immediate Occupancy	Per panel		2.0	1.0	4.0
	Per m^2		0.075	0.038	0.15
Life Safety	Per panel		6.0	3.0	12.0
	Per m^2		0.23	0.11	0.45

Table 11-10: Cladding connection repair action times

Repair action		Unit	Best estimate	Low estimate	High estimate
Remove, protect and reinstall contents adjacent to damaged area		days	1.0	0.5	2.0
Remove and re-instate internal linings and any services that obstruct access to connections		days	2.0	1.0	4.0
Inspect connections for damage		days	0.5	0.25	1.0
Replace connections or repair where possible		days	2.0	1.0	4.0
Drill panel and fix epoxy anchor for new connection		days	2.0	1.0	4.0
Install new connection to structure		days	2.0	1.0	4.0
Erect and remove scaffolding or other work platform		days	2.0	1.0	4.0
Crane in and mount new cladding panel		days	5.0	2.5	10.0
Immediate Occupancy	Per panel		3.5	1.75	7.0
	Per m^2		0.13	0.066	0.26
Life Safety	Per panel		5.0	2.5	10.0
	Per m^2		0.19	0.094	0.38

Hazards Reduced	Per panel	7.0	3.5	14.0
	Per m^2	0.26	0.13	0.53
Failure	Per panel	12.0	6.0	24.0
	Per m^2	0.45	0.23	0.91

Similarly to repair cost, the uncertainty in repair time can be represented as a log-normal distribution for each performance level. The repair time functions for the four performance levels of connections are presented in Figure 11-15.

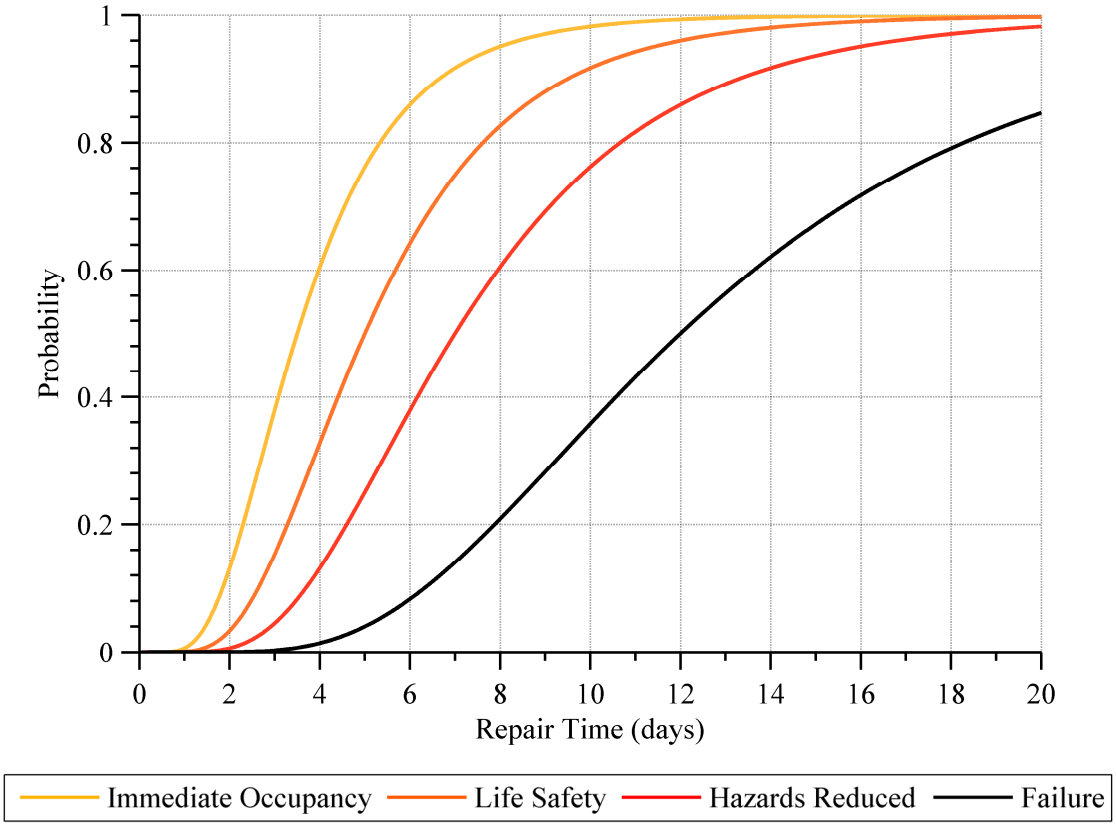

Figure 11-15: Cladding connection repair time functions

The use of the lognormal distribution results in a large amount of uncertainty for the failure performance, as would be expected due to the complicated repairs that are associated with this outcome.

11.5.1 Expected Repair Time

The expected repair time for a given demand can be found in the same way as that used to determine expected repair cost: by summing the mean repair time for each performance level and multiplying by the probability of that performance level for a given demand. This is again presented in terms of the maximum lateral displacement (of either the connection or

panel component), as this was the engineering demand parameter used to determine the cladding component performance

The cladding connection repair times are shown in Figure 11-16 for the long threaded rod, short threaded rod, slotted and UFP connection types. The repair time include all of the possible performance levels and their corresponding repair actions and are presented considering the maximum unit repair time, i.e. no economy of scale is taken into account. The mean repair time in each figure is shown by the black line and the 16th and 84th percentile repair times are shown by the grey shaded region.

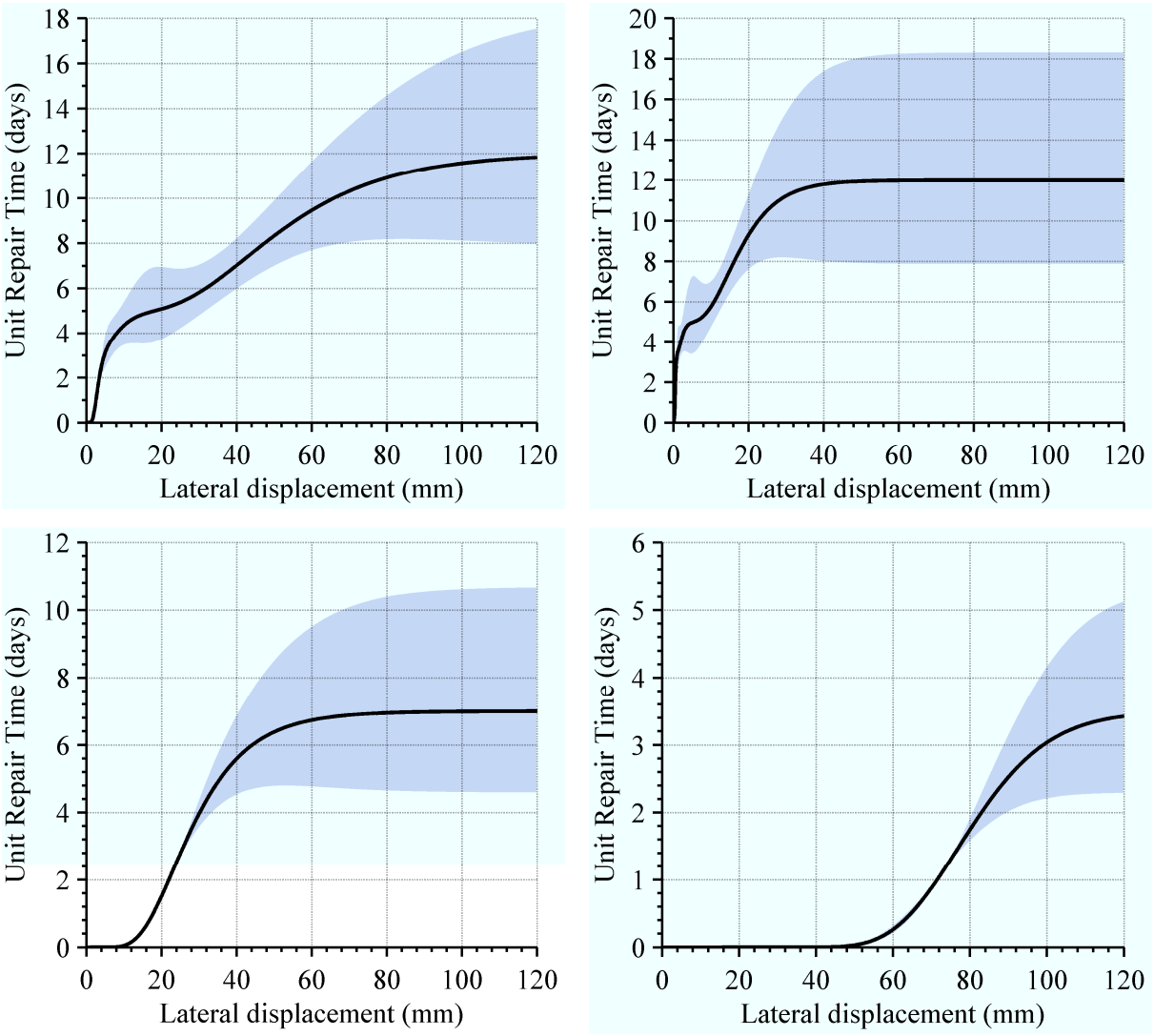

Figure 11-16: Expected repair time for each cladding connection: long threaded rod (top left), short threaded rod (top right), slotted connection (bottom left) and UFP (bottom right)

The shape of the repair time functions when presented in terms of lateral displacement are very similar to those developed for repair cost, particularly when comparing the various connection types. This is expected due to the parallel way in which both the repair time and

repair cost functions have been developed. The repair time of the short threaded rods escalates the fastest of the cladding connections, with the repair time of the long threaded rods eventually matching the short threaded rods at very large lateral displacements. Since no failure performance level has been considered for the slotted connections or UFP connections it can be seen that the maximum repair times are much less for these connections than those associated with the threaded rod connections.

The cladding panel repair time is shown in Figure 11-17. The repair time includes the two performance levels considered for the cladding panel (Immediate Occupancy and Life Safety) and their corresponding repair actions. Like that for the connections, the cladding panel repair time is also presented considering the maximum unit repair time.

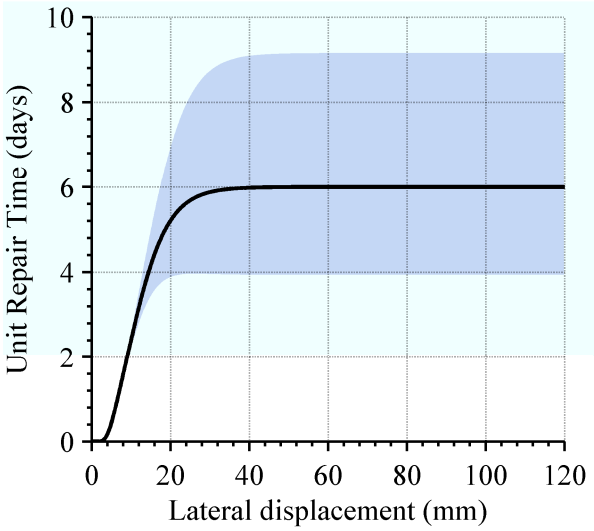

Figure 11-17: Expected repair time for cladding panel

The mean unit repair time for all of the cladding components considered here are presented in Figure 11-18 for comparison purposes. Just like those of the repair costs, these functions are useful since they are general relationships that are true regardless of where the component is located. However, it should be remembered that these repair time functions have been developed considering the Christchurch, New Zealand construction market during 2012 and 2013.

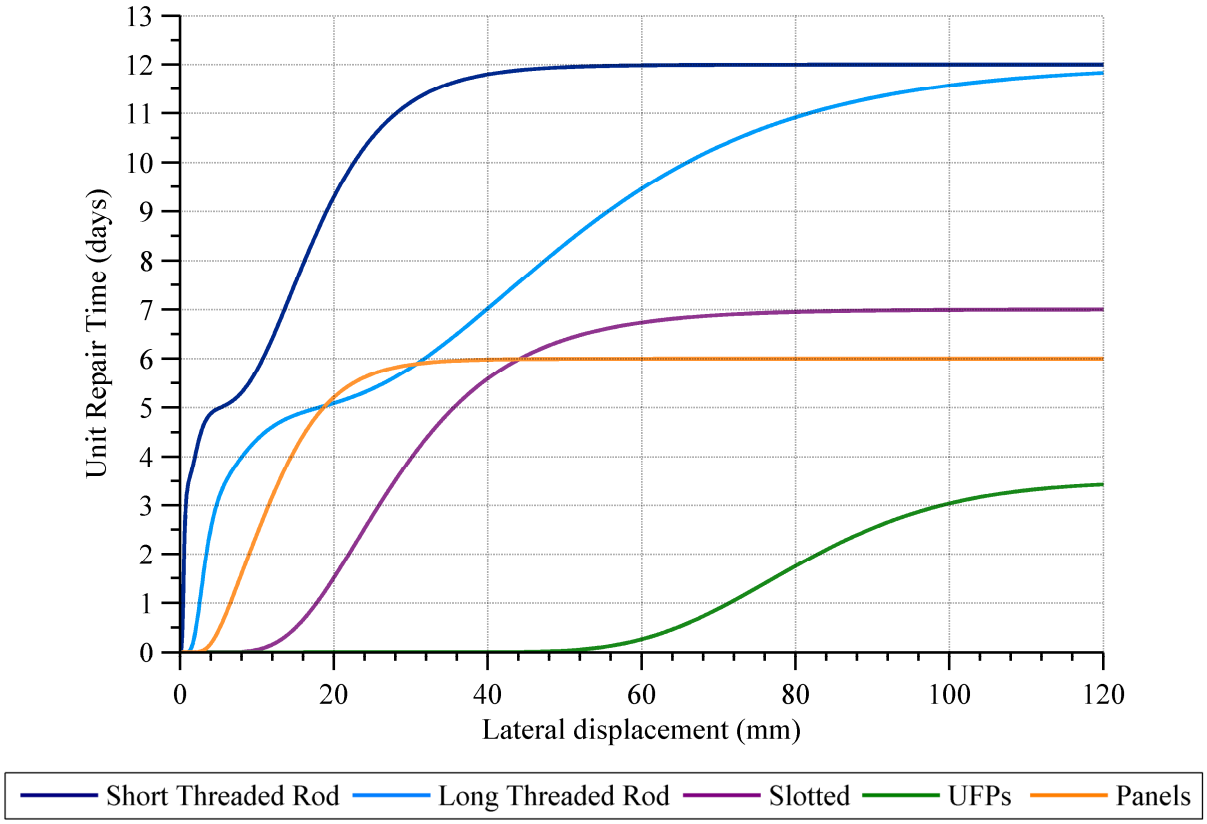

Figure 11-18: Comparison of mean unit repair time for cladding components

As was the case for repair costs, it is also possible to determine the expected repair time when the demand upon the component is defined by the structure. This is achieved by combining the repair time relationship with the seismic response relationship for a particular location in the structure. The result defines the repair time as a function of the ground motion intensity.

As introduced previously, the seismic response relationship is defined for a particular component in a particular location in the structure. In our case it defines the probability density function of the expected maximum lateral displacement for a given ground motion intensity.

The repair time functions in terms of ground motion intensity of the four connection types are presented in Figure 11-19. The ground motion intensity is presented in terms of the spectral acceleration at a period of two seconds. The repair time functions are based on the seismic response functions of the third floor connections of the case study building analysed in previous chapters. The mean repair time in each figure is shown by the black line and the 16th and 84th percentile repair times are shown by the grey shaded region.

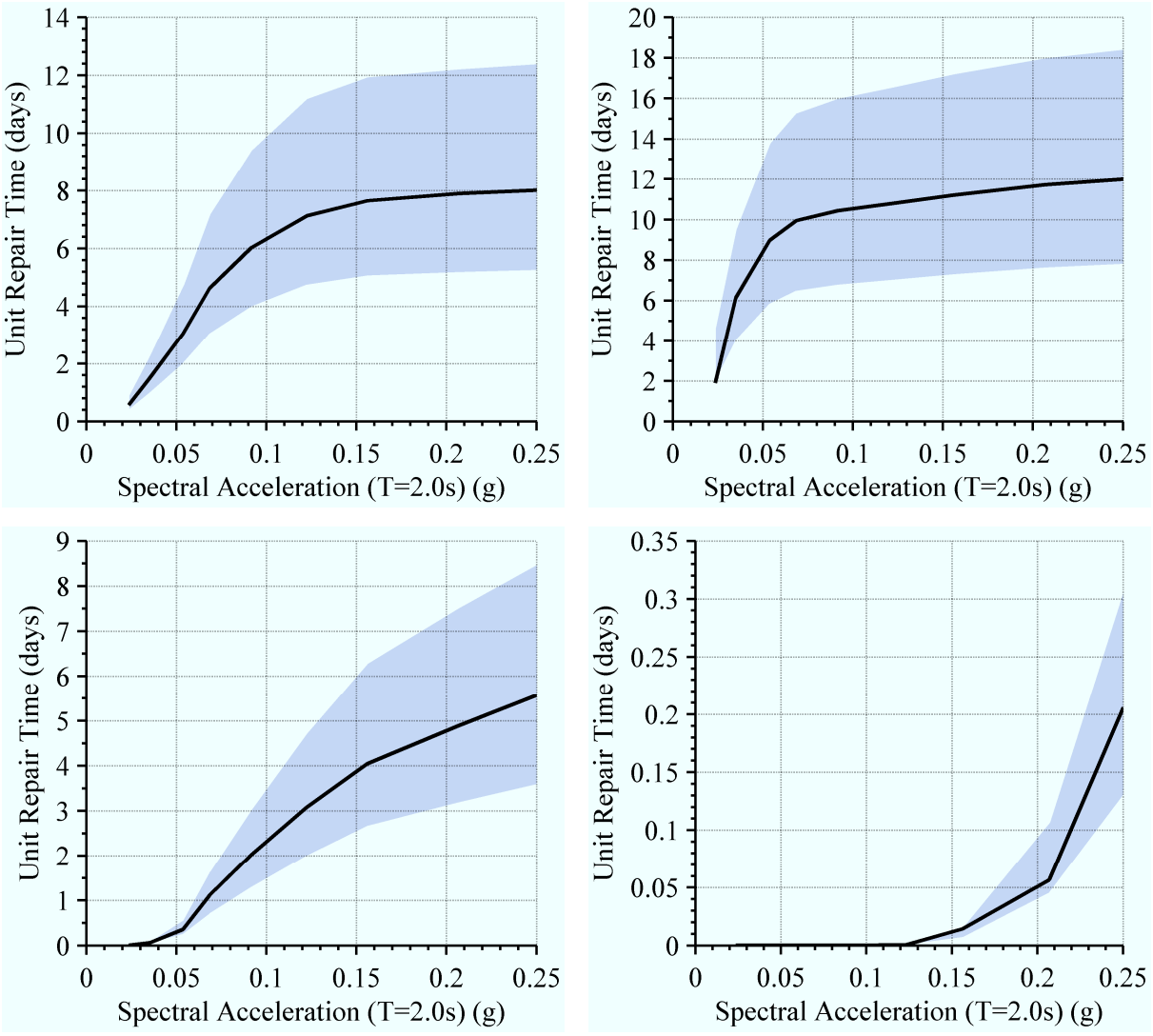

Figure 11-19: Expected repair time for third floor cladding connection: long threaded rod (top left), short threaded rod (top right), slotted connection (bottom left) and UFP (bottom right)

The repair time functions of the cladding panel are presented for each of the four connections in Figure 11-20. These are also developed using the seismic response relationships of the third floor cladding panels of the case study building. Different cladding panel repair time functions are required for each connection type since when presented in terms of ground motion intensity, the cladding panel damage is dependent upon the connection type. The mean repair time in each figure is shown by the black line and the 16th and 84th percentile repair times are shown by the grey shaded region.

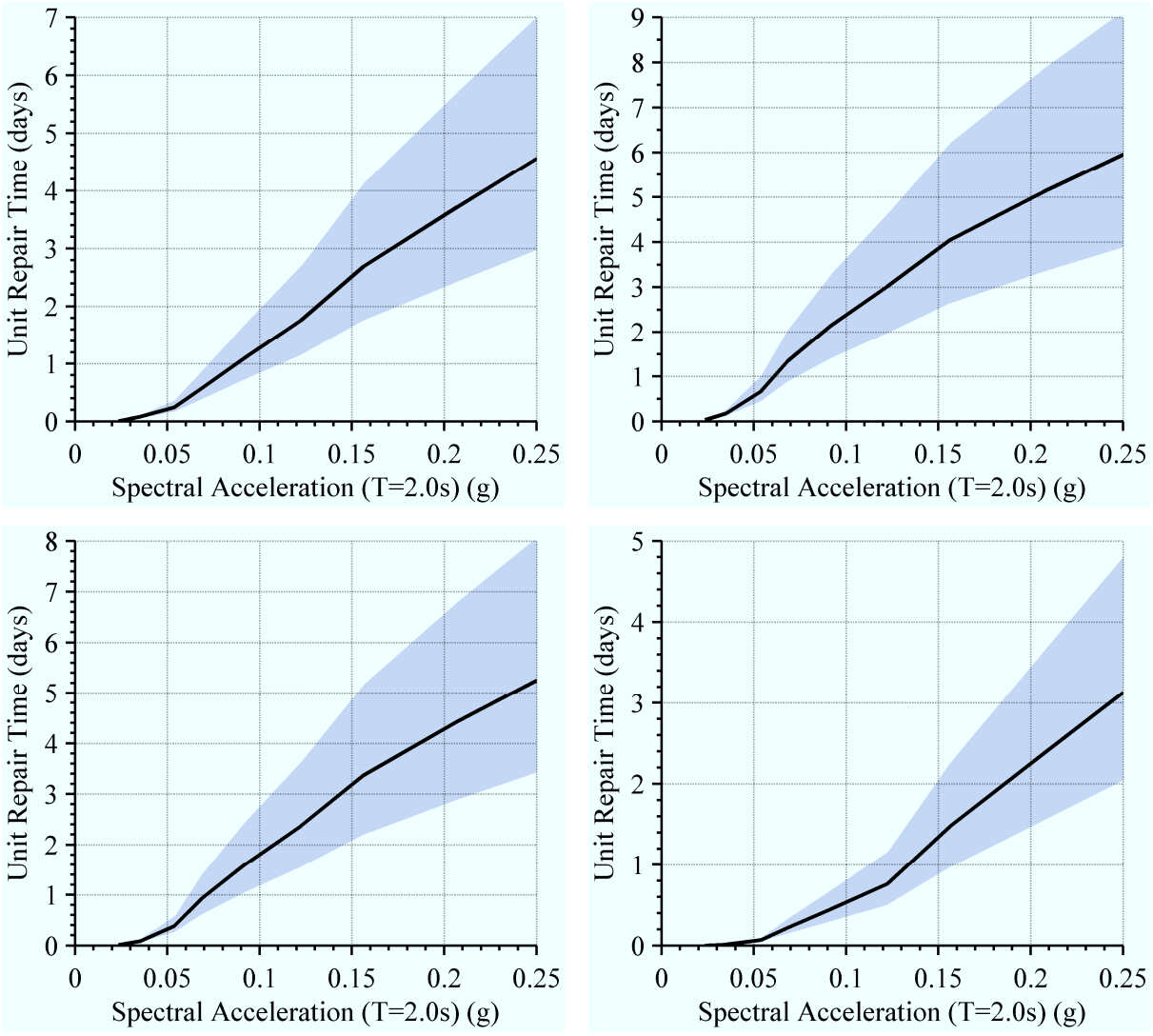

Figure 11-20: Expected repair time for third floor cladding panel with different connection: long threaded rod (top left), short threaded rod (top right), slotted connection (bottom left) and UFP (bottom right)

The mean connection and panel repair times for the four cladding connections are shown in Figure 11-21. It can be seen that the expected connection repair time of the short threaded rods are greatest for all levels of spectral acceleration considered. The repair time also begins to plateau as the probability of connection failure becomes almost certain. Like that for the repair costs, it can also be seen that the expected repair time associated with the UFP connections is virtually negligible for all of the levels of spectral acceleration considered.

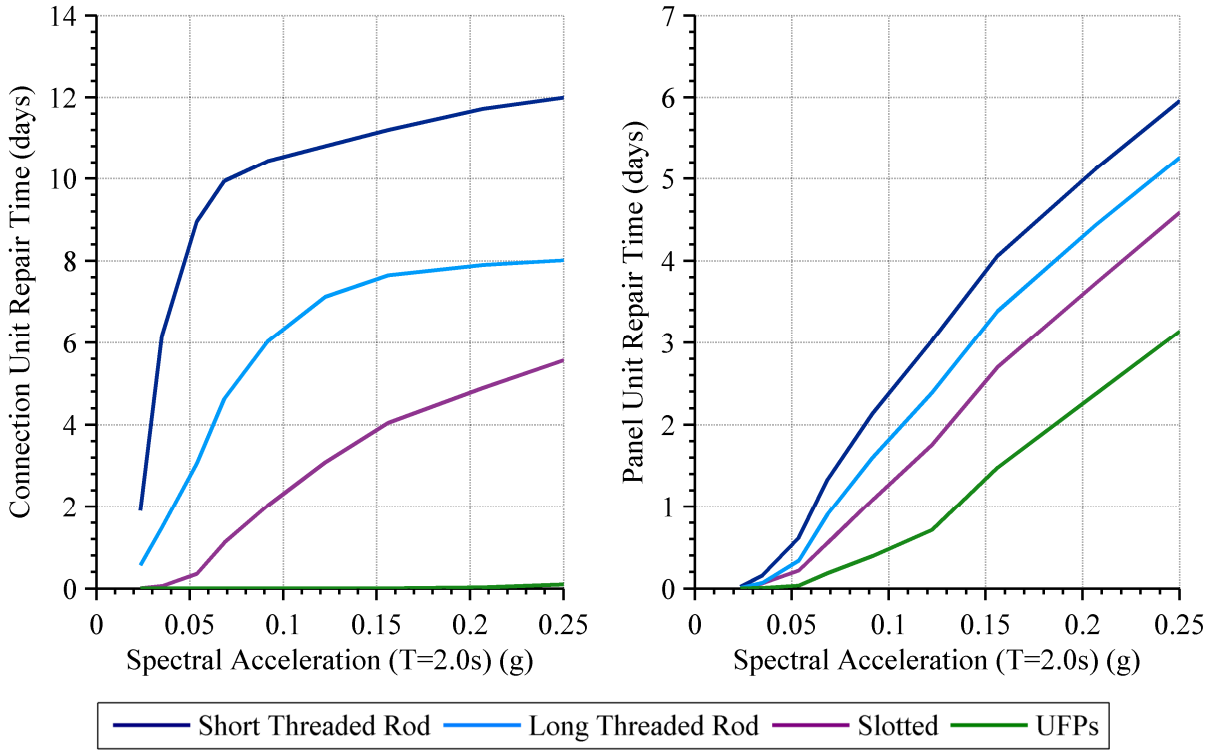

Figure 11-21: Comparison of mean connection (left) and panel (right) repair time for the four cladding connections

The repair time of the cladding panel is similarly dependent upon the connection type; with the short threaded rod connection resulting in the greatest number of days required for repair to the cladding panel. Where the UFP connection results in negligible repair time to the connection, it can be seen that the connection does not guarantee negligible damage to the cladding panel, as shown by the required numbers of days of repair time to the cladding panel for this connection type. However, the UFP connection does result in a decrease to the expected repair time to the cladding panel when compared to all other connection types considered.

11.5.2 Repair Time Consequence Functions

To estimate repair time, each damage state includes a time-related consequence function that adjusts the repair time according to the number of cladding components that requires repair. The repair time consequence function builds upon the unit repair costs obtained in the previous section to include consideration of economies of scale and efficiencies in construction operations. When a large quantity of the same type of work is necessary, efficiencies are achieved which results in the average repair time being reduced. A

typical consequence function taken from FEMA P-58-1 (2012) for repair time is illustrated in Figure 11-22.

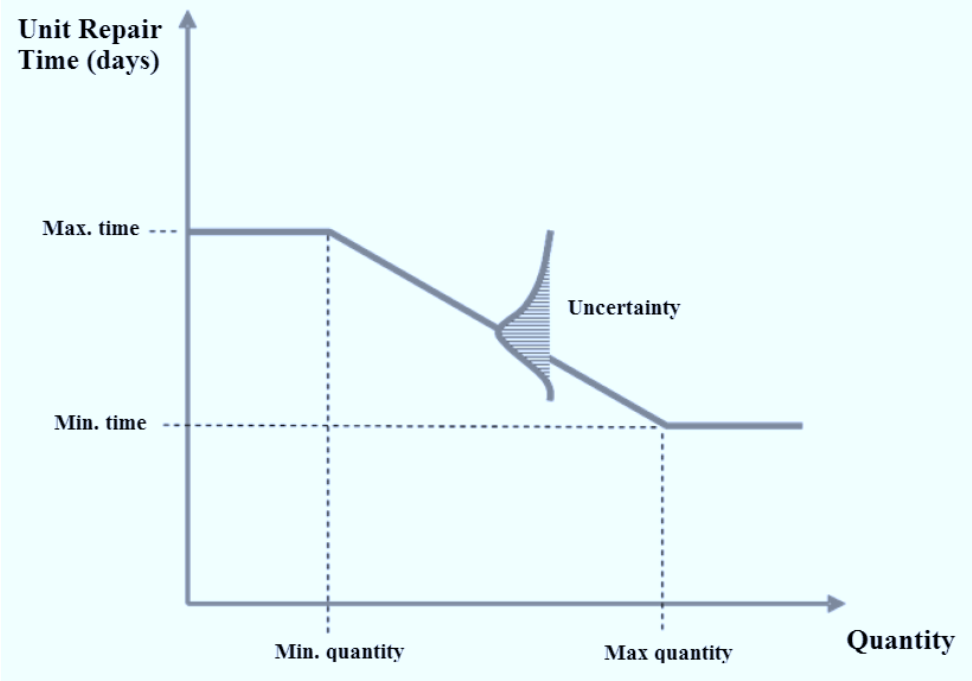

Figure 11-22: Typical consequence function for repair time (FEMA P-58-1, 2012)

For each performance level, repair times are described using the following parameters:

- **Minimum quantity:** Quantity of repair actions of a give type, below which there is no reduction in time reflecting economies of scale or efficiencies in operation.
- **Maximum quantity:** Quantity of repair work, above which no further economies of scale or efficiencies in operation are attainable.
- **Minimum time:** The minimum time necessary to perform a repair action, considering all possible economies of scale and efficiencies in operation.
- **Maximum time:** The maximum time necessary to perform a repair action, excluding any economies of scale or efficiencies in operation.

At each point along the consequence function, the uncertainty in repair time is represented by a distribution of potential repair times. As presented earlier in Figure 11-15, the dispersion of the lognormal distribution used to represent the uncertainty in time is based on the best, low and high estimates found for the repair action time.

The repair consequence data for cladding panels and cladding connections are presented in Table 11-11 and Table 11-12, respectively. The repair time is based on repair to a single cladding panel that is 26.5 m^2 with two cladding connections. The best estimates of

the repair times have been selected to represent the minimum unit repair time of the consequence functions. This was decided since the best estimate data was obtained considering large quantities of repair. The maximum unit repair times were chosen using economies of scale as similar activities in PACT (FEMA P-58-1, 2012). Similarly to the repair cost, this economy of scale is largely representative of the time associated with the repair actions that involve preparation and clean-up, e.g. removing and instating wall linings, rather than the repair actions involving the cladding.

Table 11-11: Cladding panel repair time consequence data

	Quantity		Unit Repair Time (days)	
Performance Level	Min	Max	Min	Max
Immediate Occupancy	4	40	1.25	2.0
Life Safety	4	40	4.5	6.0

Table 11-12: Cladding connection consequence repair time data

	Quantity		Unit Repair Time (days)	
Performance Level	Min	Max	Min	Max
Immediate Occupancy	5	25	2.75	3.5
Life Safety	5	25	4.0	5.0
Hazards Reduced	5	25	5.0	7.0
Failure	5	25	7.5	12.0

The repair time consequences for each of the performance levels of the cladding panels and connections are presented graphically in Figure 11-23.

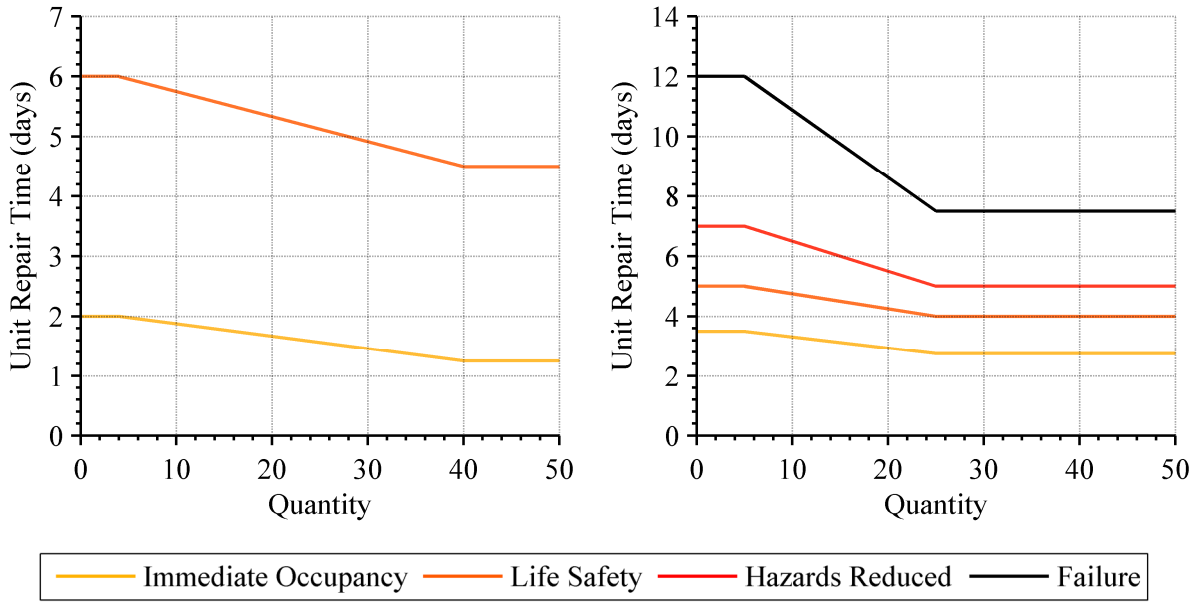

Figure 11-23: Repair time consequence functions of precast panels (left) and cladding connections (right)

11.5.3 Total Repair Time

The total repair time for the entire extent of cladding damage throughout the structure can be calculated using the same approach as that used to develop the repair times in Section 11.5.1. Since the repair actions are assumed to occur in sequential order, the total repair time is also presented here by assuming repair to each cladding component also occurs in series. The total repair time is therefore the greatest possible repair time, however, it should be noted that this is not equivalent to the greatest possible downtime. The building downtime, even when only considering cladding damage, must also include a lead-in time to commence repairs. Research has shown that this lead-in time following a large earthquake is often greater than the time to perform the actual repairs (Comerio, 2006).

The assumption that repairs occur in series is highly conservative as it presumes that only one repair action can be taking place at any given time. For a multi-storey building, this is highly unlikely as it would be expected multiple crews could work on the building at various locations, performing various repair actions at once. As mentioned previously, the repair time data gathered here represents the time to repair a single component by a team of workers. However, by presenting the total repair time in this conservative format, it is reasonable to assume that when multiple crews are assigned to the repair actions that they can proportionately reduce this 'worst-case' scenario, i.e. two crews can perform the same repairs in half the time. This relationship will not be purely elastic, and there will of course be a point whereby increasing the number of crews will not reduce the repair time at all, however this has not been considered here because it moves outside the scope of repair time and into the calculation of repair strategy which is more a downtime consideration which involves many external pressures.

Although repair strategies have not been considered, at this step it is necessary to consider the consequence functions presented in Section 11.5.2 to account for economies of scale in repairing multiple connections. Similarly to when calculating total repair cost, the height adjustment factor has been used to account for the additional difficulty and hence increased repair time to repair cladding damage in higher floors. The height adjustment factor is again presumed as being equivalent to a 5% increase to the base repair time for each floor above ground level and is presented graphically previously in Figure 11-10.

The total repair time sums both the connection and panel repair time throughout the structure. Shown in Figure 11-24 are the total repair times for each of the four connection types. The contribution to the total repair time from the panel and connection repair is shown

by the different shaded regions, with the panel contribution being the lower, dark coloured region and the connection contribution being the upper, lighter coloured region.

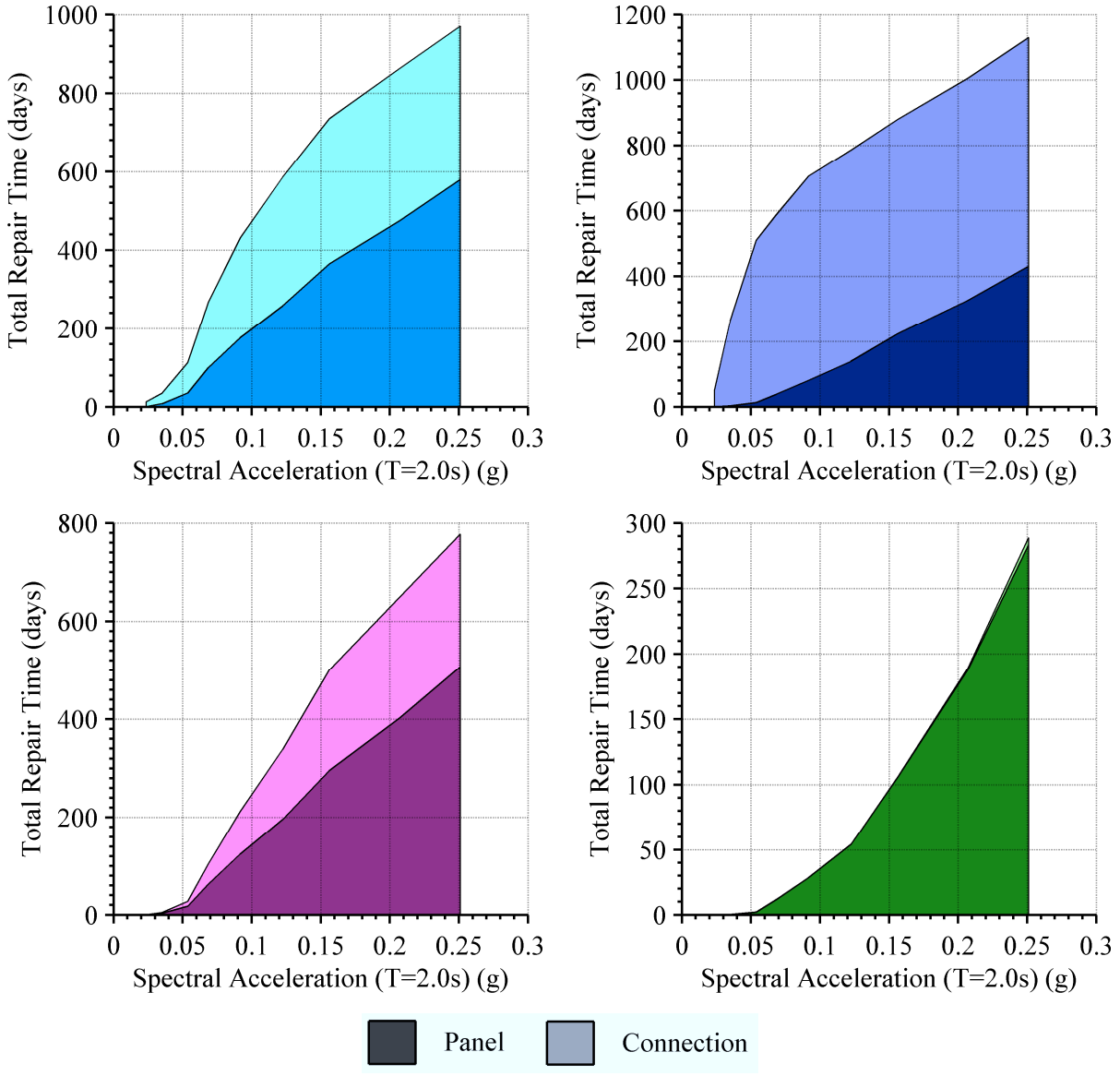

Figure 11-24: Total repair time of long threaded rod (top left), short threaded rod (top right), slotted connection (bottom left) and UFP (bottom right) cladding systems

It can be seen that the panel repair time makes up the majority of the repair time for the cladding systems that utilise long threaded rod connections, slotted connections and UFP connections. The total repair times for each of the four connections (including connection and panel repair time) are shown for comparison in Figure 11-25. Although cladding systems with short threaded rod connections predict the longest repair time, it can be seen that the difference in repair times is not as strongly dependent upon connection type when compared to the analogous figure for total repair cost, Figure 11-13. This showed that the expected repair cost for short threaded rods far exceeded the expected repair cost of the other

connection types. The total repair time for the UFP connections is significantly less than that of the other connection types.

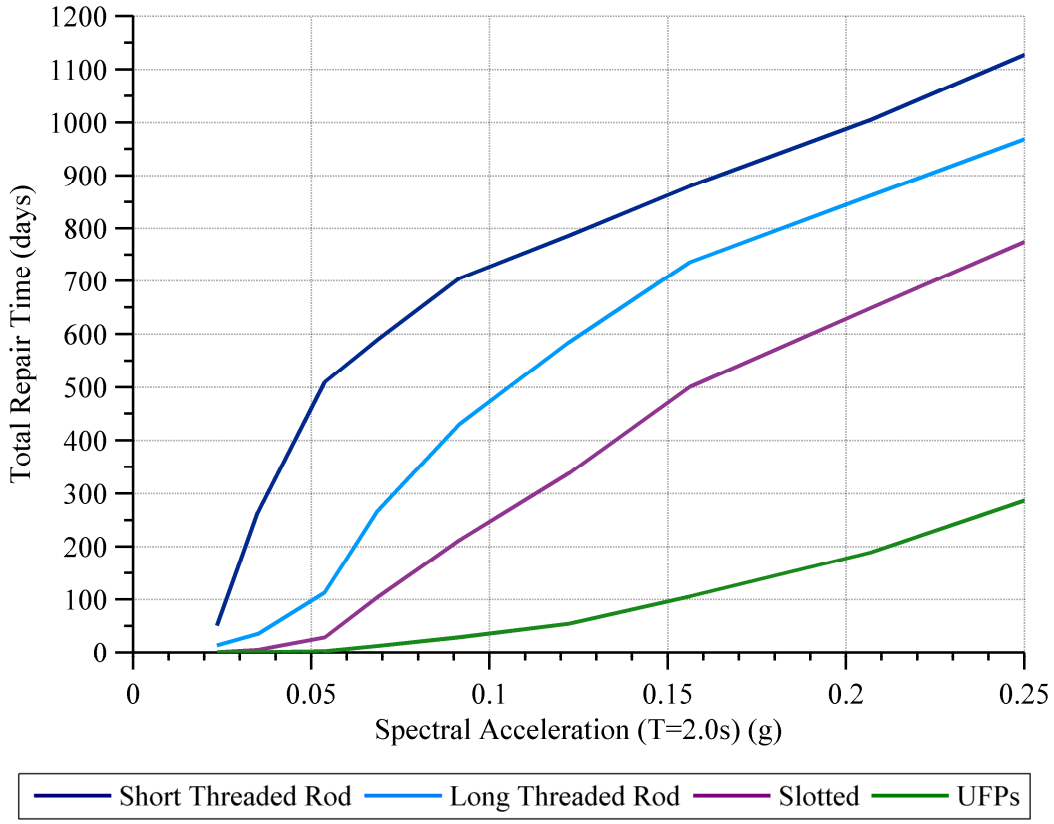

Figure 11-25: Comparison of total repair time for the four cladding systems

11.5.4 Repair Time Hazard

The repair time hazard is calculated similarly to the repair cost hazard and relates the likelihood of various levels of ground shaking at a site to the expected total repair time. It combines the expected repair time from a range of possible intensity levels. The repair time hazard is therefore defined as the integral of the probability of repair time for a given intensity measure multiplied by the incremental probability of that intensity measure occurring, as given by Equation (11-7).

$$\lambda_{RT} = \int_0^\infty P_{RT|IM}(rt|im) \left| \frac{d\lambda_{IM}(im)}{dIM} \right| dIM \qquad \textbf{(11-7)}$$

where

λ_{RT} = Annual frequency of exceedance of repair time

$P_{RT|IM}(rt|im)$ = Probability of repair time for a given intensity measure

$\frac{d\lambda_{IM}(im)}{dIM}$ = Incremental probability of a given intensity measure

The repair time hazard curves are presented in terms of the annual frequency of exceedance for each of the four connection types considered. The annual frequency of exceedance is equivalent to the reciprocal of the return period and has been presented here in logarithmic scale. The total repair time is presented in linear scale. Shown in Figure 11-26 are the total repair time hazard curves for each of the four cladding connection types considered.

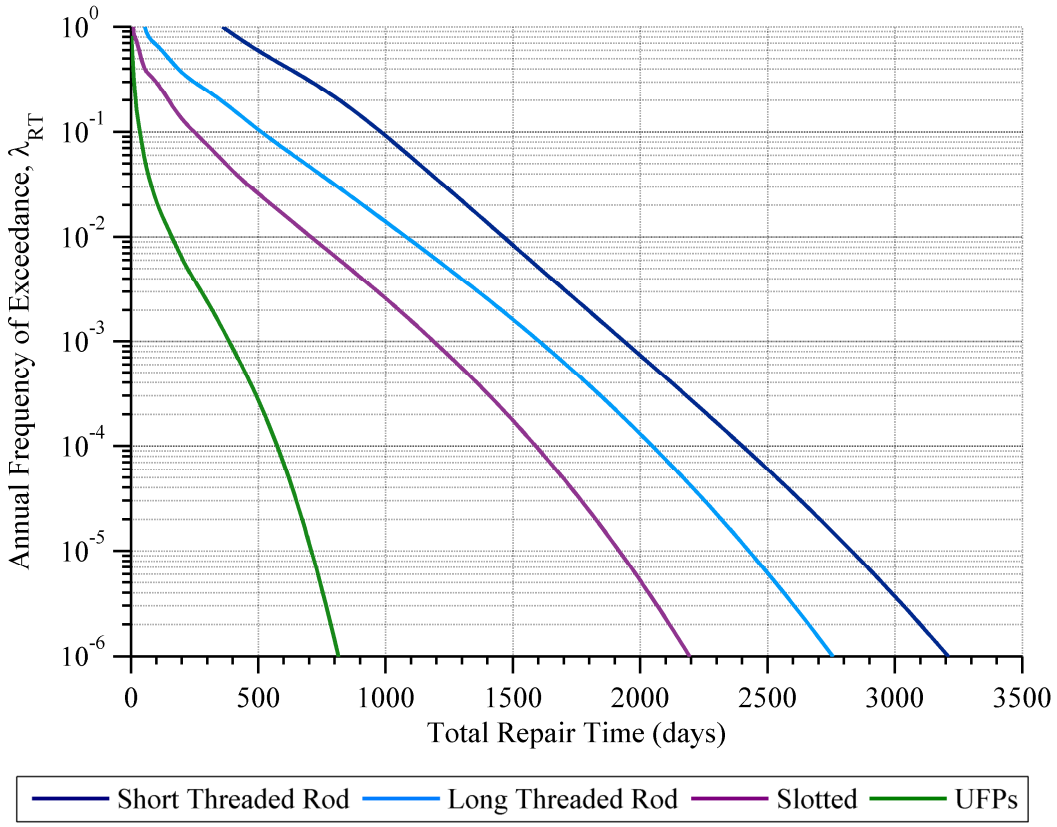

Figure 11-26: Comparison of repair time hazard curves for four cladding connections

The expected repair time for a building clad with short threaded rod connections is significantly greater than that of the other connection typologies. The total repair time for long threaded rod connections and slotted connections is approximately 75% and 55% that of short threaded rod connections. The total expected repair time for cladding systems utilising UFP connections is significantly less than that of the other connection types, on average 15% that of the short threaded rod connections. The total expected repair time at 50%, 10% and 2% probability of exceedance in 50 years are presented in Table 11-13.

Table 11-13: Expected cladding total repair time (days)

	Probability of Exceedance in 50 years		
Connection Type	**50%**	**10%**	**2%**
Long Threaded Rod	1000	1400	1800
Short Threaded Rod	1400	1800	2100
Slotted	600	1000	1400
UFP	100	300	500

11.6 Casualties

Building collapse is the principle cause of earthquake casualties (FEMA P-58-1, 2012). Casualties caused by building collapse are based on the probability of the building collapse for a given earthquake intensity and the estimated number of building occupants. The estimated building occupancy is determined using a population model based on the building type. Building population models are relatively well understood and consider the occupancy type of the structure for certain times of the day. Obviously for casualties associated with cladding failure, the risk is not to the building occupancy population but, rather to the footpath population. The building occupancy likely influences the footpath population, for example a large office building will undoubtedly have a large pedestrian population, however, a small residential property directly adjacent to an office building will have the same footpath population, therefore, it has been decided that basing footpath population on building occupancy is not a suitable model.

Common knowledge would suggest that a footpath population model would vary during the day. We would expect foot traffic to be highest during the morning and evening when people are going to and from work, as well as during lunch. Evidently, these periods of time are associated with the periods of time when vehicle movements are at their highest. Therefore, in order to develop a footpath population for casualty consequence calculation, it has been proposed to base the footpath population upon vehicle traffic data.

It should also be mentioned that the word ‘casualty’ has been deliberately chosen as it refers to both death and injury. Since many uncertainties surround the likelihood of death following a building or cladding collapse it has been decided to use the word casualty rather than assume some percentage of casualties are fatal.

11.6.1 Footpath Population Model

The link between vehicle movements and pedestrian movements is proposed by research undertaken by the U.S. Department of Transportation in order to estimate non-motorised travel data for infrastructure development (FHA, 1999). Obviously there are many factors to take into account, such as the walking environment, the walking route, climate, and the distance between likely walking destinations, however, on a basic level, the likely number of pedestrians can be linked to the likely number of vehicles in an urban setting.

The ratio of vehicle movements to pedestrian movements in an urban setting is typically around 10:1 (Bhat et al., 2005). This ratio holds true for Christchurch, the location of the case study structure, where walking is used for 9.3% of all trips in the Greater Christchurch area (CCC, 2012) in comparison with the car which is used for 85% of all trips. Based on the above, pedestrian movements on a street were taken to be 10% of the vehicle movements.

The time of day that pedestrian movements are made is believed to be closely proportional to vehicle movements. Therefore, the time of day of vehicle movements has been incorporated into the pedestrian population models developed. Vehicle movement data has been obtained from the Christchurch City Council, which provides public access to such information on its website (CCC, 2013).

As the pedestrian population models are based on an average ratio of pedestrian to vehicle movements, there may be significant inaccuracy in the pedestrian population on a case-by-case basis. To minimise this level of inaccuracy, three Christchurch CBD locations have been chosen to represent the location of the case-study structure in order to develop three different footpath populations. These locations have been chosen on streets that have large variation in the amount of vehicle movements to present a range of possible pedestrian populations. The quantity of movements for the three streets is herein described as busy, moderate and quiet. The three locations are shown in Figure 11-27 with the three respective streets being Lichfield Street (busy), Colombo Street (moderate) and Latimer Square (quiet).

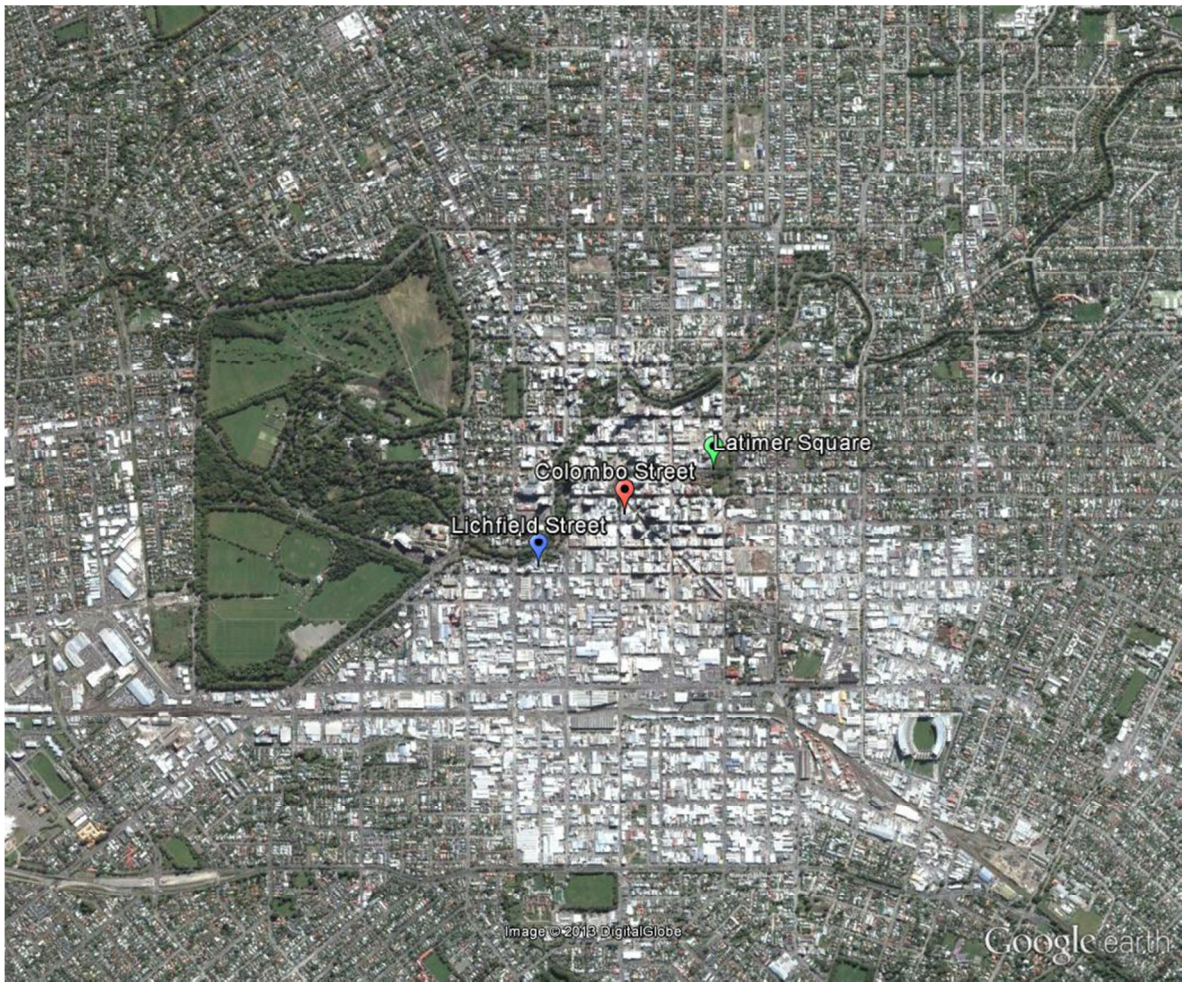

Figure 11-27: Location of three Christchurch CBD sites

The vehicle movements for each hour of the day are shown for these three sites in Figure 11-28. Seven lines are shown for each site representing the different days of the week. Evidently, the Lichfield Street site is the busiest, followed by Colombo Street and Latimer Square being the quietest.

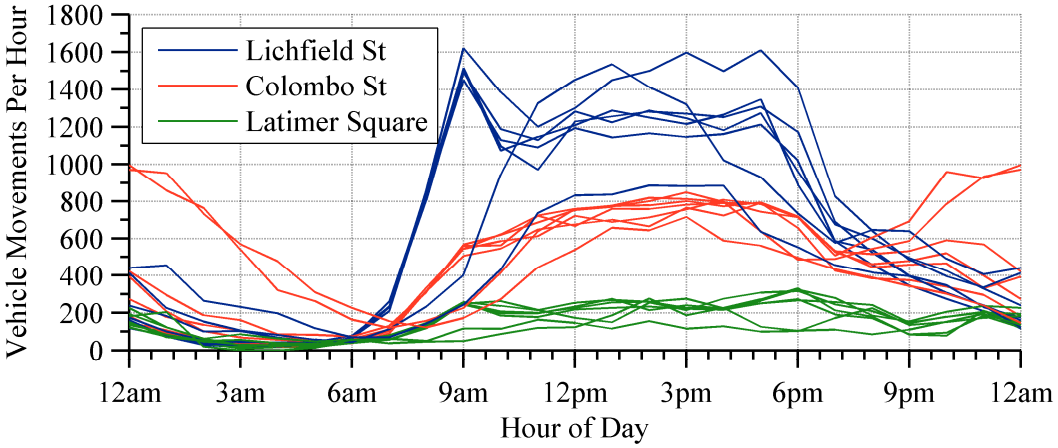

Figure 11-28: Vehicle movements per hour of three sites over a full week

Saturday and Sunday of the Lichfield Street site are easily distinguishable as they do not have a large peak around 9am due to the lack of commuter traffic at this time in the weekend. The Colombo Street site has significant movements on a Friday and Saturday night due to it being in the middle of the central city where bars and nightclubs are located. Vehicle movements on Latimer Square are relatively steady, with very few movements at night.

As introduced previously, the number of pedestrian movements per hour is assumed to be 10% of the vehicle movements per hour presented in Figure 11-28. The pedestrian population outside the case-study structure at any given time can be calculated since the building width occupies 30 m of footpath space and assuming a pedestrian is walking at 1.4 m/s (Levine & Norenzayan, 1999). The expected pedestrian population for each hour of the day is shown for the three sites in Figure 11-29.

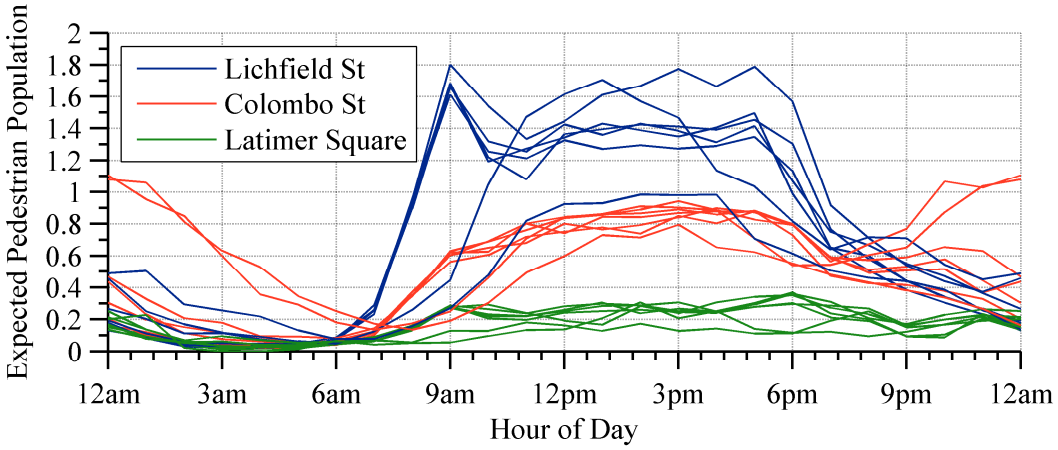

Figure 11-29: Expected pedestrian population of three sites over a full week

It can be seen that at any given time the number of pedestrians outside the building is expected to be between zero and two. Since this number is very low, when calculating the casualty risk, it has been decided to represent the expected pedestrian population in terms of the probability of an individual being present. This has been done using a Poisson distribution. The probability of at least one individual being present is shown in Figure 11-30 for each of the three sites for each hour of the day. It can be seen that there is a high probability of a pedestrian being present during the day for the Lichfield Street site but for the other sites it can be seen that the even if cladding failure were to occur there is a low probability that a pedestrian will be present.

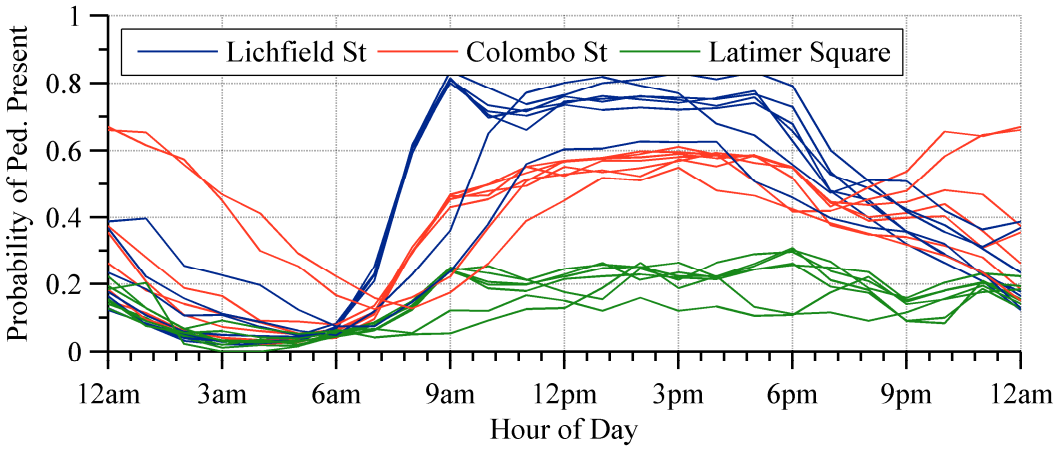

Figure 11-30: Probability of at least one pedestrian being present at three sites over a full week

11.6.2 Casualty Hazard

The casualty hazard is calculated based on the likelihood of various levels of ground shaking at a site, the relationship between the ground shaking and the seismic response, the relationship between the seismic response and the cladding performance and finally the relationship between the cladding performance and the pedestrian population. The casualty hazard is defined as the integral of the probability of a casualty for a given intensity measure multiplied by the incremental probability of that intensity measure occurring, as shown in Equation (11-8).

$$\lambda_C = \int_0^\infty P_{C|IM}(c|im) \left| \frac{d\lambda_{IM}(im)}{dIM} \right| dIM \qquad \textbf{(11-8)}$$

where

λ_C = Annual frequency of exceedance of pedestrian casualty

$P_{C|IM}(c|im)$ = Probability of pedestrian casualty for a given intensity measure

$\frac{d\lambda_{IM}(im)}{dIM}$ = Incremental probability of a given intensity measure

The steps used to determine the casualty hazard of earthquake induced cladding failure from a single building are summarised below:

1. Given the hazard level, a single ground motion is generated at a random time of the day and on a random day of the week;

2. Given this ground motion, the expected response of the structure is found using a non-linear response history analysis;
3. Given this response, the expected probability of a cladding connection failure is found;
4. Given the time of day and day of the week of the ground motion, the expected pedestrian population outside the structure is found based on the footpath population model;
5. Steps 1-5 are repeated 20 times using a newly generated ground motion to obtain a lognormal probability density function of the number of casualties based upon the expected pedestrian population and the probability of connection failure;
6. The probability of the casualty number exceeding a certain number is computed using this probability density function;
7. The probability in step 6 is multiplied by the incremental probability of that intensity level occurring. This is obtained directly from the seismic hazard curve.
8. Steps 1-7 are repeated for each intensity level considered and the result is summed

Rather than repeating the non-linear response history analyses that have been performed in previous chapters, the simulation will assume that the twenty ground motions selected are those that have already been analysed at each hazard level and thus the probability of cladding failure is already established. The simulation thus only requires that twenty different earthquake rupture times are generated and these compared with the expected pedestrian population. The probability of failure is calculated based on the probability that at least one panel has both cladding panel connections fail. Since it is assumed that if one panel fails and a pedestrian is present then they are killed, if more than one panel fails this does not affect the hazard calculation. The probability of at least one panel failing for each of the given hazard levels is shown in Figure 11-31 for both the long threaded rod (left) and short threaded rod connection (right). The data points from the analyses are presented along with the cumulative probability of connection failure in Figure 11-31 as a function of the spectral acceleration at two seconds.

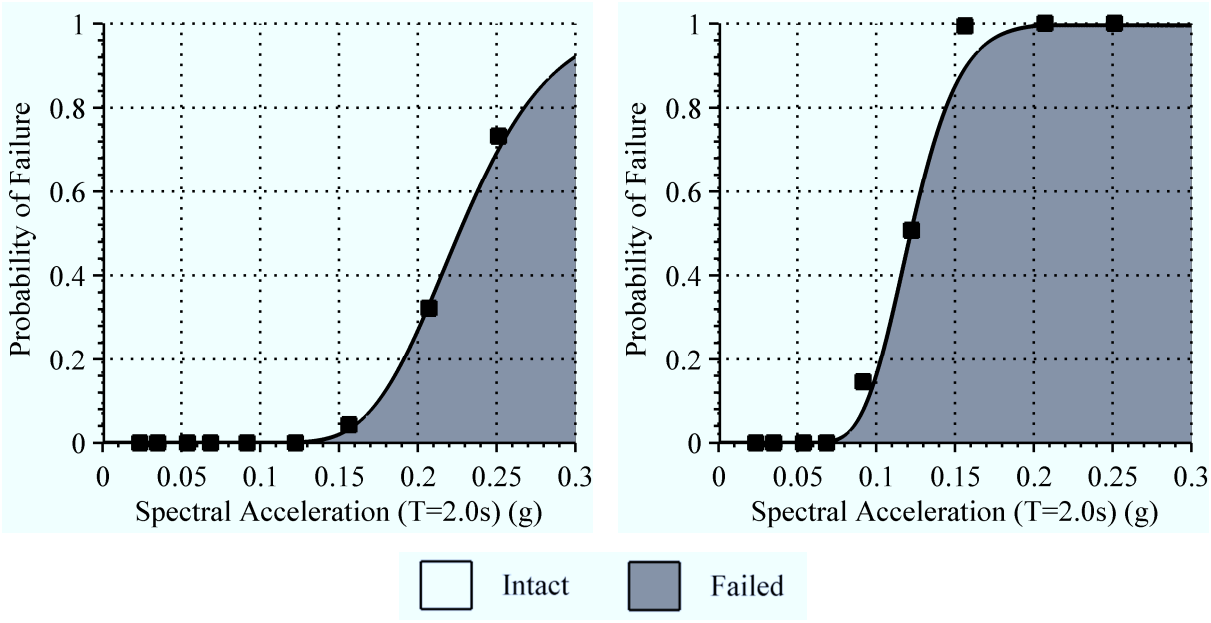

Figure 11-31: Connection failure probability of long threaded rod (left) and short threaded rod (right)

It is assumed that if a cladding connection failure occurs then any pedestrians present are casualties. The word 'casualty' has been deliberately chosen as it refers to both death and injury. Since many uncertainties surround the likelihood of death following cladding collapse it has been decided to use the word 'casualty' rather than assume some percentage of casualties are fatal. There is also some degree of uncertainty over whether the panel will indeed fall from the structure (several panels with fractured connections were observed in the post Christchurch assessment with panels that did not fall) but that has not been considered.

The casualty hazard curves are presented in terms of the annual frequency of exceedance for each of the three sites considered. The number of casualties is presented in linear scale. Shown in Figure 11-32 are the casualty hazard curves due to earthquake induced cladding failure from a single building with long threaded rod cladding connections. It can be seen that in a probabilistic sense, even when considering an annual frequency of exceedance of 10^{-6}, equivalent to a one million year return period, not a single casualty would be expected.

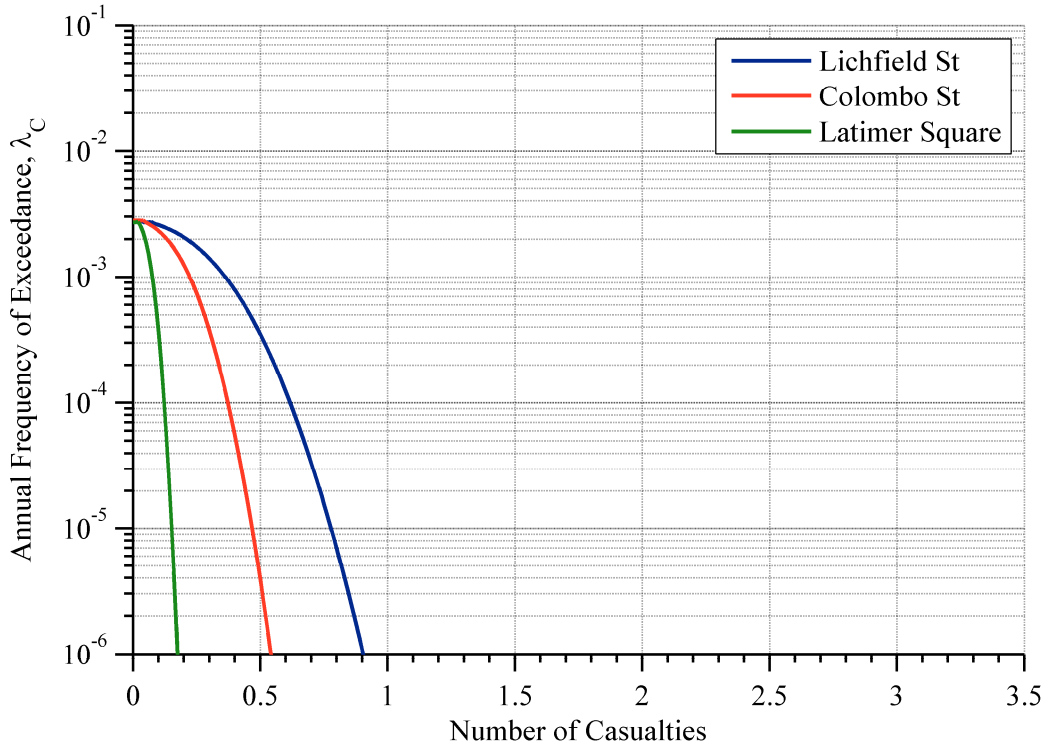

Figure 11-32: Casualty hazard curves for long threaded rod connection

The casualty hazard curves when considering the probability of earthquake induced cladding failure when short threaded rods connections are used are shown in Figure 11-33.

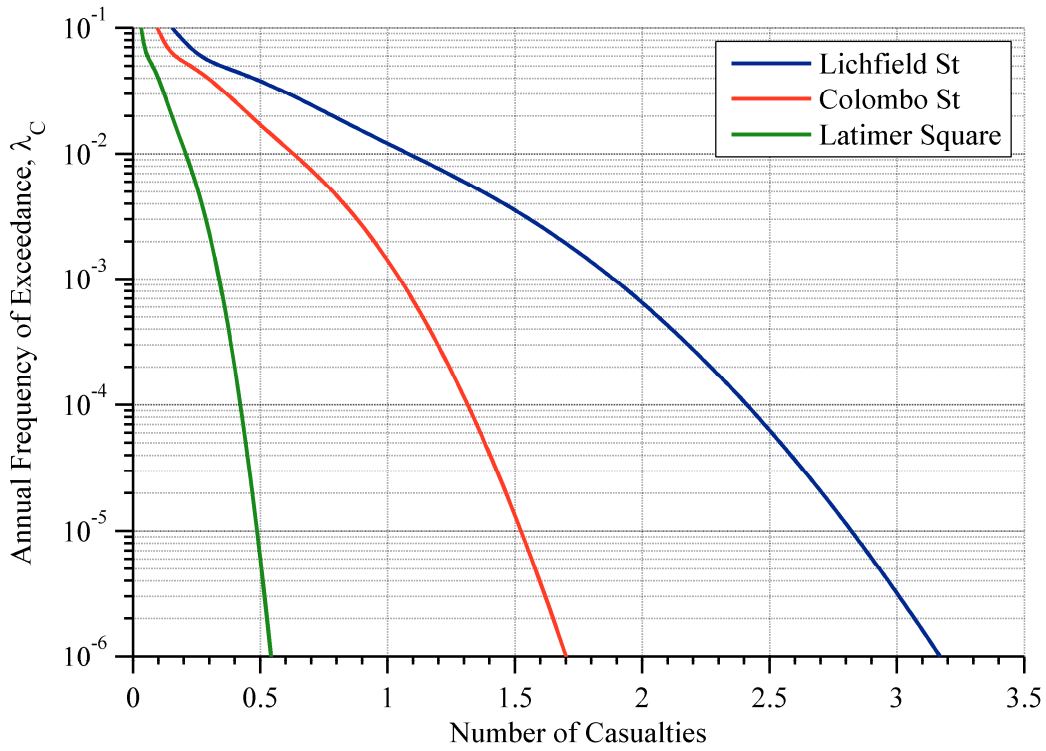

Figure 11-33: Casualty hazard curves for short threaded rod connection

The results for the short threaded rod connections register more meaningful levels of probability compared to that of the long threaded rod connections. It is possible to determine the annual frequency of exceedance that we would expect a given number of casualties. This information is more logical when presented in terms of probability of exceedance, as done so in Table 11-14 when considering a period of 50 years. This shows that there is a 45% chance that we would expect at least one casualty on Lichfield Street over 50 years. If we were to expect two casualties this reduces to a 3.9% probability and if we were to expect three or more, the probability is virtually negligible. When considering Colombo Street, there is a 9.1% probability of at least one casualty, but negligible probability of more than one. Finally, when considering Latimer Square, the probability of even a single death due to cladding failure is considered negligible. It is also worth noting that the probability of collapse of the structure in a 50 year period is less than 1%. Hence the risk to life safety inside the building is almost negligible, however, the risk to life safety outside the building is not insignificant.

Table 11-14: Probability of expected casualties in 50 years

	Number of Casualties		
Site	**1**	**2**	**3**
Lichfield Street	45%	3.9%	0.016%
Colombo Street	9.1%	-	-
Latimer Square	-	-	-

11.7 Conclusions

This chapter described the probabilistic seismic loss assessment (PSLA) of both traditional and innovative cladding systems. PLSA expresses the expected performance in terms of tangible outcomes, namely repair costs, repair time and casualties. Estimates of potential repair costs and repair time were found using the cladding fragility functions developed in previous chapters combined with loss consequence functions. Loss consequence functions are relationships that indicate the potential distribution of losses as a function of damage state. These were developed based on repair data obtained after the Canterbury earthquakes in combination with discussions with professionals including contractors, quantity surveyors, and engineering consultants. Repair costs and repair times were based upon all of the necessary construction activities to return the damaged cladding panel or cladding connection to its pre-earthquake condition. These activities were established for each damage state of the cladding panel and connection, respectively.

The mean cost to repair cladding connections was found to be between $1,000 and $10,000 depending on the level of damage. The general shape of the expected repair cost function was found to be the same for each cladding connection type, with the highest repair costs being for the short threaded rod connection type. The expected repair cost for the long threaded rod connection was on average 47% of that of the short threaded rod connections. The expected repair cost of the slotted connections was on average 23% that of the short threaded rod connections. It was also found that the expected repair cost associated with UFP connections is virtually negligible for all of the levels of spectral acceleration considered.

The mean cost to repair cladding panels was found to be between $350 and $3,600 depending on the level of damage. Only two levels of damage were considered, as found from the experimental testing undertaken in previous chapters. Again, short threaded rod connections resulted in the highest repair costs. The panel repair costs when connected with long threaded rod connections were found to be on average 66% of that when connected with short threaded rods. The panel repair costs when connected with slotted connections were on average 48% of that when connected with short threaded rods. Finally, the panel repair costs when connected with UFP connections were on average 20% of that when connected with short threaded rods.

The total repair costs summed both the connection and panel repair costs throughout the structure. At the maximum seismic hazard level considered, the expected repair cost for a building clad with cladding panels connected with short threaded rod connection was found to be $775,000. For the long threaded rod connections, slotted connections and UFP connections, this total repair cost was found to be $400,000, $315,000 and $80,000, respectively.

The time to repair the cladding was calculated in a similar way to the repair cost. This study focussed solely on the time needed to return the cladding back to its undamaged state. This portion of time is often referred to as the rational downtime component, and although seemingly straightforward, this repair effort is still highly variable depending on the repair scheme and will vary from one owner to another. The remaining portion of building downtime is difficult to model because it is highly dependent on irrational components, which include financing, relocation of functions, human resources, and economic and regulatory uncertainty. This study did not capture these aspects since these irrational components are strongly dependent upon not only the cladding damage, but the entire extent of damage throughout the building.

The mean time to repair the cladding connections was found to be between 3.5 and 12.0 days depending on the level of damage. The shape of the repair time functions were very similar to those developed for repair cost, particularly when comparing the various connection types. The mean time to repair cladding panels was found to be between 2 and 6 days, depending on the level of damage.

The total repair time summed both the connection and panel repair time throughout the structure. At the maximum seismic hazard level considered, the expected repair time for a building clad with cladding panels connected with short threaded rod connection was found to be 1,100 days. For the long threaded rod connections, slotted connections and UFP connections, this total repair time was found to be 970, 780 and 290 days, respectively.

Finally, the casualty loss assessment was undertaken based on expected footpath population models. Three footpath population models were developed for different Christchurch CBD sites based on vehicle traffic data. Based on the cladding connection failure fragility data, the casualty hazard of earthquake induced cladding failure was calculated. The results showed there was only a measureable chance of a casualty resulting from cladding failure when short threaded rod connections were used. The casualty hazard function showed a 45% chance that at least one casualty would result from cladding failure on the Lichfield Street CBD site over 50 years. This reduces to a 3.9% probability for two or more casualties. When considering the Colombo Street CBD site, there is a 9.1% probability of at least one casualty, but negligible probability of more than one. Finally, when considering Latimer Square, the probability of even a single death due to cladding failure is considered negligible.

The explicit loss consequences (casualties, repair cost and repair time) may be viewed as the ultimate measure of seismic performance for decision making. These showed that short threaded rod connections present significantly greater risk of losses compared to the other connections. Slotted connections and long threaded rod connections had similar expected losses, and UFP connections had significantly lower risk of losses.

11.8 References

Bhat, C. R., Guo, J. Y., & Sardesai, R. (2005). Non-Motorized Travel in the San Francisco Bay Area. Department of Civil Engineering: University of Texas.

Bradley, B. A. (2009). *Structure Specific Probabilistic Seismic Risk Assessment.* Ph.D. Thesis, University of Canterbury, Christchurch, New Zealand.

Bradley, B. A., Dhakal, R. P., Cubrinovski, M., MacRae, G. A., & Lee, D. S. (2009). Seismic loss estimation for efficient decision making. *Bulletin of the New Zealand Society of Earthquake Engineering, 42*(2), 96-110.

Carr, A. J. (2010). *Ruaumoko Programme for Inelastic Dynamic Analysis - User Manual*: Department of Civil Engineering, University of Canterbury, New Zealand.

CCC. (2012). Greater Christchurch Travel Demand Management Strategy and Action Plan. Urban Development Strategy: Christchurch City Council, Environment Canterbury.

CCC. (2013). Traffic Volume Count Retrieved 8th August 2013, from http://www.ccc.govt.nz/cityleisure/projectstoimprovechristchurch/transport/trafficcount/index.aspx

Comerio, M. C. (2006). Estimating downtime in loss modeling. *Earthquake Spectra, 22*.

Comerio, M. C., & Stallmeyer, J. C. (2002). *Nonstructural loss estimation: the UC Berkeley case study*: Berkeley: Pacific Earthquake Engineering Research Center, University of California.

FEMA P-58-1. (2012). Seismic Performance Assessment of Buildings *Volume 1 - Methodology*. Washington, DC., USA: Federal Emergency Management Agency.

FHA. (1999). Guidebook on Methods to Estimate Non-Motorized Travel: Overview of Methods. McLean, VA., USA: U.S. Department of Transportation, Federal Highway Administration.

Krawinkler, H., & Miranda, E. (2004). Performance-based earthquake engineering *Earthquake Engineering: From Engineering Seismology to Performance-Based Engineering*. Boca Raton, FL., USA: CRC Press.

Levine, R. V., & Norenzayan, A. (1999). The Pace of Life in 31 Countries. *Journal of Cross-Cultural Psychology, 30*(2).

Mitrani-Reiser, J. (2007). *An Ounce of Prevention: Probabilistic Loss Estimation for Performance-based Earthquake Engineering.* Ph.D. Thesis, California Institude of Technology.

Moehle, J., & Deierlein, G. (2004). *A Framework Methodology for Performance-Based Earthquake Engineering.* Paper presented at the 13th World Conference on Earthquake Engineering, Vancouver, British Columbia, Canada.

12 Conclusions and Recommendations for Future Work

12.1 Introduction

Recent earthquakes have placed a greater demand on engineers to provide societies with high performing structures that are able to minimise damage and business interruption following a major earthquake event. This demand has been the driving force behind considerable research over the past two decades. Consequently, it is evident that significant progress has been made in recent years towards the development of low damage structures as well as in modelling and predicting the performance of structures during earthquakes. However, despite the enormous contribution of non-structural components to total economic losses, non-structural components have received much less attention.

While there is greater recognition within the engineering community that non-structural damage is an important issue, the development of methods to assess non-structural damage as well as the technical solutions to prevent such damage is lacking. This is believed to be due to a lack of understanding, a lack of solutions and a reluctance of ownership in regards to the performance of non-structural elements.

This research has provided an experimental and analytical investigation into the seismic behaviour and performance of cladding systems. The key outcomes from this research are summarised in this chapter. Limitations to the research are also identified and finally, recommended future work is suggested.

12.2 Research Objectives

The holistic objective proposed in the opening chapter of this thesis was to better understand the performance of cladding systems in earthquakes, the losses associated with

this performance and propose solutions to reduce such damage. Eight key objectives were identified as necessary to achieve these overall research goals. These were as follows:

1. Collate the current state-of-art relating to the seismic performance of cladding systems;
2. Identify the most hazardous cladding systems that require research attention;
3. Experimentally gain a better understanding of the seismic behaviour of cladding components and their interaction with the structure;
4. Develop simple modelling tools for the assessment of cladding performance, including the implementation in numerical building models;
5. Examine the dynamic behaviour of cladding systems and their influence upon the structure using robust numerical modelling methods;
6. Quantify the expected seismic performance of cladding systems using qualitative damage limits;
7. Propose and evaluate innovative low-damage cladding system solutions;
8. Collect seismic loss data to perform probabilistic seismic loss assessment of cladding systems.

The previous eleven chapters have explored each of these objectives, with particular respect to the in-plane response and performance of precast concrete cladding systems. By limiting the research to a single cladding typology, it was possible to investigate the system following through the entire performance based seismic assessment process. Various other cladding systems can subsequently be investigated following the same process presented here.

12.3 Research Conclusions

The main conclusions from this research are presented here in relation to the seven key objectives stated above.

Collate the current state-of-art relating to the seismic performance of cladding systems

Previous research has shown that cladding has an influence on the behaviour of the structure it is attached to. This includes the free vibration characteristics of the structure, the displacement of the structure under static loading and the displacement of the structure under dynamic loading. Analytical research showed that cladding can decrease the translational

periods by up to 34% and the torsional periods by up to 48%. Various other studies also showed the potential lateral stiffening effect cladding has to a bare frame structure. However, several flaws were identified in the methods used to illustrate the stiffening effect of cladding. These were typically attributed to simplifications made in the modelling approach, or due to erroneous assumptions made in the modelling of the cladding. The majority of previous research also concluded that the seismic performance of cladding is most dependent on the connection between the cladding and structure.

Finally, research has shown that direct replacement costs of cladding only forms a small part of the total damage cost. This total damage cost includes the loss of function, repair costs and repair time. Such indirect costs can be two to three times the cost of replacing the damaged structure. Consequently, cladding systems in low-moderate seismic regions still require attention even in situations where the risk of structural damage appears very low.

Identify the most vulnerable cladding systems that require research attention

The seismic vulnerability of cladding systems was established through a desktop background study, literature review, and post-earthquake reconnaissance survey of their seismic performance. A cladding classification framework was proposed for assessing the seismic performance of cladding systems. This classification framework was a necessary step in order to simplify the task of assessing the multitude of cladding systems and arrangements that exist. The proposed classification system categorises cladding systems according to the cladding typology, cladding panel modularity, connection typology and connection modularity.

A survey of 217 buildings and their 266 respective cladding systems showcased all types of damage to all the different typologies of cladding systems. The poorest performing cladding system was frameless glazing; with 50% of systems being categorised as having a Hazards Reduced performance level.

It was evident that many cladding connections did not have adequate movement allowance. Several slotted connections were also welded in place, eliminating the ability of the cladding to accommodate earthquake movement.

Unfortunately the failure of heavy cladding panels on one building within the Christchurch CBD caused the panels to fall onto a car parked below, killing its occupant. This cladding system was identified as posing the most significant hazard to life-safety. Heavy cladding panels are also often included within a structural engineer's scope of work so

it was believed that addressing their performance provides the most immediate benefit to the earthquake engineering community.

Experimentally gain a better understanding of the seismic behaviour of cladding components and their interaction with the structure

Traditional heavy cladding panel connection typologies (tie-back rod and slotted) were tested in order to investigate the effect of heavy cladding systems upon the lateral resistance of a typical reinforced concrete frame. A test frame which represents a single-storey, single-bay portion of a reinforced concrete building was used to test the cladding systems. The cladding-frame system was tested under uni-directional quasi-static cyclic loading.

The magnitude of the lateral resistance provided by the cladding was found to vary significantly depending on the type of top connection used. The minimum lateral force provided by the cladding was found to be 5.6 kN. The maximum lateral force provided was found to be 62.0 kN. When slotted connections were used, the cladding added between 7.0 – 52.0 kN to the lateral resistance of the frame.

Long threaded rods were repeatedly found to fail during the 1.5 – 2.0% inter-storey drift cycles of the test frame. No connection failure was observed in the slotted connections, even when the slot length was exceeded over multiple cycles. Short threaded rods were also found to repeatedly fail during the 1.5% drift cycle. However, it was also observed that the cladding panel underwent significant lateral deformation during the testing of the short-threaded rod connections. Consequently, the 1.5% drift of the frame was accommodated both by deformation of the connections and the cladding panel. This mechanism was likely critical in order for the short threaded rods to not fail until a drift of 1.5%.

Develop simple modelling tools for the assessment of cladding performance, including the implementation in numerical building models

Analytical derivations based on fundamental engineering principles were used to derive modelling parameters of cladding connections and cladding panels. However, analytical models were not always able to accurately represent all of the parameters necessary to develop the cladding models. Therefore, finite element analyses of cladding components were also used to expand the experimental dataset.

The suitability of the proposed modelling parameters was verified by developing numerical models in the seismic response analysis programme Ruaumoko2D to represent the cladding systems tested experimentally. Two types of cladding models were then

implemented into the test frame model: the quadrilateral model and the spring model. The quadrilateral model requires less derivation but is more computationally expensive, whereas the spring model requires more derivation but is computationally efficient.

The force-displacement results were compared against the experimental behaviour. A good to excellent fit was observed for all for all of the connection types considered, with the numerical model capturing the increase and strength and stiffness the connections to the system. The failure of the connections when the 1.5% drift cycle was exceeded was also captured. However, the models were unable to capture the non-linear degradation of the cladding panel strength and stiffness.

Examine the dynamic behaviour of cladding systems and their influence upon the structure using robust numerical modelling

The cladding models developed were implemented into a 2D model of a theoretical reinforced concrete structure. A total of 18 frame model configurations with cladding were examined. The 18 frame models included the three cladding configurations (mono panel, dual panel and fully clad), two cladding models types (quadrilateral and spring) and three connection hysteretic rules (long threaded rod, short threaded rod, slotted).

Static push-over analyses showed that the inclusion of cladding increases the base shear by between 3 – 17% depending on the connection typology used. The inclusion of cladding was found to increase the stiffness of the frame by between 4 – 28%. Accordingly the inclusion of cladding in the modal analysis of the structure resulted in the peak floor displacements reducing by 6 – 7% and the peak floor forces increasing by 10 – 13%.

The inclusion of cladding caused an increase in base shear of between 2 – 12% when subject to the same ground motion record using response history analyses. Minimal reductions in maximum and residual inter-storey drifts were observed for the clad frame cases. The cladding presence also had a negligible influence upon the structure's maximum floor accelerations, regardless of the connection type or earthquake intensity.

Investigation of the maximum lateral displacements demands observed in the cladding connection and cladding panel revealed that the sum of these dynamic displacement demands exceeded the inter-storey displacement demand of the structure. This research showed that an amplification factor of between 1.25 – 1.60 should be used to determine the maximum cladding system displacement demand in relation to the maximum inter-storey drift.

It was also found that the cladding connection acceleration varied from between 80 – 120% of the floor acceleration. This result was not highly dependent upon connection type,

intensity level or floor height. This result suggests that the acceleration demand provided by Section 8 of NZS 1170.5 (2004) which multiplies the peak ground acceleration by an acceleration coefficient may be overly conservative for determining in-plane cladding acceleration demands.

Quantify the expected seismic performance of cladding systems using qualitative damage limits

The expected damage to both the structure and cladding was quantified using a performance-based assessment methodology. This methodology calculates the probability of exceeding a specified level of demand which corresponds to a qualitative level of damage. It was observed that all of the clad frame configurations reduced the expected quantity of structural damage for the same seismic demand. This reduction agrees with the result found previously that the presence of cladding reduces inter-storey drifts. This is because beam and column curvatures are intrinsically linked to frame deformation.

The expected damage to the cladding components showed that significantly higher levels of damage are expected in the cladding connections compared to the structure for the same level of hazard. Most notably, the probability of failure in the connection is significantly greater than failure of the beams. This result is not irrational, as if the beams fail, then structural collapse may be imminent and the performance of other structural and non-structural components is irrelevant. Conversely, failure of the cladding connections will most likely have no effect upon the performance of the structure. Hence it is entirely practical to expect a lower probability of structural failure than cladding failure. However, the proportion of damage is much less practical. For example, the probability of the beams in the third floor being deemed Immediate Occupancy is 56% for a 2% in 50 year seismic event, whereas, the probability of the cladding connections being in the same performance level is zero. This result tells us that there is a 56% chance that the structure will be able to be occupied without the need for structural repair, but that repair of the cladding will essentially be a certainty.

Propose and evaluate innovative low-damage cladding system solutions

Instead of attempting to isolate the structure-panel interaction, it has been proposed to instead take advantage of the cladding to form an integrated building-cladding system. Such a system is here deemed to be an ‘innovative’ cladding system. The following requirements were proposed for a cladding connection to be deemed an innovative connection:

- Low-damage, i.e. able to withstand multiple seismic events without the need for repair or replacement;
- Cost comparable to a traditional cladding connection;
- Flexible and simple in its design and implementation;
- Able to provide a positive value to the seismic performance of the structure.

The U-shaped flexural plate (UFP) was selected to determine its suitability as a possible innovative cladding connection. UFPs are a form of flexural dissipator which utilise the post-yield ductility of steel to dissipate energy. Component testing found that the UFPs produced a stable hysteretic loop with the maximum force in a single UFP of approximately 12.5 kN. The shape of the UFPs was also found to not change significantly during testing. Full-scale testing was subsequently carried out which utilised the UFP as the top connection between precast concrete cladding panels and the test-frame structure. UFPs produced stable hysteretic behaviour and were able to withstand large displacements while transferring limited force into the cladding.

Finite element modelling was undertaken in order to develop parameters that defined the non-linear behaviour of UFPs. Non-linear parameters based on the Ramberg-Osgood function were proposed and verified to provide all of the necessary information required to model UFPs as cladding connections.

The seismic performance of UFP cladding connections was examined using two theoretical design cases. Static analyses showed that the inclusion of UFP cladding systems increased the stiffness of the case-study building by between 22% and 32%. Dynamic analyses showed that the inclusion of the cladding system increased the base shear by between 8 – 13% and reduced the inter-storey drift by between 18 – 30%. Similarly to that found for traditional connections, the UFP connections had a very minimal influence upon the structure's maximum floor accelerations and residual drifts.

The use of UFP cladding connection reduced the probability of beam damage being deemed Life Safety level or worse by between 14% and 29% for a 2%/50 year seismic event. This is a significant improvement and confirms that as well as being low-damage, UFP connections can theoretically provide positive value to a structure by improving its seismic performance. However, the use of innovative cladding connections must be applied with care, due to the stiffening effect of the cladding possibly leading to undesired damage mechanisms, such as soft-storeys. It is recommended that a significant degree of conservatism be taken

when the designer intends for the cladding to contribute to the lateral resistance of the structural system, particularly if seeking a low-damage outcome.

Collect seismic loss data to perform probabilistic seismic loss assessment of cladding systems

Probabilistic seismic loss assessment (PSLA) was used to compare the performance of both traditional and innovative cladding systems in terms of tangible outcomes, namely repair costs, repair time and casualties. This was based on repair data obtained after the Canterbury earthquakes in combination with discussions with professionals including contractors, quantity surveyors, and engineering consultants. Repair costs and repair times were based upon all of the necessary construction activities to return the damaged cladding panel or cladding connection to its pre-earthquake condition. These activities were established for each damage state of the cladding panel and connection, respectively.

The mean cost to repair cladding connections was found to be between $1,000 and $10,000 and the mean time between 3.5 and 12.0 days depending on the level of damage. At the maximum seismic hazard level considered, the total repair cost for a building clad with heavy cladding panels connected with short threaded rod connection was found to be $775,000. For the long threaded rod connections, slotted connections and UFP connections, this total repair cost was found to be $400,000, $315,000 and $80,000, respectively. Similarly, the expected repair time considering short threaded rod connection was found to be 1,100 days. For the long threaded rod connections, slotted connections and UFP connections, this total repair time was found to be 970, 780 and 290 days, respectively.

Finally, the casualty loss assessment was undertaken based on expected footpath population models for different Christchurch CBD sites. The results showed there was only a measureable chance of a casualty resulting from cladding failure when short threaded rod connections were used. The casualty hazard function showed a 45% chance that at least one casualty would result from cladding failure on the Lichfield Street CBD site over 50 years. This reduces to a 3.9% probability for two or more casualties.

The explicit loss consequences (casualties, repair cost and repair time) showed that short threaded rod connections present an unacceptably high level of risk compared to the other connections. Slotted connections and long threaded rod connections had similar expected losses and UFP connections had significantly lower losses compared to all of the connections considered.

12.4 Recommendations for Future Research

As mentioned in the opening of this thesis, the myriad of increasingly complex and costly non-structural systems in modern buildings will continue to present new challenges to improving the overall seismic performance of buildings. While this research aims to provide a step towards simplifying and solving some of these challenges, there is obviously a significant amount of further research required. Some specific aspects that have been identified from this thesis are listed below:

- The characteristics of the cladding components have been determined using only quasi-static cyclic loading. Far more dynamic cyclic test data is required to understand the degradation and damping characteristics of these components, particularly the cladding connections. It is recommended that varying loading protocols are used to gain a broader understanding of how displacement demands determine the performance of cladding components.
- Furthermore, this research focussed solely upon the in-plane displacement demands upon cladding systems. It is vital that future research also considers out-of-plane demands to provide a complete picture of the seismic performance.
- Both structural and cladding performance has been quantified here using the maximum deformation demand upon each component. This does not in any way consider cumulative demands and further research is required to understand how such cumulative demands equate to damage. Energy analysis methods provide one possible means for quantifying these cumulative demands. Preliminary results from this research indicate that the additional hysteretic damping provided by UFP cladding connections can significantly reduce the total structural hysteretic energy demands upon a structure. Further research is necessary in order to quantify to what extent these reductions in hysteretic energy equate to damage reduction.
- It is recommended that the low-cycle fatigue characteristics of threaded rod-connections are further explored. This would provide opportunities to define the connection damage states in a more accurate way. This research assumed that the connection damage (performance level) was dependent upon only the connections peak displacement demand. A more useful representation of the level of damage may be a measure of the residual capacity of the connection. It is possible this could be based on low-cycle fatigue characteristics.

- The modelling parameters were verified based on the experimental tests undertaken. Further verification of these parameters using other experimental testing would be very useful to determine their suitability and reliability.
- The cladding models proposed are believed to be relatively straight-forward for a user familiar with structural modelling software such as Ruaumoko or OpenSees, however, the future development and verification of cladding models in mainstream software, such as ETABS or SAP2000, would be highly recommended in order to provide a greater number of users with tools they can implement in software that they are familiar with.
- The case-study building chosen for quantifying both the structural and cladding performance was that of a concrete moment resisting frame. This building is often used for research purposes since it serves as a design example for the New Zealand Concrete Code (NZS 3101, 2006). Future research should consider a greater range of structural typologies. Moment frames are a flexible structural system and so future research should consider stiffer structural systems, such as wall dominant structures.
- Although originally envisaged as a new-design solution, innovative cladding connections could also theoretically be employed as a retrofit solution as a way of providing additional stiffness and damping to a structure. Further research, including dynamic testing, is necessary to provide assurance that the UFP cladding connections is a viable retrofit solution.
- Research into UFPs has predominantly considered their performance when subjected to low-cycle, high-strain demands. Further research into the medium to high-cycle fatigue performance of UFPs is required.
- The repair cost and repair time data obtained following the Canterbury earthquakes is limited and sometimes based on a single quote. It is critical that this data is scrutinised and refined upon in future research in order to provide more reliable loss assessment outcomes.
- Finally, this research focussed predominantly upon two precast concrete cladding panel systems. Consequently, it is recommended that future research consider different cladding panel configurations, e.g. column cover and beam spandrel arrangements, as well as various other cladding system typologies.

12.5 Closure on Improving Non-structural Seismic Performance

The requirement to coordinate with many people, across many different disciplines, such as designers, engineers, architects, manufacturers and contractors, will continue to present a significant hurdle to improving non-structural seismic performance. One of the outcomes from the Canterbury Earthquakes Royal Commission was that engineers and architects should collaborate to minimise the potential distortion applied to non-structural elements. This is a clear recognition of the improvements that can be made by simply coordinating better. Advances in computer technology, such as the introduction of Building Information Modelling (BIM), will be hugely influential in helping to improve this coordination.

Post-earthquake functionality and operability will not be delivered until effective strategies are devised to minimize non-structural damage. It is the author's opinion that technical solutions alone will not solve all of the issues regarding non-structural damage. It is essential that equal effort is also directed at improving all aspects of the construction industry involved with non-structural elements.

Appendix A: Cladding Damage Survey Form

Facade Damage Assessment Form

New Form

Submit

Building Identification

Date And Time: ID:

Building Name: Number of Storeys:

Address: Building Size: x

Built Between: and

Structural Typology: ○ Concrete Shear Wall ○ Reinforced Masonry ○ Steel ○ Concrete Moment Frame ○ Unreinforced Masonry

Structural Regularity: ○ Yes ○ No

Occupancy Type: ○ Commercial ○ Residential ○ Industrial

Structural Assessment: ○ Green ○ Yellow ○ Red ○ N/A

Facade Classification

Facade Type A: ○ Curtain wall ○ Stick curtain ○ Double skin ○ Frameless glazing ○ Monolithic cladding ○ Heavy panels ○ Masonry veneer ○ Lightweight panels

Facade Type B: ○ Curtain wall ○ Stick curtain ○ Double skin ○ Frameless glazing ○ Monolithic cladding ○ Heavy panels ○ Masonry veneer ○ Lightweight panels

Facade Modularity: ○ Low ○ Medium ○ High

Connection Type: ○ Metal Angle ○ Sub-frame ○ Direct Attachment ○ Unknown Other:

Connection Modularity: ○ Discrete ○ Continuous ○ Unknown

Facade Age: ○ Same as Building ○ Retrofitted ○ Unknown

Facade Damage

Damage Visible: ○ Yes (A) ○ Yes (Both) ○ No

Level of Damage: ○ Minor (easily repairable, e.g. broken seals) ○ Moderate (significant repairs required) ○ Severe (large repairs / complete failure)

Approximate % of Damage:

Vertical Damage Distribution: ○ Lower ○ Middle ○ Upper ○ Even

Horizontal Damage Distribution: ○ Corner ○ Central ○ Even

Description of Damage: ○ Connection Damage ○ Cladding Damage ○ Connection Failure ○ Cladding Failure

Glazing Damage: ○ Cracked ○ Broken/Fallen ○ N/A ○ No

Comments:

Appendix B: Cladding Damage Survey Data

Building Information									
ID	Number	Street	Name	Placard	Number of Stories	Built Before	Building Type	Occupancy Type	Info
1	78	Park Terrace	Terrace on the Park A	Red	8	2010	Concrete Frame w/ Concrete Shear Walls	Apartment	
2	78	Park Terrace	Terrace on the Park B	Red	5	2010	Concrete Frame w/ Concrete Shear Walls	Apartment	
3	78	Park Terrace	Terrace on the Park C	Red	10	2010	Concrete Frame w/ Concrete Shear Walls	Apartment	
4	78	Park Terrace	Terrace on the Park D	Red	5	2010	Concrete Frame w/ Concrete Shear Walls	Apartment	
5	15	Peterborough St	The Peterborough Apartments	Green	5	2000	Concrete Frame w/ Masonry Walls	Apartment	
6	91	Victoria St	Victoria Mansions	Yellow	4	1940	Concrete Frame w/ Concrete Shear Walls	Apartment	
7	89	Victoria St	Argosy House	Red	4	1990	Concrete Frame w/ Masonry Walls	Retail	
8	99	Victoria St	Abley Consultants	Yellow	4	1980	Concrete Frame w/ Masonry Walls	Office	
9	123	Victoria St	Cranfields	Yellow	7	1990	Concrete Frame w/ Concrete Shear Walls	Office	Drawings
10	133	Victoria St	Murray & Company	Yellow	6	2010	Concrete Frame w/ Masonry Walls	Office	
11	104	Victoria St	Wise Group	Yellow	5	1990	Concrete Frame w/ Concrete Shear Walls	Office	
12	110	Park Terrace	Dorset Towers	Red	8	1990	Reinforced Masonry	Apartment	
13	82	Park Terrace	Unknown	Green	4	2010	Unknown	Apartment	
14	100	Westwood Terrace	Bishopcourt Retirement Apartments	Red	7	1980	Reinforced Masonry	Apartment	
15	142	Park Terrace	Parkbridge	Green	4	2010	Unknown	Apartment	
16	138	Victoria St	Lumley Centre	Yellow	7	2000	Concrete Frame w/ Concrete Shear Walls	Office	
17	148	Victoria St	BDO House	Yellow	7	2000	Concrete Frame w/ Concrete Shear Walls	Office	Drawings
18	167	Victoria St	Fidelity House	Yellow	4	1990	Concrete Frame w/ Masonry Walls	Office	Drawings
19	550	Hagley Ave	CDHB Dialysis Centre	Yellow	4	2000	Unknown	Hospital	
20	36	St Asaph St	Canterbury Brewery	Yellow	4	1980	Concrete Frame w/ Masonry Walls	Manufacturing	
21	4	Oxford Terrace	Terrace House	Green	4	1980	Reinforced Masonry	Office	
22	10	Oxford Terrace	Unknown	Green	5	1980	Concrete Frame w/ Concrete Shear Walls	Office	
23	32	Oxford Terrace	Deloitte	Yellow	5	2000	Concrete Moment Frame	Office	
24	38	Oxford Terrace	Oxford Clinic	Yellow	4	1990	Concrete Moment Frame	Office	
25	54	Oxford Terrace	TimeZoneOne	Yellow	4	1990	Concrete Moment Frame	Office	
26	66	Oxford Terrace	66 Oxford	Yellow	11	2010	Concrete Frame w/ Concrete Shear Walls	Apartment	
27	72	Oxford Terrace	University of Otago Building	Yellow	4	1980	Reinforced Masonry	Office	
28	74	Oxford Terrace	Psychiatric Emergency	Green	5	1980	Concrete Moment Frame	Office	
29	248	Montreal St	Cambridge Court	Yellow	6	1980	Concrete Frame w/ Masonry Walls	Apartment	
30	1	Cashel St	Ranui House	Green	4	2010	Concrete Frame w/ Concrete Shear Walls	Apartment	
31	1	Cashel St	Ranui House B	Green	6	2010	Concrete Frame w/ Concrete Shear Walls	Apartment	

Building Information									
ID	Number	Street	Name	Placard	Number of Stories	Built Before	Building Type	Occupancy Type	Info
32	35	Cambridge Terrace	Rolleston Court	Red	6	1980	Reinforced Masonry	Apartment	Drawings
33	41	Cambridge Terrace	Cambridge Apartments	Red	4	1980	Reinforced Masonry	Apartment	
34	245	Montreal St	Unknown	Green	5	2010	Concrete Frame w/ Concrete Shear Walls	Apartment	
35	61	Cambridge Terrace	AEQ	Yellow	4	1990	Reinforced Masonry	Office	
36	69	Cambridge Terrace	Unknown	Green	5	1990	Reinforced Masonry	Office	
37	79	Cambridge Terrace	Unknown	Green	7	2000	Concrete Moment Frame	Office	
38	64	Cashel St	Age Concern Canterbury	Yellow	4	1990	Concrete Moment Frame	Office	
39	62	Cashel St	BridgeWater	Green	10	2000	Concrete Frame w/ Concrete Shear Walls	Apartment	Geotech
40	56	Cashel St	Westpark	Yellow	10	2000	Concrete Moment Frame	Office	
41	254	Montreal St	Scales House	Yellow	4	1980	Concrete Frame w/ Masonry Walls	Office	
42	33	Cashel St	Ronald McDonald House	Yellow	5	2010	Unknown	Hospital	
43	32	Cashel St	Unknown	Green	4	2000	Reinforced Masonry	Apartment	
44	14	Cashel St	Unknown	Green	4	2010	Unknown	Apartment	
45	12	Hereford St	YMCA N.H. Rudkin Court	Green	6	2010	Unknown	Apartment	
46	28	Gloucester St	The Gloucester	Green	10	2010	Unknown	Apartment	
47	62	Gloucester St	Gallery Apartments	Yellow	15	2010	Concrete Frame w/ Concrete Shear Walls	Apartment	Drawings
48	70	Gloucester St	Unknown	Yellow	5	2000	Reinforced Masonry	Office	
49	84	Gloucester St	Warren House	Green	6	1980	Concrete Frame w/ Masonry Walls	Office	
50	287	Durham St North	URS House	Yellow	7	1990	Concrete Moment Frame	Office	
51	293	Durham St North	Amuri Courts	Yellow	5	1980	Concrete Frame w/ Masonry Walls	Office	Drawings
52	299	Durham St North	Contours	Red	4	1990	Concrete Moment Frame	Office	
53	66	Armagh St	West Fitzroy	Green	7	2010	Concrete Frame w/ Concrete Shear Walls	Apartment	
54	2	Cranmer Square	Braemar	Green	4	2010	Unknown	Apartment	
55	294	Montreal St	Cowlishaw Mews	Green	4	2010	Concrete Frame w/ Masonry Walls	Apartment	
56	53	Hereford St	Christchurch City Council	Green	7	1980	Concrete Moment Frame	Office	Drawings
57	62	Worcester St	HSBC Tower	Green	11	2010	Steel Frame	Office	
58	65-67	Worcester St	York House	Red	5	1980	Reinforced Masonry	Office	
59	141	Cambridge Terrace	Unknown	Yellow	7	2000	Concrete Frame w/ Masonry Walls	Office	
60	50	Park Terrace	The George Hotel	Green	4	2000	Unknown	Hotel	
61	353	Montreal St	Chateau Blanc Suites	Red	5	1990	Concrete Frame w/ Masonry Walls	Apartment	
62	52	Peterborough St	The Establishment	Red	11	2010	Concrete Moment Frame	Apartment	

Building Information									
ID	Number	Street	Name	Placard	Number of Stories	Built Before	Building Type	Occupancy Type	Info
63	50	Victoria St	NZ College of Early Childhood Education	Red	4	1990	Reinforced Masonry	Office	
64	374	Montreal St	Strategy Building	Red	5	2010	Concrete Frame w/ Masonry Walls	Office	
65	31	Victoria St	Riverlands House	Yellow	5	1990	Concrete Moment Frame	Office	Drawings
66	335	Durham St North	Copthorne Hotel	Red	11	2000	Concrete Frame w/ Concrete Shear Walls	Hotel	
67	70	Kilmore St	Crowne Plaza Hotel	Red	11	2000	Concrete Frame w/ Concrete Shear Walls	Hotel	
68	329	Durham St North	Spicers Building	Yellow	5	1990	Concrete Frame w/ Concrete Shear Walls	Office	
69	51	Chester St West	Radio New Zealand House	Yellow	4	1990	Concrete Frame w/ Masonry Walls	Office	
70	64	Kilmore St	Pegasus Building	Red	4	1990	Concrete Frame w/ Concrete Shear Walls	Office	
71	58	Kilmore St	ECan	Yellow	6	1990	Concrete Frame w/ Concrete Shear Walls	Office	
72	50	Kilmore St	Ernst and Young	Yellow	6	1990	Concrete Moment Frame	Office	
73	9	Cranmer Square	Charan	Yellow	4	2000	Concrete Frame w/ Masonry Walls	Apartment	
74	868	Colombo St	St Mary's	Green	4	2010	Reinforced Masonry	Apartment	
75	136	Salisbury St	Unknown	Green	4	2010	Reinforced Masonry	Apartment	
76	280	Bealey Ave	Amuri Park	Red	4	2010	Reinforced Masonry	Apartment	
77	169	Fitzgerald Ave	Unknown	Green	4	2010	Unknown	Apartment	
78	400	Durham St North	Madison Apartments	Green	4	2010	Concrete Frame w/ Masonry Walls	Apartment	
79	90	Armagh St	Craig's House	Red	9	1990	Unknown	Office	Drawings
80	100	Armagh St	Victoria Square Apartments	Yellow	14	2010	Concrete Frame w/ Concrete Shear Walls	Apartment	Drawings
81	101	Armagh St	Nokia Building	Yellow	4	2000	Concrete Frame w/ Concrete Shear Walls	Carpark	
82	110	Armagh St	Isaac House	Yellow	4	1930	Concrete Frame w/ Masonry Walls	Office	
83	764	Colombo St	Forsyth Barr House	Red	17	2000	Concrete Moment Frame	Office	Geotech
84	776	Colombo St	Copthorne Central Hotel	Yellow	10	1990	Concrete Frame w/ Concrete Shear Walls	Hotel	Drawings
85	210	Oxford Terrace	Allan McLean Building	Yellow	4	1970	Concrete Frame w/ Masonry Walls	Office	
86	119	Armagh St	PricewaterhouseCoopers Building	Yellow	20	2000	Concrete Moment Frame	Office	Geotech
87	127	Armagh St	Unknown	Red	7	1990	Reinforced Masonry	Office	
88	230	Oxford Terrace	Unknown	Red	4	1980	Reinforced Masonry	Office	
89	137	Armagh St	BNZ Building	Green	10	2000	Concrete Frame w/ Masonry Walls	Office	
90	143	Armagh St	ASB Building	Yellow	6	1990	Reinforced Masonry	Office	
91	250	Oxford Terrace	Charles Luney House	Yellow	5	1990	Concrete Frame w/ Concrete Shear Walls	Office	
92	218	Manchester St	Bob Browns Hi-Fi	Yellow	4	1970	Concrete Frame w/ Concrete Shear Walls	Retail	

Building Information									
ID	Number	Street	Name	Placard	Number of Stories	Built Before	Building Type	Occupancy Type	Info
93	262	Oxford Terrace	ACC Building / Trust House	Red	5	2010	Concrete Frame w/ Concrete Shear Walls	Office	
94	76	Chester St East	Community & Public Health	Yellow	4	1990	Concrete Frame w/ Masonry Walls	Office	Drawings
95	82	Chester St East	Poplar Apartments Hotel	Green	6	1980	Concrete Moment Frame	Hotel	Drawings
96	291	Madras St	Leister House	Red	5	2000	Concrete Frame w/ Concrete Shear Walls	Office	
97	199	Armagh St	Canterbury Trade Union Centre	Red	6	1990	Concrete Frame w/ Concrete Shear Walls	Office	Drawings
98	271	Madras St	Grenadier House	Red	5	2000	Concrete Frame w/ Masonry Walls	Office	Drawings
99	221	Gloucester St	Securities House	Red	7	2000	Concrete Moment Frame	Office	Drawings
100	217	Gloucester St	Tower Insurance House	Red	8	1990	Concrete Frame w/ Concrete Shear Walls	Office	
101	23-35	Latimer Square	AMI Building	Red	8	1990	Concrete Frame w/ Concrete Shear Walls	Office	
102	215	Gloucester St	Latimer View House	Red	5	1990	Reinforced Masonry	Office	
103	202	Gloucester St	TVNZ	Red	4	1930	Concrete Frame w/ Concrete Shear Walls	Office	Drawings
104	166	Gloucester St	C1 Tower / Pacific Tower Apartments	Green	21	2010	Steel Frame	Apartment	Drawings
105	148-156	Gloucester St	New Press Building	Yellow	8	2010	Steel Frame	Office	
106	728	Colombo St	Mums 24 Restaurant	Yellow	7	1980	Concrete Moment Frame	Office	
107	822	Colombo St	Unknown	Red	4	1990	Concrete Frame w/ Masonry Walls	Office	
108	151	Kilmore St	Natcoll House	Green	7	2010	Unknown	Office	Drawings
109	137	Kilmore St	Medlab	Yellow	6	1980	Concrete Moment Frame	Office	
110	315	Manchester St	Unknown	Green	5	1980	Concrete Frame w/ Masonry Walls	Office	
111	321	Manchester St	Sinclair Knight Merz House	Green	4	1990	Concrete Frame w/ Masonry Walls	Office	
112	161	Kilmore St	The Laptop Company / Amsterdam House	Green	4	2000	Concrete Frame w/ Masonry Walls	Office	
113	155	Kilmore St	McPhil Gibson & Zwart House	Green	4	1990	Reinforced Masonry	Office	Drawings
114	144	Kilmore St	Markhams	Yellow	6	2010	Concrete Frame w/ Concrete Shear Walls	Office	Geotech
115	129	Kilmore St	Unknown	Red	5	2010	Concrete Frame w/ Concrete Shear Walls	Office	
116	227	Cambridge Terrace	Ernst & Young House	Green	7	2000	Concrete Moment Frame	Office	Drawings
117	115	Kilmore St	Golder Associates	Yellow	5	2010	Concrete Frame w/ Concrete Shear Walls	Office	
118	818	Colombo St	Unknown	Yellow	5	2000	Concrete Frame w/ Masonry Walls	Office	
119	87-89	Kilmore St	Scenic Suites Christchurch	Green	7	2010	Unknown	Hotel	
120	736	Colombo St	Cathedral Square PostShop	Red	4	1950	Concrete Frame w/ Concrete Shear Walls	Retail	
121	749	Colombo St	Mutual Funds House	Yellow	8	1980	Concrete Frame w/ Concrete Shear Walls	Office	
122	91	Gloucester St	Central Christchurch Library	Red	4	2000	Concrete Frame w/ Concrete Shear Walls	Library	

Building Information									
ID	Number	Street	Name	Placard	Number of Stories	Built Before	Building Type	Occupancy Type	Info
123	170	Oxford Terrace	Rydges Hotel	Yellow	14	1990	Concrete Frame w/ Concrete Shear Walls	Hotel	
124	106	Gloucester St	Unknown	Red	6	1990	Concrete Frame w/ Masonry Walls	Office	
125	86	Gloucester St	Brannigans	Red	8	2000	Concrete Frame w/ Concrete Shear Walls	Office	Drawings
126	78	Worcester St	Clarendon Tower	Red	17	1990	Concrete Frame w/ Concrete Shear Walls	Office	Drawings
127	152	Oxford Terrace	Public Trust Office	Yellow	5	1930	Concrete Moment Frame	Office	
128	77	Hereford St	Equitable House	Yellow	7	1990	Concrete Moment Frame	Office	
129	76	Hereford St	Royal Sun Alliance House	Green	7	2010	Unknown	Office	
130	76	Cashel St	DTZ House	Red	11	2000	Concrete Frame w/ Concrete Shear Walls	Office	
131	83	Hereford St	Guardian Assurance House	Yellow	7	1970	Concrete Frame w/ Concrete Shear Walls	Office	
132	48	Hereford St	Police Building	Yellow	12	1980	Concrete Moment Frame	Office	Geotech
133	93-95	Cambridge Terrace	Harvey Cameron Building	Green	5	1990	Concrete Frame w/ Masonry Walls	Office	Drawings
134	47	Hereford St	St Elmo Courts	Red	8	1930	Concrete Moment Frame	Office	
135	282	Durham St North	Court House	Green	7	1990	Concrete Frame w/ Concrete Shear Walls	Office	
136	190	Armagh St	Costas Souvlaki Bar	Yellow	5	1980	Concrete Frame w/ Masonry Walls	Retail	
137	218	Manchester St	Orion	Yellow	4	1990	Concrete Frame w/ Concrete Shear Walls	Office	
138	180	Manchester St	SBS Bank	Yellow	9	2010	Concrete Frame w/ Concrete Shear Walls	Office	
139	151	Worcester St	Video Production Centre	Red	9	1990	Concrete Frame w/ Concrete Shear Walls	Office	Drawings
140	155	Worcester St	Radio Network House	Yellow	13	2000	Concrete Frame w/ Concrete Shear Walls	Office	Drawings
141	12	Latimer Square	Park Tower on Latimer	Yellow	7	2010	Concrete Frame w/ Masonry Walls	Apartment	
142	30	Latimer Square	Latimer Hotel	Red	4	2010	Concrete Frame w/ Masonry Walls	Hotel	
143	253	Hereford St	Hereford St Apartments	Green	4	2010	Concrete Frame w/ Concrete Shear Walls	Apartment	
144	224	Cashel St	IRD Building	Green	8	2010	Concrete Frame w/ Concrete Shear Walls	Office	Geotech
145	130	Madras St	CPIT - N Block	Green	6	1990	Concrete Frame w/ Concrete Shear Walls	Office	
146	130	Madras St	CPIT - S Block	Green	6	1990	Concrete Frame w/ Concrete Shear Walls	Office	
147	130	Madras St	School of Art and Design	Green	4	1980	Concrete Frame w/ Concrete Shear Walls	Office	
148	209	Tuam St	Old High St Post Office Building	Green	4	1940	Concrete Moment Frame	Retail	
149	179	Tuam St	Old Real Groovy	Green	4	1980	Concrete Moment Frame	Office	
150	163-175	Tuam St	Old CCC Building	Yellow	6	1980	Concrete Frame w/ Concrete Shear Walls	Office	
151	33	Lichfield St	CCC Lichfield Carpark	Yellow	5	1980	Concrete Frame w/ Concrete Shear Walls	Carpark	
152	79-81	Lichfield St	Lincoln House	Red	4	1980	Concrete Moment Frame	Office	
153	96	Lichfield St	Minx / Living Space	Yellow	4	1950	Concrete Frame w/ Concrete Shear Walls	Apartment	

Building Information									
ID	Number	Street	Name	Placard	Number of Stories	Built Before	Building Type	Occupancy Type	Info
154	122-126	Manchester St	Majestic Theatre	Yellow	4	1940	Concrete Frame w/ Masonry Walls	Theatre	
155	34	Bedford Row	Wilson Parking Bedford Row	Red	5	1990	Concrete Frame w/ Concrete Shear Walls	Carpark	Drawings
156	203	Hereford St	Interiors House	Yellow	6	1920	Concrete Moment Frame	Office	
157	195	Hereford St	Torrents House	Green	4	1980	Concrete Frame w/ Concrete Shear Walls	Office	
158	183	Hereford St	Ibis House	Yellow	8	1990	Concrete Frame w/ Masonry Walls	Office	
159	186	Hereford St	Unknown	Yellow	6	2000	Concrete Frame w/ Concrete Shear Walls	Office	
160	172	Hereford St	Metropolitan Life Building	Yellow	6	1980	Concrete Frame w/ Concrete Shear Walls	Office	
161	165	Hereford St	Broadlands House	Green	5	1980	Concrete Frame w/ Concrete Shear Walls	Office	
162	164	Hereford St	National Bank Building	Yellow	8	2000	Concrete Frame w/ Concrete Shear Walls	Office	
163	161	Hereford St	161 Hereford Suites and Apartments	Yellow	10	1990	Concrete Frame w/ Concrete Shear Walls	Apartment	
164	159	Hereford St	Malvern House	Yellow	6	1980	Concrete Frame w/ Concrete Shear Walls	Office	
165	153	Hereford St	Allan Pyatt House	Yellow	7	1990	Concrete Frame w/ Concrete Shear Walls	Office	
166	158	Hereford St	Te Waipounamu House	Yellow	11	2000	Concrete Frame w/ Concrete Shear Walls	Office	Drawings
167	152	Hereford St	The Link Centre	Yellow	7	2000	Concrete Frame w/ Concrete Shear Walls	Office	
168	141	Hereford St	Christchurch Community House	Red	6	1980	Concrete Frame w/ Concrete Shear Walls	Office	
169	137	Hereford St	Unknown	Green	4	1950	Concrete Frame w/ Concrete Shear Walls	Office	
170	135	Hereford St	Unknown	Green	4	1950	Concrete Frame w/ Concrete Shear Walls	Office	
171	2	Cathedral Square	BNZ House	Red	12	1990	Concrete Frame w/ Concrete Shear Walls	Office	
172	3	Cathedral Square	ANZ Bank House	Yellow	4	2000	Concrete Frame w/ Concrete Shear Walls	Office	
173	705	Colombo St	Night 'n Day Building	Yellow	4	1980	Concrete Frame w/ Concrete Shear Walls	Office	
174	703	Colombo St	Burger King Building	Yellow	4	1950	Concrete Frame w/ Concrete Shear Walls	Office	
175	120	Hereford St	Wendys Building	Red	4	1930	Unreinforced Masonry	Theatre	
176	118	Hereford St	The Boardroom Café Building	Red	4	1920	Concrete Frame w/ Concrete Shear Walls	Office	
177	116	Hereford St	Hereford Court	Red	4	1930	Unreinforced Masonry	Office	
178	107	Hereford St	Ibis Hotel	Yellow	9	2000	Concrete Frame w/ Concrete Shear Walls	Hotel	Geotech
179	96	Hereford St	Department of Internal Affairs	Yellow	9	1980	Concrete Frame w/ Concrete Shear Walls	Office	Drawings
180	93	Hereford St	Former Post Office	Yellow	5	1950	Concrete Moment Frame	Office	
181	90	Hereford St	Gough House	Red	4	1940	Unreinforced Masonry	Office	
182	14	Cathedral Square	Millenium Hotel	Yellow	12	1990	Concrete Frame w/ Concrete Shear Walls	Hotel	
183	28	Cathedral Square	Heritage Hotel	Yellow	12	1980	Concrete Frame w/ Concrete Shear Walls	Hotel	Drawings
184	63-69	Cathedral Square	Tower Building	Red	9	1980	Concrete Frame w/ Concrete Shear Walls	Office	Drawings

Building Information									
ID	Number	Street	Name	Placard	Number of Stories	Built Before	Building Type	Occupancy Type	Info
185	47	Cathedral Square	Grant Thornton / Anthony Harper Building	Yellow	12	1980	Concrete Frame w/ Concrete Shear Walls	Office	Drawings
186	66	Cathedral Square	Camelot Cathedral Square Hotel	Red	7	1980	Concrete Frame w/ Concrete Shear Walls	Hotel	
187	50	Cathedral Square	Warners Historic Hotel	Red	4	1910	Unreinforced Masonry	Hotel	
188	50	Cathedral Square	Novotel Hotel	Red	12	2010	Concrete Frame w/ Concrete Shear Walls	Hotel	
189	15-31	Cathedral Square	Old Chief Post Office Building	Yellow	8	2010	Concrete Frame w/ Concrete Shear Walls	Office	
190	123	Worcester St	Intercity & Newmans Coachlines	Red	6	1990	Reinforced Masonry	Office	Drawings
191	116	Worcester St	Design and Arts College Facade	Yellow	7	1910	Unreinforced Masonry	Office	
192	116	Worcester St	Design and Arts College	Yellow	8	1990	Concrete Frame w/ Concrete Shear Walls	Office	
193	113	Worcester St	Quest Hotel	Yellow	9	1990	Concrete Frame w/ Concrete Shear Walls	Hotel	
194	190-192	Hereford St	Kenton Chambers	Red	4	1930	Unreinforced Masonry	Office	Drawings
195	187	Cashel St	Oaks I-Stay Hotel	Green	12	1990	Concrete Frame w/ Concrete Shear Walls	Hotel	Drawings
196	200	Cashel St	Development House	Green	5	1980	Concrete Frame w/ Masonry Walls	Office	
197	202	Cashel St	Avonmore Tertiary Academy	Red	10	1980	Concrete Frame w/ Concrete Shear Walls	Office	Drawings
198	203	Cashel St	Les Mills	Green	4	2000	Concrete Frame w/ Concrete Shear Walls	Office	Drawings
199	199-201	Cashel St	Christchurch Business Centre	Red	5	1980	Concrete Frame w/ Concrete Shear Walls	Office	
200	192	Cashel St	Insignis House	Yellow	6	1980	Concrete Frame w/ Concrete Shear Walls	Office	Drawings
201	193	Cashel St	Union House / Christchurch Development Corporation	Yellow	6	1990	Concrete Frame w/ Concrete Shear Walls	Office	
202	182	Cashel St	Double Happy	Red	4	1960	Concrete Frame w/ Concrete Shear Walls	Office	
203	178	Cashel St	Malbas	Red	4	1930	Concrete Moment Frame	Office	
204	172	Cashel St	The Grumpy Mole Saloon	Red	6	1980	Concrete Frame w/ Concrete Shear Walls	Office	
205	170	Cashel St	Holiday Inn	Red	13	1990	Concrete Frame w/ Concrete Shear Walls	Hotel	
206	165	Cashel St	All Seasons Hotel	Red	7	2000	Concrete Frame w/ Concrete Shear Walls	Hotel	
207	166	Cashel St	Westpac Tower	Red	14	2000	Concrete Frame w/ Concrete Shear Walls	Office	Drawings
208	161	Cashel St	Grand Chancellor Hotel	Red	26	2000	Concrete Frame w/ Concrete Shear Walls	Hotel	
209	141	Cashel St	Wilson Parking Cashel St	Red	7	2000	Concrete Frame w/ Concrete Shear Walls	Carpark	
210	160	Cashel St	Glassons Building	Yellow	5	1990	Concrete Frame w/ Masonry Walls	Office	
211	137	Cashel St	Hallensteins Building	Green	7	2010	Concrete Frame w/ Concrete Shear Walls	Office	Geotech
212	7	Liverpool St	Unknown	Yellow	6	1980	Concrete Frame w/ Concrete Shear Walls	Office	
213	130	Manchester St	Peaches & Cream	Red	4	1970	Concrete Moment Frame	Office	
214	146	Manchester St	Boogie Nights	Green	4	2010	Concrete Frame w/ Concrete Shear Walls	Retail	

Building Information									
ID	**Number**	**Street**	**Name**	**Placard**	**Number of Stories**	**Built Before**	**Building Type**	**Occupancy Type**	**Info**
215	159	Manchester St	Unknown	Red	6	1980	Concrete Moment Frame	Office	
216	222	High St	Stewart Dawson Building	Yellow	4	1920	Concrete Moment Frame	Office	
217	243	High St	Cheapskates	Yellow	4	1960	Concrete Frame w/ Concrete Shear Walls	Retail	

Cladding Damage						
ID	Cladding Type A	Cladding A Performance Level	Cladding A % of Damage	Cladding Type B	Cladding B Performance Level	Cladding B % of Damage
1	Curtain Wall	Immediate Occupancy	50	Concrete Panels	Operational	30
2	Curtain Wall	Immediate Occupancy	50	Concrete Panels	Operational	30
3	Curtain Wall	Immediate Occupancy	50	Concrete Panels	Operational	30
4	Curtain Wall	Immediate Occupancy	50	Concrete Panels	Operational	30
5	Glazing Infill	Operational	0	Stucco	Operational	0
6	Masonry Infill	Life Safety	25	Glazing Infill	Operational	0
7	Curtain Wall	Hazard Reduced Level	70	None	N/A	0
8	Curtain Wall	Hazard Reduced Level	80	Lightweight Panels	Immediate Occupancy	20
9	Curtain Wall	Immediate Occupancy	10	Concrete Panels	Operational	0
10	Curtain Wall	Operational	0	Lightweight Panels	Operational	0
11	Stick Curtain	Operational	0	None	N/A	0
12	Glazing Infill	Operational	0	None	N/A	0
13	Glazing Infill	Operational	0	Stucco	Operational	0
14	Glazing Infill	Immediate Occupancy	5	None	N/A	0
15	Brick Veneer	Operational	0	Curtain Wall	Operational	0
16	Stick Curtain	Immediate Occupancy	10	None	N/A	0
17	Stick Curtain	Immediate Occupancy	10	None	N/A	0
18	Glazing Infill	Life Safety	60	Stick Curtain	Operational	0
19	Lightweight Panels	Immediate Occupancy	5	Curtain Wall	Operational	0
20	Glazing Infill	Life Safety	10	Lightweight Panels	Operational	0
21	Glazing Infill	Life Safety	40	None	N/A	0
22	Stone Panels	Operational	0	Curtain Wall	Operational	0
23	Curtain Wall	Operational	20	Lightweight Panels	Operational	0
24	Concrete Panels	Immediate Occupancy	70	None	N/A	0
25	Lightweight Panels	Life Safety	10	Curtain Wall	Life Safety	10
26	Curtain Wall	Operational	0	Lightweight Panels	Operational	0
27	Curtain Wall	Immediate Occupancy	10	Lightweight Panels	Operational	0
28	Glazing Infill	Immediate Occupancy	15	Stone Panels	Operational	0
29	Curtain Wall	Operational	0	Glazing Infill	Operational	0
30	Glazing Infill	Operational	0	Stucco	Operational	0
31	Glazing Infill	Operational	0	Lightweight Panels	Operational	0
32	Glazing Infill	Life Safety	10	None	N/A	0

Cladding Damage						
ID	Cladding Type A	Cladding A Performance Level	Cladding A % of Damage	Cladding Type B	Cladding B Performance Level	Cladding B % of Damage
33	Glazing Infill	Operational	5	None	N/A	0
34	Glazing Infill	Operational	0	Stucco	Operational	0
35	Glazing Infill	Life Safety	30	None	N/A	0
36	Curtain Wall	Operational	0	None	N/A	0
37	Concrete Panels	Operational	0	Curtain Wall	Operational	0
38	Concrete Panels	Life Safety	5	Curtain Wall	Operational	0
39	Lightweight Panels	Hazard Reduced Level	30	Curtain Wall	Operational	0
40	Stick Curtain	Operational	0	Concrete Panels	Immediate Occupancy	5
41	Concrete Panels	Operational	5	Curtain Wall	Life Safety	5
42	Curtain Wall	Operational	0	Stucco	Operational	0
43	Glazing Infill	Operational	0	None	N/A	0
44	Brick Veneer	Operational	2	Glazing Infill	Operational	0
45	Glazing Infill	Operational	0	Lightweight Panels	Operational	0
46	Stucco	Operational	20	Glazing Infill	Operational	0
47	Curtain Wall	Hazard Reduced Level	20	Lightweight Panels	Operational	5
48	Glazing Infill	Life Safety	40	None	N/A	0
49	Glazing Infill	Immediate Occupancy	5	None	N/A	0
50	Concrete Panels	Life Safety	20	Curtain Wall	Operational	0
51	Lightweight Panels	Immediate Occupancy	10	None	N/A	0
52	Concrete Panels	Operational	0	Curtain Wall	Life Safety	40
53	Lightweight Panels	Operational	0	Curtain Wall	Operational	0
54	Lightweight Panels	Operational	0	Curtain Wall	Operational	10
55	Stucco	Operational	5	Glazing Infill	Operational	0
56	Double Skin	Immediate Occupancy	20	Spider Glazing	Hazard Reduced Level	80
57	Lightweight Panels	Operational	0	Curtain Wall	Operational	0
58	Concrete Panels	Operational	0	Curtain Wall	Life Safety	80
59	Concrete Panels	Immediate Occupancy	30	Curtain Wall	Immediate Occupancy	1
60	Lightweight Panels	Operational	0	Curtain Wall	Operational	0
61	Glazing Infill	Operational	5	Stucco	Operational	30
62	Concrete Panels	Immediate Occupancy	10	Spider Glazing	Operational	0
63	Glazing Infill	Life Safety	40	Stucco	Hazard Reduced Level	80
64	Lightweight Panels	Immediate Occupancy	20	Curtain Wall	Hazard Reduced Level	60

Cladding Damage						
ID	Cladding Type A	Cladding A Performance Level	Cladding A % of Damage	Cladding Type B	Cladding B Performance Level	Cladding B % of Damage
65	Glazing Infill	Life Safety	80	Stucco	Immediate Occupancy	40
66	Concrete Panels	Operational	0	Curtain Wall	Hazard Reduced Level	5
67	Concrete Panels	Immediate Occupancy	2	Curtain Wall	Hazard Reduced Level	20
68	Concrete Panels	Operational	0	Curtain Wall	Operational	0
69	Lightweight Panels	Life Safety	5	Curtain Wall	Operational	10
70	Curtain Wall	Life Safety	30	Concrete Panels	Operational	0
71	Concrete Panels	Operational	0	Curtain Wall	Life Safety	20
72	Glazing Infill	Operational	0	Lightweight Panels	Operational	0
73	Curtain Wall	Life Safety	70	Stucco	Operational	0
74	Glazing Infill	Operational	0	None	N/A	0
75	Glazing Infill	Operational	0	Stucco	Operational	0
76	Glazing Infill	Operational	0	Stucco	Operational	30
77	Glazing Infill	Operational	0	Lightweight Panels	Operational	0
78	Glazing Infill	Operational	0	Stucco	Operational	5
79	Stick Curtain	Operational	0	None	N/A	0
80	Glazing Infill	Life Safety	2	Lightweight Panels	Operational	0
81	Lightweight Panels	Operational	0	Spider Glazing	Immediate Occupancy	1
82	Glazing Infill	Immediate Occupancy	10	Brick Veneer	Operational	0
83	Curtain Wall	Operational	0	Lightweight Panels	Operational	0
84	Curtain Wall	Operational	0	Lightweight Panels	Operational	0
85	Glazing Infill	Hazard Reduced Level	40	Stucco	Operational	0
86	Curtain Wall	Operational	5	Lightweight Panels	Operational	0
87	Glazing Infill	Operational	0	Concrete Panels	Operational	0
88	Glazing Infill	Immediate Occupancy	5	None	N/A	0
89	Curtain Wall	Life Safety	2	Concrete Panels	Operational	0
90	Concrete Panels	Operational	5	Glazing Infill	Operational	0
91	Stick Curtain	Operational	5	Lightweight Panels	Operational	0
92	Glazing Infill	Life Safety	40	Stucco	Operational	0
93	Stick Curtain	Immediate Occupancy	2	None	N/A	0
94	Glazing Infill	Life Safety	10	Stone Panels	Operational	0
95	Glazing Infill	Life Safety	10	Lightweight Panels	Operational	0
96	Glazing Infill	Operational	5	Concrete Panels	Operational	50

Cladding Damage						
ID	Cladding Type A	Cladding A Performance Level	Cladding A % of Damage	Cladding Type B	Cladding B Performance Level	Cladding B % of Damage
97	Curtain Wall	Life Safety	10	Concrete Panels	Operational	0
98	Glazing Infill	Hazard Reduced Level	30	Brick Veneer	Hazard Reduced Level	10
99	Glazing Infill	Life Safety	30	None	N/A	0
100	Glazing Infill	Operational	5	Concrete Panels	Operational	0
101	Glazing Infill	Hazard Reduced Level	5	Concrete Panels	Operational	0
102	Glazing Infill	Life Safety	30	None	N/A	0
103	Glazing Infill	Life Safety	20	None	N/A	0
104	Concrete Panels	Operational	0.1	Curtain Wall	Operational	0
105	Spider Glazing	Hazard Reduced Level	20	Lightweight Panels	Operational	0
106	Concrete Panels	Operational	5	None	N/A	0
107	Glazing Infill	Hazard Reduced Level	90	Curtain Wall	Operational	0
108	Concrete Panels	Life Safety	5	Stick Curtain	Operational	0
109	Masonry Infill	Hazard Reduced Level	2	Curtain Wall	Operational	0
110	Curtain Wall	Operational	2	None	N/A	0
111	Lightweight Panels	Operational	0	Curtain Wall	Operational	0
112	Glazing Infill	Life Safety	10	Curtain Wall	Operational	0
113	Curtain Wall	Life Safety	20	Concrete Panels	Operational	0
114	Glazing Infill	Immediate Occupancy	30	Concrete Panels	Operational	0
115	Glazing Infill	Operational	15	Stick Curtain	Hazard Reduced Level	40
116	Concrete Panels	Operational	0	Curtain Wall	Operational	0
117	Stick Curtain	Operational	0	Lightweight Panels	Operational	0
118	Stick Curtain	Operational	10	Masonry Infill	Operational	0
119	Glazing Infill	Operational	0	Stucco	Operational	0
120	Glazing Infill	Hazard Reduced Level	70	None	N/A	0
121	Concrete Panels	Operational	0	Curtain Wall	Operational	0
122	Curtain Wall	Operational	10	Concrete Panels	Operational	0
123	Curtain Wall	Immediate Occupancy	2	Concrete Panels	Operational	0
124	Glazing Infill	Life Safety	30	Concrete Panels	Operational	0
125	Spider Glazing	Hazard Reduced Level	90	Concrete Panels	Immediate Occupancy	20
126	Concrete Panels	Immediate Occupancy	1	None	N/A	0
127	Glazing Infill	Immediate Occupancy	20	None	N/A	0
128	Concrete Panels	Operational	5	None	N/A	0

Cladding Damage						
ID	Cladding Type A	Cladding A Performance Level	Cladding A % of Damage	Cladding Type B	Cladding B Performance Level	Cladding B % of Damage
129	Lightweight Panels	Operational	0	Curtain Wall	Operational	0
130	Stick Curtain	Life Safety	2	None	N/A	0
131	Stone Panels	Operational	5	None	N/A	0
132	Concrete Panels	Operational	0	Curtain Wall	Operational	0
133	Glazing Infill	Operational	10	None	N/A	0
134	Masonry Infill	Hazard Reduced Level	80	None	N/A	0
135	Stone Panels	Operational	0	Concrete Panels	Operational	0
136	Stick Curtain	Operational	0	Lightweight Panels	Operational	0
137	Concrete Panels	Operational	0	Curtain Wall	Operational	0
138	Curtain Wall	Operational	0	Glazing Infill	Life Safety	10
139	Curtain Wall	Immediate Occupancy	40	Lightweight Panels	Operational	20
140	Curtain Wall	Operational	0	Lightweight Panels	Operational	0
141	Glazing Infill	Operational	10	Stucco	Operational	0
142	Glazing Infill	Immediate Occupancy	2	Stucco	Operational	10
143	Curtain Wall	Operational	0	Lightweight Panels	Operational	0
144	Stick Curtain	Operational	0	Concrete Panels	Operational	0
145	Curtain Wall	Operational	0	Concrete Panels	Operational	0
146	Curtain Wall	Operational	0	Concrete Panels	Operational	0
147	Glazing Infill	Operational	0	Concrete Panels	Operational	0
148	Glazing Infill	Operational	0	None	N/A	0
149	Glazing Infill	Immediate Occupancy	10	Brick Veneer	Operational	0
150	Curtain Wall	Hazard Reduced Level	40	None	N/A	0
151	Concrete Panels	Hazard Reduced Level	50	None	N/A	0
152	Masonry Infill	Operational	0	Glazing Infill	Operational	0
153	Glazing Infill	Life Safety	20	Curtain Wall	Operational	0
154	Glazing Infill	Life Safety	30	None	N/A	0
155	Concrete Panels	Immediate Occupancy	10	None	N/A	0
156	Masonry Infill	Immediate Occupancy	10	Glazing Infill	Hazard Reduced Level	40
157	Curtain Wall	Operational	0	Concrete Panels	Operational	0
158	Concrete Panels	Operational	0	Curtain Wall	Operational	0
159	Lightweight Panels	Operational	20	Glazing Infill	Immediate Occupancy	1
160	Glazing Infill	Operational	0	None	N/A	0

Cladding Damage						
ID	Cladding Type A	Cladding A Performance Level	Cladding A % of Damage	Cladding Type B	Cladding B Performance Level	Cladding B % of Damage
161	Concrete Panels	Operational	0	None	N/A	0
162	Lightweight Panels	Operational	5	Spider Glazing	Hazard Reduced Level	10
163	Stick Curtain	Immediate Occupancy	10	None	N/A	0
164	Curtain Wall	Immediate Occupancy	10	None	N/A	0
165	Concrete Panels	Operational	10	Glazing Infill	Operational	0
166	Curtain Wall	Operational	0	Concrete Panels	Operational	0
167	Concrete Panels	Operational	0	Curtain Wall	Operational	0
168	Curtain Wall	Life Safety	10	Concrete Panels	Operational	0
169	Glazing Infill	Operational	0	None	N/A	0
170	Glazing Infill	Operational	0	None	N/A	0
171	Concrete Panels	Operational	0	Spider Glazing	Operational	0
172	Stick Curtain	Operational	0	Glazing Infill	Hazard Reduced Level	100
173	Glazing Infill	Life Safety	10	None	N/A	0
174	Glazing Infill	Life Safety	10	None	N/A	0
175	Glazing Infill	Life Safety	10	None	N/A	0
176	Glazing Infill	Life Safety	10	Stucco	Immediate Occupancy	10
177	Glazing Infill	Hazard Reduced Level	50	Stucco	Immediate Occupancy	10
178	Concrete Panels	Immediate Occupancy	10	None	N/A	0
179	Concrete Panels	Operational	0	Curtain Wall	Operational	0
180	Glazing Infill	Operational	5	Stucco	Operational	0
181	Glazing Infill	Hazard Reduced Level	50	Stucco	Immediate Occupancy	10
182	Concrete Panels	Operational	0	None	N/A	0
183	Lightweight Panels	Immediate Occupancy	10	Glazing Infill	Operational	0
184	Curtain Wall	Immediate Occupancy	2	Glazing Infill	Immediate Occupancy	5
185	Glazing Infill	Immediate Occupancy	2	Stucco	Operational	0
186	Concrete Panels	Operational	0	None	N/A	0
187	Glazing Infill	Immediate Occupancy	10	Stucco	Life Safety	20
188	Concrete Panels	Immediate Occupancy	10	None	N/A	0
189	Concrete Panels	Operational	0	None	N/A	0
190	Glazing Infill	Hazard Reduced Level	70	Concrete Panels	Operational	0
191	Glazing Infill	Life Safety	20	Stucco	Immediate Occupancy	5
192	Glazing Infill	Operational	0	Stucco	Operational	0

Cladding Damage						
ID	Cladding Type A	Cladding A Performance Level	Cladding A % of Damage	Cladding Type B	Cladding B Performance Level	Cladding B % of Damage
193	Glazing Infill	Operational	0	Stucco	Operational	0
194	Glazing Infill	Hazard Reduced Level	70	None	N/A	0
195	Concrete Panels	Operational	0	None	N/A	0
196	Curtain Wall	Operational	0	Concrete Panels	Operational	0
197	Curtain Wall	Operational	0	Concrete Panels	Operational	0
198	Lightweight Panels	Operational	0	Stick Curtain	Operational	0
199	Concrete Panels	Operational	0	None	N/A	0
200	Curtain Wall	Immediate Occupancy	10	Concrete Panels	Operational	0
201	Curtain Wall	Hazard Reduced Level	40	None	N/A	0
202	Glazing Infill	Hazard Reduced Level	60	Brick Veneer	Operational	0
203	Glazing Infill	Hazard Reduced Level	50	None	N/A	0
204	Glazing Infill	Operational	0	None	N/A	0
205	Curtain Wall	Operational	0	Concrete Panels	Operational	0
206	Curtain Wall	Operational	0	Concrete Panels	Operational	0
207	Curtain Wall	Hazard Reduced Level	10	Spider Glazing	Hazard Reduced Level	80
208	Curtain Wall	Hazard Reduced Level	10	Concrete Panels	Life Safety	5
209	Concrete Panels	Operational	0	None	N/A	0
210	Curtain Wall	Operational	0	Lightweight Panels	Operational	0
211	Stick Curtain	Operational	0	Lightweight Panels	Operational	0
212	Glazing Infill	Operational	0	None	N/A	0
213	Glazing Infill	Life Safety	10	None	N/A	0
214	Glazing Infill	Operational	0	Lightweight Panels	Operational	0
215	Glazing Infill	Hazard Reduced Level	80	Masonry Infill	Operational	0
216	Glazing Infill	Operational	0	None	N/A	0
217	Glazing Infill	Hazard Reduced Level	50	None	N/A	0

Appendix C: Test Frame Design

A moment-resisting frame subassembly usually requires that the connections of the subassembly to the laboratory floor/wall and loading apparatus are located at points of zero moment. This allows the use of pinned connections at these zero moment locations. The columns of a frame subassembly would therefore typically be extended above and below the beam level approximately half the inter-storey height. Extending the columns 1500 mm above and below the beam level was not possible for the test frame due to the height restriction of the gantry crane in the laboratory. Consequently, the moment-curvature of the columns is not an entirely accurate representation of what would be observed in a typical moment resisting frame. It was decided that this inaccuracy was acceptable due to the fact that the columns were going to be of such high enough stiffness that the curvature in the columns would be insignificant. Essentially this meant that the columns were going to be so close to rigid that there were negligible rotations in the portions of the column above and below the frame. This is due to the inter-storey drift, θ_d, being comprised of several individual rotations, as described in Figure A2-1 and Equation (A2-1).

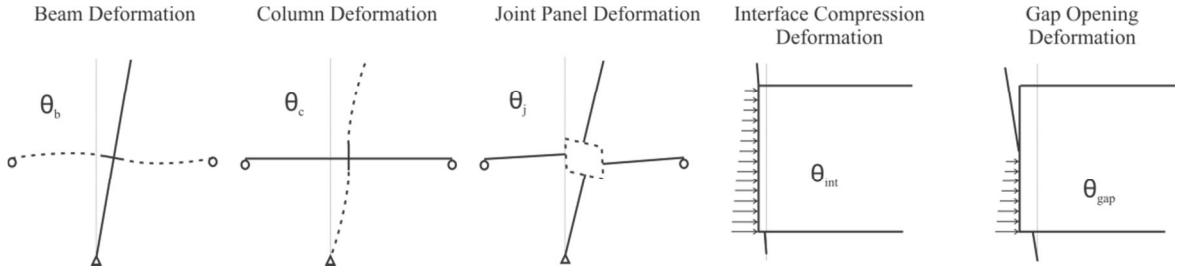

Figure A2-1: Individual rotation contributions to inter-storey drift

$$\theta_d = \theta_b + \theta_c + \theta_j + \theta_{int} + \theta_{gap} \quad \textbf{(A2-1)}$$

The stiff frame members resulted in the beam, column, joint and interface deformations all being negligible and thus the rotation being concentrated as gap opening deformation.

This is often incorrectly assumed to always be the case, however, for this frame, it does hold true. The stiffness of the concrete frame members was relatively high in order to ensure they remained elastic. By having stiff frame members, the gapping of the PRESSS beam-column joint connections was accentuated.

Due to geometry, the inter-storey drift rotation, θ_d, is amplified when calculating the gap opening rotation. This can be related by the expression in Equation (A2-2), which shows that for the test frame a gap opening of 4.53% was expected if all other rotations are zero.

$$\theta_{gap} = \frac{\theta_d}{1 - \frac{h_c}{L_b}} \quad \textbf{(A2-2)}$$

$$\theta_{gap} = \frac{4.0\%}{1 - \frac{400mm}{3400mm}} = 4.53\%$$

Having the rotation concentrated in the gap meant that the elongation of the post-tensioning was significant according to Equation (A2-3) and thus, so was the increased force in the post tensioning. It was thus important to ensure that the elongation of the post-tensioning at 4.0% drift would not result in yielding.

$$\Delta_{PT} = \theta_{gap}(0.5h_b - c) \quad \textbf{(A2-3)}$$

$$\Delta_{PT} = 0.0453 \times (0.5 \times 450 - 28) = 8.9\ mm$$

Macalloy 1030 post-tensioning bars were used to provide the post-tensioning force. The Macalloy bar is a high strength carbon chrome steel bar with high strength properties achieved by either cold working or heat treatment. The maximum post-tensioning force at 4.0% drift was limited to 85% of the yield capacity, as shown in Equation (A2-4), in order to ensure elastic behaviour of the bars. Once the total increment in post-tensioning force was computed, as shown in Equation (A2-5), then the initial post-tensioning force could be found using Equation (A2-6).

$$T_{PT(4.0\%)} = 0.85 A_{PT} f_y \quad \textbf{(A2-4)}$$

$$T_{PT(4.0\%)} = 0.85 \times 804\ mm^2 \times 835 = 571\ kN$$

$$\Delta T_{PT} = \varepsilon_{PT} E_{PT} = \frac{n\Delta_{PT}}{l_{ub}} E_{PT} \quad \textbf{(A2-5)}$$

$$\Delta T_{PT} = \frac{2 \times 8.9\ mm}{4700\ mm} 170{,}000\ MPa = 520\ kN$$

$$T_{PT(initial)} = T_{PT(4.0\%)} - \Delta T_{PT} \quad \textbf{(A2-6)}$$

$$T_{PT(initial)} = 571 - 520 = 51\ kN$$

With the initial and final post-tensioning forces computed, the moment-rotation response for the PRESSS connections could be found. The moment at decompression can be defined when the stress at the outer most fibre is equal to zero and is given in Equation (A2-7). The rotation of the connection is equal to zero.

$$M_{dec} = \left(\frac{eT_{PT(initial)}}{Z} + \frac{T_{PT(initial)}}{A}\right) Z \quad \textbf{(A2-7)}$$

$$M_{dec} = \left(\frac{0\ m \times 51\ kN}{0.0135\ m^2} + \frac{51\ kN}{0.18\ m^2}\right) 0.0135\ m^2 = 3.8\ kNm$$

The moment capacity at 4.0% drift requires iteration to determine the neutral axis depth. Once the neutral axis is determined, the moment capacity is a simple section analysis, as given in Equation (A2-8). It should be remembered that this corresponds to a connection rotation of 4.52% as per Equation (A2-2).

$$M_{4.0\%} = T_{PT(4.0\%)} \left(d_{PT} - \frac{a}{2}\right) \quad \textbf{(A2-8)}$$

$$M_{4.0\%} = 571\ kN \left(225\ mm - \frac{23.8\ mm}{2}\right) = 122\ kNm$$

Appendix D: Test Results

Order of tests

Mono Panel Tests	
Test number	**Test ID**
1	MP-LTR1-1
2	MP-LTR1-2
3	MP-LTR1-3
4	MP-LTR2-1
5	MP-LTR2-2
6	MP-LTR2-3
7	MP-LTR3-1
8	MP-LTR3-2
9	MP-LTR3-3
10	MP-LTR4-1
11	MP-LTR4-2
12	MP-LTR4-3
13	MP-LTR5-1
14	MP-LTR5-2
15	MP-LTR5-3
16	MP-SL1-1
17	MP-SL1-2
18	MP-SL1-3
19	MP-SL2-1
20	MP-SL2-2
21	MP-SL2-3
22	MP-SL3-1
23	MP-SL3-2
24	MP-SL3-3
25	MP-SL4-1
26	MP-SL4-2
27	MP-SL4-3
28	MP-STR1-1
29	MP-STR1-2
30	MP-STR1-3

Mono Panel Tests	
Test number	
31	MP-STR1-1
32	MP-STR1-2
33	MP-STR1-3
34	MP-UFP1
35	MP-UFP2
36	MP-UFP3
37	MP-UFP4
38	MP-UFP5
39	MP-UFP6
40	MP-UFP7

Dual Panel Tests	
Test number	**Test ID**
1	DP-LTR1-1
2	DP-LTR1-2
3	DP-LTR1-3
4	DP-SL1-1
5	DP-SL1-2
6	DP-SL1-3
7	DP-STR1-1
8	DP-STR1-2
9	DP-STR1-3
10	DP-UFP1
11	DP-UFP2

Long threaded rod connection test results

Test ID	MP-LTR1
Rod Size	20 mm
Location	2 Beam
Steel Grade	4.6
End Fixity	Fix-fix

Test #	Pushover Force (1.5% Drift)	Force Increase (1.5% Drift)	Failure Drift (Cycle Number)
1	46.8 kN	7.5 kN	2.0% (1)
2	46.4 kN	7.1 kN	1.5% (3)
3	46.4 kN	7.1 kN	2.0% (1)
Av.	46.5 kN	7.2 kN	-

Test ID	MP-LTR2
Rod Size	20 mm
Location	2 Beam
Steel Grade	8.8
End Fixity	Fix-fix

Test #	Pushover Force (1.5% Drift)	Force Increase (1.5% Drift)	Failure Drift (Cycle Number)
1	53.1 kN	13.6 kN	2.0% (1)
2	53.1 kN	13.6 kN	2.0% (2)
3	51.7 kN	12.2 kN	2.0% (1)
Av.	52.6 kN	13.1 kN	-

Test ID	MP-LTR3
Rod Size	20 mm
Location	2 Beam
Steel Grade	4.8
End Fixity	Fix-pin

Test #	Pushover Force (1.5% Drift)	Force Increase (1.5% Drift)	Failure Drift (Cycle Number)
1	47.8 kN	7.2 kN	2.0% (2)
2	50.1 kN	9.5 kN	2.0% (1)
3	48.2 kN	7.6 kN	2.0% (2)
Av.	48.7 kN	8.1 kN	-

Test ID	MP-LTR4
Rod Size	20 mm
Location	2 Column
Steel Grade	4.8
End Fixity	Fix-fix

Test #	Pushover Force (1.5% Drift)	Force Increase (1.5% Drift)	Failure Drift (Cycle Number)
1	54.8 kN	15.1 kN	1.5% (3)
2	54.5 kN	14.8 kN	1.5% (2)
3	54.8 kN	15.1 kN	1.5% (3)
Av.	54.7 kN	15.0 kN	-

Test ID	MP-LTR5
Rod Size	12 mm
Location	2 Beam
Steel Grade	4.8
End Fixity	Fix-fix

Test #	Pushover Force (1.5% Drift)	Force Increase (1.5% Drift)	Failure Drift (Cycle Number)
1	44.2 kN	4.9 kN	2.75% (1)
2	45.1 kN	5.8 kN	2.75% (2)
3	45.4 kN	6.1 kN	2.75% (2)
Av.	44.9 kN	5.6 kN	-

Test ID	DP-LTR1
Rod Size	20 mm
Location	4 Beam
Steel Grade	4.8
End Fixity	Fix-fix

Test #	Pushover Force (1.5% Drift)	Force Increase (1.5% Drift)	Failure Drift (Cycle Number)
1	54.8 kN	15.0 kN	1.5% (3)
2	54.9 kN	15.1 kN	1.5% (3)
3	55.9 kN	16.1 kN	2.0% (1)
Av.	55.2 kN	15.4 kN	-

Slotted connection test results

Test ID	MP-SL1
Slot Length	300 mm
Tube Spacer	None
Location	2 Beam

Test #	Pushover Force		Force Increase	
	1.5% Drift	3.5% Drift	1.5% Drift	3.5% Drift
1	45.9 kN	110.0 kN	7.9 kN	7.9 kN
2	45.9 kN	*	7.9 kN	*
3	45.7 kN	109.6 kN	7.7 kN	7.5 kN
Av.	45.8 kN	109.8 kN	7.8 kN	7.7 kN

* Bolt became stuck in slotted connection

Test ID	MP-SL2
Slot Length	300 mm
Tube Spacer	Present
Location	2 Beam

Test #	Pushover Force		Force Increase	
	1.5% Drift	3.5% Drift	1.5% Drift	3.5% Drift
1	45.4 kN	109.1 kN	7.2 kN	7.3 kN
2	45.4 kN	109.2 kN	7.2 kN	7.5 kN
3	45.5 kN	109.3 kN	7.3 kN	7.4 kN
Av.	45.4 kN	109.2 kN	7.2 kN	7.4 kN

Test ID	MP-SL3
Slot Length	150 mm
Tube Spacer	None
Location	2 Beam

Test #	Pushover Force		Force Increase	
	1.5% Drift	3.5% Drift	1.5% Drift	3.5% Drift
1	46.3 kN	155.6 kN	8.5 kN	50.3 kN
2	46.2 kN	150.3 kN	8.4 kN	45.0 kN
3	45.9 kN	150.5 kN	8.1 kN	45.2 kN
Av.	46.1 kN	152.1 kN	8.3 kN	46.8 kN

Test ID	MP-SL4
Slot Length	150 mm
Tube Spacer	Present
Location	2 Beam

Test #	Pushover Force		Force Increase	
	1.5% Drift	3.5% Drift	1.5% Drift	3.5% Drift
1	44.8 kN	157.2 kN	7.1 kN	51.5 kN
2	44.8 kN	155.2 kN	7.1 kN	49.5 kN
3	44.9 kN	157.9 kN	7.2 kN	52.2 kN
Av.	44.8 kN	156.8 kN	7.1 kN	51.1 kN

Test ID	DP-SL1
Slot Length	300 mm
Tube Spacer	Present
Location	4 Beam

Test #	Pushover Force		Force Increase	
	1.5% Drift	3.5% Drift	1.5% Drift	3.5% Drift
1	50.6 kN	115.7 kN	13.0 kN	13.7 kN
2	50.8 kN	115.9 kN	13.2 kN	13.9 kN
3	50.4 kN	115.3 kN	12.8 kN	13.3 kN
Av.	50.6 kN	115.6 kN	13.0 kN	13.6 kN

Short threaded rod connection test results

Test ID	MP-STR1
Rod Size	20 mm
Location	2 Beam
Steel Grade	4.8
End Fixity	Fix-fix

Test #	Pushover Force (1.5% Drift)	Force Increase (1.5% Drift)	Failure Drift (Cycle Number)
1	73.4 kN	32.8 kN	2.0% (1)
2	70.5 kN	29.9 kN	1.5% (3)
3	70.7 kN	30.1 kN	1.5% (3)
Av.	71.5 kN	30.9 kN	-

Test ID	MP-STR2
Rod Size	20 mm
Location	4 Beam
Steel Grade	4.8
End Fixity	Fix-fix

Test #	Pushover Force (1.5% Drift)	Force Increase (1.5% Drift)	Failure Drift (Cycle Number)
1	101.5 kN	60.9 kN	1.5% (3)
2	101.8 kN	61.2 kN	1.5% (3)
3	104.6 kN	64.0 kN	2.0% (1)
Av.	102.6 kN	62.0 kN	-

Test ID	DP-STR1
Rod Size	20 mm
Location	4 Beam
Steel Grade	4.8
End Fixity	Fix-fix

Test #	Pushover Force (1.5% Drift)	Force Increase (1.5% Drift)	Failure Drift (Cycle Number)
1	102.1 kN	61.3 kN	1.5% (3)
2	100.6 kN	59.8 kN	1.5% (3)
3	101.0 kN	60.2 kN	1.5% (3)
Av.	101.2 kN	60.4 kN	-

UFP connection test results

Test ID	MP-UFP1
Quantity	2
Housed	No
Config.	1

Pushover Force		Force Increase	
1.5% Drift	3.5% Drift	1.5% Drift	3.5% Drift
62.1 kN	-	22.4 kN	-

Test ID	MP-UFP2
Quantity	2
Housed	No
Config.	1

Pushover Force		Force Increase	
1.5% Drift	3.5% Drift	1.5% Drift	3.5% Drift
67.2 kN	-	27.1 kN	-

Test ID	MP-UFP3
Quantity	2
Housed	Yes
Config.	1

Pushover Force		Force Increase	
1.5% Drift	3.5% Drift	1.5% Drift	3.5% Drift
67.5 kN	127.8 kN	27.6 kN	26.8 kN

Test ID	MP-UFP4
Quantity	4
Housed	Yes
Config.	1

Pushover Force		Force Increase	
1.5% Drift	3.5% Drift	1.5% Drift	3.5% Drift
94.3 kN	163.8 kN	54.4 kN	62.8 kN

Test ID	MP-UFP5
Quantity	2
Housed	Yes
Config.	2

Pushover Force		Force Increase	
1.5% Drift	3.5% Drift	1.5% Drift	3.5% Drift
68.3 kN	128.6 kN	28.4 kN	27.6 kN

Test ID	MP-UFP6
Quantity	2
Housed	Yes
Config.	3

Pushover Force		Force Increase	
1.5% Drift	3.5% Drift	1.5% Drift	3.5% Drift
69.2 kN	129.5 kN	29.3 kN	28.5 kN

Test ID	MP-UFP7
Quantity	2
Housed	Yes
Config.	4

Pushover Force		Force Increase	
1.5% Drift	3.5% Drift	1.5% Drift	3.5% Drift
69.0 kN	129.1 kN	29.1 kN	28.1 kN

Test ID	DP-UFP1
Quantity	2
Housed	Yes
Config.	1

Pushover Force		Force Increase	
1.5% Drift	**3.5% Drift**	**1.5% Drift**	**3.5% Drift**
66.7 kN	134.6 kN	26.8 kN	27.5 kN

Test ID	DP-UFP2
Quantity	4
Housed	Yes
Config.	1

Pushover Force		Force Increase	
1.5% Drift	**2.75% Drift**	**1.5% Drift**	**2.75% Drift**
84.6 kN	136.9 kN	44.6 kN	61.2 kN

Appendix E: Numerical Modelling Parameters

Frame Model Parameters

```
a = 3.6;                                %Interstorey height       [m]
a1 = 4.0;                               %Bottom floor interstorey height
b = 7.35;                               %Dimension of horizontal beam    [m]
n = 3;                                  %Number of spans in x direction
m = 10;                                 %Number of floors in y direction
g = 9.81;                               %Acceleration of gravity       [m/s^2]
Load_y= -260;
Weight_x= 650;

%=========================================================================
%Prepare the input file

    %COLUMN top
    E_c   = 28000000;
    G_c   = 11666666.67;
    A_c   = 0.414;
    AS_c  = 0.345;
    I_c   = 0.01956;
    WGT_c = 9.729;
    END1_c = 0.45;
    END2_c = 0.45;
    END1_c_bot = 0;

    RA_c = 0.005;
    RF_c = 0.005;
    H1_c = 0.484;
    H2_c = 0.484;

    PYC_c = -18736.2;
    PB_c = -6831;
    MB_c = 2058.6;
    M1B_c = 1905.5;
    M2B_c = 1505.1;
    MO_c = 849.64;
    PYT_c = 2073.5;
    IEND_c = 0;

    ALFA_c = 0.5;
```

```
    BETA_c = 0.3;
    NF_c = 1;
    KKK_c = 1;

    %BEAM
    E_b   = 28000000;
    G_b   = 11666666.67;
    A_b   = 0.36;
    AS_b  = 0.30;
    I_b   = 0.00972;
    WGT_b = 8.46;
    END1_b = 0.45;
    END2_b = 0.45;

    RA_b = 0.001;
    RF_b = 0.001;
    H1_b = 0.363;
    H2_b = 0.363;

    PYT_b = 1295.9;
    PYC_b = -11511.78;
    MY1p_b = 544;
    MY1m_b = -544;
    MY2p_b = 544;
    MY2m_b = -544;

    ALFA_b = 0.3;
    BETA_b = 0.2;
    NF_b = 1;
    KKK_b = 1;

    ILOS_b = 0;
    IDAMG_b = 1;
    DUCT1_b = 16.59;
    DUCT2_b = 46.27;
    RDUCT_b = 0;

%=========================================================================
%Nodes
p=n+1;
q=m+1;
totalnodes=q*p;

for i=1:q                              %Floor number
    for j=1:p                          %Bay number
        nodes(j+i*p-p,1)=j+i*p-p ;     %Node number
        nodes(j+i*p-p,2)=j*b-b;        %X coord
        if i==1
        nodes(j+i*p-p,3)=0;            %Y coord
        else
        nodes(j+i*p-p,3)=i*a-2*a+a1;   %Y coord
        end
        nodes(j,4:6)=1;                %Fixity
        nodes(j,7:10)=0;               %Zeros
    end
end

%Elements
totalelements=m*n+m*p;
```

```
elementtypes=3;

for r=1:m*n+m*p
    elements(r,1)=r;                %Element number
end

%Beams
for i=1:m*n                         %Beam definition
    elements(i,2)=1;                %Element = beam
end

for i=1:m
    for j=1:n
        elements(j+i*n-n,3)=i*p+j;    %1st node
        elements(j+i*n-n,4)=i*p+j+1; %2nd node
        elements(j+1*n-n,5:7)=0;      %zeros
    end
end

%Columns
%Bottom columns
for i=m*n+1:m:m*n+m*p                 %Column definition
    elements(i,2)=2;                %Element = columns
end

%Other columns
for k=2:m
    for i=m*n+k:m:m*n+m*p                %Column definition
        elements(i,2)=3;               %Element = columns
    end
end

for i=1:p
    for j=1:m
        elements(j+i*m-m+n*m,3)=j+j*n-n+i-1;    %1st node
        elements(j+i*m-m+n*m,4)=j+j*n-n+i+n;    %2nd node
        elements(j+1*m-m+n*m,5:7)=0;      %zeros
    end
end

%Weights
for i=1:q                             %Floor number
    for j=1:p                         %Bay number
        weights(j+i*p-p,1)=j+i*p-p;       %Node number
        if i==1
            weights(j+i*p-p,2)=0;     %x Weight at first floor
        else
            weights(j+i*p-p,2)=Weight_x;   %x Weight at other nodes
        end
        weights(j+i*p-p,3:4)=0;     %Y*Z weight = zeros
    end
end

%Loads
for i=1:q                             %Floor number
    for j=1:p                         %Bay number
        loads(j+i*p-p,1)=j+i*p-p;       %Node number
        loads(j+i*p-p,2)=0;          %x load = zeros
        if i==1
```

```
            loads(j+i*p-p,3)=0;      %y Load at first floor
        else
            loads(j+i*p-p,3)=Load_y;    %y Load at other nodes
        end
        loads(j+i*p-p,4)=0;          %z load = zero
    end
end
```

Cladding Model Parameters

```
%Use 9999 if no third line data required for hysteretic rule

if CType==1 %Long threaded rod
                %TYPE   %IHYST  %ILOS   %IDAMG  %KX     %KY     %GJ
    pfline1=[   1       40      0       0       0       600     0  ...
            ... %WGT    %RF     %RT     %PSX    %PSY    %PSZ    %THETA
%ITRUSS
                0       13      0       0       0       0       0       0];
                %FX+    %FX-    %FY+    %FY-    %MZ+    %MZ-
    pfline2=[   0       0       1.9     -1.9    0       0];
                %DUCT1  %DUCT2  %RDUCT  %DUCT3  %RCYC
    pfline3=[9999];

elseif CType==2 %Slotted (infinite)
                %TYPE   %IHYST  %ILOS   %IDAMG  %KX     %KY     %GJ
    pfline1=[   1       2       0       0       0       2800    0  ...
            ... %WGT    %RF     %RT     %PSX    %PSY    %PSZ    %THETA
%ITRUSS
                0       0       0       0       0       0       0       0];
                %FX+    %FX-    %FY+    %FY-    %MZ+    %MZ-
    pfline2=[   0       0       3.0     -3.0    0       0];
                %DUCT1  %DUCT2  %RDUCT  %DUCT3  %RCYC
    pfline3=[9999];
                %TYPE   %IHYST  %ILOS   %IDAMG  %KX     %KY     %GJ
    addline1=[  1       15      0       0       0       1       0  ...
            ... %WGT    %RF     %RT     %PSX    %PSY    %PSZ    %THETA
%ITRUSS
                0       1       0       0       0       0       0       0];
                %FX+    %FX-    %FY+    %FY-    %MZ+    %MZ-
    addline2=[  0       0       0.1     -0.1    0       0];
                %DUCT1  %DUCT2  %RDUCT  %DUCT3  %RCYC
    addline3=[9999];

elseif CType==3  %Slotted (finite)
                %TYPE   %IHYST  %ILOS   %IDAMG  %KX     %KY     %GJ
    pfline1=[   1       2       0       0       0       2800    0  ...
            ... %WGT    %RF     %RT     %PSX    %PSY    %PSZ    %THETA
%ITRUSS
                0       0       0       0       0       0       0       0];
                %FX+    %FX-    %FY+    %FY-    %MZ+    %MZ-
    pfline2=[   0       0       3.0     -3.0    0       0];
                %DUCT1  %DUCT2  %RDUCT  %DUCT3  %RCYC
    pfline3=[9999];
                %TYPE   %IHYST  %ILOS   %IDAMG  %KX     %KY     %GJ
    addline1=[  1       9       0       0       0       2800    0  ...
```

```
            ... %WGT    %RF     %RT     %PSX    %PSY    %PSZ    %THETA
%ITRUSS
                0       1       0       0       0       0       0       0];
                %FX+    %FX-    %FY+    %FY-    %MZ+    %MZ-
    addline2=[  0       0       20      -20     0       0];
                %FU     %FI     %PTRI   %PUNL   %GAP+   %GAP-   %BETA
%ALPHA  %LOOP
    addline3=[  10      0.01    5       4       0.05    -0.05   1       0.1
1];

elseif CType==4  %Short threaded rod
                %TYPE   %IHYST  %ILOS   %IDAMG  %KX     %KY     %GJ
    pfline1=[   1       40      0       0       0       75000   0  ...
            ... %WGT    %RF     %RT     %PSX    %PSY    %PSZ    %THETA
%ITRUSS
                0       8       0       0       0       0       0       0];
                %FX+    %FX-    %FY+    %FY-    %MZ+    %MZ-
    pfline2=[   0       0       9.4     -9.4    0       0];
                %DUCT1  %DUCT2  %RDUCT  %DUCT3  %RCYC
    pfline3=[9999];

end
```

Appendix F: Seismic Hazard

Seismic Hazard Disaggregation

The seismic hazard disaggregation plots for a soft soil site (Vs_{30}=250 m/s) in Christchurch, New Zealand are illustrated in Figure A4-1 using the ground motion prediction equation developed by Bradley (2010). The disaggregation plots are shown for each of the three intensity levels investigated for spectral acceleration at a period of 2 seconds.

The seismic hazard disaggregation is a visual representation of the PSHA hazard curve. It displays the relative contribution of the magnitude, M_W, or rupture distance, R_{rup}, to the overall seismic hazard as well as the number of standard deviations, ε, from the median ground motion as predicted by an attenuation equation (Baker, 2008; Bazzurro & Cornell, 1999) .

The disaggregation plots show how the seismic hazard is dominated by the Alpine, Hope and Porter's Pass faults. These faults represent significant earthquake events ($M_w \geq 6.0$) of various rupture distances from Christchurch.

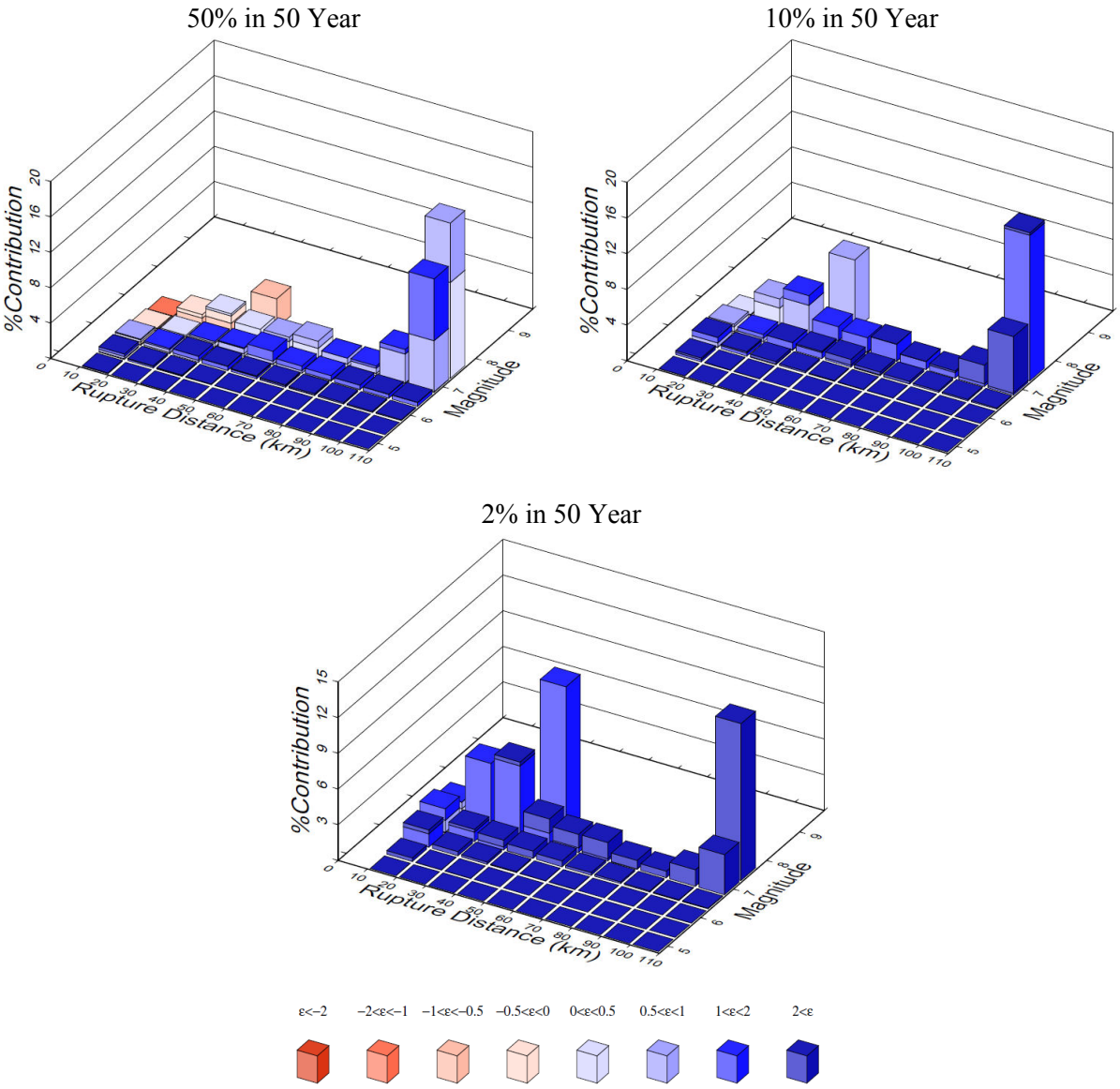

Figure A4-1: Spectral acceleration seismic hazard disaggregation for Christchurch, New Zealand

Ground Motion Record Selection

The basis of the GCIM approach is the construction of probability distributions for a number of ground motion IM (e.g. peak ground acceleration (PGA), peak ground velocity (PGV), spectral acceleration (SA)) that are conditioned on the occurrence of a specific ground motion intensity measure (Bradley, 2012).

The construction of the GCIM distributions is typically done via simulation which involves two steps. Firstly, a random earthquake rupture is obtained for the seismic hazard disaggregation that was obtained using PSHA. Secondly, given that the randomly drawn earthquake rupture has a ground motion intensity measure equal to that specified (e.g. PGA =

0.2 g), a random realization of the set of other intensity measures is found using their probability distributions. This requires several correlation computations to link all of the different IM's considered, e.g. the correlation between PGA and PGV.

The benefit of the GCIM approach is that the construction of the IM distributions provides the exact distribution of the other intensity measures, given the IM specified. The GCIM distributions are therefore the 'target' used in selecting a set of ground motions for seismic response analysis. The ground motions that best fit these distributions are selected from the PEER database using a statistical goodness-of-fit test (Bradley, 2012).

Ten ground motions were selected for each level of seismic hazard, each containing two orthogonal components, giving a total of twenty ground motions for each level of seismic hazard. The levels of seismic hazards will be expanded upon in the following section.

The ground motion amplitude was scaled based on the geometric mean of the two orthogonal components (Boore et al., 2006). A further constraint of an amplitude scale factor in the range of 0.33 to 3.0 was used as this is specified by NZS 1170.5 (2004) and aids to reduce response bias for non-linear structural drift responses (Luco & Bazzurro, 2007).

50% in 50 Year Exceedance Probability Ground Motions

A 50% in 50 year exceedance probability corresponds to a return period of 73 years and will herein be referred to as the 50%/50 intensity level. The 50%/50 ground motions represent the lowest seismic hazard considered for the seismic response analysis in this chapter.

Referring to the performance objectives matrix developed by SEAOC (1995), the Basic Safety Objective is attained when a structure achieves the Immediate Occupancy performance level for the 50%/50 intensity level. Since research has shown damage to cladding is often initiated at low intensity levels (Cohen, 1995), the inclusion of this low intensity level is important to assess the response of cladding at low intensity earthquakes.

A summary of the important characteristics of the ten ground motions is given in Table A4-1 and the spectral accelerations of the twenty individual ground motion records are illustrated in Figure A4-2. Also shown in Figure A4-2 is the mean spectral acceleration of the twenty records and the uniform hazard spectra for the 50%/50 year seismic hazard. It can be seen that on average the ground motion records represent the uniform hazard spectrum reasonably well.

Table A4-1: Twenty ground motion records representing 50%/50 year seismic hazard

EQ ID	Event	Year	M_w	Epi. Dist. (km)	Vs30 (m/s)	PGA (g)	SA (g) (T=2s)	k1
892	Landers	1992	7.28	182.7	309	0.033	0.042	1.27
1307	Chi-Chi, Taiwan	1999	7.62	154.3	474	0.026	0.040	1.33
1355	Chi-Chi, Taiwan	1999	7.62	143.5	286	0.028	0.034	1.56
1638	Manjil, Iran	1990	7.37	216.0	275	0.029	0.028	1.89
1799	Hector Mine	1999	7.13	186.6	349	0.032	0.032	1.66
2652	Chi-Chi, Taiwan-03	1999	6.20	48.4	215	0.044	0.064	0.84
2744	Chi-Chi, Taiwan-04	1999	6.20	48.9	273	0.078	0.049	1.09
3261	Chi-Chi, Taiwan-06	1999	6.30	105.1	191	0.038	0.068	0.79
3272	Chi-Chi, Taiwan-06	1999	6.30	88.9	198	0.076	0.070	0.76
3416	Chi-Chi, Taiwan-06	1999	6.30	130.1	261	0.033	0.053	1.01

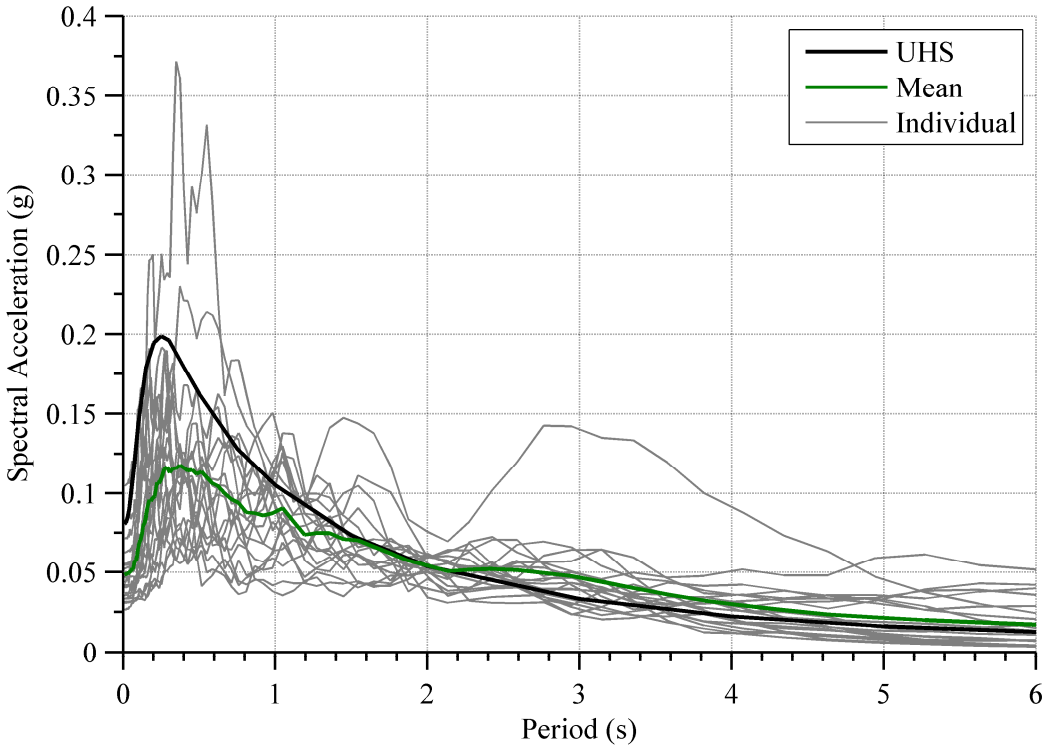

Figure A4-2: Spectral acceleration curves of 50%/50 year seismic hazard

10% in 50 Year Exceedance Probability Ground Motions

A 10% in 50 year exceedance probability corresponds to a return period of 475 years and will herein be referred to as the 10%/50 intensity level. This intensity level represents the typical design level seismic hazard. Referring to the performance objectives matrix developed by SEAOC (1995), the Basic Safety Objective is attained when a structure achieves the Life Safety performance level under the 10%/50 intensity level.

A summary of the important characteristics of the ten ground motions is given in Table A4-2 and the spectral accelerations of the twenty individual ground motion records are illustrated in Figure A4-3. Also shown in Figure A4-3 is the mean spectral acceleration of the twenty records and the uniform hazard spectra for the 10%/50 year seismic hazard. It can be seen that on average the records slightly under-represent the uniform hazard spectrum, particularly for short periods.

Table A4-2: Twenty ground motion records representing 10%/50 year seismic hazard

EQ ID	Event	Year	M_w	Epi. Dist. (km)	Vs30 (m/s)	PGA (g)	SA (g) (T=2s)	k1
286	Irpinia, Italy-01	1980	6.90	23.3	1000	0.089	0.150	0.82
736	Loma Prieta	1989	6.93	61.5	450	0.114	0.132	0.93
756	Loma Prieta	1989	6.93	74.5	271	0.073	0.098	1.25
833	Landers	1992	7.28	146.1	235	0.041	0.095	1.55
1209	Chi-Chi, Taiwan	1999	7.62	54.9	273	0.182	0.155	0.79
1220	Chi-Chi, Taiwan	1999	7.62	103.9	247	0.064	0.056	2.17
2467	Chi-Chi, Taiwan-03	1999	6.20	44.0	233	0.095	0.139	0.88
2473	Chi-Chi, Taiwan-03	1999	6.20	54.1	273	0.053	0.077	1.60
2884	Chi-Chi, Taiwan-04	1999	6.20	47.7	213	0.060	0.083	1.48
3311	Chi-Chi, Taiwan-06	1999	6.30	54.8	254	0.078	0.134	0.92

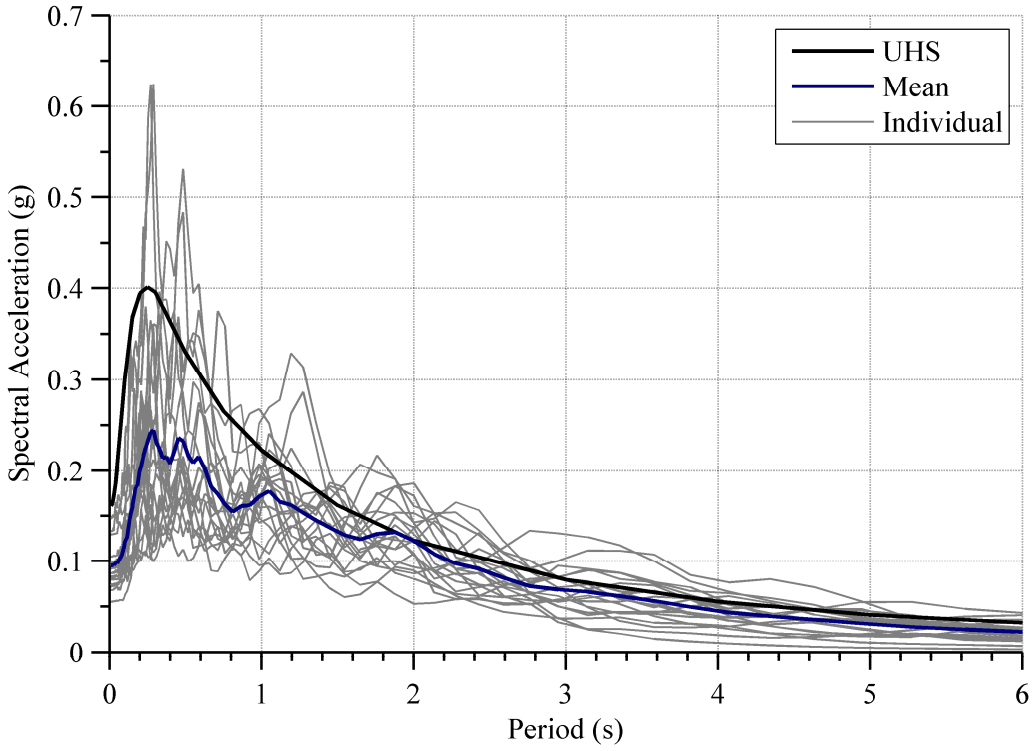

Figure A4-3: Spectral acceleration curves of 10%/50 year seismic hazard

2% in 50 Year Exceedance Probability Ground Motions

A 2% in 50 year exceedance probability corresponds to a return period of 2475 years and will herein be referred to as the 2%/50 intensity level. The 2%/50 ground motions represent the largest seismic hazard considered for the seismic response analysis in this chapter.

Referring to the performance objectives matrix developed by SEAOC (1995), the Basic Safety Objective is attained when a structure achieves Collapse Prevention performance level under the 2%/50 intensity level.

A summary of the important characteristics of the ten ground motions is given in Table A4-3 and the spectral accelerations of the twenty individual ground motions are illustrated in Figure A4-4. Also shown in Figure A4-4 is the mean spectral acceleration of the twenty records and the uniform hazard spectra for the 2%/50 year seismic hazard. It can be seen that on average the records match the hazard spectrum well, however, the short period seismic hazard is under-represented, having a plateau in this range as is similar to that given by the design spectra in NZS 1170.5 (2004).

Table A4-3: Twenty ground motion records representing 2%/50 year seismic hazard

EQ ID	Event	Year	M_w	Epi. Dist. (km)	Vs30 (m/s)	PGA (g)	SA (g) (T=2s)	k1
286	Irpinia, Italy-01	1980	6.90	23.3	1000	0.089	0.150	1.38
731	Loma Prieta	1989	6.93	62.3	392	0.095	0.124	1.67
778	Loma Prieta	1989	6.93	45.1	216	0.263	0.178	1.17
1243	Chi-Chi, Taiwan	1999	7.62	84.8	230	0.067	0.088	2.35
1269	Chi-Chi, Taiwan	1999	7.62	81.1	273	0.139	0.109	1.89
1294	Chi-Chi, Taiwan	1999	7.62	78.5	273	0.148	0.110	1.89
1417	Chi-Chi, Taiwan	1999	7.62	152.2	215	0.081	0.140	1.47
1422	Chi-Chi, Taiwan	1999	7.62	145.7	195	0.069	0.102	2.02
1547	Chi-Chi, Taiwan	1999	7.62	33.8	273	0.149	0.265	0.78
2754	Chi-Chi, Taiwan-04	1999	6.20	37.0	223	0.050	0.108	1.92

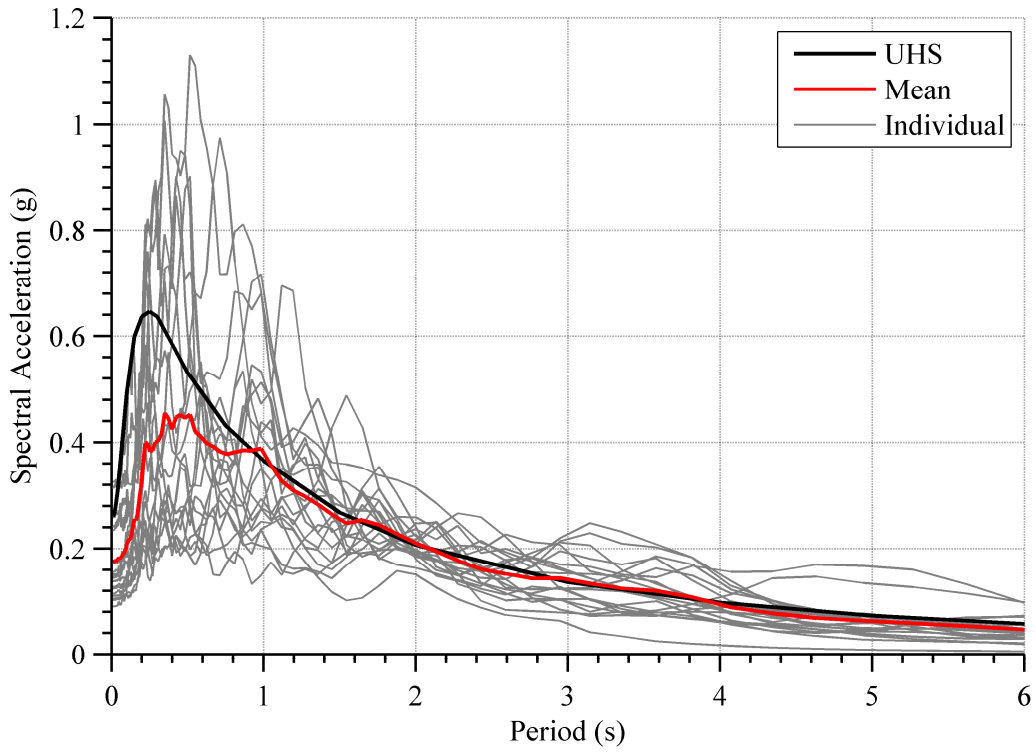

Figure A4-4: Spectral acceleration curves of 2%/50 year seismic hazard

References

Baker, J. W. (2008). An Introduction to Probabilistic Seismic Hazard Analysis (PSHA) (Version 1.3 ed., pp. 72): Stanford University.

Bazzurro, P., & Cornell, C. (1999). Disaggregation of Seismic Hazard. *Bulletin of the Seismological Society of America, 89*(2), 501 - 520.

Boore, D. M., Watson-Lamprey, J., & Abrahamson, N. A. (2006). Orientation-independent measures of ground motion. *Bulletin of the Seismological Society of America, 96*(4), 1502-1511.

Bradley, B. A. (2010). NZ-Specific Pseudo-Spectral Acceleration Ground Motion Prediction Equations Based on Foreign Models: University of Canterbury.

Bradley, B. A. (2012). A ground motion selection algorithm based on the generalized conditional intensity measure approach. *Soil Dynamics and Earthquake Engineering, 40*, 48-61.

Cohen, J. M. (1995). Seismic Performance of Cladding: Responsibility Revisited. *Journal of Performance of Constructed Facilities, 9*(4), 254-270.

Luco, N., & Bazzurro, P. (2007). Does amplitude scaling of ground motion records result in biased nonlinear structural drift responses? *Earthquake Engineering & Structural Dynamics, 36*(13), 1813-1835.

NZS 1170.5. (2004). Structural Design Actions, Part 5: Earthquake Actions - New Zealand. Wellington: Standards New Zealand.

SEAOC. (1995). Performance-based seismic engineering. Sacramento, CA: Structural Engineers Associate of California.